THE JOURNAL
OF
CHEMICAL PHYSICS

VOLUME 20, NUMBER 4 APRIL, 1952

Hindered Intermolecular Rotation in the Solid State: Thermal and Dielectric Phenomena in Long-Chain Compounds

JOHN D. HOFFMAN
General Electric Research Laboratory, Schenectady, New York
(Received October 22, 1951)

It has been assumed that the potential energy barrier hindering rotation of chain molecules about their long axes in the solid state has one deep minimum and Ω other minima with a potential energy V above that of the deeper well. Molecular models suggest Ω should be between 8 and 18. Application of the Bragg-Williams cooperative approximation to this system leads to first-order thermal and dielectric transitions. Dielectric and thermal data on n-$C_{22}H_{45}Br$, n-$C_{30}H_{61}Br$, and n-$C_{28}H_{58}$ show that the transitions are first-order. The static dielectric constant of the polar compounds calculated from Onsager's equation on the basis $\Omega=12$ agree closely with experiment. The model suggests the existence of two Debye-type loss regions below the transition temperature. Loss data confirm this and further indicate Ω is close to 12. There is no evidence of resonance absorption. Ω may also be found from the entropy of transition at constant volume, $R\ln\Omega$. Thermal data on all three compounds are consistent with a value of Ω of 12. The theory indicates that the transition temperatures of a homologous series should arise almost linearly with increasing chain length if the chains do not twist appreciably. Data from the literature confirm this.

I. INTRODUCTION

IN 1932 Müller[1] deduced from x-ray data that long-chain paraffin molecules showed hexagonal symmetry about their long axes in the solid state above a transition temperature T_t and suggested that this signified that the ribbon-shaped molecules were in a state of hindered rotation. Further work on long-chain paraffins,[2] esters,[3,4] bromides,[5] alcohols,[4,6,7] and solid solutions of ketones in paraffins[8] by x-ray and other methods served to confirm Müller's suggestion.

The aim of this paper is to develop a simple theory giving the relationship between the hindered rotation and the thermal and dielectric properties of long-chain compounds and to compare theory with experiment.

Before proceeding, however, it is necessary to point out that the transitions and melting points of chemically and allotropically pure long-chain compounds are of the first order (i.e., they possess a latent heat) and are not broad lambda-points or second-order transitions as suggested by Ubbelohde.[9] His calorimetric data on n-octadecane ($C_{18}H_{38}$) indicates an extremely broad melting point on warming,[9] but other work shows that on cooling both the transition and freezing point are sharp.[10] It has also been clearly demonstrated that a large number of longer paraffins and paraffin derivatives[2–6] have first-order freezing and transition points.*

[1] A. Müller, Proc. Roy. Soc. (London) **A138**, 514 (1932).
[2] E. R. Andrew, J. Chem. Phys. **18**, 607 (1950).
[3] R. W. Crowe and C. P. Smyth, J. Am. Chem. Soc. **73**, 5401 (1951).
[4] W. O. Baker and C. P. Smyth, J. Am. Chem. Soc. **60**, 1229 (1938).
[5] J. D. Hoffman and C. P. Smyth, J. Am. Chem. Soc. **72**, 171 (1950).
[6] J. D. Hoffman and C. P. Smyth, J. Am. Chem. Soc. **71**, 431 (1949).
[7] H. Ott, Z. physik. Chem. **193**, 218 (1944).
[8] V. Daniel, Nature **163**, 725 (1949).
[9] A. R. Ubbelohde, Trans. Faraday Soc. **34**, 289 (1938).
[10] Seyer, Patterson, and Keays, J. Am. Chem. Soc. **66**, 179 (1944).

* The reason for the broadening of the transition and melting points of compounds containing 18 to 22 carbon atoms is that a transformation of an entirely different character from that due to molecular rotation may interfere with the measurements. This transformation is between the vertical (≡|≡) and tilted (≡/≡) packing arrangements of long-chain hydrocarbons and their derivatives. Compounds which exceed a chain length of 24 carbon atoms usually remain in the vertical configuration in the solid state. Only vertical phases undergo rotational transitions. In molecules with 18 to 22 carbon atoms the vertical form slowly converts to the tilted form with the result that a nonequilibrium mixture of the two forms is apt to be studied. This often leads to the observation of unsharp melting and transition phenomena. The above difficulty may generally be avoided in the 18 to 22 carbon atom region by making rapid runs with *lowering* temperature or simply by employing compounds which exceed a chain length of 24. In the latter case the transitions are reversible.

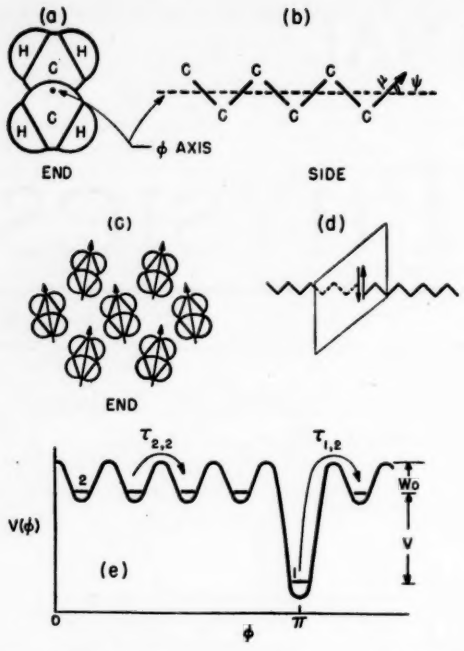

FIG. 1. (a, b) Molecular structure of paraffins, (c, d) crystal structure, (e) assumed potential function for hindered rotation.

In the theoretical development which follows, it will be assumed that the molecules freeze into the vertical phase and remain in this condition above and below T_t. For convenience the molecules will be referred to as "rotationally melted" and "rotationally frozen" above and below T_t. Sometimes the phases above and below T_t are given the name[5] "rotator" and "prerotator." Only nonpolar molecules or molecules with terminal dipoles will be considered.

II. THEORY

1. Model

Some pertinent details of the molecular[1] and crystal structure of long-chain molecules are shown in Fig. 1. In Fig. 1(a) an end view of a model of a paraffin molecule is depicted, and Fig. 1(b) shows a schematic side view of the carbon skeleton which is ribbon-shaped in solid phases. The ϕ-axis is the axis about which rotation occurs, and ψ is the angle subtended by the dipole and the ϕ-axis. In Fig. 1(c) an end view of the crystal array of paraffin molecules in the ground state is shown. It is assumed that end groups in this particular layer point in the same direction. If the molecules are polar, they arrange themselves in a dipole-to-dipole arrangement[11] as shown in Fig. 1(d). These dipole pairs in the plane of the end groups arrange themselves in a head-to-tail manner so that there is no permanent polarization in the ground state. The molecules are strongly constrained to a linear configuration by their neighbors. This puts a severe restraint on bending of the molecules as a whole, but some torsional twisting may be possible.

Paraffin molecules are frequently supposed to have a single fixed position[1] in the ground state. This implies that there is a single narrow minimum on the potential energy. The single minimum cannot be entirely a result of the ribbon-like shape of the molecules, otherwise two or more such positions would be evident. It may therefore be surmised that the deep well is caused in part by the interaction of end groups. In polar compounds dipolar interaction may deepen the well. In the event that a molecule in the ground state is disturbed by thermal agitation, a large number of nearly equivalent equilibrium positions of higher potential energy should become accessible to the molecule as it rotates about its ϕ-axis. This is suggested by the molecular model [Fig. 1(c)] where it is seen that a hydrogen on the central molecule fits between at least 8 but probably no more than 18 of the hydrogens on the adjacent molecules, as the central molecule is rotated between 0 and 2π. The above considerations lead to a potential barrier of the type shown in Fig. 1(e).

2. Calculation of Rotational Order as a Function of Reduced Temperature

In Fig. 1(e) V will be taken as the difference in depth of the deep and shallow wells and W_0 the depth of the wells of higher potential energy. It is clear that the molecule is a librator in such a system and that "rotation" consists in passing over a potential barrier into another well.

The ground state will be designated "1" and the upper states by "2," and Ω will be taken as the degeneracy of the upper level. It seems natural to identify Ω with the number of equivalent wells suggested by the model, and as a consequence Ω should be between 8 and 18.

According to statistical mechanics the ratio of the population of levels 1 and 2 is

$$n_2/n_1=\Omega\exp(-V/RT). \tag{1}$$

The long-range rotational order x is defined as the fraction of molecules in the deep wells so that

$$x=n_1/(n_1+n_2). \tag{2}$$

It is now assumed that the forces locking the molecules in the deep well are broken cooperatively. It seems reasonable to believe that if one end group is out of place it cannot interact so effectively with its neighbors. This cooperative effect will be accounted for by the Bragg-Williams zeroth-order approximation

$$V=V_0x. \tag{3}$$

These relations lead directly to

$$x=1/[1+\Omega\exp(-xT_c/T)], \tag{4}$$

where $V_0/R=T_c$. Equation (4) permits the fraction of

[11] Francis, Collins, and Piper, Proc. Roy. Soc. (London) **A158**, 691 (1937).

molecules in the deep well to be computed as a function of reduced temperature T/T_c for different values of Ω. Plots of x *versus* T/T_c for values of Ω of 6, 12, and 18 are shown in Fig. 2. When Ω reaches a value greater than e^2, x becomes triple-valued over a certain temperature range, and this suggests that a first-order transition occurs in this region; this transition temperature will be located precisely by considerations based on free energy. Frank[12] has derived Eq. (4) from a different model in which the degeneracy of the upper states was that of a free rotator and noted such a model led to first-order transitions, but the implication that the molecules in the upper states are free rotators is unsatisfactory in the present case.

3. Thermodynamic Quantities

The energy involved in the disordering process may be calculated from[13]

$$dE=-V_0 x dx, \tag{5}$$

which leads to

$$E=-\int_1^x V_0 x dx=(V_0/2)(1-x^2). \tag{6}$$

Straightforward procedures then lead to the heat capacity, entropy, and Helmholtz free energy which are

$$C_v=-V_0 x dx/dT=-Rx dx/d\theta; \quad \theta=T/T_c \tag{7}$$

$$S-S_0=R[(1-x)\ln\Omega-x\ln x-(1-x)\ln(1-x)] \tag{8}$$

$$A=(V_0/2)(1-x^2) -RT[(1-x)\ln\Omega-x\ln x-(1-x)\ln(1-x)]. \tag{9}$$

T_t is the temperature at which the two roots of

$$(\partial A/\partial x)_{T_t}=0, \tag{10}$$

which correspond to minima in a plot of A *versus* x, give equal values of A. Thus, the free energy of the two phases in equilibrium at T_t must be equal and at a minimum. It can easily be verified by the substitution in Eq. (9) of

$$T_t=V_0/2R\ln\Omega, \tag{11}$$

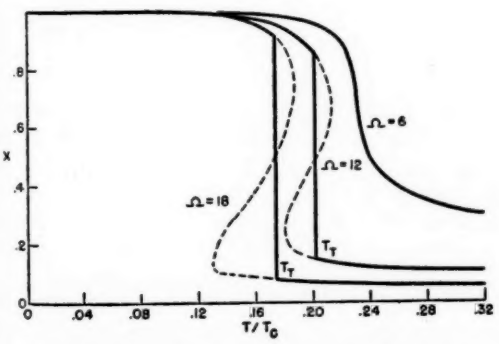

FIG. 2. Rotational order as a function of reduced temperature for various values of Ω.

[12] F. C. Frank, Trans. Faraday Soc. **A42**, 32 (1946).
[13] F. C. Nix and W. Shockley, Revs. Modern Phys. **10**, 1 (1938).

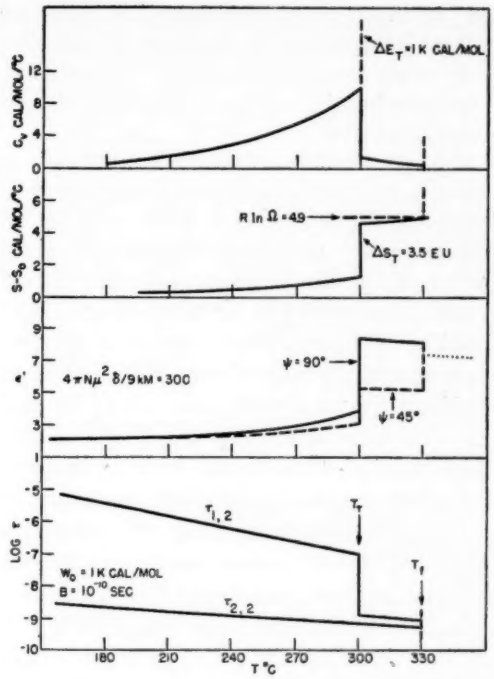

FIG. 3. Calculated thermal and dielectric properties; $T_t=300°K$ $\Omega=12$.

that $A_{(x)}=A_{(1-x)}$ for all x, and that $\partial A/\partial x=0$ is satisfied by a certain value of x, say x_1, and by $(1-x_1)$. Thus, the desired values of x at T_t are symmetrically disposed† about the value $x=\frac{1}{2}$. The value $x=\frac{1}{2}$ also satisfies the conditions of equilibrium except that it represents a maximum in free energy. A vertical line constructed through $x=\frac{1}{2}$ on an x *versus* T/T_c plot serves as the simplest way[12] to locate T_t (see Fig. 2).

C_v and $S-S_0$ have been calculated for the case $\Omega=12$ and $T_t=300°K$ and plotted in Fig. 3. The theory leads to a gradual rise in entropy and specific heat (in excess of that resulting from other causes) in the rotationally frozen state and a first-order transition at T_t if Ω is greater than e^2. There is a remnant of the effect of hindered rotation above T_t.

4. Static Dielectric Constant

We shall use the Onsager[14] equation in the form

$$(\epsilon'-n^2)=\frac{4\pi N\alpha}{3V_m}\left[\frac{\epsilon'(n^2+2)^2}{2\epsilon'+n^2}\right] \tag{12}$$

to calculate the static dielectric constant ϵ' from the orientational polarizability α. n is the index of refraction and V_m the molar volume M/d. While Eq. (12) is most commonly applied to liquids, there is no objection to applying it to solids consisting of rotating spherical molecules. In the present case where the dipoles are

† A plot of A *versus* x near T_t shows two minima and one maximum in A. At T_t the ordinates at the minima are equal.
[14] L. Onsager, J. Am. Chem. Soc. **58**, 1486 (1936).

arranged in sheets in which rotation is 2-dimensional, the Onsager internal field is probably not strictly valid, but it is surely more correct than the Lorentz field, which leads to infinite values of the dielectric constant at low temperatures.

For a polycrystalline substance consisting of molecules constrained to rotate about the ϕ-axis in a symmetrical potential well having three or more minima (or rotating freely) α is $(\mu^2 \sin^2\psi)/3kT$, since only the component of the dipole moment μ perpendicular to the ϕ-axis can contribute to the polarizability.[5] The polarizability will be further reduced if the potential well is asymmetric as for the case $x>0$. For the present, we consider only the simple case where the unit cell contains two molecules [Fig. 1(d)]. The probability that both molecules are frozen in is x^2 and the contribution of these to the polarizability is zero; the probability that both will rotate is $(1-x)^2$ and we assume that each contributes independently to the polarizability. If one molecule and the other is fixed, the probability is $2x(1-x)$ and the pair contributes $(g\mu^2 \sin^2\psi)/3kT$ to the polarizability. The correlation factor g, which plays the role of Kirkwood's correlation parameter,[15] $1+z\langle\cos\gamma\rangle_{Av}$, is entered here, as one might expect the rotating member of the pair not to be random with respect to the fixed member.[16] One might also include a correlation for unit cells in which both dipoles rotate, but these will probably be weaker than those already considered. Using the above arguments, the polarizability is found to be

$$\alpha=(\mu^2 \sin^2\psi/3kT)(1-x)(gx+1-x). \quad (13)$$

TABLE I. Static dielectric constants at 1 and 10 kc in the region of the freezing and transition points.

$C_{22}H_{45}Br$		n-$C_{28}H_{58}$		n-$C_{29}H_{61}Br$	
T°C	ϵ'	T°C	ϵ'	T°C	ϵ'
50.7	3.13	77.7	2.020	78.7	2.62
46.7	3.14	72.4	2.025	73.7	2.64
42.8	3.17	64.7	2.036	71.7	2.65_5
41.0	3.18	61.7	2.041	68.2	2.65_5
40.0	3.19	60.68[a]	2.044	66.40[a]	2.67_5
40.0[a]	3.20	60.68	2.112	66.4	2.71
40.0	3.10	60.67	2.150	66.1	2.72
40.0	2.99	60.60	2.202	65.7	2.72
39.0	2.91	59.0	2.214	60.7	2.71
36.0	2.90	58.2	2.220	58.0	2.70_5
33.8	2.90	55.7	2.232	57.0[b]	2.70
31.8	2.90	54.7	2.236	56.7	2.65
29.8	2.84	53.5[b]	2.240	56.7	2.63
29.8[b]	2.82	53.1	2.220	56.5	2.61
29.7	2.65	53.1	2.214	56.4	2.54
28.3	2.51	52.8	2.190	53.7	2.51
26.5	2.48	52.2	2.190	50.0	2.50
23.8	2.47	49.9	2.185	39.2	2.48
22.0	2.46	30.1	2.183	24.7	2.46

[a] Freezing point.
[b] Transition point.

[15] J. G. Kirkwood, J. Chem. Phys. 7, 911 (1939).
[16] H. Fröhlich, *Theory of Dielectrics* (Oxford University Press, London, 1949), p. 59.

In the event that $g=1$, i.e., there is no local ordering and hence no correlation, the polarizability is simply

$$\alpha=(\mu^2/3kT) \sin^2\psi(1-x), \quad (14a)$$

but if a strong correlation exists as for $g=2$, we find

$$\alpha=(\mu^2/3kT) \sin^2\psi(1-x^2). \quad (14b)$$

A much weaker correlation will lead to Eq. (14b) if more neighbors are included. Eq. (14b) is just the dependence of α on x found by Frank[12] by a different method which involves arbitrary assumptions of its own.

It is impossible to decide on the exact dependence of α on x unless detailed information is available concerning local ordering. Fortunately, however, the quantitative difference between Eqs. (14a) and (14b) (which results from drastically different degrees of local ordering) is rather small in the important ranges of x. Following Frank, we have chosen Eq. (14b) as a working equation, but it must be remembered that this choice rests on specialized assumptions; the use of Eq. (14a) which is based on the supposition that the molecules are independent must be regarded as equally probable. Owing to a fortunate coincidence, the *change* in ϵ' at T_t, computed from either Eq. (14a) or (14b) with (13) is the same for the important case $\Omega=12$.

The dielectric constant is calculated by first converting $x(T/T_c)$ for an assumed value of Ω to $x(T)$ by matching the observed value of T_t with the first-order transition in an x *versus* T/T_c plot. $x(T)$ is then substituted in Eq. (14) and α calculated as a function of temperature. Substitution of this quantity in Eq. (12) then yields $\epsilon'(T)$.

The theoretical effect of hindered rotation on the static dielectric constant is shown in Fig. 3 for the case $\Omega=12$, $T_t=300$°K, $4\pi N\mu_0^2 d/9kM=300$, and $n^2=2.00$. ψ was set at $\pi/2$ and $\pi/4$. The theory predicts a gradual rise in ϵ' which culminates in a first-order transition at T_t. The factor $1-x^2$ is nearly unity above T_t, so the reduction in ϵ' in the rotationally melted state is principally caused by ψ.

5. Dielectric Relaxation Effects

The model implies there are two Debye-type relaxation times below T_t. Molecules may occasionally reorient under the influence of an applied field over the barrier W_0 from one position to another in state 2; in addition, molecules may occasionally be lifted out of the deep well over the barrier W_0+V into one of the upper wells. Thus we may write

$$\tau_{1,2}=B \exp(W_0+V)/RT \quad (15)$$

$$\tau_{2,2}=B \exp(W_0/RT), \quad (16)$$

where $\tau_{1,2}$ is the relaxation time of the transition from the deep well to the upper well, and $\tau_{2,2}$ is the relaxation time of the transitions in the upper well. There is no *a priori* way to compute B with the required accuracy, so we shall proceed in a manner which avoids the

necessity of knowing either B or W_0. This may be done by taking logarithms of Eqs. (15, 16) and subtracting. This yields

$$\log\tau_{1,2}-\log\tau_{2,2}=V/2.303RT. \quad (17)$$

Thus the difference of the relaxation times (in decades) is equal to $2x\ln\Omega/2.303$ at T_t. For the case $\Omega=12$ where $x=0.86$ just below T_t, the two relaxation peaks should occur two decades apart. Below T_t the two relaxation times will diverge. Above T_t the relaxation times will be so close as to be virtually indistinguishable.‡

The behavior of the two relaxation times with temperature is illustrated in Fig. 3, where B has been set at 10^{-10} sec, $\Omega=12$, $T_t=300°K$, and W_0 at 1 kcal/mole.

The ratio of the intensities of the two loss peaks, $I_{2,2}/I_{1,2}$, will be of the order of magnitude

$$\frac{I_{2,2}}{I_{1,2}}\cong\frac{n_2\exp[-W_0/RT]}{n_1\exp[-(W_0+V)/RT]}\cong\Omega. \quad (18)$$

The numerator of Eq. (18) shows that the intensity of the 2,2 line should drop with decreasing temperature.

6. Properties as a Function of Chain Length

If the molecules are assumed to be rigid rods, Ω should be constant with chain length, and the barrier V_0 as a function of chain length may be written

$$V_0(m)=2V_{e.g.}+(m-2)V_{CH_2}, \quad (19)$$

where m is the chain length, $V_{e.g.}$ the barrier caused by one of the end groups, and V_{CH_2} the barrier caused by each $-CH_2-$ group. Combination of (11) and (19) yields

$$T_t(m)=[2V_{e.g.}+(m-2)V_{CH_2}]/2R\ln\Omega. \quad (20)$$

This shows T_t will vary in a linear way with chain length if the molecules behave as rigid rods and if $V_{e.g.}$ is not temperature dependent.

The effect of torsional twisting of the chains on $T_t(m)$ would be to cause T_t to be lower than expected from Eq. (20) for very long chains. Part of this effect would be a result of an increase of Ω with chain length and part of it a result of curvature in $V_0(m)$. The latter may be taken into account using a modification of Fröhlich's theory of chain twisting (reference 16, p. 128) which gives $V_0(m)=V_{CH_2}\cdot\bar{m}\tanh(m/\bar{m})$. $\bar{m}$ is interpreted as the chain length where twisting becomes appreciable. In the present application we prefer to include the interactions caused by the end groups, so that

$$T_t=[2V_{e.g.}+\bar{m}V_{CH_2}\cdot\tanh(m-2/\bar{m})]/2R\ln\Omega(m). \quad (21)$$

If the twisting is not so severe as to cause $\Omega(m)$ to change appreciably, Eq. (21) may be used to analyze T_t *versus* m plots for a homologous series. It should be remembered that $V_{e.g.}$ may vary slightly with temperature. If $\bar{m}$ is large compared to m, then $\tanh(m-2/\bar{m})\cong m-2/\bar{m}$ and Eq. (21) reverts to (20).

The entropy of transition at constant volume (for the case where Ω is large) is given by§

$$\Delta S_T\cong R\ln\Omega. \quad (22)$$

Thus, ΔS_T should be independent of chain length unless the molecules twist appreciably, and so cause Ω to increase with chain length. It would be a mistake, however, to compare Eq. (22) with the observed entropy of transition because the observed value contains a large contribution as a result of expansion. If one adopts the view that a melting or transition process may be regarded as an expansion at constant order followed by a disordering at constant volume,[17] the observed entropy will consist of $R\ln\Omega+\Delta S_{(expansion)}$ where

$$\Delta S_{(expansion)}=2.34\cdot10^{-5}\Delta V\alpha/\beta. \quad (23)$$

In this equation α, the cubical coefficient of expansion, is in deg^{-1}; β, the cubical compressibility, is in $cm^2\ g^{-1}$; and ΔV, the change in molar volume at T_t, is in cm^3/mole.

Table II. Dielectric constants and loss factors in the rotationally frozen state.

	n-$C_{22}H_{45}Br$		n-$C_{30}H_{61}Br$			
	10 kc		1 kc		10 kc	
T°C	ϵ'	ϵ''	ϵ'	ϵ''	ϵ'	ϵ''
20	...	...	2.45	...	...	0.017
10	2.40	0.008	2.45	0.01	...	0.031
0	2.37	0.008	2.42	0.027	2.41	0.040
−10	2.34	0.009	2.37	0.038	2.35	0.035
−20	2.32	0.012	2.33	0.031	2.30	0.022
−25	...	0.014	...	...	...	0.017
−30	2.31	0.014	2.28	0.016	2.25	0.015
−35	2.29	0.012	...	...	...	0.015
−40	2.28	0.009$_5$	2.25	...	2.23	0.011
−50	2.27	0.008	2.23	...	2.21	0.005
−60	2.26	...	2.22	...	2.20	0.003
−70	2.26	...	2.21	...	2.20	...

III. EXPERIMENTAL

The dielectric constant ϵ' and dielectric loss ϵ'' (at 1 and 10 kc) of n-docosyl bromide ($C_{22}H_{45}Br$), n-octacosane ($C_{28}H_{58}$), and n-tricontyl bromide ($C_{30}H_{61}Br$) have been measured over a wide temperature range covering the liquid, rotationally melted, and rotationally frozen states. These measurements were made in a cell of 14.95 $\mu\mu$f capacitance on an impedance bridge. The results are shown in Tables I and II. The ϵ' values are accurate to ±1 percent and the ϵ'' values to better than ±0.003. The values on $C_{22}H_{45}Br$ are very close to those measured previously.[5] The temperature measurements were made with a platinum resistance thermometer. $C_{22}H_{45}Br$ and $C_{30}H_{61}Br$ were purified by vacuum distillation. The physical properties of the compounds

‡ If $10>\Omega>\epsilon^2$, two relaxation processes might be resolved above T_t.

§ Eq. (8) may be employed if a more exact value of ΔS_T is desired.

[17] R. A. Oriani, J. Chem. Phys. **19**, 93 (1951).

TABLE III. Physical properties of the compounds.

	M.W.	T_f, °C This work	T_f, °C Lit.	T_T, °C This work	T_T, °C Lit.	n_D(liquid)	ϵ_∞ (solid)	Density Liquid	Density Solid
$C_{22}H_{45}Br$	389.3	40.0	40.5[5]	29.8	30.5[5]	1.458(40°)	2.26	1.00(40°)	1.15(35°)[a]
$C_{28}H_{58}$	394.5	60.7	61.2[10]	53.5	54.0[10]	1.428(61°)	2.18	0.78(61°)[10]	0.89(55°)
$C_{30}H_{61}Br$	501.4	66.4	···	57.0	···	1.414(67°)	2.21	0.92(67°)[a]	1.06(60°)[a]

[a] Estimated from data in reference 18.

are shown in Table III. Some of the density data have been taken from the literature.[18]

The loss tangent, tanδ, was measured on the rotationally frozen phase of $C_{22}H_{45}Br$ at 25°C over a wide frequency range (Table IV). The methods are given in the table. The error in tanδ probably does not exceed ± 0.0003. Values of ϵ' and ϵ'' were obtained on the rotationally melted phase of $C_{22}H_{45}Br$ at 35°C at 3.12 cm (Sec. IV).

The specific heat and cooling curve data (Sec. IV) on these compounds were obtained in a differential calorimeter.[19] A summary of the thermodynamic data is given in Table V. It is believed the data are correct to about ± 5 percent. The runs on $C_{28}H_{58}$ and $C_{30}H_{61}$ were made on warming. The data on $C_{22}H_{45}Br$ were first obtained on cooling and then on warming after standing 48 hr at 0°C.

IV. COMPARISON OF THEORY AND EXPERIMENT

1. Calculation of the Static Dielectric Constant

The required values of M, d, and ϵ_∞' (which replaces n^2) for use in the Onsager formula are given in Table I. The proper moment for use in Eq. (14) is the *gas* moment which is 2.15 Debye for the chain bromides.[20] ψ is 35° if the dipole is assumed to be rigidly connected to the rest of the molecule.

When $\epsilon'(T)$ is computed for solid n-$C_{22}H_{45}Br$ and n-$C_{30}H_{61}Br$ for the case $\Omega = 12$ (Figs. 4, 5) a good fit is obtained. If Ω is taken as 18, the subtransitional rise in ϵ' is too small, and if Ω is taken as 8, the discontinuity in ϵ' at T_t is too small. It may be concluded from these calculations that $\Omega = 12 \pm 4$.

The general features of the dielectric transitions seem correctly predicted. In particular, a first-order discontinuity occurs at T_t. This is in contrast with the results obtained with a two-position theory (reference 16, p. 146) which yields second-order transitions. It should be remarked that the rotation of the molecules is hindered above and below T_t. α always contains a factor of $\sin^2\psi$ in the solid state because the rotation is restricted to one degree of freedom.‖

[18] Heston, Hennelly, and Smyth, J. Am. Chem. Soc. **72**, 2071 (1950).

[19] J. D. Hoffman, J. Am. Chem. Soc. (to be published).

[20] C. P. Smyth and A. L. McAlpine, J. Chem. Phys. **3**, 347 (1935).

‖ If the value 2.15 Debye is used to compute ϵ' for the liquid bromides, the results are too high. This means g is less than unity for the liquid. Since x-ray evidence indicates some aligning of long-chain molecules in the liquid state, part of this reduction in g may in fact be a result of a $\sin^2\psi$ factor.

The nonpolar compound $C_{28}H_{58}$ will now be considered. Just above T_f, ϵ' is 2.044, and just above T_t it is 2.240. If these data are inserted in the Clausius-Mossoti formula

$$[(\epsilon'-1)/(\epsilon'+2)]M/d = P_e, \tag{24}$$

where P_e is the molar electronic polarization, it is found that $d_s/d_l = 1.13_4$ for this nonpolar substance in good agreement with the value $d_s/d_l = 1.14$ found by direct density measurement (Table I). The dielectric constant of the rotationally melted phase increases about one percent between T_f and T_t. This is probably caused by a slight increase of the amount of material between the condenser plates. Surprisingly, at T_t, ϵ' drops one percent even though the density increases a few percent. This effect at T_t is very small compared to that in the polar compounds, and may be a result of a drop in electronic polarizability, or more likely, to cracks in the dielectric. The dashed line in Fig. 5 (lower) shows the value of ϵ' that would be obtained using $d_s/d_l = 1.13$ with the density assumed constant below T_f, just as was done for the polar materials.

2. Dielectric Relaxation Phenomena

It has already been mentioned that when $\Omega = 12$ and $T_t = 300$°K, two relaxation regions approximately two decades apart should appear just below T_t because of the assymmetry of the potential energy barrier. The frequency sweep of n-docosyl bromide (Fig. 6) at 25°C clearly shows two relaxation regions. They are 2.2 ± 0.1 decades apart. This again shows Ω is close to 12.

Another method of finding the two relaxation times in the rotationally frozen state is to examine ϵ'' *versus* T at

TABLE IV. Tanδ of n-$C_{22}H_{45}Br$ at 25°C (rotationally frozen phase from 10^4 to 10^{10} cycles/sec).

Frequency cps	Tanδ	Method
1.0×10^4	0.0012	Bridge[b]
3.0×10^4	0.0013	
1.0×10^5	0.0017	
1.5×10^6	0.0040	Susceptance variation
2.4×10^6	0.0043	
5.0×10^6	0.0051	
8.5×10^6	0.0053	
2.0×10^7	0.0046	
8.0×10^7	0.0044	
5.5×10^8	0.0070	Re-entrant cavity
3.0×10^9	0.0070	Wave guide
1.0×10^9	0.0044[a]	

[a] $\epsilon' = 2.27$.

[b] These measurements were made with a 40 $\mu\mu$f cell.

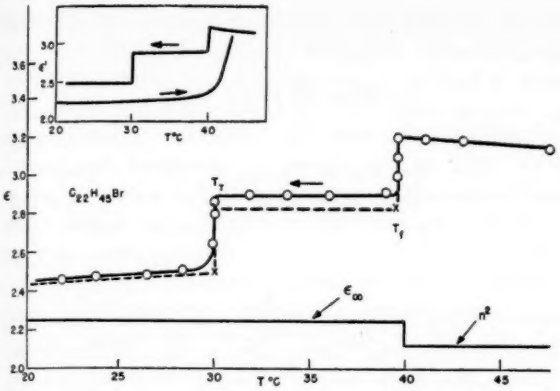

FIG. 4. Dielectric constant of *n*-docosyl bromide as a function of temperature in the transition region. Arrows indicate direction in which temperature is changing. Dashed lines indicate theoretical values.

low temperatures for two loss peaks at constant frequency. The data for $C_{30}H_{61}Br$ show these two peaks at 0°C and −35°C at 10 kc (Fig. 7). A loss region was also detected in $C_{22}H_{45}Br$ at low temperatures, but it could not definitely be proved to be a double maximum because the loss was near the limit of observation. In any event strong evidence of the two predicted relaxation times in the subtransitional state has been found in both polar compounds.

Fröhlich (reference 16, p. 146) has suggested that a high frequency peak may appear in polar long-chain compounds as a result of resonance (Lorentz) absorption. This theory indicates τ should be $\sim 10^{-12}$ sec (corresponding to an f_{max} of $\sim 10^{11}$ cycles/sec). The upper peak in $C_{22}H_{45}Br$ ($\tau_{2,2}$) occurs at too low a frequency (10^9 cycles/sec) to be accounted for by such a mechanism, and it is extremely unlikely that either of

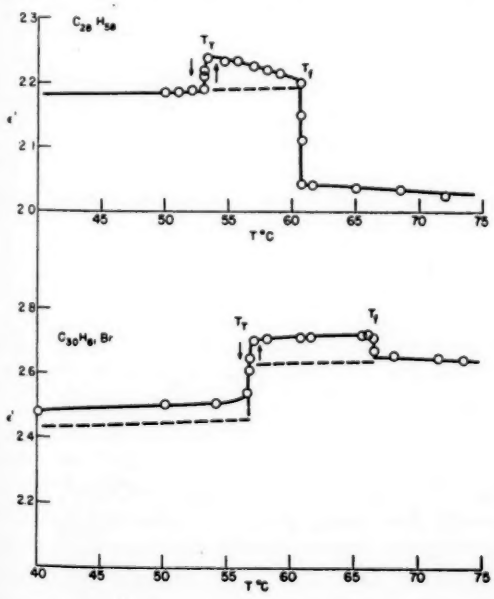

FIG. 5. Dielectric constant of *n*-octacosane and *n*-tricontyl bromide in the transition region. Transitions are reversible. Dashed lines indicate theoretical values.

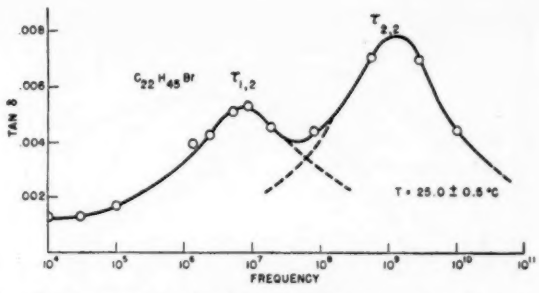

FIG. 6. Loss tangent of *n*-docosyl bromide as a function of frequency in rotationally frozen state.

the two peaks in $C_{30}H_{61}Br$ observed at 10^4 cycles/sec could be resonance absorption. Furthermore, the data of Cook and Buchanan on $C_{15}H_{31}COOCH_3$ show that the intensity of the high frequency line in this compound drops markedly with decreasing temperature, in

TABLE V. Thermal data.

	n-$C_{22}H_{45}Br$	*n*-$C_{28}H_{58}$	*n*-$C_{30}H_{61}Br$
Δh_T(cal/g)	11.8	12.8	9.5
ΔS_T(cal/mole/°C)	15.1 eu	15.0 eu	14.4 eu
Δh_f(cal/g)	23.0 (cooling) 48.5 (warming)[a]	38.1	38.0

[a] After standing 48 hr at 0°C.

contrast to what would be expected for resonance absorption but in accord with Eq. (18). Our conclusion is that both of the peaks observed in this research, as well as those of Cook and Buchanan[21] are of the Debye type. Higasi and Ozawa[22] have arrived at the same conclusion on different grounds.

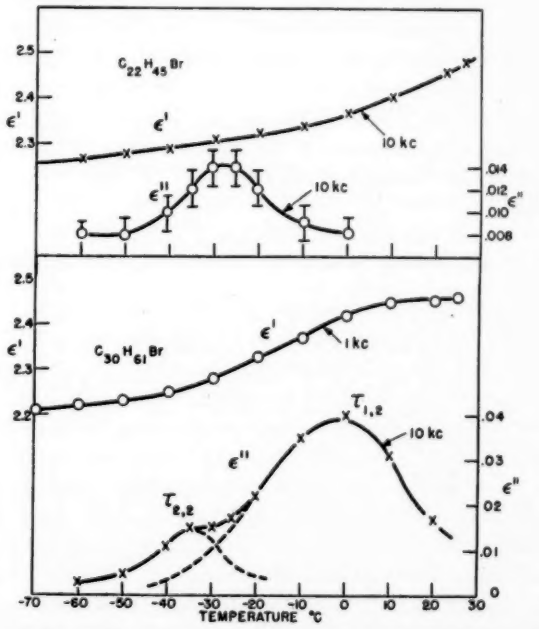

FIG. 7. Dielectric constant and loss factor of *n*-docosyl bromide and *n*-tricontyl bromide in the rotationally frozen state as a function of temperature.

[21] H. F. Cook and T. J. Buchanan, Nature **165**, 358 (1950).
[22] H. Higasi and M. Ozawa, J. Phys. Soc. Japan **6**, 280 (1951).

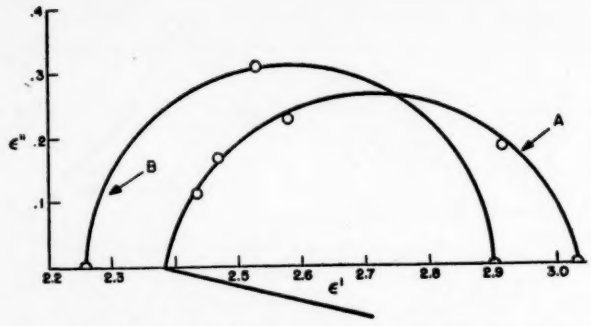

FIG. 8. Cole plot of *n*-dodecyl stearate (a) after Crowe and Smyth, and *n*-docosyl bromide (b) in the rotationally melted phase.

In accord with expectation, the $\tau_{2,2}$ line is stronger than the $\tau_{1,2}$ line (Fig. 6). Quantitative agreement of the observed value of I_{22}/I_{12} and the value obtained from Eq. (18) is not to be expected since such details as the exact barrier shape have not been taken into account.

The present study of relaxation phenomena in the rotationally melted state, where the potential barrier is nearly symmetrical, is confined to the measurement of ϵ' and ϵ'' at 3.12 cm on $C_{22}H_{45}Br$ at 35°C. These data are shown in Fig. 8 with appropriate ϵ_0' and ϵ_∞' values in a Cole[23] plot. The fact that a full semicircle is found suggests a small distribution of relaxation times apparently limited to a single relaxation region. Fortunately, the above data may be strengthened by those of Crowe and Smyth[3] who have succeeded in obtaining sufficient points in the rotationally melted phase of *n*-dodecyl stearate ($C_{17}H_{35}COOC_{12}H_{25}$) to make a virtually complete Cole plot. These data are also shown in Fig. 8. It seems clear there is but one large relaxation region of the 2,2 type; a small distribution of relaxation times in this compound is indicated by the fact that the center of the circle is below the ϵ'-coordinate. Very detailed measurements of the kind described above may succeed in revealing a remnant of the $\tau_{1,2}$-peak above T_T.

3. Calculation of Ω from Thermodynamic Data

The observed entropies of transition of the compounds are all close to 15 eu (Table V). This must be the sum of the entropy of expansion and the configurational entropy $R\ln\Omega$. The values[10] of α (cubical) for hydrocarbons 20 to 30 carbon atoms long all lie close to 45×10^{-5} deg^{-1}, and Müller's data[24] on the compressibility of n-$C_{23}H_{48}$ and commercial paraffin wax give β (cubical) $=2.06\times10^{-8}$ cm^2 g^{-1} and 1.7×10^{-8} cm$^2\cdot$g^{-1}, respectively. ΔV is 16.5 to 18 cm^3/mole for compounds containing 20 to 30 carbon atoms.[10] With these data in Eq. (23) it is found that $\Delta S_{(\text{expansion})}=9.7\pm2.0$ eu. If this is added to $R\ln12=4.9$ eu, the result is 14.6 ± 2.0 eu in good agreement with the observed values. It is satisfactory that this thermodynamic method suggests a value of Ω consistent with those found from dielectric properties.

4. Specific Heat Data

In order to compare the observed and theoretical specific heat values caused by hindered rotation, it would be necessary to have detailed α- and β-values for the rotationally melted and rotationally frozen states since $C_v=C_p-\alpha^2VT/\beta$. Such detailed data are not available. It may be noted, however, that there is a subtransitional rise in C_p which may be ascribed to the onset of hindered rotation (Fig. 9). The values of C_p in the rotationally melted phases are surprisingly high. This may be a result of the fact that the α is high in these phases.[10] The rapid rise of C_p in $C_{28}H_{58}$ just below

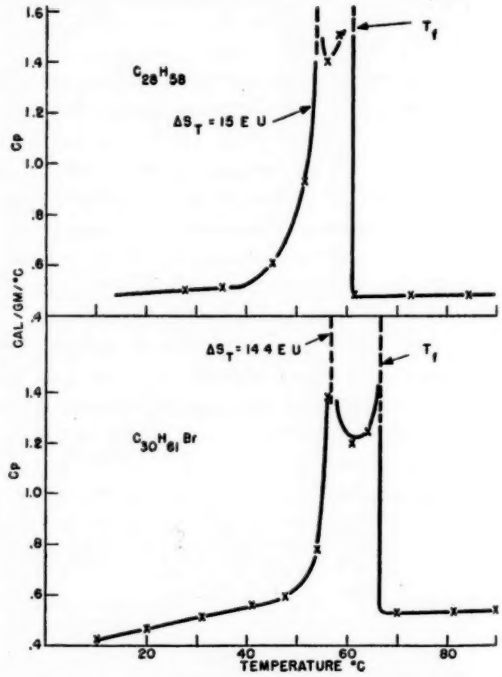

FIG. 9. Specific heat of *n*-tricontyl bromide and *n*-octacosane in the region of the transition and melting points.

T_t is probably a result of the fact that this compound is not as pure as the other materials.

5. Order of Transition: Vertical-Tilted Transformations

The automatically recorded cooling curve of $C_{22}H_{45}Br$ is shown in Fig. 10. This curve shows that the freezing and transition points are first order despite the fact that this compound is in the critical 18 to 24 carbon chain length where vertical-tilted transformations occur readily. The vertical-tilted transformation was deliberately induced in $C_{22}H_{45}Br$ by allowing the material to stand in the calorimeter for 48 hr at 0°C. When ϵ was measured on rewarming, virtually no transition effect appeared, and the melting point was unsharp as shown in Fig. 4 (inset). This illustrates what a vertical-tilted transformation can do to induce "second-order"

[23] K. S. Cole and R. H. Cole, J. Chem. Phys. **9**, 341 (1941).
[24] A. Müller, Proc. Roy. Soc. (London) **A178**, 227 (1941).

melting and transition effects. The other two compounds exhibit completely reversible first-order rotational transitions and melting points in similar experiments because the vertical-tilted transformation does not intervene.

By subtracting $(\Delta h_{\text{freezing}}+\Delta h_T)$ from Δh_{fusion}¶ for $C_{22}H_{45}Br$, it was found that the enthalpy change of the vertical-tilted transformation was approximately

$$\Delta H_{\text{vertical}\rightarrow\text{tilted}}=5.3 \text{ kcal/mole.} \quad (25)$$

The tilted form of $C_{22}H_{45}Br$ is more stable, has a higher melting point, and no rotational transition. The corresponding transformation** in the $C_{22}H_{46}$ liberates 6.4 kcal/mole.[25]

6. Physical Properties as a Function of Chain Length: Chain Twisting and Internal Rotation Effects

It may be seen in Fig. 11(a) that T_T varies in a nearly linear manner with chain length for the *n*-paraffins[10] as indicated by Eq. (20). This supports the hypothesis

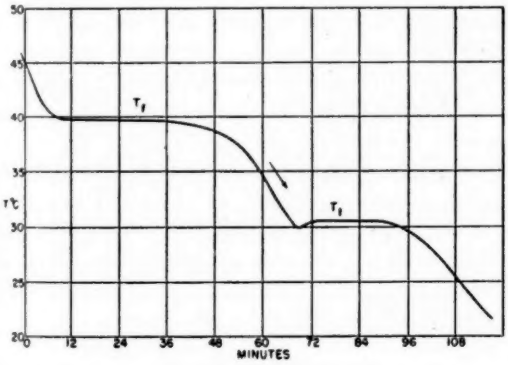

FIG. 10. Tracing of automatically recorded cooling curve of *n*-docosyl bromide.

that the chains may be regarded as rigid rods to a fair approximation. The curvature is so slight that if Eq. (21) is used, $\bar{m}$ must be set at a value greater than 100 to obtain a fit. It may therefore be concluded that chain twisting causes no large effects for the chain lengths studied. Analysis of the T_T *versus* m data, using Eq. (20) with $\Omega=12$, shows then $V_{\text{e.g.}}$ is $\sim$1.0 kcal/mole and V_{CH_2} is $\sim$25 cal/CH_2.

If the entropy of fusion of the *n*-hydrocarbons with 8 to 16 carbon atoms (which have no transitions) are extrapolated to longer chain lengths, the sum of the entropy of transition and melting of the longer members falls fairly close to this line (Fig. 11(b)). This suggests

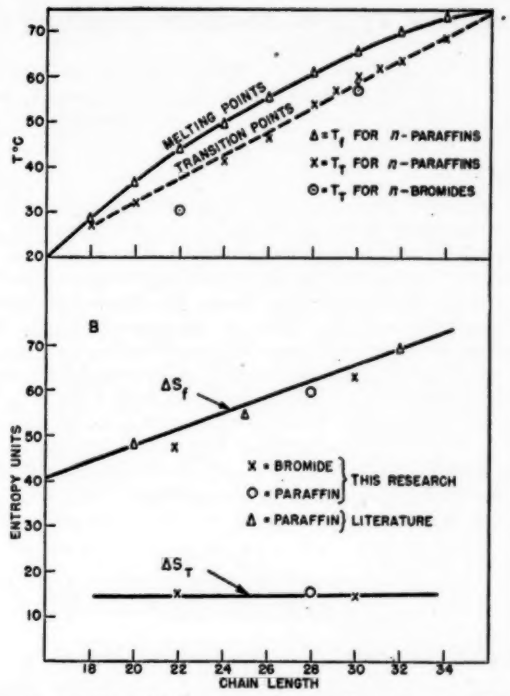

FIG. 11. (a) Transition and melting points of *n*-paraffins and transition points of *n*-bromides as a function of chain length. (b) Entropies of fusion and transition of *n*-bromides and *n*-paraffins as a function of chain length.

that the melting process in the longer molecules is divided into two parts: rotational melting at T_T and total melting at T_f.

It could be argued that the bromine atom in the polar molecules is orienting independently of the rest of the molecule, and that this internal rotation leads to one of the two observed dielectric relaxation times. An orientation of the dipole of this type would require a severe distortion of the neighboring molecules and seems rather unlikely.

One indication that long chain molecules rotate as a unit may be had in the fact that unsymmetrical esters[3] and solid solutions of ketones in paraffins[8] (where the dipole is rigidly connected to the molecule) exhibit hindered rotational transitions of exactly the same general character as those found in paraffins and bromides. Another indication that the polar group does not orient independently is given by the fact that x-ray[7] and dielectric data[6] on long-chain alcohols both lead to the same conclusion concerning the nature of rotation above and below T_T. This could not be true unless the $-$OH group were affixed to the hydrocarbon part of the molecule with an effective barrier considerably greater than the barrier to intermolecular rotation.

ACKNOWLEDGMENT

The author wishes to thank Mr. S. I. Reynolds for valuable assistance in making the high frequency measurements and Dr. J. R. Ladd for preparing the docosyl bromide. Thanks are also due Dr. B. H. Zimm and Dr. J. K. Bragg for many helpful conversations.

¶ Measured after standing 48 hours.

** The enthalpy change in a process of this type is often called the heat of "transition" in the literature. The vertical-tilted change is an irreversible and time-dependent effect which occurs over a wide temperature range in these compounds, while the rotational transition occurs reversibly at a definite temperature. It seems best to differentiate between these two effects by using the term *transformation* for the vertical-tilted change and *transition* for the first-order rotational change.

[25] Garner, VanBibber, and King, J. Chem. Soc., 1553 (1931).

A New Type of Disorder Affecting the Dielectric Properties of Long-Chain Esters

ROBERT W. CROWE, JOHN D. HOFFMAN AND CHARLES P. SMYTH
General Electric Research Laboratory, Schenectady, New York, and Frick Chemical Laboratory, Princeton University, Princeton, New Jersey

(Received November 23, 1951)

The dielectric properties of a series of long-chain esters have been investigated in the solid state. Like other long-chain molecules containing 20 or more carbon atoms, most of the ester molecules showed evidence of hindered molecular rotation about their long axes in the crystal lattice. It was also found that higher dielectric constants resulted when the samples were rapidly frozen than when they were allowed to solidify gradually, the effect being more pronounced as the chain length was increased. In order to explain this behavior, it has been assumed that the esters may crystallize in an ordered lattice in which the dipoles are in a plane, or in a longitudinally disordered lattice in which some of the chains are reversed. In the latter case, the dipoles may or may not form two planes depending upon the position of the polar group in the chain. It has also been assumed that the degree of longitudinal disorder increases with increase in freezing rate. Once frozen in, however, it remains fixed until the sample is remelted.

The potential barrier hindering rotation has been assumed to be much higher in the ordered state than in the disordered state because separation of the dipoles should lower steric and dipole interaction in the latter. Since the rotational transition temperature is proportional to a potential energy difference V_0 related to the barrier against rotation, the transition temperature should increase with increase in longitudinal order. In a completely ordered ester or a nearly symmetrical disordered ester, the barrier may be sufficiently high to raise the transition point to a temperature near or above that of fusion. The experiments agree with these assumptions.

I. INTRODUCTION

SINCE the conclusion reached by Müller[1] in 1932 that long-chain hydrocarbon molecules may assume a state of hindered rotation about their long axes in the solid state, dielectric constant measurements have shown that this behavior persists even when a polar group is introduced at the end of the chain. These polar molecules include long-chain alcohols,[2,6] bromides[3,4] and ethyl esters.[5,6] Andrew[7] has recently confirmed Müller's original conclusion by nuclear resonance studies on crystalline *n*-octacosane (n-$C_{28}H_{58}$) and dicetyl (n-$C_{32}H_{66}$). It is now clearly understood that the chains do not rotate freely in the lattice and that rotational oscillation is a more accurate description. Inasmuch as the rotation of molecules in this sense appears to be a typical order-disorder phenomenon culminating in a first-order transition, we will refer to this effect as rotational disorder.

A recent investigation of the dielectric properties of a number of long-chain alkyl esters[8] has revealed that rotational disordering of chains is also possible when the polar group is introduced near the center of the molecule. During the course of this investigation, however, two unusual phenomena were observed: (1) a definite dependence of the dielectric constants and transition points of the solid esters upon rate of solidification, and (2) a striking dissimilarity in dielectric behavior depending upon the symmetry of the molecule in respect to the placement of the polar group. This paper is an attempt to explain, at least qualitatively, these phenomena in terms of permanent *longitudinal disorder* or reversal of chains in the crystals realized during solidification (Fig. 1).

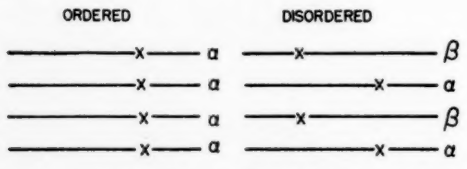

FIG. 1. Longitudinally ordered and disordered phases in crystalline long-chain esters.

II. EXPERIMENTAL

The esters investigated include *n*-decyl palmitate, *n*-dodecyl palmitate, *n*-tetradecyl palmitate, *n*-hexa-

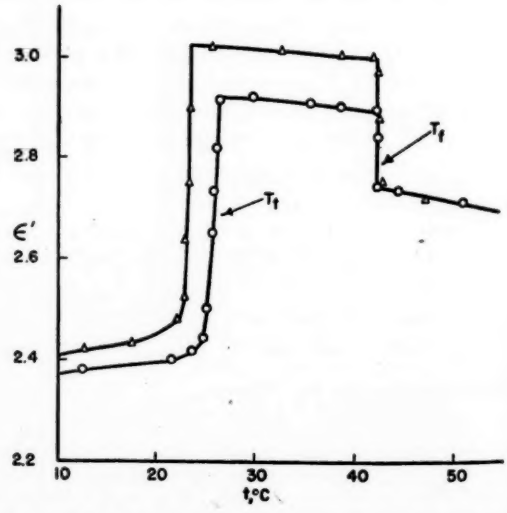

FIG. 2. Variation of the dielectric constant of *n*-dodecyl stearate with increasing temperature after freezing times of one-half hour Δ and two hours ○.

[1] A. Müller, Proc. Roy. Soc. (London) **A138**, 514 (1932).
[2] J. D. Hoffman and C. P. Smyth, J. Am. Chem. Soc. **71**, 431 (1949).
[3] J. D. Hoffman and C. P. Smyth, see ref. 2, **72**, 171 (1950).
[4] J. D. Hoffman, J. Chem. Phys. **20**, 541 (1952).
[5] R. Buckingham, Trans. Faraday Soc. **30**, 377 (1934).
[6] W. O. Baker and C. P. Smyth, J. Am. Chem. Soc. **60**, 1229 (1938).
[7] E. R. Andrew, J. Chem. Phys. **18**, 607 (1950).
[8] R. W. Crowe and C. P. Smyth, J. Am. Chem. Soc. **73**, 5401 (1951).

decyl palmitate, *n*-dodecyl stearate, *n*-tetradecyl stearate, *n*-octadecyl stearate, and *n*-octadecy acetate. The methods of preparation, purification, and measurement of dielectric properties have been described in an earlier publication.[8] Approximately eight grams of sample were required to fill the measuring cell. The measurements were made for the most part at five kilocycles, and in some cases at a lower frequency to insure that the *static* dielectric constant was always obtained. Dielectric relaxation phenomena will not be considered here. In order to make the picture more complete, data taken from the literature for ethyl stearate[6] ($C_{17}H_{35}COOC_2H_5$) and ethyl behenate[5] ($C_{21}H_{43}COOC_2H_5$) have been included in the discussion.

III. DISCUSSION

Dielectric evidence for hindered molecular rotation or rotational disorder of polar molecules in the crystal lattice consists in the solid having a dielectric constant

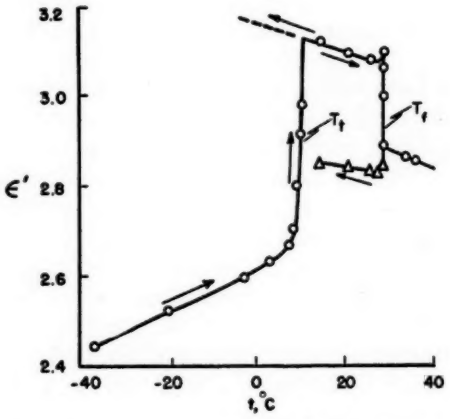

FIG. 3. Temperature dependence of the dielectric constant of *n*-decyl palmitate after freezing times of one-half hour ○ and two hours Δ.

similar to that of the liquid, i.e., one considerably larger than n^2, the square of the refractive index. This effect should not be confused with subtransitional dielectric phenomena, which often cause the dielectric constant to be slightly above n^2. Normally, molecules containing 20 or more carbon atoms in the chain show evidence of molecular rotation between the freezing point and a first-order rotational transition point. In the shorter molecules, the rotational transitions are normally monotropic because of an irreversible transformation to a third crystalline form with a higher melting point.[3] Above 24 carbon atoms, however, the transitions are completely reversible and the higher melting form usually can be realized only by crystallization from solvent.

Contrary to expectation, certain of the esters showed little or no evidence of rotational disorder in the solid state even though the chain length was much longer than is usually necessary to induce rotation (Fig. 6), while closely related members of the series showed the

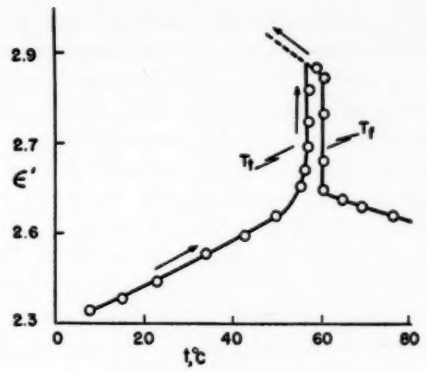

FIG. 4. Temperature dependence of the dielectric constant of *n*-octadecyl stearate. Little dependence upon rate of freezing.

expected behavior (Figs. 2–5). Furthermore, the absolute values of the dielectric constants of the rotator phases of the latter depended strongly and uniquely upon the rate of solidification. We wish to advance the following hypothesis to explain these phenomena.

It is believed that the long molecules may arrange themselves in a more or less ordered or disordered array in the crystal lattice, depending upon the rate of solidification. A simplified picture of this type of behavior is shown in Fig. 1.

A. Longitudinal Disorder and Rate of Solidification

Whenever, in the present investigation, rotational disorder was evident in the solid esters, the dielectric constants were found to be dependent upon rate of solidification, higher values being obtained after rapid freezing as shown in Figs. 2, 3, and 5. Once the samples

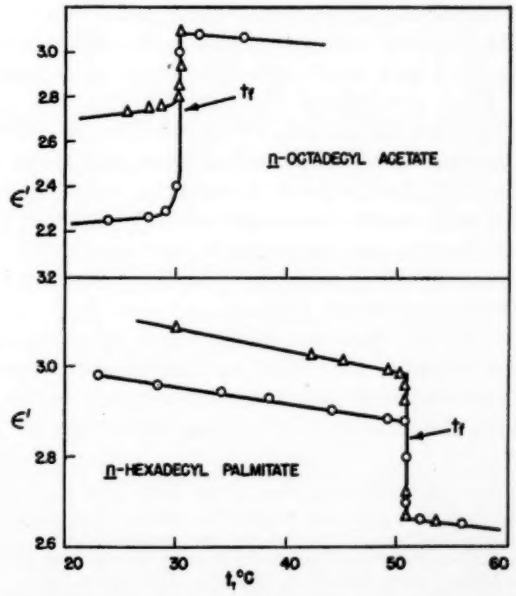

FIG. 5. Variation of the dielectric constants of *n*-octadecyl acetate and *n*-hexadecyl palmitate with decreasing temperature after freezing times of one-half hour Δ and two hours ○.

were frozen, their dielectric constants assumed time-independent values for any given temperature below the freezing point.* If the longitudinal disordering of chains does exist in these compounds, it is obvious that the degree of disorder will be promoted by rapid freezing. It is also logical that the dipoles do not form a continuous plane in the disordered state as they do in the ordered, providing the polar group is not in the center of the molecule. It has been found that pure symmetrical ketones, in which longitudinal disorder is impossible, do not show rotational disorder in the solid.[9,10] This would lead us to expect that hindered molecular rotation would be difficult in the ordered state of esters because of similar steric or dipole interaction effects. The dielectric constants of the longitudinally ordered esters should therefore be comparable to those of symmetrical ketones. In a region of longitudinal disorder, however, polar groups in adjacent chains may be sufficiently separated from one another that their interaction is no longer so important and the chains may rotate. Variations in the degree of longitudinal disorder that can be frozen into the samples can thus result in corresponding variations in orientation polarization as has been observed. *An important characteristic of longitudinal disorder is that, once frozen in, it remains unchanged until the sample is remelted.*

It can be seen in Figs. 2, 3, and 5 that the dielectric constant and thus the degree of longitudinal disorder increases not only with increase in freezing rate, but also with increase in total chain length for a given freezing rate. An extreme example of this behavior is illustrated in Fig. 5. The relatively short *n*-octadecyl acetate exhibited a dielectric constant near n^2 after gradual solidification, while even rapid freezing yielded a value far below that of the liquid. The much longer *n*-hexadecyl palmitate, on the other hand, invariably yielded a solid dielectric constant significantly above that of the liquid,† with much less dependence upon freezing rate. With *n*-octadecyl stearate (Fig. 4), the chain length was apparently long enough that nearly complete longitudinal disorder was realized when the sample was solidified gradually. Such a trend is to be expected since a more severe rearrangement is undoubtedly required for very long molecules to form an ordered configuration in going from the disordered liquid to the longitudinally ordered solid.

Contrary to what one might expect from the foregoing statements concerning the unsymmetrical esters, it has been reported that unsymmetrical ketones do not rotate in the solid state.[10] The possible reason for this is that molecules of sufficient chain length have not been investigated with the techniques employed here, i.e., variation in freezing rate.

Buckingham[5] concluded from a dielectric investigation of ethyl behenate that variations in dielectric constant with rate of solidification were the result of variations in the manner in which the crystallites aligned themselves between the plates of the measuring condenser. Although such behavior could lead to differences in the value of the dielectric constant because of the anisotropic nature of the crystals, it seems unlikely that such slight variations in solidification rate could have such a profound effect upon crystal alignment. Further evidence against Buckingham's hypothesis will be mentioned later.

B. Rotational Transitions in Longitudinally Disordered Phases of Esters

The rotational transitions in the long-chain esters were, in some cases, difficult to find because of the tendency of their rotationally disordered phases to super-cool. The rotator phase of *n*-dodecyl stearate could be super-cooled as much as 17° before the transition took place, while the transition in *n*-decyl palmitate could be found only on warming. Because of this uncertainty, transition temperatures are reported only as observed during warming. In only two members of the series, *n*-octadecyl acetate and *n*-hexadecyl plamitate, was it impossible with the techniques employed to locate the transition temperature. Since *n*-dodecyl stearate was examined more completely in the region of its transition point than the other esters in the present work, its behavior will be used as an example in the following discussion.

n-Dodecyl stearate exhibited a first-order and reversible rotational transition (Fig. 2) similar in nature to those found in long-chain bromides,[4] alcohols,[2] and paraffins.[1,4] The temperature of this transition was found, however, to shift to lower values with increase in degree of longitudinal disorder, but remained sharp. Such a shift cannot be accounted for by Buckingham's conclusion. Apparently, almost any degree of longitudinal disorder may be frozen into a sample, and the rotational transition temperature then depends uniquely on the degree of this disorder.

The shift in transition temperature T_t with degree of longitudinal disorder may be understood in terms of a recent treatment[4] of hindered molecular rotation in long-chain compounds, in which the potential energy difference V_0 associated with rotation is assumed to be as shown in Fig. 7(b). A consequence of this treatment is that T_t is proportional to V_0.

If longitudinal disorder is present, the average value of V_0 should be different than that observed for the ordered state. Let $V_0(\sigma)$ be the value of V_0 averaged over a lattice whose long-range longitudinal order is

* In some of the shorter alcohols,[2] different rates of freezing led to different dielectric constants in the solid state, but the dielectric data were time-dependent. The effects in alcohols were due to an irreversible vertical-tilted transformation in the rotator phase. Such a transformation does not take place in long esters.

[9] A. Müller, Proc. Roy. Soc. (London) **A158**, 403 (1937).

[10] V. Daniel and K. H. Stark, Trans. Faraday Soc. **47**, 149 (1951).

† The increase in dielectric constant at the freezing point is due to the normal increase in density accompanying solidification.

TABLE I.

Ester Name	Formula	Chain length (m_1+m_2+1)	Symmetry (m_1-m_2)	Rotation	T_f	T_t
(1) Ethyl behenate	$C_{21}H_{43}COOC_2H_5$	25	18	yes	47.8	43
(2) *n*-Octadecyl acetate	$CH_3COOC_{18}H_{37}$	21	18	yes	30.1	?
(3) Ethyl stearate	$C_{17}H_{35}COOC_2H_5$	21	14	yes	30.5	23.6
(4) *n*-Decyl palmitate	$C_{15}H_{31}COOC_{10}H_{21}$	27	4	yes	29.0	10
(5) *n*-Dodecyl stearate	$C_{17}H_{35}COOC_{12}H_{25}$	31	4	yes	42.0	23
(6) *n*-Hexadecyl palmitate	$C_{15}H_{31}COOC_{16}H_{33}$	33 } Type *A*	2	yes	51.0	?
(7) *n*-Octadecyl stearate	$C_{17}H_{35}COOC_{18}H_{37}$	37 } Type *A*	2	yes	60.0	57
(8) *n*-Dodecyl palmitate	$C_{15}H_{31}COOC_{12}H_{25}$	29 } Type *B*	2	no	38.5	None
(9) *n*-Tetradecyl stearate	$C_{17}H_{35}COOC_{14}H_{29}$	33 } Type *B*	2	no	50.1	None
(10) *n*-Tetradecyl palmitate	$C_{15}H_{31}COOC_{14}H_{29}$	31	0	no	47.0	None

specified by an order parameter σ,

$$\sigma=(n_\alpha-n_\beta)/(n_\alpha+n_\beta), \quad 0\leqslant\sigma\leqslant 1. \tag{1}$$

Here n_α is the number of molecules whose long axes are oriented in a specified direction, and n_β is the number oriented in the opposite direction (see Fig. 1).

It may then be shown that (see Appendix I)

$$V_0(\sigma)=V_0(1)-(1-\sigma^2)\Delta V: \quad \Delta V=V_0(1)-V_0(0). \tag{2}$$

In the present application, ΔV is positive‡ because of the interactions of carbonyl groups of neighboring pairs of α-type or β-type molecules. Therefore, the transition temperature is lowered by disordering according to the relation,

$$T_t(\sigma)\propto V_0(1)-(1-\sigma^2)\Delta V. \tag{3}$$

If ΔV is large enough, one may observe a transition in a disordered phase of a substance whose ordered phase possesses only a virtual transition above its ordinary melting point.

If a sample were cooled at an extremely nonuniform rate, it should be possible to obtain microphases with rather wide fluctuations in σ. This would lead to variations in T_t which would broaden the transition points. No such experiments are at hand.

It is very curious that, in certain of these esters, one can permanently freeze in practically any desired degree of longitudinal order (σ), and that this in turn affects the first-order transition temperature associated with a cooperative change in *rotational* order.

C. Calculation of the Dielectric Constant of *n*-Dodecyl Stearate

In order to estimate the static dielectric constant ϵ_0 of long-chain compounds it is necessary to know μ, the dipole moment perpendicular to the chain axis, and the degree of rotational order x. The latter is essentially the fraction of molecules frozen in deep wells (Fig. 7(b)) as opposed to those of higher energy. In the present case μ may be estimated by assuming that the keto and ether group moments are opposed. For long ketones $\mu=2.75$, and for ethers $\mu=1.15$, so that a

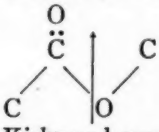

C moment should be roughly 1.60. The Kirkwood equation[11] is

$$4\pi N\mu^2 g/9kT=\frac{M}{d}\cdot\frac{(\epsilon-n^2)(2\epsilon+n^2)}{\epsilon(n^2+2)^2}, \tag{4}$$

where the constants have their usual significance. In the present case it seems reasonable to assume that $g=1-x^2$ as was shown to be the case for the *n*-bromides.[4] Details of the calculation of x from T have been given previously.[4] For *n*-dodecyl stearate $T_t=296°$K, $M=428$, $d=0.97$ and $\epsilon_\infty\cong n^2\cong 2.30$. In the rotationally melted phase which has virtually no rotational order, $g\cong 1$ and the calculated dielectric constant is 3.11. This is slightly higher than the observed value of 3.02 for the rapidly frozen sample. The calculated value just below T_t where $x\cong 0.85$ is 2.53 in good agreement with the observed value of 2.50. In the latter calculation Ω, the degeneracy of the upper states, was assumed to be 12 as was found for other long-chain molecules.

D. Longitudinal Disorder and Molecular Symmetry

In Table I are summarized the significant structural, symmetry, and orientational disorder data for the esters under consideration. In this table, m_1 and m_2 represent the chain length on either side of the polar carbonyl group.§ m_1 always refers to the longer of the two. As can be seen, rotation does not disappear until the carbonyl group approaches the center of the chain. If $m_1-m_2=0$, ΔV is certainly very small, while if $m_1-m_2=2$, it may still be so small that $T_t(\sigma)$ is above the ordinary melting point for all σ (Fig. 6).

However, it may be seen from Table I that certain compounds for which $m_1-m_2=2$ do show the rotational transition for at least some values of σ. This may be because of the following circumstance. In compounds

‡ It should be noted that ΔV will always be small since the interactions of the carbonyl groups furnish only a small part of the total barrier to rotation. Large changes in T_t will therefore never be expected.

[11] J. G. Kirkwood, J. Chem. Phys. **7**, 911 (1939); H. Fröhlich, *Theory of Dielectrics*, Oxford University Press, London (1949), p. 52.

§ The total chain length m, counting the carbonyl group, is m_1+m_2+1.

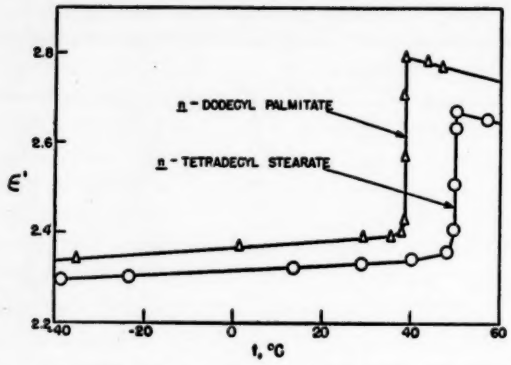

FIG. 6. Temperature dependence of the dielectric constant of *n*-dodecyl palmitate Δ and *n*-tetradecyl stearate ○. No dependence upon rate of freezing.

of type *A*, e.g., *n*-octadecyl stearate, the chain oxygen atom of the upper chain lies between the two carbonyl dipoles and should show a small dipole repulsion effect between it and the lower carbonyl (Fig. 7a). This would serve to lower V_0, and therefore T_t in compounds of type *A*. No such repulsion occurs in type *B* where the chain oxygens do not intervene.

E. An Alternative Model of Longitudinal Disorder

In the foregoing discussion it has been assumed that the dipoles in the longitudinally disordered phase in esters are staggered while the end groups remain in a plane (Fig. 1). A closely related but different picture of longitudinal disorder may be obtained by allowing the dipoles to remain in a plane while the end groups are staggered (not shown). In this new scheme the shift of T_t with σ could be ascribed to the difference in end-group forces instead of differences in polar forces. It is not obvious that the end-group forces will be very different when the end groups are staggered, but it is clear that dipole-dipole forces will diminish as $\sim\mu^2/(m_1-m_2)^3$ for the model where longitudinal disorder is as shown on Fig. 1. If the dipoles were always in the same plane, it would be more difficult to explain the variation of the dielectric constant with cooling rate. Neither of the above arguments permits rejection of the alternative model of longitudinal disorder, however. A somewhat better indication that the model of the disordered state shown in Fig. 1 is the better one may be had by consideration of the esters where $m_1-m_2=2$. If the alternative model of reversal of chains were employed, it would be found that both the dipolar and end-group forces were very nearly identical for all four cases, so that the observed differences in dielectric behavior could not be explained.¶ There is no reason to believe that the alternative arrangement may not appear in other compounds, however.

¶ A. Bondi and L. B. Scott [Nature **167**, 486 (1951)] have found that certain pairs of long-chain esters form a continuous series of solid solutions, and interpret this to mean the dipoles do not form a single sheet. This is in accord with the picture of disorder presented in this paper.

A direct determination of the structure of the disordered phases in long-chain compounds by x-ray methods aimed at differentiating the two models of the disordered state would probably be difficult unless longitudinal disorder could be found in a system where the polar group had a high atomic weight.

APPENDIX I

Calculation of the Average Value of V_0 as a Function of the Order Parameter σ

Let V_1 = the value of V_0 for a chain which is completely surrounded by chains longitudinally oriented in the same direction, *viz.*,

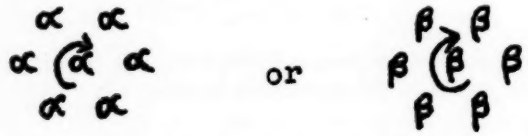

Let V_2 = the value of V_0 for a chain completely surrounded by chains longitudinally oriented in the opposite direction, *viz.*,

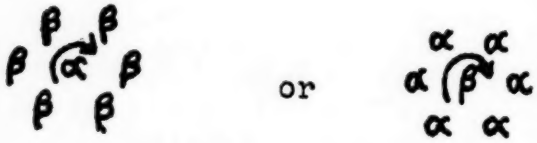

The average value of V_0 experienced by an α-type molecule in the disordered lattice is

$$V_{0\alpha}=(n_\alpha V_1/N)+(n_\beta V_2/N) \quad (1)$$

and for a β-type molecule,

$$V_{0\beta}=(n_\beta V_1/N)+(n_\alpha V_2/N). \quad (2)$$

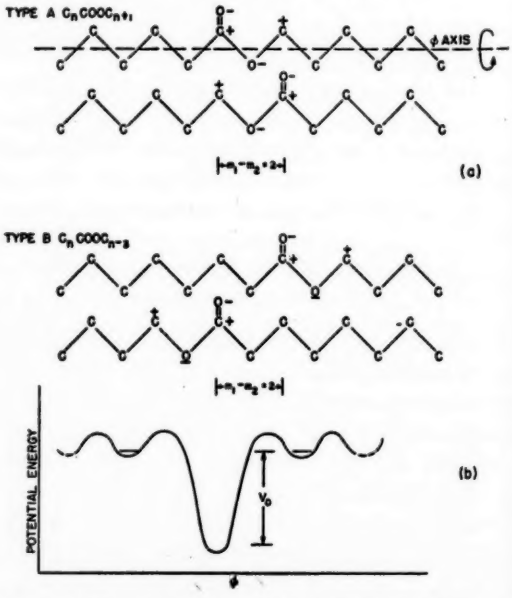

FIG. 7. (a) The two types of longitudinal disorder in esters where $m_1-m_2=2$. (b) Assumed potential energy function for rotation about ϕ axis.

If V_0 is then averaged over the entire lattice, it is found that

$$V_0 = V_1 - [2n_\alpha n_\beta/N^2](V_1 - V_2). \quad (3)$$

The order parameter is defined as

$$\sigma = (n_\alpha - n_\beta)/N, \quad (4)$$

which, when substituted in Eq. (3), gives

$$V_0(\sigma) = V_1 - (1-\sigma^2)(V_1/2 - V_2/2). \quad (5)$$

Although V_1 is the energy difference of a molecule in the ordered state, $V_0(1)$, it must be remarked that complete disorder results in a molecule having on the average three α and three β nearest neighbors. For this disordered state, then, $V_0(0) = \frac{1}{2}(V_1 + V_2)$. Defining ΔV as $V_0(1) - V_0(0)$, Eq. (5) becomes

$$V_0(\sigma) = V_0(1) - (1-\sigma^2)\Delta V, \quad (6)$$

which is the required form.

THE JOURNAL OF CHEMICAL PHYSICS VOLUME 20, NUMBER 4 APRIL, 1952

The Molecular Structure of 1,2-Dichloropropane

WILLIAM W. WOOD* AND VERNER SCHOMAKER
Gates and Crellin Laboratories of Chemistry, California Institute of Technology, Pasadena, California†

(Received July 16, 1951)

Under the assumption of $V(\varphi) = V_0[1-\cos(\varphi-\varphi_0)]/2$ for the potential hindering internal rotation, visual interpretation of the electron-diffraction pattern leads to the results (best values and estimated limits of error): C−Cl, 1.79±0.035A; C···Cl, 2.715±0.025A; C−C, 1.56A (range: 1.49–1.60A); ∠C−C−Cl, 108±4°; $|\varphi_0| \leqslant 30°$ (i.e., essentially *trans* in the chlorine atoms), with a small positive value of φ_0 (increasing $CH_3\cdots Cl_{primary}$) most likely; $V_0 \geqslant 4$ kcal/mole. The best value for V_0 ranges from 10 kcal/mole for $\varphi_0 = 0°$ to 30–40 kcal/mole for $\varphi_0 = 25°$. The diffraction pattern is almost indifferently compatible with fractions ranging up to 50 percent of a *skew*-isomer with $\varphi_0 \sim 120°$ and a sufficiently low value of V_0, but consideration of dipole moment data provides some further evidence on its structure while showing the fraction present to be about 20 percent with an upper limit of about 30 percent.

THE present investigation of propylene chloride was undertaken primarily to obtain structural information needed for an application[1] of Kirkwood's theory of optical activity,[2] which in this case predicts a strong dependence of the optical activity upon internal rotation quite different from that of the conspicuous aspects of the diffraction pattern. Our electron-diffraction data alone were accordingly inadequate, but dipole moment data were fortunately made available which made possible a fairly complete structure determination.

In an x-ray diffraction study of the gas Berger found satisfactory agreement[3] on the assumption of reasonable values for the bond distances, tetrahedral bond angles, and the potential function $V(\varphi) = V_0(1-\cos\varphi)/2$, with $V_0 = 0.88$ kcal/mole, for the dihedral angle of displacement φ of the $Cl-C_1-C_2$ and C_1-C_2-Cl planes from the *trans*-orientation. The structure of the related molecule, 1,2-dibromopropane, has been investigated by electron diffraction by Schomaker and Stevenson,[4] who reported normal values for the bond distances and bond angles and a root-mean-square torsional vibration of ±20° around the *trans*-position, again with no indication of the possible occurrence of other internal-rotation isomers.

THE ELECTRON DIFFRACTION INVESTIGATION

Experimental

Two sets of photographs were prepared, the first at the 11-cm camera distance from some of the commercial Paragon product that had been distilled through a 40-cm column packed with glass helices (n_D^{25} 1.4367, b.p. on redistillation through a similar 60-cm column 95.6–96.4°) and the second, partly at 11 cm and partly at 20 cm, from an independent sample prepared from propylene glycol by Dr. H. K. Garner (b.p. 96.2–96.5°, n_D^{25} 1.4368; see lit.[5]: b.p. 96.2°, n_D^{25} 1.43638), in the apparatus described by Brockway.[6] For the photographs actually used the sample temperature was about 25°.

The Photographs

Curve V_1 was drawn from the appearance and measurements of the photographs of the first set, the shape and height of the central maximum being guessed from past experience, while V_2, which was drawn after

* Present address: Los Alamos Scientific Laboratories, Los Alamos, New Mexico.
† Contribution No. 1595.
[1] Wood, Fickett, and Kirkwood, J. Chem. Phys. **20**, 561 (1951).
[2] J. G. Kirkwood, J. Chem. Phys. **5**, 479 (1937).
[3] H. Berger, Physik. Z. **38**, 370 (1937). Berger's data extended to only $q = (40/\lambda)\sin\vartheta/2 = 22$, however.
[4] V. Schomaker and D. P. Stevenson, J. Am. Chem. Soc. **62**, 2423 (1940).
[5] R. R. Dreisbach and R. A. Martin, Ind. Eng. Chem. **41**, 2875 (1949).
[6] L. O. Brockway, Revs. Modern Phys. **8**, 231 (1936). The wavelength, about 0.06A, was determined from ZnO photographs (C. S. Lu and E. W. Malmberg, Rev. Sci. Instr. **14**, 271 (1943): $a = 3.2492$A, $c = 5.20353$A). Corrections were made for film expansion.

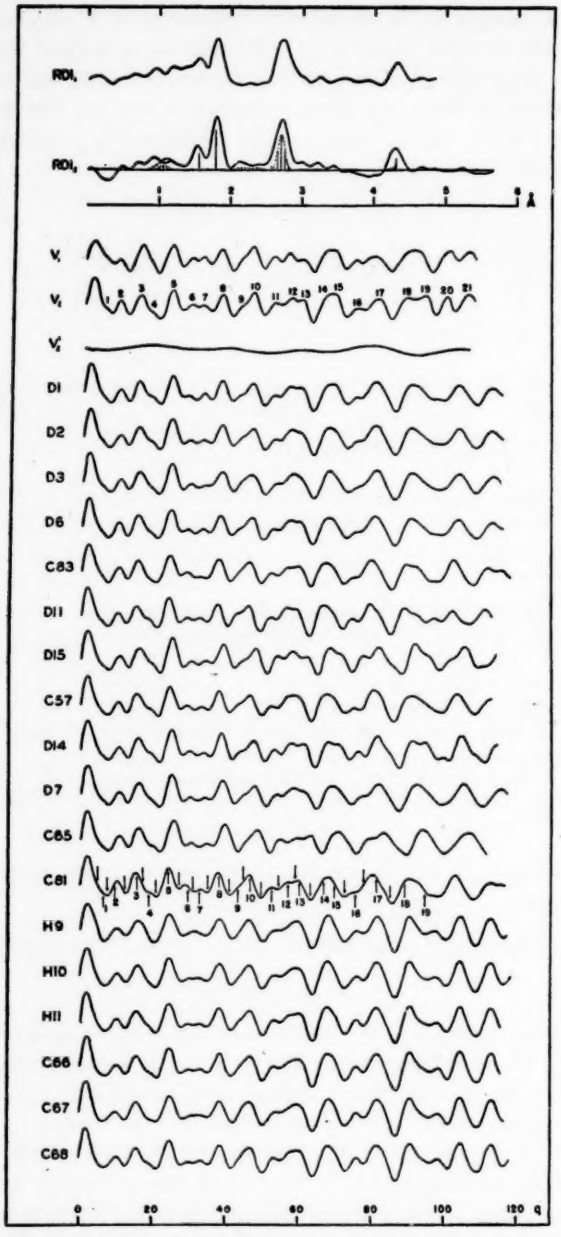

FIG. 1. Radial distribution and visual curves. Intensity curves for models defined in Table I and the text.

comparisons with a number of theoretical curves had shown persistent discrepancies suggestive of errors in V_1, incorporates changes based upon the second set of photographs and observations by Dr. Kenneth Hedberg, who had no knowledge of the nature of the discrepancies. (See Fig. 1 and Table I.) (The second set shows no significant differences from the first but is much more distinct, especially at the triplet 11–12–13.) We have used both curves, emphasizing V_2, however, where the differences between them[7] are significant.

[7] In V_2 the depth of min 2 *vs* min 3, the height of max 2 *vs* max 3, the position of shelf 4 on max 3, and the position of shelf 9 on max 10 reflect reinterpretations in agreement with Dr. Hedberg. The depth of min 6 *vs* min 8 is difficult to determine and represents an average of the observers' differing opinions. The relative heights of maxima 11, 12, and 13, and the shape and positions of maxima 17 and 18–19 and minima 18, 20, and 21 show changes from V_1 based on the second set of pictures. (Beyond $q \approx 90$ both sets are unclear and the film edge is close enough to be bothersome.)

Radial Distribution Curves

Curves RDI_1 and RDI_2 were calculated[8,9] respectively from V_1 and V_2 according to the equation

$$rD(r) = \sum_{q=1,\,2,\,\cdots}^{q_{max}} V(q) \exp(-aq^2) \sin \pi qr/10, \quad (1)$$

with $q = 10s/\pi = (40/\lambda) \sin\vartheta/2$, ϑ the scattering angle, and a chosen to make the convergence factor $\exp(-aq^2)$ equal to 0.10 at $q = 100$. The interpretation of the main peaks is clear in terms of a molecule approximately *trans* with respect to the chlorine atoms: 4.32A in RDI_1 and 4.30A in RDI_2, Cl···Cl (somewhat broad); 2.73 and 2.72, C···Cl (width indicates temperature factor with $a_{Cl\cdots Cl} = 10^{-4}$ or a symmetrical splitting of the three nonequivalent C···Cl distances, with separations of about 0.05); 1.82 and 1.81, C—Cl; and 1.56 and 1.53, C—C (poorly resolved). The more important remaining terms, some probably negligible and all weak, are the following: 2.16 and 2.45, C···H and Cl···H pairs having a common ligand (moderately heavy a); 2.52, C···C; 2.8–3.5 (if $|\varphi| < 30°$), rotation dependent C···Cl (large a); and 1.09, C—H. Agreement for these is fair, at least with RDI_2, but there are evidently errors, especially at low r and extending into the C—H peak.[10]

TABLE I. Models of propylene chloride represented in Fig. 1.

Model[a]	C—Cl, A	C···Cl, A[b]	V_φ, kcal/mole	φ_0, deg	$a_{Cl\cdots Cl}$[b]	$a_{Cl\cdots Cl}$
*D*1	1.79	2.70	30	10	0.00010	0.00010
*D*2	1.79	2.70	30	20	0.00010	0.00010
*D*3	1.79	2.70	30	30	0.00010	0.00010
*D*6	1.79	2.70	10	0	0.00010	0.00010
*C*83	1.80	2.73	4	0	0.00010	0
*D*11	1.82	2.74	60	25	0.00010	0
*D*15	1.76	2.64	60	20	0.00010	0
*C*57	1.79	2.72	30	20	0.00010	0.00010
*D*14	1.76	2.68	60	15	0.00010	0
*D*7	1.76	2.66	30	20	0.00010	0.00010
*C*65	1.73	2.60	30	15	0.00010	0.00010
*C*81[a]	1.80	2.73	10	0	0.00010	0.00010
*H*9[c]	1.79	2.70	30	20	0	0
*H*10[c]	1.79	2.70	30	20	0	0
*H*11[c]	1.79	2.70	30	20	0	0
*C*66[c]	1.79	2.70	···	···	0	0
*C*67[c]	1.79	2.70	···	···	0	0
*C*68[c]	1.79	2.70	···	···	0	0

[a] C—C, 1.54A and C—H, 1.09A, except that *C*81 has C—C, 1.57A and C—H, 1.06A.
[b] The three rotation-independent terms.
[c] Mixtures of *skew* and *trans:* see text.

[8] R. Spurr and V. Schomaker, J. Am. Chem. Soc. **64**, 2693 (1942).
[9] Shaffer, Schomaker, and Pauling, J. Chem. Phys. **14**, 648, 659 (1946).
[10] Not unusual for complicated molecules and ordinarily corresponding to inconsequential low frequency errors in the visual curve. It here became necessary, however, to attempt direct comparisons of the intensities of rather widely separated features of the pattern and in the comparisons to allow for these errors which had been made obvious by the radial distribution curves.

Altogether, the indication was that except for these errors the diffraction pattern could be accounted for with a model having conventional distances and angles with the possible exception of C−Cl, which might be 0.04A longer than usual, and only a small amplitude of libration about the *trans*-orientation $\varphi=0$.[11]

Theoretical Intensity Curves

As the appropriate simplified intensity function we have taken

$$I(q)=\{\sum_i (Z-f)_i^2\}^{-1}\sum_{ij}' (Z-f)_i(Z-f)_j r_{ij}^{-1} \times\exp(-a_{ij}q^2)\sin\pi r_{ij}q/10 \quad (2)$$

with $a_{ij}=\frac{1}{2}(\pi/10)^2\langle\delta r_{ij}^2\rangle_{Av}$, omitting the form factors f_i, however (trial calculations showed them to be unimportant in this case), and, whenever necessary for the internal-rotation dependent terms, replacing the factors $r_{ij}^{-1}\exp(-a_{ij}q^2)\sin\pi r_{ij}q/10$ by adequate explicit approximations to the integrals[9] $\int rD_{ij}'(r)\sin\pi rq/10dr$ over the distribution functions $r^2D_{ij}'(r)$ as defined by the assumed potential function and classical statistics. The effective value of Z_H was taken as 1.25. Except where otherwise stated the following special assumptions were made: all bonded C−C, bonded C−Cl, and next-to-bonded C···Cl distances respectively equal; ∠C−C−C and all bond angles involving hydrogen atoms tetrahedral; $a_{C-H}=0.00016$; $a_{C\cdots H}=a_{Cl\cdots H}=0.00030$; and all hydrogen terms except C−H and next-to-bonded X−H negligible, as was verified by test calculations.

The remaining shape parameters were taken (holding C−C constant), as (1) C−H, (2) C−Cl, (3) C···Cl, (4) the positions of the minima of the potential hindering internal rotation around the C_1-C_2 bond, (5) the shape of the potential barrier in the neighborhood of the minima,[12] and (6) the skeletal vibrational temperature factors. The number of these parameters and the complex nature of the ones most important for us prolonged and complicated the work, while making impracticable systematic investigation; we can only summarize, showing a few of the theoretical curves.

Assumption of a Single Potential Minimum

At first the potential $V(\varphi)=V_0[1-\cos(\varphi-\varphi_0)]/2$ was assumed. (*We quote V_0 in kcal/mole throughout. A positive displacement of φ, at $\varphi=0$, increases* $CH_3\cdots Cl_{primary}$.)

It was not found possible to get general agreement including maxima 11–12–13 and 18–19 without widening the C···Cl distribution about as indicated by the *RDI*'s. For most of the later curves, therefore, a temperature factor with $a_{C\cdots Cl}=10^{-4}$ was used, there being no apparent reason for the three nonequivalent distances to be significantly different, whereas considerations of the probable amplitudes of vibration seemed to justify an even greater a value.[13,14] The same considerations seemed to require a vibrational a of about 10^{-4} for Cl···Cl also. For the long C···Cl term, finally, a considerably more severe factor would be reasonable but none was used, since its effect would be small compared to the librational attenuation.

A best value of φ_0 is easily chosen if the other parameters, including V_0, are arbitrarily fixed. This is illustrated by Curves *D*1, *D*2, and *D*3; *D*1 and *D*3 we regard as unacceptable, in relative amplitude of maxima 6 and 7 particularly, whereas *D*2 is quite good. There is, however, already a strong interaction of the parameters V_0 and φ_0. This arises (1) from the increase of $|dr_{Cl\cdots Cl}/d\varphi|$ with $|\varphi|$, so that even at constant V_0 the attenuation of the Cl···Cl term increases with $|\varphi_0|$ in the way shown by the series *D*1−*D*2−*D*3, and (2) directly from the variation of

The expected C−H peak was joined onto RDI_2 as shown by the dashed line. The difference between RDI_2 so modified and RDI_2 itself was then Fourier-inverted, adjusted to allow for the use of a convergence factor in the inversion, and taken as a correction (V_2') to be added to V_2: the hump at $q\approx18$ points to an unimportant mistake but the wave with node at $q\approx85$ is interesting, since the correction serves to raise max 17 above the line of max 14–15 and max 18–19, as is required by all otherwise acceptable theoretical intensity curves. Even though all observers were here in agreement, therefore, V_2 must be in error in this respect.

[11] For asymmetric components of the distribution function the relation $rD(r)\propto\int_{-\infty}^{\infty} r'D'(r')\{\exp[-(r-r')^2/4a]+\exp[-(r+r')^2/4a]\}dr'$ (with $rD(r)\propto\int_0^{s_{max}} I(s)\exp(-as^2)\sin rsds$ and $rD'(r)\propto\int_0^{\infty} I(s)\sin rsds$) between the true distribution function $r^2D'(r)$ and the one, $r^2D(r)$, corresponding to Eq. (1) is rather complex. In particular, the positions of the maxima do not coincide: for the *trans* Cl···Cl distance in propylene chloride, for example, reasonable amplitudes of libration could cause differences of 0.05A or more. This circumstance, the uncertainty in the pertinent C−C distance, and the fact that the maximum of the angular distribution does not necessarily occur at the angle corresponding to the maximum of the distance distribution prevent an immediate reliable determination of φ.

In the earlier study of propylene bromide (see reference 4) neither these circumstances nor, in the calculation of theoretical curves, even the variation of Br···Br with the amplitude of φ, at $\bar{\varphi}=0$, were considered. Since the C−Br, C···Br, and Br···Br terms predominate in this molecule, the situation may be interpreted merely as indicating somewhat different values of C−C and ∠C−C−Br than were reported.

[12] The temperature of the vapor was assumed to be 300°K but was not actually known and may possibly have been significantly lower.

[13] Extension of the normal coordinate analysis of ethylene chloride (S. Mizushima and Y. Morino, Sci. Papers I. P. C. R. (Tokyo) **26**, 1 (1934); Bull. Chem. Soc. Japan **13**, 189 (1938); we used the same force constants and frequencies, and neglected the motions of the hydrogen atoms as in the first paper) leads to the following mean-square displacements: C−Cl, 0.0030A²; C−C, 0.0026A²; C···Cl, 0.0063A²; Cl···Cl, 0.0070A². Referred to $a_{C-C}=0$, the resulting a's are: for C−Cl, ∼0; C···Cl, 0.00018; Cl···Cl, 0.00020. Also, the frequencies and diagrams of the normal modes given by P. C. Cross and J. H. Van Vleck (J. Chem. Phys. **1**, 350 (1933)) for the skeletal motions of ethyl chloride lead to the values, roughly estimated, $a_{C-Cl}\approx0$ and $a_{C\cdots Cl}\approx0.00027$, again referred to $a_{C-C}=0$. These estimates are uncertain in that the valence-force potential functions assumed are not necessarily correct, but they at least suggest the assumption of considerable vibrational amplitudes for C···Cl and Cl···Cl in propylene chloride.

[14] It has been usual to assume a rigid heavy-atom skeleton (excepting internal rotations) unless large amplitudes of vibration were obviously to be expected or unless it was found impossible or seemed unreasonable (as for C···Cl here) to obtain a fit otherwise. But the possibility of getting agreement with a rigid skeleton does not guarantee the results so obtained—compare the possible conclusion for propylene chloride that the three C···Cl distances were significantly split. Moreover, the simultaneous contributions of vibrations and libration can become important in the same sense, particularly at *trans*, where the resulting attenuations may well be comparable. To be sure, the finer effects do differ, notably the variation with q of the effective value of r in the case of libration.

The value 0.004 reported for $a_{Br\cdots Br}$ (s scale) in reference 4 corresponds to a torsional amplitude greater than the reported ±20°, unless allowance, not mentioned in the article, is made for a vibrational contribution.

TABLE II. Comparison of observed and calculated q values Model $C81$.

Max	Min	q_0[a]	q_c/q_0	Max	Min	q_0[a]	q_c/q_0
	1	4.6	(0.913)		12	54.8	0.994
1		6.2	(0.935)	12		57.5	0.995
	2	7.4	(1.000)		13	59.4	0.988
2		9.5	(1.063)	13		60.6	0.998
	3	12.2	(1.033)		14	63.6	1.003
3		15.6	0.987	14		67.3	0.992
	4	17.2	(1.058)		15	68.8	0.993
4		19.0	(1.042)	15		70.2	0.994
	5	20.9	1.005		16	73.0	1.000
5		24.3	1.004	16		76.0	0.993
	6	27.3	1.004		17	78.3	0.983
6		29.9	0.970	17		81.8	0.980
	7	31.2	1.013		18	85.6	1.008
7		33.0	1.012	18		89.6	(1.003)
	8	35.3	0.992		19	92.4	(0.990)
8		38.4	0.971	19		95.2	(0.978)
	9	41.2	1.005				
9		43.7	0.986	Average, 28 terms[b]			0.995
	10	45.1	0.989	Average deviation			0.008
10		47.0	0.998	Scale factor[c]			0.993
	11	50.0	1.000				
11		53.0	0.992				

[a] Weighted averages from both sets of photographs.
[b] Excluding unreliable values in parentheses.
[c] Corrected for change in λ from tentative value 0.0608A used for q_0 to calibration value 0.0606₁A.

$r_{Cl\cdots Cl}$ with φ and the consequent dependence of the effective value of $r_{Cl\cdots Cl}$ on both φ_0 and V_0 (as well as q[13]), so that, for example, the combination $V_0=30$, $\varphi_0=10°$ ($D1$) is unsatisfactory in a way that could be corrected by making $|\varphi_0|$ greater, whereas $V_0=10$, $\varphi_0=0°$ ($D6$) is acceptable. Curve $C83$, with $V_0=4$ and $\varphi_0=0°$, is again unacceptable, but here other parameter variations are also involved.

Further investigation indicated more generally that for $|\varphi_0|>30°$ no satisfactory curves exist, that for $|\varphi_0|\approx 20°$, $V_0=30$ is satisfactory, and that for the *trans*-position $\varphi_0=0$, $V_0\approx 10$ is required.[15] Curves $D11\cdots D65$ illustrate several combinations of C−Cl and C···Cl, each for its best φ_0 and a roughly corresponding V_0. If, as in $C65$, C−Cl is 1.73A and C···Cl is selected for shape of max 18–19, there is no φ_0 which makes satisfactory the inner features, particularly maxima 6 and 7, whereas with a longer C···Cl distance the situation is reversed: there seems to be no satisfactory choice with C−Cl this small. For C−Cl$\geq$1.82A, on the other hand, the height of max 18–19 decreases while further deviations occur, notably degeneration of the triplet into an excessively strong[16] doublet and a weak, too well separated, inside member (see $D11$) and, for C−Cl=1.85A, excessive growth of max 13 *vs* max 12. Our use of max 18–19 is illustrated by $D2$, $D11$, and $D15$ (not symmetrically doubled: component 19 too weak), $C57$ (too weak, but shape acceptable), and $D14$ (both shape and height somewhat improved).

All curves so far called acceptable have certain deficiencies associated with the height of max 10 *vs* maxima 8 and 11–12–13, the depth of min 9 *vs* minima 8 and 11, and the depth of min 11 *vs* minima 9 and 14. Dr. Hedberg agreed that the pictures seem to require max 10 to be higher, min 9 deeper, and min 11 shallower than the respective lines joining the mentioned adjacent features, but tangency of line and feature was finally deemed acceptable for each.[17] We find $C44$, $D6$, $D11$, and $D15$ barely acceptable at max 10 and $D2$, $D11$, and $C57$ unacceptable; $D2$, $D7$, $D11$, $C44$, $C57$, $D14$, and $C65$ barely acceptable or acceptable at minima 9 and 11; and $D15$ unacceptable at min 11 and doubtful at min 9. None is everywhere satisfactory; $D11$, for example, fails at max 18–19, while similar models having longer C···Cl (2.76A, say), although even better as regards max 10 and the shape of max 18–19, make the latter feature rather too weak (even on allowing the correction V_2') while showing the deterioration of the triplet. Shortening C−H to about 1.04A ameliorates the relations at max 10 but not at minima 9 and 11.

Altogether, model $C81$ has about the optimum shape. The scale determination for it (Table II) together with the range of qualitative acceptability of the intensity curves and the estimated scale uncertainty (both direct and as consequence of the uncertainty in shape) leads to the following parameter values and approximate limits of error for the single-minimum model: C−H, (1.05A);[18] C−C, 1.56A (1.49−1.60A); C−Cl, 1.79±0.035A; C···Cl, 2.715±0.025A; ∠C−C−Cl, 108±4°; and $V_0\geq 4$ (upper limit not determined)[14] and $|\varphi_0|\leq 30°$, with best values not separately determined but only related as indicated by the pairs $\varphi_0=0°$, $V_0=10$ and $\varphi_0=25°$, $V_0=30-40$. The sign of φ_0 remains somewhat uncertain: librational attenuation renders the odd C···Cl, the only pertinent term, unimportant despite its having half the weight of Cl···Cl. For the larger values of $|\varphi_0|$, however, V_0 has to be so large as to diminish this attenuation considerably (for $V_0=30$ and $\varphi_0=0°$, as would correspond roughly to the best models with $\varphi_0=\pm 20°$, the term retains a quarter of its initial amplitude at $q=35$), and positive φ_0 gives the better agreement. This is satisfactory, since the approximate equality of van der Waal's radii for methyl and chlorine suggests that the value 10° reported[19] for 1,1,2-trichloroethane might hold approximately here also.

Consideration of Other Conformations

The steric similarity of chloro and methyl groups and the analogy to trichloroethane,[19] as well as the existence of internal-rotation isomers even in ethylene chloride,[20] suggest that for propylene chloride there may be a significant population of *skew*-molecules with $\varphi_0\approx 120°$, i.e., with $-CH_3$ rather than $-Cl$ *trans* to the primary

[15] The question of an upper limit of V_0 was not investigated, because the optical activity does not depend critically on it. Discrepancies do appear for very large V_0, due to the too-long persistence of the libration-dependent terms; but this indication is unreliable, since more severe vibrational a's than were used would not be unreasonable. For the larger values of V_0 (and $|\varphi_0|$) the factor for Cl···Cl (with $a=0.00010$) tends to eliminate an otherwise bad hump on the outside of max 17, while causing a not unsatisfactory coalescence of maxima 18 and 19 into a single broad feature, but for low values of V_0 its inclusion has little effect on the curves or the optimum for the other parameters. For many of the curves it was omitted.

[16] The following doublet (14–15) appears *much* the stronger, but this may be only a visual consequence of the greater width of the triplet.

[17] Curves V_1 and V_2 would imply more stringent requirements on the relative amplitudes of *pairs* of adjacent features in this series: e.g., max 10 higher than max 8. We have been forced to discount these judgments, as is reasonable in view of the difficulty of estimating and allowing for the slope of the apparent background, and have emphasized the presumably more reliable comparisons of *triples* of adjacent features.

[18] The small weight, severe temperature factor, and evidently large corresponding error in the radial distributions justify regarding C−H as *assumed* (relative to C−C), even though it was chosen in the effort to improve max 10. Use of the more likely value 1.09A leaves the other shape parameters and the scale determination essentially unchanged.

[19] A. Turkevitch and J. Y. Beach, J. Am. Chem. Soc. **61**, 3127 (1939).

[20] W. D. Gwinn and K. S. Pitzer, J. Chem. Phys. **16**, 303 (1948).

chlorine atom.[21] Since the calculated optical activity[1] depends critically on internal rotation, being of comparable magnitude but different sign for the *trans*- and *skew*-isomers, a limiting estimate of the fraction of *skew* is essential, even though the photographs give no clear indication that any is present. For reasonable hindering potentials, we find that 25 percent of *skew* is equally acceptable with pure *trans* while 50 percent or more is unacceptable; the diffraction data do not afford a much lower limit. On the other hand, a fraction somewhere between the half-fractions $\frac{1}{10}$ and $\frac{1}{2}$ for ethylene chloride[20] and trichloroethane[21] would correspond to the plausible sequence of steric effectiveness $-H<-CH_3<-Cl$.

Sums of *skew*- and *trans*-curves in various proportions were examined, taking *D*2 without the C···Cl and Cl···Cl temperature factors for *trans*,[22] and the same basic model for *skew*, with various values V_{0s} and φ_{0s} for the constants of the assumed onefold cosinusoidal potential. For Curves *H*9, *H*10, and *H*11 the further assumption was made that V_{0s} is sufficiently low to wash out completely the contribution of the rotation-dependent *skew*-terms, as is reasonable for Cl···Cl, which now varies rapidly with φ, and not too unsatisfactory for C···Cl, which, although at about its maximum distance in any *skew*-model, has low weight. Curve *H*9 (75 percent *skew*) is out of the question, *H*10 (50 percent *skew*) is doubtful, and *H*11 (25 percent *skew*) is as good as *D*2, i.e., as 100 percent *trans*. The results obtained on including specific *skew*-terms are illustrated by the last three curves. Curve 66 (25 percent *skew*, $V_{0s}=30$, $\varphi_{0s}=120°$) is similar to *H*11 (justifying the preceding special assumption) and acceptable, *C*67 (50 percent *skew*, $V_{0s}=30$, $\varphi_{0s}=120°$) is at least as poor as *H*10, and *C*68 (25 percent *skew*, $V_{0s}=80$, $\varphi_{0s}=120°$) is satisfactory for moderate q[22] except possibly in showing max 7 higher than max 6 (see V_2), a difficulty improvable either by slightly increasing φ_{0t} or (as would be structurally reasonable) decreasing φ_{0s}. Other variations of the *skew*-structure were tried, also after the *trans*-parameters had been frozen, but none were successful. More nearly quantitative intensity data than can be got by the visual method would no doubt better define the diffuse Cl···Cl term and abundance of the *skew*-isomer as well as the diffuse C···Cl term of the *trans*.

THE DIPOLE MOMENT BEHAVIOR

For the interpretation of the moment values (Table III), from the work of Oriani and Smyth,[23] we have used the expression $\mu(\varphi)=2\mu_\perp \sin\varphi/2 = 2\mu_0 \sin\angle C-C-Cl \sin\varphi/2$, assuming the molecular dipole moment $\mu(\varphi)$ to be the sum of $-CH_2Cl$ and $-CH(CH_3)Cl$ group moments of equal magnitude μ_0 which lie along the respective C−Cl lines at equal angles to the connecting C−C bond, all independent of the angle of internal rotation φ.[24] Two sets of calculations were made, the first on the further assumption that effectively there is simply an equilibrium between *trans*- and *skew*-species, each with temperature-independent characteristics, and the second with the explicit use of various possible forms of the hindering potential.

In the first case the equation

$$\langle\mu^2(T)\rangle_{Av}=\{\mu_t^2+\mu_s^2 a\exp(-\Delta E/RT)\}/\{1+a\exp(-\Delta E/RT)\} \quad (3)$$

is an appropriate approximation, μ_t and μ_s being the moments of *trans* and *skew*, a the ratio of partition functions referred to the separate origins $\bar{E}_s$ and $\bar{E}_t$ (or, roughly, the ratio of torsional vibration periods), and ΔE the difference $\bar{E}_s-\bar{E}_t$ in average energy.[25] Least-squares fits to this equation in the logarithmic form (Mizushima and Morino)[13]

$$\ln\{\mu_s^2-\mu^2(T)\}-\ln\{\mu^2(T)-\mu_t^2\}=-\ln a+\Delta E/RT \quad (4)$$

with plausible assumed values of φ_t, φ_s, and $\mu_\perp$ are all good, and about equally good, as perhaps can be seen from the small, relatively nearly constant standard errors (estimated from the residuals) of the derived values of a and ΔE (Table IV).[26] Nevertheless, the insensitivity of ΔE and the rapid variation of a with $\mu_\perp$ and φ_s, i.e., with the moment of the *skew*-molecule, taken together with inferences from related molecules, do limit φ_s and the fraction of *skew* at room temperature fairly well: $\mu_\perp$ will surely be close to the 1.59*D* found by Gwinn and Pitzer for ethylene chloride[20] or some-

TABLE III. Dipole moment of propylene chloride according to two treatments of the atom polarization.

T, °K	$\mu\times10^{18}$, e.s.u.	
344.7	1.46[a]	1.40[b]
381.7	1.50	1.44
393.8	1.53	1.47
432.2	1.59	1.52
465.6	1.63	1.56
505.7	1.68	1.61

[a] On the assumption $P_A+P_E=M_D$. (See reference 23.)
[b] Recalculated on the assumption $P_A=P_E/10$, with P_E set equal to the mole refraction as extrapolated from M_R to infinite wavelength by analogy to the known behavior for ethylene chloride. The second set of moment values is used here, the nearly constant differences between the two sets corresponding essentially to a negligible difference in the value of the group moment.

[21] Only the "staggered" conformations are at all likely, and of these the third, with $\varphi_0\sim-120°$ (tertiary −H *trans* to primary −Cl), is probably about as unstable, relatively, as in 1,1,2-trichloroethane ($\Delta E>2.5$: J. R. Thomas and W. D. Gwinn, J. Am. Chem. Soc. **71**, 2785 (1949)) and therefore negligible for ordinary temperatures.

[22] Not the best *trans*-model, but good enough except at large q (see reference 14). Omission of the Cl···Cl temperature factor partly compensates for the inclusion of *skew* and so tends to keep conservative our estimate of the upper limit of *skew*.

[23] R. A. Oriani and C. P. Smyth, J. Chem. Phys. **17**, 1174 (1949).

[24] We are confident the inaccuracies of these assumptions will not vitiate the essential conclusions to be drawn.
Since most of the average dipole moment is due to the *skew*-isomer, the value of $\mu_\perp$ will refer essentially to it.

[25] K. S. Pitzer (J. Chem. Phys. **14**, 239 (1946)) has shown that in the classical partition function the effects of the dependence on φ of the vibrational frequencies and of the external moments of inertia cancel, if the potential energy is free of cross terms between φ and the vibrational coordinates, so that the simple factor $a\exp(-\Delta E/RT)$ may be used to weight classical averages over φ. For ethylene chloride, furthermore, Gwinn and Pitzer (see reference 20) were able to show in detail that the same is true of the quantum-mechanical averages.
It may be seen that μ_t and μ_s can really be constant only if the minima of $V(\varphi)$ are very narrow; and a, only if the minima are fairly wide and suitably similar in shape, or so narrow as to make $a=1$, with only one torsional energy level occupied for each isomer. Rough estimates make it clear, however, that both conditions are probably satisfied.

[26] In both treatments the lowest-temperature point deviates badly, as if the observed moment were too high, and has been ignored in the calculations. It probably is in error.

TABLE IV. Equation (4) fitted to the dipole behavior.

Assumed			Calculated		
$\mu_\perp$, D	φ_t, deg	φ_s, deg	a	ΔE kcal mole^{-1}	Fraction *skew*, 300°K
1.59	0	120	1.34±0.05	0.96±0.03	0.21
1.59	0	90	3.54±0.19	1.23±0.04	0.31
1.80	0	120	0.86±0.03	0.87±0.03	0.17
1.80	0	90	1.85±0.08	1.03±0.04	0.25
2.00	0	120	0.62±0.02	0.84±0.03	0.14
2.00	0	90	1.21±0.05	0.94±0.03	0.20
1.59	25	120	1.29±0.06	1.12±0.04	0.16
1.59	25	90	3.43±0.20	1.40±0.05	0.25

what larger due to induction in the methyl group but, due to mutual induction of the two C—Cl dipoles, not so large as for ethyl chloride; a must be about unity, the corresponding ratio being about one for ethylene chloride and necessarily one for 1,1,2-trichloroethane; and φ_s is probably forced toward *trans* away from the ideal 120°, perhaps by less than the 10° reported for trichloroethane[19] or the somewhat smaller amount indicated by Gwinn and Pitzer's potential function for ethylene chloride. Increasing φ_t to about the upper limit permitted by the diffraction pattern, it will be noted, increases ΔE substantially and correspondingly decreases the fraction of *skew*.

The explicit potentials listed in Table V also afford satisfactory fits, the parameters ΔE and $\mu_\perp$ having been adjusted to fit the 432°K point exactly and the others, excepting the lowest temperature point,[26] as well as possible. In agreement with our first treatment, ΔE is about 1.0, at least for barriers of reasonable shape, with any implausibly high ratio of widths of the two minima (numbers 6, 7, and perhaps 2) again resulting in a too low value of $\mu_\perp$). Potential 5 and the onefold barrier $V(\varphi)=V_0(1-\cos\varphi)/2$ with $V_0=2.5$ originally fitted[23] to the moment values are both incompatible with our diffraction data, the *trans*-minimum of 5 being somewhat too narrow and that of the onefold barrier much too wide. This contradiction with the onefold barrier constitutes rather direct evidence favoring the existence of auxiliary potential minima.

Similar conclusions from the dipole data have been reached by Morino, Miyagawa, and Haga.‡

In summary, we believe that the above results should lead to fairly reliable estimates of averages over φ, with the *skew*-conformation perhaps conservatively overweighted in view of our concern with the optical activity. Knowledge of the Raman and infrared spectra of the vapor, and particularly their temperature dependence, would be very helpful, however.[27]

‡ Morino, Miyagawa, and Haga, J. Chem. Phys. **19**, 791 (1951).

TABLE V. Various internal-rotation potentials and $\mu_\perp$ values adjusted to the dipole behavior.

	$V(\varphi)$, kcal mole^{-1}	φ, deg	ΔE	$\mu_\perp$, D
1.	$2.5[1-\cos\varphi]$	−40— 40	1.1	1.76
	2.1	40— 70		
	$\Delta E+2.5[1-\cos(\varphi-120°)]$	70—160		
	∞	160—320		
2.	$15[1-\cos(\varphi-20°)]$	−40— 50	1.3	1.52
	2.09	50— 80		
	$\Delta E+2.5[1-\cos(\varphi-120°)]$	80—160		
	∞	160—320		
3.	$15[1-\cos(\varphi-20°)]$	−40— 50	1.3	1.74
	1.64	50— 60		
	$\Delta E+2.5[1-\cos(\varphi-90°)]$	60—140		
	∞	160—320		
4.	$0.75[1-\cos\varphi]+0.22[1-\cos3\varphi]$	−30—150	(0.96)	1.83
	∞	150—330		
5.	$1.0[1-\cos\varphi]+1.1[1-\cos3\varphi]$	−60—180	(0.85)	1.62
	∞	180—300		
6.	0	10— 30	1.3	1.29
	2.1	30— 80		
	ΔE	80—160		
	∞	160—370		
7.	0	0— 40	1.1	1.42
	2.1	40— 80		
	ΔE	80—160		
	∞	160—360		

ACKNOWLEDGMENT

We are indebted to Dr. Hedberg for his assistance in the diffraction investigation, to Dr. Garner for the organic preparation, and to Dr. Oriani and Professor Smyth for their kindness in making available the dipole moment data before publication.

[27] The liquid spectra (K. W. F. Kohlrausch and Gr. Prin Ypsilanti, Z. physik. Chem. **B32**, 407 (1936); L. Kahovec and J. Wagner, Z. physik. Chem. **B47**, 48 (1940); H. W. Thompson and P. Torkington, Proc. Roy. Soc. (London), **A184**, 21 (1945); temperature dependence not reported) do clearly indicate the presence of at least two isomers in the same way as has been noted for ethylene chloride (see Mizushima, Morino, Watanabe, Simanouti, and Yamaguchi, J. Chem. Phys. **17**, 591 (1949)).

The Absolute Configuration of Optically Active Molecules

WILLIAM W. WOOD,* WILDON FICKETT,* AND JOHN G. KIRKWOOD†
The Gates and Crellin Laboratories of Chemistry, Institute of Technology, Pasadena, California‡
(Received July 20, 1951)

The problem of the absolute configuration of optically active molecules is investigated with the aid of the Kirkwood theory of optical rotatory power. Absolute configurations are assigned to the enantiomorphs of 2,3-epoxybutane and 1,2-dichloropropane. The assignments are consistent with the established experimental configurational relationships between these compounds. The Fischer convention is confirmed as a structurally correct representation of absolute configuration. The magnitudes of the calculated rotations of the compounds are in reasonably good agreement with experiment. The theory accounts satisfactorily for the effect of temperature and solvent on the optical rotation of 1,2-dichloropropane.

INTRODUCTION

ACCORDING to the theory of Born and Rosenfeld,[1] the optical rotatory power of an optically active substance in a gas or liquid phase is related to molecular structure through a rotatory parameter g, which for a molecule in its ground spectroscopic state is given by[1]

$$g=\frac{c}{3\pi h}\sum_n{}'\frac{Im(\boldsymbol{\mu}_{0n}\cdot\mathbf{m}_{n0})}{\nu_{0n}^2-\nu^2}, \tag{1}$$

where $Im(\boldsymbol{\mu}_{0n}\cdot\mathbf{m}_{n0})$ is the imaginary part of the scalar product of the matrix elements of the electric moment $\boldsymbol{\mu}$ and magnetic moment $\mathbf{m}$ of a molecule between the ground state 0 and excited state n, ν_{0n} the spectroscopic frequency associated with the transition in question, ν the frequency of the incident plane polarized light, c the velocity of light, and h Planck's constant. The sum extends over all excited states of the molecule. The theoretical determination of the absolute configuration of optically active molecules depends upon the determination of the sign of the parameter g. Since a direct evaluation of the right side of Eq. (1) requires the wave functions of all quantum states, a more detailed knowledge of molecular structure than we have at our command at present, attempts have been made to simplify Eq. (1) in such a manner as to allow the estimation of the rotatory power from available structural information. The polarizability theory of Kirkwood[2] and the one-electron theory of Condon, Altar, and Eyring[3] both provide simplified methods for estimating the rotatory parameter from limited structural information.

The theory of Kirkwood begins with the division of a disymmetric molecule into a convenient, but arbitrarily selected set of N structurally symmetric groups of atoms, such as an asymmetric carbon atom and the four substituent groups. The matrix elements $\mathbf{m}_{n0}$ and $\boldsymbol{\mu}_{n0}$ of the magnetic and electric moments of the molecule may then be expressed in the following manner:

$$\mathbf{m}_{n0}=\frac{e}{2mc}\sum_{k=1}^{N}\mathbf{R}_k\times\mathbf{p}_{n0}{}^{(k)}+\sum_{k=1}^{N}\mathbf{m}_{n0}{}^{(k)},$$
$$\boldsymbol{\mu}_{n0}=\sum_{k=1}^{N}\boldsymbol{\mu}_{n0}{}^{(k)}, \tag{2}$$

where $\mathbf{m}_{n0}{}^{(k)}$ and $\boldsymbol{\mu}_{n0}{}^{(k)}$ are the matrix elements of the magnetic and electric moments of group k referred to the center of mass of that group, $\mathbf{p}_{n0}{}^{(k)}$ is the matrix element of the total electronic momentum of the group, and $\mathbf{R}_k$ is the position of the center of mass of group k relative to the center of mass of the molecule as a whole. With the partition of the electric and magnetic moments into those of the set of N groups, expressed in Eq. (2), the rotatory parameter g of Eq. (1) assumes the form

$$g=g^{(0)}+\sum_{i,k=1}^{N}g_{ik},$$
$$g^{(0)}=\frac{1}{3h}\sum_{i<k=1}^{N}\sum_n{}'\frac{\nu_{0n}}{\nu_{0n}^2-\nu^2}[\mathbf{R}_{ik}\cdot(\boldsymbol{\mu}_{0n}{}^{(k)}\times\boldsymbol{\mu}_{n0}{}^{(i)})], \tag{3}$$
$$g_{ik}=\frac{c}{3\pi h}\sum_n{}'\frac{Im(\boldsymbol{\mu}_{0n}{}^{(i)}\cdot\mathbf{m}_{n0}{}^{(k)})}{\nu_{0n}^2-\nu^2},$$

where g_{kk} is the rotatory parameter of group k, referred to its own center of mass. In the polarizability theory of Kirkwood the rotatory parameter is approximated by $g^{(0)}$, which may be calculated with the use of perturbation theory in the form presented in Eq. (4) of the next section. In the one-electron theory of Condon, Altar, and Eyring the rotatory parameter is approximated by one of the group rotatory parameters g_{kk}, which is judged from empirical information on rotatory dispersion to contain the chromophoric electron responsible for the major contribution to the rotatory power. The matrix elements of the electric and magnetic moments of the

* Present address: Los Alamos Scientific Laboratories, Los Alamos, New Mexico.
† Present address: Sterling Chemistry Laboratory, Yale University, New Haven, Connecticut.
‡ Contribution No. 1596.
[1] L. Rosenfeld, Z. Physik **52**, 161 (1928); M. Born and P. Jordan, Elementare Quantenmechanik (Verlag. Julius Springer, Berlin, 1930), p. 250.
[2] J. G. Kirkwood, J. Chem. Phys. **5**, 479 (1937). The signs of the right sides of Eqs. (16), (19), (21), (24), (29), (33), and (35) of this article are in error and have been corrected in Sec. II of the present article.
[3] E. U. Condon, Revs. Modern Phys. **9**, 432 (1937); Kauzmann, Walter, and Eyring, Chem. Revs. **26**, 339 (1940).

chromophoric electron under the dissymmetric perturbation arising from the other groups of the molecule are then explicitly calculated with the use of approximate wave functions. In neither theory has attention been given to the cross terms g_{ik} of Eq. (3). The relative importance of the several terms $g^{(0)}$, and the g_{ik}, which of course depends on the manner of subdivision of the molecule into groups, is difficult to determine. However, explicit calculations have led to values of the Kirkwood term $g^{(0)}$ and of the Eyring term g_{kk} of similar magnitude and to rotatory powers of optically active substances in approximate agreement with experiment.

In the present article we shall report a study of the problem of absolute configuration under the hypothesis that the signs of the optical rotations of the molecules under investigation are determined by the Kirkwood term $g^{(0)}$, when the calculation is based upon a structurally acceptable division of each molecule into groups. On this hypothesis absolute configurations have been assigned to the enantiomorphs of 2,3-epoxybutane and 1,2-dichloropropane. The assignments are consistent with each other and both confirm the Fischer convention as a structurally correct representation of absolute configuration.[4] The magnitudes of the calculated rotations are also in reasonably good agreement with experiment. Moreover, the theory is consistent with observations on the effect of temperature and solvent on the rotation of 1,2-dichloropropane, which arise from changes in the relative populations of the *trans*- and *skew*-forms of the molecule.

While a complete theoretical solution of the problem of absolute configuration cannot be claimed in the absence of reliable estimates of the neglected terms g_{ik} of Eq. (3), the successful description of all observations relating to the rotatory power of the two substances investigated by the approximate theory makes it highly probable that the solution presented here is the correct one. It is also encouraging, though perhaps fortuitous, that our confirmation of the Fischer convention is in agreement with the conclusion reached by Eyring and his co-workers from calculations based upon the one-electron theory.

I.

The specific rotation of plane polarized light of wavelength λ by an optically active substance is related to the molecular rotatory parameter g by[2]

$$[\alpha]=2.880\times10^{4}\frac{\pi^2N}{M\lambda^2}\frac{n^2+2}{3}g, \tag{4}$$

where N is Avogadro's number, M is the molecular weight of the compound, and n is the refractive index of the solution or of the pure compound if we are referring to the specific rotation of a pure liquid. Inserting numerical values we find for the sodium D line

$$[\alpha]_D=4.930\times10^{5}[(n^2+2)/3M]g. \tag{5}$$

If all the substituent groups of the molecule have optical axes of cylindrical symmetry, then g is given by the theory of Kirkwood as[2]

$$g^{(0)}=\tfrac{1}{6}\sum_{i>k=1}^{N}\alpha_i\alpha_k\beta_i\beta_kG_{ik}\mathbf{R}_{ik}\cdot(\mathbf{b}_i\times\mathbf{b}_k),$$

$$G_{ik}=\mathbf{b}_i\cdot\mathbf{T}_{ik}\cdot\mathbf{b}_k=\frac{1}{R_{ik}^3}\left[\mathbf{b}_i\cdot\mathbf{b}_k-3\frac{(\mathbf{b}_i\cdot\mathbf{R}_{ik})(\mathbf{b}_k\cdot\mathbf{R}_{ik})}{R_{ik}^2}\right], \tag{6}$$

$$\mathbf{R}_{ik}=\mathbf{R}_k-\mathbf{R}_i.$$

The sum extends over a set of intrinsically inactive groups into which the molecule is divided on the basis of structural considerations for the purpose of calculation. The indices i and k refer to these groups, the requirement $i>k$ indicating that to any pair of such groups there corresponds one and only one term in the sum. Here $\mathbf{R}$ is the vector distance from the center of mass of the molecule to the center of mass of the group, $\mathbf{b}$ is the unit vector along the optical symmetry axis of the group, α is the mean polarizability of the group, and β is the anisotropy of the polarizability of the group. The quantities α and β are defined more precisely below.

It can be seen that $\mathbf{T}_{ik}$ is the electrical dipole-dipole interaction tensor of groups i and k. Thus each term in the sum is connected with an electrical interaction of this type between one pair of groups. It should also be noted that if the polarizability of any group is isotropic then all terms containing quantities related to that group vanish since the value of β, the anisotropy of the polarizability, will then be zero. There is another way in which a term can vanish, *viz.*, the vectors composing the triple product $\mathbf{R}_{ik}(\mathbf{b}_i\times\mathbf{b}_k)$ can all lie in the same plane. This will be the case if both groups have their optical axes of symmetry along the bond to the central group. Such would be the case, for example, for two halogens bonded to an asymmetric carbon atom.

In calculation of $g^{(0)}$ for any given molecule it is necessary first of all to decide on an appropriate subdivision of the molecule into groups. The general considerations which guide us here are concerned with the approximations involved in the theory and the necessity of evaluating properly the values of the polarizability anisotropy β for the different groups so chosen. The approximate representation of the group interactions as dipole-dipole becomes more valid as the distance between the groups is increased. On the other hand, the size and bonding of the groups must be such that the values of β can be obtained from the available experimental data. After the division into groups has been carried out the individual terms in the sum must be evaluated. Inspection of the expression for $g^{(0)}$ reveals that there are four types of quantities required for each

[4] This result is consistent with that obtained recently by x-ray diffraction utilizing the phase shift near an absorption edge: Peerdeman, Van Bommel, and Bijvoet, Proc. Koninkl. Nederland. Akad. Wetenschap. **54B**, 16 (1951).

group: its mean polarizability α_i; its anisotropy ratio β_i; the direction of its optical symmetry axis $\mathbf{b}_i$; and its spatial position $\mathbf{R}_i$.

The quantities α and β are precisely defined in terms of the polarizability tensor of the group. If $\mathbf{b}_i$ is the unit vector in the direction of the optical axis of symmetry of the group, then the polarizability tensor may be expressed in the following form:

$$\boldsymbol{\alpha}^{(i)}=\alpha_i[(1-\beta_i/3)\mathbf{1}+\beta_i\mathbf{b}_i\mathbf{b}_i], \tag{7}$$

where

$$\alpha_i=\tfrac{1}{3}(\alpha_{11}{}^{(i)}+2\alpha_{22}{}^{(i)}), \quad \beta_i=\frac{\alpha_{11}{}^{(i)}-\alpha_{22}{}^{(i)}}{\alpha_i}, \tag{8}$$

$\alpha_{11}{}^{(i)}$ and $\alpha_{22}{}^{(i)}$ being the components of $\boldsymbol{\alpha}^{(i)}$ parallel and perpendicular to $\mathbf{b}_i$.

The calculation of the mean polarizabilities of the groups from available experimental data presents little difficulty. They are given in terms of the ordinary atomic refractions A_s by

$$\alpha_i=\frac{3}{4\pi N}\sum_s{}^{(i)} A_s. \tag{9}$$

The determination of the anisotropies of the polarizabilities is somewhat more involved and has received considerable discussion in Kirkwood's original paper,[2] where values of α and β for many of the common groups of interest are given. It is sufficient to state here that these values are obtained from measurements of the degree of depolarization of scattered light or of the Kerr effect for appropriate compounds containing the group in question. The values of α and β to be used in the calculations described below are given in Table I.

The geometry of the molecule (excluding the important question of changes in internal conformation due to freedom of rotation about one or more bonds) is in many cases known from electron diffraction data. From the known form and symmetry of the groups it is possible to determine $\mathbf{b}_i$, and $\mathbf{R}_{ik}$ is readily evaluated (the question of internal conformation will be discussed later) from bond angles and bond distances obtained from electron diffraction or spectroscopic data.

TABLE I. Values of the mean polarizabilities α and of the anisotropy ratios β.

Group	$\alpha\cdot10^{24}$ (c.c.)[a]	β
CH_3	2.25	0.35[b]
CH_3		0.31[c]
Cl	2.35	0.35[b,d]
CH_2Cl	4.17	0.34[b,e]
CH_2Cl		0.33[c,e]

[a] Landolt-Börnstein, *Physikalische-Chemische Tabellen*, Hw. II, 985; Eisenlohr, Z. Physik. Chem. **75**, 585 (1910); **79**, 129 (1912).
[b] Values obtained by Cabannes; see Landolt-Börnstein, *Physikalische Chemische Tabellan*, 5th Ed., Eg. II, p. 88; Eg. III, p. 1204.
[c] Average of two values: H. A. Stuart, *Hand-und-Jahrbuch der Chemischen Physik* (Leipzig, 1939), **10 III**, p. 27, and W. M. Breazeale, Phys. Rev. **49**, 625 (1936).
[d] See reference c, H. A. Stuart.
[e] Assumed to have an approximate axis of symmetry along the C–Cl bond.

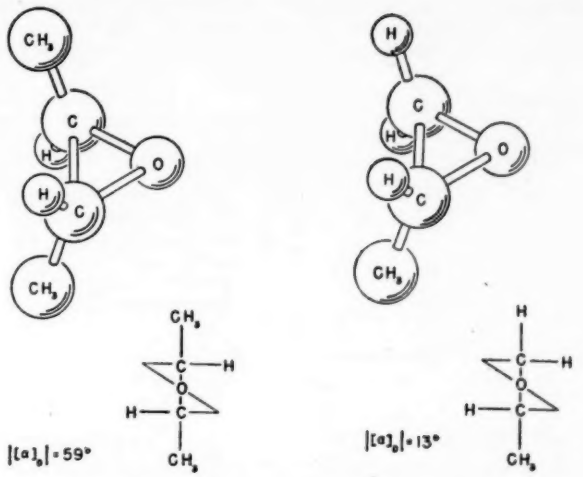

FIG. 1. Enantiomorph of 2,3-epoxybutane to which the calculations apply, the configurationally related 1,2-epoxypropane, and the corresponding Fischer projection formula.

We now apply Eqs. (5) and (6) to the calculation of the optical rotatory power of 2,3-epoxybutane. The spatial model to which the calculations apply, the configurationally related 1,2-epoxypropane, and the corresponding Fischer projection formulas are shown in Fig. 1. We first divide the molecule into groups. We consider it to be composed of three groups: the three-membered ring with its attached hydrogens, and the two methyl groups.[5] Three pairs can be chosen from these groups and therefore three terms contribute to the rotatory power: two representing the methyl-ring interactions, identical in both magnitude and sign; and one representing the methyl-methyl interaction.

Having defined the number and type of terms in the sum by our division of the molecule into groups, we proceed to the actual calculation. Since the molecule is a rigid one, no questions of internal conformation arise, and the known bond angles and distances[6] suffice for the determination of $\mathbf{b}_i$, $\mathbf{b}_k$, and $\mathbf{R}_{ik}$ in each term. The values of α are obtained from Table I. Values of β for the methyl groups are also given in Table I, but no such value is available for the three-membered ring or its component atoms as the necessary experimental data are lacking. Thus we can calculate directly the term representing the methyl-methyl interaction, but not those representing the methyl-ring interactions.

[5] We do not intend to imply by our terminology that the methyl-ring interaction must contribute only a single term to $g^{(0)}$. It is more correct and in keeping with the intent of the theory to consider it as being itself the sum of three terms describing the interactions of the methyl group with the two carbons and oxygen of the ring, plus terms describing the interactions of the ring atoms with each other. (The sum of these latter terms describing interactions within the ring is probably small since the ring has a plane of symmetry in the absence of perturbing influences.) Thus the "methyl-ring interaction term" actually comprises a sum of terms and the terminology is adopted for the sake of convenience; the optical properties of carbon and oxygen in such an environment are not sufficiently well known to allow separate calculation of these terms.

[6] L. O. Brockway and P. C. Cross, J. Am. Chem. Soc. **58**, 2407 (1936); **59**, 1147 (1937).

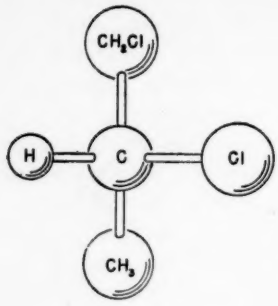

FIG. 2. Enantiomorph of 1,2-dichloropropane to which the calculations apply, and the corresponding Fischer projection formula.

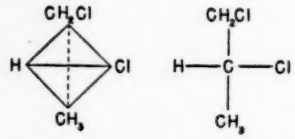

We are thus forced to resort to a quasi-empirical evaluation of these terms. To this end we consider the configurationally related 1,2-epoxypropane molecule, shown in Fig. 1. If we make an analogous division into groups, we arrive at the following result: the methyl group, the three-membered ring together with the two hydrogens chosen so as to correspond to the same group in epoxybutane, and the third hydrogen. Thus we have the following terms to consider: one representing a methyl-ring interaction of the same sign and approximately the same magnitude as in the epoxybutane isomer shown, one representing a hydrogen-methyl interaction, and one representing a hydrogen-ring interaction. Because of the small polarizability of hydrogen the terms containing it are neglected. (Even if the polarizability of hydrogen were large, the hydrogen-methyl interaction would still be zero since the optical symmetry axes and the vector connecting them would lie in the same plane and the triple vector product would vanish. The methyl group is considered free to rotate about the C—C bond, and hence has an optical symmetry axis along this bond.) Thus there remains only one term to account for the entire rotatory power of the molecule; this term involves the methyl-ring interaction. Moreover, because of the way in which the groups have been chosen, this interaction should be approximately the same as the corresponding methyl-ring interaction in 2,3-epoxybutane. The methyl-ring contribution to the rotatory power of 2,3-epoxybutane is thus equal to the observed specific rotation of the configurationally related 2,3-epoxypropane. Without making an *a priori* assumption concerning absolute configuration we obtain from the observed specific rotation of 2,3-epoxypropane only the magnitude, and not the sign, of this contribution.

Calculation of the methyl-methyl interaction in the enantiomorph of 2,3-epoxybutane shown in Fig. 1 gives $+17°$ for this contribution to the rotatory power in a medium of refractive index 1.37, corresponding to the pure liquid. The observed rotation of 2,3-epoxypropane gives a magnitude of 13 as the quasi-experimental value for the methyl-ring interaction. Remembering that in 2,3-epoxybutane there are two such interactions we obtain $+17+2\times(+13)=+43°$ as the predicted specific rotation if we take the positive sign for the methyl-ring interaction, and $+17+2\times(-13)=-9°$ if we choose the negative sign. The fact that the enantiomorphs of 2,3-epoxybutane and 1,2-epoxypropane having the same sign of rotation are configurationally related[7] allows us to reject the latter value, for since the observed rotation of the 2,3-epoxybutane is greater than can be accounted for by the two methyl-ring interactions, the methyl-methyl interaction and methyl-ring interactions must have the same sign. We therefore assign the spatial configuration of Fig. 1 to the dextrorotatory isomer. Since the dextrorotatory isomers have been assigned the *D* configuration, the Fischer convention regarding absolute configuration is in agreement with this result. The predicted rotation of 43° is in fair agreement with the observed value of 59°.[7]

The theory would be expected to apply most accurately to vapors or dilute solutions in nonpolar solvents. Since the experimental results quoted above were those of the pure liquid, a possible solvent effect was investigated for 2,3-epoxybutane. No significant change in $[\alpha]_D^{300°K}(3/n^2+2)$ was observed for this compound on passing from the pure liquid to a dilute solution in heptane. Similar information for 2,3-epoxypropane is not available, but structural considerations suggest that its behavior would not differ from that of 2,3-epoxybutane. A related rigid compound, 2,3-iminobutane, has been found to undergo only a slight change in rotation

TABLE II. The rotatory power of 1,2-dichloropropane as a function of internal conformation.

ϕ degrees	$[\alpha]_D^{300°K}(3/n^2+2)$ I[a]	II[b]	III[c]
0	+39.9	+47.3	+40.7
20	+29.5	+35.6	+32.2
40	+16.5	+20.1	+14.8
60	+1.8	+3.2	−0.7
80	−12.8	−13.9	−16.2
100	−26.7	−30.0	−30.7
120	−38.5	−41.7	−40.7
140	−43.9	−47.9	−45.4
160	−40.1	−45.4	−41.5
180	−26.7	−33.1	−28.5
200	−12.2	−19.0	−13.8
220	−4.1	−10.3	−4.6
240	−1.7	−5.6	−0.0
260	+0.9	+0.1	+4.9
280	+9.6	+12.1	+14.7
300	+24.9	+29.8	+29.2
320	+39.0	+46.1	+42.1
340	+44.1	+52.6	+46.3

[a] I. Data of Cabannes: $\beta_{CH_3}=0.35$, $\beta_{CH_2Cl}=0.35$; optical center of CH_2Cl group at center of mass.
[b] II. Data of Cabannes; optical center of CH_2Cl group at Cl.
[c] III. Data of Stuart (and Breazeale): $\beta_{CH_3}=0.31$, $\beta_{CH_2Cl}=0.33$; optical center of CH_2Cl group at center of mass. (For references see Table I.)

[7] H. J. Lucas and H. K. Garner, J. Am. Chem. Soc. 70, 990 (1948); P. A. Levene and A. Walti, J. Biol. Chem. 68, 415 (1926).

on passing from the pure liquid to a dilute solution in heptane.[8]

In calculating the optical rotatory power of 1,2-dichloropropane (Fig. 2) we proceed in the same way, dividing the molecule into groups as follows: H, CH_3, Cl, and CH_2Cl bonded to the asymmetric carbon atom as the central group. If the optical axis of the CH_2Cl group is taken to lie along the C—Cl bond, the two contributing terms correspond to the interaction of CH_3 and of Cl with CH_2Cl. Terms involving hydrogen are neglected because of its small polarizability, and that representing the interaction of CH_3 with Cl is zero because the optical axes of both groups lie along their bonds to the central group. In contrast to the case of 2,3-epoxybutane, the experimental data are sufficiently complete that values of β may be found for all of the groups involved. These are given in Table I. Thus, given the geometry of the molecule, the optical rotatory power can be calculated directly from Eqs. (5) and (6).

The possibility of internal rotation about the 1,2-carbon-carbon bond must be considered, however, and this additional degree of freedom complicates the determination of the molecular geometry. We define an angle ϕ specifying the internal conformation such that ϕ is zero when the chlorine atoms are *trans* to each other with the positive direction of rotation from zero that which increases the methyl-chlorine distance. Only two potential minima are considered to have sufficiently low energies to make appreciable contributions:[9] that at $\phi=0°$ (*trans*), and that at $\phi=+120°$ (*skew*). To obtain a result corresponding to the observed value we first calculate the optical rotation as a function of ϕ, and then take a suitably weighted average over all values of ϕ. The results of the first calculation in Table II, from Eqs. (5) and (6) with C—C 1.54Å, C—Cl 1.76Å and tetrahedral angles, indicate the necessity of taking into account the internal rotation. The calculated optical rotations of the *skew*- and *trans*-forms have nearly the same magnitude but opposite signs; if the two were nearly equally populated we would be unable to make an unambiguous prediction of the sign of the optical rotation and hence of the absolute configuration.

Using electron diffraction[9] and dipole moment data[10] Wood and Schomaker[9] estimated the energy difference between the *skew*- and *trans*-forms. Some of their results are given in Tables III and IV. The values in Table III were obtained by considering the problem as an equilibrium between the *skew*- and *trans*-isomers, so that the rotation is given approximately by

$$\alpha=(\alpha_t+\alpha_s e^{-\Delta F/RT})/(1+e^{-\Delta F/RT}),$$
$$\Delta F=\Delta E-RT\ln(f_s/f_t), \tag{10}$$

where α is the observed rotation at absolute temperature T; α_t is the optical rotation of the *trans*-form; and α_s, that of the *skew*-form. The difference between the free energy of the two forms in the vapor is denoted by ΔF and the corresponding difference in internal energy by ΔE, while f_s and f_t are the partition functions for the *skew*- and *trans*-forms each referred to its own ground state as the zero of energy. The values in Table IV were obtained with the use of the explicit potential functions shown, the averaging being carried out by numerical evaluation of the integral expression,

$$\alpha=\frac{\int_0^{2\pi}\alpha(\phi)e^{-V(\phi)/RT}d\phi}{\int_0^{2\pi}e^{-V(\phi)/RT}d\phi}, \tag{11}$$

where $V(\phi)$ is the potential of internal conformation and $\alpha(\phi)$ represents the function tabulated in Table II.

In order to ensure as far as possible that the prediction of absolute configuration on the basis of these results will be unambiguous, the assumed values of the parameters in Table III and the potential barriers in Table IV were chosen so as to afford a conservative estimate of the upper limit of the contribution of the *skew*-form. It is seen that the values obtained for the specific rotation are nevertheless unequivocal with regard to sign.

We therefore conclude that the enantiomorph shown in Fig. 2 is dextrorotatory and that its specific rotation in the vapor state is probably between +20° and +30°. The vapor value of the rotation was not measured, but reasonable agreement with this range of values was obtained on the basis of the observed rotations in

TABLE III.[a] Specific rotations of 1,2-dichloropropane calculated from Eq. (10).

ϕ degrees	ϕ_s degrees	f_s/f_t	ΔE kcal/mole	Fraction of *skew*	$[\alpha]_D^{300°K}(3/n^2+2)$
0	+120°	1.36	0.96	0.21	+29°
0	+120°	0.86	0.87	0.17	+33°
0	+90°	1.26	1.03	0.25	+30°
0	+120°	0.64	0.82	0.14	+35°
0	+90°	1.18	0.94	0.20	+33°
+25	+120°	1.41	1.12	0.16	+19°

[a] Using column II of Table II for α_s and α_t.

TABLE IV.[a] Specific rotations of 1,2-dichloropropane calculated from Eq. (11) with explicit potential functions.

	$V(\phi)$ kcal/mole	Range of ϕ degrees	ΔE kcal/mole	$[\alpha]_D^{300°K}(3/n^2+2)$
1.	$2.5(1-\cos(\phi))$	−40– 40	1.1	+26°
	2.1	40– 70		
	$\Delta E+2.5(1-\cos(\phi-120))$	70–160		
	∞	160–320		
2.	$15(1-\cos(\phi-20))$	−40– 50	1.3	+20°
	1.6	50– 60		
	$\Delta E+2.5(1-\cos(\phi-90))$	60–140		
	∞	140–320		
3.	$0.75(1-\cos(\phi))$ $+0.22(1-\cos(3\phi))$	−30–150	(0.96)	+22°
	∞	150–330		

[a] Using column II of Table II for $\alpha(\phi)$.

[8] Dickey, Fickett, and Lucas, J. Am. Chem. Soc. (to be published).
[9] W. W. Wood and V. Schomaker, J. Chem. Phys. (to be published).
[10] R. A. Oriani and C. P. Smyth, J. Chem. Phys. **17**, 1174 (1949).

TABLE V. Optical rotation of $L(-)$1,2-dichloropropane in n-heptane at different temperatures.

$T°K$	αD^{T} [a] obs.	Concentration[a]	$[\alpha]D^{T}$	nD^{T} [b]	$[\alpha]D^{T}(3/n^2+2)$
298.0	−1.113	0.02688	−20.70	0.7652	−15.84
300.7	−1.094	0.02679	−20.42	0.7659	−15.64
303.8	−1.075	0.02669	−19.91	0.7667	−15.21
307.9	−1.051	0.02655	−19.79	0.7678	−15.19
311.1	−1.020	0.02644	−19.29	0.7686	−14.83
315.7	−1.007	0.02628	−19.16	0.7698	−14.75
319.7	−0.986	0.02615	−18.85	0.7708	−14.53
324.6	−0.964	0.02598	−18.55	0.7720	−14.32
330.7	−0.923	0.02577	−17.91	0.7736	−13.86
337.5	−0.869	0.02553	−17.02	0.7754	−13.20
345.7	−0.838	0.02524	−16.60	0.7776	−12.91

[a] From coefficients of expansion of n-heptane, I. C. T. 3, 29.
[b] From dn/dT for n-octane, G. Egloff, editor, *Physical Constants of Hydrocarbons* (V. I. Reinhold Corporation, New York, 1939), p. 49.
[c] Readings were taken with an ordinary polarimeter to two decimal places. Each value in the table represents an average of at least ten such readings; the last figure was retained in the averaging, although the degree of accuracy is probably not so great as implied by its presence. The probable errors of most of the sets of observations were about 0.007.

solvents of different dipole moment, discussed in detail in the following section. The Fischer convention assigns the spatial model of Fig. 2 the D configuration; experimentally, the D configuration is assigned to the dextrorotatory isomer.[11] The Fischer convention is thus again found to be correct, in agreement with the result obtained from 2,3-epoxybutane.

II.

While the above calculation leads approximately to a predicted value for the vapor rotation of 1,2-dichloropropane, the values actually observed were for the compound in the pure liquid state and in solutions of the compound in organic solvents. Since there is a difference in energy between the two forms the rotation may be expected to exhibit a temperature dependence.[12] Experimentally, this was found to be the case. In order to make a more direct comparison between theory and experiment a quantitative investigation of these effects was carried out. From the experimental data concerning the temperature dependence it was possible to calculate approximately the free energy difference between the two forms in solution in n-heptane, and also the separate rotatory powers of the *trans*- and *skew*-forms of the molecule; these latter could then be compared directly with the theoretical values.

The variation of the rotatory power of 1,2-dichloropropane in n-heptane with temperature is shown in Table V.[13] In order to obtain the values for the separate optical rotatory powers of the *skew*- and *trans*-forms we again assume that the two minima are very narrow so that the problem may be treated as one involving an equilibrium between two isomers. The optical rotation of the equilibrium mixture is then given by Eq. (10), where ΔF now refers to the difference in free energy of the two forms under the conditions of observation, *viz.*, in the solvent n-heptane; the previous description of ΔF in terms of f_s/f_t is of course no longer valid. Equation (10) can be written in the form:

$$\alpha=(\alpha_t-\alpha_g)\left(\frac{1}{1+e^{-\Delta F/RT}}\right)+\alpha_s. \qquad (12)$$

The value of ΔF, treated as a constant, is determined from the requirement that the plot of α against $1/(1+e^{-\Delta E/RT})$ be linear, and the values of α_t and α_s can be found in terms of the slope and intercept of the line so obtained. This procedure makes evident the relative insensitivity to variations in ΔF; a series of approximate calculations indicated that the width of the range of permissible values was about the same as that resulting from the analysis of the vapor dipole moment data:[10] several hundred cal/mole. A value lying near the middle of the range was chosen, $\Delta F=760$ cal/mole. The values of α_t and α_s depend somewhat on the value of ΔF; once it is fixed they can be determined within two or three degrees. The values found for α_t and α_s were $+36°$ and $-56°$, respectively. These are to be compared with the theoretical values of α_t and α_s from Table II (with $\phi=0°$ and $\phi=+120°$), $+40°$ and $-39°$, respectively (to two significant figures).

The observed rotations of the 1,2-dichloropropane in different solvents are shown in Table VI. In order to take into account the effect of the solvent we calculate the lowering of the free energy difference through solvent polarization. Since the *trans*-form has essentially zero dipole moment we assume that the electrostatic effects of the solvent on its free energy are small. Assuming that nonelectrostatic effects are the same for both isomers we may express the free energy difference in solution, with neglect of the difference between their partial molal volumes, as

$$\Delta F=\Delta E-(N\mu^2/r^3)(D-1)/(2D+1), \qquad (13)$$

where ΔE is the difference in internal energy between the two forms in the vapor (ΔE and ΔF for the vapor are equal under the assumption of equal partition functions for the two forms). The second term represents the lowering of the free energy of the *skew*-form due to solvent polarization according to the theory of Kirkwood.[14] Here μ and r represent the dipole moment and approximate radius of the *skew*-form, D is the dielectric constant of the solvent, and N is Avogadro's number. Since the rotations of the *trans*- and *skew*-forms

[11] Fickett, Garner, and Lucas, J. Am. Chem. Soc. **73**, 5063 (1951).
[12] The effects of temperature and solvent on optical rotation have been considered previously; C. O. Beckman and K. Cohen, J. Chem. Phys. **4**, 784 (1936); Kauzmann, Walter, and Eyring, Chem. Revs. **26**, 373 (1940); H. J. Bernstein and E. E. Pedersen, J. Chem. Phys. **17**, 885 (1949).
[13] The rotations in Table V and VI are for approximately 2–5 percent solutions. Measurements at lower concentrations showed that the rotation was nearly independent of concentration in all of the solvents used. The values in Tables V and IV may therefore be taken as those at infinite dilution.
[14] J. G. Kirkwood, J. Chem. Phys. **2**, 351 (1934).

are about equal in magnitude but opposite in sign, the effect of the solvent should be to decrease the observed rotation by increasing the relative population of the *skew*-form through a decrease in its free energy. This effect should be larger for solvents of high dielectric constant.

Solving Eqs. (12) and (13) for ΔF and equating the results we obtain

$$\Delta E-\left(\frac{D-1}{2D+1}\right)(N\mu^2)\left(\frac{1}{r^3}\right)=RT\ln\left(\frac{\alpha_s-\alpha}{\alpha_t-\alpha}\right). \quad (14)$$

Here D represents the dielectric constant of the solvent; μ is the dipole moment of the *skew*-form and has been obtained from an analysis of the variation of the vapor dipole moment with temperature,[9,10] α_s and α_t have been determined above from the temperature dependence of the rotation. The unknowns are taken to be ΔE and $(1/r^3)$. The observed rotations in two different solvents of known dielectric constant provide two sets of values for the coefficients and constant term in Eq. (14). The resulting pair of simultaneous linear equations may be solved for ΔE and $(1/r^3)$. Taking the rotations in the solvents *n*-heptane and methanol (Table VI) and the value 3.1 d.u. for μ, corresponding to $\mu_\perp=1.8$ d.u.,[9] we obtain 1050 cal/mole for ΔE and 4.5A for r. This value of ΔE agrees with the approximate value 1000 cal/mole obtained from the dipole moment and electron diffraction data.[9] The value of 4.5A for r is reasonable in that it is about equal to the distance between a point midway between the centers of the C—Cl bonds and the outer edge of the methyl group when the molecule is in the *skew*-configuration.

Using the value of ΔE obtained in this way and the values of α_s and α_t obtained from the temperature dependence of the rotation, a quasi-experimental value for the vapor rotation can be calculated with the use of Eq. (10). The value obtained in this way for the vapor rotation is +23°. This is to be compared with the theoretical values of Table III and Table IV, obtained from the theoretically calculated dependence of the rotation on the internal angle and the potential functions obtained from the dipole moment and electron diffraction data.[9] The numerical agreement is seen to be satisfactory.

Another approximate check on the theory is the calculation of the rotation of the pure liquid 1,2-dichloropropane making use of its known dielectric constant and the radius of the molecule obtained above, together with Eqs. (10) and (13). The value thus calculated is +4.3°, and is to be compared with the experimental value of +4.6°.

The low observed rotation in dioxane appears at first glance to be inconsistent with this general picture, since the dielectric constant of dioxane is about the same as that of heptane. However, the strong quadrupole moment of dioxane, which could markedly affect the *trans-skew* equilibrium of the 1,2-dichloropropane, does not contribute to the dielectric constant of the material.

TABLE VI. Optical rotation of $L(-)$1,2-dichloropropane in different solvents.

Solvent	Conc. g/ml	αD^{25} observed	$[\alpha]D^{25}$	$[\alpha]D^{25}(3/n^2+2)$
Pure liquid	1.1478	−6.76	−5.87	−4.33
Heptane	0.0693	−1.44	−20.8	−15.9
Methanol	0.0618	−0.20	−3.2	−2.6
Dioxane	0.0707	−0.36	−4.5	−3.4

Comparison of the theoretical and experimental results indicates that, in general, the numerical agreement is satisfactory considering the approximations involved throughout. Probably the most valid comparison, in the sense of offering the best test of the theory, is that between the theoretical and experimental values for the separate optical rotatory powers of the *trans*- and *skew*-forms of 1,2-dichloropropane. The theoretical results for these two forms have roughly correct magnitudes and are consistent with the experimental results with regard to the signs of their rotations relative to each other.

We have assigned the absolute configuration of Fig. 2 to the dextrorotatory isomer of 1,2-dichloropropane. This was done without any experimental data concerning the optically active forms of the molecule, using only the calculated dependence of the rotatory power on conformation (Table II) and the information about the potential of internal conformation obtained from the electron diffraction and dipole moment measurements.

As stated above, it has been possible to obtain experimentally the configurational relationship between the two compounds for which calculations were made. It was found that the enantiomorphs of 2,3-epoxybutane and 1,2-dichloropropane of like sign were configurationally related. (Levorotatory 1,2-dichloropropane was prepared from dextrorotatory 2,3-epoxybutane by a series of reactions involving a single Walden inversion at the assymmetric center.) Since the theory assigns positive rotations to the configurationally related isomers of Fig. 1 and Fig. 2, it is found to be internally consistent in its predictions for these two different molecules and confidence in it is considerably strengthened.

It was shown above that there is semiquantitative agreement between the experimental and calculated temperature dependence of the rotation. Using only the direction of this effect, however, it is possible to make an assignment of absolute configuration which requires less knowledge of the potential of internal conformation than when the dependence of the rotation on temperature is not known.

From the observed temperature dependence we can determine the relationship between the over-all optical rotation on the basis of the following assumption: the principal effect of a change in temperature is an increase in the population of the *skew*-form at the expense of the *trans*, with the *skew*-form taken as having the higher free

energy of the two. It can then be shown that if the observed rotation increases with increasing temperature, the sign of the over-all rotation must be the same as that of the *skew*-form;[15] the relationship between the signs of the over-all rotation and that of the *trans*-form remains indeterminate. If, on the other hand, the observed rotation is found to decrease with increasing temperature, it can be shown that the signs of the over-all rotation and that of the *trans*-form must be the same, and the relationship between the signs of the over-all rotation and that of the *skew*-form remains indeterminate. For 1,2-dichloropropane the observed rotation was found to decrease with increasing temperature, so that under the above assumption the correct calculation of the sign of rotation of the *trans*-form alone is sufficient to determine uniquely the sign of the over-all rotation, and hence the absolute configuration.

[15] This can be shown by distinguishing three cases: (1) The isomers have optical rotations of the same sign, which is obviously the same as that of the over-all rotation. The magnitude of the over-all rotation will then either increase or decrease with increasing temperature depending on the relative magnitudes of the rotations of the two isomers. (2) The isomers have rotations of opposite sign, and the sign of the over-all rotation is the same as that of the *trans*-form. The over-all rotation will then decrease with increasing temperature. (3) The isomers have rotations of opposite sign, and the sign of the over-all rotation is the same as that of the *skew*-form. The over-all rotation will then increase with increasing temperature. If the actual effect is a decrease in the observed rotation with increasing temperature, this is consistent with (1) and (2), not with (3). Hence the signs of the over-all rotation and that of the *trans*-forms are the same. The argument is similar for the opposite temperature effect.

THE JOURNAL OF CHEMICAL PHYSICS VOLUME 20, NUMBER 4 APRIL, 1952

On the Distribution Function in Phase Space, with Application to the Stationary State of an Ideal Gas

ERNEST IKENBERRY
Alabama Polytechnic Institute, Auburn, Alabama
(Received January 3, 1951)

An infinite set of partial differential equations which are to be satisfied by the coefficients in a Bruns' series expansion of the distribution function, as a consequence of the principle of "conservation of density-in-phase," are obtained. By means of these equations there are derived meteorologically useful expressions for the density and temperature gradients in an ideal gas.

THE DIFFERENTIAL EQUATIONS

IN his application of Gibbs' principle of "conservation of density-in-phase" to the statistical theory of liquids, Jaffé[1] obtained several of the set of partial differential equations which the coefficients in a power series expansion of the distribution function must satisfy, by equating to zero coefficients of powers of the moments in the expansion of $Df=0$ where D is the operator presently to be defined. The corresponding equations which the coefficients in a Bruns' series expansion[2] (I, 2) of the distribution function satisfy are much more easily obtained, however, by utilization of the orthogonality (I, 1) of the polynomials used in the expansion.

Assuming that

$$\frac{\partial}{\partial q_i}\left(\frac{dq_i}{dt}\right)=\frac{\partial}{\partial p_i}\left(\frac{dp_i}{dt}\right)=0, \tag{1}$$

we may write the operator D (I, 5) in the form

$$D=\frac{\partial}{\partial t}+\sum_{i=1}^{3N}\left(\frac{1}{m}p_i\frac{\partial}{\partial q_i}+R_i\frac{\partial}{\partial p_i}\right), \tag{2}$$

where $p_i=(dq_i/dt)$ and $R_i=(dp_i/dt)$, $i=1, 2, \cdots 3N$. We then obtain

$$D(f\phi)\equiv f(D\phi)+\phi(Df)=f(D\phi), \tag{3}$$

where, for the present, we shall choose $\phi=\phi(h, p)=1$, H_{1i}, H_{2i}, $H_{1i}H_{1j}$, H_{3i}, $H_{1i}H_{2j}$, etc., in turn. The equation

$$\int D(f\phi)d\omega=\int f(D\phi)d\omega \tag{4}$$

then represents an infinite set of partial differential equations which the coefficients in the Bruns' series expansion of the distribution function must satisfy, as a consequence of $Df=0$. In forming these partial differential equations, it is convenient to make use of the recurrence relations

$$2hp_iH_n(hp_i)=(2n)^{\frac{1}{2}}H_{n-1}(hp_i)+(2n+2)^{\frac{1}{2}}H_{n+1}(hp_i) \tag{5}$$

and

$$\frac{\partial}{\partial p_i}H_n(hp_i)=(2n)^{\frac{1}{2}}hH_{n-1}(hp_i). \tag{6}$$

The arbitrary parameter h in the Bruns' series expansion (I, 2) of the distribution function may, in general, be chosen as any real function of the $3N$ posi-

[1] G. Jaffé, Phys. Rev. **75**, 184–196 (1949). The text refers to this paper as J, followed by the number of the equation.

[2] E. Ikenberry, J. Chem. Phys. **19**, 4, 467–470 (1951). The text refers to this paper as I, followed by the number of the equation. The notation used follows this paper.

tion coordinates, and of the time. As the polynomials H_{ni}, (I, 1), with the exception of $H_{0i}=1$, are functions of h; the coefficients, with the exception of a, are also functions of h; and the partial differential equations contain terms involving the partial derivatives of h with respect to the position coordinates and the time. A method of forming a set of differential equations in which these partial derivatives do not appear explicitly will now be developed.

Since the distribution function is independent of any particular form used for its representation, we may write

$$(\partial f/\partial h)=0, \tag{7}$$

as well as corresponding equations for all physically defined quantities, such as the density n and the temperature T. If we now define operators $(\partial'/\partial t)$, $(\partial'/\partial q_i)$, and D' by

$$\frac{\partial}{\partial t}=\frac{\partial'}{\partial t}+\left(\frac{\partial h}{\partial t}\right)\frac{\partial}{\partial h},$$
$$\frac{\partial}{\partial q_i}=\frac{\partial'}{\partial q_i}+\left(\frac{\partial h}{\partial q_i}\right)\frac{\partial}{\partial h}, \tag{8}$$

and

$$D=D'+(Dh)\partial/\partial h,$$

we obtain

$$D'f=Df=0, \tag{9}$$

and hence

$$D'(f\phi)=f(D'\phi)+\phi(D'f)=f(D'\phi). \tag{10}$$

The partial differential equations may then be written in the form

$$\int D'(f\phi)d\omega=\int f(D'\phi)d\omega. \tag{11}$$

Thus, there is no loss of generality in treating h as a constant independent of the position coordinates and of the time. This explains a result of calculations previously performed by Jaffé,[1] who found that there was no loss of physical generality in assuming that his parameter e_1, which corresponds to $2mh^2$, is independent of the position coordinates (J, following 3.21). As a further conclusion, we may say that h cannot be determined from physical considerations, but that we may arbitrarily assign h any real value, such as $h=1/(2mkT)^{\frac{1}{2}}$, (see I, preceding 5).

Upon letting $\phi=1$, H_{1j}, H_{2j}, $j=1, 2, \cdots 3N$, in turn, we obtain, as examples of the infinite set of partial differential equations to be satisfied by the coefficients in the Bruns' series expansion (I, 2) of the distribution function,

$$\frac{\partial' a}{\partial t}+(2^{\frac{1}{2}}mh)^{-1}\sum_{i=1}^{3N}\frac{\partial' b_i}{\partial q_i}=0,$$
$$\frac{\partial' b_j}{\partial t}+(2^{\frac{1}{2}}mh)^{-1}\sum_{i=1}^{3N}\frac{\partial' c_{ij}}{\partial q_i}=2^{\frac{1}{2}}haR_j, \tag{12}$$
$$\frac{\partial' c_j}{\partial t}+(2^{\frac{1}{2}}mh)^{-1}\sum_{i=1}^{3N}\frac{\partial' d_{ij}}{\partial q_i}=2hb_jR_j,$$

where $c_{jj}=a+2^{\frac{1}{2}}c_j$ and $d_{jj}=2^{\frac{1}{2}}b_j+3^{\frac{1}{2}}d_j$. It is obvious that the substitution into (11) of any quantity ϕ which is a multinomial in the momentum coordinates, with coefficients which may be polynomials in h, will lead to a partial differential equation which is a linear combination of equations of the type illustrated by (12).

The system illustrated by (12) corresponds closely to the system (J, 3.09 to 3.13) obtained by Jaffé, who assumed, in his method of treatment, that the distribution function depends only on the coordinates of the center of mass of the system, as well as on the momentum coordinates and the time. Upon closer comparison of the two systems it is found, however, that there is an important difference, arising from the fact that Jaffé retained terms only as far as those of the third order in the momentum coordinates, whereas the present method leads to equations which are complete without any terms being neglected.

Although solutions of the systems (4) or (11) may be found in a few cases, as, for example, for an ideal gas in a conservative force field, with isothermal conditions, there is at present no known solution which is satisfactory for a mechanical system consisting of a dense gas or a liquid. Furthermore, complete determination of the coefficients in the Bruns' series expansion (I, 2) would require detailed information regarding the initial and boundary conditions, which is equivalent to complete knowledge of the microscopic state of the system. The most that can be hoped for is the determination of relations between statistically defined quantities which describe the macroscopic state of the system. The author has obtained an infinite set of integro-partial differential equations satisfied by these quantities, and has obtained an approximate solution[3] of the first four of these equations, leading to expressions for the coefficients of heat conductivity and viscosity (I, 7 and 8). The method of obtaining expressions for the density and temperature gradients in an ideal gas in a gravitational field will be given here, inasmuch as it is believed that the method is of value, although the results of the final equations, (24) and (25), are well known. It may be noted that, in the case of stationary, isothermal condi-

[3] E. Ikenberry, "The conservation of systems in phase space as applied to the liquid state," doctoral dissertation, Louisiana State University (1950).

tions, Gibbs' canonical distribution function,[4]

$$f_c=(2\pi mkT)^{-3N/2}\cdot\exp(-\sum_{i=1}^{3N}p_i^2/2mkT), \quad (13)$$

is the appropriate solution of the system (12).

STATIONARY STATE OF AN IDEAL GAS

If, in the equation of transport, (I, 6), we consider the stationary case with gradients only in the direction corresponding to q_1, we obtain

$$(\partial'/\partial q_1)\int\int fp_1\phi d\omega dQ_1=m\int\int f(D'\phi)d\omega dQ_1. \quad (14)$$

In order to obtain an expression for the density gradient, it would be desirable to let $p_1\phi=1$ in (14), since $\int\int fd\omega dQ_1=\mathbf{N}n/N$ (I, 3 and 4). However, the right-hand side of (14) becomes undefined when $\phi=1/p_1$. To avoid this, we choose for ϕ a polynomial in p_1 such that $p_1\phi$ differs from unity by a term in $H_{2r,1}$, where r is any arbitrarily large integer. Setting

$$\phi=2^{\frac{1}{2}}h\sum_{s=1}^{r}a_sH_{2s-1,1},$$

we find, by means of the recurrence relation (5), that $p_1\phi=1+(2r)^{\frac{1}{2}}a_rH_{2r,1}$ if $a_s=(-2)^{s-1}\Gamma(s)/\{\Gamma(2s)\}^{\frac{1}{2}}$. Furthermore,

$$D'\phi=-mg(\partial\phi/\partial p_1)=-2h^2mg\sum_{s=0}^{r-1}(2s+1)^{\frac{1}{2}}a_{s+1}H_{2s,1},$$

where $Dp_1=-mg$ is the gravitational force acting on the representative particle. Substituting into (14), we obtain

$$(\partial'n/\partial q_1)=-2h^2nm^2g(1-\gamma+K_r)$$
$$-(2r)^{\frac{1}{2}}2^{-r}a_r(\partial'/\partial q_1)(n\gamma_{2r}), \quad (15)$$

where

$$n\gamma_s=(2^{s/2}N/\mathbf{N})\int\int fH_{s,1}d\omega dQ_1, \quad (16)$$

$\gamma=2^{-\frac{1}{2}}\gamma_2$ and

$$K_r=\sum_{s=2}^{r-1}2^{-s}(2s+1)^{\frac{1}{2}}a_{s+1}\gamma_{2s}. \quad (17)$$

Assuming that h has been chosen such that $2^{-r}r^{\frac{1}{2}}a_r\gamma_{2r}$ approaches zero as r approaches infinity,† then (15) shows that K_r approaches a limit K as r approaches infinity, and since the density n is independent of h and of r, we obtain

$$(\partial n/\partial q_1)=(\partial'n/\partial q_1)=-2h^2nm^2g(1-\gamma+K). \quad (18)$$

In order to obtain an expression for the temperature gradient, we note that the components S_{11}, S_{22}, and S_{33} of the strain tensor, where $S_{ii}=(N/m\mathbf{N})\int\int fp_i^2d\omega dQ_1$, are equal in the case of isotropic conditions. For conditions not too far from isotropism we may approximate nkT by S_{11}, since $3nkT=S_{11}+S_{22}+S_{33}$, and obtain

$$nkT\simeq S_{11}=n(1+\gamma)/(2h^2m). \quad (19)$$

Letting $\phi=p_1$, $D'\phi=-mg$, in (14), we obtain

$$(\partial/\partial q_1)(nkT)=-mgn. \quad (20)$$

Upon eliminating n from (18), (19), and (20), we obtain

$$(\partial T/\partial q_1)=2h^2m^2gT\left[K-\left(\frac{\gamma^2}{1+\gamma}\right)\right]. \quad (21)$$

The difference between expressions (18) and (21) for the density and temperature gradients and the expressions obtained by Jaffé (J, 3.18 and 3.19), may be shown to arise from terms of higher than the third order in the moments in the power series expansion of the distribution function.

If we let

$$D^*=-\left(T\frac{\partial n}{\partial q_1}\right)\Big/\left(n\frac{\partial T}{\partial q_1}\right), \quad (22)$$

and eliminate the density and temperature gradients by means of (18) and (21), we obtain

$$(D^*-1)(1+\gamma)(1-\gamma+K)=D^*. \quad (23)$$

Then, upon using this and (19) to eliminate γ and K from (18) and (21), we obtain

$$(\partial n/\partial q_1)=(nmgD^*)/\{kT(1-D^*)\} \quad (24)$$

and

$$(\partial T/\partial q_1)=-(mg)/\{k(1-D^*)\}. \quad (25)$$

It is to be noted that these expressions are independent of the parameter h used in the Bruns' series expansion of the distribution function. In the cases of isothermal, isochoric, and adiabatic temperature distributions, the dimensionless parameter D^* has the values ∞, 0, and $-c_v/R$, respectively, and (24) and (25) reduce to expressions frequently used in meteorology.

[4] J. Willard Gibbs, *Collected Works* (Longmans, Green and Company, New York, 1931), Vol. II, Pt. 1, pp. 32–45.

† For the canonical distribution function (13), $2^{-r}r^{\frac{1}{2}}a_r\gamma_{2r}=-(1-2h^2mkT)^r$ and the condition is that $0<mkTh^2<1$.

The Viscosity of Concentrated Suspensions and Solutions*

H. C. BRINKMAN
Bosscha Physics Laboratory, University of Indonesia, Bandung, Indonesia
(Received December 3, 1951)

An expression for the viscosity of solutions and suspensions of finite concentration is derived by considering the effect of the addition of one solute-molecule to an existing solution, which is considered as a continuous medium.

IN recent years much attention has been given to the viscosity of concentrated solutions and suspensions. Guth and Simha[1] have derived the quadratic term in the concentration-dependence of the viscosity of suspensions of spherical particles by considering the hydronamic interaction of two spheres as derived by von Smoluchowski.[2] Their derivation, which leads to very involved calculations, seems to contain a numerical error, as was kindly pointed out to me by Dr. Simha.

Riseman and Ullman[3] have derived formulas for the quadratic term in the concentration-dependence of the viscosity for dumbbell, rigid rod, and flexible chain macromolecules.

Burgers and, independently, Saito[4] have developed a theory for spherical solute-molecules in which a single solute-molecule is placed in a field of flow, obtained by averaging over all possible positions of a second solute-molecule. This averaging process, however, leads to diverging integrals which make the result questionable.

In this paper we wish to point out that there is a very simple method of estimating the concentration-dependence of any quantity at higher concentrations if the result for infinite dilution is known. An analogous treatment was given by Onsager in his theory of the dielectric constant.[5]

Let us consider a suspension containing n solute-particles in a total volume V. Its viscosity is a function of the concentration n/V and will be indicated by $\eta(n/V)$.

Let us now consider the effect of adding one more solute-particle. If such a particle were added to a pure solvent of volume V we could immediately give an expression for the viscosity-increase. If the solute-particle has a volume v_0 and a spherical shape, the viscosity would be multiplied by Einstein's well-known factor $(1+2.5v_0/(V+v_0))$.

Let us now assume this factor to be approximately valid for the result of the addition of one solute-molecule to an already existing solution containing n solute-molecules. This means that this solution is represented by a pure solvent of the same viscosity. The assumption would be exact if the n solute particles already present were much smaller than the one added. In our case, however, the substitution of a continuum for the solution is an approximation. In this way we obtain the difference-equation,

$$\eta\left(\frac{n+1}{V+v_0}\right)=\eta\left(\frac{n}{V}\right)\cdot\left(1+\frac{5}{2}\frac{v_0}{V+v_0}\right),$$

which leads to

$$d\eta/dc_v=5\eta/2(1-c_v),$$

where c_v is the concentration by volume nv_0/V and therefore

$$\eta=\eta_0/(1-c_v)^{5/2}.$$

By expansion we find

$$\eta_{sp}/c_w=[\eta]+0.7[\eta]^2c_w+0.42[\eta]^3c_w^2+\cdots,$$

where η_{sp} is the specific viscosity, $[\eta]$ the intrinsic viscosity, and c_w the concentration by weight. For spheres $[\eta]=2.5v_0/M$, where M is the mass of a sphere.

This equation agrees quite well up to the term indicated with very careful measurements on asphalt-emulsions by H. Eilers.[6] Eilers represents his measurements by a formula

$$\eta=\eta_0\left\{1+\frac{1.25c_v}{1-(c_v/0.78)}\right\}^2.$$

This is equivalent to

$$\eta_{sp}/c_w=[\eta]+0.76[\eta]^2c_w+0.64[\eta]^3c_w^2+\cdots.$$

The method discussed here for spherical molecules may of course be applied to any kind of molecules.

* Paper presented at the XIIth Congress of Pure and Applied Chemistry, New York, 1951.
[1] E. Guth and R. Simha, Kolloid Z. **74**, 266 (1936).
[2] M. v. Smoluchowski, Bull. Acad. de Sci. de Cracovie No. 1A (1911).
[3] J. Riseman and R. Ullman, J. Chem. Phys. **19**, 578 (1951).
[4] Private communication by Dr. Simha.
[5] L. Onsager, J. Am. Chem. Soc. **58**, 1986 (1936).
[6] H. Eilers, Kolloid Z. **97**, 313 (1941).

Note on Configuration Probabilities

A. J. F. SIEGERT
Physics Department, Northwestern University, Evanston, Illinois
(Received January 4, 1952)

The series obtained by Goldberger and Adams[1] are derived by a simpler method and generalized to include systems of particles with Bose and Fermi statistics and spin, if spin dependent terms in the Hamiltonian are neglected.

In a recent paper Goldberger and Adams[1] have given series for the probability distributions in configuration space of systems of interacting point particles obeying Boltzmann statistics. These series contain as first terms the results of Wigner[2] and Green.[3] We will first give a very simple derivation which yields the results of Goldberger and Adams in a slightly more convenient form. We will then generalize these results to include systems of particles with Bose or Fermi statistics and spin if the spin-dependent terms in the Hamiltonian can be neglected.

To obtain the series expansions we first derive an integral equation which connects the average density matrix of the system with the average density matrix of a simpler system. The series expansions of Goldberger and Adams are then obtained by solving the integral equation by iteration.

We first consider a system of N point particles obeying Boltzmann statistics with Hamiltonian $\mathcal{H}\equiv\mathcal{H}_0+U(\mathbf{q})$, where $\mathbf{q}$ denotes all the spatial coordinates of all the particles. We define the average density matrix $\rho(\mathbf{q}_0|\mathbf{q},\beta)$, where $\beta=(kT)^{-1}$ and T is the temperature of the system, by

$$\rho(\mathbf{q}_0|\mathbf{q},\beta)=\sum_\nu\psi_\nu(\mathbf{q}_0)e^{-\beta E_\nu}\psi_\nu(\mathbf{q}), \tag{1}$$

where $\psi_\nu(\mathbf{q})$ and E_ν are the eigenfunctions (chosen to be real) and eigenvalues of $\mathcal{H}$ with the boundary condition that $\psi_\nu(\mathbf{q})$ vanishes on the walls of the container. The partition function Q is given by[4] $Q=\int\rho(\mathbf{q}|\mathbf{q},\beta)dq^{3N}$ and the probability for the configurations $\mathbf{q}$ by $Q^{-1}\rho(\mathbf{q}|\mathbf{q},\beta)$. We define further the function $G(\mathbf{q}_0|\mathbf{q},\beta)$

$$G(\mathbf{q}_0|\mathbf{q},\beta)=\sum_\mu\varphi_\mu(\mathbf{q}_0)e^{-\beta W_\mu}\varphi_\mu(\mathbf{q}), \tag{2}$$

where $\varphi_\mu(\mathbf{q})$ and W_μ are the eigenfunctions and eigenvalues of $\mathcal{H}_0$, with the boundary condition that $\varphi_\mu(\mathbf{q})$ vanishes on the walls of the container.

We now consider the integral

$$\begin{aligned}I&=\int_0^\beta dt\int d^{3N}q'G(\mathbf{q}_0|\mathbf{q}',\beta-t)U(\mathbf{q}')\rho(\mathbf{q}'|\mathbf{q},t)\\&=\sum_{\mu\nu}\int_0^\beta dt\int d^{3N}q'\,\varphi_\mu(\mathbf{q}_0)e^{-(\beta-t)W_\mu}\varphi_\mu(\mathbf{q}')\\&\quad\times U(\mathbf{q}')\psi_\nu(\mathbf{q}')e^{-E_\nu t}\psi_\nu(\mathbf{q}).\end{aligned} \tag{3}$$

With

$$\int_0^\beta dt\exp[-(\beta-t)W_\mu-tE_\nu]=(e^{-\beta W_\mu}-e^{-\beta E_\nu})/(E_\nu-W_\mu) \tag{4}$$

and

$$\begin{aligned}&\int d^{3N}q'\varphi_\mu(\mathbf{q}')U(\mathbf{q}')\psi_\nu(\mathbf{q}')\\&\quad=\int d^{3N}q'\varphi_\mu(\mathbf{q}')(\mathcal{H}-\mathcal{H}_0)\psi_\nu(\mathbf{q}')\\&\quad=(E_\nu-W_\mu)\int d^{3N}q'\varphi_\mu(\mathbf{q}')\psi_\nu(\mathbf{q}'),\end{aligned} \tag{5}$$

we have

$$\begin{aligned}I&=\sum_{\mu\nu}\varphi_\mu(\mathbf{q}_0)(e^{-\beta W_\mu}-e^{-\beta E_\nu})\\&\quad\times\int d^{3N}q'\varphi_\mu(\mathbf{q}')\psi_\nu(\mathbf{q}')\psi_\nu(\mathbf{q})\\&=\int G(\mathbf{q}_0|\mathbf{q}',\beta)d^{3N}q'\textstyle\sum_\nu\psi_\nu(\mathbf{q}')\psi_\nu(\mathbf{q})\\&\quad-\int\textstyle\sum_\mu\varphi_\mu(\mathbf{q}_0)\varphi_\mu(\mathbf{q}')d^{3N}q'\rho(\mathbf{q}'|\mathbf{q},\beta)\end{aligned} \tag{6}$$

and

$$\begin{aligned}&\int_0^\beta dt\int d^{3N}q'G(\mathbf{q}_0|\mathbf{q}',\beta-t)U(\mathbf{q}')\rho(\mathbf{q}'|\mathbf{q},t)\\&\quad=G(\mathbf{q}_0|\mathbf{q},\beta)-\rho(\mathbf{q}_0|\mathbf{q},\beta).\end{aligned} \tag{7}$$

After solving the integral Eq. (7) by iteration we obtain the series

$$\begin{aligned}\rho(\mathbf{q}_0|\mathbf{q},\beta)&=G(\mathbf{q}_0|\mathbf{q},\beta)\\&\quad-\int_0^\beta dt_1\int d^{3N}q_1G(\mathbf{q}_0|\mathbf{q}_1,\beta-t_1)U(\mathbf{q}_1)G(\mathbf{q}_1|\mathbf{q},t_1)\\&\quad+\int_0^\beta dt_1\int d^{3N}q_1\int_0^{t_1}dt_2\int d^{3N}q_2G(\mathbf{q}_0|\mathbf{q}_1,\beta-t_1)\\&\quad\times U(\mathbf{q}_1)G(\mathbf{q}_1|\mathbf{q}_2,t_1-t_2)U(\mathbf{q}_2)G(\mathbf{q}_2|\mathbf{q},t_2)-\cdots.\end{aligned} \tag{8}$$

[1] M. L. Goldberger and E. N. Adams II, J. Chem. Phys. **20**, 240 (1952).
[2] E. P. Wigner, Phys. Rev. **40**, 749 (1932).
[3] H. S. Green, J. Chem. Phys. **19**, 955 (1951).
[4] All integrations over the coordinates of the particles extend over the container.

If $\mathcal{H}_0$ is the Hamiltonian for free particles

$$\mathcal{H}_0 = -(\hbar^2/2m)\sum_j(\partial^2/\partial q^{(j)2}),$$

and if the linear dimensions of the container are large compared with $(\hbar^2\beta/m)^{\frac{1}{2}}$, one may with negligible error use for $G(\mathbf{q}_0|\mathbf{q}, t)$ the approximation

$$G(\mathbf{q}_0|\mathbf{q}, t) \cong (2\pi\hbar^2 t/m)^{-3N/2} \exp\{-m(\mathbf{q}-\mathbf{q}_0)^2/2\hbar^2 t\} \quad (9)$$

and extend convergent integrals over all of $\mathbf{q}$ space.

The series (8) then beomes for $\mathbf{q}_0=\mathbf{q}$ equal to the series of Goldberger and Adams. One sees in our form that the integrations over t_k are folding integrals which can be reduced to one integration by going to the Laplace transform.

The expansion in the neighborhood of the classical value is obtained by a similar procedure. We have the integral equation

$$\rho(\mathbf{q}_0|\mathbf{q}, \beta) = e^{-\beta U}\Big[G(\mathbf{q}_0|\mathbf{q}, \beta) - \int_0^\beta dt e^{tU}\int d^{3N}q' G(\mathbf{q}_0|\mathbf{q}', \beta-t) \cdot (U(\mathbf{q}')-U)\rho(\mathbf{q}'|\mathbf{q}, t)\Big], \quad (10)$$

where U may be $U(\mathbf{q}_0)$ or $U(\mathbf{q})$ or any other value independent of $\mathbf{q}'$ and t. Eq. (10) is obtained by the same method as Eq. (7). By iteration we get, choosing $U=U(\mathbf{q})$, the series

$$\begin{aligned}\rho(\mathbf{q}_0|\mathbf{q}, \beta) = e^{-\beta U(\mathbf{q})}\Big[&G(\mathbf{q}_0|\mathbf{q}, \beta) \\ &- \int_0^\beta dt_1 \int d^{3N}q_1 G(\mathbf{q}_0|\mathbf{q}_1, \beta-t) \\ &\times (U(\mathbf{q}_1)-U(\mathbf{q}))G(\mathbf{q}_1|\mathbf{q}, t) \\ &+ \int_0^\beta dt_1 \int d^{3N}q_1 \int_0^{t_1} dt_2 \int d^{3N}q_2 G(\mathbf{q}_0|\mathbf{q}_1, \beta-t_1) \\ &\times (U(\mathbf{q}_1)-U(\mathbf{q}))G(\mathbf{q}_1|\mathbf{q}_2, t_1-t_2) \\ &\times (U(\mathbf{q}_2)-U(\mathbf{q}))G(\mathbf{q}_2|\mathbf{q}, t_2) - \cdots\Big]. \end{aligned} \quad (11)$$

Wigner's correction terms are obtained from the second and third terms of this series by expanding $U(\mathbf{q}_1)-U(\mathbf{q})$ and $U(\mathbf{q}_2)-U(\mathbf{q})$ in power series up to second-degree terms and using Eq. (9).

The integral equation and the series expansions following from it can be easily generalized to include particles with spin and Bose or Fermi statistics. We denote by $\mathbf{s}$ the spin-coordinates of all particles and define

$$\rho(\mathbf{q}_0, \mathbf{s}_0|\mathbf{q}, \mathbf{s}; \beta) = \sum_\nu{}'\psi_\nu(\mathbf{q}_0, \mathbf{s}_0)e^{-\beta E_\nu}\psi_\nu(\mathbf{q}, \mathbf{s}) \quad (12)$$

$$G(\mathbf{q}_0, \mathbf{s}_0|\mathbf{q}, \mathbf{s}; \beta) = \sum_\mu{}'\varphi_\mu(\mathbf{q}_0, \mathbf{s}_0)e^{-\beta W_\mu}\varphi_\mu(\mathbf{q}, \mathbf{s}), \quad (13)$$

where the prime indicates summation over symmetric or antisymmetric functions only. We neglect in what follows spin dependent terms in the Hamiltonians and define $\psi_\nu(\mathbf{q}, \mathbf{s})$ and E_ν, and $\varphi_\mu(\mathbf{q}, \mathbf{s})$ and W_μ as the eigenfunctions and eigenvalues of the spin-independent Hamiltonians $\mathcal{H}_0+U(\mathbf{q})$ and $\mathcal{H}_0$, respectively. We then obtain as before

$$\begin{aligned}&\int_0^\beta dt \sum_{s'}\int d^{3N}q' \\ &\quad\times G(\mathbf{q}_0, \mathbf{s}_0|\mathbf{q}', \mathbf{s}'; \beta-t)U(\mathbf{q}')\rho(\mathbf{q}', \mathbf{s}'|\mathbf{q}, \mathbf{s}; t) \\ &\quad= \sum_\mu{}'\sum_\nu{}'\varphi_\mu(\mathbf{q}_0, \mathbf{s}_0)(e^{-\beta W_\mu}-e^{-\beta E_\nu}) \\ &\quad\times \sum_{s'}\int d^{3N}q'\varphi_\mu(\mathbf{q}', \mathbf{s}')\psi_\nu(\mathbf{q}', \mathbf{s}')\psi_\nu(\mathbf{q}, \mathbf{s}). \end{aligned} \quad (14)$$

The expression

$$\sum_{s'}\int d^{3N}q'\varphi_\mu(\mathbf{q}'\mathbf{s}')\psi_\nu(\mathbf{q}'\mathbf{s}')$$

vanishes unless φ_μ and ψ_ν are of the same symmetry, and we can therefore sum over all states ν in the first term and over-all states μ in the second term and obtain δ-functions. We thus get the integral equation

$$\begin{aligned}&\int_0^\beta dt \sum_{s'}\int d^{3N}q' \\ &\quad\times G(\mathbf{q}_0, \mathbf{s}_0|\mathbf{q}', \mathbf{s}'; \beta-t)U(\mathbf{q}')\rho(\mathbf{q}', \mathbf{s}'|\mathbf{q}, \mathbf{s}; t), \\ &\quad= G(\mathbf{q}_0, \mathbf{s}_0|\mathbf{q}, \mathbf{s}; \beta) - \rho(\mathbf{q}_0, \mathbf{s}_0|\mathbf{q}, \mathbf{s}; \beta), \end{aligned} \quad (15)$$

from which a series expansion is obtained by iterations.

We would like to thank Dr. Goldberger for an interesting discussion and an advance copy of the paper by Goldberger and Adams.

Kinetics of the Decomposition of Diethyl Peroxide*

RICHARD E. REBBERT† AND KEITH J. LAIDLER
Department of Chemistry, The Catholic University of America, Washington, D. C.
(Received December 17, 1951)

The kinetics of the gas-phase decomposition of diethyl peroxide have been studied in a flow system, using excess of toluene. The main reaction products were found to be ethane and formaldehyde, and there were smaller amounts of methane and dibenzyl. The frequency factor of the reaction is 2.1×10^{13}, and the activation energy is 31.7 kcal per mole. The mechanism of the reaction is discussed, and it is shown that the measured rate must refer to the initial dissociation $C_2H_5OOC_2H_5\rightarrow 2C_2H_5O$. With a new value of 47.8 kcal for the heat of formation of gaseous diethyl peroxide, the heat of formation of the C_2H_5O radical is calculated to be 8.1 kcal, which agrees satisfactorily with estimates from other kinetic data. Thermochemical values for other reactions involving this radical are calculated.

STUDIES of the kinetics of the decompositions of peroxides have a special interest in that they provide dissociation energies for O—O bonds in these compounds and enable heats of formation of the alkoxy radicals to be calculated. The main work of this type so far carried out has been on di-t-butyl peroxide[1,2] for which dissociation energies of 39.1[1] and 36.0[2] kcal have been obtained. The decomposition of diethyl peroxide was studied in a static system by Harris and Egerton,[3] and an activation energy of 31.5 kcal was obtained. These authors concluded the reaction to be a nonchain process at lower temperatures, and the present work substantiates this view. This conclusion was not entirely certain, however, particularly as the reaction became explosive at higher temperatures. A further reason for suspecting the conclusion that 31.5 kcal represented the dissociation energy of the O—O bond was that this assumption led to a heat of formation for the radical C_2H_5O that was inconsistent with other values; this latter difficulty we have, however, traced to an error in the value for the heat of formation of the peroxide itself.[4] Walsh[5] in particular has proposed that the O—O dissociation energy in diethyl peroxide is very much greater than 31.5 kcal; the present work, however, does not support this interpretation.

With a view to establishing with more certainty the heat of dissociation of the peroxide, we have made a study of its decomposition in a flow system with excess of toluene, using the method introduced by Szwarc.[6]

TABLE I. Mass spectrographic analysis pattern of diethyl peroxide.

m/e	pattern	m/e	pattern
14	13.03	31	33.21
15	42.49	43	20.65
26	7.95	44	11.04
27	21.72	45	31.00
28	7.90	62	18.55
29	100.00	90	11.15
30	8.99		

EXPERIMENTAL

Preparation of Diethyl Peroxide

Diethyl peroxide was prepared by the method of Baeyer and Villiger[7] as modified by Harris and Egerton.[3] The crude product was first vacuum distilled to remove all volatile products which were then distilled at atmospheric pressure and the fraction from 60–70°C was collected. This was washed with sodium hydroxide solution and dried with potassium carbonate. It was then redistilled and the fraction from 63–67°C was retained. It was washed again with sodium hydroxide and dried with potassium carbonate and redistilled, the final distillation range being 64.3–65.3°C.

To test the purity of the compound a mass spectrographic analysis was made.* The main peaks are shown in Table I; peaks which were less than 5 percent of the highest peak are omitted. The absolute purity of the sample could not be determined since there is no standard of diethyl peroxide with which to compare it. However, the lack of any appreciable peak at 17 *m/e* indicates the absence of any alcohol or hydroperoxide. Also, the lack of any appreciable peak at 74 *m/e* indicates the absence of diethyl ether. The index of refraction of the compound was taken at various temperatures and the results are given in Table II along with the results given in the literature.

The toluene used was from Mallinckrodt Chemical Works, analytical reagent grade (meets A.C.S. specifications).

* Abstracted from a dissertation presented by Richard E. Rebbert to the Graduate School of the Catholic University of America, in partial fulfillment of the requirements for the degree of Doctor of Philosophy in Chemistry.

† Present address: Division of Chemistry, National Research Council, Ottawa, Canada.

[1] Raley, Rust, and Vaughan, J. Am. Chem. Soc. **70**, 88 (1948); Rust, Seabold, and Vaughan, J. Am. Chem. Soc. **70**, 95 (1948).

[2] Muraski, Szwarc, and Roberts, J. Chem. Phys. **19**, 698 (1951).

[3] E. J. Harris and A. C. Egerton, Proc. Roy. Soc. (London) **A168**, 1 (1938).

[4] E. C. Stathis and A. C. Egerton, Trans. Faraday Soc. **36**, 606 (1940).

[5] A. D. Walsh, J. Chem. Soc., 331 (1948); Trans. Faraday Soc. **42**, 264 (1946).

[6] M. Szwarc, J. Chem. Phys. **16**, 128 (1948); **17**, 431 (1949).

[7] A. von Baeyer and V. Villiger, Ber. deut. chem. Ges. **B33**, 3387 (1900).

* Courtesy of the National Bureau of Standards.

TABLE II. Index of refraction of diethyl peroxide.

Temperature	9.5°C	15°C	16.5°C	20°C
Observed	1.3752	1.3720	1.3718	1.3700
Literature	1.3758	1.3712	1.3715	1.3698

Kinetic Procedure

The apparatus, which is similar to that used by Szwarc,[6] is shown in Fig. 1. Toluene was introduced through the capillary K_2 from flask V_1 which was maintained at constant temperature. Stopcocks S_1 and S_2 and the intervening tubing were heated to about 80°C with nichrome wire in order to prevent any condensation of toluene; Dow-Corning High Vacuum grease was used in this part of the system. The peroxide was introduced through capillary K_1 from flask V_2 which is also surrounded by a constant temperature bath. The gases were passed through a spiral R which was maintained at constant temperature in a thermostatically controlled furnace. The temperature of the furnace was measured using an iron-constantan thermocouple. The first trap after the furnace, T_1, was surrounded with dry ice-acetone and condensed most of the toluene and undecomposed peroxide. The second trap T_2 was immersed in liquid nitrogen and retained the ethane and formaldehyde. The mercury diffusion pump P was capable of maintaining a steady pumping speed even when stopcock S_9 was closed and a small methane pressure built up in the vessel V_3.

Before starting a run, flasks V_1 and V_2 were weighed. They were then inserted into the system and the contents repeatedly frozen in liquid nitrogen, evacuated, and melted. Every 15 minutes during a run the pressure was read on manometer M_1 using a traveling telescope and was usually constant to 0.2 mm. The toluene, peroxide, ethane, and formaldehyde were condensed in traps T_1 and T_2, while the methane formed went into the storage vessel V_3 and its amount was determined at the end of the run. The storage vessel was then evacuated and a liquid nitrogen trap was placed around trap T_4. Stopcock S_7 was opened and a liquid ethylene trap replaced the liquid nitrogen trap about T_2. After about 15 minutes stopcock S_7 was closed and the liquid nitrogen was removed from trap T_4. The temperature and pressure of ethane and formaldehyde were measured. Finally, flasks V_1 and V_2 were removed and reweighed in order to determine the amounts of toluene and peroxide that went through the furnace. The total volume of gas that went through the furnace could be calculated from the total number of moles of toluene and peroxide and the pressure and temperature of the furnace. The contact time was then determined from this total volume passed, the volume of the furnace, and the time in which it passed. From the contact time, the amount of peroxide passed, and the amount decomposed (see later), the specific rate at the temperature of the furnace was calculated using the first-order rate equation.

RESULTS

The main products of the reaction were found to be ethane and formaldehyde, and much smaller amounts of methane and dibenzyl were found. Some polymerization of the formaldehyde occurred in the traps; the polymer was a white solid which gave the Tollen and Fehling tests. The reaction rate was calculated from the amount of ethane formed plus one-half of the amount of methane; the justification for this is given in the next section. To determine the amount of ethane from the combined pressures of ethane and formaldehyde a correction had to be made for the amount of polymerization. It was estimated that 20 percent of the formaldehyde polymerized. The error in activation energy arising from inaccuracy in this figure is only slight; thus even taking the extreme cases of zero and 100 percent polymerization, the inaccuracy is only ±2 kcal, and therefore is, in fact, very much smaller than this.

The results are summarized in Table III. The rate constants are shown plotted against $1/T$ in Fig. 2. The activation energy is found to be 31.7±1 kcal, and the frequency factor is 2×10^{13} sec^{-1}. The latter value is consistent with the values found by Szwarc[5] for reactions of this type, including the di-*t*-butyl peroxide reactions.[2] The activation energy is in excellent agreement with the value (31.5 kcal) given by Harris and Egerton[3] for the over-all process in a static system.

DISCUSSION

Kinetic Mechanism

The products obtained for this reaction indicate that the main processes are

$$C_2H_5OOC_2H_5 \rightarrow 2C_2H_5O, \quad (1)$$

$$C_2H_5O \rightarrow CH_3 + CH_2O, \quad (2)$$

$$2CH_3 \rightarrow C_2H_6. \quad (3)$$

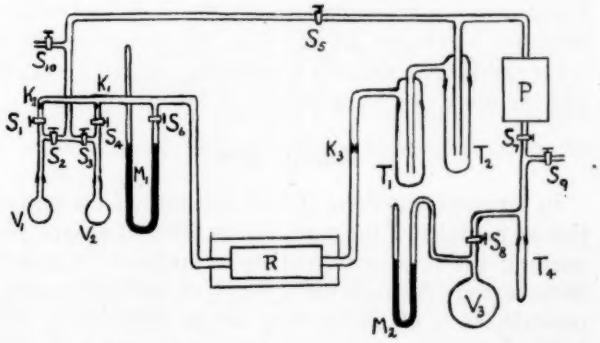

FIG. 1. Schematic diagram of apparatus. The stopcock S_9 is connected to the forepump, S_{10} to a McLeod gauge.

[5] M. Szwarc, Chem. Revs. 47, 75 (1950).

TABLE III. Summary of results.

T°C	Total pressure (mm)	Ratio toluene peroxide	Contact time (sec)	% decomp	$k\times10^2$ (sec^{-1})
239	12.15	68/1	0.863	31	42.4
245	12.62	74/1	0.850	42	64.3
234	12.51	76/1	0.858	26	35.0
234	12.05	73/1	0.857	28	38.6
218	11.91	73/1	0.894	10	14.7
213	10.91	74/1	0.893	6	6.63
210	11.13	78/1	0.888	7	8.30
206	11.99	91/1	0.900	6	6.41
242	12.01	84/1	0.832	24	57.4
226	12.04	89/1	0.856	17	22.3
241	11.48	78/1	0.850	39	57.6
200	11.39	79/1	0.914	3	3.58
210	11.53	77/1	0.910	6	6.76

In addition the reactions

$$CH_3+C_6H_5CH_3\rightarrow CH_4+C_6H_5CH_2 \quad (4)$$

$$2C_6H_5CH_2\rightarrow C_6H_5CH_2CH_2C_6H_5 \quad (5)$$

must occur to a small extent to account for the fact that methane and dibenzyl are minor products. The fact that no ethyl alcohol is formed shows that reaction (2) is more rapid than the process $C_2H_5O+C_6H_5CH_3\rightarrow C_2H_5OH+C_6H_5CH_2$. The small amounts of dibenzyl formed are consistent with the result[9] that the activation energy of (4) is 8.3 kcal higher than that of (3); dibenzyl will therefore only be formed in large amounts at higher reaction temperatures.

The reaction under our conditions is much simpler than as studied by Harris and Egerton[3] who found appreciable amounts of acetaldehyde, ethyl alcohol, and carbon monoxide in addition to the products we obtained. These products are presumably formed by the following reactions:

$$C_2H_5O+C_2H_5OOC_2H_5\rightarrow C_2H_5OH+CH_3CHOOC_2H_5 \quad (6)$$

$$CH_3CHOOC_2H_5\rightarrow CH_3CHO+C_2H_5O \quad (7)$$

$$CH_3CHO\rightarrow CH_4+CO \text{ via chain processes.} \quad (8)$$

The absence of these complicating reactions in our investigation is to be attributed to the very low peroxide pressures employed, so that the bimolecular reactions occur slowly; reaction (3) is probably a surface reaction and therefore can occur readily at low pressures.

Kinetic Law

In terms of reactions (1)–(5) the rate of decomposition of peroxide is the rate of formation of ethane plus one-half the rate of formation of methane; this is so because every peroxide molecule gives rise to two methyl radicals, each of which may either dimerize to give $1/2C_2H_6$ or may react with toluene to give CH_4. The rates given in Table III are in fact determined in this way. Since diethyl peroxide only disappears by reaction (1), the over-all rate is

$$-\frac{d[C_2H_5OOC_2H_5]}{dt}=k_1[C_2H_5OOC_2H_5],$$

so that the over-all activation energy is applicable to reaction (1).

The O–O Dissociation Energy

The activation energy of 31.7 kcal for reaction (1) is almost certainly the energy of dissociation of the O–O bond in the peroxide, since the activation energy of the reverse reaction is probably zero. It is of interest to compare this value with that for other O–O bonds, the values for which are as follows:

$D(HO-OH)=54$ kcal per mole
$D(C_2H_5O-OC_2H_5)=31.7$ kcal per mole
$D(C_3H_7O-OC_3H_7)=35$ kcal per mole
$D((CH_3)_3CO-OC(CH_3)_3)=36$, 39 kcal per mole.

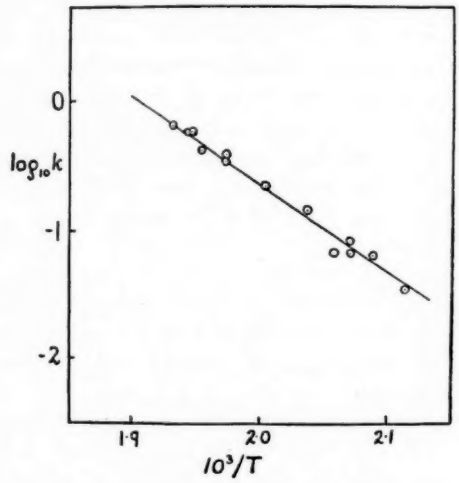

FIG. 2. Plot of $\log_{10}k$ *vs* $1/T$. The least squares activation energy is 31.7 kcal per mole.

Thermochemistry of the C_2H_5O Radical

Assuming the activation energy of 31.7 kcal to be the energy of dissociation of the O–O bond, the heat of formation of the C_2H_5O radical can be calculated provided that for the peroxide is known. Stathis and Egerton's value[4] of 68.0 for the liquid peroxide gave rise to inconsistent results (see below), and we arranged for a redetermination of the heat of combustion to be carried out on our sample; this was very kindly done by Mr. F. A. Zihlman at the U. S. Naval Powder Factory at Indian Head, Maryland. His value (662.2 kcal per mole) leads to 55.6 kcal per mole for the heat of formation of the liquid peroxide, and a correction based on Trouton's rule gives 47.8 kcal for the gaseous substance. The heat of formation for C_2H_5O calculated from this value is 8.1 kcal per mole.

[9] A. F. Trotman-Dickenson and E. W. R. Steacie, J. Chem. Phys. 19, 329 (1951).

Values for this quantity may also be calculated from other data. The activation energy of 37.7 kcal for the decomposition of ethyl nitrite[10] is almost certainly the dissociation energy of the N—O bond in the molecule, and heats of formation are available for the nitrite and for nitric oxide. Two activation energies, 34.6 and 39.9 kcal, have been obtained for the decomposition of ethyl nitrate,[11,12] and these again almost certainly correspond to the dissociation energy of the bond. Unfortunately, the heat of formation of the nitrate is not certain since various values have been quoted.

In Table IV are presented a number of possible combinations of values for the peroxide, nitrite, and nitrate data; the value for the heat of formation of the C_2H_5O radical is given in each case. The value obtained on the basis of the Stathis-Egerton heat of formation of the peroxide is seen to be much higher than the remaining values. The value of 8.1 from the peroxide work agrees satisfactorily with that from the nitrite study. It also

TABLE IV. Data for reactions $C_2H_5OX \rightarrow C_2H_5O+X$.

X	$Q_f(C_2H_5OX)$	$Q_f(X)$	D	$Q_f(C_2H_5O)$
C_2H_5O	47.8[a]	...	31.7[b]	8.1[l]
C_2H_5O	60.2[c]	...	31.7[b]	14.3
NO	25.9[b]	−21.6[c]	37.7[f]	9.8[l]
NO_2	33.4[d]	−8.0[g]	34.6[h]	6.8
NO_2	33.4[d]	−8.0[g]	39.9[i]	1.5
NO_2	34.9[j]	−8.0[g]	34.6[h]	8.3[l]
NO_2	34.9[j]	−8.0[g]	39.9[i]	3.0
NO_2	35.8[k]	−8.0[g]	34.6[h]	9.2[l]
NO_2	35.8[k]	−8.0[g]	39.9[i]	3.9

[a] F. A. Zihlman (private communication).
[b] Present investigation.
[c] E. C. Stathis and A. C. Egerton, Trans. Faraday Soc. **36**, 606 (1940); value corrected for the gaseous peroxide.
[d] J. Thomsen, *Thermochemische Untersuchungen* (Barth, Leipzig, 1882–6).
[e] M. P. E. Barthelot, Ann. chim. et phys. (5) **20**, 255 (1880).
[f] E. W. R. Steacie and S. Katz, J. Chem. Phys. **5**, 125 (1937).
[g] M. Randall, *International Critical Tables*, Vol. VII, p. 239.
[h] L. Phillips, Nature **160**, 753 (1947).
[i] G. K. Adams and C. E. H. Bawn, Trans. Faraday Soc. **45**, 494 (1949).
[j] E. Schmidt, Z. ges. Schiess-u. Sprengstoffw. **29**, 262 (1934).
[k] Landolt-Bornstein, *Physik. Chem. Tabellen*, **II**, 1619.
[l] These values are mutually consistent within experimental error.

agrees well with the results of the nitrate work, provided that Phillips's activation energy is used. The Adams and Bawn activation energy seems to be too high to give agreement using any of the heats of formation for the nitrate. The values marked with an asterisk in Table IV are the ones that appear to be most mutually consistent.

By assuming the heat of formation of C_2H_5O to be 8.1 kcal, other interesting heats of dissociation can be deduced. Those for C_2H_5O-H, $CH_3CO-OC_2H_5$, and

[10] E. W. R. Steacie and S. Katz, J. Chem. Phys. **5**, 125 (1937).
[11] L. Phillips, Nature **160**, 753 (1947).
[12] G. K. Adams and C. E. H. Bawn, Trans. Faraday Soc. **45**, 494 (1949).

TABLE V. Derived heats of dissociation.

Dissociation $AB \rightarrow A+B$	Heats of formation AB	A	B	Heats of dissociation kcal per mole
$C_2H_5OH \rightarrow C_2H_5O+H$	57.0[a]	8.1[b]	−51.9[a]	100.8
$C_2H_5OC_2H_5 \rightarrow C_2H_5O+C_2H_5$	59.6[e]	8.1[b]	−26.0[d]	77.5
$C_2H_5OH \rightarrow C_2H_5+OH$	57.0[a]	−26.0[d]	−10.0[a]	93.0
$CH_3COOC_2H_5 \rightarrow CH_3CO+C_2H_5O$	106.6[e]	6.6[d]	8.1[b]	91.9
$C_2H_5O \rightarrow CH_3+CH_2O$	8.1[b]	−31.0[d]	28.7[a]	10.4
$C_2H_5O \rightarrow C_2H_5+O$	8.1[b]	−26.0[d]	−59.2[a]	93.3
$C_2H_5O \rightarrow H+CH_3CHO$	8.1[b]	−51.9[a]	44.0[a]	16.0

[a] F. D. Rossini *et al.*, "Selected values of properties of hydrocarbons," Natl. Bur. Standards.
[b] Present investigation.
[c] F. Stohmann, J. prakt. Chem. (2) **35**, 40, 136 (1887).
[d] E. Butler and M. Polanyi, Trans. Faraday Soc. **39**, 19 (1943).
[e] E. Schjanberg, Z. physik. Chem. **A172**, 197 (1935).

CH_3-CH_2O, together with related dissociations, are given in Table V. The value of 10.4 for the reaction $C_2H_5O \rightarrow CH_3+CH_2O$ clearly places a lower limit on the activation energy of this reaction which plays a part in many reaction mechanisms.

The low value of 77.5 kcal for the dissociation $C_2H_5OC_2H_5 \rightarrow C_2H_5O+C_2H_5$ is of special interest in that it suggests that this reaction will be the first step in the decomposition of the ether; the alternative process $C_2H_5OC_2H_5 \rightarrow CH_3+CH_2OC_2H_5$ proposed by Rice and Herzfeld[13] probably has a higher dissociation energy. The mechanism for the decomposition is thus probably

$$C_2H_5OC_2H_5 \rightarrow C_2H_5O+C_2H_5$$
$$C_2H_5O \rightarrow CH_2O+CH_3$$
$$C_2H_5+CH_3CH_2OC_2H_5 \rightarrow C_2H_6+CH_3CHOC_2H_5$$
$$CH_3+CH_3CH_2OC_2H_5 \rightarrow CH_4+CH_3CHOC_2H_5$$
$$CH_3CHOC_2H_5 \rightarrow CH_3CHO+C_2H_5.$$

If chain ending occurs mainly by recombination of CH_3 and C_2H_5 with $CH_3CHOC_2H_5$, the kinetics are first order in agreement with experiment.[14] This scheme seems preferable to that of Rice and Herzfeld in avoiding the unlikely step

$$CH_3+C_2H_5OC_2H_5 \rightarrow C_2H_6+CH_2OC_2H_5.$$

ACKNOWLEDGMENT

The authors are indebted to the Mass Spectroscopy Section of the National Bureau of Standards for their analysis of the diethyl peroxide. They are also grateful to Mr. F. A. Zihlman of the U. S. Naval Powder Factory, Indian Head, Maryland, for measuring the heat of combustion of the peroxide and for advice on various thermochemical matters.

[13] F. O. Rice and K. F. Herzfeld, J. Am. Chem. Soc. **56**, 284 (1934).
[14] K. J. Laidler, *Chemical Kinetics* (McGraw-Hill Book Company, Inc., New York, 1950), pp. 269–270.

The Reaction of Methyl Radicals with Some Halogenated Methanes

F. A. RAAL* AND E. W. R. STEACIE
Division of Chemistry, National Research Council, Ottawa, Canada

(Received December 7, 1951)

The reactions of methyl radicals formed by the photolysis of acetone with several halogenated methanes have been investigated between 110°C and 220°C. The activation energies of these reactions have been determined relative to the activation energy of the combination of methyl radicals and are found to be (in kcal): methyl fluoride 8.7, methylene fluoride 6.2, methyl chloride 9.4, methylene chloride 7.2, chloroform 5.8, methyl bromide 10.1, methylene bromide 8.7. The steric factors of the reactions are in the range 10^{-2}–10^{-4}.

INTRODUCTION

THIS paper is a continuation of the quantitative survey of the reactions of methyl radicals with various compounds[1] and the experiments described here were carried out to determine the rate of abstraction of hydrogen atoms, by methyl, from a series of halogenated methanes. The methyl radicals were produced in the photolysis of acetone at temperatures above 100°C in which case the production of methane and ethane is compatible with the reactions:

$$CH_3+CH_3=C_2H_6, \tag{2}$$

$$CH_3+CH_3COCH_3=CH_4+CH_2COCH_3. \tag{3}$$

If R_{CH_4} and $R_{C_2H_6}$ are the rates of formation of methane and ethane, respectively, $[CH_3]$ and $[CH_3COCH_3]$ the concentrations of methyl and acetone, and k_2 and k_3 the rate constants corresponding to reactions (2) and (3), it follows that

$$k_3/k_2^{\frac{1}{2}}=R_{CH_4}/R_{C_2H_6}^{\frac{1}{2}}\cdot[CH_3COCH_3].$$

In the presence of a compound containing hydrogen, RH, methane is most likely also produced by the reaction

$$CH_3+RH=CH_4+R. \tag{1}$$

If k_1 is the rate constant for this reaction and $[RH]$ the corresponding concentration, it can be shown that

$$k_1/k_2^{\frac{1}{2}}=R_{CH_4}/R_{C_2H_6}^{\frac{1}{2}}\cdot\frac{1}{[RH]}-k_3/k_2^{\frac{1}{2}}\cdot\frac{[CH_3COCH_3]}{[RH]}.$$

Since we can obtain a value for $k_3/k_2^{\frac{1}{2}}$ by the photolysis of acetone alone at any temperature, it is possible, by using this relation, to determine $k_1/k_2^{\frac{1}{2}}$.

TABLE I. The photolysis of acetone alone.

Temp. (°K)	Acetone concentration (molecules/cc $\times10^{-18}$)	Time (sec)	Products (molecules/cc $\times10^{-16}$) CO	Methane	Ethane	$k_3/k_2^{\frac{1}{2}}\times10^{12}$
			No filter			
488	1.90	1800	21.0	11.0	8.52	46.5
405	2.25	1800	18.2	2.29	14.0	6.40
565	1.51	1200	21.6	14.4	2.61	170
439	2.10	1800	17.8	4.71	12.3	15.1
532	1.75	1800	18.5	17.0	4.10	114
434	2.24	1800	5.66	2.56	3.41	14.6
			Filter No. 1			
456	2.10	5400	6.82	7.02	2.89	26.8
400	2.27	5400	4.56	2.05	3.88	6.24
493	1.97	5400	5.23	9.32	1.14	60.3
425	2.26	5400	4.89	3.41	2.95	12.0
431	2.18	1800	16.1	5.23	13.9	15.2
523	1.71	1800	18.0	17.0	5.11	104

EXPERIMENTAL

Apparatus

The light source was a Hanovia *S*-500 medium pressure arc and was operated with a constant current of 9.6 amp through the primary of the lamp transformer. The light from the arc was roughly collimated by a highly polished aluminum cylinder having approximately the same diameter as the reaction vessel.

The volume of the light beam within the reaction cell was 120 cc, and this volume has been used throughout in the calculation of the rate constants. The volume of the vessel was only slightly greater than that of the beam (the beam passed within 2–3 mm of the walls), so that no appreciable change would result if the cell volume were used in the calculations instead of the light volume. The following filters were periodically included in the optical system:

Filter 1: A Corning 9–54 filter with a cutoff below 2200A.
Filter 2: A Corning 9–53 filter with a cutoff below about 2700A.

In the case of each halide used, blank experiments were made to ensure that no direct photolysis occurred, and this factor governed the choice of filter in each case.

The cylindrical silica reaction vessel was contained in an aluminum block furnace whose temperature was maintained constant to within ±0.5°C during each run by manual control. The furnace was made to slide on a rail to facilitate removal of the reaction vessel when necessary.

The analysis system was of the conventional type and included a modified Ward still,[2] McLeod gauge, Toepler

* National Research Council of Canada Postdoctorate Fellow, 1950–51.

[1] A. F. Trotman-Dickenson and E. W. R. Steacie, J. Chem. Phys. **18**, 1097 (1950); **19**, 169, 329 (1951); Trotman-Dickenson, Birchard, and Steacie, J. Chem. Phys. **19**, 163 (1951).

[2] D. J. LeRoy, Can. J. Research **B28**, 492 (1950).

TABLE II. The reaction of methyl radicals with halogenated methanes.

Temp. (°K)	Concentration (molecules/cc ×10⁻¹⁷) Acetone	RH	Time (sec)	Products (molecules/cc ×10⁻¹⁶) CO	Methane	Ethane	$k_1/k_2^{\frac{1}{2}}$ ×10¹³
			Acetone-methyl fluoride no filter				
431	22.3	22.1	3600	10.3	9.66	5.97	16.8
484	19.6	19.8	3600	10.7	15.2	1.93	48.9
398	23.8	24.4	3600	9.77	4.42	6.70	6.64
451	21.0	20.8	3600	10.2	10.9	3.92	23.4
415	22.6	23.3	3600	9.66	5.94	4.88	11.0
			Acetone-methylene fluoride no filter				
434	22.2	22.1	3600	9.66	7.95	4.71	13.7
402	23.6	23.7	3600	8.97	4.77	5.45	8.60
446	21.3	21.5	3600	9.54	8.44	3.26	17.4
410	23.3	23.5	3600	8.75	5.30	5.02	9.47
465	20.6	20.6	3600	9.88	10.5	2.47	25.0
421	22.7	22.7	3600	9.09	6.11	3.96	12.4
			Acetone-methyl chloride no filter				
436	22.1	21.6	5400	9.77	8.24	2.82	16.5
480	19.4	20.3	5400	8.63	13.1	0.97	50.5
413	22.0	23.2	5400	7.16	5.79	3.64	10.2
454	20.0	21.2	5400	7.38	10.2	1.59	30.3
400	23.3	23.9	5400	6.48	4.74	4.18	7.50
			Acetone-methylene chloride filter No. 1				
433	21.5	4.25	5400	5.00	5.85	2.90	40.5
402	23.1	5.66	5400	5.00	3.98	3.98	23.6
484	19.8	3.60	5400	5.00	8.97	0.91	104
414	22.1	4.56	5400	4.77	4.09	3.24	27.5
453	21.1	3.95	5400	4.66	6.82	1.65	63.4
			Acetone-chloroform filter No. 1				
432	22.1	4.10	5400	4.20	5.86	2.27	56.1
405	23.9	3.71	5400	3.75	3.75	3.01	38.6
444	21.8	4.04	5400	3.41	6.36	1.59	71.6
418	22.7	4.40	5400	3.30	4.94	2.39	51.2
457	21.4	4.13	5400	3.69	6.99	1.14	86.0
476	20.9	4.07	5400	3.41	7.73	0.74	114
			Acetone-methyl bromide filter No. 1				
418	21.5	22.9	5400	7.95	8.29	3.41	18.1
450	20.8	21.7	5400	9.43	12.6	1.76	39.5
481	19.5	19.9	5400	9.09	14.8	0.49	104
394	23.4	23.2	5400	5.97	4.87	3.74	10.2
438	20.7	22.1	5400	6.25	9.37	1.69	29.9
455	20.3	21.2	5400	5.23	12.2	1.36	43.8
401	23.3	23.3	5400	5.23	5.30	3.65	10.5
463	20.4	20.8	5400	5.79	12.3	0.91	57.3
			Acetone-methylene bromide filter No. 2				
402	24.9	5.78	1800	12.6	15.1	4.43	266
432	21.4	2.46	1800	9.66	10.8	1.82	634
399	23.5	2.79	1800	7.95	6.59	3.18	262
450	20.9	2.58	1800	8.07	11.7	0.97	897
413	22.5	2.81	1800	6.59	7.16	1.88	367
426	22.7	2.73	1800	6.25	8.35	1.47	490

pump, and calibrated gas burette. A small copper oxide furnace operated at 216°C was used to determine the amount of carbon monoxide in the "noncondensable" fraction of the reaction products.

Materials

Acetone was a Mallinckrodt Analytical Reagent product which had been refluxed over potassium permanganate prior to distillation. It was dried over dreierite and kept in the dark.

Methyl fluoride was prepared by the Swarts[3] method. Mercurous fluoride was slowly added to a solution of iodine in methyl iodide (in a molar ratio of 1:2). The effluent gases were passed through a condenser at −40°C, then washed with water to remove silicon tetrafluoride and condensed in Pyrex traps cooled in liquid air. The product was distilled through a Podbielniak Column and center cuts taken at a constant boiling point. The molecular weight was 33.8 (theoretical 34.0).

Methylene fluoride was prepared by the reaction of mercurous fluoride with an equimolar mixture of methylene iodide and iodine. The gaseous products were distilled and the fraction boiling at −51° to −52° collected. The gas was bubbled through 10 percent sodium hydroxide solution and dried with concentrated sulfuric acid. This was redistilled and the fraction boiling at −51.6° was removed. The molecular weight was 51.4 (theoretical for methylene fluoride 52.0).

Methylene chloride was an Eastman Kodak Company product. It was washed with sodium carbonate, dried over calcium chloride, and then distilled from phosphorous pentoxide.

Chloroform and carbon tetrachloride were research grade Anachemia products.

Methyl bromide (99.5 percent), methylene bromide, and bromoform were obtained from the Matheson Company.

RESULTS

The results given in Table I and plotted in Fig. 1 are those obtained in the photolysis of acetone alone. The value of 9.5 kcal arrived at for the activation energy of the reaction of a methyl radical with acetone in both cases compares favorably with the value of 9.7 kcal previously established in this laboratory.

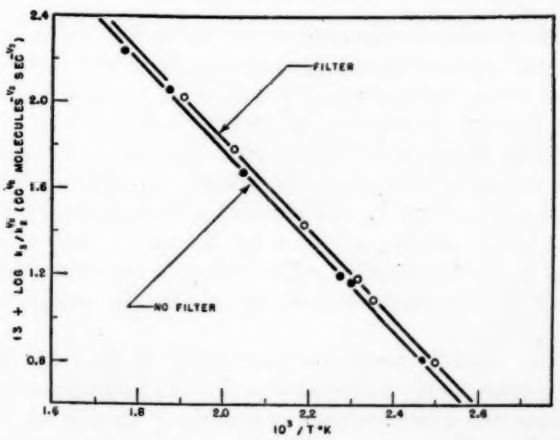

FIG. 1. Arrhenius plot for the reaction of methyl radicals with acetone.

[3] F. Swarts, Bull. Soc. Chim. Belg. 46, 10 (1937).

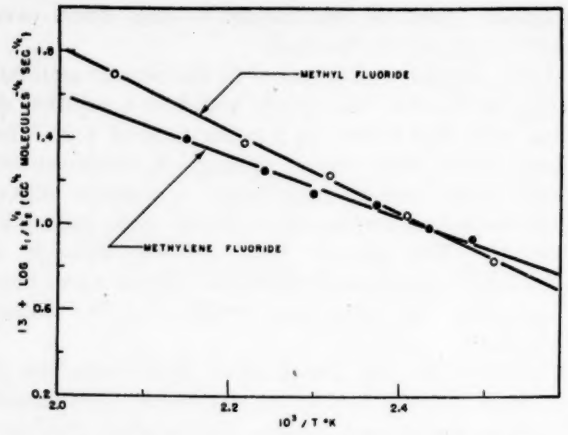

FIG. 2. Reaction of methyl radicals with fluorinated methanes.

The results obtained on the photolysis of acetone in the presence of various halogenated methanes are given in Table II and Figs. 2–4. Certain members of the series have not been done, either because of low vapor pressure (bromoform) or because of difficulty in separating the products from the reactant (fluoroform). It is hoped that work with these will be done later.

It will be noted from the results that the rate of carbon monoxide production fluctuated from one series of experiments to the next, and since the carbon monoxide production functions as an internal actinometer, it follows that the intensity of illumination changed accordingly. This was caused in part by the introduction of different filters into the optical system as indicated and also to the formation of a deposit on the windows of the reaction cell. Whereas the deposit did not affect the intensity of illumination appreciably in any one series of experiments, it was found necessary to "flame" the reaction vessel from time to time, and each such flaming produced a sharp rise in transmission in the succeeding series.

DISCUSSION

The results we obtained are summarized in Table III. Several interesting conclusions may be drawn at once from these observations. First of all, it is evident that the ease of interaction of methyl radicals with the different halogenated methanes varies markedly with the nature of the particular halogen substituent. The activation energy for the removal of a hydrogen atom, by methyl radicals, from methyl fluoride is lower than that for methyl chloride, which in turn is lower than that for methyl bromide. This is also true for the methylene compounds.

The second conclusion we arrive at is that the activation energy for the abstraction of a hydrogen atom in any one series becomes progressively smaller as the number of halogen atoms in the methane is increased. Thus, a methyl radical removes a hydrogen atom from methylene chloride more readily than from methyl chloride but less readily than from chloroform. This is also in general agreement with the work of Kistiakowsky and van Artsdalen[4] who concluded that there was a progressive decline in the magnitude of the C—H bond strength with increased halogenation. It is also in line with the general conclusions of organic chemistry regarding the "activity" of the hydrogen atoms in substituted methanes.

In calculating the ratio of the steric factors, a collision diameter of 5A was assumed for all the halogenated methanes and of 3.5A for the methyl radical. The uncertainties introduced by assuming these values are certainly less than the experimental error.

If one accepts a value of 0.1 for the best value of the steric factor of reaction (2),[5] then the absolute values of the steric factors will be equal to $\frac{1}{3}$ the value of $P_1/P_2^{\frac{1}{2}}$ given in the last column of Table III.

The results in Table III indicate that, as with other hydrogen-abstraction reactions, the steric factors of these reactions are significantly lower than unity.[6] The values for the bromides are, however, decidedly larger

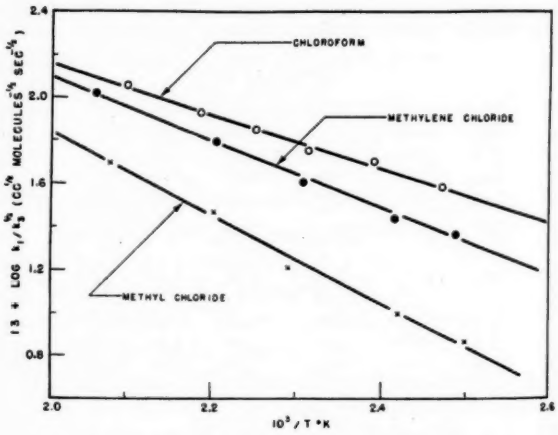

FIG. 3. Reaction of methyl radicals with chlorinated methanes.

than is the case with hydrocarbons and most other substances.[7]

In the interpretation of the above results the only important assumption is that methane and ethane are formed solely by reactions (1), (2), and (3). Provided that this is true, other fates of the methyl radical will not affect the interpretation of the results.

It is, of course, obvious that chlorine-abstraction reactions may also occur, e.g.,

$$CH_3+CHCl_3=CH_3Cl+CHCl_2.$$

In the case of methyl chloride and methyl bromide this

[4] G. B. Kistiakowsky and E. R. van Artsdalen, J. Chem. Phys. **12**, 469 (1944).

[5] R. W. Durham and E. W. R. Steacie, J. Chem. Phys. (to be published).

[6] For a discussion of the status of investigations of such factors, see E. W. R. Steacie and M. Szwarc, J. Chem. Phys. **19**, 1309 (1951).

[7] A. F. Trotman-Dickenson and E. W. R. Steacie, J. Chem. Phys. **19**, 329 (1951).

can make no difference, since the only result is an exchange of the chlorine or bromine atom.

In the case of chloroform the result is to form methyl chloride and a partially chlorinated methyl radical. Since the conversion is small and since methyl chloride is less reactive than the more highly substituted methanes, no serious complication can result from the presence of CH_3Cl. The fate of the radical $CHCl_2$ will be of no importance unless methane or ethane are formed from it, and this seems most unlikely. The abstraction of chlorine would not, therefore, be expected to introduce complications.

It is, in fact, possible to make a rough estimate of the extent of chlorine abstraction. If methyl radicals combined only with each other, then in the photolysis of acetone alone the ratio $(C_2H_6+\frac{1}{2}CH_4)/CO$ would be unity. If, however, all acetonyl radicals formed by hydrogen-abstraction combined with methyl, then the above ratio would be less than unity, and the ratio

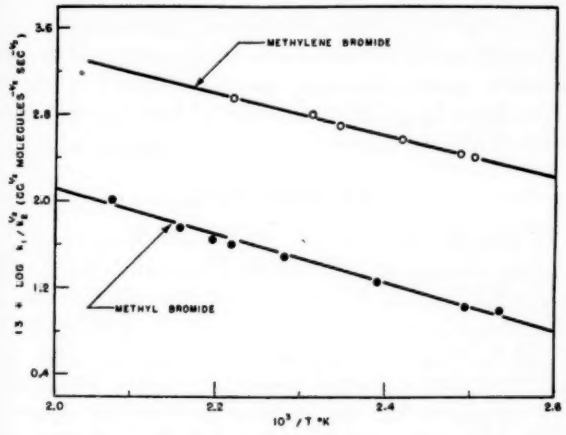

FIG. 4. Reaction of methyl radicals with brominated methanes.

$(C_2H_6+CH_4)/CO$ would equal unity. In fact the real situation lies between these two extremes. In the presence of an added substance, RH, similar considerations will apply, depending on the presence or absence of processes such as

$$R+CH_3=RCH_3.$$

If chlorine-abstraction were the major process, most methyl radicals would be expected to disappear by reactions such as

$$CH_3+CH_2Cl=C_2H_5Cl,$$

TABLE III. Activation energies and steric factors for the reaction of methyl radicals with some halogenated methanes.

Compound	$E_1-\frac{1}{2}E_2$ kcal	$P_1/P_2^{\frac{1}{2}}\times10^4$
Methyl fluoride	8.7	13
Methylene fluoride	6.2	1
Methyl chloride	9.4	28
Methylene chloride	7.2	6
Chloroform	5.8	2
Methyl bromide	10.1	96
Methylene bromide	8.7	45

which do not form methane or ethane. The ratio $(C_2H_6+\frac{1}{2}CH_4)/CO$ would thus be expected to become very small. In fact it is found that the value of this ratio is not appreciably affected by the presence of halides. It may, therefore, be concluded that chlorine-abstraction reactions are at least not faster than hydrogen-abstraction, and the rates found for hydrogen-abstraction may be taken as an upper limit for the rate of chlorine-abstraction.

Finally, one peculiar effect should be mentioned. Experiments have been performed in which acetone was photolyzed in the presence of carbon tetrachloride. Under these circumstances methane formation is *increased* and ethane formation becomes almost zero. A part of this effect is a result of traces of HCl as an impurity in the carbon tetrachloride. This is, however, by no means responsible for the major part of the effect. It seems very difficult to explain the increased formation of methane unless HCl is formed in small amounts in the reaction. A detailed investigation of this problem is under way. In the meantime the possibility of complications of this sort introduces some uncertainty into the above results. However, in view of the reproducibility of the results, the way in which the kinetics fit in with work on other systems, and the reasonableness of the activation energies obtained, we feel that it is most unlikely that the present results are greatly in error from such a cause.

ACKNOWLEDGMENT

We are greatly indebted to Mr. M. Chmilar and Mr. R. M. MacDonald of the Defence Research Chemical Laboratories, Ottawa, for the preparation of methyl fluoride and methylene fluoride.

The Reaction of Methyl Radicals with Nitric Oxide, and the Rate of Combination of Methyl Radicals

R. W. DURHAM* AND E. W. R. STEACIE
Division of Chemistry, National Research Council, Ottawa, Canada

(Received November 16, 1951)

Radioactive tellurium mirrors have been used to investigate the rate of reaction of methyl radicals with nitric oxide in a flow system. The collision efficiency of this reaction has been found to be 1.5×10^{-4}, which is higher by a factor of 10 than the previous value obtained by Forsyth. This value when applied to results obtained by Miller and Steacie for the ratio of the two reactions

$$CH_3+CH_3\rightarrow C_2H_6, \quad (1)$$
$$CH_3+NO\rightarrow \text{products}, \quad (2)$$

leads to a collision efficiency or steric factor, assuming the activation energy to be zero, of 0.01 for methyl combination. A comparison of this value with those obtained by other authors from photochemical studies suggests the value for the collision efficiency of methyl combination is between 0.5 and 0.05.

INTRODUCTION

THE collision efficiency of the reaction between methyl radicals and nitric oxide has been estimated by Forsyth[1] to be 1.4×10^{-5}. The experimental technique entailed finding the rate of disappearance of methyl radicals as they flowed along a reaction tube in the presence of several different concentrations of nitric oxide. The relative concentrations of radicals at points along the tube were obtained from the rates of removal of tellurium mirrors at those points; radicals were produced by heating diethyl ether vapor, flowing through the system, to 800°C.

This value for the collision efficiency of methyl and nitric oxide has been used by Miller and Steacie[2] to evaluate the collision efficiency of the combination of methyl radicals. They allowed the two reactions

$$CH_3+CH_3\xrightarrow{k_1}C_2H_6,$$

$$CH_3+NO\xrightarrow{k_2}\text{products},$$

to take place simultaneously and measured the ratio $k_1^{\frac{1}{2}}/k_2$. The collision efficiency of methyl and nitric oxide was then multiplied by the collision frequency of this reaction in order to find the value of the reaction constant k_2. When this value was substituted in their results a value of 4.4×10^{-5} was obtained for the collision efficiency of methyl combination. Results obtained by Gomer and Kistiakowsky,[3] Lucas and Rice,[4] and Dodd,[5] however, all point towards a value near unity for this efficiency, and as the methyl combination reaction occurs as a competing reaction in all investigations involving the reaction of methyl radicals with other molecules, it is important that the reason for this discrepancy in the values for the collision efficiency be found. The value for the ratio of reaction of methyl with nitric oxide occurs as a squared term in Miller and Steacie's calculation and therefore Forsyth's experiments have been repeated with certain refinement in order to obtain as accurate a value as possible for k_2.

EXPERIMENTAL

In principle the method used is the same as that of Forsyth though several modifications affecting radical production and measurement have been introduced. In order that there should be no ambiguity over the nature of the radicals investigated, di-*t*-butyl peroxide was used in place of diethyl ether as a source of radicals. This substance has been shown by Vaughan *et al.*[6] to decompose into methyl radicals and acetone at comparatively low temperatures. In the present work a vapor pressure of about 0.2-mm di-butyl peroxide was maintained in the reaction tube by allowing liquid di-butyl peroxide to evaporate from a reservoir held slightly below room temperature into a large bulb, and from there through a capillary into the reaction tube. A furnace temperature of 325°C gave a reasonable yield of radicals so that a Pyrex reaction tube could be used in place of quartz.

Matheson nitric oxide, specified purity 98 percent, was obtained from a cylinder and passed at atmospheric pressure through a trap at −120°C to remove NO_2, then into a ballast vessel which was connected to the reaction tube through a capillary downstream from the furnace. The capillary was removable and could be replaced by a variety of tubes in order to vary the partial pressure of NO in the system. The input rate of NO could be found by cutting off the calibrated ballast vessel from the NO input and observing the drop in pressure in a given time with an oil manometer; over a pressure drop of 2 or 3 mm of mercury the partial pressure of NO in the

* National Research Council of Canada Postdoctorate Fellow, 1950–52.

[1] J. S. A. Forsyth, Trans. Faraday Soc. **37**, 312 (1941).

[2] D. M. Miller and E. W. R. Steacie, J. Chem. Phys. **19**, 73 (1951).

[3] R. Gomer and G. B. Kistiakowsky, J. Chem. Phys. **19**, 85 (1951).

[4] V. E. Lucas and O. K. Rice, J. Chem. Phys. **18**, 993 (1950).

[5] R. E. Dodd, Trans. Faraday Soc. **47**, 56 (1951).

[6] Raley, Rust, and Vaughan, J. Am. Chem. Soc. **70**, 88 (1948).

reaction tube was not affected. In order to calculate the partial pressure of NO in the reaction tube Forsyth assumed that the flow rates of NO and ether vapor along the tube were equal and independent of each other. The partial pressures of NO and vapor would then be in the same ratio as their input rates at atmospheric pressure, both of which could be measured. A measurement of the pressure with ether vapor alone passing through the tube at a known input rate then made possible an estimation of the NO partial pressures for different NO input rates. It would appear that this method could lead to a considerable error in the absolute value for the NO partial pressure so that a more direct method was applied to measure this quantity. The total pressure was measured with a McLeod gauge while the apparatus was operating under known conditions of flow, the mixed gas in the McLeod was then isolated from the apparatus and the butyl peroxide frozen out in a small side tube at $-120°C$. The pressure of NO was then measured and taken to be the partial pressure of NO in the reaction tube; cooling the side tube with NO alone in the McLeod did not alter the NO pressure. The difference between this NO pressure and the total pressure was found to equal the pressure obtained when di-butyl peroxide vapor alone was passing and hence shows that the flow rates are independent. Using this method it was found that the flow rate of NO differed from that of di-butyl peroxide, and therefore a source of error would arise in Forsyth's equating of the flow rates.

Radioactive tellurium mirrors were used in order that the rate of removal could be followed directly. Pure tellurium was irradiated in the Chalk River pile producing Te^{127} and Te^{129} with half-lives of 90 and 32 days, respectively, and also 8-day I^{131}. Since high activities of the tellurium isotopes could be obtained, the iodine activity was removed by allowing the irradiated material to decay for about three months. Most of the activity reaching an annular Geiger tube[7] surrounding the reaction tube consisted of γ-rays from Te^{129}. The annular counter could be moved along the reaction tube, and when in operation, it surrounded the mirror. Mirrors were deposited inside a cylindrical glass rider movable up and down the tube by means of a steel counterweight and external magnet. To deposit a mirror the rider was lowered to the bottom of the tube where a small sidearm was used to store a pellet of Te*, whereupon gentle heating caused a mirror to be deposited on the inside of the rider. The thin front edge of the mirror so formed was then distilled away, leaving a uniformly thick mirror about 1 cm in length. The annular counter was used in conjunction with a counting rate meter, the output from this being fed into an automatic recorder. In this way the decrease in activity of the mirror due to radical attack was directly plotted against time, and the slope of this graph was therefore proportional to the rate of removal of the mirror. The initial slopes of these graphs were found to be straight lines which later became exponential curves after the initial activity had dropped to more than half its value. This was to be expected as the mirror would cease to remove all the radicals reaching it when its size was greatly diminished so that the initial slope was taken as representative of the radical concentration. The counting geometry was such that a displacement of the mirror by 0.5 cm either way from the plane of the annular counter did not materially affect the counting rate, so it would appear safe to assume that the decrease in counting rate of the mirror did represent the removal of an equivalent amount of tellurium from the mirror.

Gomer and Kistiakowsky have suggested that the decrease in rate of removal of a mirror in the presence of NO in Forsyth's work was due to a poisoning effect on the mirror by the NO. Using this radioactive technique, it was possible to follow the rate of removal of a mirror with no NO present, then admit NO for a time, cut it off, and see if the removal rate recovered its original value. It was found that the original rate was regained without any appreciable time lag and thus no poisoning could have occurred.

In order to show that the increase in mass flow through the tube caused by admittance of NO to the system did not upset the radical concentration, helium, which has a similar viscosity to NO and is inert, was admitted in place of NO. The rate of removal of a mirror was observed to be unaffected on introducing helium; therefore the decrease in removal rate of a mirror with NO is not caused by a diluting effect of the NO on the radical concentration.

Although the absolute concentration of methyl radicals is not necessary in order to find the collision efficiency, it was nevertheless estimated, as all that is required to convert the decrease in activity of a mirror into amounts of tellurium removed is the specific activity of the tellurium as measured with the annular counter. In order to find this value the activity of a mirror deposited under normal operating conditions was measured using the annular counter, and then the rider was removed from the tube and the mirror dissolved in dilute nitric acid. An aliquot of this solution was then evaporated on a small watchglass under a heat lamp along with an aliquot of a standard solution of Te* prepared by weighing accurately about 50 mg Te*, dissolving in dilute nitric acid and making up to known volume. Comparison of the two activities using standard β-particle counting technique then gave the amount of tellurium in the mirror and hence the counting rate per mg Te* as measured by the annular counter. The rates of removal of several mirrors were then found at a point in the tube immediately after measuring the specific activity of the Te* so that no decay correction was necessary. The average value of these determinations was then converted to moles tellurium removed per sec, and twice this value, when divided by the volume flow rate at that point in the tube, gave the concentration of

[7] G. Ensell and S. C. Chatterjee, Rev. Sci. Instr. 22, 700 (1951).

TABLE I.

Partial pressure of NO in mm Hg	Input rate NO at atmos pressure cc/sec	Time of flight of radical sec $\times 10^3$	Rate of mirror removal counts/min/min
0	0	9.02	960
		10.02	1000
		11.60	690
		12.96	520
		14.76	410
0.019	0.00286	9.02	640
		10.02	460
		11.60	400
		12.96	290
		14.15	250
		14.76	240
0.039	0.00604	9.02	686
		10.02	580
		11.60	350
		12.96	320
		14.76	200
0.056	0.00859	9.02	600
		10.02	480
		11.60	400
		12.96	240
		14.15	160
0.083	0.0127	9.02	460
		10.02	320
		10.77	335
		11.60	200
		12.96	170
0.087	0.0134	9.02	500
		10.02	360
		10.77	200
		11.60	290
		12.96	125
		14.15	90

radicals in moles per cc. It has been assumed that $Te(CH_3)_2$ is formed by the reaction of methyl radicals with tellurium at room temperature, as no trace was found of the red compound reported by Rice and Glazebrook[8] to be $(TeCH_3)_2$, and obtained using heated mirrors. The concentration at a point in the tube 10.0 millisec from the mouth of the furnace was found to be 5.5×10^{-12} mole of radicals per cc. Forsyth obtained a value of 1.94×10^{-11} mole of radicals per cc 26.2 millisec from the furnace by determining the time required for removal of a mirror of known weight. These methods of estimating the radical concentration actually only give a lower limit to the value as very probably all the radicals in the gas stream are not removed on reaching the mirror. Miller and Winkler[9] find this efficiency to be about 70 percent for methyl with tellurium under their experimental conditions.

RESULTS

The flow rate of butyl peroxide vapor was determined by measuring the rate of evaporation of peroxide from a calibrated reservoir and converting this to the pressure of vapor in the reaction tube. The reaction tube was 1 cm in diameter and was found to produce a pressure gradient of 0.003 mm per cm length, which meant the flow rate was changing appreciably along the tube. In order to correct for this, use was made of the following equation[10] to find the time required for a radical to traverse the distance between the mouth of the furnace and center of the mirror.

$$t=\frac{X}{V_0}-\frac{(P_1-P_2)X^2}{2V_0P_1L}.$$

X corresponds to the distance of the mirror center from the furnace mouth, at which point the pressure is P_1 and V_0 is the flow rate. $(P_1-P_2)/L$ is the pressure gradient along the reaction tube.

The expansion effect on concentration pointed out by Gomer[11] to be inherent in flow system has been calculated for the flow conditions used in these experiments.

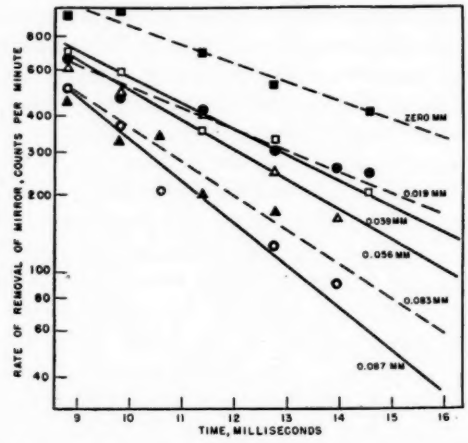

FIG. 1. Decrease in radical concentration along reaction tube for different partial pressures of nitric oxide.

For a flow rate of 1100 cm/sec at the furnace the radical concentration would fall by 12 percent over the range of actual concentrations measured. As these concentration changes are of the order of three to five times, no correction was made for expansion.

The mirror removal rates obtained from the automatic recorder were plotted against the times required for a radical to reach the mirror for a series of NO partial pressures using semilogarithmic graph paper. These results are given in Table I and shown in graph form in Fig. 1. The slopes of these graphs, $d/dt \log[CH_3]$, were calculated by reading off the time required for the initial removal rate to fall to half its value $T_{\frac{1}{2}}$, then substituting in the equation $K=0.693/T_{\frac{1}{2}}$. Table II shows the values obtained for K from the slopes of the graphs in Fig. 1. As the concentration of NO is high compared with that of methyl, K is the apparent first-order reaction constant for a given partial pressure of

[8] F. O. Rice and A. L. Glazebrook, J. Am. Chem. Soc. **56**, 2472 (1934).
[9] D. M. Miller and C. A. Winkler, Can. J. Chem. **29**, 537 (1951).
[10] F. Paneth and W. Lautsch, Ber. **64**, 2708 (1931).
[11] R. Gomer, J. Chem. Phys. **19**, 284 (1951).

NO. The graph of K against NO pressure is then represented by the equation

$$K=k'+k''[\mathrm{NO}],$$

where k' is the reaction constant for the normal decay of radicals along the tube and k'' the reaction constant when NO is present. From Fig. 2

$$k'=152 \text{ sec}^{-1},$$

$$k''=1940 \text{ sec}^{-1} \text{ per mm NO.}$$

The collision efficiency of methyl with NO is then given by

$$\frac{\text{Number of mols reacting}}{\text{Number of mols colliding}}=\frac{1.94\times10^3\times1\times[\mathrm{CH_3}]}{Z\times[\mathrm{CH_3}]}$$

$$=\frac{1.94\times10^3}{1.3\times10^7}=1.5\times10^{-4},$$

where Z is the collision frequency of a methyl radical with NO molecules at a pressure of 1 mm Hg. This collision efficiency is higher than Forsyth's value by a factor of about 10.

TABLE II.

Partial pressure of NO in mm Hg	$T\frac{1}{2}$ sec$\times10^3$	K sec^{-1}
0	4.10	169
0.019	3.62	192
0.039	3.08	225
0.056	2.64	263
0.083	2.28	304
0.087	1.58	374

THE RATE OF COMBINATION OF METHYL RADICALS

Using the rotating sector technique in the photolysis of acetone and dimethyl mercury, Gomer and Kistiakowsky obtain the value 4.47×10^{-16} for $s\sigma^2$ where s is the steric factor for the recombination reaction of two methyl radicals and σ is the collision diameter. Substituting 3.5A for the collision diameter of methyl as computed by Hill,[12] s is found to be 0.36. Dodd investigated the intermittent photolysis of acetaldehyde and obtained a value for the rate constant of the bimolecular termination reaction which was presumed to be recombination of methyls to give ethane, although reaction products were not identified. This rate constant was found to be between 10^{13} and 10^{14} cc M^{-1} sec^{-1} in agreement with the value of 6×10^{13} cc M^{-1} sec^{-1} quoted by Lucas and Rice for a similar investigation of the photolysis of acetaldehyde. Since the collision frequency of methyl radicals is 1.1×10^{14} cc M^{-1} sec^{-1}, calculated using a value for σ of 3.5A, it is apparent that the above results lead to a collision efficiency of between 1 and 0.1.

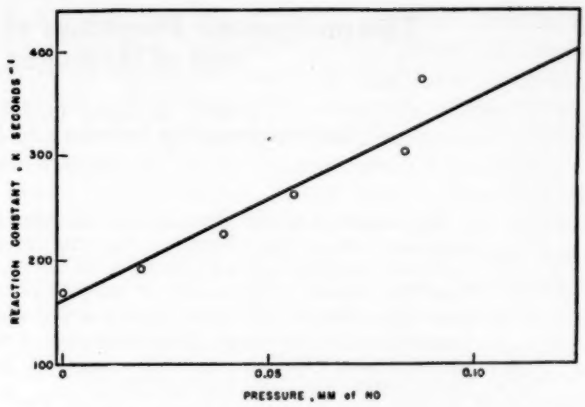

FIG. 2. Effect of NO on reaction constant.

The collision frequency of methyl with nitric oxide is calculated to be 2.2×10^{14} cc M^{-1} sec^{-1}, assuming 3.75A as a reasonable collision diameter for the reaction. Combining this with the value of 1.5×10^{-4} for the collision efficiency obtained in this work, k_2 is found to be 3.3×10^{10} cc M^{-1} sec^{-1}. Miller and Steacie found the ratio $k_1{}^{\frac{1}{2}}/k_2=3.1\times10^{-5}$ so that k_1 is 1.1×10^{12} cc M^{-1} sec^{-1}. This result used in conjunction with the collision frequency evaluated earlier leads to a value of 0.01 for the collision efficiency of methyl combination. It has been pointed out to us by Dr. Gomer that the pressure obtained in our experiments is about 20 times lower than in Miller and Steacie's, so one would expect some falling off in rate of the methyl-NO reaction owing to third-body effects. This means that the value of k_2 used in combination with Miller and Steacie's value for $k_1{}^{\frac{1}{2}}/k_2$ is actually too low and hence the collision efficiency of 0.01 so calculated would be a lower limit.

Taking into account the lack of any real knowledge of the entity σ and attaching reasonable weight to the results of Gomer and Kistiakowsky, Dodd, and Lucas and Rice, it would appear that all existing data are compatible with a value of between 0.5 and 0.05 for the collision efficiency of methyl combination.

[12] T. L. Hill, J. Chem. Phys. 17, 1125 (1949).

Thermodynamic Properties of the Fluorine Atom and Molecule and of Hydrogen Fluoride to 5000°K*

LELAND G. COLE,† M. FARBER, AND G. W. ELVERUM, JR.
California Institute of Technology, Jet Propulsion Laboratory, Pasadena, California

(Received November 29, 1951)

The evaluation of the thermodynamic functions C_p^0, S^0, $-(F^0-E_0^0)/T$, and $(H^0-E_0^0)/T$ of the fluorine atom and molecule and of hydrogen fluoride from 100°K to 5000°K have been made by statistical calculations from available spectral constants for the atom and for hydrogen fluoride; for fluorine the constants have been derived or estimated from the Raman shift in gaseous fluorine, the equilibrium internuclear distance from electron diffraction measurements, and the heat of dissociation obtained recently by R. N. Doescher at this Laboratory. These results have been combined with the thermodynamic functions of hydrogen to evaluate the heats and free energies of dissociation and dissociation constants for the equilibria $F_2 \rightleftharpoons 2F$, $HF \rightleftharpoons \frac{1}{2}H_2+\frac{1}{2}F_2$, and $HF \rightleftharpoons H+F$.

QUANTITATIVE statistical calculations of the thermodynamic functions for the fluorine molecule have not been possible heretofore because of the lack of sufficient spectral data. Fluorine does not exhibit banded absorption presumably because the upper potential curve is not sufficiently stable.[1] In addition, considerable uncertainty has been attached to the reported dissociation energies of fluorine with values obtained by many different and indirect methods ranging from 30.6 kcal mole^{-1} [2] to 81 kcal mole^{-1} [3,4] so that only estimates of equilibria involving fluorine have been possible. Murphy and Vance,[5] however, have made statistical calculations of the thermodynamic functions of fluorine and hydrogen fluoride to 2000°K. For fluorine they initially estimated a fundamental vibration frequency of 856±17 cm^{-1} by Badger's rule[6] making use of Brockway's electron diffraction measurements of the internuclear distance of the atoms in fluorine of 1.45±0.05A.[7] Subsequently, Butkow and Rozenbaum[8] have evaluated the thermodynamic functions of the fluorine molecule and atom and the equilibrium constant for the reaction $F_2 \rightleftharpoons 2F$ from 298.1°K to 5000°K using an estimated ω^0 of 907 cm^{-1} and a D_0^0 of 72.0 kcal mole^{-1}.

Garner and Yost[9] had previously observed no Raman lines in liquid fluorine and this approach to a quantitative evaluation of the first vibrational quantum appeared fruitless. Andrychuk, however, using recent improvements in light sources and photographic plates has found[10] two weak Raman lines in an irradiated 14-inch quartz tube containing gaseous fluorine corresponding to the two mercury lines 4047A and 4358A. The observed shifts were 891.4 cm^{-1} and 892.8 cm^{-1}, respectively, from which a mean value for $\Delta G_{\frac{1}{2}}$ of 892.$_1$±2 cm^{-1} was derived. Murphy and Vance have subsequently revised their data on molecular fluorine to 2000°K[11] on the basis of this value for the first vibrational quantum and an improved value of 1.435A for the equilibrium internuclear distance from electron diffraction measurements of Rogers, Schomaker, and Stevenson.[12]

Recently, at this Laboratory, Doescher[13] has determined the heat of dissociation of fluorine to be 37.7±0.4 kcal mole^{-1} in the range of 759°K to 1115°K by direct equilibrium pressure measurements in a coated nickel tube. The results of the electron diffraction, Raman, and dissociation measurements have now been combined to evaluate the thermodynamic functions C_p^0, S^0, $-(F^0-E_0^0)/T$, and $(H^0-E_0^0)/T$ of fluorine in the temperature interval from 100°K to 5000°K for the rigid-rotator, harmonic oscillator diatomic model to which the anharmonic contributions have been added for higher temperatures by the methods of Mayer and Mayer.[14] For fluorine below 1000°K and for hydrogen fluoride below 4200°K it is not possible to use the expanded form of Mayer's equation (7.42) for $\ln Q_c$, which they have defined as the difference between $\ln Q_{vjm}$ and the sum of $\ln Q_v$ and $\ln Q_j$. The unexpanded equations used to evaluate contributions to the functions resulting from the anharmonicity of vibration and the increase of moment of inertia with increasing v and j values, are summarized here because of their general utility between ambient temperature and temperatures at which $h\nu/kt \geqslant 0.75$

* This paper presents the results of one phase of research carried out at the Jet Propulsion Laboratory under Contract No. DA-04-495ORD18, sponsored by the U. S. Army Ordnance Department.

† Present address: Chemistry and Chemical Engineering Section, University of Michigan, Willow Run Research Center.

[1] A. G. Gaydon, *Dissociation Energies and Spectra of Diatomic Molecules* (John Wiley and Sons, Inc., New York, 1947).

[2] H. Schmitz and H. J. Schumacher, Z. Naturforsch. **2a**, 359 (1947).

[3] C. H. D. Clark, Trans. Faraday Soc. **36**, 370 (1940).

[4] J. H. Simons, *et al.*, *Fluorine Chemistry* (Academic Press Inc., New York), Vol. 1.

[5] G. M. Murphy, and J. E. Vance, J. Chem. Phys. **7**, 806 (1939).

[6] R. M. Badger, J. Chem. Phys. **2**, 128 (1934), **3**, 710 (1935).

[7] L. O. Brockway, J. Am. Chem. Soc. **60**, 1348 (1938).

[8] K. V. Butkow and R. B. Rozenbaum, Zhur. Fiz. Khim. **24**, 706–31 (1950).

[9] C. S. Garner and D. M. Yost, J. Am. Chem. Soc. **59**, 2738 (1938).

[10] D. Andrychuk, J. Chem. Phys. **18**, 233 (1950).

[11] G. M. Murphy and J. E. Vance, J. Chem. Phys. **18**, 1514 (1950).

[12] Rogers, Schomaker, and Stevenson, J. Am. Chem. Soc. **63**, 2610 (1941).

[13] R. N. Doescher, J. Chem. Phys. **19**, 1070 (1951).

[14] J. E. Mayer and M. G. Mayer, *Statistical Mechanics* (John Wiley and Sons, Inc., New York, 1940), first edition.

(i.e., <1000°K for F_2 and <4200°K for HF). These unexpanded anharmonic contributions can be shown, in the nomenclature of Mayer,[14] to be

$$-F_e/RT=u^{-1}\left[8\gamma+\delta\left(\frac{u}{e^u-1}\right)+2x\left(\frac{u^2}{(e^u-1)^2}\right)\right]$$

$$E_e/RT=8\gamma u^{-1}+\frac{u}{(e^u-1)^2}(\delta e^u-2x)+\frac{4xu^2e^u}{(e^u-1)^3}$$

$$S_e/R=16\gamma u^{-1}+\frac{\delta}{e^u-1}+\frac{\delta u e^u}{(e^u-1)^2}+\frac{4xu^2e^u}{(e^u-1)^3}$$

and

$$C_{pe}/R=16\gamma u^{-1}-\frac{\delta u^2e^u}{(e^u-1)^2}+\frac{u^2e^u}{(e^u-1)^3}(2\delta e^u-4xu-8x)+\frac{12xu^3e^{2u}}{(e^u-1)^4},$$

in which $u=h\nu/kT$, $\sigma=Bhc/kT$, $x\cong x_e\cong x_0$, $\gamma=\sigma/u$ and $\delta=6(\gamma^{\frac{1}{2}}x^{\frac{1}{2}}-\gamma)$.

The anharmonicity constant, x_e, was evaluated to a first approximation for fluorine from its heat of dissociation D_0 and the usual relationships between D_0, D_e, ω_e, $x_e\omega_e$, and $\Delta G_{\frac{1}{2}}$ from which ω_e and $x_e\omega_e$ were calculated to be 926 cm^{-1} and 16.9 cm^{-1}, respectively, assuming that ΔG is a linear function of v. A value for the anharmonicity constant x_e for the next higher molecular weight halogen, chlorine, calculated from these relationships agrees within 0.1 percent with that observed spectroscopically. The observed and calculated values for bromine and iodine, however, show considerably less agreement.

Walsh[15] had predicted a force constant for fluorine of 4×10^5 dynes cm^{-1} in accord with Badger's relationship and showed that higher values such as Gale and Monk's value of 7.1×10^5 dynes cm^{-1} [16] and Gordy's value for k of 7.93 dynes cm^{-1} [17] were in conflict with the similarity in properties of isoelectronic molecules. Using ω_e, as derived above from $\Delta G_{\frac{1}{2}}$ and the experimental heat of dissociation of fluorine, and assuming a linear relationship between ΔG and v, the force constant of fluorine was calculated to be 4.80×10^5 dynes cm^{-1}.

The evaluation of the electron affinity ΔE_{0i}^0 of fluorine from its new heat of dissociation is also of theoretical interest; applying the Born-Haber cycle to the five alkali metal fluorides, ΔE_{0i}^0 was estimated to be 84±1 kcal, whereas chlorine, bromine, and iodine have electron affinities evaluated by the same technique of 92.5 kcal, 87.1 kcal, and 79.2 kcal, respectively. Glockler, from an empirical relationship between ionization potentials and atomic number, had previously estimated somewhat lower values of ΔE_{0i}^0 for fluorine and chlorine; he reported an electron affinity for fluorine of 89.9 kcal and 85.3 kcal for chlorine.[18] This latter value has been confirmed by McCallum and Mayer who have obtained a value of 85.8$_4$ kcal for chlorine experimentally.[19] Direct determinations of the electron affinity of other halogens by this technique have yielded an electron affinity for bromine of 80.5 kcal,[20] and an electron affinity for iodine of 72.4 kcal.[21] There is nearly a constant difference between the affinities obtained from the Born-Haber cycle and the results from measurement of the ion current of the dissociated halogens, the difference being 6.66, 6.60, and 6.80 kcal for chlorine, bromine, and iodine. On this basis the electron affinity of fluorine might be expected to be still lower than the Born-Haber cycle calculation indicates, e.g., 84.0, −6.70 or 77.0 kcal or 7 kcal lower than chlorine and 3–4 kcal lower than bromine. At first hand the value of ΔE_{0i}^0 (and of D_0^0) appears unexpectedly low; however, not all of the properties of the halogens show continuous progression. The change in physical properties is often greatest in passing from chlorine to fluorine. The internuclear distance changes 0.554A in going from fluorine to chlorine while the differences between chlorine-bromine, and bromine-iodine are only 0.295A and 0.383A, respectively. Similarly, the force constant increments, using the presently proposed value for fluorine (0.48 md cm^{-1}), are 0.07, 0.08, and 0.15 md cm^{-1} for iodine-bromine, bromine-chlorine, and chlorine-fluorine, respectively. Such progressions are not peculiar to the Group VII elements; the properties of the Group V and the Group VI elements have physical properties which also exhibit irregularities. The internuclear distances in diatomic tellurium and selenium differ by 0.40A, in selenium and sulfur by 0.30A, but in sulfur and oxygen by 0.72A.

The dissociation (or bond) energy increments between elements in the first and second periods show a progression on going from Group IV to VII which indicates that a dissociation energy (and hence ΔE_{0i}^0) for fluorine less than chlorine is tenable. The increments are based on the bond energies of Skinner[22] with the exception of that for the N−N bond, which has been increased from 43 kcal to 60 kcal,[23] and on a heat of sublimation of carbon of 170 kcal. For Groups IV, V, VI, and VII, the bond energy differences progress from +33.7, to +13, −2, and −23 kcal on subtracting the second period elements' properties from the first.

Physical constants used in the calculations of functions are from Dumond and Cohen.[24] The atomic

[15] A. D. Walsh, J. Chem. Soc. 331 (1948).
[16] H. G. Gale and G. S. Monk, Astrophys. J. 69, 77 (1929).
[17] W. Gordy, J. Chem. Phys. 14, 305 (1946).
[18] G. Glockler, Phys. Rev. 46, 111 (1934).
[19] K. J. McCallum and J. E. Mayer, J. Chem. Phys. 11, 56 (1943).
[20] P. M. Doty and J. E. Mayer, J. Chem. Phys. 12, 323 (1944).
[21] P. P. Sutton and J. E. Mayer, J. Chem. Phys. 3, 20 (1935).
[22] H. A. Skinner, Trans. Faraday Soc. 41, 645 (1945).
[23] M. Szwarc, Proc. Roy. Soc. (London) A198, 267 (1949).
[24] J. W. M. Dumond and E. R. Cohen, "A Least Squares Adjustment of the Atomic Constants as of December 1950. A Report to the National Research Council Committee on Constants and Conversion Factors of Physics." California Institute of Technology, Pasadena, 1951 (privately printed).

TABLE I. Thermodynamic functions of the fluorine molecule.

T°K	C_p^0 cal mole^{-1} deg^{-1}	S^0 cal mole^{-1} deg^{-1}	$-(F^0-H_0^0)/T$ cal mole^{-1} deg^{-1}	$(H^0-H_0^0)/T$ cal mole^{-1} deg^{-1}
100	6.9568	40.756	33.804	6.9499
200	7.0969	45.604	38.630	6.9789
298.16	7.4870	48.506	41.432	7.0785
300	7.4950	48.553	41.475	7.0812
400	7.8947	50.761	43.534	7.2363
500	8.1998	52.562	45.165	7.4001
600	8.4204	54.077	46.527	7.5528
700	8.5813	55.388	47.702	7.6888
800	8.7023	56.272	48.737	7.8048
900	8.7962	57.573	49.673	7.9131
1000	8.8716	58.504	50.503	8.0053
1100	8.9339	59.352	51.269	8.0869
1200	8.9868	60.131	51.976	8.1598
1300	9.0328	60.852	52.632	8.2251
1400	9.0737	61.524	53.243	8.2842
1500	9.1108	62.151	53.818	8.3383
1600	9.1448	62.741	54.357	8.3876
1700	9.1765	63.296	54.866	8.4331
1800	9.2062	63.821	55.349	8.4752
1900	9.2295	64.320	55.808	8.5144
2000	9.2617	64.794	56.247	8.5512
2100	9.2874	65.246	56.665	8.5856
2200	9.3125	65.679	57.065	8.6180
2300	9.3369	66.094	57.449	8.6487
2400	9.3608	66.496	57.816	8.6779
2500	9.3841	66.874	58.171	8.7058
2600	9.4071	67.243	58.516	8.7324
2700	9.4257	67.597	58.846	8.7576
2800	9.4526	67.941	59.161	8.7820
2900	9.4739	68.273	59.471	8.8055
3000	9.4957	68.595	59.769	8.8282
3100	9.5171	68.906	60.062	8.8501
3200	9.5385	69.208	60.341	8.8711
3300	9.5596	69.503	60.614	8.8917
3400	9.5807	69.792	60.881	8.9117
3500	9.6012	70.067	61.139	8.9312
3600	9.6217	70.338	61.392	8.9501
3700	9.6431	70.601	61.638	8.9684
3800	9.6636	70.859	61.877	8.9864
3900	9.6842	71.111	62.109	9.0041
4000	9.7046	71.356	62.337	9.0215
4100	9.7251	71.595	62.560	9.0384
4200	9.7454	71.830	62.780	9.0548
4300	9.7656	72.060	62.992	9.0711
4400	9.7860	72.284	63.201	9.0872
4500	9.8060	72.505	63.406	9.1030
4600	9.8262	72.721	63.604	9.1186
4700	9.8462	72.931	63.803	9.1336
4800	9.8662	73.139	63.992	9.1488
4900	9.8863	73.343	64.184	9.1637
5000	9.9063	73.542	64.369	9.1783

weights are from Mattauch and Fluegge.[25] The separation of the $^2P_{\frac{1}{2}}$ and $^2P_{\frac{3}{2}}$ terms in the fluorine atom was taken to be 404 cm^{-1};[26,27] the contribution of the next energy level to the internal partition function can be shown to be negligible at temperatures considerably in excess of 5000°K. The spectral constants for hydrogen fluoride, $\omega_e=4138.52$ cm^{-1}, $\omega_e x_e=90.069$ cm^{-1}, $\omega_e y_e=0.980$ cm^{-1}, $B_e=20.939$ cm^{-1}, and $\alpha=0.771$ cm^{-1} are those summarized by Herzberg.[28] The contributions of nuclear spin to the entropy and free energy function have not been included in the reported values of the entropy and free energy function. The perfect gas thermodynamic functions for the fluorine molecule and atom

TABLE II. Thermodynamic functions of the fluorine atom.

T°K	C_p cal mole^{-1} deg^{-1}	S^0 cal mole^{-1} deg^{-1}	$-(F^0-E_0^0)/T$ cal mole^{-1} deg^{-1}	$(H^0-E_0^0)/T$ cal mole^{-1} deg^{-1}
100	5.068	32.132	27.147	4.985
200	5.403	35.755	30.641	5.120
298.16	5.436	37.933	32.707	5.224
300	5.435	37.966	32.739	5.225
400	5.361	39.521	34.250	5.269
500	5.282	40.708	35.428	5.280
600	5.220	41.663	36.388	5.275
700	5.171	42.464	37.198	5.264
800	5.134	43.152	37.902	5.250
900	5.108	43.755	38.520	5.235
1000	5.084	44.292	39.071	5.221
1100	5.067	44.776	39.567	5.208
1200	5.053	45.216	40.020	5.196
1300	5.042	45.620	40.435	5.184
1400	5.033	45.993	40.818	5.174
1500	5.025	46.340	41.177	5.164
1600	5.019	46.664	41.509	5.155
1700	5.014	46.968	41.821	5.147
1800	5.009	47.255	42.114	5.139
1900	5.005	47.525	42.393	5.133
2000	5.002	47.782	42.656	5.126
2100	4.999	48.027	42.906	5.120
2200	4.996	48.259	43.144	5.115
2300	4.994	48.480	43.371	5.109
2400	4.992	48.692	43.588	5.104
2500	4.990	48.897	43.800	5.100
2600	4.989	49.092	43.996	5.096
2700	4.987	49.281	44.189	5.092
2800	4.986	49.462	44.375	5.088
2900	4.985	49.637	44.552	5.084
3000	4.984	49.805	44.723	5.081
3100	4.983	49.969	44.890	5.078
3200	4.982	50.128	45.053	5.075
3300	4.981	50.281	45.206	5.072
3400	4.980	50.429	45.359	5.069
3500	4.980	50.574	45.506	5.067
3600	4.979	50.714	45.650	5.064
3700	4.978	50.850	45.789	5.062
3800	4.978	50.984	45.921	5.060
3900	4.977	51.113	46.056	5.058
4000	4.977	51.239	46.180	5.056
4100	4.977	51.361	46.307	5.054
4200	4.976	51.481	46.428	5.052
4300	4.976	51.597	46.549	5.050
4400	4.975	51.713	46.666	5.048
4500	4.975	51.825	46.778	5.047
4600	4.975	51.934	46.889	5.045
4700	4.975	52.041	46.996	5.044
4800	4.974	52.145	47.104	5.042
4900	4.974	52.248	47.200	5.041
5000	4.974	52.348	47.306	5.040

[25] J. Mattauch and S. Fluegge, *Nuclear Physics Tables* (Interscience Publishers, Inc., New York, 1946).

[26] B. Edlen, Physik **98**, 453 (1936).

[27] C. E. Moore, "Atomic Energy Levels, Vol. I: The Spectra of Hydrogen, Deuterium, Tritium, Helium, Lithium, Beryllium, Boron, Carbon, Nitrogen, Oxygen, Fluorine, Neon, Sodium, Magnesium, Aluminum, Silicon, Phosphorous, Sulfur, Chlorine, Argon, Potassium, Calcium, Scandium, Titanium, and Vanadium," U. S. Natl. Bur. Standards, Circ. No. 467, U. S. Gov't. Printing Office, Washington, D. C. (June 15, 1949).

[28] G. Herzberg, *Molecular Spectra and Molecular Structure I. Spectra of Diatomic Molecules* (D. Van Nostand Company, Inc., New York, 1950), second edition.

and for monomeric hydrogen fluoride from 100°K to 5000°K are summarized in Tables I, II, and III.

The equilibrium constants for the reactions $F_2 \rightleftharpoons 2F$, $HF \rightleftharpoons \frac{1}{2}H_2+\frac{1}{2}F_2$, and $HF \rightleftharpoons H+F$ have been calculated using the free energy functions from Tables I to III inclusive and the dissociation energies, ΔE_0^0, of 35.3 kcal mole^{-1}, 64.2$_2$ kcal mole^{-1}, and 133.5$_4$ kcal mole^{-1}; the free energy function for molecular hydrogen was derived from the work of Woolley, Scott, and Brickwedde[29] from which the contribution for nuclear spin was removed by adding R ln4 to the values of $(F^0-E_0^0)/T$. The equilibrium constants for the several reactions derived from these functions and the above dissociation energies are summarized in Table IV with the heats of reaction indicated as quotients with temperature for the sake of tabulation convenience.

Murphy[30,31] has proposed an interpolation equation for the free energy function which is useful at temperatures other than those recorded in Tables I, II, III, and IV. Constants for the equation, which may be readily differentiated to obtain the other functions,

$$-(F^0-E_0^0)/T=a/T+b\ \ln T+cT+dT^2+eT^3+j$$

are tabulated in Table V for H_2 from the data of Scott, Woolley, and Brickwedde,[29] and for F_2, F, and HF from the results herein reported. The maximum error in the free energy function for molecular hydrogen amounts to 0.030 cal mole^{-1} deg^{-1} at 500°K being progressively less in going to higher and lower temperatures so that at 300°K and 800°K the error is only 0.002 cal mole^{-1} deg^{-1} and 0.008 cal mole^{-1} deg^{-1}, respectively; at 1000°K the error is 0.001 cal mole^{-1} deg^{-1}. The maximum error in the free energy function for the fluorine molecule and atom calculated from the interpolation equations are 0.035 cal mole^{-1} deg^{-1} and 0.007 cal mole^{-1} deg^{-1}, respectively; that for hydrogen fluoride has a maximum error of .030 cal mole^{-1} deg^{-1} at 500°K.

The value of ΔE_0^0 for the dissociation reaction of hydrogen fluoride into the atoms was evaluated from the new heat of dissociation of fluorine[13] and the best available heats of formation of HF (64.22 kcal mole^{-1})[32] and of H (103.24 kcal mole^{-1})[32] to be 133.5 0.2 kcal mole^{-1}; this value falls well below the upper limit of 138 kcal mole^{-1} obtained by the usual Birge-Sponer plot from the first five vibrational levels of the ground state of HF. Such a low value of the D_0^0 of HF (5.83$_3$ ev) does not invalidate the conclusions of Glockler with respect to the NH heat of dissociation of 3.74 ev.[33] The constants for his empirical relationship for D_0^0 have been re-evaluated using the new heat of dissociation of fluorine and the D_0^0 of NH was calculated to be 3.77 ev which value is in close agreement with that derived from the N−H bond energy by Cole and Gilbert[34] from the heat of dissociation of hydrazine as reported by Szwarc.[23]

The complete thermodynamic properties of chlorine monofluoride would be known if a reliable heat of formation for this interhalogen was available. The values of ΔH_f^0 reported to date range from −27.4 kcal mole^{-1} [35–37]

TABLE III. Thermodynamic functions of hydrogen fluoride.

T°K	C_p cal mole^{-1} deg^{-1}	S^0 cal mole^{-1} deg^{-1}	$-(F^0-E_0^0)/T$ cal mole^{-1} deg^{-1}	$(H^0-E_0^0)/T$ cal mole^{-1} deg^{-1}
100	6.961	33.974	27.162	6.757
200	6.959	38.745	31.884	6.859
298.16	6.960	41.526	34.629	6.893
300	6.960	41.569	34.670	6.894
400	6.961	43.573	36.655	6.912
500	6.973	45.127	38.202	6.923
600	6.987	46.399	39.495	6.933
700	7.015	47.479	40.536	6.942
800	7.063	48.418	41.462	6.954
900	7.129	49.254	42.286	6.970
1000	7.210	50.011	43.021	6.990
1100	7.304	50.702	43.687	7.014
1200	7.401	51.340	44.281	7.043
1300	7.503	51.936	44.842	7.075
1400	7.604	52.495	45.386	7.108
1500	7.703	52.925	45.881	7.144
1600	7.798	53.524	46.342	7.182
1700	7.886	54.001	46.779	7.221
1800	7.974	54.453	47.193	7.260
1900	8.054	54.887	47.586	7.300
2000	8.129	55.302	47.962	7.340
2100	8.1994	55.683	48.317	7.366
2200	8.264	56.082	48.664	7.417
2300	8.326	56.452	48.997	7.456
2400	8.383	56.808	49.314	7.493
2500	8.436	57.148	49.535	7.530
2600	8.486	57.482	49.915	7.566
2700	8.532	57.802	50.202	7.600
2800	8.576	58.116	50.481	7.634
2900	8.617	58.416	50.748	7.668
3000	8.656	58.709	51.009	7.700
3100	8.691	58.979	51.246	7.732
3200	8.727	59.270	51.507	7.762
3300	8.760	59.538	51.747	7.793
3400	8.790	59.802	51.980	7.821
3500	8.819	60.058	52.208	7.849
3600	8.847	60.306	52.429	7.876
3700	8.874	60.547	52.645	7.903
3800	8.899	60.785	52.856	7.924
3900	8.923	61.017	53.063	7.954
4000	8.946	61.242	53.264	7.979
4100	8.969	61.465	53.461	8.002
4200	8.990	61.681	53.655	8.026
4300	9.011	61.893	53.844	8.048
4400	9.028	62.100	54.030	8.070
4500	9.045	62.304	54.211	8.092
4600	9.066	62.501	54.387	8.113
4700	9.084	62.697	54.562	8.134
4800	9.102	62.888	54.735	8.154
4900	9.119	63.076	54.902	8.174
5000	9.135	63.260	55.068	8.192

[29] Woolley, Scott, and Brickwedde, J. Research Natl. Bur. Standards **41**, 379–475 (1948).
[30] G. M. Murphy, J. Chem. Phys. **5**, 637 (1937).
[31] G. M. Murphy and J. E. Vance, J. Chem. Phys. **7**, 808 (1939).
[32] F. D. Rossini, *et al.*, "Selected Values of Chemical Thermodynamic Properties," U. S. Natl. Bur. Stnds. U. S. Gov't. Printing Office, Washington, D. C., (Dec. 31, 1947).
[33] G. Glockler, J. Chem. Phys. **16**, 602 (1948).
[34] Leland G. Cole and E. C. Gilbert, J. Am. Chem. Soc. **75**, 5423 (1951).
[35] O. Ruff and W. Menzel, Z. anorg. u. allgem. Chem. **198**, 375 (1931).
[36] O. Ruff, Z. angew. Chem. **42**, 806 (1929).
[37] O. Ruff and F. Laass, Z. anorg. u. allgem. Chem. **183**, 214 (1929).

TABLE IV. Heats, free energies and equilibrium constants for the dissociation reactions of HF and F_2.

Temp. °K	$HF \rightleftharpoons \frac{1}{2}H_2+\frac{1}{2}F_2$ $\Delta H^0/T$	$\Delta F^0/T$	$K=\frac{P_{H_2}^{\frac{1}{2}}P_{F_2}^{\frac{1}{2}}}{P_{HF}}$	$HF \rightleftharpoons H+F$ $\Delta H^0/T$	$\Delta F^0/T$	$K=\frac{P_H P_F}{P_{HF}}$	$F_2 \rightleftharpoons 2F$ $\Delta H^0/T$	$\Delta F^0/T$	$K=\frac{P_F^2}{P_{F_2}}$
298.16	215.43	217.09	3.590×10^{-48}	451.16	427.36	4.544×10^{-94}	122.06	94.712	1.998×10^{-21}
300	214.11	215.77	6.980×10^{-48}	448.42	424.59	1.831×10^{-93}	121.34	93.967	2.908×10^{-21}
400	160.67	162.23	3.512×10^{-36}	337.16	312.36	6.175×10^{-68}	91.777	63.509	1.319×10^{-14}
500	128.65	130.08	3.719×10^{-29}	270.39	245.48	2.239×10^{-54}	73.940	45.089	1.399×10^{-10}
600	107.31	108.66	1.789×10^{-24}	225.87	199.77	2.194×10^{-44}	61.980	32.734	7.019×10^{-7}
700	92.097	93.296	4.078×10^{-21}	196.48	167.44	2.554×10^{-37}	53.396	23.863	6.095×10^{-6}
800	80.683	81.776	1.343×10^{-18}	170.18	143.15	5.187×10^{-32}	46.933	17.171	1.767×10^{-4}
900	71.814	72.804	1.227×10^{-16}	151.60	124.22	7.097×10^{-28}	41.879	11.955	2.439×10^{-3}
1000	64.716	65.621	4.558×10^{-15}	136.74	109.05	1.472×10^{-24}	37.827	7.7510	2.023×10^{-2}
1200	54.066	54.804	1.054×10^{-12}	114.40	86.198	1.451×10^{-19}	31.724	1.4280	4.874×10^{-1}
1400	46.454	47.088	5.118×10^{-11}	98.416	69.842	5.447×10^{-16}	27.342	−3.1150	4.812
1600	40.736	41.277	9.528×10^{-10}	86.400	57.520	2.686×10^{-13}	24.041	−6.5422	2.690×10^{1}
1800	36.321	36.747	9.312×10^{-9}	77.072	47.907	3.388×10^{-11}	21.464	−9.2181	1.034×10^{2}
2000	32.755	33.114	5.794×10^{-8}	69.562	40.193	1.644×10^{-9}	19.396	−11.370	3.055×10^{2}
2500	26.285	26.474	1.638×10^{-6}	55.952	26.161	1.917×10^{-6}	15.650	−15.273	2.177×10^{3}
3000	21.993	22.172	1.427×10^{-5}	46.861	16.904	2.022×10^{-4}	13.131	−17.880	8.085×10^{3}
3500	18.927	19.027	6.947×10^{-5}	40.339	10.195	5.915×10^{-3}	11.314	−19.762	2.084×10^{4}
4000	16.630	16.657	2.290×10^{-4}	35.429	5.1438	7.513×10^{-2}	9.9380	−21.175	4.245×10^{4}
4500	14.848	14.808	5.804×10^{-4}	31.597	1.1974	5.474×10^{-1}	8.8550	−22.286	7.424×10^{4}
5000	13.431	13.323	1.225×10^{-3}	28.523	−1.9640	2.687	7.9797	−23.165	1.155×10^{5}

to −11.6 kcal mole^{-1}.[38] The energy of dissociation of fluorine may be combined with the results of Wahraftig's studies on the λ4800 band system of ClF[39] and the dissociation energy of normal chlorine[32] to yield the heat of formation of ClF directly. The dissociation products of ClF are first taken to be $Cl(^2P_{\frac{1}{2}})$ and $F(^2P_{\frac{1}{2}})$;[39] the reactions may be written:

	ΔH_0^0 (kcal mole^{-1})
$ClF \rightleftharpoons Cl(^2P_{\frac{1}{2}})+F(^2P_{\frac{1}{2}})$	61.472
$F(^2P_{\frac{1}{2}}) \rightleftharpoons F(^2P_{\frac{1}{2}})$	− 1.16
$F \rightleftharpoons \frac{1}{2}F_2$	−17.7±0.2

and

$Cl \rightleftharpoons \frac{1}{2}Cl_2$	−28.61

from which ΔE_0^0 for the formation of ClF is −14.0±0.2 kcal mole^{-1}. Had the dissociation been to normal atoms (for $D_0^0(ClF)=2.666$ ev), $\Delta H_f^0(ClF)$ would be 15.2±0.2 kcal mole^{-1}. Similarly, had the dissociation products consisted of an excited chlorine atom and an unexcited fluorine atom[40] the $-\Delta H_f^0(ClF)$ would be 12.6±0.2 kcal mole^{-1}. Schmitz and Schumacher have reported a value of $-\Delta H_f^0$ for ClF of 15.0±0.5 kcal mole^{-1} at 18°C from calorimetric determinations of the heats of two reactions.[41] The heat of reaction of fluorine and sodium chloride was measured by them and found to be 39.5±0.5 kcal mole^{-1}, which value is in excellent agreement with an earlier value for this reaction.[42] This value was combined with the heat of reaction of chlorine monofluoride with sodium chloride which they had determined to be 24.5 within 0.2 kcal mole^{-1}. Schmitz and Schumacher's result has been combined[43] with the free energy and heat content functions for fluorine from this paper, for chlorine monofluoride from the recent work of Potter up to 2000°K, and for chlorine to yield the heat and free energy changes for the dissociation reactions of chlorine fluoride

$$ClF \rightleftharpoons \tfrac{1}{2}F_2+\tfrac{1}{2}Cl_2$$

and

$$ClF \rightleftharpoons F+Cl;$$

the ΔE_0^0 for the dissociation to atoms was taken to be 61.31 kcal mole^{-1}. At 298.16°K the heats of dissociation were assumed to be the same as at 0°K within the limits of error of the experimental heats of reaction involved and the free energy changes were calculated to be 15,363 cal mole^{-1} and 54,687 cal mole^{-1}, respectively.

TABLE V. Constants for interpolation equations of the form $-(F^0-E_0^0)/T=(a/T)+b\ln T+dT^2+eT^3+j$.

	HF	F_2	F	H_2
a	-2.17217×10^{2}	3.85319×10^{2}	1.91510×10^{1}	-1.462467×10^{2}
b	6.16936	7.986085	5.39394	6.289966
c	6.24534×10^{-4}	4.80248×10^{-4}	-1.85666×10^{-4}	5.207196×10^{-4}
d	-2.28325×10^{-8}	-2.6403×10^{-7}	1.37835×10^{-8}	-5.152480×10^{-9}
e	0.00000	0.00000	0.00000	-1.036496×10^{-12}
j	0.020084	−5.50214	1.96369	−11.079834

[38] E. Wicke, Nachr. Akad. Wiss. Gottingen, Math.-physik. Kl., 1946, 89.
[39] A. L. Wahraftig, J. Chem. Phys. **10**, 248 (1942).
[40] R. A. Durie, Proc. Roy. Soc. **A207**, 388 (1951).
[41] H. Schmitz and H. J. Schumacher, Z. Naturforsch **2a**, 362 (1947).
[42] H. V. Wartenberg and H. Fitzner, Z. anorg. u. allgem. Chem. **151**, 313 (1926).
[43] Leland G. Cole and G. W. Elverum, Jr. (unpublished data from a paper in preparation on the thermodynamic properties of the interhalogens).

The Microwave Spectra and Molecular Structures of Trifluoromethyl Bromide, Iodide, and Cyanide*

JOHN SHERIDAN† AND WALTER GORDY
Department of Physics, Duke University, Durham, North Carolina
(Received November 23, 1951)

The pure rotational spectra of trifluoromethyl bromide, iodide, and cyanide have been studied in the microwave region. The B_0 values in Mc/sec were determined as follows: 2098.06 for CF_3Br^{79}; 2078.50 for CF_3Br^{81}; 1523.23 for CF_3I; 2945.535 for CF_3CN^{14}; 2855.859 for CF_3CN^{15}. The nuclear quadrupole couplings, eQq, are in Mc/sec: 619 for Br^{79}; 517 for Br^{81}; −2150 for I^{127}; −4.70 for N^{14}. With any reasonable assumption of bond angles, d_{CF} is found to be 1.33±0.015A in each molecule. The other distances depend more strongly on the assumption of the bond angles. With ∠FCF assumed to be 108°±1°, as suggested from other similar molecules, the values, $d_{CBr}=1.91\pm0.02$A, $d_{CI}=2.14\pm0.02$A, $d_{CC}=1.46\pm0.02$A, are obtained, where the additional assumptions $d_{CF}=1.332$A for CF_3I and $d_{CN}=1.158$A for CF_3CN are made.

INTRODUCTION

INTERATOMIC distances in fluorocarbon derivatives are of special interest from the viewpoint of structural theory, and a number of such compounds have been studied by electron diffraction[1] and by spectroscopy.[2] The symmetric top molecules in which a CF_3 group is joined to another atom or axially symmetric group are especially suited to study by means of their pure rotational spectra in the microwave region, and investigations of this type have already been reported for CF_3H,[3] CF_3Cl,[4] and CF_3CCH.[5] The present paper is a fuller account of microwave studies of CF_3Br, CF_3I, and CF_3CN which were briefly described in a preliminary publication.[6] No structural information has previously been available for these molecules.

EXPERIMENTAL

The trifluoromethyl bromide and iodide were the gift of Imperial Chemical Industries, Ltd., General Chemical Division, England, and are gratefully acknowledged. About 10 g of each was distilled at low pressure and the center fractions used.

Trifluoromethyl cyanide was prepared as described by Gilman and Jones[7] and similarly fractionated. The CF_3CN^{15} was made by the same means, using ammonia containing 7.5 atom percent of N^{15}.

The microwave measurements were made with a video sweep spectroscope[8] at −70° and gas pressures of about 10^{-3} mm. Frequencies were measured with a frequency standard monitored with station WWV.

RESULTS

The unperturbed frequencies of the indicated transitions are given in Table I, with the values of B_0, moment of inertia I_B, distortion coefficients D_J and D_{JK}, and nuclear quadrupole coupling factors (eQq) for the bromine, iodine, and N^{14} nuclei. The results for CF_3Br are in close agreement with those obtained by Shar-

TABLE I. Spectral constants.

Molecule	$J\rightarrow J'$	Unperturbed frequency Mc/sec ±0.1 Mc/sec	B_0 Mc/sec	I_B[a] g cm² ×10⁻⁴⁰	D_J kc/sec	D_{JK} kc/sec	eQq Mc/sec
CF_3Br^{79}	10→11	46,157.41	2098.06	399.847	0 (assumed)	1.26	619
CF_3Br^{81}	10→11	45,726.89	2078.50	403.612	0 (assumed)	1.22	517±3
CF_3I^{127}	9→10	30,464.6	1523.23	550.741	0 (assumed)	0.6	−2150
CF_3CN^{14}	5→6 7→8	35,346.03 47,127.74	2945.535	284.806	0.4	5.8	−4.70
CF_3CN^{15}	5→6 7→8	34,269.81 45,692.94	2855.859	293.749	0.4	5.6	—

[a] The value of Planck's constant was taken as 6.62373×10^{-27} erg sec and 1 a.m.u. as 1.65972×10^{-24} g (J. W. M. Dumond and E. R. Cohen, Revs. Modern Phys. **21**, 651 (1949)).

* The research reported in this paper has been sponsored by the Geophysical Research Directorate of Air Force Cambridge Research Laboratories under Contract No. W19-122-ac-35.

† Present address: Department of Chemistry, University of Birmingham, Birmingham 15, England.

[1] P. W. Allen and L. E. Sutton, Acta Cryst. **3**, 46 (1950).
[2] G. Herzberg, Infrared and Raman Spectra, (D. Van Nostrand Company, Inc., New York, 1945), p. 322.
[3] Gilliam, Edwards, and Gordy, Phys. Rev. **75**, 1014 (1949).
[4] D. K. Coles and R. H. Hughes, Phys. Rev. **76**, 858 (1949).
[5] Anderson, Trambarulo, Sheridan, and Gordy, Phys. Rev. **82**, 58 (1951).
[6] J. Sheridan and W. Gordy, Phys. Rev. **77**, 292 (1950).
[7] H. Gilman and R. G. Jones, J. Am. Chem. Soc. **65**, 1458 (1943).
[8] W. Gordy and M. Kessler, Phys. Rev. **72**, 644 (1947).

TABLE II. Observed and calculated hyperfine structure for the $J=10\rightarrow11$ transition of CF_3Br^{79}. Frequencies are calculated with $B_0=2098.064$ Mc/sec, $D_J=0$ kc/sec, $D_{JK}=1.26$ kc/sec, and $eQq=+619$ Mc/sec.

K	Transition $F\rightarrow F'$		Calc frequency Mc/sec	Obs frequency Mc/sec
9	21/2→23/2		46,188.03	46,187.96
9	19/2→21/2		46,182.76	46,182.44
8	21/2→23/2		46,181.44	46,181.24
9	19/2→21/2		46,178.16	46,177.98
7	21/2→23/2		46,175.61	46,175.44
8	19/2→21/2		46,174.06	46,173.94
6	21/2→23/2		46,170.57	46,170.44
7	19/2→21/2		46,170.90	
6	19/2→21/2		46,167.28	46,167.24
5	21/2→23/2		46,166.30	46,166.14
5	19/2→21/2		46,164.62	46,164.58
4	21/2→23/2		46,162.81	46,162.68
4	19/2→21/2		46,162.25	46,162.40
3	19/2→21/2		46,160.74	46,160.70
3	21/2→23/2		46,160.08	46,160.02
2	19/2→21/2		46,159.53	46,159.50
1	19/2→21/2		46,158.80	46,158.80
0	19/2→21/2,	17/2→19/2	46,158.52	46,158.56
2	21/2→23/2		46,158.14	46,158.06
1	17/2→19/2		46,158.10	
1	21/2→23/2		46,156.98	46,156.98
0	23/2→25/2,	21/2→23/2	46,156.59	46,156.60
2	17/2→19/2		46,156.72	
1	23/2→25/2		46,156.28	46,156.28
2	23/2→25/2		46,155.33	46,155.32
3	17/2→19/2		46,154.41	46,154.28
3	23/2→25/2		46,153.76	46,153.72
4	23/2→25/2		46,151.56	46,151.52
4	17/2→19/2		46,151.18	46,151.04
5	23/2→25/2		46,148.72	46,148.76
5	17/2→19/2		46,147.03	46,146.92
6	23/2→25/2		46,145.24	46,145.34
6	17/2→19/2		46,141.95	46,141.80
7	23/2→25/2		46,141.15	46,141.18
8	23/2→25/2		46,136.42	46,136.42
7	17/2→19/2		46,135.95	46,135.84
9	23/2→25/2		46,131.05	46,130.54
8	17/2→19/2		46,129.04	46,128.96
9	17/2→19/2		46,121.19	46,121.20

baugh, Pritchard, and Madison[9] from the $J=4\rightarrow5$ and $J=5\rightarrow6$ transitions.

The hyperfine structures calculated using these values of D_{JK} and eQq are compared with the observed frequencies in Tables II–VI.

Table VII gives some combinations of structural parameters which are in accord with the observed moments of inertia. Microwave measurements on different isotopically substituted molecules are desirable in order that a final choice of parameters can be made. While we hope, with somewhat improved sensitivity, to observe spectra for CF_3CN containing C^{13} in natural concentration, spectra for different isotopic combinations in the other substances are only likely to be observed after difficult isotopic enrichments.

DISCUSSION

CF_3Br and CF_3I

To obtain the molecular structures it is at present necessary to assume one parameter for CF_3Br and two parameters for CF_3I. The results are fairly sensitive to the value of $\angle FCF$ assumed, and while this angle is known for fluoroform both from electron diffraction and from microwave spectroscopy, there are no similar results for CF_3Br, CF_3I, or CF_3CN.

In fluoroform, $\angle FCF$ has been found from microwave studies by Ghosh, Trambarulo, and Gordy[10] to be $108°\,48'\pm45'$ and the CF distances as 1.332 ± 0.008A. These results are in agreement with a recent reinvestigation of CF_3H by electron diffraction using the rotating sector method.[11]

In CF_3 derivatives we might expect $\angle FCF$ to be nearly the same as in CF_3H, or perhaps somewhat smaller on account of the substitution of a larger group in place of the hydrogen atom. This, however, is by no means certain, since if F is substituted for H in CF_3H $\angle FCF$ must clearly increase to $109°\,28'$; but steric

TABLE III. Observed and calculated hyperfine structure for the $J=10\rightarrow11$ transition of CF_3Br^{81}. Frequencies are calculated with $B_0=2078.495$ Mc/sec, $D_J=0$ kc/sec, $D_{JK}=1.22$ kc/sec, and $eQq=+517$ Mc/sec.

K	$F\rightarrow F'$	Calc frequency Mc/sec	Obs frequency Mc/sec
9	21/2→23/2	45,752.19	45,752.20
10	19/2→21/2	45,747.72	45,747.52
8	21/2→23/2	45,746.73	45,746.74
9	19/2→21/2	45,743.95	45,743.94
7	21/2→23/2	45,741.93	45,741.90
8	19/2→21/2	45,740.57	45,740.64
6	21/2→23/2	45,737.66	45,737.66
7	19/2→21/2	45,737.59	45,737.56
6	19/2→21/2	45,735.01	45,735.00
5	21/2→23/2	45,734.24	45,734.22
5	19/2→21/2	45,732.84	45,732.88
4	21/2→23/2	45,731.36	45,731.36
4	19/2→21/2	45,730.89	45,731.06
3	19/2→21/2	45,729.66	45,729.66
3	21/2→23/2	45,729.11	45,729.10
2	19/2→21/2	45,728.66	45,728.70
1	19/2→21/2	45,728.06	45,728.12
0	19/2→21/2	45,727.87	45,727.88
0	17/2→19/2	45,727.87	
1	17/2→19/2	45,727.48	45,727.50
2	21/2→23/2	45,727.50	
1	21/2→23/2	45,726.54	45,726.60
0	23/2→25/2	45,726.23	45,726.26
0	21/2→23/2	45,726.23	
2	17/2→19/2	45,726.31	
1	23/2→25/2	45,725.96	45,726.02
2	23/2→25/2	45,725.16	45,725.18
3	17/2→19/2	45,724.37	45,724.34
3	23/2→25/2	45,723.83	45,723.84
4	23/2→25/2	45,721.96	45,722.12
4	17/2→19/2	45,721.65	45,721.66
5	23/2→25/2	45,719.56	45,719.66
5	17/2→19/2	45,718.14	45,718.16
6	23/2→25/2	45,716.61	45,716.70
6	17/2→19/2	45,713.86	45,713.80
7	23/2→25/2	45,713.14	45,713.24
8	23/2→25/2	45,709.14	45,709.20
7	17/2→19/2	45,708.80	45,708.80
9	23/2→25/2	45,704.60	45,704.58
8	17/2→19/2	45,702.97	45,702.98
10	23/2→25/2	45,699.53	45,699.46
9	17/2→19/2	45,696.36	45,696.34

[9] Sharbaugh, Pritchard, and Madison, Phys. Rev. **77**, 302 (1950).

[10] Ghosh, Trambarulo, and Gordy (to be published).

[11] Private communication from Dr. L. O. Brockway.

TABLE IV. Observed and calculated hyperfine structure for the $J=9\rightarrow10$ transition of CF_3I^{127}. Frequencies are calculated with $B_0=1523.23$ Mc/sec, $D_J=0$ kc/sec, $D_{JK}=0.6$ kc/sec, and $eQq=-2150$ Mc/sec.

K	Transition $F\rightarrow F'$	Calc frequency Mc/sec	Obs frequency Mc/sec
6	13/2→15/2	30,533.11	30,532.05
7	23/2→25/2	30,531.33	30,531.33
6	23/2→25/2	30,514.55	30,514.83
2	19/2→19/2	30,514.97	
5	13/2→15/2	30,510.66	30,509.58
6	23/2→23/2	30,508.17	
5	23/2→25/2	30,500.32	
5	17/2→17/2	30,499.57	30,500.73
3	19/2→19/2	30,499.18	
4	13/2→15/2	30,492.30	30,491.56
9	15/2→17/2	30,490.08	
4	23/2→25/2	30,489.69	30,489.17
8	21/2→21/2	30,489.08	
8	15/2→17/2	30,482.84	
0	21/2→23/2	30,480.58	
3	23/2→25/2	30,479.63	30,480.14
1	21/2→23/2	30,479.32	
3	13/2→15/2	30,478.02	30,477.65
7	15/2→17/2	30,477.08	
4	19/2→19/2	30,477.02	
2	21/2→23/2	30,476.49	30,476.54
6	15/2→15/2	30,476.20	
2	23/2→25/2	30,473.16	30,473.55
6	15/2→17/2	30,471.00	30,470.95
7	23/2→25/2	30,469.31	30,470.02
3	21/2→23/2	30,469.31	30,469.63
0	23/2→25/2	30,468.00	30,468.32
2	13/2→15/2	30,467.83	30,467.72
			30,467.09[a]
5	15/2→17/2	30,466.29	30,466.29
0	19/2→21/2	30,465.66	30,465.76
1	19/2→21/2	30,464.19	30,464.26
4	15/2→17/2	30,462.48	30,462.46
1	13/2→15/2	30,461.69	30,462.16
4	21/2→23/2	30,460.57	30,461.76
2	19/2→21/2	30,459.76	30,459.83
3	15/2→17/2	30,459.60	30,459.51
0	13/2→15/2	30,459.49	
7	21/2→21/2	30,459.24	30,459.00
0	17/2→19/2	30,459.00	
1	17/2→19/2	30,458.13	30,458.15
2	15/2→17/2	30,457.35	30,457.42
1	15/2→17/2	30,456.08	30,456.13
0	15/2→17/2	30,455.66	30,455.63
2	17/2→19/2	30,455.48	30,455.46
3	19/2→21/2	30,452.39	30,452.49
3	17/2→19/2	30,451.12	30,451.31
5	21/2→23/2	30,499.30	30,449.49
			30,446.96
4	17/2→19/2	30,444.98	30,445.32
4	19/2→21/2	30,442.08	30,442.17
5	17/2→19/2	30,437.11	30,437.54
			30,436.74
5	21/2→23/2	30,435.97	30,436.24
			30,434.89
6	21/2→21/2	30,433.39	30,432.06
6	17/2→17/2	30,431.02	
5	19/2→21/2	30,429.67	30,428.97
6	17/2→19/2	30,427.45	30,427.99
			30,426.25[a]
			30,425.23[a]
			30,421.04[a]
7	21/2→23/2	30,419.28	30,420.49
7	17/2→19/2	30,416.01	30,416.42
			30,414.44
6	19/2→19/2	30,413.72	30,413.84
6	19/2→21/2	30,412.60	30,412.64
5	21/2→21/2	30,411.48	30,412.09
8	17/2→19/2	30,402.93	30,402.76
8	21/2→23/2	30,400.50	30,400.97
			30,397.85[a]
			30,395.37[a]
7	19/2→21/2	30,393.43	30,393.47
			30,392.19[a]
			30,391.03[a]
			30,390.29[a]
9	17/2→19/2	30,388.02	30,387.87
			30,387.43[a]
			30,386.82[a]
			30,386.08[a]
7	19/2→19/2	30,372.51	
8	19/2→21/2	30,371.32	30,371.50
2	21/2→21/2	30,369.74	30,369.52
9	19/2→21/2	30,347.27	30,346.49

[a] These are observed frequencies for which there is no corresponding theoretical value. They probably arise from molecules in excited vibrational states.

effects may be active in CF_3Cl, CF_3Br, and CF_3I. If we take $\angle FCF$ as $108°\pm1°$ in CF_3Cl, the microwave data of Coles and Hughes[4] give $d_{CF}=1.328\mp0.005$A and $d_{CCl}=1.740\pm0.018$A. This value of d_{CCl} is naturally somewhat shorter than the 1.765A calculated by these authors, assuming tetrahedral angles, but the angle FCF assumed here appears more probable. A tendency for $\angle FCF$ to be slightly less than the tetrahedral angle is supported by the value ($107°\pm30'$) found for this angle by Stewart and Nielsen[12] in CF_2H_2 from the infrared spectrum, and such a tendency would be analogous to the behavior of $\angle FSiF$ in SiF_3H,[13] SiF_3Cl[1] and of $\angle FGeF$ in GeF_3Cl.[14] There are also indications from preliminary electron diffraction studies that d_{CCl} in CF_3Cl may be shorter than the 1.76A found in CCl_4,[15] which would require $\angle FCF$ to be smaller than the tetrahedral angle.

In CF_3Br, if $\angle FCF$ is again taken as $108°\pm1°$ we obtain $d_{CF}=1.330\mp0.005$A and $d_{CBr}=1.908\pm0.018$A. It is possible, however, that $\angle FCF$ may be slightly smaller than this on account of the size of the bromine atom, and if $\angle FCF$ is assumed to be $107.5°\pm1°$ we find $d_{CF}=1.333\mp0.005$A and $d_{CBr}=1.899\pm0.018$A.

In CF_3I we have assumed $d_{CF}=1.332$A, which is close to the values consistently found in these compounds with all reasonable valency angles. If, in addition, $\angle FCF$ is $108°\pm1°$, then $d_{CI}=2.134\pm0.016$A. If $\angle FCF$ is assumed to have decreased to $107°\pm1°$, then $d_{CI}=2.118\pm0.016$A.

It is seen that d_{CF} can be determined as 1.33 ± 0.015A in CF_3Br and CF_3Cl with all reasonable allocations of valency angles. This distance is in agreement with that for CF_3H and for CF_3CN (see below). The other distances are much more dependent on the assumed angles.

[12] H. B. Stewart and H. H. Nielsen, Phys. Rev. **75**, 640 (1949).
[13] J. Sheridan and W. Gordy, J. Chem. Phys. **19**, 965 (1951).
[14] Anderson, Sheridan, and Gordy, Phys. Rev. **81**, 819 (1951).
[15] See R. L. Livingston and L. O. Brockway, J. Am. Chem. Soc. **66**, 97 (1944). We understand that Dr. Brockway is reinvestigating CF_3Cl by electron diffraction.

TABLE V. Observed and calculated hyperfine structures for the $J=5\rightarrow6$ and $J=7\rightarrow8$ transitions of CF_3CN^{14}. Frequencies were calculated with $B_0=2945.535$ Mc/sec, $D_J=0.4$ kc/sec, $D_{JK}=5.8$ kc/sec, $eQq=-4.70$ Mc/sec.

Transition $J\rightarrow J'$	K	$F\rightarrow F'$	Calc frequency Mc/sec	Obs frequency Mc/sec
5→6	0	4→5, 5→6, 6→7	35,346.04−6.09	35,346.03
	1	4→5, 5→6, 6→7	35,345.97−6.03	
	2	4→5, 5→6	35,345.86	35,345.90
	2	5→6	35,345.65	
	3	5→6	35,345.63	35,345.60
	3	6→7	35,345.56	
	4	4→5	35,345.32	
	3	5→6	35,345.15	35,345.15
	4	6→7	35,345.14	
	5	4→5	35,344.92	35,344.91
	5	6→7	35,344.64	35,344.65
	4	5→6	35,344.42	35,344.44
	5	5→6	35,343.49	35,343.50
7→8	0	6→7, 7→8, 8→9	47,127.72−0.75	47,127.74
	1	6→7, 7→8, 8→9	47,127.64−0.67	
	2	6→7, 7→8, 8→9	47,127.31−0.40	47,127.44
	3	6→7, 8→9	47,126.96−0.97	47,127.02
	3	7→8	47,126.77	47,126.83
	4	6→7, 8→9	47,126.35−0.38	47,126.46
	4	7→8	47,126.03	47,126.07
	5	6→7, 8→9	47,125.56−0.64	47,125.62
	6	6→7	47,124.72	47,124.68
	6	8→9	47,124.60	47,124.58
	6	7→8	47,123.90	47,123.88
	7	6→7	47,123.63	47,123.60
	7	8→9	47,123.46	47,123.48
	7	7→8	47,122.50	47,122.48

Table VIII summarizes the sets of parameters obtained with $\angle$FCF assumed as 108°. The results can profitably be regarded in the following way. In Table IX are compared the values of d_{CX} in CH_3X with those obtained for CF_3X (X=Cl, Br, I) assuming $\angle FCF=108°$ in all cases. The distance d_{CX} is shorter in CF_3X, but the contraction caused by replacing CH_3 by CF_3 falls off in the sequence X=Cl, Br, I. From a 2.2 percent contraction when X=Cl it declines to almost zero in CF_3I. (If tetrahedral angles are assumed, it has been shown[6] that d_{CI} becomes greater in CF_3I than in CH_3I.)

TABLE VI. Observed and calculated hyperfine structures for the $J=5\rightarrow6$ and $J=7\rightarrow8$ transitions of CF_3CN^{15}. Frequencies were calculated with $B_0=2855.859$ Mc/sec, $D_J=0.4$ kc/sec, and $D_{JK}=5.6$ kc/sec.

Transition $J\rightarrow J'$	K	Calc frequency Mc/sec	Obs frequency Mc/sec
5→6	0	34,269.91	
	1	34,269.84	34,269.81
	2	34,269.64	
	3	34,269.30	34,269.30
	4	34,268.83	34,268.83
	5	34,268.23	34,268.24
7→8	0	45,692.98	45,692.94
	1	45,692.89	
	2	45,692.62	45,692.74
	3	45,692.17	45,692.16
	4	45,691.55	45,691.56
	6	45,690.74	45,690.72
	7	45,689.76	45,689.82
	8	45,688.59	45,688.54

TABLE VII. Parameters consistent with I_B values. (Zero-point energy effects are neglected.)

Molecule	$\angle$FCF	d_{CF}(A)	d_{CX}(A)
CF_3Br	106° 28′	1.338	1.881
	107° 28′	1.333	1.899
	108° 28′	1.327	1.917
	109° 28′	1.322	1.935
CF_3I	106° 28′	1.332	2.110
	107° 28′	1.332	2.126
	108° 28′	1.332	2.142
	109° 28′	1.332	2.158
	109° 28′	1.322	2.164
CF_3CN, assuming $d_{CN}=1.158$A	106° 28′	1.343	1.432
	107° 28′	1.338	1.452
	108° 28′	1.333	1.472
	109° 28′	1.328	1.492

Atomic masses used were: *Carbon:* 12.00386 (R. T. Birge, Revs. Modern Phys. **13**, 233 (1941)). *Fluorine:* 19.00452 (M. S. Livingston and H. A. Bethe, Revs. Modern Phys. **9**, 373 (1937)). *Bromine:* 78.9417 and 80.9400 (F. W. Aston, Nature **141**, 1096 (1938)). *Iodine:* 126.932 (F. W. Aston, Proc. Roy. Soc. (London) **A115**, 487 (1927)). *Nitrogen:* 14.00750 and 15.00489 (M. S. Livingston and H. A. Bethe, Revs. Modern Phys. **9**, 373 (1937)).

If it is assumed that d_{CX} is always 2.2 percent shorter in CF_3X than in CH_3X, and the values which $\angle$FCF must then take are calculated, it is found that $\angle$FCF falls from 108° when X=Cl progressively to 105° 40′ when X=I. This, however, does not seem probable.

The contractions in d_{CX} which occur are presumably to be accounted for by contributions to the structure from types (I) and (II), which are expected to be more important here than the analogous structures for CH_3X on account of the high electronegativity of fluorine. Against this must be set the possibility of contributions from type (III) opposing a contraction of the CX bond. When X is fluorine, forms (I) and (III) must contribute equally, but as X

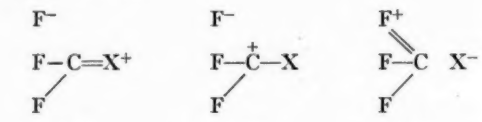

(I) (II) (III)

changes in the sequence Cl, Br, I, the decline in the ability of X to form double bonds may be faster than its decline in electronegativity, and form (III) may increase in relative importance compared with (I) as X changes in this way.[6] This would correspond to a decline in the contraction of the CX bond in the sequence X=Cl, Br, I.

TABLE VIII. Parameters for CF_3X and CF_3CN.

Molecule	$\angle$FCF assumed	d_{CF} (A)	d_{CX} (A)
CF_3Cl	108°±1°	1.328∓0.008	1.740±0.02
CF_3Br	108°±1°	1.330∓0.008	1.908±0.02
CF_3I	108°±1°	1.332 (assumed)	2.134±0.02
CF_3CN (d_{CN} assumed 1.158A)	108°±1°	1.335∓0.008	1.464±0.02

Further evidence can be obtained by comparison of the nuclear quadrupole couplings of Cl, Br, and I in the series CF_3X and CH_3X (Table X). The couplings are always numerically greater in CF_3X, and the percentage increase in coupling caused by substitution of CF_3 for CH_3 increases from 4 percent in the case of Cl, through that of Br, to 11 percent in that of I. Since forms (I) to (III) do not account for the increased coupling, this increase suggests the possible occurrence of some type (IV) coupled with smaller contributions from type (V) than in the analogous CH_3X case. Form (IV) should increase in importance

(IV) (V)

in the sequence X = Cl, Br, I. This is in agreement with the sequence of observed changes in coupling, which

TABLE IX. Values of d_{CX} (assuming $\angle$FCF) compared with d_{CX} in the CH_3X series.

X	$\angle$FCF	d_{CX} (A) CF_3X	CH_3X	$d_{CF_3}-d_{CH_3}$ (A)
(F	109° 28′	1.34[a]	1.385[b]	−0.045)
Cl	108°	1.740	1.779[c]	−0.039
Br	108°	1.908	1.936[c]	−0.028
I	108°	2.134	2.139[c]	−0.005

[a] We have taken the lower limit allowed by the electron diffraction results for CF_4 (reference 1). A reinvestigation of CF_4 by electron diffraction seems desirable to decide whether d_{CF} in it is appreciably longer than that now found in CF_3 derivatives and CF_2H_2.
[b] Reference 3.
[c] Gordy, Simmons, and Smith, Phys. Rev. **74**, 243 (1948).

could be accounted for by relatively small contributions from (IV). The factors affecting the structures discussed here are very similar to those which affect the analogous silane derivatives.[13]

CF_3CN

To determine this structure we must at present assume two of the four parameters. We have taken d_{CN} to be 1.158A as found in methyl cyanide.[16] This assumption may be made with some confidence since the quadrupole coupling of N^{14} in CF_3CN is close to that in methyl cyanide, and it has been shown[16] that a relationship exists between this coupling and the CN bond length. Actually the coupling in CF_3CN (−4.70 Mc/sec) is slightly more than that in methyl cyanide (−4.35 Mc/sec) which probably corresponds to a very slightly shorter bond in CF_3CN, but such a difference in length (0.001A or less) is smaller than other unavoidable errors. It is, moreover, known that triple bonds of

[16] Kessler, Ring, Trambarulo, and Gordy, Phys. Rev. **79**, 54 (1950).

TABLE X. Nuclear quadrupole couplings of halogens (X) in CF_3X and CH_3X.

X	CH_3X[a]	eQq in (Mc/sec) CF_3X	Percent increase in coupling in CF_3X
Cl^{35}	−75.13	−78.05[b]	3.9
Cl^{37}	−59.03	−61.44[b]	4.1
Br^{79}	+577.0	+619	7.3
Br^{81}	+482.0	+517	7.3
I^{127}	−1934	−2150	11.2

[a] From Gordy, Simmons, and Smith, Phys. Rev. **74**, 243 (1948).
[b] From reference 4.

the type of C≡N change little in length despite rather wide variations in the nature of the attached groups.

If, in addition, we assume $\angle$FCF to be 108°±1°, we find $d_{CF}=1.335\mp0.008$A and $d_{CC}=1.464\pm0.02$A. Once more, d_{CF} can be obtained quite closely, and its value agrees well with that found in other CF_3 derivatives, while the other distance, here d_{CC}, depends considerably on the assumed angle. With the above angle, d_{CC} is almost as short as the 1.460A found[16] in methyl cyanide, and would equal this distance if $\angle$FCF were 107° 48′. If tetrahedral angles are assumed, d_{CC} is found as 1.492A, which is distinctly longer than in methyl cyanide; this, however, seems less probable. The situation is very similar to that in trifluoromethyl acetylene[5] where the analogous d_{CC} was found to be 1.493A on the assumption of tetrahedral angles; it seems that more probable parameters for this molecule also would be d_{CC} close to 1.460, as in methyl acetylene[17] with an angle $\angle$FCF slightly less than tetrahedral.

In methyl cyanide, the shortness of d_{CC} has been attributed in part to hyperconjugation involving structures such as (VI), but it is not probable that analogous structures would be important

(VI) (VII)

for CF_3CN. Without hyperconjugation, but with the acetylenic carbon radius, d_{CC} would be about 1.50A. There is, however, evidence, for example from the electron diffraction by the trifluoracetic acid dimer,[1] that attachment of three fluorine atoms to a carbon atom lowers the carbon radius towards its fourth partner, even when no shortening of the fourth bond by double-bond character appears likely, and such an effect would lead to d_{CC} in CF_3CN being less than 1.50A. It may perhaps be attributed to a lowering of the carbon radius in form (VII), analogous to (II) above. It appears probable that the CC bond length so produced is quite close to that in methyl cyanide.

[17] R. F. Trambarulo and W. Gordy, J. Chem. Phys. **18**, 1613 (1950).

The Infrared and Raman Spectra of F_2CO, FClCO, and Cl_2CO*

A. H. Nielsen, T. G. Burke, P. J. H. Woltz, and E. A. Jones†
K-25 Laboratories, Carbide and Carbon Chemicals Company, Oak Ridge, Tennessee and the University of Tennessee, Knoxville, Tennessee

(Received August 30, 1951)

This paper combines earlier preliminary reports on F_2CO, FClCO and Cl_2CO into a complete report on the Raman and infrared spectra of these molecules. Details of measurement and handling of the samples are given. The fundamental frequencies observed in both Raman effect (liquid) and infrared (gas) and a large number of overtone and combination frequencies observed in the infrared have been identified and are collected in tables. The observed infrared band envelopes are described and compared with the band envelopes predicted on the basis of the molecular models. Resonance between ν_2 and $2\nu_1$ in F_2CO and ν_2 and $\nu_1+\nu_4$ in FClCO is discussed.

INTRODUCTION

THIS paper combines into a single report results of infrared and Raman investigations performed over a period of several years on the molecules F_2CO, FClCO, and Cl_2CO, some of which have been reported elsewhere in preliminary fashion.[1] Of this group of carbonyls only Cl_2CO has been previously investigated in the Raman or infrared regions of the spectrum. The most recent Raman measurements found in the literature were those of Ananthakrishnan[2] who observed 5 lines at 302, 442, 573, 832, and 1807 cm^{-1}, which have been designated as the fundamentals. Shortly after the publication of this Raman work, Bailey and Hale[3] observed the infrared spectrum from about 2–19μ and reported sixteen absorption bands, among which were three of the fundamentals. They also assigned the remainder of their bands as overtones and combination frequencies and computed force constants. Electron diffraction measurements which served to fix the model as planar and similar to H_2CO were made by Brockway, Beach, and Pauling.[4]

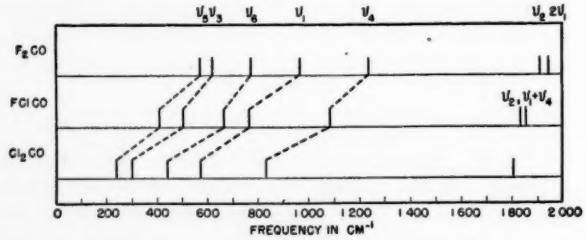

FIG. 1. Scale drawing of the Raman spectra of F_2CO, FClCO, and Cl_2CO.

In the present investigation, the Raman spectra have been photographed for F_2CO and FClCO, and repeated for Cl_2CO. The infrared spectra of F_2CO and FClCO have been observed from about 2–38μ, and the infrared spectrum of Cl_2CO has been repeated from 2–20μ and extended to 38μ. Assignment of the fundamentals, and overtone and combination bands has been made.

EXPERIMENTAL DETAILS

Raman Spectra

A Lane-Wells Raman spectrograph and source unit were employed to obtain the spectra of all three molecules. The exciting line was the Hg 4358A filtered by Rhodamine 5GDN extra and paranitrotoluene. Exposures with 100μ slits ranged from 1–4 hr.

F_2CO

F_2CO cooled to −100°C is a colorless liquid. The gas was condensed into a glass Raman tube through a copper tube from a copper storage cylinder, and was kept liquid by blowing cooled N_2 into a Dewar flask surrounding the Raman tube. The exposures were made on Eastman XXX PAN film. The F_2CO was prepared by W. Simon, A. V. Faloon, and W. B. Kenna.

FClCO

The technique of handling FClCO was the same as outlined above, but the temperature of the colorless liquid was about −60°C. For the photographs obtained in this case, Eastman 103 AJ film was used. The FClCO was prepared by A. V. Faloon and W. B. Kenna.

Cl_2CO

Cl_2CO is also a colorless liquid when cooled to about 0°C. It was obtained from Matheson Company and was handled in the same way as the other molecules. Eastman 103 AJ film was used for all exposures. In this case, slits of 150μ were used and the exposures shortened to 40 min.

---

* This document is based on work performed for the AEC by Carbide and Carbon Chemicals Company at Oak Ridge, Tennessee.

† Department of Physics, Vanderbilt University, Nashville, Tennessee.

[1] The Ohio State Symposium on Molecular Structure (June 1949, 1950). Woltz, Jones, and Nielsen, Phys. Rev. **76**, 200A (1949). P. J. H. Woltz and E. A. Jones, J. Chem. Phys. **17**, 502 (1949). E. A. Jones and T. G. Burke, J. Chem. Phys. **18**, 1308 (1950).

[2] R. Ananthakrishnan, Proc. Indian Acad. Sci. **5A**, 285 (1937).

[3] C. R. Bailey and J. B. Hale, Phil. Mag. **25**, 98 (1938).

[4] Brockway, Beach, and Pauling, J. Am. Chem. Soc. **57**, 2693 (1935).

TABLE I. Observed Raman frequencies for liquid F_2CO, FClCO and Cl_2CO.

F_2CO		FClCO		Cl_2CO		
Frequency	Intensity	Frequency	Intensity	Frequency	Intensity	Ananthakrishnan[2]
1944 cm^{-1}	vw	1858 cm^{-1}	m	1807 cm^{-1}	m	1807 cm^{-1}
1909	m	1832	m	...	...	...
1238	vvw	1085	vvw	832	vw	832
965	vs	765	vs	573	vs	573
771	vw	665	vw	442	m	442
620	m	506	s	302	s	302
571	w	410	m	240	vvw	...

Infrared Spectra

The infrared spectra of these three molecules were made with Perkin-Elmer spectrographs, Models 12C and 21 equipped with NaCl, LiF, CaF_2, KBr, and KRS-5 prisms. The cells used for most of the absorption measurements were of fluorothene,[5] and 10 cm long. Windows of NaCl, KBr, AgCl, and KRS-5 were used, in the appropriate regions. They were attached to the cells with a low melting polymer of trifluorochloroethylene. Gas pressures in the cells varied from less than 1 mm of Hg to an atmosphere as indicated in the legends accompanying each figure. In order to discover as many overtone and combination bands as possible records also were made using a modified Perkin-Elmer 1 m cell. A number of records utilizing different gas pressures and slit-widths were made for each band to obtain the optimum in envelope structure to aid in identification. Some difficulty was encountered in handling the F_2CO because of its instability. It was, however, discovered that measurements could be made for quite a long time with a given sample if the cell and transfer system were properly conditioned with gas. No difficulties arose with FClCO and Cl_2CO. Grating records were made across several bands. For these records the University of Tennessee prism-grating spectrograph was used with 7200 and 3600 lines/in. gratings. It was in fact noted that a long-wavelength band in F_2CO could be resolved into rotational fine structure. The analysis of this band has been published as a separate paper.[6] Grating records were made across the C=O absorption region between 1800 cm^{-1} and 2000 cm^{-1} for F_2CO and FClCO to investigate the existence of two overlapping bands which was suggested by the presence in that region of two close and fairly intense Raman lines.

EXPERIMENTAL RESULTS

Raman Spectra

Figure 1 shows the Raman spectra of the three molecules drawn to scale from prints of the original negatives. The original prints are not shown here because the contrast is not sufficiently good to reproduce all the lines well. Reference to Fig. 1 immediately shows the great similarity of the spectra and the shift of the lines to lower frequencies from F_2CO to Cl_2CO.

For F_2CO, 7 lines varying in intensity from very, very weak to very strong were observed. As there are six Raman-active fundamentals, the seventh line requires explanation in some other way. For FClCO, 7 lines also were observed while for Cl_2CO only six lines were found. Explanation of the additional line in F_2CO and FClCO will be made in a later section.

The observed Raman frequencies for all three molecules are collected in Table I, together with the estimated relative intensities. Also listed in Table I are the frequencies given by Ananthakrishnan[2] for Cl_2CO. The agreement is perfect with one exception. He found only five lines, and concluded that his line at 302 cm^{-1} was composed of two degenerate frequencies. In this investigation, a line was found at 240 cm^{-1} in addition to the 302 cm^{-1} line. By comparison with the Raman spectrum of the similar molecule Cl_2CS in which there is a low-frequency Raman line at 200 cm^{-1}, Thompson[7] had made an estimate of 230 cm^{-1} for the low frequency fundamental of Cl_2CO. This estimate is in excellent agreement with the observed line.

Infrared Spectra

The discussion of the infrared spectra of these molecules has been divided into three sections covering the absorption regions 250–1300, 1300–2300, and 2300–4200 cm^{-1} for convenience and clarity. The spectra, thus divided, are shown in Figs. 2, 4, and 5.

250–1300 cm^{-1} *Region*

F_2CO

Figure 2(a) shows this region of the spectrum plotted in percent absorption *versus* frequency in cm^{-1}. Four

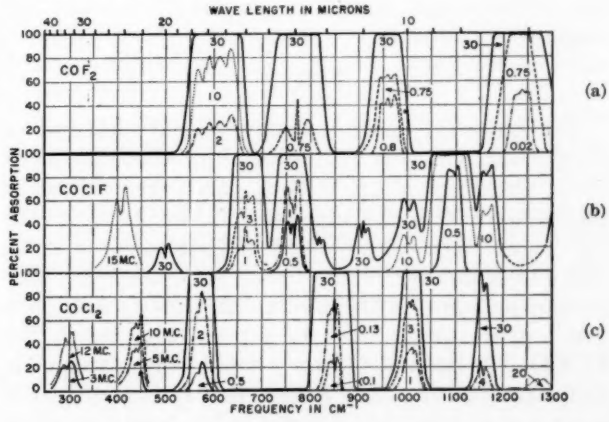

FIG. 2. Prism spectra of F_2CO, FClCO and Cl_2CO for 250 cm^{-1}–1300 cm^{-1} region. (Pressures are as indicated, in inches. Cell lengths are 10 cm except where pressure value is followed by M. C., indicating that a one-meter cell was used.)

[5] J. S. Kirby-Smith and E. A. Jones, J. Opt. Soc. Am. **39**, 780 (1949).

[6] A. H. Nielsen, J. Chem. Phys. **19**, 98 (1951).

[7] H. W. Thompson, Trans. Faraday Soc. **37**, 251 (1941).

quite intense regions of absorption may be seen. The absorption for the various gas pressures in the 10-cm cell may be found in the legend accompanying Fig. 2(a). KBr and NaCl prisms were used for all the bands shown in this region for F_2CO. The KRS-5 region also was explored for F_2CO, but no bands were detected.

The region around 600 cm^{-1} appears to consist of two overlapping bands centered at 584 cm^{-1} and 626 cm^{-1}. This is probably the correct interpretation because of the two Raman lines at 571 cm^{-1} and 620 cm^{-1}. The band at 584 cm^{-1} appears to have a central branch, but three maxima for the 626 cm^{-1} band were not resolved possibly because of the overlapping.

The absorption at 774 cm^{-1} is distinctive because of its very sharp and intense Q branch. It was this band which was resolved into rotational structure and which gave information about the moments of inertia of the molecule. This band is about four times as intense as the ones at 584 cm^{-1} and 626 cm^{-1}. Good agreement exists between the frequency of this band and the Raman line at 771 cm^{-1}.

Of about equal intensity with the band at 774 cm^{-1} is the one at 965 cm^{-1}. Three peaks are clearly discernible in this band showing that there is a gathering of Q branches near the center. The general appearance is quite different from that of the 774 cm^{-1} band showing that it results from a completely different type of vibration. The corresponding Raman line also is at 965 cm^{-1}.

By far the most intense infrared absorption band occurs at 1249 cm^{-1} and contrasts with its corresponding Raman line at 1238 cm^{-1} which is very weak. This band too has three peaks, and has much the same appearance as the band at 965 cm^{-1}.

These five lowest frequency bands are so intense that there seems little doubt about their being identified as fundamentals. The fact that there are five Raman lines whose frequencies differ by only a few cm^{-1} from the infrared band centers in the gas also makes this assignment reasonable.

FClCO

The long-wave section of the infrared spectrum of FClCO is shown in Fig. 2(b) plotted in percent absorption *versus* frequency in cm^{-1}. Nine bands were found in this region. With the exception of the band at 415 cm^{-1}, which required a pressure of $\frac{1}{2}$ atmos in the meter cell, the remainder of the bands were observed with various pressures in the 10-cm cell. KRS-5, KBr, and NaCl prisms were used to explore this region for FClCO. The band at 415 cm^{-1} doubtlessly corresponds to the medium intensity Raman line at 410 cm^{-1}. It is quite a weak band and appears to be doublet in character. A somewhat more intense band, also apparently a doublet, was observed at 501 cm^{-1} in good agreement with the strong Raman line at 506 cm^{-1}.

Two quite intense bands were observed at 667 cm^{-1} and 776 cm^{-1}. These correspond to the very weak Raman line at 665 cm^{-1} and the very intense one at 765 cm^{-1}. Both of these bands have three branches which are fairly prominent and well resolved. The central branch of the 667 cm^{-1} band is more prominent than the one in the 776 cm^{-1} band. Two fairly weak bands with prominent central lines were observed at 818 cm^{-1} and 910 cm^{-1}. A moderately intense one of doublet type occurs at 1004 cm^{-1}.

The most intense band in this region for FClCO is the one at 1095 cm^{-1}. From the prism curve it appears to have three branches with the central branch shading into the low frequency side of the band. To show this better, the record shown in Fig. 3 was made with the 3600 lines/in. grating. It may be seen that the central branch is very sharp on its high frequency side but shades off into the low frequency side of the band. This band corresponds to the extremely weak Raman line at 1085 cm^{-1}. At slightly higher frequency, 1165 cm^{-1}, lies a fairly intense band which also appears to have three branches.

Cl_2CO

The seven observed bands for Cl_2CO in this region are shown in Fig. 2(c). It was necessary to resort to the 1-m cell to observe some of them satisfactorily. KRS-5, KBr, and NaCl prisms were used to observe all the bands in this region. The longest wavelength band observed for Cl_2CO is a doublet occurring at 297 cm^{-1} which undoubtedly corresponds to the Raman frequency at 302 cm^{-1}. This band was not observed by Bailey and Hale because of lack of instrument range.

A band having three maxima and occurring at 440 cm^{-1}, which corresponds to the Raman line at 442 cm^{-1}, was observed with the 1-m cell. This band also was not reported by Bailey and Hale because of instrument limitations. An intense band, which has the appearance of a doublet with a strong R branch was observed at 575 cm^{-1} in agreement with the very intense Raman line at 571 cm^{-1}. This frequency also agrees well with the average position of the two maxima at 563 cm^{-1} and 576 cm^{-1} reported by Bailey and Hale and which they label *N*. The envelope of their curve is also a doublet.

The most intense infrared band in this region for Cl_2CO occurs at 849 cm^{-1}. The very weak corresponding Raman line falls at 832 cm^{-1}. Bailey and Hale report a band, which they call *K*, at 845 cm^{-1}. They show this band as a single maximum while in Fig. 2(c) three branches are clearly seen. This band doubtlessly corresponds to the same vibration mode as the very intense bands at 1249 cm^{-1} in F_2CO and 1095 cm^{-1} in FClCO. Another quite intense band which exhibits three branches occurs at 1011 cm^{-1}. This agrees in position with Bailey and Hale's band *I* at 1009 cm^{-1}.

The band of somewhat lower intensity at 1159 cm^{-1} appears to be a doublet in Fig. 2(c). It corresponds to band *H* at 1157 cm^{-1} in Bailey and Hale's work. A fairly

weak doublet band occurs at 1276 cm^{-1} in agreement with band G at 1285 cm^{-1} reported by Bailey and Hale.

Bailey and Hale also reported bands at 740, 698, and 660 cm^{-1}, which they labeled L, M_1, and M_2, respectively. These bands were not observed in the present investigation even with much more gas than they used, and are thought to be impurities. These bands fall in a region where there is CO_2 absorption, and as CO_2 was an impurity in all of the samples of the carbonyl molecules, it may well be that their bands could be ascribed to CO_2.

Summary

The region 250–1300 cm^{-1} for these three molecules clearly is the region in which most of the fundamentals occur. The only observed Raman lines for which infrared bands have not been thus far discussed are the ones occurring between 1800 and 2000 cm^{-1} which essentially correspond to the C=O vibration.

For F_2CO, only the fundamentals were observed. For FClCO and Cl_2CO, four and two additional bands, respectively, which are combinations and overtones, were observed.

1300–2300 cm^{-1} *Region*

This is the region in which the highest frequency fundamentals occur and contains in addition a number of overtones and combination bands. This region was explored by means of the NaCl, CaF_2, and LiF prisms. For most of the bands, the 10-cm cell was used, but for FClCO a record also was made with the 1-m cell at about 1-atmos pressure.

F_2CO

A band of very irregular contour, shown in Fig. 4(a), was observed the center of which appears to be about 1560 cm^{-1}. This region is interfered with by the 6.26μ atmospheric water band and it is not certain whether the structure as indicated is real. However, in a number of records made with various amounts of gas the details seemed to repeat. If this structure were ignored the general contour of the band would be that it had three maxima with the central one being most intense. An alternative interpretation, which is probably the correct one, would be that two bands with centers at 1546 cm^{-1} and 1583 cm^{-1}, respectively, overlap to give this envelope.

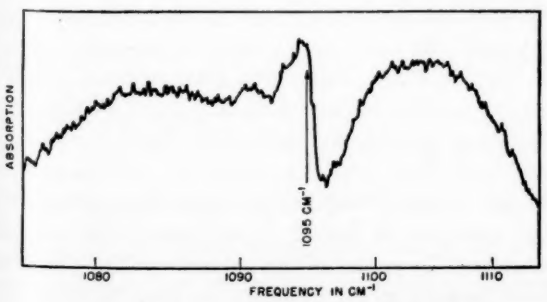

FIG. 3. Grating record of ν_4 for FClCO.

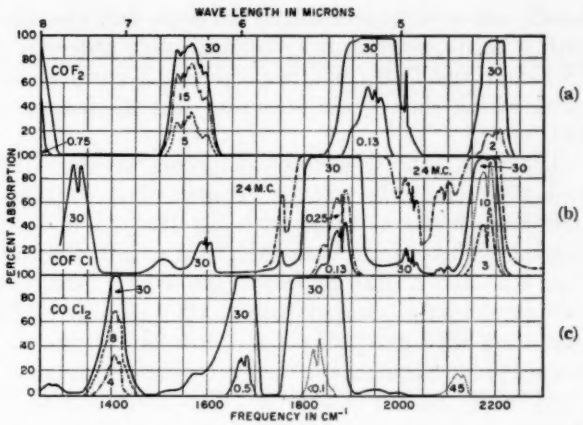

FIG. 4. Prism spectra of F_2CO, FClCO and Cl_2CO for 1300 cm^{-1}–2300 cm^{-1} region. (Pressures are as indicated, in inches. Cell lengths are 10 cm except where pressure value is followed by M. C., indicating that a one-meter cell was used.)

The most intense absorption region is that between 1900 and 2000 cm^{-1}. At much reduced pressure, there is one prominent band with three maxima at 1944 cm^{-1}. There is, however, a shoulder on this band at about 1900 cm^{-1} which overlaps the principal absorption. It must be recalled that the Raman photographs exhibit two lines in this region, an intense one at 1909 cm^{-1} and a very weak one at 1944 cm^{-1}. An exploration of this region was made with the grating spectrometer. Because of interference by the rotation lines of the intense atmospheric water vapor band the appearance of the absorption was not much improved over the prism record in Fig. 4(a) and is not reproduced. The grating record does, however, show the shoulder to somewhat better advantage, and that the envelope is distorted toward lower frequencies. There seems little doubt of the existence of two bands and the best estimate of the frequencies is that they lie at 1907 cm^{-1} and 1942 cm^{-1}. The Raman line separation is 35 cm^{-1} and the separation of the infrared bands also appears to be 35 cm^{-1}.

A sharp line, reminiscent of the sharp Q branch in the band at 774 cm^{-1}, occurs at 2010 cm^{-1}. The band associated with this Q branch is quite weak and does not appear except with fairly high pressure in the 10 cm cell. The last band observed in this region is the one at 2195 cm^{-1}. This band is intense, has three maxima, but no prominent central branch.

FClCO

As shown in Fig. 4(b), 8 absorption regions were observed in this spectral interval for FClCO, one of which is the C=O fundamental between 1800 and 1900 cm^{-1}. A doublet band of moderate intensity was observed at 1327 cm^{-1} in the 10-cm cell at atmospheric pressure. With the same amount of gas two weak

bands, one with undetermined envelope and the other with a fairly prominent Q branch, were observed at 1508 cm^{-1} and 1594 cm^{-1}, respectively. A much weaker band which showed no structure was discovered at 1752 cm^{-1}.

The most intense absorption occurs between 1800 and 1900 cm^{-1}. It will be recalled that 2 Raman lines were found at 1832 cm^{-1} and 1858 cm^{-1}. There is good evidence from both the prism record, shown in Fig. 4(b) and a grating record not shown here, that two overlapping infrared bands occur at about 1847 cm^{-1} and 1876 cm^{-1}. The band envelope is distorted toward lower frequencies as in F_2CO. The low frequency band is the weaker of the two. The separation of the Raman lines and of the infrared bands is 26 cm^{-1} and 29 cm^{-1}, respectively.

Near 2000 cm^{-1} in Fig. 4(b) is a fairly weak but complicated absorption envelope. Two alternatives present themselves: that 2 bands with centers at 2015 cm^{-1} and 2025 cm^{-1} exist here; or, what is perhaps more likely, that one band with center at 2020 cm^{-1} represents the region. Two more bands, a doublet at 2091 cm^{-1} and a doublet at 2182 cm^{-1}, were observed.

Cl_2CO

Five bands, of which the most intense is the C=O frequency, were observed for Cl_2CO in the 1300–2300 cm^{-1} region. A band which could not be adequately resolved was discovered at 1412 cm^{-1}. Because of the rather intense absorption near the center and the lack of resolution, this band was assumed to have three close maxima. It corresponds to the Bailey and Hale band *F* at 1403 cm^{-1}. A weak band showing no structure and unreported by Bailey and Hale was found at 1570 cm^{-1}. These authors also reported a band *E* at 1666 cm^{-1} which appeared as a doublet at 1677 cm^{-1} in this investigation.

The C=O fundamental at 1827 cm^{-1} is the band Bailey and Hale called *D*. In their work it appears as a single maximum, but here it is clearly a doublet. Only one Raman line at 1807 cm^{-1} and one infrared band at 1827 cm^{-1} were discovered in this interval. This is in contrast to F_2CO and FClCO where two were found.

A weak doublet not reported in the earlier work was found at 2130 cm^{-1} with 1.5 atmos of gas in the 10-cm cell. Bailey and Hale reported a band *C* at 2062 cm^{-1} which was not found in the present work. It is suggested that this band may be caused by CO as an impurity.

Summary

The investigation of this region produced the remaining fundamental for each molecule as well as a number of overtone and combination bands. It also gave evidence that the two close Raman lines in F_2CO and FClCO were accompanied by two infrared bands.

2300–4200 cm^{-1} *Region*

For all three molecules a number of weak bands which may be explained as overtone and combination frequencies were discovered in this region. The 10-cm cell and the 1-m cell were both used with pressures up to 1.5 atmos. Most bands were examined with the LiF prism. The results are shown in Figs. 5(a), 5(b), and 5(c).

F_2CO

As shown in Fig. 5(a), 9 bands located at 2474, 2682, 2712, 2875, 2912, 3179, 3412, 3851, and 4830 cm^{-1} were found; two of these bands exhibit sharp Q branches while the others have three more or less equally intense maxima. Another band of unknown envelope was found at 5703 cm^{-1}.

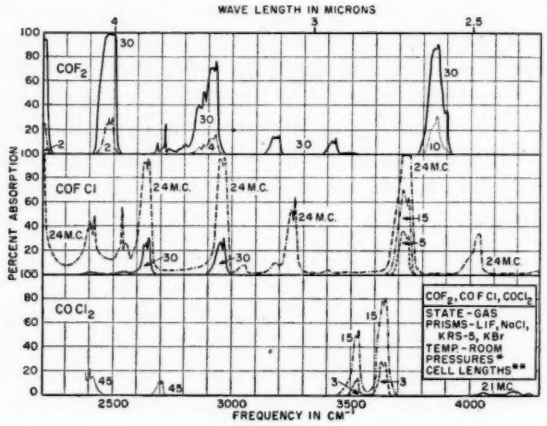

FIG. 5. Prism spectra of F_2CO, FClCO and Cl_2CO for 2300 cm^{-1}–4200 cm^{-1} region. (Pressures are as indicated, in inches. Cell lengths are 10 cm except where pressure value is followed by M. C., indicating that a one-meter cell was used.)

FClCO

For FClCO, eleven bands located at 2413, 2538, 2634, 2958, 3045, 3177, 3255, 3400, 3730, 4033, and 5500 cm^{-1} were discovered. Their structures, as shown in Fig. 5(b), exhibit either two or three maxima.

Cl_2CO

Seven bands located at 2405, 2705, 3527, 3639, 4073, 4180, and 4255 cm^{-1} were discovered and are shown in Fig. 5(c). Of these, Bailey and Hale reported bands at 2714 cm^{-1}, which is part of their A_3, and at 3630 cm^{-1}, which they labeled A_1. They also listed bands A_2 at 3058, A_3 at 2780, and B at 2336 cm^{-1} which were not detected in this investigation, even with considerably larger amounts of gas. It is suggested that they are impurities. The center of the ν_3 band of CO_2, which was always present as an impurity, is close to their 2336 cm^{-1} band.

DISCUSSION OF RESULTS

General

The molecules comprising this group of carbonyls are planar and geometrically similar to H_2CO and D_2CO. F_2CO and Cl_2CO belong to a class of molecules whose symmetry is that of the point group C_{2v} while FClCO belongs to the C_s group. There are six nondegenerate fundamental frequencies, the forms of which are well known[8] and whose symmetry species are A_1 for ν_1, ν_2, and ν_3, B_1 for ν_4 and ν_5, and B_2 for ν_6. Thus, if the electric moment oscillates along the C_2 or twofold axis, an A_1 symmetry results; if it oscillates along an axis perpendicular to the C_2 but in the plane of the model, a B_1 symmetry results; and if it oscillates perpendicularly to the plane of the model, a B_2 results. Briefly described: ν_1 is essentially the inphase C−X vibration, ν_2 is the C=O vibration, ν_3 is the bending of the X−C−X angle, ν_4 is the out-of-phase C−X, ν_5 is the rocking of the X−C−X triangle, and ν_6 is the out-of-plane vibration. Thus there are electric moment changes possible along all three principal axes of inertia. Because of the symmetry type the principal inertial axes in FClCO make an angle with the direction of the C=O bond. All of the planar vibrations, therefore, have components along both the least and intermediate axes for this molecule.

From the grating measurements[6] and the microwave measurements by Smith and co-workers,[9] it appears that F_2CO is very nearly an oblate symmetrical top with $\rho=I_A/I_B\approx1$. The out-of-the-plane oscillation ν_6 is thus the only one of the six fundamental modes which could be a parallel type band. Only one band with an intense and sharp Q branch is observed and this immediately identifies ν_6. The remaining fundamentals all have about the same appearance with three more or less equal maxima. The parameter $\beta=\rho-1$, defined by Gerhard and Dennison,[10] is about -0.5 for F_2CO. The envelopes of perpendicular bands for this value of β have 3 maxima of about the same intensity. The Q branches of the $\Delta K=\pm1$ transitions gather near the band center to form the rather intense central maximum. All of the observed bands in F_2CO are of the types described, parallel and perpendicular.

From the electron diffraction data given by Allen and Sutton,[11] the moments of inertia of Cl_2CO may be calculated. It is found that the molecule is quite asymmetric with the intermediate axis of inertia lying along the C_2 axis and the least axis of inertia perpendicular to the C_2 axis in the plane of the figure. The parameter $\rho=I_A/I_B\approx0.4$. Using Figs. 19 and 20 in Dennison's[12] review article, it may be seen that a type A band should have a fairly strong central branch while a type B band should appear as a doublet. Type C bands should also have a central line not unlike type A bands. The molecule Cl_2CO should therefore have three fundamentals of type A, two of type B, and one of type C.

The molecule FClCO is clearly an asymmetric rotor because its spectrum is composed of type A, B, and C bands of much the same form as the spectrum of Cl_2CO. As there is no C_2 axis for this model, the principal axes of inertia do not lie along any bond direction as in the other two molecules. An attempt has been made to orient the principal axes by guessing at a molecular shape which seems reasonable in terms of the other two molecules. The C=O distance was chosen as the average of the values for F_2CO and Cl_2CO. The O−C−F angle was retained from F_2CO, and the O−C−Cl angle from Cl_2CO. The Cl−C−F angle then becomes the average of the F−C−F and Cl−C−Cl angles for the other molecules. Transformation to principal axes puts the least axis at an angle of about 9° with the C−Cl bond, and the intermediate axis at an angle of about 25° with the C=O bond. As the parameter $\rho=I_A/I_B\approx0.45$, the type A and type B bands should have about the same appearance as in Cl_2CO. It is no longer possible to say that the vibrations ν_1, ν_2, and ν_3 cause dipole moment changes entirely along a principal axis and, therefore, that they should have the same character because all the planar vibrations have components along both the least and intermediate axis. In fact, the bands identified as ν_1 and ν_2 have three maxima and are of type A, but ν_3 appears to be a doublet. This is

TABLE II. Assignment, symmetry, and envelopes of observed bands in F_2CO.[a]

Assignment	Symmetry	Obs freq	Calc freq	Obs envel	Pred envel
ν_1	A_1	965 cm^{-1}		Perp[d]	Perp
ν_2	A_1	1942[b]		Perp	Perp
ν_3	A_1	626		Perp	Perp
ν_4	B_1	1249		Perp	Perp
ν_5	B_1	584		Perp	Perp
ν_6	B_2	774		Parallel	Parallel
$2\nu_1$	A_1	1907[b]	1930 cm^{-1}	?	Perp
$2\nu_2$	A_1	3851	3856[c]	Perp	Perp
$2\nu_4$	A_1	2474	2498	Perp	Perp
$2\nu_6$	A_1	1546?	1548	Perp	Perp
$\nu_1+\nu_2$	A_1	2912	2893[c]	Perp	Perp
$\nu_1+\nu_3$	A_1	1583	1591	Perp	Perp
$\nu_1+\nu_4$	A_1	2195	2214	Perp	Perp
$\nu_1+\nu_5$	B_1	1546?	1549	Perp	Perp
$\nu_2+\nu_4$	B_1	3179	3177[c]	Perp	Perp
$\nu_2+\nu_6$	B_2	2712	2702[c]	Parallel	Parallel
$3\nu_1$	A_1	2875	2895	Perp	Perp
$\nu_1+2\nu_4$	A_1	3412	3463	Perp	Perp
$2\nu_1+\nu_6$	B_2	2682	2704	Parallel	Parallel
$2\nu_3+\nu_6$	B_2	2010	2026	Parallel	Parallel
$5\nu_1$	A_1	4830	4825	Perp	Perp
$2\nu_2+\nu_4+\nu_5$	B_1	5703	5689	?	Perp

[a] The assumption is made that F_2CO is very nearly an oblate symmetric top.
[b] Perturbed values of ν_2 and $2\nu_1$ caused by Fermi-type resonance.
[c] Calculated values obtained by using unperturbed value of $\nu_2=1928$ cm^{-1}.
[d] Type A and type B bands are virtually identical for a model as close to a symmetric top as this.

[8] G. Herzberg, *Infrared and Raman Spectra* (D. Van Nostrand Company, Inc., New York, 1945), p. 65.
[9] Smith, Tidwell, Williams, and Senatore, Phys. Rev. **83**, 485(A) (1951).
[10] S. L. Gerhard and D. M. Dennison, Phys. Rev. **43**, 197 (1933).
[11] P. W. Allen and L. E. Sutton, Acta Cryst. **3**, 47 (1950).
[12] D. M. Dennison, Revs. Modern Phys. **3**, 280 (1931).

TABLE III. Assignment, symmetry, and envelopes of observed bands in FClCO.

Assignment	Symmetry	Observed frequency	Calculated frequency	Observed envelope
ν_1	A'	776 cm^{-1}	...	Type A
ν_2	A'	1876[a]	...	Type A
ν_3	A'	501	...	Type B
ν_4	A'	1095	...	Type A
ν_5	A'	415	...	Type B
ν_6	A''	667	...	Type C
$2\nu_2$	A'	3730	3736[b] cm^{-1}	Type B
$2\nu_3$	A'	1004	1002	Type B
$2\nu_4$	A'	2182	2190	Type B
$2\nu_5$	A'	818	830	Type A
$2\nu_6$	A'	1327	1334	Type B
$\nu_1+\nu_2$	A'	2634	2644[b]	Type A
$\nu_1+\nu_4$	A'	1847[a]	1871	?
$\nu_2+\nu_4$	A'	2958	2963[b]	Type B
$\nu_2+\nu_6$	A''	2538	2535[b]	Type C
$\nu_3+\nu_4$	A'	1594	1596	Type A
$\nu_3+\nu_5$	A'	910	916	Type A
$\nu_3+\nu_6$	A''	1165	1168	Type C?
$\nu_4+\nu_5$	A'	1508	1510	?
$\nu_4+\nu_6$	A''	1752	1762	?
$\nu_1+2\nu_2$	A'	4487	4512	?
$\nu_1+2\nu_4$	A'	3045?	2966	?
$2\nu_1+\nu_2$	A'	3400	3420[b]	?
$\nu_2+2\nu_4$	A'	4033	4058[b]	Type A
$\nu_2+2\nu_6$	A'	3177	3202[b]	?
$2\nu_1+\nu_3$	A'	2020	2053	Type A
$2\nu_3+\nu_4$	A'	2091	2097	Type B
$3\nu_4$	A'	3255	3285	Type B
$\nu_4+2\nu_6$	A'	2413	2429	Type B
$2\nu_2+\nu_4+\nu_6$	A''	5500?	5498	?

[a] Perturbed values of ν_2 and $\nu_1+\nu_4$ caused by resonance.
[b] Calculated values obtained by using unperturbed value of $\nu_2=1868$ cm^{-1}.

reasonable if the suggested model is correct, and means that the component of the changes of electric moment along I_B in ν_1 and ν_2 nearly cancel out, and that the component along I_A in ν_3 nearly cancels out. With the same kind of argument, ν_4 could very well be essentially type A, and ν_5 essentially type B, as is observed. The envelopes of the overtones and combinations cannot be predicted as in F_2CO and Cl_2CO with the exception of possibly the ones involving ν_6 in such a ways as to give A'' symmetry. Such a band $\nu_2+\nu_6$ is observed at 2538 cm^{-1} with a sharp Q branch not unlike ν_6 itself. The other overtones and combination bands are type B and type A.

F_2CO

The fundamental bands, and overtone and combination bands have been identified and may be found listed in Table II together with the calculated frequencies and the observed and predicted band envelopes. Identification of the fundamentals was accomplished by an elimination process. As has been previously pointed out, ν_6 is the only parallel-type vibration in the molecule. Only one band at 774 cm^{-1} was found which was resolvable, and which had a Q branch compatible with this type structure. This band was, therefore, assigned to ν_6. The fundamental mode which corresponds essentially to the C=O vibration would probably be numerically somewhere near the C=O frequency in H_2CO and D_2CO and other molecules containing the C=O group. The band at 1944 cm^{-1} was, therefore, assigned to ν_2. There are two frequencies, ν_1 and ν_4, which would very likely fall fairly close together because they are essentially C−F valence bond oscillations. Of these, ν_4, the out-of-phase vibration, is generally of higher frequency than ν_1, the in-phase one. Therefore, ν_1 was taken to be 965 cm^{-1} and ν_4 was taken to be 1249 cm^{-1}. There remain the bending frequency ν_3 and the rocking frequency ν_5 both of which would be low frequencies. It seems reasonable to believe that the rocking frequency would be lower than the bending one. Therefore, ν_3 is taken to be 626 cm^{-1} and ν_5 is 584 cm^{-1}. This assignment is also reasonable on the basis of the observed Raman intensities. The totally symmetrical vibrations ν_1, ν_2, and ν_3 should be polarized and hence should be intense in Raman effect. The strongest Raman lines are indeed the ones at (1909, 1944) cm^{-1}, 965 cm^{-1}, and 620 cm^{-1}, while the weakest ones are those at 1238 cm^{-1}, 771 cm^{-1}, and 571 cm^{-1}. The C=O frequency ν_2 is clearly related to the pair at (1909, 1944) cm^{-1} and ν_1 is certainly larger than ν_3 which fixes the strong Raman lines as ν_2, ν_1, and ν_3, respectively. Among the weak lines, ν_6 is certainly 774 cm^{-1}, and ν_4 is obviously larger than ν_5. This establishes the weak lines as ν_4, ν_6, and ν_5, respectively.

As there are no prohibitions on overtones or combination bands there are many possibilities for transitions throughout the spectrum. They are by no means all observed as the intensities may be low on a great many. Exclusive of the 6 fundamentals, fifteen bands which are ascribed to overtones and combinations were found in F_2CO. These are listed in Table II with the appropriate assignment and calculated frequency using the observed fundamentals. It is worth noting that among the overtones and combinations observed three have sharp Q branches and should, therefore, be parallel-type vibrations of the B_2 symmetry species. These are the bands at 2010, 2704, and 2712 cm^{-1} which can indeed be identified as $\nu_6+2\nu_3$, $\nu_6+2\nu_1$, and $\nu_2+\nu_6$, respectively.

FClCO

With the fundamentals identified in F_2CO the identification of the fundamentals in FClCO is not difficult. The assignments and observed frequencies are given in Table III along with the calculated frequencies and observed envelopes. ν_2 should be nearly the same value as in F_2CO, but a little lower in frequency, and is assigned to the absorption (1847, 1876) cm^{-1}. There are three intense Raman lines which must be ν_1, ν_2, and ν_3. Thus ν_1 must be 776 cm^{-1} and ν_3 is taken to be 501 cm^{-1}. The three weak lines are ν_4, ν_5, and ν_6, of which ν_6 is undoubtedly 667 cm^{-1} as it exhibits a fairly prominent Q branch as in F_2CO. The out-of-phase valence frequency ν_4 is, therefore, 1095 cm^{-1} and ν_5 is 415 cm^{-1}.

A great many overtone and combination bands were discovered, this spectrum being much richer than the F_2CO probably because of the lower symmetry. The twenty-four bands, exclusive of fundamentals which were observed, have been fitted into Table III with identifications which agree closely with the calculated values.

Cl_2CO

The same arguments used previously on F_2CO and FClCO to identify the fundamentals were applied to Cl_2CO. The fundamentals and their present assignments are given in Table IV. An apparent disagreement between these results and those of Bailey and Hale is explained when it is noted that ω_1 and ω_2 have been interchanged in order to use the notation of Herzberg.[8]

Fourteen overtone and combination bands were discovered and have been fitted into Table IV with proper assignment. Several bands were found that were unreported by Bailey and Hale, and several reported by them were not found even with more gas in the cells.

Resonance

Attention has already been directed to the fact that in F_2CO and FClCO there exist close pairs of Raman lines and close pairs of infrared bands in the C=O region, while in Cl_2CO there exists only a single Raman line and single infrared band. This can be explained in F_2CO by a Fermi-type resonance between ν_2 and $2\nu_1$ and in FClCO by a resonance between ν_2 and the binary combination $\nu_1+\nu_4$. No resonance occurs

TABLE IV. Assignment, symmetry, and envelopes of observed bands in Cl_2CO.

Assign	Sym	Obs freq	Calc freq	Obs envel	Pred envel	Bailey and Hale[a] Obs freq	Bailey and Hale[a] Assignment
ν_1	A_1	575 cm^{-1}	···	Type *B*	Type *B*	570 *N*	ω_2[a]
ν_2	A_1	1827	···	Type *B*	Type *B*	1827 *D*	ω_1[a]
ν_3	A_1	297	···	Type *B*	Type *B*	···	
ν_4	B_1	849	···	Type *A*	Type *A*	845 *K*	ω_4
ν_5	B_1	240	···	Type *A*	Type *A*	···	···
ν_6	B_2	440	···	Type *C*	Type *C*	···	···
$2\nu_1$	A_1	1159	1150	Type *B*	Type *B*	1157 *H*	$2\omega_2$[a]
$2\nu_2$	A_1	3639	3654	Type *B*	Type *B*	3630 A_1	$2\omega_1$[a]
$2\nu_4$	A_1	1677	1698	Type *B*	Type *B*	1666 *E*	$2\omega_4$
$\nu_1+\nu_2$	A_1	2405	2402	Type *B*	Type *B*	···	···
$\nu_1+\nu_4$	B_1	1412	1424	Type *A*	Type *A*	1403 *F*	$\omega_2+\omega_4$[a] $\omega_2+2\omega_6$[a] $\omega_3+2\omega_2$[a]
$\nu_1+\nu_6$	B_2	1011	1015	Type *C*	Type *C*	1009 *I*	$\omega_2+\omega_6$[a]
$\nu_2+\nu_3$	A_1	2130	2124	Type *B*	Type *B*	···	···
$\nu_2+\nu_5$	B_1	···	2067	···	Type *A*	2062[b] *C*	$\omega_1+\omega_{3,5}$ $\omega_6+2\omega_4$
$\nu_3+\nu_6$	B_2	···	737	···	Type *C*	746[b] 735[b]	$\omega_6+\omega_{3,5}$
$\nu_4+\nu_6$	A_2	1276	1289	Type *B*	···	1285 *G*	$\omega_4+\omega_6$
$\nu_3+\nu_6$	A_2	···	680	···	···	660[b] M_1 698[b] M_2	$2\omega_2$ $2\omega_5$
$\nu_1+2\nu_2$	A_1	4255	4224	Type *B*	Type *B*	···	···
$2\nu_1+\nu_2$	A_1	···	3067	···	Type *B*	3058[b] A_2	$2\omega_1-\omega_2$[a] $\omega_1+2\omega_2$[a]
$\nu_2+2\nu_6$	A_1	2705	2707	Type *B*	Type *B*	···	···
$2\nu_2+\nu_6$	B_2	4073	4094	?	Type *C*	···	···
$3\nu_1+\nu_2$	A_1	3527	3552	Type *B*	Type *B*	···	···
$\nu_4+2\nu_1$	B_2	1570	1590	?	Type *C*	···	···
?	?	4180	?	?	?	···	···
?		5335	?	?	?	···	···
?		5408	?	?	?	···	···

[a] ω_1 and ω_2 have been interchanged to agree with Herzberg's notation.
[b] Probably an impurity.

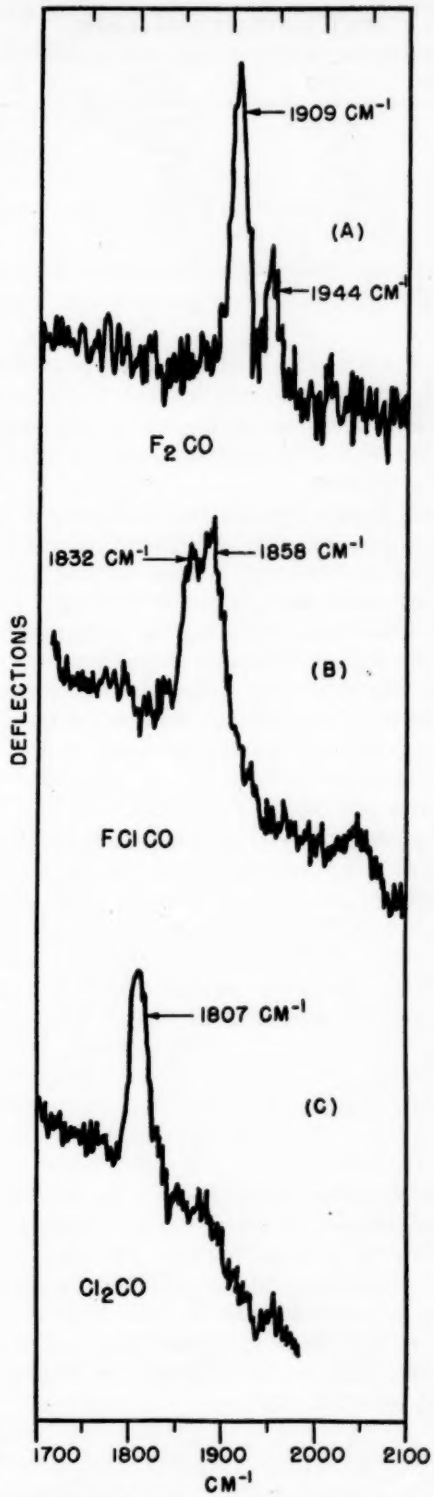

FIG. 6. Raman lines in the C=O region showing resonance of ν_2 and $2\nu_1$ in F_2CO, and ν_2 and $\nu_1+\nu_4$ in FClCO.

in Cl_2CO because there are no close frequencies of the proper character.

In F_2CO the level $V_1=1$, $V_2=V_3=V_4=V_5=V_6=0$ is observed to be 965 cm^{-1} above the ground state. Ignoring the anharmonic terms the level $V_1=2$, would

TABLE V. The fundamental frequencies for F_2CO, FClCO and Cl_2CO (gaseous state).

Assignment	F_2CO	FClCO	Cl_2CO
ν_1	965 cm^{-1}	776 cm^{-1}	575
ν_2	1928[a]	1868[a]	1827
ν_3	626	501	297
ν_4	1249	1095	849
ν_5	584	415	240[b]
ν_6	774	667	440

[a] Unperturbed values.
[b] Raman line.

fall at 1930 cm^{-1}. The level $V_2=2$ is observed at 3851 cm^{-1} and if resonance were ignored $V_2=1$ would fall at 1926 cm^{-1}. Thus, ν_2 and $2\nu_1$ are virtually equal and as they are both of symmetry species A_1 they are in position to resonate.

The two Raman lines for the liquid may be seen in Fig. 6(a), an intense one at 1909 cm^{-1} and a medium intensity one at 1944 cm^{-1}. In the infrared the absorption frequencies in the gas fall at 1907 cm^{-1} and 1942 cm^{-1}, with the weak one being the low frequency one, and the strong one being the high frequency one, as shown in Fig. 4(a). The intensities of corresponding frequencies are thus reversed. Because the C=O vibration is polarized and should be strong in the Raman spectrum the line at 1909 cm^{-1} is associated with ν_2 and the line at 1944 is associated with $2\nu_1$. For the liquid, the energy level $V_2=1$ is perhaps a little lower than $V_1=2$. The resonance interaction would then shift the $V_2=1$ level up to 1944 cm^{-1} and the $V_2=2$ level down to 1909 cm^{-1}. Because of the mixing of the wave functions $2\nu_1$ borrows some intensity from ν_2 but still remains somewhat weaker. Normally, the frefrequencies in the gas are somewhat larger than in the liquid. For the infrared it might, therefore, be expected that the levels $V_2=1$ and $V_1=2$ would be a little higher than for the liquid. It is suggested that perhaps the level $V_2=1$ is a little higher than $V_1=2$ in the gas which would mean that in going from liquid to gas the V_2 levels are shifted more than the V_1 levels and thus cross over. If this were the case, the resonance would shift the $V_2=1$ level to 1942 cm^{-1} and the $V_1=2$ level to 1907 cm^{-1} making the higher frequency band ν_2 and consequently more intense. It can, therefore, be explained how ν_2 is the more intense frequency both in the Raman effect and in the infrared. The estimated, unperturbed ν_2 is 1928 cm^{-1}.

In FClCO the situation is a little different. The two Raman lines fall at 1832 cm^{-1} and 1858 cm^{-1}, but unlike F_2CO their intensities are virtually identical, as is shown in Fig. 6(b). This is probably indicative that, at least in the liquid, the resonance is much closer than it was in F_2CO. The two infrared bands shown in Fig. 4(b) occur at 1847 cm^{-1} and 1876 cm^{-1}, with the low frequency one being the weaker for F_2CO. The resonating levels in this case are $V_2=1$ and the combination level $V_1=V_4=1$. An estimate of the unperturbed levels in the gas may be had from the observed value, 3730 cm^{-1}, of $2\nu_2$. If the anharmonic terms are ignored the level $V_2=1$ falls at about 1865 cm^{-1}. The unperturbed position of $V_1=V_4=1$ can be had from the observed positions of ν_1 and ν_4 and is found to be 1871 cm^{-1}. These levels are of the symmetry species A' and may resonate. For the liquid it is probably not possible to determine the relative positions of the levels ν_2 and $\nu_1+\nu_4$ because the intensities of the Raman lines are so nearly equal. For the gas it is presumed, however, that the level $V_2=1$ is the higher because the high frequency infrared band is the more intense.

In Cl_2CO it is clear from Fig. 6(c) that only a single Raman line occurs at 1807 cm^{-1} and from Fig. 4(c) that only one infrared band occurs at 1827 cm^{-1}. There are no overtones or combination bands which have frequencies in this vicinity and no resonance occurs. It seems reasonable, therefore, to put the unperturbed frequency ν_2 at about 1928 cm^{-1} in F_2CO and at 1868 cm^{-1} in FClCO. The use of these values brings the calculated frequencies in Tables II and III into better agreement with the observed frequencies. Table V has been prepared to summarize the fundamental frequencies for the three molecules, using the infrared values for the gaseous state.

Finally, several very weak infrared bands could not be identified with low or reasonable combinations of the fundamentals. They are, however, believed to be real as they were observed for several samples.

ACKNOWLEDGMENT

The authors express their gratitude to A. V. Faloon, W. B. Kenna, and W. Simon for their careful sample preparation. One of us (AHN) acknowledges a Frederick Gardner Cottrell grant of the Research Corporation of New York which aided materially in completing the grating spectrometer used in part of this work.

Microwave Spectra and Molecular Structures of Fluoroform, Chloroform, and Methyl Chloroform*

S. N. Ghosh,† Ralph Trambarulo, and Walter Gordy
Department of Physics, Duke University, Durham, North Carolina

(Received December 11, 1951)

Sufficient isotopic combinations have been studied to make complete structural determinations of fluoroform and chloroform from microwave rotational spectra. The dimensions of CHF_3 are $d_{CH}=1.098$A, $d_{CF}=1.332$A, and $\angle FCF=108°48'$; those of $CHCl_3$ are $d_{CH}=1.073$A, $d_{CCl}=1.767$A, and $\angle ClCCl=110°24'$. Measurements were made on only the most abundant isotopic species of CH_3CCl_3. If the CCl_3 configuration as in chloroform and the CH_3 configuration as in methane are assumed, the CC distance in CH_3CCl_3 is found to be 1.55A.

INTRODUCTION

ALTHOUGH fluoroform and chloroform have been the subject of several previous structural investigations both with electron diffraction and with spectroscopy, no complete determination of either structure has before been made. Because of the low electron scattering power of H, no estimate of the CH distance could be made with electron diffraction. The earlier microwave investigations of chloroform[1,2] and fluoroform[3] did not employ sufficient isotopic combinations to make possible unambiguous assignments of the parameters. In the present study the structural determinations of both these molecules have been completed, and a partial evaluation of the structure of methyl chloroform has been made, from measurements on their microwave rotational spectra.

EXPERIMENTAL METHOD

Observations were made with a Stark-modulation spectrograph employing 100-kc square-wave modulation. Frequency measurements were made in the usual way with a secondary frequency standard monitored by comparison with station WWV.

Deuterated fluoroform was prepared by heating ordinary fluoroform with a tenfold molar excess of heavy water at 120°C in the presence of potassium carbonate for eight days. A portion of the fluoroform was removed from the reaction mixture after one day, and a very weak absorption line corresponding to the species CDF_3 was found. At the end of eight days the CDF_3 absorption line was much stronger indicating that an exchange between D and H had taken place. This research suggests the possibility of using microwave spectroscopy to study exchange reactions. Spectra of other isotopic species of both chloroform and fluoroform were observed for the naturally occurring concentrations.

SPECTRAL CONSTANTS

Frequencies of the rotational lines measured in this research are listed in Table I. Spectral constants derived from these frequencies as well as the previously reported values for other isotopic combinations are listed in Table II. Gilliam, Edwards, and Gordy[3] made observations of the most abundant isotopic species, $C^{12}HF_3$. The I_B value of this species has also been determined from optical spectra with very good accuracy by Bernstein and Herzberg.[4] Isotopic combination $C^{12}HCl_3^{35}$ has been measured by Smith and Unterberger[1] and $C^{12}DCl_3^{35}$ by Unterberger, Trambarulo, and

Table I. Observed rotational absorption frequencies of some isotopic combinations of CHF_3, $CHCl_3$, and CH_3CCl_3.

Isotopic species	Transition	Frequency (Mc)
$C^{13}HF_3$	$J=1\rightarrow2$	41,287.98±0.40
$C^{12}DF_3$	$J=0\rightarrow1$	19,842.69±0.40
$C^{12}HCl_3^{37}$	$J=5\rightarrow6$	37,554.11±0.40
$C^{12}H_3C^{12}Cl_3^{35}$	$J=7\rightarrow8$	37,955.88±0.40

Table II. Derived spectroscopic constants of some isotopic combinations of CHF_3, $CHCl_3$, and CH_3CCl_3.

Isotopic species	B_0 (Mc)	I_0[a] ($\times10^{-40}$ g cm²)	Reference
$C^{12}HF_3$	10,348.74	81.0641	b
$C^{13}HF_3$	10,422.00	81.2741	c
$C^{12}DF_3$	9,921.35	84.5561	c
$C^{12}HCl_3^{35}$	3,301.94	254.066	d
$C^{12}HCl_3^{37}$	3,129.51	268.065	c
$C^{12}DCl_3^{35}$	3,250.17	258.113	e
$C^{12}H_3C^{12}Cl_3^{35}$	2,372.6	353.58	c

[a] Calculated from B_0 using Planck's constant =6.623773 erg sec.
[b] See reference 3.
[c] Present work.
[d] See reference 1.
[e] See reference 2.

* The research reported in this paper has been made possible through sponsorship extended by the Geophysical Research Directorate of Air Force Cambridge Research Laboratories under Contract No. W19-122-ac-35.

† On leave from the Department of Physics, The University of Calcutta, India.

[1] W. V. Smith and R. R. Unterberger, J. Chem. Phys. **17**, 1348 (1949).

[2] Unterberger, Trambarulo, and Smith, J. Chem. Phys. **18**, 565 (1950).

[3] Gilliam, Edwards, and Gordy, Phys. Rev. **75**, 1014 (1949).

[4] H. J. Bernstein and G. Herzberg, J. Chem. Phys. **16**, 30 (1948).

TABLE III. Molecular structures of CHF_3, $CHCl_3$, and CH_3CCl_3.

	d_{CH}	d_{CF}	∠FCF
CHF_3	1.098	1.332	108°48′
	d_{CH}	d_{CCl}	∠ClCCl
$CHCl_3$	1.073	1.767	110°24′
CH_3CCl_3	$d_{CH}=1.093$, $d_{CCl}=1.767$, ∠HCH = 109°28′, ∠ClCCl = 110°24′ (assumed parameters)	d_{CC}	1.55

Smith.[2] These earlier microwave measurements have been combined with ours in our structural evaluations.

Hyperfine structures resulting from the Cl nuclear quadrupole coupling in chloroform and methyl chloroform were not resolved. Nevertheless, because the coupling is small and because the strongest hyperfine components are close to the position of the undisplaced rotational lines, it is possible to obtain an accurate measurement of the position of the rotational lines without resolution and analysis of these structures.

STRUCTURES

Table III lists the structural parameters which were calculated from the rotational constants. The CF distance and FCF angle for fluoroform are in good agreement with the electron diffraction values, 1.34±0.02A and 109°±2°, measured by Bauer and Beach.[5] Similar electron diffraction results have recently been obtained by Brockway.[6] Our results on chloroform also agree well with the electron diffraction values $d_{CCl}=1.77\pm0.02$A and ∠ClCCl = 112°±2° for chloroform.[7]

A significant difference in the zero-point vibrational energies of the hydrogen and deuterium containing molecules can cause a rather large possible error in the determination of the CH distance. Since only a minimum number of isotopic combinations for the structural evaluations were measured, no estimate of the limits of error could be made from the internal consistency test. From such tests on other molecules where substitutions or D for H have been made, the limits of error in the CH distance are estimated as 0.02A. Fortunately, because of the small weight of H, such a large possible error in the CH distance does not cause a correspondingly large error in the other parameters.

It is interesting that the bond angles and the CH distance in fluoroform are so close to those for methane. The CH length suggests that this bond is formed primarily with an sp^3 hybridized orbital of the C. Although the CF distance, 1.332A, is considerably shorter than the added covalent radii of C and F, 1.51A, the three C orbitals which form bonds to fluorine are presumably also sp^3 hybrides. The most likely cause for the marked shortening of the CF bonds is the ionic resonance of Form II with I, as suggested by Schomaker and Stevenson,[8] and the resonance of I with Form III, as proposed by Pauling.[9] The Schomaker-Stevenson rule which predicts a decrease of about

$$0.09|x_A-x_B|=0.13\text{A}$$

would account for the greater part of the shortening.

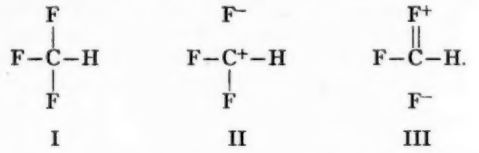

I II III

Although the bond angles are nearly tetrahedral in CHF_3, it does not seem probable that the CF distance would be significantly smaller in this molecule than it is in CF_4. A single, early electron-diffraction measurement gives the CF distance in CF_4 as 1.36±0.02A. A remeasurement of CF_4 with electron diffraction seems worthwhile. The CF distances in CF_3Cl reported by Coles and Hughes[10] and in other CF_3X molecules found by Sheridan and Gordy[11] are in good agreement with the fluoroform value.

It is interesting to compare the structures of fluoroform and chloroform. In fluoroform, the CH distance and ∠HCF are slightly larger than those expected for tetrahedral carbon, whereas in chloroform the corresponding values appear to be slightly smaller than the tetrahedral values. Differences in angles can be explained on the basis of the larger size of the Cl, which causes a repulsion of the Cl atoms and thus increases ∠ClCCl above the tetrahedral value of 109°28′. The surprising feature is that the CH distance in chloroform is shorter than that in fluoroform and even shorter than that in methane, 1.093A. Although the error caused by the difference in zero-point energy mentioned above might barely account for the deviation in the methane value, it is not probable that this accounts for the observed CH distance in chloroform being shorter by 0.03A than that in fluoroform since deuterium substitution was employed in both determinations. Nevertheless, it is difficult to account for the shorter chloroform distance. From the fact that ∠HCCl is smaller than 109°28′, one might predict that the C bonding orbital in CH would have less than 25 percent *s* character and hence that the CH bond length would be longer than that in methane. For similar reasons, one might expect the CH in fluoroform to be slightly shorter than 1.093A. Actually, the opposite trend is indicated by the present structural determinations.

As the lines of CCl_3CH_3 were rather weak, it was possible to measure only the most abundant isotopic

[5] S. H. Bauer and J. Y. Beach, quoted by P. W. Allen and L. E. Sutton, Acta Cryst. 3, 46 (1950).
[6] L. Brockway (private communication to J. Sheridan).
[7] L. Brockway, Revs. Modern Phys. 8, 231 (1936).
[8] V. Schomaker and D. P. Stevenson, J. Am. Chem. Soc. 63, 37 (1941).
[9] L. Pauling, *The Nature of the Chemical Bond* (Cornell University Press, Ithaca, New York, 1945), second edition, p. 236.
[10] D. K. Coles and R. H. Hughes, Phys. Rev. 76, 858 (1949).
[11] J. Sheridan and W. Gordy (to be published).

combination. Nevertheless, it is believed that the CC distance estimated for this molecule is reasonably accurate. There is no obvious reason why the CH_3 and CCl_3 configuration should be significantly different from those of methane and chloroform which are assumed in the determination of d_{CC}. The value obtained for d_{CC}, 1.55A, is in accord with CC single bond lengths in other hydrocarbons. No evaluation of the CC distance in this molecule by other methods has been made.

We would like to thank Dr. A. F. Benning of the Jackson Laboratories of the E. I. duPont de Nemours Company for the sample of fluoroform, and the Texas Division of the Dow Chemical Company for the sample of methyl chloroform.

THE JOURNAL OF CHEMICAL PHYSICS VOLUME 20, NUMBER 4 APRIL, 1952

Spectroscopic Studies in the Near Ultraviolet of the Three Isomeric Dimethylbenzene Vapors.* I. Absorption and Fluorescence Spectra of *Para*-Dimethylbenzene†

C. D. Cooper‡ and M. L. N. Sastri§
Department of Physics, Duke University, Durham, North Carolina

(Received December 7, 1951)

The absorption spectrum of *para*-xylene between 2850 and 2350A was photographed using a 3-meter grating spectrograph, and the corresponding fluorescence spectrum between 3125 and 2720A was photographed with a Bausch and Lomb medium quartz spectrograph. The electronic transition involved is interpreted as $^1A_{1g}-{}^1B_{3u}$ with the 0, 0 band at 36733 cm^{-1}. Progressions in the fluorescence spectrum involve the totally symmetric vibrations 829 and 1208 cm^{-1}, while progressions of the corresponding frequencies 775 and 1185 cm^{-1} appear in the absorption spectrum. A weak portion of the spectrum is identified with a so-called forbidden transition involving the β_{1g}-component of the $606\epsilon_g{}^+$ benzene vibration. This β_{1g}-vibration has a frequency of 648 cm^{-1} in the ground state and of 552 cm^{-1} in the upper state. The α_{1g}-component of the $\epsilon_g{}^+$ benzene vibration in *para*-xylene has a lower state frequency of 458 cm^{-1} and the upper state value of 367 cm^{-1}. The Tesla luminescence spectrum is interpreted in relation to the fluorescence and absorption spectra.

INTRODUCTION

CONSIDERABLE spectroscopic data in the form of absorption, emission, fluorescence, phosphorescence, infrared, and Raman spectra have been recorded for the dimethylbenzenes $C_6H_4(CH_3)_2$ (more commonly known as the xylenes). Among the earliest investigations, if not the earliest, of the absorption spectra of the xylenes are those by Pauer[1] in 1897 who studied them in solution and in the vapor phase. Recent reliable data for the solution spectra have been published by Conrad-Billroth[2] and Wolf and Herold.[3] Optical density curves may also be found in the *Catalog of Ultraviolet Spectrograms*.[4] Kronenberger[5] has studied the near ultraviolet absorption of *meta*-xylene in the vapor and in the solid state. He mentions that he compared his plates of the vapor absorption with corresponding enlargements of V. Henri. No later publication of these results from Henri's laboratory could be found. M. B. Hall and P. Cole photographed the xylene spectra in 1943,[6] but because of war research these spectroscopic studies were not pursued further.

Absorption studies in the vacuum ultraviolet of the individual xylenes in a *n*-heptane solution have been carried out by Platt and Klevens.[7] In this same spectral region Price[8] and co-workers have obtained the spectra of the xylenes in the vapor phase.

Emission spectra in the near ultraviolet which must be considered as the counterpart of the absorption in this region have been obtained in a Tesla discharge through xylene vapor by McVicker[9] and co-workers. The near ultraviolet fluorescence spectrum of *ortho*-xylene was reported by Marsh[10] in 1923, but similar data could not be found for the vapors of the other two isomers. Fluorescence of the xylenes in alcoholic solutions, as well as other related facts, have been included in the recent book on fluorescence and phosphorescence by Pringsheim.[11] The Raman spectra of

* This work was assisted by the ONR under contract N60ri-107, Task Order I, with Duke University.

† Based on parts of two theses submitted in partial fulfillment of the requirements for the degree of Doctor of Philosophy in the Graduate School of Arts and Sciences of Duke University during 1950 and 1951.

‡ Present address: Physics Department, University of Georgia, Athens, Georgia.

§ Present address: Pithapuram (M.S.M. Rly.), India.

[1] J. Pauer, Ann. Physik und Chem. **61**, 363 (1897).

[2] H. Conrad-Billroth, Z. physik. Chem. **B29**, 170 (1935)

[3] K. L. Wolf and W. Herold, Z. physik. Chem. **B13**, 201 (1931).

[4] American Petroleum Institute Research Project 44 at the National Bureau of Standards, *Catalog of Ultraviolet Spectrograms*. Serial No. 55, 56, and 57. *O*-xylene, *M*-xylene and *P*-xylene, contributed by the Texas Company, Beacon, New York.

[5] A. Kronenberger, Z. Physik **63**, 494 (1930).

[6] Communication to Dr. H. Sponer from Dr. M. B. Hall.

[7] J. R. Platt and H. B. Klevens, Chem. Revs. **41**, 301 (1947).

[8] Price, Hammond, Teegan, and Walsh, Disc. Faraday Soc. **9**, 53 (1950).

[9] McVicker, Marsh, and Stewart, J. Chem. Soc. **125**, 1743 (1924).

[10] J. K. Marsh, J. Chem. Soc. **123**, 3315 (1923); Phil. Mag. **49**, 971 (1925).

[11] P. Pringsheim, *Fluorescence and Phosphorescence* (Interscience Publishers, Inc. New York, 1949).

the xylenes can be found in the publications of Paulsen,[12] Kohlrausch,[13] and Herz.[14] Recent work by Plyler[15] has extended and supplemented the work of Lecomte,[16] Barnes,[17] and others,[18] so that infrared spectra of the dimethylbenzenes are known between 250 cm^{-1} and 2000 cm^{-1}.

The present work was undertaken as part of a program on the structure of electronic levels in substituted benzenes. Since the near ultraviolet absorption spectra of toluene[19,20] and mesitylene[21] have been analyzed, it was felt that a study of the xylene spectra would fill the remaining gap between these methylbenzenes and at the same time offer some interesting comparisons. Also, much unpublished information, both experimental and theoretical, has been obtained in this laboratory on the spectra of other disubstituted benzenes. These spectral data will furnish comparisons and serve as guides in the choice of assignments for the dimethylbenzenes.

EXPERIMENTAL

The *para*-xylene sample used in this research was purchased from Eimer and Amend and was their cp grade. Further purification of the sample was carried out by a fractional recrystallization of five steps to obtain a final sample with a freezing point of 13.2°C.

The experimental details involved in obtaining the fluorescence spectrum reported here will be published with other fluorescence data in the near future by M. L. N. Sastri. They follow, in general, procedures used in previous fluorescence research.[22]

For the absorption spectra reported here, the optical arrangement was the same as in previous similar studies from this laboratory. The 25-cm quartz absorption cell used for *para*-xylene was loaded and its temperature controlled in much the same manner as that reported by Sponer and Lowe[23] for benzotrifluoride. This method gives the spectra as a function of the vapor pressure inside the cell. The vapor pressures for the different temperatures were obtained from the measurements of Stuckey and Saylor.[24]

As a continuous light source a hydrogen lamp of conventional design was employed and operated at 2300 volts. The light from this lamp was rendered approximately parallel by a quartz condensing lens and then allowed to pass through the absorption cell and was focused on the spectrographic slit with a cylindrical quartz lens. The spectrograph utilizes a Rowland 3-meter reflection grating in a modified Eagle mounting. The grating was used in the first order giving a practically linear dispersion of 5.535 A/mm.

Eastman Kodak III-0 and II-0 spectroscopic plates were used with the best results being obtained on II-0 plates. Exposure times varied from ten to sixty minutes and the plates were developed for five minutes in a tray of D19 developer at 20°C. An iron arc was used to supply a comparison spectrum. Measurement of the spectra was carried out with a Hilger comparator so that in general the bands are accurate to within 2 or 3 cm^{-1}.

EXPERIMENTAL RESULTS

The near ultraviolet absorption spectrum of *para*-dimethylbenzene lies in the region between 2850 and 2350A. This spectrum was studied in dependence of the pressure of the substance for temperatures ranging between −40° and 100°C. The bands of the spectrum have slightly diffuse heads and are degraded toward the red. At −30°C (0.05 mm Hg) only four bands are present on the photographic plate. They appear at 2721.52A (36,733 cm^{-1}), 2665.8A (37,508 cm^{-1}), 2663.4A (37,535 cm^{-1}), and 2636.5A (37,918 cm^{-1}). When the temperature is increased to −20°C (0.16 mm Hg), an additional band is found at 2681.3A (37,285 cm^{-1}) as well as five bands of shorter wavelengths which belong to combinations or progressions of the first bands, as will be shown later. Also at this temperature three bands appear on the red side of the 36,733-cm^{-1} band and are separated from it by 54, 94, and 192 cm^{-1}. For higher temperatures similar companions appear on the long-wavelength side of the other bands cited above. Referring to Fig. 1, which shows both the absorption and fluorescence spectra, we see that similar band groups of medium intensity, which are only partially developed, appear toward the violet from the 37,918-cm^{-1} band. Also, for the temperature of 10°C (3.29 mm Hg), the absorption spectrum shows a few widely spaced, very weak bands toward the red from the well-developed 36,733-cm^{-1} group. These bands are accompanied by weaker ones at increased temperatures to develop at least three more of the groups similar to these observed in the stronger region. For these temperatures above 30°C (11.72 mm Hg) the stronger bands of the spectrum have broadened to a continuous absorption.

In addition to the near ultraviolet electronic spectrum discussed above, there is another absorption system around 2100A for *para*-xylene. A study of this system with ultraviolet sensitized plates revealed only the edge of a continuous absorption which gradually moves toward the red with increasing temperatures to merge

[12] O. Paulsen, Monatsh. Chem. **72**, 244 (1939).
[13] K. W. F. Kohlrausch and associates, Monatsh. Chem. **72**, 268 (1939); **74**, 175 (1942); **76**, 200 (1947).
[14] E. Herz, Monatsh. Chem. **76**, 1 (1947).
[15] E. K. Plyler, Disc. Faraday Soc. **9**, 100 (1950).
[16] J. Lecomte, J. phys. radium **9**, 13 (1938); Ann. phys. **10**, 503 (1938).
[17] Barnes, Gore, Liddel, and Williams, *Infrared Spectroscopy* (Reinhold Publishing Corporation, New York, 1944).
[18] American Petroleum Institute Research Project 6 at the National Bureau of Standards, *Catalog of Infrared Spectrograms*.
[19] J. Savard, Ann. chim. et phys. **21**, 287 (1929).
[20] Ginsburg, Robertson, and Matsen, J. Chem. Phys. **14**, 511 (1946).
[21] H. Sponer and M. J. Stallcup, paper in V. Henri memorial Volume, *Contributions à l'Etude de la Structure Moléculaire* (Desoer, Liège, 1948), p. 211.
[22] A. M. Bass and H. Sponer, J. Opt. Soc. Am. **40**, 389 (1950).
[23] H. Sponer and D. S. Lowe, J. Opt. Soc. Am. **39**, 840 (1949).
[24] J. M. Stuckey and J. H. Saylor, J. Am. Chem. Soc. **62**, 2922 (1940).

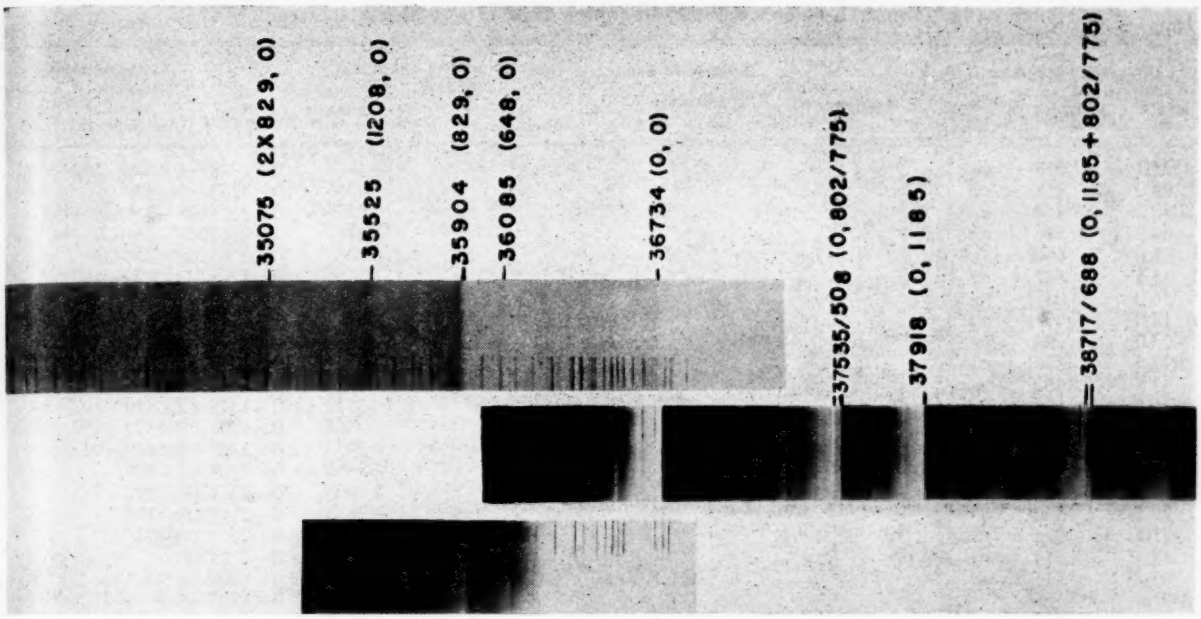

FIG. 1. Top—fluorescence spectrum of *para*-xylene excited by Mn spark; exposure time 48 hours; slit width 50μ; vapor pressure 5 mm Hg; Corning #9863 filter. Middle—absorption spectrum of *para*-xylene; vapor pressure 1.4 mm Hg. Bottom—absorption spectrum of *para*-xylene; vapor pressure 11.7 mm Hg.

with the system of longer wavelengths for temperatures above 50°C.

The fluorescence of *p*-xylene was obtained by using a condensed Mn spark as light source. Table I gives the emission of Mn and the corresponding absorption bands of *p*-xylene for comparison. The exciting lines are rather weak, but it is exceptional to find strong lines which coincide in wavelength with the strong absorption bands. It was found that the fluorescence spectrum extends from 3125 to 2720A and consists of about 45 rather diffuse bands. In appearance the spectrum is very similar to the Tesla luminescence spectrum of *p*-xylene taken by McVicker and Marsh.[9] The fluorescence bands agree with the emission bands, but the fluorescence spectrum is much richer in bands. In fluorescence a region of weak emission is observed in the neighborhood of the 0, 0 band. The same observation has been made in the other cases studied as may be seen from the fluorescence spectra of benzotrifluoride,[25] toluene,[26] fluorobenzene,[22] and benzonitrile.[26] This effect has been interpreted as caused by partial reabsorption of the emitted radiation in the cell.

In the region of overlap the bands coincide in most cases with absorption bands. The wavelengths, wave numbers, intensities, and assignments of both fluorescence and absorption bands are listed in Table II. The intensity measurements are only visual estimates based on the following scale: *vs*—very strong, *s*—strong, *ms*—medium strong, *m*—medium, *mw*—medium weak, *w*—weak, *vw*—very weak, and *ew*—extremely weak. The wave numbers used in the assignment column are those obtained from the absorption measurements since they are the more accurate.

DISCUSSION AND ANALYSIS

On the basis of the known molecular configuration of *para*-dimethylbenzene it is assigned to the point group D_{2h}, considering the CH_3 group as a single atom, as was done by Pitzer and Scott[27] in their discussion of the Raman data. In this discussion the z axis has been chosen to be perpendicular to the plane of the benzene ring, and the y axis coincides with a line joining the two substituents. Thus for *para*-xylene the electronic transition $^1A_{1g}-{}^1B_{3u}$ is allowed with the transition moment in the x direction. In addition to this allowed transition a so-called forbidden part of the transition of much weaker intensity may also be produced by a vibration moment just as was the case in benzene. This moment can be produced in the y direction by a β_{1g} vibration or in the z direction by a β_{2g} vibration.

TABLE I. Comparison of Mn lines[a] with the absorption bands of *p*-xylene in A units.

Mn lines	Absorption bands of *p*-xylene	Assignment
2722.1	2721.5	0,0
2695.4	2694.6	0,367
2681.7	2681.3	0,552
2666.8	2665.5	0,775
2664.0	2663.4	0,802
2637.2	2636.5	0,1185

[a] From MIT wavelength tables.

[25] M. L. N. Sastri, Ph.D. dissertation, Duke University (1951).
[26] A. M. Bass, J. Chem. Phys. 18, 1403 (1950).
[27] K. S. Pitzer and D. W. Scott, J. Am. Chem. Soc. 65, 803 (1943).

TABLE II. Fluorescence and absorption bands of *para*-dimethylbenzene.

[Fluorescence bands Wave-length A	Wave number cm^{-1}	Int.	Absorption bands Wave-length A	Wave number cm^{-1}	Int.		Separation from 0, 0 36,733 cm^{-1}	Assignments
3122.3	32,018	*ew*					−4715	0−1208−4×829−192
03.0	218	*ew*					−4515	0−1208−4×829
3080.0	458	*ew*					−4275	0−2×1208−2×829−192
69.8	566	*ew*					−4167	0−2×1208−2×829−94
61.0	660	*w*					−4073	0−2×1208−2×829
43.5	847	*ew*					−3886	0−1208−3×829−192
26.0	33,037	*w*					−3696	0−1208−3×829
12.0	191	*ew*					−3542	0−2×1208−829−192−94
03.0	290	*ew*					−3443	0−2×1208−829−192
2994.4	386	*vw*					−3347	0−2×1208−829−94
85.8	482	*w*					−3251	0−2×1208−829
76.1	591	*wd*					−3142	0−1208−2×829−192−94
69.0	672	*wd*					−3061	0−1208−2×829−192
60.0	774	*w*					−2959	0−1208−2×829−94
51.9	867	*m*					−2866	0−1208−2×829
36.8	34,040	*mw*					−2693	0−2×1208−192−94
29.1	130	*mw*					−2603	0−2×1208−192
21.1	224	*s*					−2509	0−2×1208−94
13.1	318	*s*					−2415	0−2×1208
05.2	411	*m*					−2322	0−1208−829−192−94
2897.3	505	*s*					−2228	0−1208−829−192
89.1	603	*vs*					−2130	0−1208−829−94
81.5	694	*vs*					−2039	0−1208−829
74.2	782	*mw*					−1951	0−2×829−192−94
66.6	874	*m*					−1859	0−2×829−192
57.8	982	*m*					−1751	0−2×829−94
					$t=85°C$ $p=135.0$ mm Hg	$t=35°C$ $p=15.70$ mm Hg		
50.2	35,075	*vs*	2850.2	35,075	*ew*		−1658	0−2×829
44.8	142	*ew*					−1591	0−1208−2×192
			42.1	175	*ew*		−1558	
36.5	244	*m*					−1490	0−1208−192−94
			35.3	259	*w*		−1474	0−829−648
29.3	334	*s*	29.1	335	*mw*		−1398	0−1208−192
21.4	433	*vs*	21.4	433	*ew*		−1300	0−1208−94
			15.9	502	*ew*		−1231	
14.1	525	*vs*	14.1	525	*s*	*vw*	−1208	0−1208
06.7	619	*s*					−1114	0−829−192−94
2799.5	710	*s*	2799.5	710		*vw*	−1023	0−829−192
			98.7	720		*vw*	−1013	0−829−2×94
91.6	811	*vs*	91.6	811		*mw*	−922	0−829−94
			88.5	851		*ew*	−882	0−829−54
			85.3	892		*w*	−841	0−829−12
84.4	904	*vs*	84.4	904		*ms*	−829	0−829
77.5	993	*vw*	77.5	993		*vw*	−740	0−648−94
			75.1	36,024		*ew*	−709	0−648−54?
			71.3	073		*mw*	−660	0−648−12
					$t=10°C$ $p=3.29$ mm Hg			
70.4	36,085	*s*	70.4	085	*ew*	*m*	−648	0−648; 0−458−192
			65.0	155		*ew*	−578	0−458−94−27
62.9	184	*vw*	62.9	184		*vw*	−549	0−458−94
			59.6	227		*ew*	−506	0−458−54
			57.8	250		*ew*	−483	0−458−27
55.9	275	*s*	55.9	275	*vw*	*s*	−458	0−458
50.5	346	*mw*					−387	0−2×192; 0−387?
			49.4	361	*w*		−372	0−192−2×94
42.8	448	*s*	42.5	452	*vw*		−281	0−192−94
			39.9	488	*w*		−245	0−192−54
			38.8	502	*w*		−231	0−192−27−12
			38.0	512	*w*		−221	0−192−27
35.8	541	*s*	35.8	541	*s*		−192	0−192
						$t=0°C$ $p=1.30$ mm Hg		
			35.5	545	*m*	*m*	−188	0−2×94
			30.6	611		*w*	−122	0−94−27
			29.7	624		*vw*	−109	0−94−12?

TABLE II—*Continued.*

Fluorescence bands			Absorption bands				Separation from 0, 0 36,733 cm^{-1}	Assignments
Wave-length Å	Wave number cm^{-1}	Int.	Wave-length Å	Wave number cm^{-1}	Int.			
28.4	641	*s*	28.4	641		*m*	−92	0−94
			26.9	661		*vw*	−72	0−72
			25.5	680		*mw*	−53	0−54; 0−2×27
			24.5	694		*mw*	−39	0−12−27
			23.5	706		*mw*	−27	0−27
			22.4	721		*mw*	−12	0−12
21.5	733	*s*	21.5	733	*vs*	*vs*	0	0, 0
						$t=15°C$ $p=5.00$ mm Hg		
			20.8	743	*w*	*vs*	10	
			18.6	773		*ew*	40	
			17.6	786	*ew*	*vw*	53	
			15.6	816		*mw*	83	
			08.5	910	*vw*	*w*	177	0+367−192
			00.2	37,023		*ew*	290	
			2698.6	049		*ew*	316	0+367−54
			95.3	091	*ms*	*vs*	358	0+552−192?
			94.6	100	*ms*	*s*	367	0+367; 0+552−2×94
			90.3	159	*w*	*ms*	426	
			88.0	191	*w*	*mw*	458	0+552−94
			85.2	231	*ew*		498	0+552−54
			81.9	275	*ms*	*vs*	542	0+552−12?
			81.3	285	*s*	*vs*	552	0+552
			78.7	320	*w*	*mw*	587	0+775−192; 0+775−2×94
			76.6	349	*w*		616	0+802−192; 0+802−2×94
			72.0	414	*w*		681	0+775−94
			70.1	440	*mw*		707	0+802−94
			65.5	508	*vs*		775	0+775
			63.4	535	*vs*	*vs*	802	0+802
			52.2	694	*w*	*mw*	961	
			49.7	729	*mw*	*mw*	996	0+1185−2×94
			42.9	827	*ew*		1094	0+1185−94
			42.0	838	*mw*		1105	0+2×552
			40.3	864	*w*		1131	0+1185−54
			36.5	918	*vs*	*vs*	1185	0+1185
			31.0	997	*ew*	*ew*	1264	
			27.5	38,047	*w*		1314	0+552+775−12
			26.9	057	*w*	*mw*	1324	0+552+775
			25.5	076	*ew*		1343	
			25.0	084	*w*		1351	0+552+802
			24.3	093	*vw*	*w*	1360	0+2×775−192
			23.2	110	*ew*	*ew*	1377	0+1565−192
			16.8	203	*vw*		1470	0+1565−94
			11.2	286	*vw*		1553	0+2×775; 0+1565−12?
			10.3	298	*s*	*vs*	1565	0+1565; 0+775+802
			07.4	342	*m*	*s*	1609	0+2×802
			2599.5	457		*ew*	1724	0+552+1185−12
			98.7	469	*w*	*mw*	1736	0+552+1185
			97.5	487	*w*	*w*	1754	
			96.6	500	*w*	*w*	1767	0+1185+775−2×94
			94.2	535	*w*	*w*	1802	0+1185+802−2×94
			90.2	595	*vw*		1862	0+1185+775−94
			88.1	627	*ew*		1894	0+1185+802−94
			85.8	661	*ew*		1928	0+1185+802−54
			84.0	688	*s*		1955	0+1185+775
			82.0	717	*ms*	*vs*	1984	0+1185+802
			73.4	848	*w*	*w*	2115	0+552+1565
			70.9	885		*vw*	2152	0+552+2×802
			69.3	910	*vw*	*vw*	2177	0+2×1185−2×94
			63.0	39,005	*vw*		2272	0+2×1195−94
			59.5	059	*ew*		2326	0+3×775
			57.4	090	*s*		2357	0+1565+802
			56.9	098	*ms*	*vs*	2365	0+2×1185; 0+1565+802
			53.5	151	*ew*	*ew*	2418	0+552+1185+775−94
			51.5	181	*ew*	*ew*	2448	0+552+1185+802−94
			47.8	238	*w*	*mw*	2505	0+552+1185+775
			45.9	268	*vw*	*w*	2535	0+552+1185+802
			43.7	301		*ew*	2568	
			38.0	389		*ew*	2656	0+1185+1565−94
			32.3	478	*m*	*vs*	2745	0+1185+1565

TABLE II—*Continued.*

Fluorescence bands			Absorption bands					
Wave-length A	Wave number cm^{-1}	Int.	Wave-length A	Wave number cm^{-1}	Int.		Separation from 0, 0 36,733 cm^{-1}	Assignments
			29.5	521	*vw*	*vw*	2788	0+1185+2×802
			21.3	650		*ew*	2917	0+552+802+1565
			20.3	666		*ew*	2933	0+552+2×1185
			13.2	778		*ew*	3045	0+2×1185+775−94
			11.5	805		*ew*	3072	0+2×1185+802−94
			07.6	867	*ms*	*vs*	3134	0+2×1185+775; 0+2×1565
			05.8	899	*mw*	*s*	3166	0+2×1185+802
					$t=30°C$ $p=11.72$ mm Hg			
			2497.0	40,036	*ew*		3303	0+552+1185+1565
			95.8	055	*ew*		3322	
			94.4	078		*ew*	3345	0+552+1185+2×802
			82.2	275	*s*	*vs*	3542	0+3×1185; 0+1565+1185+802
			73.2	421	*w*	*vw*	3688	0+552+2×1185+775
			71.4	451	*vw*	*vw*	3718	0+552+2×1185+802
			58.7	659	*s*	*s*	3926	0+2×1185+1565
			56.4	698	*w*	*ew*	3965	0+2×1185+2×802
			49.0	821	*w*		4088	0+552+3×1185
			46.9	856	*ew*		4123	
			44.6	894	*ew*		4161	
			41.2	951	*ew*		4218	
			38.9	990	*ew*		4257	
			37.8	41,008	*ew*		4275	
			34.1	070	*w*		4337	0+3×1185+802
			32.0	106	*ew*		4373	
			26.1	206	*ew*		4473	0+552+2×1185+1565
			18.9	329	*ew*		4596	
			17.1	359	*ew*		4626	0+4×1185−94
			14.4	406	*ew*		4673	
			11.8	450	*vw*		4717	0+4×1185
			01.6	626	*ew*		4893	0+552+3×1185+802
			2389.7	833	*vw*		5100	0+3×1185+1565

From group theoretical considerations and from the Franck-Condon principle[28] totally symmetric vibrations are expected to appear in strong bands, and they should form progressions. Nontotally symmetric vibrations will appear in $v-v$ transitions according to their Boltzmann factors. They may also, with the exception of the classes β_{1u}, β_{2u}, and β_{3u}, appear singly excited in "forbidden" bands for which the electronic transition moment would not be in the x direction but perpendicular to it. Since these β_u-vibrations are all infrared active, it follows that for *para*-xylene infrared active vibrations can occur, in the electronic absorption spectrum here discussed, in $v-v$ transitions only, or excited in even multiples.

Of the four strong bands that are observed in absorption at a temperature of −30°C (0.05 mm Hg) the band of longest wavelength 2721.52A (36,733 cm^{-1}) is chosen as the 0, 0 band of the allowed spectrum. The other three bands found at 37,508, 37,535, and 35,918 cm^{-1} represent frequency differences from the 0, 0 band of 775, 802, and 1185 cm^{-1}. All three frequencies appear in progressions. Table II shows that 775 and 802 combine with the 1185 progression and probably with each other. The band at 38,298 cm^{-1} with the frequency of 1565 cm^{-1} may be the slightly anharmonic combination 775+802=1577. The frequency separations 775, 802, and 1185 cm^{-1} are interpreted as vibrational frequencies in the upper electronic state. From Raman data[11] we find polarized Raman lines at 809, 828, and 1204 cm^{-1}; and on both our fluorescence and absorption spectrograms, bands separated to the red from the 0, 0 band by 829, 1208, and 2×829 cm^{-1} have been observed at the respective positions of 35,904, 35,525, and 35,057 cm^{-1}. These bands are the strongest in the fluorescence spectrum and all bands toward the red from the 35,904 cm^{-1} band can be assigned as members of progressions or combinations of the 829 and 1208 cm^{-1} frequencies if frequency differences involved in v, v transitions are taken into consideration. Furthermore, an interpretation of the ultraviolet emission spectrum of *para*-xylene obtained in a Tesla discharge by Marsh[9] reveals that the frequencies 830 and 1210 cm^{-1} appear in progressions and combinations. There is no doubt that the 1185 cm^{-1} upper state vibration corresponds to the 1208 ground state vibration. Appearance and intensity of the 1185 progression make it certain that this frequency is to be correlated with a totally symmetric vibration. Of the two bands involving the frequencies 775 and 802, the first is considerably stronger than the 802 band (see Fig. 1 and experimental results). Since the 828 is a highly polarized Raman line and a band is not found in the electronic spectra which can reasonably be assigned to a 809 vibration in the ground state, the 775 frequency

[28] H. Sponer and E. Teller, Revs. Modern Phys. **13**, 76 (1941).

in the excited state is correlated with the totally symmetric 829 frequency in the ground state. Considering the correlation of the 1208 and 828 frequencies to modes of vibration, different assignments have been suggested.[13,27] It can be said safely that at least one of them is a carbon ring vibration, and the other one may be associated with the C—CH_3 valence vibration.

As mentioned earlier, a vibration moment may be formed in the y direction by a β_{1g}-vibration once excited, or in the z direction by a β_{2g}-vibration once excited. Superposed on these 0—1 transitions may occur transitions of totally symmetric vibrations. All these bands should be weaker than those in which the electronic transition is in the x direction, and they constitute the "forbidden" part of the spectrum. Now the ϵ_g^+ (606 cm^{-1}) vibration, which makes the "forbidden" spectrum of benzene allowed in the second order, splits for D_{2h} symmetry into an α_{1g} and β_{1g}-vibration. The polarized Raman line 457 has been associated with the α_{1g}-component. It is represented by the band 36,725 cm^{-1}. The weak band at 37,100 cm^{-1} in the absorption spectrum may be interpreted as representing this vibration in the upper electronic state, thus giving a value of 367 cm^{-1}. This frequency is not found in any combinations or progressions because of too great a weakness of the corresponding bands which in most cases would be close to other strong bands.

From absorption and fluorescence studies and Tesla luminescence spectra the β_{1g}-component of the ϵ_g^+ benzene vibration is chosen as 648 in the ground state and 552 in the upper state as represented by the bands at 36,085 and 37,285 cm^{-1}. Support for assignment of these bands to a "forbidden" transition is gained from estimated intensities. The band 37,285, as well as those superimposed on it, is about ten times weaker than bands belonging to the allowed part of the spectrum (see Table II). The vibration involved gives rise to a depolarized Raman line at 643 cm^{-1}. Using an average value of 646 we find the difference of this vibration in the two states as 646—552=94. It is suggested that the bands separated to the red from all the prominent bands by this amount involve 1—1 transition of this vibration. Still further, the progressively weaker bands 36,545, 36,452, and 36,361, which are separated from the 0, 0 band by 188, 281, and 372 cm^{-1}, do fit numerically to $v-v$ transitions of the same vibration where $v=2$, 3 and 4. However, it is difficult to reconcile the intensity of some of these bands with a Boltzmann distribution of the vibrational levels. Other companions of the main bands with separations of 12, 27, 39, 54, and 72 cm^{-1} may be produced by $v-v$ transitions of almost any vibration below 600 cm^{-1}. Also, the 12 cm^{-1} separation may be associated with rotation structure. The prominent band at 37,541 cm^{-1} is separated from the 0, 0 band by 192 cm^{-1}. This band is different from and much stronger than the one separated by 188 cm^{-1} which was mentioned previously. The 192 band is therefore attributed to a $v-v$ transition of a low-lying vibration. The intensity ratio is that expected for a vibration of about 400 cm^{-1}. It is possible that the vibration partaking in this transition is analogous to the ϵ_u^+ vibration of 400 cm^{-1} which produces the 160 cm^{-1} frequency difference observed in benzene. This vibration is of type α_{1u} or β_{1u} in the *para*-compound. It is also possible that a deformation or out-of-plane vibration of low frequency of the CH_3 groups is involved in this $v-v$ transition. Plyler's[15] recent investigation of the infrared spectrum between 700 and 250 cm^{-1} revealed only three bands within this region. Their frequencies and tentative assignments were listed[b] as 645—β_{1g}, 483—α_{1g}, and 292—β_{3g}. Since both the 645 and 292 cm^{-1} bands are weak, their assignment to inactive modes is tenable, but an association of the very strong 483 cm^{-1} frequency with the β_{1u} component of the 400 ϵ_u^+ benzene vibration seems to be a more likely assignment. This would mean that the 483 cm^{-1} infrared band is not to be associated with the 458 α_{1g}-band in the Raman spectrum. Then the 192 frequency difference found in electronic spectra may possibly be assigned to a 1—1 transition involving a β_{1u} vibration of 483 cm^{-1} in the ground state and 291 cm^{-1} in the excited state. The 2—2 transition of this vibration might produce the 36,346 cm^{-1} band with a separation of 387 cm^{-1} in the fluorescence spectrum.

TABLE III. Comparison of some fundamental frequencies obtained by different means of excitation.

Raman[13]	Fluorescence	Tesla luminescence[9]	Absorption lower	Absorption upper	Symmetry
457(7)	458		458	367	α_{1g}
643(5)	648	650	648	552	β_{1g}
828(10)	829	830	829	775	α_{1g}
1204(8)	1208	1210	1208	1185	α_{1g}

On the basis of the assignments discussed most of the *para*-xylene bands may be interpreted as in Table II. The fundamental frequencies obtained from absorption, fluorescence, and Tesla luminescence are collected with the corresponding Raman values in Table III. Symmetry assignments are given in the last column of this table.

The authors are indebted to Professor H. Sponer for her suggestions and helpful discussions in directing this research.

[b] Plyler's notations of β_{3g} and β_{2g} are changed here to β_{1g} and β_{3g}, respectively.

The Mechanism of Hydrogen Evolution at Nickel Cathodes in Aqueous Solutions

J. O'M. Bockris and E. C. Potter
Department of Chemistry, Imperial College of Science and Technology, London S.W. 7, England
(Received September 24, 1951)

Hydrogen overpotential at nickel cathodes has been measured under very pure conditions in aqueous solutions of hydrogen chloride (0.001N−1.0N) and in aqueous sodium hydroxide (0.001N−0.2N). The measurements have been made in the current density range $10^{-8}-10^{-1}$ amp/apparent cm², and in the temperature range 0°–50°C. Observations were also made of the build-up and rate of decay of overpotential and of the capacity of the electrode/electrolyte interface. Direct measurements were made of the number of acts of the rate-determining step associated with one act of the over-all hydrogen evolution reaction (i.e., the stoichiometric number μ). The application of μ has been extended to hydrogen overpotentials greater than about −20 millivolts. The experimental data were treated statistically and show that the most probable mechanism of hydrogen overpotential at nickel cathodes is that of a rate-determining discharge step followed by a recombination of hydrogen atoms. The discharge probably takes place from hydroxonium ions in acid solution. In alkaline solution the observed *p*H effect on overpotential is best explained by assuming that the discharge occurs from water molecules whose activity depends on the electrode field. Consideration of the role of chemisorption in the hydrogen electrode process indicates that a rate-determining discharge step can take place from a nickel surface substantially occupied with hydrogen atoms.

I. INTRODUCTION

In recent years considerable progress has been made in deciding the relevance and interpretation attached to certain specific studies of the kinetics of cathodic hydrogen evolution. For example, Agar[1] has demonstrated how knowledge of the effects of temperature and reactant concentration assists in elucidating electrochemical reaction mechanisms. Bockris[2] and also Lukovzew[3] have pointed out the value of several parameters open to experimental study in providing distinguishing criteria for reaction mechanisms. The theoretical bases of these criteria have recently been clarified by Parsons,[4] and by Bockris and Potter,[5] and it is the aim of this paper to report the results of an application of the principles described by these authors to the deposition of hydrogen at nickel cathodes.

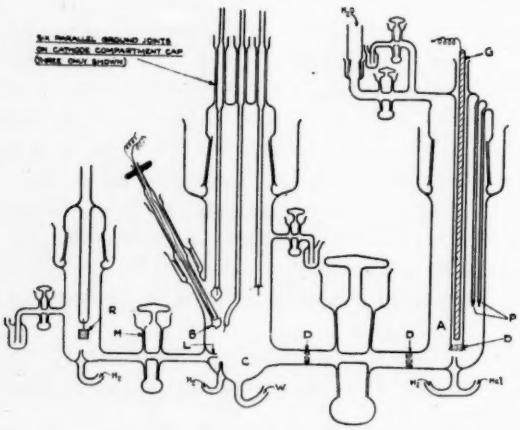

FIG. 1. Electrolytic cell.

[1] J. N. Agar, Disc. Faraday Soc., No. 1, 81, (1947).
[2] J. O'M. Bockris, Chem. Revs. **43**, 525 (1948).
[3] P. Lukovzew, J. Phys. Chem. Russ. **21**, 589 (1947).
[4] R. Parsons, Trans. Faraday Soc. **47**, 1332 (1951).
[5] J. O'M. Bockris and E. C. Potter, J. Electrochem. Soc. (to be published).

II. PREVIOUS CONCEPTS OF THE MECHANISM OF HYDROGEN EVOLUTION AT NICKEL CATHODES

Most concepts of the mechanism of hydrogen evolution at nickel cathodes have been based on studies of hydrogen overpotential in aqueous solutions. According to Frumkin and his co-workers,[6–10] the observed phenomena correspond to a dual mechanism in which the reaction is controlled over part of the electrode by a discharge step involving the hydrogen ion or a water molecule, and over the remaining area by the recombination of hydrogen atoms. Thus, the observed *p*H effects on overpotential and the reported variation[9] of μ, the stoichiometric number,[11] with *p*H in alkaline solutions can be interpreted by the dominance of either type of area. Bockris and Conway[12] attributed the effect of minute amounts of catalytic poisons on overpotential at a nickel cathode to a dual rate-determining desorption step involving recombination of hydrogen atoms and electrochemical desorption.[13] Okamoto, Horiuti, and Hirota[14] have applied the transition state theory to the recombination of hydrogen atoms at a nickel cathode, but this treatment assumes that the Nernst emf equation applies to hydrogen atoms in an irreversible reaction, and this has not been validly demonstrated.

[6] Lukovzew, Lewina, and Frumkin, Acta Physicochimica, U.R.S.S. **11**, 21 (1939).
[7] A. Legran and S. Lewina, Acta Physicochimica, U.R.S.S. **12**, 243 (1940).
[8] J. Kolotyrkin and A. Frumkin, Compt. rend. acad. Sci. U.R.S.S. **33**, 445 (1941).
[9] P. Lukovzew and S. Lewina, J. Phys. Chem. Russ. **21**, 599 (1947).
[10] A. Frumkin, Disc. Faraday Soc., No. 1, 63 (1947).
[11] J. Horiuti, J. Research Inst. Catalysis Hokkaido Univ. **1**, 8 (1948).
[12] J. O'M. Bockris and B. E. Conway, Trans. Faraday Soc. **45**, 989 (1949).
[13] $MH+H_3O^+ + e \rightarrow H_2$, where M is a metal atom and e is an electron.
[14] Okamoto, Horiuti, and Hirota, Sci. Papers Inst. Phys. Chem. Research (Tokyo) **29**, 223 (1936).

III. SCOPE OF THE PRESENT INVESTIGATION

In the present investigation the course of the Tafel line[15] for nickel cathodes in acid (HCl) and alkaline (NaOH) aqueous solutions at several temperatures and concentrations was traced, and data of known accuracy were obtained therefrom by statistical procedures. Supplementary information was derived from studies of the transient build-up and decay of overpotential and from the effect of ac superimposed on the polarizing current.

IV. EXPERIMENTAL TECHNIQUE

Throughout the experimental work very pure conditions were reached and maintained in the electrode-electrolyte system by methods previously described.[16] The electrolytic cell, made of arsenic-free borosilicate glass, is shown diagrammatically in Fig. 1. The cathode compartment C accommodated six nickel wire electrodes each supported on a parallel ground glass joint allowing full rotation and movement through a vertical distance of about 8 cm.[17] The electrodes were sealed in pure dry hydrogen in fragile glass bulbs[18] so that when these were broken by the retractable thermocouple sheath B under the purified electrolyte, any one of the cathodically polarized nickel electrodes could be moved to touch the Luggin capillary *L*. Equilibrium water, refluxed in hydrogen for 6 hours, was distilled into *A*, the anode compartment of the cell, and gaseous HCl or aqueous NaOH was passed in until the required concentration (estimated conductometrically at P or with a calibrated glass float) was obtained. Waste wash liquor was discarded through W, and interdiffusion of anolyte and catholyte was retarded both by the sintered glass disks D, and by the closed tap between these. The anode G was of spectroscopically pure graphite and a platinized-platinum reference electrode R was used. All connections of subsidiary apparatus to the cell were of glass using water-sealed joints and taps as at M.

TABLE I. Conditions of pre-electrolysis for various concentrations of electrolyte.

Concentration	Cathodic c.d. amp/cm²	Time	Coulombs
1.0N	10^{-1}	18 hr	1800–2000
0.1N	10^{-1}	18 hr	1800–2000
0.01N	8×10^{-3}	18 hr	100–125
0.001N	1×10^{-3}	18 hr	10

Hydrogen chloride was prepared by the action of sulfuric acid on potassium chloride, previously heated to 500°C in a stream of hydrogen for 1 hour, and was passed through a trap cooled to −80°C before leading to the cell. Pure aqueous sodium hydroxide was prepared by recrystallizing three times as pentahydrate at −12°C in hydrogen, followed by prolonged electrolysis at platinum electrodes in the same all-glass apparatus. Hydrogen used in the preparation of electrodes and electrolytes was freed from oxygen and carbon monoxide, and passed through three traps at −196°C. The cell was regularly cleaned with a mixture of nitric acid and sulfuric acid or aqua regia, and repeatedly washed with equilibrium water before final rinsing with conductivity water in hydrogen.

Before fracturing the bulbs surrounding the five nickel test electrodes (average apparent area 0.25 cm² each), pre-electrolysis[16] was carried out under the conditions given in Table I by using the sixth electrode. In this way nearly all traces of impurities (especially oxygen) were removed from the catholyte.

Accurate estimates of current between 10^{-9} and 10^{-6} amp were made by measuring the potential drop across

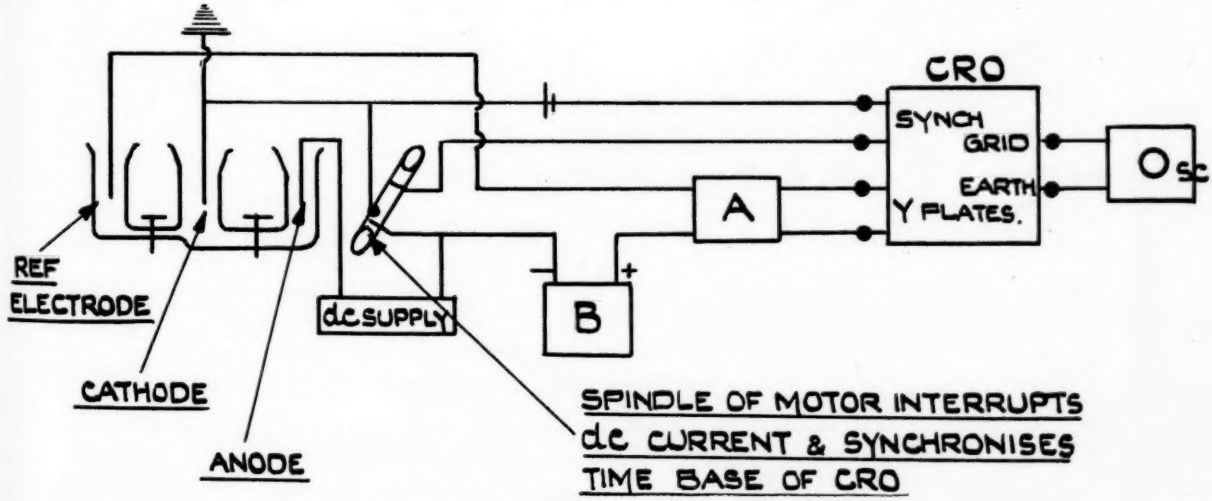

FIG. 2. Circuit for dc charging and decay curves.

[15] The line obtained when hydrogen overpotential is plotted as ordinate against common logarithm of current density as abscissa.
[16] Azzam, Bockris, Conway, and Rosenberg, Trans. Faraday Soc. **46**, 918 (1950).
[17] E. C. Potter, J. Sci. Instr. (to be published).
[18] J. O'M. Bockris and B. E. Conway, J. Sci. Instr. **25**, 283 (1948).

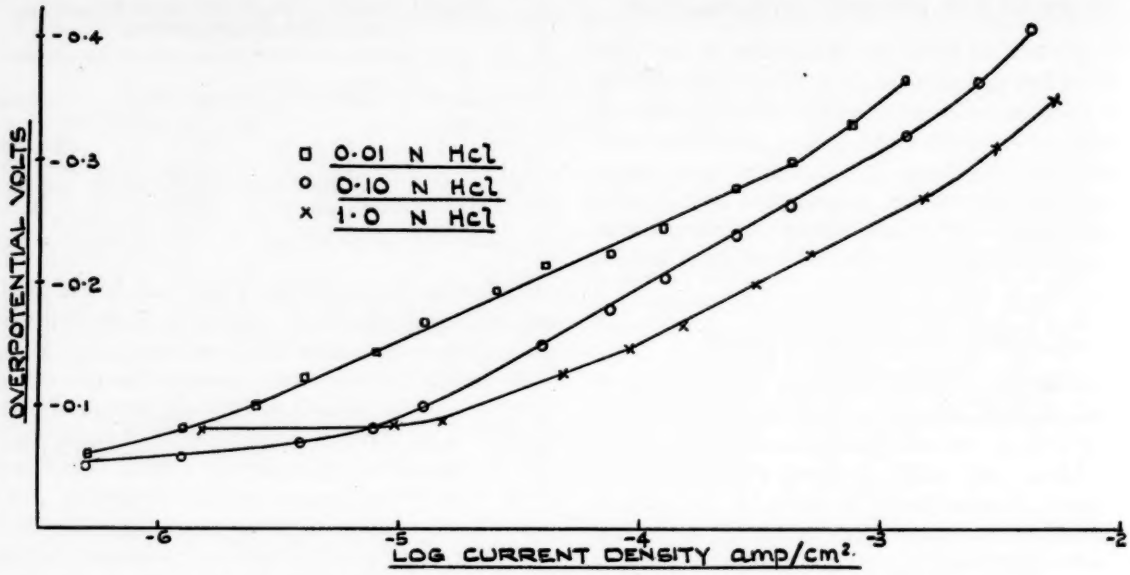

FIG. 3. Hydrogen overpotential at nickel cathodes at 20°C in aqueous HCl solutions.

a megohm resistance in the cell circuit using a G.E.C. portable valve potentiometer. Currents above 10^{-6} amp were directly measured with a Cambridge unipivot multirange instrument. The overpotential was measured to one millivolt with the abovementioned potentiometer. All electrical instruments and auxiliary controls were mounted on paraffin wax, and connections were made with screened, polymer-coated wire. The cell was fully enclosed in a double-walled air thermostat controlled to $\pm\frac{1}{2}$°C. A water thermostat could not be used owing to the electrical leaks thereby introduced.

The circuit for measuring the build-up and decay of overpotential is given in Fig. 2. The varying cathode potential was "backed out" by an opposing potential from B so that the resultant potential varied within the range of linear response of the amplifier A. By synchronizing the interruption of the polarizing current with the time-base of the cathode ray oscillograph (CRO), a stationary pattern could be photographed which appeared as a dotted trace on connecting an oscillator to the grid of the CRO. The horizontal distance between the dots corresponded to the period of the oscillator, and was used to calibrate the horizontal time axis. The vertical potential axis was found from the shifts produced by the known variations in backing-out potential. The method used for the measurement of differential electrode capacity by means of superimposed ac was similar to that described by Borissova

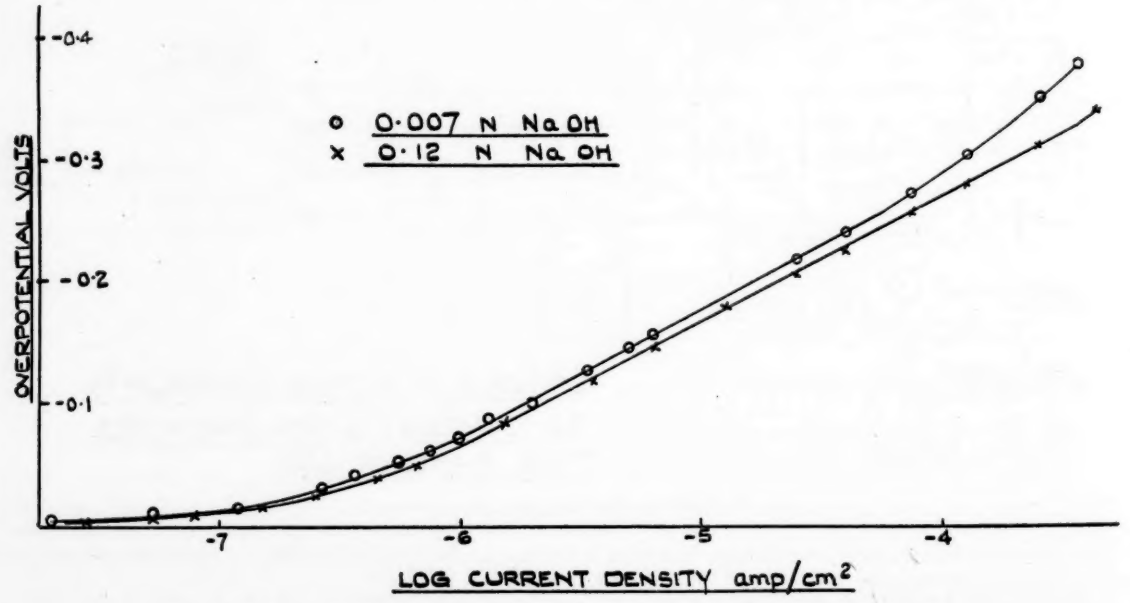

FIG. 4. Hydrogen overpotential at nickel cathodes at 20°C in aqueous NaOH solutions.

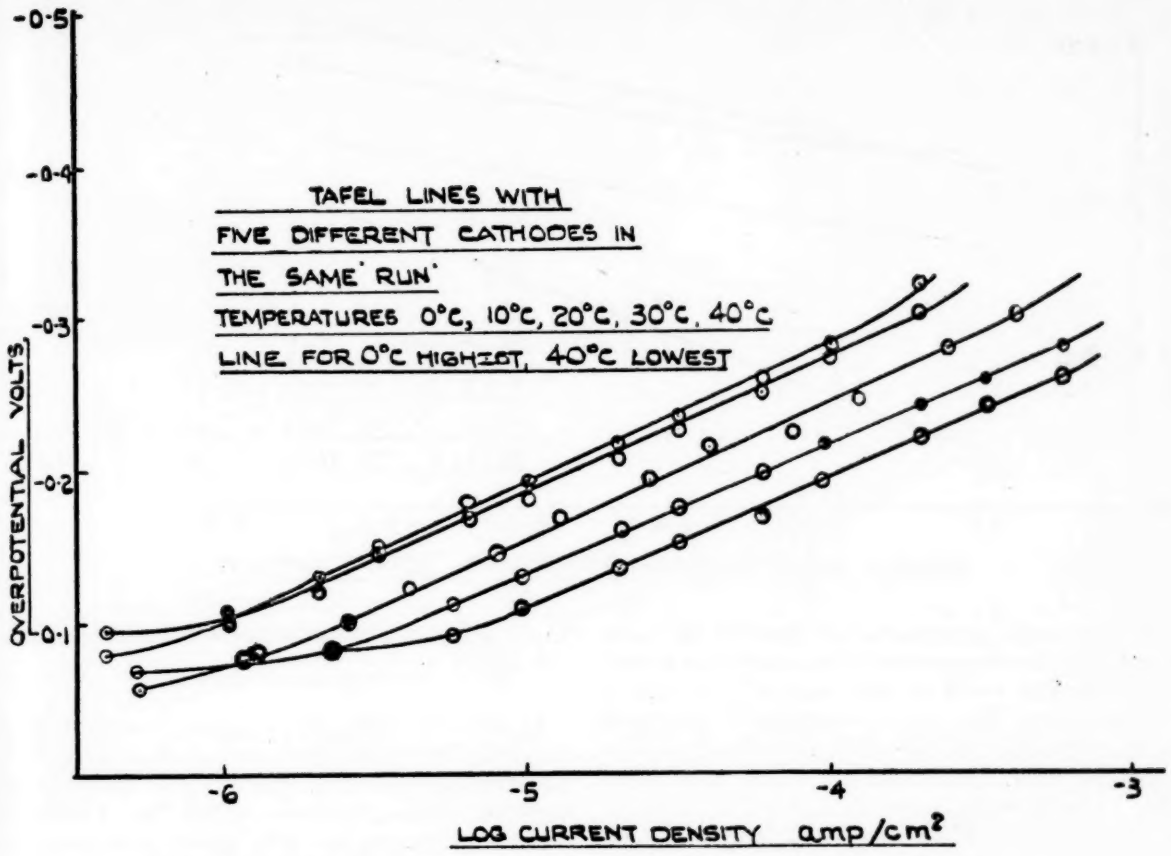

FIG. 5(a). Hydrogen overpotential at nickel cathodes in 0.01N HCl at different temperatures.

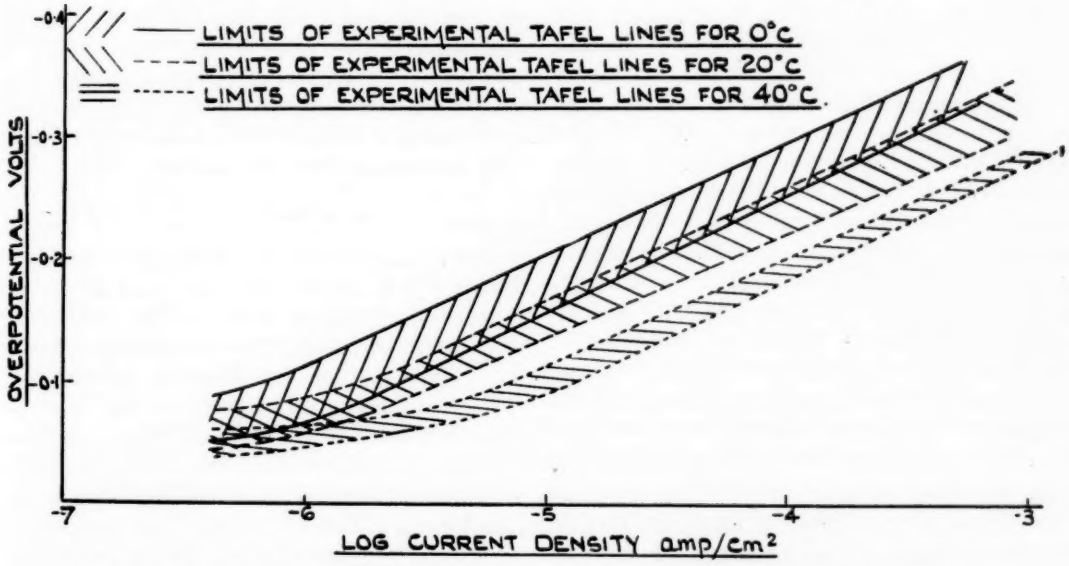

FIG. 5(b). Limits of replicate Tafel lines for nickel cathodes in 0.01N HCl at different temperatures.

and Proskurnin.[19] The amplitudes of the alternating currents passing either a standard condenser or the electrode-electrolyte interface were measured on the CRO screen, and the electrode capacity calculated.

[19] T. Borissova and M. Proskurnin, Acta Physicochimica, U.R.S.S. 4, 819 (1936).

V. EXPERIMENTAL RESULTS

Since it has been shown in previous work that in very pure solutions the potential of a nickel cathode reaches a steady value after about 1 hour of polarization[12,20]

[20] This behavior is probably a result of the surcharging of the metal with hydrogen. Tafel lines obtained using such surcharged

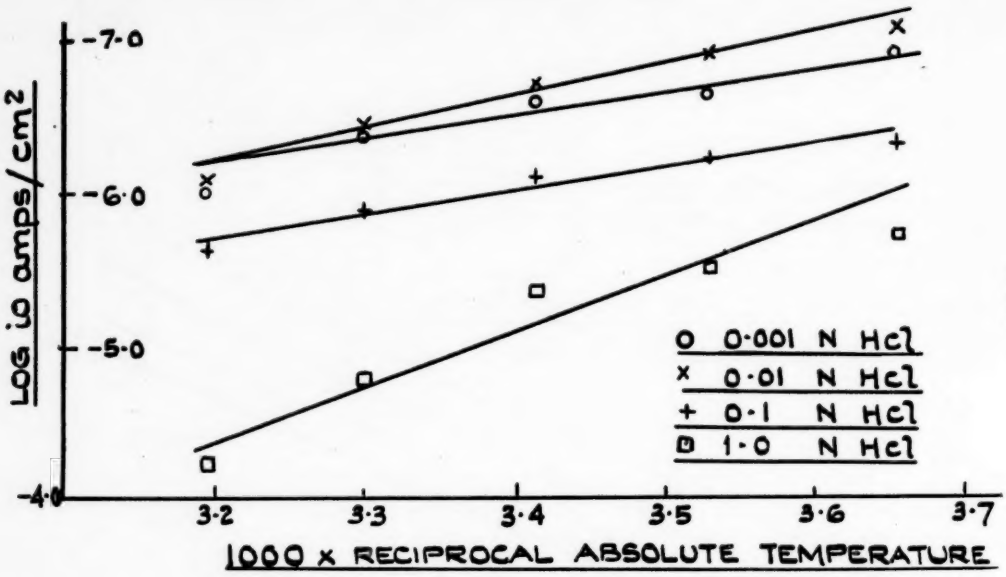

FIG. 6. Relationship between $\log i_0$ and $1/T$ for nickel cathodes in aqueous HCl solutions.

and that the rapid technique of establishing the Tafel line yields the most reproducible results,[16] it was clear that an electrode could be used once only to trace a Tafel line for any given set of conditions. It was found that the variations among different electrodes sometimes caused a scatter of results of the same order as the effects it was desired to estimate, and it became necessary to replicate the measurements as much as sixfold, and to treat the results statistically. The characteristic forms of the Tafel lines[21] are seen in Fig. 3 for acid solutions and in Fig. 4 for alkaline solutions. In acid solutions above about 10^{-5} amp/apparent cm², the line is straight with a slope near to 0.100 volt, and below about 10^{-5} amp/apparent cm² tends to become horizontal at a potential between 50 and 100 millivolts more cathodic than the reversible hydrogen potential. This trend of the Tafel line at low c.d.'s is more marked in concentrated acid solutions at elevated temperatures, and is attributed to dissolution of the metal.[8] In alkaline solutions at overpotentials more negative than about 50 millivolts, the Tafel line is straight with a temperature-dependent slope of about 0.11 volt. At low current densities the line curves towards the reversible hydrogen potential as the ionization of hydrogen atoms becomes appreciable. When no current passes, the "rest potential" of the nickel electrode lies within a few millivolts of the reversible potential provided no agitation of the electrolyte is permitted to transport minute quantities of depolarizers to the metal surface. In both acid and alkaline solutions above about 10^{-4}–10^{-2} amp/cm² depending on the rapidity with which observations are made and on the concentration of the solution, the line shows a gradual bend-up.

electrodes are not linear, and probably do not correspond to the same physical condition of the metal throughout the whole range of current density (see reference 16).

[21] Traced rapidly in the direction of increasing current density.

1. Effect of Temperature on the Tafel Line

(a) *Acid Solutions*

In any one "run" employing five temperatures and using each test electrode once only for observations at a particular temperature, a set of Tafel lines of the same slope was obtained as shown in Fig. 5(a). The replicate Tafel lines for any one temperature from several runs lay within a relatively wide band, and Fig. 5(b) shows that the position of such a band is temperature dependent. The main quantity of interest derived from temperature effects on the Tafel line is ΔH_0^*, the standard heat of activation of the forward (cathodic) direction of the rate-determining step of the hydrogen evolution reaction at the reversible hydrogen potential, and this is obtained from the relation,

$$\log i_0 = \log B - (\Delta H_0^*/2.303RT), \qquad (1)$$

where i_0 is the exchange current, B is Eyring's entropy factor,[22] R is the gas constant, and T is the absolute temperature. The equation[23] of the straight section of the Tafel line passing through the experimental points for every electrode was found by the method of least squares taking overpotential as the dependent variable. The ratios a/b for all Tafel lines at each electrolyte concentration were identified with the values of $\log i_0$ and were themselves subjected to a least squares treatment using $1/T$ as the independent variable. ΔH_0^* was then readily obtained from the computed slope of the relation between $\log i_0$ and $1/T$ (see Fig. 6). The results of the analysis are given in Table II, from which it appears that ΔH_0^* is a complex function of concentration.

[22] Eyring, Glasstone, and Laidler, J. Chem. Phys. 7, 1053 (1939).

[23] That is $\eta = a - b \log i_c$, where a is characteristic for each metal at constant temperature and electrolyte concentration, b is of the order of 100 millivolt, and i_c is the observed cathodic current density in amp/apparent cm² of cathode.

TABLE II. Statistically computed average Tafel lines and derived data for nickel cathodes in acid solutions at 0–40°C.

Activity HCl	Temp. °C	Straight section of Tafel Line units of $\log i_c$	n[a]	$-a$ volt	b volt	95% limits	$-\log i_0$ amp/cm²	95% limits	ΔH_0^* kcals	95% limits	$\log B$ amp/cm²	95% limits
	0	6.25−4.0	5	0.704	0.099	±0.007	6.9	±0.2	···	···	···	···
	10	6.0 −4.25	4	0.688	0.104	±0.017	6.6	±0.2	···	···	···	···
0.001N	20	5.75−3.25	5	0.617	0.093	±0.012	6.6	±0.2	6.7	±1.2	−1.5	±2.0
	30	5.75−3.25	7	0.625	0.099	±0.008	6.4	±0.2	···	···	···	···
	40	5.5 −3.5	4	0.628	0.104	±0.003	6.0	±0.3	···	···	···	···
	0	6.0 −3.25	7	0.639	0.090	±0.005	7.1	±0.2	···	···	···	···
	10	5.75−3.75	6	0.623	0.090	±0.003	6.9	±0.2	···	···	···	···
0.01N	20	5.5 −3.25	6	0.611	0.091	±0.003	6.7	±0.1	9.9	±0.9	+0.8	±1.4
	30	5.25−3.25	6	0.576	0.090	±0.006	6.4	±0.2	···	···	···	···
	40	5.0 −3.0	8	0.571	0.094	±0.005	6.1	±0.1	···	···	···	···
	0	5.5 −2.5	6	0.641	0.101	±0.006	6.3	±0.1	···	···	···	···
	10	5.5 −2.75	4	0.642	0.103	±0.006	6.2	±0.3	···	···	···	···
0.10N	20	5.0 −2.0	7	0.626	0.104	±0.006	6.0	±0.2	6.9	±1.3	−0.9	±2.1
	30	5.0 −2.5	4	0.602	0.102	±0.006	5.9	±0.2	···	···	···	···
	40	4.75−2.0	5	0.598	0.106	±0.004	5.7	±0.1	···	···	···	···
	0	4.5 −2.0	5	0.670	0.116	±0.011	5.7	±0.3	···	···	···	···
	10	4.5 −2.0	6	0.581	0.105	±0.004	5.5	±0.2	···	···	···	···
1.0N	20	4.25−2.0	9	0.594	0.109	±0.009	5.4	±0.1	16.3	±2.1	+7.1	±2.5
	30	3.75−2.0	7	0.543	0.113	±0.009	4.8	±0.1	···	···	···	···
	40	3.25−2.0	3	0.510	0.120	±0.006	4.2	±0.5	···	···	···	···

[a] n = number of replicate Tafel lines used to obtain a, b, and $\log i_0$. 95% limits = (variance × t) where the value of t is taken from tables at the 0.05 probability level and for the appropriate number of degrees of freedom.

(b) *Alkaline Solutions*

The Tafel lines for temperatures between 0°C and 50°C were found to be almost coincident for each electrolyte concentration used. It was evident, however, that the slopes of the Tafel lines and the corresponding values of $\log i_0$ were temperature dependent, and values of ΔH_0^* were computed as for acid solutions. Table III gives the results of the analysis for alkaline solutions, and it is seen that the values of ΔH_0^* are effectively independent of concentration. After ascertaining by graphical inspection that there was no evidence for a concentration effect on b at constant temperature or of a change in temperature effect on b with concentration, the sixty-five b values obtained for alkaline solution were bulked and the correlation coefficient between b and absolute temperature was found to be 0.721. This value is extremely significant for 63 degrees of freedom. The best linear relation between b and absolute temperature was found to be $b=-0.056+5.47\times10^{-4}T$, in which the constant term is significantly different from zero with a confidence greater than 1000 to 1. This means that b does not vary with temperature as required by the well-known equation $b=2.303RT/\alpha F$, where α is independent of temperature as has been assumed by several former workers (cf. reference 1).

2. Effect of Electrolyte Concentration on the Tafel Line

(a) *Acid Solutions*

The quantity $d\eta/d(p\text{H})$ is complex and varies somewhat with temperature pH and current density, as shown in Table IV.

(b) *Alkaline Solutions*

Here the experimental data are more scanty, and it is not possible to state if $d\eta/d(p\text{H})$ is dependent on current density or pH at constant temperature. The

TABLE III. Statistically computed average Tafel lines and derived data for nickel cathodes in alkaline solutions.

Activity NaOH	Temp. °C	Straight section of Tafel line units of $\log i_c$	n	$-a$ volts	b volts	95% limits	$-\log i_0$ amp/cm²	95% limits	ΔH_0^* kcals	95% limits	$\log B$ amp/cm²	95% limits
	2	6.75−5.0	4	0.74	0.104	±0.004	7.1	±0.3	···	···	···	···
0.001N	20	6.75−4.75	1	0.72	0.103	···	7.0	···	7.6	±2.4	−1.1	±4.0
	40	6.0 −4.5	4	0.79	0.121	±0.013	6.3	±0.5	···	···	···	···
	2	6.25−4.5	3	0.62	0.088	±0.011	7.0	±0.4	···	···	···	···
0.006N	20	6.25−3.75	6	0.66	0.101	±0.009	6.6	±0.2	4.9	±1.1	−3.0	±1.8
	40	6.25−3.5	4	0.69	0.108	±0.014	6.4	±0.1	···	···	···	···
	2	6.0 −3.25	10	0.65	0.097	±0.004	6.6	±0.2	···	···	···	···
0.10N	20	6.0 −3.0	15	0.65	0.101	±0.004	6.4	±0.2	5.7	±1.1	−2.1	±1.8
	40	5.75−3.0	4	0.76	0.125	±0.012	6.1	±0.2	···	···	···	···

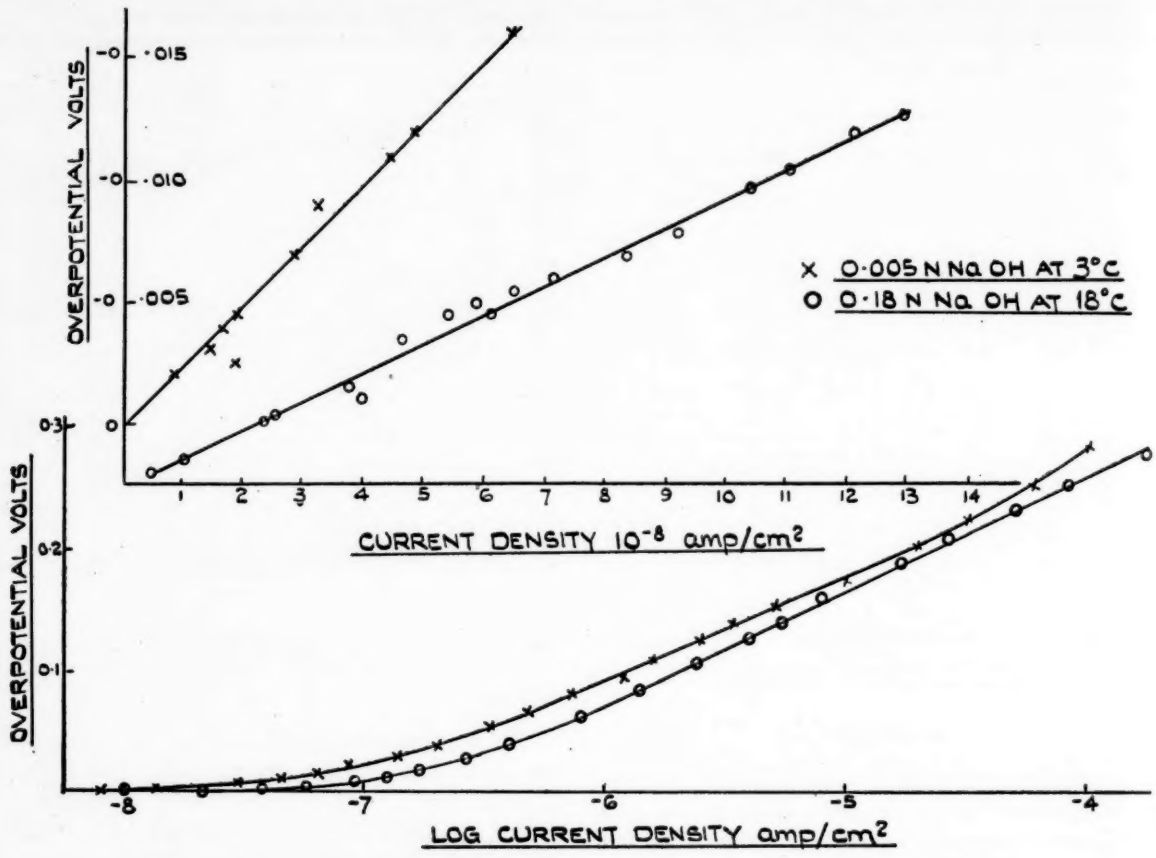

FIG. 7. Experimental data for determination of μ at nickel cathodes in aqueous NaOH solutions.

average values of $d\eta/d(p\mathrm{H})$ at 2°C, 20°C, and 40°C are, respectively, +23, +10, and +14 millivolts.

3. Estimation of the Stoichiometric Number in Alkaline Solution

The expression for μ, the stoichiometric number,[11] i.e., the number of acts of the rate-determining step accompanying one act of the over-all hydrogen evolution reaction, is

$$\mu=\frac{-2i_0F}{RT}\left(\frac{d\eta}{di_c}\right)_{\eta=0}, \qquad (2)$$

where F = the Faraday.

The above equation requires that in order to measure μ the complete Tafel line from the reversible potential must be traced. Figure 7 shows two typical Tafel lines traced from the "resting potential" and the corresponding η, i_c curves near the reversible potential. It was sometimes found possible to return a cathode (which had been already studied) to a potential close to that of the reversible hydrogen electrode. In these instances any time variation of μ accompanying the usual time variation of the Tafel line could be measured. Table V gives the values of μ which were obtained for various concentrations of alkaline solutions at several temperatures. Table VI shows that no detectable time variation of μ exists.

It is evident from Table V that there is no detectable variation of μ with temperature or with concentration, (cf. the conclusion of Lukovzew and Lewina).[9] Owing to the fact that the errors in μ are not normally distributed, it is difficult to assess the error of a single determination of μ. It may be expected, however, that since the somewhat skew distribution of i_0 gives a bias towards high values of i_0, a similar bias in the values of μ occurs. Hence, assuming by analogy to $\log i_0$ that the errors in $\log\mu$ are normally distributed, it was calculated that the 95 percent limits of error for the fifth entry in Table V ($\mu=1.8$) were −0.3 and +0.5. Bearing in mind that this limit of error for μ does not include a source of error arising from the differences among electrodes and experimental "runs," it is reasonable to conclude

TABLE IV. Concentration effect on overpotential in acid solutions.

Temp. °C	$d\eta/d(p\mathrm{H})$ at $i_c=10^{-3.5}$ amp/cm²		
	pH3 −2	pH2 −1	pH1 −0
0	...	−35 mv	−23 mv
10	...	−29 mv	−65 mv
20	−0 mv	−31 mv	−53 mv
30	−16 mv	−16 mv	−102 mv
40	−17 mv	−17 mv	−140 mv

TABLE V. Values of μ for alkaline solutions of various concentrations.

Concn. NaOH	Temp. °C	amp/cm² i_0	ohms/cm² $-\left(\frac{d\eta}{di_c}\right)_{\eta=0}$	μ	Concn. NaOH	Temp. °C	amp/cm² i_0	ohms/cm² $-\left(\frac{d\eta}{di_c}\right)_{\eta=0}$	μ
0.18N	3	1.6×10^{-7}	11.2×10^{4}	1.6	0.012N	20	1.5×10^{-7}	15.0×10^{4}	1.8
	3	2.1×10^{-7}	10.7×10^{4}	1.8		20	1.7×10^{-7}	16.0×10^{4}	2.1
	18	3.3×10^{-7}	7.4×10^{4}	2.0	0.006N	2	1.0×10^{-7}	31.0×10^{4}	2.7
	18	3.0×10^{-7}	10.0×10^{4}	2.3		2	1.5×10^{-7}	12.9×10^{4}	1.6
	18	2.5×10^{-7}	9.4×10^{4}	1.9		3	7.7×10^{-8}	24.8×10^{4}	1.6
	18	2.0×10^{-7}	11.1×10^{4}	1.8		18	5.0×10^{-7}	6.9×10^{4}	2.8
	18	1.7×10^{-7}	12.2×10^{4}	1.7		18	3.0×10^{-7}	8.6×10^{4}	2.0
	20	1.5×10^{-7}	16.0×10^{4}	2.0		20	1.8×10^{-7}	12.0×10^{4}	1.7
	37	1.1×10^{-6}	2.6×10^{4}	2.2		20	1.4×10^{-7}	17.5×10^{4}	1.9
	39	6.0×10^{-7}	5.6×10^{4}	2.5		20	1.1×10^{-7}	18.2×10^{4}	1.6
	41	7.1×10^{-7}	4.0×10^{4}	2.1		37	1.5×10^{-7}	22.5×10^{4}	2.5
	51	8.7×10^{-7}	3.1×10^{4}	1.9		40	3.0×10^{-7}	10.6×10^{4}	2.3
0.12N	15	4.2×10^{-7}	4.6×10^{4}	1.6		40	3.9×10^{-7}	6.5×10^{4}	1.9
	17	1.3×10^{-6}	2.2×10^{4}	2.2		40	4.3×10^{-7}	5.1×10^{4}	1.6
	25	2.9×10^{-7}	9.6×10^{4}	2.2	0.001N	2	8.0×10^{-8}	40.0×10^{4}	2.7
	35	7.2×10^{-7}	2.6×10^{4}	1.4		42	9.4×10^{-7}	2.8×10^{4}	2.0
0.06N	1	1.3×10^{-7}	20.2×10^{4}	2.3					
	3	1.2×10^{-7}	17.6×10^{4}	1.8					
	20	1.1×10^{-7}	22.0×10^{4}	2.0					
	20	8.5×10^{-8}	25.8×10^{4}	1.8					
	20	4.0×10^{-7}	8.7×10^{4}	2.8					

that the scatter of the μ-values in Table V is no more than would be expected under the experimental conditions. On averaging all the μ-values given in Table V, and calculating the variance of $\log\mu$, it follows that for nickel cathodes in alkaline solution $\mu=2.0\pm0.1$.

It has been shown[5] that another less accurate method of measuring μ is by estimating the overpotential η_s at which the Tafel line begins to deviate from its linear path as a result of the increase to significance of the ionization of hydrogen atoms. Thus, when several observations near to η_s have been made,

$$\mu=-\eta_s/0.038$$

at 20°C where η_s is in volts. Application of the above relation to the experimental results yielded 15 values of μ lying between 1.3 and 2.2, the average value being 1.8.

4. Differential Capacity of Nickel Cathodes

The values of differential electrode capacity obtained by the superimposed ac method and from the dc charging and decay curves were very similar, and showed no variation with time or with potential up to $\eta=-0.25$ volt (Table VII). At greater overpotentials the ac method became inaccurate owing to the great increase in the ohmic as opposed to the capacitative component of the interfacial impedance, and the dc method indicated a gradual 50 percent increase in capacity up to about -0.4 volt.

5. The Decay of Overpotential at Nickel Cathodes

Using the dc transient method previously described, the decay curve of overpotential with time was found to be steep and linear for the first 20 mv of decay. The succeeding decay became logarithmic with time, the slope of the logarithmic decay curve (Fig. 8 and Table VIII) approximating to the slope b of the Tafel line. The last stage of decay to near the reversible potential occupied some minutes and gave a linear relation between $\log\eta$ and time. This type of behavior of the complete curve of the decay is in accordance with expectation.[5]

6. Behavior of the Tafel Line at Current Densities Greater than 10^{-4} amp/cm²

As previously mentioned, an upward trend of the Tafel line was observed in acid and alkaline solutions above about $10^{-4}-10^{-2}$ amp/cm². The appearance of the upward trend at lower c.d.'s in weaker solutions is characteristic of resistance overpotential, but in view of the observed increase in the effect with time, it was desirable to ascertain if the Tafel line would remain straight if this resistance overpotential were eliminated.

TABLE VI. Constancy of μ for six electrodes as the Tafel line varies with time.

Electrode No.	Description of Tafel line	b volts	μ
1	1st ascent of c.d.	0.093	2.0
	2nd ascent of c.d.	0.105	1.8
2	2nd ascent of c.d.	0.100	1.8
	3rd ascent of c.d.	0.105	2.1
3	3rd ascent of c.d.	0.110	2.0
	4th ascent of c.d.	0.115	2.4
4	1st ascent of c.d.	0.115	1.9
	2nd ascent of c.d.	0.120	1.8
5	1st ascent of c.d.	0.095	1.6
	2nd ascent of c.d.	0.113	1.8
6	1st ascent of c.d.	0.109	1.7
	2nd ascent of c.d.	0.110	1.9
	3rd ascent of c.d.	0.115	1.6

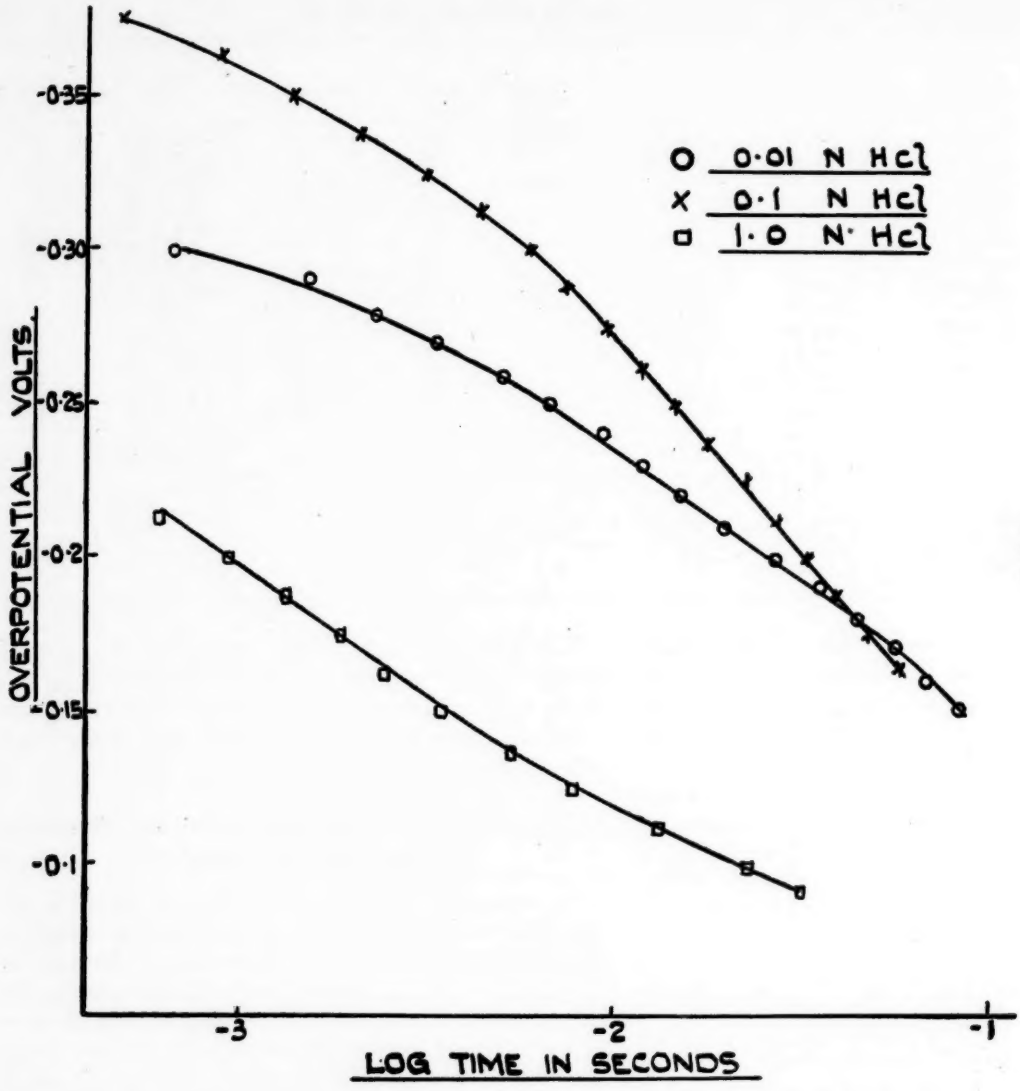

FIG. 8. Decay curves of hydrogen overpotential at nickel cathodes in aqueous HCl solutions.

In the dc method described above for tracing charging and decay curves, any resistance overpotential present was manifest as a vertical gap at the instant decay began. By making measurements of the constant depth of the gap (constant with time) at various currents, it was possible to correct the Tafel line for resistance overpotential. The method was tested with a silver cathode and the corrected Tafel line for this metal was found to be straight to above 10^{-2} amp/cm². The result of applying the method to a nickel cathode is shown in Fig. 9, and it is evident that the upward trend of the Tafel line is in part an effect connected with activation overpotential, and not entirely a result of resistance overpotential.

VI. DISCUSSION

1. Derivation of the Stoichiometric Number μ

The hydrogen evolution reaction may be represented by the over-all reactions,

$$2\,BH^{\cdot}+2\epsilon \rightleftharpoons H_2 \quad \text{(acid solution)} \qquad (3)$$

$$2\,HOH+2\epsilon \rightleftharpoons H_2+2\,OH' \quad \text{(aqueous alkaline solution)}, \qquad (4)$$

where B is a solvation sheath. If there is one step in the over-all reaction which is rate-determining then the rate v_1 of the forward direction of this step is

$$v_1=\kappa a_1(kT/h)\exp\left[\frac{-\Delta G_1^*+\beta(\Delta\phi_e-\zeta)2F/\mu}{RT}\right], \qquad (5)$$

where κ=transmission coefficient, a_1=product of the

TABLE VII. Differential capacity of nickel cathodes in aqueous solutions at 20°C.

No. of electrodes	Electrolyte concentration	Average differential capacity μF/apparent cm²	Range of observed capacities μF/app. cm²
4	0.01N HCl	28	25–29
6	0.1N HCl	37	31–41
3	1.0N HCl	41	38–45
2	0.006N NaOH	22	20–23
3	0.12N NaOH	27	20–30

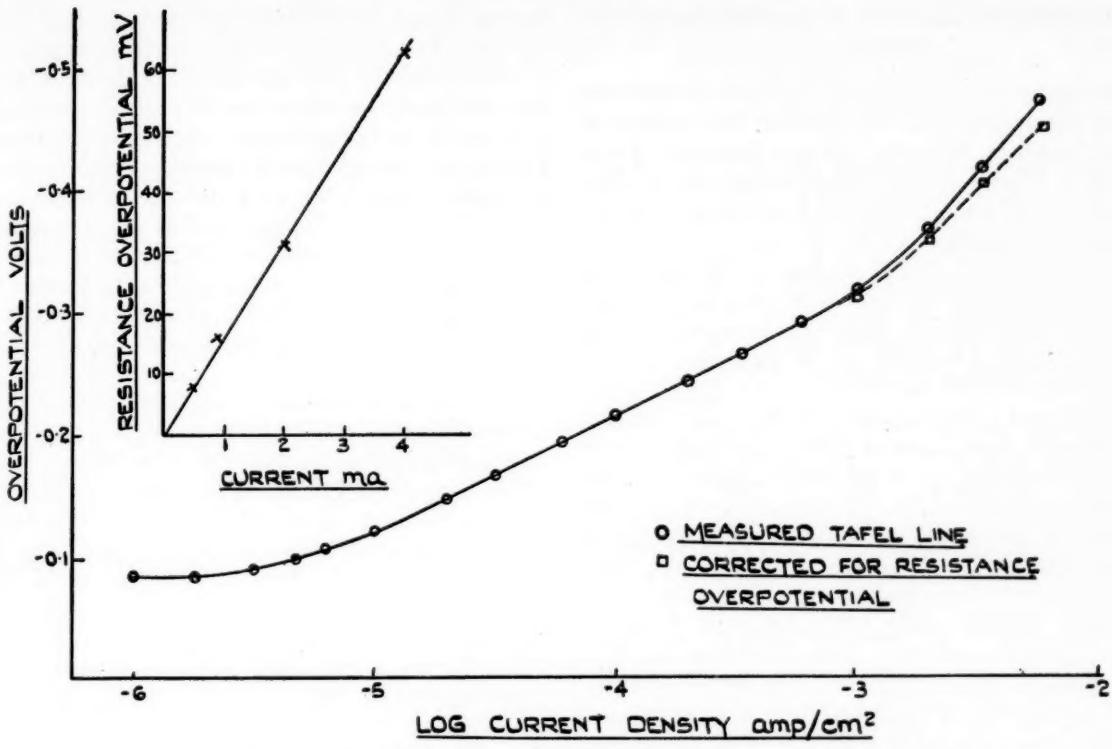

FIG. 9. Experimental data for correction of the Tafel line at a nickel cathode in 0.1N aqueous HCl for resistance overpotential.

activities of the reactants of the rate-determining step at the site of reaction, k=Boltzmann's constant, h=Planck's constant, ΔG_1^*=standard free energy of activation for the forward direction of rate-determining step, $\Delta\phi_c$=inner potential of the electrode minus the inner potential of the solution, ζ=that part of $\Delta\phi_c$ in the diffuse double layer, β=a fraction (<1) of $(\Delta\phi_c-\zeta)$ operating to facilitate the forward direction of the rate-determining step, F=Faraday, R=the gas constant, and μ=the number of acts of the rate-determining step necessary for one act of the over-all reaction. The velocity v_2 of the reverse direction of the rate-determining step is analogously given by

$$v_2=\kappa a_2\frac{kT}{h}\exp\left[-\frac{\Delta G_2^*-(1-\beta)(\Delta\phi_c-\zeta)2F/\mu}{RT}\right], \quad (6)$$

where a_2=product of the activities of the products of the rate-determining step at the site of reaction, and ΔG_2^*=standard free energy of activation for the reverse direction of rate-determining step. The currents i_1 and i_2 corresponding to v_1 and v_2 are

$$i_1=2\epsilon v_1/\mu \quad (7)$$

and

$$i_2=2\epsilon v_2/\mu, \quad (8)$$

where ϵ=the electronic charge. When $\Delta\phi_c=\Delta\phi_r$ the reversible hydrogen potential, $i_1=i_2=i_0$ (the exchange current). In general, since $\Delta\phi_r+\eta=\Delta\phi_c$ and $i_c=i_1-i_2$, it follows,

$$i_c=i_0\{\exp[-2\beta\eta F/\mu RT]-\exp[2(1-\beta)\eta F/\mu RT]\}. \quad (9)$$

At appreciable negative values of η the above equation reduces to

$$i_c=i_0\exp[-2\beta\eta F/\mu RT], \quad (10)$$

which is equivalent to Tafel's equation where

$$b=2.303\mu RT/2\beta F. \quad (11)$$

At small values of η (more positive than -20 mv), the two exponential terms may be expanded so that

$$i_c=-2i_0\eta F/\mu RT. \quad (12)$$

Differentiating and rearranging,

$$\mu=\frac{-2i_0F}{RT}\left(\frac{d\eta}{di_c}\right)_{\eta=0}. \quad (2)$$

TABLE VIII. Logarithmic decay of overpotential at nickel cathodes in aqueous solutions at 20°C.

Electrode No.	Electrolyte concentration	Slope of η, log$t$ curve, volts
1	0.01N HCl	0.11
2	0.01N HCl	0.08
3	0.1N HCl	0.12
4	0.1N HCl	0.09
5	0.1N HCl	0.11
6	1.0N HCl	0.09
7	0.006N NaOH	0.10
8	0.06N NaOH	0.10
9	0.06N NaOH	0.10
10	0.06N NaOH	0.12

2. Interpretation and Use of the Stoichiometric Number

From the definition of the stoichiometric number, the μ-values characteristic of the common mechanisms of cathodic hydrogen evolution are rate-determining discharge step, $H^{\cdot}+e\rightarrow H$: $\mu=2$; rate-determining electrochemical step, $H^{\cdot}+H+e\rightarrow H_2$: $\mu=1$; and rate-determining recombination step, $H+H\rightarrow H_2$: $\mu=1$.

It has been shown[5] that in the case of the rate-determining recombination step, $\beta=1$, whereas for the rate-determining electrochemical step, $\beta>\frac{3}{4}$. Hence from the expression (11) $b_{20°C}=0.029$ volt for the former mechanism, and $b_{20°C}<0.044$ volt for the latter. Therefore the quantities μ and b may be used to differentiate between the three main mechanisms of cathodic hydrogen evolution. The use of Eq. (2) is confined to those low overpotentials where it is valid, and the criterion η_s, i.e., the overpotential at which the slope b of the Tafel line is reached,[5] is used to find μ_{η_s}. For potentials more negative than η_s, the following argument may be used. Over the current density range that the slope b of the Tafel line remains constant, it is clear from Eq. (11) that at constant temperature μ/β must also remain constant. Even allowing for the possibility that nonintegral values of μ may exist under the above conditions, there is no reason to suppose μ can vary directly with β, and hence, throughout the straight section of the Tafel line μ retains the value μ_{η_s}. Clearly the ability to estimate μ, not only near the reversible potential but also in the overpotential region most commonly encountered in practice, is very valuable in the determination of electrode reaction mechanism.

3. Application of μ to Nickel Cathodes

(a) *Alkaline Solutions*

Consideration of the experimental results shows that for solutions of concentration 0.001N NaOH–0.2N NaOH at 0°C–50°C and from the reversible hydrogen potential to the overpotential (approx −300 mv) at which the Tafel line shows an upward trend, $\mu=2$. Therefore, under these conditions the rate-determining step of hydrogen evolution is a discharge step.

(b) *Acid Solutions*

Here dissolution of the metal at low c.d.'s prevents the application of Eq. (2). However, since b is constant at approximately 0.1 mv, the rate-determining step cannot be the recombination step, and μ remains constant at least in the region where the Tafel line remains straight.

4. Further Evidence of Mechanism for Nickel Cathodes

It has been shown[5] that the observed tendency[24] for the slope of the Tafel line to reach infinity in acid solutions at about 10^1 amp/cm^2 may be identified with the approach to a maximum rate of the recombination step of the hydrogen evolution reaction. Hence it appears that the desorption step of the over-all reaction at nickel cathodes is the recombination step, there being no suggestion that electrochemical desorption may replace or accompany atomic recombination at current densities below 10^1 amp/cm^2.[25] It follows that the rate-determining step for acid solutions is a discharge step, since the slope b of the Tafel line is not 0.029 volt. Furthermore, the constancy of differential electrode capacity with potential at overpotentials numerically up to 0.25 volt indicates that the coverage of the electrode with adsorbed hydrogen does not change as the velocity of the rate-determining step is varied, which is in accord with a slow discharge mechanism. However, the coincidence of the increase in differential electrode capacity and of the upward trend of the Tafel line at overpotentials more negative than about −300 mv suggests that the limiting current associated with the maximum rate of the recombination step is being reached as the surface coverage of the cathode tends to 100 percent.

It is therefore probable that the mechanism of hydrogen evolution for nickel cathodes in aqueous acid and alkaline solutions is that of a rate-determining discharge step followed by a recombination step involving adsorbed hydrogen atoms.

5. The Effect of *p*H on the Discharge Step in Acid Solutions

It has been shown that the Tafel line should be independent of hydrogen ion concentration in pure dilute acid solutions when the rate-determining step of the electrode reaction is a discharge step.[26] This is so whether the discharge step involves a hydrogen ion or a water molecule. The assumptions attached to the derivation of the *p*H effect on the Tafel line have perhaps not been fully stressed in the past, and may, as seen below, obscure effects which have hitherto been regarded as anomalous.

In general, for a rate-determining discharge step, it follows (neglecting the reverse reaction),

$$i_c=Fk_1a_{dl}\exp\left[\frac{-\beta(\Delta\phi_c-\zeta)F}{RT}\right], \tag{13}$$

where k_1 is the velocity constant of the discharge step, a_{dl} is the activity of the entity discharged at the interface between Helmholtz and diffuse double layers, and ζ is the potential drop across the diffuse double layer. Putting $\Delta\phi_c=\Delta\phi_r+\eta$ and $\Delta\phi_r=(RT/F)\ln a_{H^{\cdot}}$, where $a_{H^{\cdot}}$ = activity of hydrogen ions in the bulk of the electrolyte,

$$\eta=\text{const}-\frac{RT}{\beta F}\ln i_c+\frac{RT}{\beta F}\ln a_{dl}-\frac{RT}{F}\ln a_{H^{\cdot}}+\zeta. \tag{14}$$

[24] A. M. Azzam and J. O'M. Bockris, Nature **165**, 403 (1950).

[25] J. O'M. Bockris and A. M. Azzam (to be published).

[26] Frumkin, Z. physik. Chem. **164A**, 121 (1933).

There are now two cases to consider:

(a) *The Entity Discharged Is a Hydrogen Ion*

Here

$$a_{dl}=a_{H\cdot}\exp\left[-\frac{\zeta F}{RT}\right], \tag{15}$$

and (14) becomes

$$\eta=\text{const}-\frac{RT}{\beta F}\ln i_e+\frac{1-\beta}{\beta}\frac{RT}{F}\ln a_{H\cdot}-\left(\frac{1-\beta}{\beta}\right)\zeta. \tag{16}$$

From (16),

$$\left[\frac{\partial\eta}{\partial(\ln a_{H\cdot})}\right]_{i_e}=\frac{1-\beta}{\beta}\left[\frac{RT}{F}-\frac{\partial\zeta}{\partial(\ln a_{H\cdot})}\right]. \tag{17}$$

(b) *The Entity Discharged Is a Water Molecule*

In this case let it be assumed that

$$a_{dl}=a_w, \tag{18}$$

where a_w is the activity of water in the bulk of the electrolyte and is effectively constant except in very concentrated solutions. (The assumption implicit in (18) is further treated in Sec. 6(c).) From (14),

$$\eta=\text{const}-\frac{RT}{\beta F}\ln i_e-\frac{RT}{F}\ln a_{H\cdot}+\zeta. \tag{19}$$

From (19),

$$\left[\frac{\partial\eta}{\partial(\ln a_{H\cdot})}\right]_{i_e}=\frac{-RT}{F}+\frac{\partial\zeta}{\partial(\ln a_{H\cdot})}. \tag{20}$$

Equations (17) and (20) show that the pH effect on the Tafel line, as expressed by the term $[\partial\eta/\partial(\ln a_{H\cdot})]_{i_e}$ depends on the value of $\partial\zeta/\partial(\ln a_{H\cdot})$. Under the assumptions that (1) the electrolyte is dilute, (2) that specific adsorption at the electrode is absent, and (3) that the potential conditions are not near those of the electrocapillary maximum, the Stern treatment of the electrical double layer simplifies so that

$$\partial\zeta/\partial(\ln a_{H\cdot})=RT/F.$$

Hence under these conditions for both cases (a) and (b) above, $[\partial\eta/\partial(\ln a_{H\cdot})]_{i_e}=0$, i.e., the Tafel line is independent of pH of the electrolyte.

When the electrolyte contains an excess of a neutral salt (e.g., KCl, $BaCl_2$, $LaCl_3$) the diffuse double layer disappears and $\partial\zeta/\partial(\ln a_{H\cdot})=0$. Under these conditions (17) becomes

$$\left[\frac{\partial\eta}{\partial(\ln a_{H\cdot})}\right]_{i_e}=\frac{1-\beta}{\beta}\frac{RT}{F}=\frac{RT}{F}, \quad \text{if} \quad \beta=0.5; \tag{21}$$

and (20) becomes

$$\left[\frac{\partial\eta}{\partial(\ln a_{H\cdot})}\right]_{i_e}=\frac{-RT}{F}. \tag{22}$$

It is evident from (21) and (22) that in the presence of excess neutral salt in acid solution the direction of the pH effect on the Tafel line depends on the nature of the entity discharged and is numerically of the order of 60 mv/pH unit at ordinary temperature.

As is shown below, it was not necessary in the case of the nickel cathode to carry out measurements of neutral salt effects in order to ascertain the nature of the entity discharged.

As the potential conditions at the electrode approach those of the electrocapillary maximum, it becomes less valid to simplify the Stern treatment of the double layer, and as a result $\partial\zeta/\partial(\ln a_{H\cdot})<RT/F$ in pure dilute acid solution. Under these conditions (17) and (20) show that not only is there a pH effect on the Tafel line, but also that the direction of the pH effect distinguishes the entity discharging. It is probable[5] that the electrocapillary maximum of nickel lies at a potential about 0.3 volt more positive than that of the reversible hydrogen electrode, and hence, for nickel cathodes in pure acid solutions of concentration $>10^{-1}$N approx, $\partial\zeta/\partial(\ln a_{H\cdot})<RT/F$. From the experimental data of Table IV, it is seen that $[\partial\eta/\partial(\ln a_{H\cdot})]_{i_0}$ is positive, so that (21) must be applicable. Hence, the experimental data indicate that the *entity discharged during the hydrogen evolution reaction at nickel cathodes in acid solution is the hydrogen ion.*

The use of the direction of a pH effect on the Tafel line to determine the entity discharged in a rate-determining discharge step at a cathode near its electrocapillary maximum represents a new useful criterion in electrode kinetics.

In order to ascertain the relevant values of $\partial\zeta/\partial(\ln a_{H\cdot})$ for nickel cathodes in acid solutions, the full Stern expression was used to calculate the relationship between ζ and $\Delta\phi_c$ at hydrogen ion activities of 10^{-3}, 10^{-2}, 10^{-1}, 10^{0}, and 10^{1} g ions/liter. The relation between ζ and $\ln a_{H\cdot}$ was then found at several chosen values of $\Delta\phi_c$. Only at relatively high values of $\Delta\phi_c$ and at low electrolyte concentrations is the value of $\partial\zeta/\partial(\ln a_{H\cdot})$ maintained at RT/F. At low values of $\Delta\phi_c$ even at low concentrations of electrolyte the value of $\partial\zeta/\partial(\ln a_{H\cdot})$ is appreciably below RT/F, so that under these conditions a slow discharge mechanism of hydrogen evolution is associated with a pH effect on the Tafel line. By using the $\zeta/\ln a_{H\cdot}/\Delta\phi_c$ data given by Bockris and Conway[27] and the experimental values for β and η at nickel cathodes in aqueous acid solutions of various concentrations, the expected pH effects on η were calculated and are compared with the observed values in Table IX.

[27] J. O'M. Bockris and B. E. Conway, Trans. Faraday Soc. (to be published).

TABLE IX. Expected and observed changes in hydrogen overpotential at nickel cathodes in aqueous acid solutions of various concentrations at 25°C.

	Change in overpotential in millivolts					
	$i_c=10^{-4}$ amp/cm²			$i_c=10^{-2}$ amp/cm²		
	*p*H3−2	*p*H2−1	*p*H1−0	*p*H3−2	*p*H2−1	*p*H1−0
Expected	nil	nil	+20	nil	nil	+10
Observed	nil	+35	+50	nil	+10	+40

Although the numerical agreement is only fair in Table IX, the calculated *p*H effects reflect two of the observed trends, *viz.*, the *p*H effect increases from zero as the electrolyte becomes more concentrated, and the effect is less at higher current densities. This latter effect is observed as a result of an increased slope of the Tafel line with increasing electrolyte concentration at constant temperature (see Table II).

When $\partial\zeta/\partial(\ln a_{H\cdot})$ is zero, Eq. (21) shows that the change in overpotential (at constant current) per unit change in *p*H is about 58 mv at ordinary temperatures. However, Table IV shows that this value is exceeded in strong acid solutions, especially at elevated temperatures, and thus it appears that the arguments presented above are oversimplified possibly as a result of neglect of specific adsorption at the electrode.

6. The Effect of *p*H on the Discharge Step in Alkaline (NaOH) Solutions

In alkaline solutions it seems inconceivable that the direct discharge of hydrogen ions can occur because their stationary concentration is so small.[28] Hence, the discharge of hydrogen either takes place from a water molecule or by reaction of a discharged alkali metal atom with water. Owing to the observed similarities in double layer capacity for acid and alkaline (NaOH) solutions, it is reasonable to assume that the hydrogen ions present in the double layer in acid solutions are replaced by sodium ions in alkaline solutions.

(a) *The Discharge of Hydrogen Takes Place from a Water Molecule*

In this case the Eq. (20) expresses the *p*H effect on the Tafel line. Under the previously mentioned assumptions enabling a simplified Stern treatment of the electrical double layer to be carried out,

$$\frac{d\zeta}{\partial(\ln a_{H\cdot})}=\frac{-d\zeta}{\partial(\ln a_{Na\cdot})}=\frac{-RT}{F},$$

where $a_{Na\cdot}$ is the activity of sodium ions in the bulk of the electrolyte. Hence under these conditions $[\partial\eta/\partial(\ln a_{H\cdot})]_{i_0}=-2RT/F$. When the electrolyte contains an excess of a neutral salt, $\partial\zeta/\partial(\ln a_{H\cdot})=0$, and the *p*H effect is again expressed by (22) when the potential conditions at the electrode approach those of the electrocapillary maximum $\partial\zeta/\partial(\ln a_{H\cdot})>-RT/F$ and the value of $[\partial\eta/\partial(\ln a_{H\cdot})]_{i_c}$ lies between $-RT/F$ and $-2RT/F$.

It is thus evident that when a rate-determining discharge step takes place from a water molecule in dilute alkaline solution, a relatively large effect of *p*H on the Tafel line may be expected, being equivalent in pure solutions at high cathodic potentials to a vertical shift of about 116 mv per *p*H unit at ordinary temperature. The present work indicates that at constant current density and temperature, the overpotential becomes more positive by 10–25 mv per unit increase in *p*H in pure dilute NaOH solutions.[29] This effect is much less than the expected one, although it is in the same direction, and furthermore, it should be noted that the expected result cannot decrease numerically below 58 mv/*p*H unit even under conditions close to the electrocapillary maximum.

(b) *The Hydrogen Originates from Sodium Atoms and Water*

If the rate-determining step of the electrode reaction is

$$Na/Ni+H_2O\rightarrow Na\cdot+OH'+Ni-H, \qquad (23)$$

it has been shown[30] that the current is given by

$$i_c=\text{const}\times a_w(a_{Na\cdot})^n{}_{dl}\exp\left[-\frac{n(\Delta\phi_c-\zeta)F}{RT}\right], \qquad (24)$$

where $(a_{Na\cdot})_{dl}$ is the concentration of sodium ions at the interface between Helmholtz and diffuse double layers, and n is the order of step (23) with respect to Na atoms. Putting $\Delta\phi_c=\Delta\phi_r+\eta$, $\Delta\phi_r=(RT/F)\ln a_{H\cdot}$, and $(a_{Na\cdot})_{dl}=(a_{Na\cdot})\exp[-\zeta F/RT]$, it follows,

$$[\partial\eta/\partial(\ln a_{H\cdot})]_{i_c}=-2RT/F. \qquad (25)$$

It is seen from Eq. (25) that when step (23) is rate-determining, the *p*H effect on the Tafel line is independent of ζ, i.e., independent of potential and of the presence of neutral salt. It also appears that the observed *p*H effect is much less than that characteristic of the above mechanism of hydrogen evolution.

(c) *The Effect of Oriented Water Dipoles at the Cathodic Surface*

In the foregoing treatments of hydrogen discharge from alkaline solutions it has been assumed that the value of a_w, the activity of water, is the same in the bulk of the electrolyte as in the double layer adjacent to the cathode. It is probable, however, that the high

[28] About one hydrogen ion within the electrical double layer adjacent to 1 cm² of cathode in a solution of *p*H 13. For further quantitative considerations see reference 30.

[29] The value of about 40 mv/*p*H unit obtained by Lukovzew and Lewina[9] may be high since the same cathode was used more than once during an experiment. An unknown amount of "time variation" is thereby introduced into the results.

[30] J. O'M. Bockris and R. G. H. Watson, J. chim. phys. 49, 1 (1952).

field close to the cathode orients the water dipoles so as to produce an increase in the activity of the water in the double layer. Let it be assumed that the water dipoles adjacent to the cathode surface are completely oriented in the direction of the field, and that the plane of the interface between Helmholtz and diffuse double layers passes through the centers of the water dipoles. The potential energy P of such a dipole is equal to $X\mu_w$, where X is the absolute field strength in the plane where the potential is ζ with respect to the bulk of the electrolyte, and μ_w is the dipole moment of water. Since

$$X=4\pi\sigma/d=4\pi C_d\zeta/d, \tag{26}$$

where σ=absolute charge density over the ζ-plane, d=dielectric constant at the ζ-plane, and C_d=integral capacity of the diffuse double layer, it follows,

$$P=4\pi\mu_w C_d\zeta/d. \tag{27}$$

According to the Maxwell-Boltzmann distribution law,

$$(a_w)_{dl}=a_w\exp[-P/RT], \tag{28}$$

where $(a_w)_{dl}$ is the activity of water at the ζ-plane. Hence,

$$\ln(a_w)_{dl}=\ln a_w-(4\pi\mu_w C_d\zeta/dRT). \tag{29}$$

Equation (29) may now be introduced into (14) to give a modified form of (20), and hence the modified pH effect for discharge from a water molecule in alkaline solution is given by

$$\left[\frac{\partial\eta}{\partial(\ln a_{H^\cdot})}\right]_{i_c}=\frac{-RT}{F}+\frac{\partial\zeta}{\partial(\ln a_{H^\cdot})}\left\{1-\frac{4\pi\mu_w C_d}{d\beta F}\right\}. \tag{30}$$

In applying Eq. (30) to the case of the nickel cathode in alkaline solution, values of C_d were taken from the data of Grahame,[31] β was taken to be 0.5 at 25°C, d was taken to be 4, μ_w was taken as 1.83×10^{-18} esu, and relevant values of ζ were derived[27] using overpotentials at $10^{-4.5}$ amp/cm². The results are given in Table X.

As mentioned previously, the observed value of $[\partial\eta/\partial(\log a_{H^\cdot}]_{i_c}$ is between −10 and −25 mv, and as indicated in Table V, does not change appreciably with pH. It is evident from Table X that Eq. (30) correctly indicates the direction and order of magnitude of the pH effect. All the experimental data cannot be claimed to have received an adequate theoretical explanation, however, particularly because the theory requires a change in pH effect with pH which is much greater than that observed.

7. The Coverage of Nickel Cathodes with Adsorbed Hydrogen Atoms

The method of preparation of cathodes used in the present work would be expected to produce a nickel surface covered with adsorbed hydrogen atoms. Thus when the bulb surrounding the nickel electrode was broken, the hydrogen-saturated electrolyte made contact with a cathodic surface fully occupied with hydrogen atoms. Assuming that the discharge step is rate-determining at nickel cathodes in acid and alkaline aqueous solutions, the succeeding desorption of hydrogen as molecules proceeds so that only a low stationary concentration of adsorbed hydrogen from the discharge step exists on the cathode surface. It would be reasonable to suppose, on this account, that the initial monolayer of hydrogen atoms almost disappears when the nickel electrode contacts the electrolyte as a cathode. This question is now considered.

TABLE X. Expected changes in hydrogen overpotential at nickel cathodes in aqueous NaOH solutions of various concentrations at 25°C.

pH	C_d $\mu F/cm^2$	$\frac{\partial\zeta}{\partial(\log a_{H^\cdot})}$ mv	$\frac{4\pi\mu_w C_d}{d\beta F}$	$\left(\frac{\partial\zeta}{\partial(\log a_{H^\cdot})}\right)_{i_c}$ mv
11	21	−51	0.44	−87
12	38	−52	0.82	−67
13	84	−45	1.82	−21

There would appear to be two ways in which this adsorbed hydrogen could be removed: (a) by ionization, and (b) by replacement with adsorbed oxygen or hydroxyl radicals. In the former case the separation of charges which occurs would be manifest as a change in capacity during the process. If approximately 10^{-9} g atoms of hydrogen constitute a monolayer over 1 cm² of electrode, about 10^{-4} coulomb pass to remove these atoms as molecules. At the reversible hydrogen potential the rate of this process is given by i_0, which is approximately 10^{-6} amp/cm² for a nickel electrode, and hence a monolayer of hydrogen atoms would be removed under these conditions in about 100 seconds. No capacity change corresponding to such an ionization process was observed in the present work, and the capacity remained constant to 2 $\mu F/cm^2$ at constant potential for some hours after contact of a nickel electrode with the electrolyte.[32] In the latter case, in which oxygen or hydroxyl (from water) may replace adsorbed hydrogen, Hillson and Rideal[33] have calculated from approximate data that hydrogen replaces oxygen (or hydroxyl) on a nickel cathode at a potential of −0.2v with respect to the reversible hydrogen electrode. It would not appear to follow, however, as stated by these authors, that a nickel electrode cannot function as a reversible hydrogen electrode; for a high concentration of adsorbed hydrogen is not necessarily essential for an electrode to act in this way. Moreover, the present work and also that of Foresti[34] shows that the reversible hydrogen potential is taken up by the nickel electrode, and it must be regarded as uncertain to what extent oxygen or hydroxyl is adsorbed on nickel cathodes in aqueous solutions.

[31] D. C. Grahame, Chem. Revs. **41**, 441 (1947).

[32] It was possible to measure the electrode capacity within five seconds of breaking the electrode sheath.

[33] P. Hillson and E. K. Rideal, Proc. Roy. Soc. (London) **199A**, 295 (1949).

[34] B. Foresti, Atti congr. intern. chim. **2**, 226 (1938).

On the other hand, the following argument may also be advanced. The limiting current, which has been observed for nickel cathodes in acid solutions by Bockris and Azzam[24] and which, as is indicated by the present work, probably occurs also in alkaline solutions, shows that the atomic hydrogen recombination reaction is desorptive. The maximum rate at which this reaction can take place is given by the value of the limiting current and corresponds to the complete occupation of the cathode surface with adsorbed hydrogen. It therefore follows that at currents below the limiting current, the cathode surface is not completely occupied with adsorbed hydrogen, and indeed, at overpotentials more positive than about −0.30 volt, i.e., at currents below that at which the Tafel line begins tending towards a limiting current, it appears that the stationary concentration of adsorbed hydrogen atoms emanating from the discharge step is inappreciable.

The two apparently conflicting views that during hydrogen evolution when η is more positive than −0.30 volt nickel cathodes may be virtually covered with adsorbed hydrogen atoms and yet the desorption of hydrogen atoms is a rapid process, are reconcilable by consideration of the recent conclusions of Rideal and Trapnell.[35] These workers have given evidence to show that the heat of adsorption of hydrogen atoms on tungsten and nickel surfaces not only decreases with increasing coverage of the surface, but falls considerably at coverages above about 70 percent until at about 90 percent coverage the heat of adsorption is about 5 kcal. This evidence is supported by that of Beeck, Smith, and Wheeler[36] who observed that about 20 percent of a chemisorbed hydrogen layer on a nickel surface can be pumped off *in vacuo*, indicating that this amount of hydrogen requires a heat of desorption which is markedly lower than that for the remainder of the surface (15–30 kcal). It is therefore suggested that in the case of hydrogen being evolved at a nickel cathode, the discharge step forms adsorbed atoms on a surface already highly covered (about 80 percent) with hydrogen atoms,[37] but that the desorption step involves only those atoms (or an equivalent number of the original adsorbed atoms) which emanated from the discharge step. The desorption step occurs relatively rapidly at the nickel cathode as a consequence of a low heat of desorption at high surface coverage. As the rate of the electrode reaction is increased, the coverage with adsorbed hydrogen increases slightly, thereby allowing the desorption rate to increase by virture of both an increased concentration of reactants and a decreased heat of desorption. This increase in coverage probably corresponds to the increase in differential electrode capacity observed for nickel cathodes at overpotentials more negative than about −0.30 volt. The beginning of the tendency to the limiting current, which also occurs at this potential, then becomes a result of the "sluggishness" of the atomic desorption step relative to the discharge step.

It is relevant to consider the effect of poisons on the electrode reaction on the views expressed above. It is known that carbon monoxide can be adsorbed onto a nickel surface and leaves any remaining uncovered surface unpoisoned in that hydrogen will adsorb on it. Furthermore, carbon monoxide is not capable of displacing adsorbed hydrogen from a nickel surface.[38] Consequently, on introducing a small amount of carbon monoxide into a nickel cathode/electrolyte system, the coverage of the surface with adsorbed gas (supposed originally about 80 percent) increases. As a result the desorption step is rendered easier, by virtue of a decreased heat of desorption, but the discharge step, the velocity of which depends on the number of free sites available on the cathode, is made more difficult. As the over-all rate of reaction is given by the over-all current and the discharge step is rate-determining, the overpotential must become more negative to accommodate the new electrode conditions. It is thus possible to account qualitatively for the fact, observed by Bockris and Conway,[12] that amounts of carbon monoxide sufficient to cover only a fraction of a nickel cathode surface measurably increase the overpotential.

The authors are indebted to Dr. R. Parsons for the use of the electronic apparatus used for charging curve, decay curve, and capacity studies.

[35] E. K. Rideal and B. M. W. Trapnell, "Colloque sur L'Adsorption et la Cinetique, Hétérogène," Lyon, 1949; J. chim. phys. 47, 126 (1950).
[36] Beeck, Smith, and Wheeler, Proc. Roy. Soc. 177A, 62 (1940).
[37] Or with oxygen or hydroxyl from water (see aforementioned).
[38] O. Beeck, *Advances in Catalysis* (Academic Press, Inc., New York, 1950), Vol. II.

Interchange of Fission-Product Bromine with Carrier Bromine*

ANDREW F. STEHNEY†‡
Argonne National Laboratory, Department of Chemistry and Institute for Nuclear Studies
University of Chicago, Chicago, Illinois

AND

NATHAN SUGARMAN
Institute for Nuclear Studies, University of Chicago, Chicago, Illinois

(Received October 4, 1951)

Experiments on the interchange of the fission products 2.4-hr Br^{83} and 55.6-sec Br^{87} with carrier bromine have been performed. Essentially the same degree of interchange is effected by the following chemical procedures: carrier added as BrO_3^- and reduced by H_2S, carrier added as BrO_3^- and reduced by excess carrier Br^-, and carrier added as Br^- to HCl and irradiated uranium metal dissolved.

INTRODUCTION

IN the study of the radiations and fission yield[1] of 55.6-sec Br^{87}, some experiments were performed on the extent of interchange of carrier bromine with Br^{87} using different carrier species and chemical procedures. Since it had been noted that the interchange of fission-product iodine with carrier iodine was not complete except under very special chemical conditions,[2] it was thought that perhaps similar difficulties might be encountered in the interchange of bromine.

Some indication of interchange difficulties of bromine was present in the work of Langsdorf and Segrè[3] who observed that the recovery of tracer Br^{83} from the decay of Se^{83} in a solution containing macroquantities of $SeO_3^=$ was incomplete when carrier bromine was added as Br^- and AgBr was precipitated. They found it necessary first to oxidize $SeO_3^=$ to $SeO_4^=$ with Br_2 before the chemical separation was complete. A procedure was developed by Edwards, Gest, and Davies[4] for the separation of Br^{83} from solutions containing macro-$SeO_3^=$ in which complete interchange was effected by adding carrier BrO_3^-, and reducing the BrO_3^- to Br^- with H_2S. This H_2S procedure has been used subsequently for the radiochemical analysis of bromine in fission,[5] and in the study[6] of the isomeric states of Se^{83}.

In the experiments reported here, comparisons were made of the extent of interchange of carrier bromine with Br^{87} obtained by three different chemical procedures. The recovery of Br^{87} was found to be essentially the same when the radiobromine was separated by the H_2S procedure, by solution of uranium metal in HCl in the presence of Br^- carrier, and by the use of BrO_3^- and excess Br^- carriers. Similar concordant results were achieved in the study of 2.4-hr Br^{83} where the time spent by the radioactive atoms in solution was much greater. It would appear from these experiments that complete interchange between carrier and fission-product bromine is effected, using carrier bromine as BrO_3^- and Br^-, whereas the analogous carriers (plus periodate) do not achieve complete interchange for radioiodine.

INTERCHANGE STUDIES OF 55.6-SEC Br^{87}

The reduction of BrO_3^- with H_2S, shown[4] to give complete recovery of Br^{83}, was used first in the interchange study of 55.6-sec Br^{87}. A 500-mg sample of uranyl nitrate was irradiated in the "rabbit" of the Argonne Heavy-water Pile for 45 seconds, then transferred and dissolved in 7 ml water containing an aliquot of standardized $KBrO_3$ solution and some KIO_3. The solution was gassed with H_2S for 1 min, the minimum time necessary for complete reduction of the BrO_3^- to Br^-. The Br^- was oxidized to Br_2 by addition of a heated solution containing 15 ml $0.5M$ $KMnO_4$ and 5 ml $6M$ HNO_3; simultaneously the I^- was oxidized[7] to IO_3^-; and the excess H_2S was destroyed. The solution was then poured into a distillation apparatus and the Br_2 was distilled by heating the solution and passing air through it. This procedure is similar to that used by Strassmann and Hahn[8] in their study of short-lived bromine activities in fission. The air stream containing Br_2 was passed through an acid solution of Ag^+ and Fe^{++} for the precipitation of AgBr. Trial runs with BrO_3^- absent in the original solution showed that neither I_2 nor H_2S was being carried in the air stream, since no precipitate formed in the Ag^+-Fe^{++} solution.

* This document is based on work performed at the Argonne National Laboratory, Chicago, Illinois.
† Presented in partial fulfillment for the Ph.D. degree in the Department of Chemistry, University of Chicago.
‡ Now at the Argonne National Laboratory, Chicago, Illinois.
[1] A. F. Stehney and N. Sugarman (to be published elsewhere).
[2] Glendenin, Metcalf, Novey, and Coryell, Paper 279, *National Nuclear Energy Series* (McGraw-Hill Book Company, Inc., New York, 1951), Vol. 9, Div. IV; Katcoff, Dillard, Finston, Finkle, Seiler, and Sugarman, Paper 141, *ibid.*
[3] A. Langsdorf and E. Segrè, Phys. Rev. **57**, 105 (1940).
[4] Edwards, Gest, and Davies, Paper 22, *National Nuclear Energy Series* (McGraw-Hill Book Company, Inc., New York, 1951), Vol. 9, Div. IV.
[5] Glendenin, Edwards, and Gest, Paper 232, *National Nuclear Energy Series* (McGraw-Hill Book Company, Inc., New York, 1951), Vol. 9, Div. IV.
[6] J. R. Arnold and N. Sugarman, J. Chem. Phys. **15**, 703 (1947).
[7] R. K. McAlpine and B. A. Soule, *Prescott and Johnson's Qualitative Chemical Analysis* (D. Van Nostrand and Company, Inc., New York, 1933), p. 550.
[8] F. Strassmann and O. Hahn, Naturwiss. **28**, 817 (1940).

TABLE I. Interchange experiments on 55.6-sec Br^{87}.

Experiment	Fission product isolated	Activity, $c/m \times 10^{-5}$	Activity ratio Br^{87}/Ba^{139}
H_2S reduction procedure—500 mg uranyl nitrate, BrO_3^- carrier, H_2S reduction			
1	Br^{87}	7.78	3.69
	Ba^{139}	2.11	
2	Br^{87}	7.60	3.35
	Ba^{139}	2.27	
3	Br^{87}	7.99	3.43
	Ba^{139}	2.33	
	Average activity ratio = 3.49±0.13[a]		
Uranium metal procedure—200 mg uranium metal dissolved in HCl containing Br^- carrier			
4	Br^{87}	8.57	3.58
	Ba^{139}	2.39	
5	Br^{87}	9.00	3.91
	Ba^{139}	2.30	
	Average activity ratio = 3.75±0.17[a]		
BrO_3^-—Br^- procedure—500 mg uranyl nitrate, BrO_3^- and excess Br^- carriers			
6	Br^{87}	9.34	3.79
	Ba^{139}	2.46	
7	Br^{87}	9.75	3.66
	Ba^{139}	2.66	
8	Br^{87}	5.90	3.71
	Ba^{139}	1.59	
9	Br^{87}	7.56	4.25
	Ba^{139}	1.78	
10	Br^{87}	8.27	3.32
	Ba^{139}	2.49	
11	Br^{87}	10.2	3.70
	Ba^{139}	2.76	
	Average activity ratio = 3.74±0.19[a]		

[a] Mean deviation from average value.

The AgBr precipitate was filtered through a filter paper disk in a Hirsch funnel, washed with water, alcohol, and ether, and mounted on a cardboard card for activity determination. After the counting was completed, the filter paper disk was removed from the mounting card, dried in an oven at 110°C for 10 min, and weighed to determine the chemical yield of the bromine carrier.

Several determinations of Br^{87} activity were also made by irradiating uranium metal, a strongly reducing medium in which the fission-product bromine might be expected to be in a reduced state, and thus would interchange readily with carrier Br^- when the metal is dissolved in HCl containing Br^-. This procedure is analogous to that used on iodine by Katcoff *et al.*[2] in their determination of the fission yield of 6.7-hr I^{135}, and by Stanley and Katcoff[9] in their work on the fission yield of 86-sec I^{136}. A 200-mg sample of uranium was irradiated for 45 sec and then dissolved in dilute HCl containing standardized Br^- carrier and some I^- carrier. The small amount of oxide remaining in the solution was dissolved by the addition of 1 ml 6*M* HNO_3. Attempts to dissolve the uranium metal quickly in H_2SO_4 or H_3PO_4 were unsuccessful, and HNO_3 was not desirable because of the possible oxidation of radiobromine during the solution process. The permanganate oxidation-distillation procedure was used for the separation of bromine, and special pains were taken to prevent the distillation of Cl_2 along with Br_2; namely, the use of a minimum quantity of HCl to dissolve the uranium (1 ml 6*N* HCl in 4 ml solution) and a preliminary CCl_4 extraction of the Br_2 after adding only a slight excess of $KMnO_4$. The bromine was extracted into $NaHSO_3$ solution and then reoxidized with HNO_3—$KMnO_4$ solution, after which the distillation was carried out as in the H_2S-reduction procedure. The method was tested for chlorine interference and no precipitate was found in the Ag^+—Fe^{++} solution when no Br^- carrier was added.

The third chemical procedure used was the reduction of BrO_3^- carrier with excess Br^- and the subsequent oxidation of the remaining Br^- with $KMnO_4$. In this procedure, 500 mg of irradiated uranyl nitrate was dissolved in a solution containing 5 ml 6*M* H_2SO_4 and 4 ml 0.05*M* KBr, then 1 ml 0.01*M* $KBrO_3$ was added. After stirring for 15 sec, I^- carrier was added, followed by 15 ml 0.5*M* $KMnO_4$. The distillation procedure was then performed. The I^- carrier addition was delayed to ensure the reduction of BrO_3^- by Br^-.

Activity measurements were started on the isolated bromine samples 3 to 4 minutes after the end of the irradiation. Since much of the 55.6-sec Br^{87} had disintegrated during this time interval, thick absorbers were used to distinguish the hard β- and γ-radiations[1] of Br^{87} from the relatively weaker radiations[10] of 3.00-min Br^{85}. Under these conditions only the 55.6-sec activity and a much less intense component of about 32-min half-life (Br^{84}) were observed in the decay curves.

Since only one determination of Br^{87} was made for each irradiation, because of the short half-life of Br^{87}, the activity of Br^{87} was compared with that of 85-min Ba^{139} from the same irradiation. The ratio of the activity of Br^{87} to Ba^{139} is then a measure of the radiochemical yield of Br^{87}. Extra samples of uranyl nitrate were included in each irradiation for the isolation of duplicate samples of barium activity, which was done by the HCl-ether procedure given by Glendenin.[11] The activities of Br^{87} and Ba^{139} were each measured under standard conditions. The results of these measurements are given in Table I. Column 3 gives the activity of the fission product denoted in column 2 measured with a standard absorber, calculated to the end of the irradiation, and corrected for chemical yield. The activity of the Br^{87} was measured through 1029 mg/cm² of aluminum absorber. The activity of Ba^{139} was measured through zero or 47.6 mg/cm² of aluminum absorber and calculated to zero total absorber. The ratio of the activity of Br^{87} to that of Ba^{139} in each experiment is

[9] C. W. Stanley and S. Katcoff, J. Chem. Phys. **17**, 653 (1949).

[10] N. Sugarman, J. Chem. Phys. **17**, 11 (1949).

[11] L. E. Glendenin, Paper 288, *National Nuclear Energy Series* (McGraw-Hill Book Company, Inc., New York, 1951), Vol. 9, Div. IV.

given in column 4; the constancy of this ratio is a measure of the reproducibility of the interchange of Br^{87} with carrier bromine.

An examination of the activity ratios of Table I shows that the interchange effected by all three chemical procedures is the same within the determined precision of about 5 percent. Since the procedure using metallic uranium would in principle be expected to provide complete interchange of Br^{87} with carrier, it appears that the other two procedures also give complete interchange.

INTERCHANGE STUDIES OF 2.4-HR Br^{83}

Studies of the interchange of 2.4-hr Br^{83} with carrier bromine were made by the H_2S reduction and the BrO_3^--Br^- procedures to see if the formation of Br^{83} from the decay of the 25-min Se^{83} and 67-sec Se^{83m} parents leads to chemical states that are not interchangeable with carrier bromine in these procedures. Although it had now been established that 55.6-sec Br^{87} interchanges to the same extent in each of these procedures, it was possible that some difficulty might be encountered in the case of Br^{83} because of the appreciable half-life of the parent species, and the length of time the radiobromine existed in solution before the radiochemical analysis.

In these experiments, the results of the two methods were compared directly, since the half-life of Br^{83} is long enough to allow for several analyses from the same solution of irradiated uranyl nitrate. Thus, it was not necessary to analyze for Ba^{139} and to compare the bromine activities with those of Ba^{139} from the same irradiation, as was done in the case of Br^{87}. Two experiments were performed in which uranyl nitrate was irradiated in the Argonne Graphite Pile and dissolved two to three hours later and a stock solution prepared. Aliquots were taken for bromine analysis after a wait of 3 hr or more from the end of the irradiation, to allow for the decay of the 25-min Se^{83} parent. In each case the sample was mounted as AgBr and the decay was followed for 3 half-lives. Corrections for chemical yield and decay were made to compare the activity recovered by each procedure. The results are given in Table II.

In the entries designated "H_2S, Extract," the analyses were performed according to the procedure given for fission-product bromine by Glendenin *et al.*[5] Carrier BrO_3^- was reduced for 5 min by H_2S to Br^-, and the bromine was subjected to several cycles of oxidation and reduction, using $KMnO_4$ for oxidation and $NH_2OH \cdot HCl$ or $NaHSO_3$ for reduction. The "Br^-, Extract" experiments were made in the same way except that the BrO_3^- carrier was reduced by excess Br^- before the oxidation-reduction cycles. The "H_2S, Sweep, $NaHSO_3$" and "Br^-, Sweep, $NaHSO_3$" experiments were done by the distillation procedure used for Br^{87} except that the Br_2 was absorbed in 15 ml of 0.01*M* $NaHSO_3$ instead of the $Ag^+ - Fe^{++}$ solution. The bisulfite solution was acidified with 1 ml of 6*M* HNO_3 and boiled for 1 min to expel SO_2 before the precipitation of AgBr.

TABLE II. Interchange experiments on 2.4-hr Br^{83}.

Experiment	Procedure	Activity, *c/m*	Recovery,[a] %
1	H_2S, Extract	13600	100
	Br^-, Extract	13000	96
2	H_2S, Extract	6900	100
	Br^-, Extract	6520	95
	H_2S, Sweep, $NaHSO_3$	6820	99
	Br^-, Sweep, $NaHSO_3$	6660	96

[a] Percent recovery based on "H_2S, Extract" set equal to 100.

A comparison of the data of Table II shows that the activity of Br^{83} recovered from the reduction of BrO_3^- by H_2S is consistently about 4 percent higher than that recovered from the reduction of BrO_3^- by excess Br^-. If this difference is truly significant of more complete interchange in the H_2S-reduction procedure, then the reason it was not noted in the Br^{87} interchange experiments may be due to the larger scatter of the values in those experiments.

SUMMARY

The experiments on the interchange of fission-product Br^{87} and Br^{83} with carrier bromine show that there is no apparent difficulty in achieving interchange. There is, apparently, some significant difference between the chemistry of bromine and iodine such that using the analogous chemistry for iodine complete interchange is not effected.

It is a pleasure to acknowledge the assistance given to one of us (A. F. S.) by the Atomic Energy Commission in the form of a predoctoral fellowship.

Statistical Mechanics of Rubber

F. W. Boggs
United States Rubber Company, General Laboratories, Passaic, New Jersey
(Received August 27, 1951)

It is shown in this paper that above the second-order transition the partition function of a rubber can be represented to a reasonably good approximation by the product of the partition function of a liquid formed of molecules similar to the chain elements and the partition function of the noninteracting chains divided by the partition function of a perfect gas. In terms of the free energy this means that the free energy of rubber will be equal to the sum of the free energy of the chain network without interactions and that of a liquid formed of the chain elements alone minus the free energy of a perfect gas having the same number of molecules as the rubber has chain elements.

This same procedure has permitted the calculation of the free energy and partial pressure of a rubber solution. This is, however, by no means the only possible application. All the thermodynamic properties of elastomer solvent systems can be obtained.

This is a generalization of the methods previously used in the statistical studies of rubber and rubber solvent mixtures.

INTRODUCTION

IT was not until the proposal of the statistical theory of Guth and Mark in 1934[1] and Kuhn in 1936[2] that a satisfactory explanation of the elastic properties of rubber was available. Since then papers by Treloar,[3] Flory,[4] Guth, and James,[5] and many others have extended their ideas. For all these theories the statistical treatment is based on the assumption that rubber is formed of chain elements which do not interact with one another except through the chain links. This has been justified by the argument that the variation in potential energy of the chain elements resulting from near neighbor interaction between nonlinked neighbors is negligible in the interior of the rubber. It has, of course, been recognized almost from the start that such a model could not predict all of the properties of rubber any more than the properties of a liquid can be predicted from those of a perfect, even though dense, gas. To account for the approximate incompressibility of rubber in these treatments it has been necessary to superimpose some special additional assumptions. Usually the partition function of chains is deduced from statistical considerations and the volume is assigned as an arbitrary function of the temperature similar to that characteristic of liquids of similar density and composition.

In this paper we will attempt to validate this procedure by integrating the theory of chains with existing theories of liquid structures, notably that of Lennard-Jones and Devonshire.[6] In subsequent papers we will show how somewhat more elaborate theories of liquid structures will give even better results. Despite the obvious imperfections of the present theories of liquid structure they are, nevertheless, sufficiently refined to throw considerable light on the more primitive concepts of the structure and properties of rubber. We will start out by assuming that the macroscopic properties of the system can be deduced from the canonical ensemble of Gibbs and we will show how certain approximations will lead quite naturally to the existing theories.

Let us suppose that we have a set of long chain molecules which are tied together to form an irregular three-dimensional network. It is just such a network which is usually supposed to account for the properties of rubber. We know that the total energy H in such a system of chains would be given as a sum of the kinetic and potential energy,

$$H=\sum_{ij} A_{ij}p_ip_j+V(q_1\cdots q_n), \tag{1}$$

where the p_i are the generalized momentum coordinates and the q_i the generalized position coordinates. The matrix elements A_{ij} are functions of $q_1\cdots q_n$, and the external parameters. They will be functions of the external parameters because the ends of some chains may be considered to be fastened to the external boundaries which will consequently appear as external restrictions on the movements of the chains. Moving the outer boundaries of the sample will consequently change these restrictions which limit the motion of the chain segments. $V(q_1\cdots q_n)$, on the other hand, will be the potential energy of these elements with respect to one another. It is this quantity which is neglected in the previous theories of rubber.

THE PARTITION FUNCTION FOR RUBBER

It is known from statistical mechanics that the Helmholtz[7] free energy will be given by the expression in Eq. (2):

$$A=-kT\log\frac{1}{h^n}\int\cdots\int\exp-\frac{H}{kT}dp_1\cdots dq_n. \tag{2}$$

[1] E. Guth and H. Mark, Monatsh. **65**, 93 (1934).
[2] W. Kuhn, Kolloid-Z. **76**, 258 (1936).
[3] L. R. G. Treloar, Proc. Phys. Soc. **55**, 345 (1943).
[4] P. J. Flory and J. Rehner, J. Chem. Phys. **11**, 512 (1943).
[5] H. M. James and E. Guth, J. Chem. Phys. **11**, 455 (1943).
[6] J. E. Lennard-Jones and A. F. Devonshire, Proc. Roy. Soc. (London) **A163**, 53 (1937).
[7] R. H. Fowler, *Statistical Mechanics* (Cambridge University Press, London, England, 1936).

Our object will be to find suitable approximations for the integral appearing in Eq. (2), which is the partition function. We will see that the nature of the approximation which we use will determine the type of behavior predicted and, further, that each approximation which we will discuss is related rather directly to approximations used in existing theories of the liquid state. This will permit us to inset the corresponding expression for liquids into the partition function of rubber and thus lead quite naturally to a more complete description of its behavior.

If we substitute the expression given in Eq. (1) into the partition function we will obtain Eq. (3):

$$Z_r=\frac{1}{h^n}\int\cdots\int \times\exp-\frac{1}{kT}[\sum_{ij} A_{ij}p_ip_j+V(q_1\cdots q_n)]dp_1\cdots dq_n. \quad (3)$$

Now it has been shown[8,9] that if we integrate first with respect to the momenta alone, Eq. (3) will take the new form given in Eq. (4),

$$Z_r=\frac{(kT)^{n/2}}{h^n}\int\cdots\int |\alpha_{ij}|^{\frac{1}{2}} \times\exp\left[\frac{-V(q_1\cdots q_n)}{kT}\right]dq_1\cdots dq_n, \quad (4)$$

where (α_{ij}) represents the inverse of the matrix A_{ij} and $|\alpha_{ij}|$ represents its determinant. This is, of course, a perfectly general expression in which nothing has been neglected aside from the internal structure of the individual elements. If the interaction potential $V(q_1\cdots q_n)$ is vanishingly small then Eq. (4) will become Eq. (5):

$$Z_r=\frac{(kT)^{n/2}}{h^n}\int\cdots\int |\alpha_{ij}|^{\frac{1}{2}}dq_1\cdots dq_n. \quad (5)$$

It can be shown that this will be identical with the expression that would be obtained in any specific case from the hypothesis of noninteracting chains. That this must be so follows among other things from the work of Frank on the nature of entropy.[10]

In a dense, disordered aggregate such as we suppose rubber to be when there is no crystallinity present, it is usually assumed that the potential energy of the intermolecular forces is adequately approximated by assuming that it is a sum of terms each of which depends on the relative distance and orientation between molecules. Unfortunately, it is quite difficult to solve the integrals that are obtained under these assumptions so that further approximations are necessary. It is, however, possible to use other approximations which have already proved successful in the calculation of the partition functions for liquids. These allow the development of general relations between the partition function of rubber and that of a liquid formed of particles which are not tied together but which have the same intermolecular forces.

[8] M. V. Eidenoff and J. G. Aston, J. Chem. Phys. **3**, 379 (1935).
[9] J. W. Gibbs, *Statistical Mechanics* (Longmans, Green and Company, New York, 1928), Chapter V.
[10] H. S. Frank, J. Chem. Phys. **13**, 478 and 492 (1945).

RELATION TO THE THEORY OF LENNARD-JONES AND DEVONSHIRE

One of the simplest and most successful approximations which has been made for the intermolecular potential field of liquids is that of Lennard-Jones and Devonshire in which the contribution to V of all but nearest neighbor pairs is neglected. $\sum V_{ij}$ is further approximated by a sum $\sum V_{(r_i)}$ where $V_{(r_i)}$ is a potential of spherical symmetry obtained by averaging all the near neighbor contributions over all configurations. This approximation has, of course, as principal advantage the simplicity of the results to which it leads. It results quite directly in a partition function which is the product of the partition function of a chain network, the partition function of a liquid, and an additional factor depending on the volume. It is clear that such an expression will lead to the constancy of volume which is one of the outstanding characteristics of rubber as it is of liquids. It will also lead to the familiar expression of the stress-strain relations. The assumption that such a partition function is possible has been implicit in all previous statistical theories of rubber.

According to the Lennard-Jones and Devonshire theory the potential of an element will become very large when it leaves the center of the spherical "cell." Consequently, one would expect that this would happen relatively infrequently. On the other hand, $|\alpha_{ij}|^{\frac{1}{2}}$, being a slowly varying function of the variables $q_1\cdots q_n$, will not change greatly when the potential energy of one of the chain elements deviates from its minimum. If we integrate, therefore, each chain element merely over the volumes of the cell which it is occupying, we will obtain a simple expression for the partition function which is given in expression (6),

$$\frac{1}{h^n}|\alpha_{kl}|^{\frac{1}{2}}\prod_{i=1}^{N}\int\exp\left[\frac{-V_{(r_i)}}{kT}\right]d\tau_i, \quad (6)$$

where $V_{(r_i)}$ is the potential of the chain element as a function of the distance r_i from the center (potential minimum) of its cell and $d\tau_i$ is the volume element of i. As the integration has been carried out, it is assumed tacitly that the chain element is confined to a given cell by its near neighbors which create a potential barrier; $|\alpha_{ij}|^{\frac{1}{2}}$ could therefore be assigned the value which it has when each chain element is at the center of the cell it happens to be occupying. Since interchange of elements between cells must be considered possible, we must sum up all these configurations giving the parti-

tion function in Eq. (7).

$$Z_r=\frac{1}{h^n}\sum_k |\alpha_{ij}(q_{1k}\cdots q_{nk})|^{\frac{1}{2}}\prod_{i=1}^{N}\int \exp\left[\frac{-V_{(r_i)}}{kT}\right]d\tau_i. \quad (7)$$

$q_{1k}\cdots q_{nk}$ are the values assumed by the variables q_i when the chain elements are in the kth set of cells. If we replace the summation by integration of the variables $q_1\cdots q_n$ over the volume of the sample, then Eq. (7) will become Eq. (8),

$$Z_r=\frac{1}{h^n}\int\cdots\int\frac{|\alpha_{ij}|^{\frac{1}{2}}}{{v_1}^N}dq_1\cdots dq_n\prod_{i=1}^{N}\int\exp\left[\frac{-V_{(r_i)}}{kT}\right]d\tau_i, \quad (8)$$

where v_1 is the volume of the unit cell. Let v be the total volume, T the absolute temperature, L_x, L_y, L_z the lengths of the sample in the x, y, and z directions. If we make the substitutions

$$\Omega(vT)=\int\exp\left[\frac{-V_{(r_i)}}{kT}\right]d\tau_i;$$

$$C(L_xL_yL_z)=\int\cdots\int|\alpha_{ij}|^{\frac{1}{2}}dq_1\cdots dq_n, \quad (9)$$

we will obtain the expression in Eq. (10) for the partition function of rubber.

$$Z_r=\frac{(kT)^{n/2}}{h^n}C(L_x,L_y,L_z)\left[\frac{N\Omega(vT)}{v}\right]^N. \quad (10)$$

This has the form postulated. To see that this must be the case it will suffice to write the partition function for a liquid on the same assumptions. This is given in Eq. (11).

$$Z_L=\frac{1}{h^{3N}}(2\pi mkT)^{3N/2}[\Omega(vT)]^N\frac{1}{N!}. \quad (11)$$

Equations (10) and (11) differ in the fact that one has the partition function for a chain divided by ${v_1}^N$ as a factor and the other has $1/N!$. The differences occur, therefore, in the term which expresses the communal entropy. The communal entropy in rubber will depend on the external parameters and in particular on the external stresses. It is this which gives rise to the characteristic elastic properties. If now we find expressions for the Helmholtz free energy for both these systems, we will obtain Eqs. (12) and (13).

$$A_r=-kT\left[\frac{n}{2}\log\frac{kT}{h^2}-N\log\frac{v}{N}+N\log\Omega\right]; \quad (12)$$

$$A_L=-kT\left[\frac{3N}{2}\log\frac{2\pi mkT}{h^2}-\log N!+N\log\Omega\right]. \quad (13)$$

A_r will be the Helmholtz free energy of rubber and A_L that of the corresponding liquid. By elimination between (12) and (13) it is possible to obtain Eq. (14),

$$A_r=A_L-kT\left[\frac{-(3N-n)}{2}\log\frac{kT}{h^2}-\frac{3N}{2}\log 2\pi m+\log C-N\log\frac{v}{N}+\log N!\right]. \quad (14)$$

We know from previous work that $\log C$ will be equal to $N\Gamma(L_x^2+L_y^2+L_z^2)$ where Γ is a constant proportional to the concentration of crosslinks in the system and L_x, L_y, L_z are the dimensions of the sample. If the forces acting on the sample are F_x, F_y, and F_z in the xyz direction, respectively, then we must have F_x,

$$F_x=NkT\left[2\Gamma L_x-\frac{L_yL_z}{v}\right]+\frac{\partial A_L}{\partial v}L_yL_z. \quad (15)$$

Similar relations will hold for F_y and F_z. If F_y and F_z are 0 we will obtain the usual equation for the stress-strain relations:

$$2\Gamma NkT\left[L_x-\frac{v}{{L_x}^2}\right]=F_x. \quad (16)$$

If we wish to calculate the volume of the sample of rubber as a function of the temperature, we can first obtain an expression for the pressure by writing $L_x=L_y=L_z=v^{\frac{1}{3}}$; then we will obtain Eq. (17) for the pressure.

$$-2\Gamma NkTv^{-\frac{1}{3}}+\frac{\partial A_L}{\partial v}-\frac{NkT}{v}=-p. \quad (17)$$

The volume will of course be obtained by setting Eq. (17) equal to 0. If we make the dubious assumption that Van der Waals' equation is a valid approximation for the equation of state of a liquid at high temperature and small volumes it is possible to obtain an equation which when solved will give us a qualitative idea as to how the volume behaves as a function of the temperature. The relation is shown in Eq. (18) and its solution is plotted in Fig. 1,

$$\frac{2\Gamma b^{\frac{1}{3}}}{(v/b)^{\frac{1}{3}}}=\frac{1}{v/b-1}-\frac{1}{v/b}-\frac{a/b}{(v/b)^2kT}. \quad (18)$$

It is apparent that at high temperatures the volume approaches a constant, while at low temperatures there will be a temperature coefficient of expansion. The volume obtained is of reasonable magnitude, something of the order of b. It will increase with the temperature and decrease slightly with increasing modulus; that is, with an increasing number of crosslinks. Both of these effects have been observed. Had a better equation of state been used we would obtain still more plausible results but much numerical work would be required.

THE THEORY OF SWELLING

If rubber is immersed in an appropriate solvent it will absorb the solvent and increase in volume. The degree of swelling is related to the number of crosslinks in the sample and to the nature of the solvent. The expression of Flory and Rehner[11] relating the percent swelling of the sample to the energy of interaction of the polymer and the solvent can be obtained from the model of rubber which we are developing as we shall show. There are many other possible theoretical developments which will occur to the reader and which can be carried out without great difficulty.

We will suppose that there are, in the interior of the polymer sample, two types of spherical molecules of which types one is strung in an irregular network, and the other is completely free to move about. The partition function of such a system will be given by Eq. (19) which is similar to Eq. (4).

$$Z_r=\frac{(2\pi m)^{3N_2/2}(kT)^{(n'+3N_2)/2}}{h^{n'+3N_2}N_2!}$$

$$\times\int\cdots\int|\alpha|^{\frac{1}{2}}e^{-V/kT}dq_1\cdots dq_n. \quad (19)$$

n' is the number of degrees of freedom of the network of N_1 units and N_2 is the number of unattached units. We divide by $N_2!$ because of the free interchange of the molecules 2, but we do not divide by $N_1!$ because this type is tied together in long chains. We will have two types of cells in such a system. Let us, therefore, divide our sample into N_1 cells of volume v_1 having the first type of molecule at their center, and N_2 cells of volume v_2 having the second. Let V_1 be the potential field acting on the particle in the cell of type 1, and V_2 be that acting on the particle in the cell of type 2. If $\Omega_1=\int\exp(-V_1/kT)d\tau_1$ and $\Omega_2=\int\exp(-V_2/kT)d\tau_2$ by a reasoning similar to that previously used, we will obtain the partition function given in Eq. (20).

$$Z_r=\frac{(2\pi m)^{3N_2/2}}{h^{n'+3N_2}N_2!}\frac{C\Omega_1^{N_1}\Omega_2^{N_2}}{[(N_1v_1+N_2v_2)/N_1]^{N_1}}. \quad (20)$$

Since the average potentials V_1 and V_2 will depend on the composition of the sample, this must also be true of Ω_1 and Ω_2. The total volume v will, of course, be equal to $N_1v_1+N_2v_2$. Following the procedure which we used in the previous case, we will write the partition function for a liquid mixture similar to the polymer. This partition function is given in Eq. (21).

$$Z_L=\frac{(2\pi mkT)^{\frac{3}{2}(N_1+N_2)}\Omega_1^{N_1}\Omega_2^{N_2}}{N_1!N_2!h^{3(N_1+N_2)}}. \quad (21)$$

The chemical potentials of the second component of the rubber and of the corresponding liquid will be obtained by differentiating the logarithms of Eqs. (20) and (21) with respect to N_2. We can eliminate the terms in Ω_1 and Ω_2 between these two equations, which gives us Eq. (22).

$$v_2\left[\frac{\partial}{\partial v}\log C-\frac{N_1}{v}\right]=\frac{\mu_r-\mu_L}{kT}. \quad (22)$$

In Eq. (22) μ_r is the chemical potential of component 2 in the rubber, and μ_L is the chemical potential in a similar liquid.

If the swollen rubber is in equilibrium with the liquid phase, then the chemical potential μ_r must be equal to the chemical potential μ_S of the liquid in the pure state. If in addition we suppose that $\log C=3N_1\Gamma v^{\frac{1}{3}}$ as we did in Eq. (17), we obtain Eq. (23),

$$\frac{v_2}{v_1}\left[2\Gamma v_0^{\frac{1}{3}}\left(\frac{v_0}{v}\right)^{\frac{1}{3}}-\frac{v_0}{v}\right]=\frac{\mu_S-\mu_L}{kT}, \quad (23)$$

where v_0 is the volume of the unswollen sample. Equation (23) indicates that the percent swelling would increase as μ_S approaches μ_L. This is, of course, what we would expect. The expression does not hold exactly when $\mu_S=\mu_L$ because at this point it predicts that the percent swelling should be infinite. This means that the chains would be infinitely extended. The Gaussian approximations for the number of chain configurations which gives $\log C=N_1\Gamma v^{\frac{1}{3}}$ is not valid so that the theory of the finite chain should be used.

Equation (23) is closely related to the results obtained by Flory and Rehner.[11] Its advantages are that it is valid for molecules of different volumes and that it justifies the use of partition functions of liquids which are already known in the calculations of the partition function of rubber. It also justifies the use for these calculations of certain empirical or semiempirical relations which have been found to be applicable to liquids. In this way it is possible to extend considerably the theory of high polymer solutions. We illustrated this point for a one-component system when we used Van der Waals' equation to calculate the volume of rubber as a function of the temperature and the number of crosslinks. We will illustrate this again by calculating

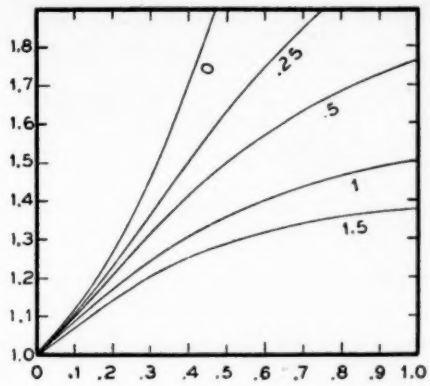

FIG. 1. v/b as a function of bkT/a for different values of $2\Gamma b^{\frac{1}{3}}$.

[11] P. J. Flory and J. Rehner, J. Chem. Phys. 11, 521 (1943).

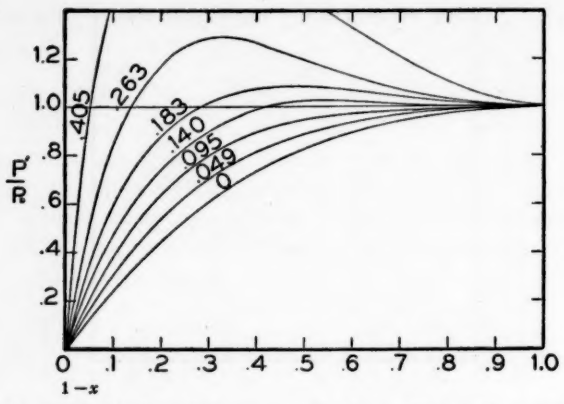

FIG. 2. Ratio of partial pressure of solvent P' in rubber to the vapor pressure of pure solvent P_0 as a function of volume fraction of solvent.

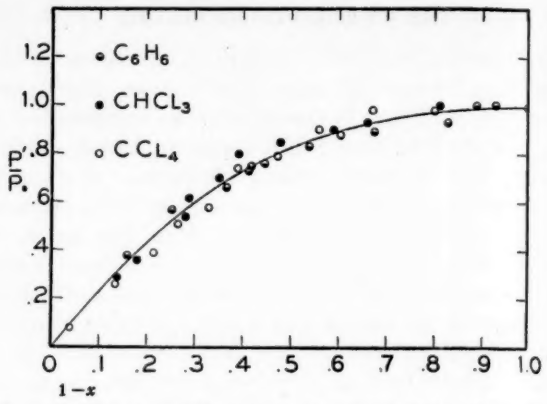

FIG. 3. Ratio of partial pressure of solvent P' in rubber to the vapor pressure of the pure solvent P_0 as a function of volume fraction.

the partial pressure of a solvent over a solution of rubber in the solvent as a function of the volume fraction.

If we let $v_1=v_2$, Eq. (23) can be rewritten to give us Eq. (24),

$$\frac{p'}{p_0}=\frac{p}{p_0}\exp(2\Gamma v_0^{\frac{1}{3}}x^{\frac{1}{3}}+x), \tag{24}$$

where p is the partial pressure of the solvent over a solution of which one component is essentially the monomer, and the other solvent p' is the partial pressure over the swollen polymer, and p_0 is the vapor pressure of the solvent. x is the volume fraction of the rubber. It is possible to substitute for p/p_0 expressions for the partial pressure of the liquid mixture of the monomer and the solvents which may be obtained from the theory of liquids or from direct measurements.

If we use the expression calculated from the theory of strictly regular solutions developed by Rushbrooke[12] then we can calculate p'/p_0 and we will obtain the set of curves given in Fig. 2. These curves have been calculated assuming that the number of crosslinks is negligibly small. p'/p_0 is plotted for different values to $2W_{AB}/ZRT$ where W_{AB} is defined by Rushbrooke as the energy required to change a pair of like molecules of one type (AA) and a pair of molecules of a type (BB) into two pairs of type AB. It is, therefore, closely related to the difference in cohesive energy density. Z is the number of nearest neighbors of a given molecule. We see that when $2W_{AB}/ZRT$ is sufficiently small there will always be a one-phase system. However, when $2W_{AB}/ZRT$ increases, the system will separate into two phases, one of which is pure solvent and the other the polymer solution.

If the number of crosslinks is appreciable, the curves plotted in Fig. 2 will all be raised above the values which we have given. If the degree of swelling is large, it would, as was previously indicated, be necessary to use the partition function for a finite chain rather than a Gaussian approximation. In any case, the effect of the cross links will be to reduce the swelling, a result which is, of course, familiar. In Fig. 3 we have a comparison between the partial pressure of various solvents in rubber for various volume fractions. The solutions are supposed to be ideal. The data is taken from the article of Lens.[13] It can be seen that the results fit the experimental facts.

[12] G. S. Rushbrooke, Proc. Roy. Soc. (London) **A166**, 296 (1938).

CONCLUSIONS

The existing theories of rubber can be related to the theory of liquid structure of Lennard-Jones and Devonshire and approximate relations can be found between the partition function for a liquid formed of interacting spheres and a rubber model consisting of chains of spheres in which the forces of interaction are the same. These results allow us, among other things, to explain the incompressibility of rubber. Although this work, so far, has not yielded anything essentially new, it places on a much firmer basis the relations which have previously been obtained for the modulus and the swelling of rubberlike materials.

We have not touched, in this paper, on the possibility of explaining the different transitions which are known to occur in elastomers. Although it is formally possible to suppose that below a certain temperature free interchange of particles becomes impossible, one cannot predict *a priori* at what temperature this would occur. A recent discussion of this same point in connection with the theory of liquids was published by Kirkwood.[14] This immobilization of chain elements would, however, clearly lead to embrittlement. In a subsequent paper we hope to consider the results of using, not the simple model of Lennard-Jones and Devonshire, but a model in which the mean force of interaction between pairs is used.

ACKNOWLEDGMENT

This work was carried out under the sponsorship of the Chemicals and Plastics Section, Research and Development Branch of the Office of the Quartermaster General.

[13] J. Lens, Rec. trav. chim. **V51**, 971 (1932).
[14] J. G. Kirkwood, J. Chem. Phys. **18**, 38 (1950).

The Influence of First-Order Rotational Resonance Interaction on Certain Bands in the Infrared Spectrum of the Allene Molecule*

J. DE HEER
Department of Physics and Astronomy, Ohio State University, Columbus, Ohio
(Received November 16, 1951)

The Coriolis coupling between two degenerate vibrations in allene has been discussed. This theoretical treatment gives a satisfactory explanation of the main features of two perpendicular bands, which have been observed in the infrared absorption spectrum of this molecule between 8 and 14μ. An analysis of the nuclear spin statistics has been carried out in order to account for the intensity alternations and to help in identifying the Q branches. A derivation of the frequency formula has been given on the basis of ordinary first-order perturbation theory. Some emphasis is laid on the ambiguity in notation and the relation of this formula to others, reported in the literature. After making some reasonable assumptions with regard to the geometry of the molecule, we have obtained numerical values for the band centers and the various Coriolis coupling coefficients. A tentative suggestion has been made in partial explanation for the appearance of satellites between the main Q branches in the spectrum.

I. GENERAL INTRODUCTION

IN this paper we present a theoretical discussion of two perpendicular type of bands in the infrared absorption spectrum of the allene molecule, which were measured by Miller and Thompson.[1] These authors reported a convergence of the Q branches in the fundamentals towards the sides of the bands, which are adjacent to each other, and a divergence of these Q branches towards the outer sides (see Fig. 1). They recognized that this phenomena was the result of a Coriolis coupling of two twofold degenerate frequencies, which lie fairly close together.

The allene molecule, C_3H_4,[2] belongs to the point group $D_{2d}(\equiv V_d)$. In the equilibrium configuration the three carbon atoms lie on a straight line (taken to be the z axis) and the two CH_2 groups are oriented in such a way that two hydrogen atoms, e.g., a and b, lie in the xz plane, and the other two, c and d, in the yz plane (see Fig. 2). The classical vibration problem has been discussed by Herman and Shaffer.[3] Figure 3, taken from their paper, shows the independent degenerate modes of oscillation; the actual normal vibrations will be linear combinations of these. The location of the bands to be discussed in this paper (8–14μ) strongly suggests that we are dealing with C−C−C bending vibrations. This means that the two interacting modes of oscillations are essentially ω_{10} and ω_{11}, mixed to a small degree with some of the ω_8 and ω_9 (in the notation of Herman and Shaffer; see Fig. 3). Since we cannot obtain the exact linear combination owing to a lack of our knowledge of the various force constants involved, we shall simply denote the interacting vibrations by ω_s and $\omega_{s'}$.

Rotational resonance interactions (Coriolis coupling between frequencies, which are accidentally degenerate) have first been discussed by Nielsen, mainly in connection with the formaldehyde molecule.[4–6] Miller and Thompson[1] succeeded in fitting their data on allene approximately into a formula of the form of the one derived for formaldehyde. In doing so they rather arbitrarily identified the lines at 836.5 cm^{-1} and at 1028.5 cm^{-1} as the first lines of the ^rQ branches of bands A and B, respectively.

We shall first consider the nuclear spin statistics of allene, and this investigation leads to the result that the first line of the ^rQ branches has to be strong in a scheme of strong weak intensity alternation. We shall therefore relocate the band centers and show that the experimental data, properly reinterpreted, fit excellently into an equation which was first derived by Nielsen[7] within the scope of his general theory of the rotation vibration energies of polyatomic molecules. In this paper we shall briefly indicate how the resonance interaction problem involved may be treated more directly by ordinary first-order perturbation theory. We shall stress the fact that in allene, where we are dealing with resonance between vibrations which are twofold degenerate, the formula for the frequencies, although similar to that derived for resonance between nondegenerate frequencies (such as in formaldehyde) will differ from it in some important respects.

After making reasonable assumptions about the geometry of the allene molecule, our analysis will lead to numerical values for the band centers, the Coriolis coupling constant between the two frequencies, and the two Coriolis interaction constants between the two components of each degenerate vibration.

Miller and Thompson[1] have pointed out that between the intense Q branches other absorption maxima occur which cannot be entirely the result of an overlapping by the subsidiary P and R branches. Clearly, one recognizes certain "satellites" and the main Q branch at

* This work was assisted by the ONR under Contract No. 6 onr-22526, NR 019–123 with the Ohio State University.
[1] C. H. Miller and H. W. Thompson, Proc. Roy. Soc. (London) A200, 1 (1949).
[2] Throughout this paper we are referring to the C^{12} isotope.
[3] R. C. Herman and W. H. Shaffer, J. Chem. Phys. 17, 30 (1949).
[4] H. H. Nielsen, Phys. Rev. 55, 289 (1939).
[5] H. H. Nielsen, J. Opt. Soc. Am. 34, 521 (1944).
[6] H. H. Nielsen, Phys. Rev. 68, 181 (1945).
[7] H. H. Nielsen, Revs. Modern Phys. 23, 90 (1951).

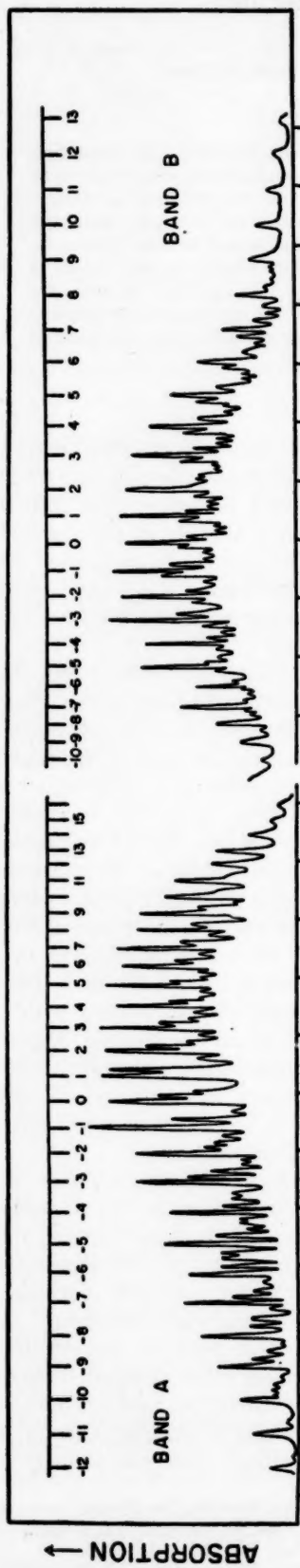

FIG. 1. Fundamental absorption bands of two degenerate vibrations in allene. (Taken from Miller and Thompson, reference 1. The arbitrary indices used by these authors have been replaced by the $\mathfrak{K}$ values as introduced in section III of the present paper. Hence, the index 1 corresponds to the first lines of the ^rQ branches, etc.)

845.5 cm^{-1} has an almost equally strong neighbor at 847.5 cm^{-1} (Fig. 1). We suggest that the irregularities may be partially understood by taking into account the difference in effective moments of inertia between the ground state and the excited state. However, certain anomalies remain and we feel that a completely satisfactory explanation requires the results of new experiments with a higher resolution.

II. NUCLEAR SPIN FUNCTIONS AND THE STATISTICAL WEIGHT OF THE ROTATIONAL VIBRATIONAL LEVELS; ALTERNATING INTENSITIES IN THE INFRARED ABSORPTION SPECTRUM

Since nuclei with spin $\frac{1}{2}$ obey Fermi-Dirac statistics, the total wave function for the allene molecule must be antisymmetrical with respect to the interchange of any pair of protons. Consequently, the quantum statistical weights of the vibration rotation levels in the (electronic and vibrational) ground state can be determined by using group theoretical methods outlined by Wilson.[8] The results of such an analysis, details of which need not be reported, are given in Table I.

Within the scope of this paper, we are interested in the intensities of the infrared absorption bands corresponding to excitation of the fundamentals of certain degenerate vibrations (see the general introduction above, and Fig. 3) and associated with transitions $\Delta J=0$, $\Delta K=\pm 1$. As is well known, the square of the transition moment, summed over all orientations of J, is given by[9,10]

$$(A_{JK\to J,K\mp 1})^2=\frac{(J\pm K)(J\mp K+1)}{16J(J+1)} \qquad (1)$$

for $K\neq 0$. For $K=0$, Eq. (1) would lead to a value $\frac{1}{16}$, but the correct number is $\frac{1}{8}$.[9,10] This factor 2 compensates for the fact that the average statistical weight

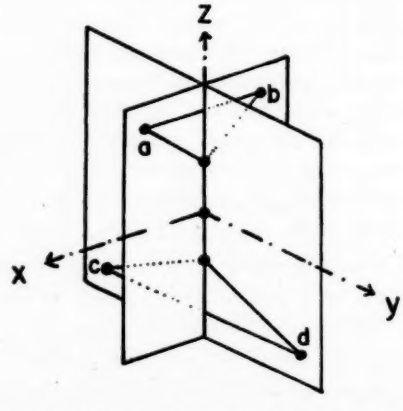

FIG. 2. Equilibrium configuration of the allene molecule.

[8] E. Bright Wilson, Jr., J. Chem. Phys. 3, 276 (1935); further references given in this paper.

[9] G. Herzberg, *Infrared and Raman Spectra of Polyatomic Molecules* (D. Van Nostrand Company, Inc., New York, 1945), Chapter IV.

[10] D. M. Dennison, Revs. Modern Phys. 3, 280 (1931).

for the state $K=0$ is only half that number for the states $|K|=2p$ ($p=1, 2, 3, \cdots$; see Table I). Hence, the final result is that throughout the entire absorption band there will be a 5/3 alternation; the lines of strong intensities originate from transitions $|K|=2q \rightarrow |K|=2q\pm1$, and the lines of weak intensities are associated with $|K|=2q\pm1 \rightarrow |K|=2q$, where $q=0, 1, 2, 3, \cdots$ (hence, q, contrary to the parameter p previously used in this section, includes the value 0).[11]

This analysis shows that the lines at 836.5 cm^{-1} and at 1028, 5 cm^{-1} cannot be associated with the transition $K=0 \rightarrow K=1$ (as was assumed by Miller and Thompson[1]), but rather suggests that the next lines on the high frequency side should be identified with these (if we choose the next lines on the low frequency side instead, the distribution of lines on both sides of the center would become rather asymmetrical).

III. THE PERTURBATION PROBLEM

The energy formula for the perturbed states has been derived by Nielsen[7] within the scope of his general theory of the rotation vibration energies of polyatomic molecules. In Nielsen's treatment the Hamiltonian is first subjected to a certain type of contact transformation. Although such a procedure provides an elegant and relatively simple way of dealing with second-order perturbation problems, it obscures the first-order perturbation calculation to which the present paper is restricted. Therefore, we shall briefly indicate how the formula concerned may be derived by direct ordinary perturbation theory.

The Coriolis coupling, which we discuss, arises from the presence in the Hamiltonian of the following terms:

$$(1/hc)\{\zeta_{s1s'2}^{(zz)}[(\omega_{s'}/\omega_s)^{\frac{1}{2}}q_{s1}p_{s'2}-(\omega_s/\omega_{s'})^{\frac{1}{2}}q_{s'2}p_{s1}] + \zeta_{s2s'1}^{(zz)}[(\omega_{s'}/\omega_s)^{\frac{1}{2}}q_{s2}p_{s'1} - (\omega_s/\omega_{s'})^{\frac{1}{2}}q_{s'1}p_{s2}]\}(P_z/I_e^{(zz)}). \quad (2)$$

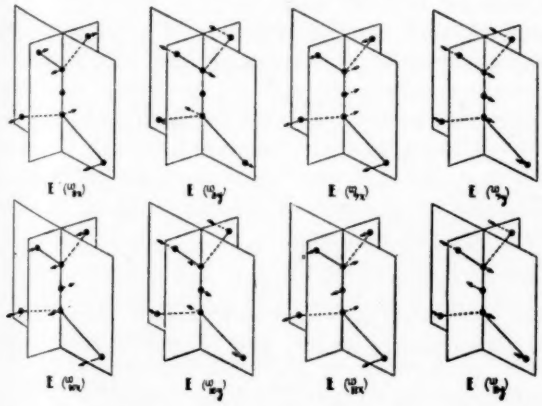

FIG. 3. Degenerate modes of oscillation of the allene molecule. (Taken from Herman and Shaffer, reference 3.)

[11] In exactly the same way we may derive the corresponding results for fully deuteriorated allene, C_3D_4. We get an alternation of the same type as in C_3H_4, but with a strong/weak ratio of 5/4 instead of 5/3. Hence, we can predict that the intensity alternation in the corresponding bands of C_3D_4 will be less pronounced than in C_3H_4.

TABLE I. Weights of the vibration rotation levels in the electronic and vibrational ground state of the allene molecule.

($p=1, 2, 3, \cdots$; multiply all weights by $2J+1$)		Weights
$K=0$	J even	7
	J odd	3
	Average	5
$\|K\|=2p$	All J values	10
$\|K\|=2p\pm1$	All J values	6

Here the $q_{s\sigma}$ refer to the normal coordinates of the degenerate vibrations with frequency ω_s; the $p_{s\sigma}$ are the conjugate momenta. P_z is the z component of the total angular momentum, which in the usual representation is diagonal in the quantum number K, and $I_e^{(zz)}$ is the equilibrium moment of inertia along the z axis. The $\zeta_{s\sigma s'\sigma'}^{(zz)}$ are Coriolis coupling coefficients, which depend in a complicated manner on the normal coordinates associated with ω_s and $\omega_{s'}$, and it follows from their definition that

$$-\zeta_{s1s'2}^{(zz)}=\zeta_{s2s'1}^{(zz)}. \quad (3)$$

Next we replace the $q_{s\sigma}$ and $p_{s\sigma}$ by their equivalents in cylindrical polar coordinates r, χ. The matrix components for the transformed expression may then be obtained from those for $r_s e^{\pm i\chi_s}$ and $e^{\pm i\chi_s}$. ($p_{r_s}\pm ip_{\chi_s}$), evaluated by Shaffer[12] and by Nielsen,[13] respectively, and recalling that the matrix components of P_z are simply $K\hbar$. The work is quite straightforward and need not be reported in detail. It shows that the Coriolis interaction between the vibrations ω_s and $\omega_{s'}$ couples the states ($V_s=1, l_s=1, V_{s'}=0, l_{s'}=0, K$) with ($V_s=0, l_s=0, V_{s'}=1, l_{s'}=1, K$) on the one hand, and ($V_s=1, l_s=-1, V_{s'}=0, l_{s'}=0, K$) with ($V_s=0, l_s=0, V_{s'}=1, l_{s'}=-1, K$) on the other hand. In both cases the interaction term (nondiagonal element) is equal to

$$KB_e^{(zz)}\zeta_{ss'}^{(zz)}[(\omega_{s'}/\omega_s)^{\frac{1}{2}}+(\omega_s/\omega_{s'})^{\frac{1}{2}}] \backsimeq 2KB_e^{(zz)}\zeta_{ss'}^{(zz)}. \quad (4)$$

Here, $B_e^{(zz)}=h/(8\pi^2 I_e^{(zz)}c)$ as usual and, in view of Eq. (3), we have written $\zeta_{ss'}^{(zz)}$ for $\zeta_{s1s'2}^{(zz)}$ and for $-\zeta_{s2s'1}^{(zz)}$. Replacing the expression $[(\omega_{s'}/\omega_s)^{\frac{1}{2}}+(\omega_s/\omega_{s'})^{\frac{1}{2}}]$ by the factor 2 is legitimate, because ω_s and $\omega_{s'}$ lie fairly close together.[14] To obtain the energies we diagonalize the two secular determinants which have the nondiagonal elements given by (4) and diagonal elements of the type,

$$E_{\text{vibr}}+B_V^{(zz)}J(J+1)+(B_V^{(zz)}-B_V^{(zz)})K^2 - 2B_V^{(zz)}K\textstyle\sum_s \zeta_{ss}^{(zz)}l_s. \quad (5)$$

The constants $\zeta_{ss}^{(zz)}$ determine the Coriolis interaction between the two components of the degenerate pair of vibrations associated with ω_s. We shall neglect centrif-

[12] W. H. Shaffer, Revs. Modern Phys. 16, 245 (1944).

[13] H. H. Nielsen, Phys. Rev. 77, 130 (1950); see also reference 7.

[14] One may verify this *a posteriori* by using the numerical values for $\omega_{s'}$ and ω_s as computed in section IV.

ugal stretching terms in E_{vibr} and put all B_V equal to B_e. We easily obtain the roots of the secular determinants, which after subtracting the energy of the molecule in the normal state, in our approximation

$$E_{\text{vibr}}{}^0+B_e{}^{(xx)}J(J+1)+(B_e{}^{(zz)}-B_e{}^{(xx)})K^2, \quad (5a)$$

yield the frequencies of the two fundamentals A and B of Fig. 1:

$$\omega({}_A{}^B)=\frac{\omega_s+\omega_{s'}}{2}-(B_e{}^{(zz)}-B_e{}^{(xx)})$$
$$\pm\sqrt{\left[\left\{\frac{\omega_{s'}-\omega_s}{2}+\mathcal{K}(\zeta_{ss}{}^{(zz)}-\zeta_{s's'}{}^{(zz)})B_e{}^{(zz)}\right\}^2\right.}$$
$$\left.+4\mathcal{K}^2(B_e{}^{(zz)}\zeta_{ss'}{}^{(zz)})^2\right]$$
$$+2\mathcal{K}\left\{\left[1-\left(\frac{\zeta_{ss}{}^{(zz)}+\zeta_{s's'}{}^{(zz)}}{2}\right)\right]B_e{}^{(zz)}-B_e{}^{(xx)}\right\}, \quad (6)$$

where the index $\mathcal{K}$ can take on all values 0, ±1, ±2, ±3, $\cdots$. Positive $\mathcal{K}$ values refer to the ${}^rQ$ branches ($\Delta K=+1$) with the understanding that the first line of this branch ($K=0\rightarrow K=1$) corresponds to $\mathcal{K}=1$. $\mathcal{K}=0$ and negative $\mathcal{K}$ values in Eq. (6) yield the ${}^pQ$ branches in such a way that $\mathcal{K}=0$ corresponds to the first line ($K=1\rightarrow K=0$). The $\mathcal{K}$ index of each line, thus defined, is given in the upper half of Fig. 1. Several remarks must be made in connection with Eq. (6):

(1) We have assigned $\mathcal{K}$ values in accordance with the convention adopted by some authors (e.g., Dennison, Nielsen; see, however, remark (2) below). Others (e.g., Herzberg) assign $\mathcal{K}$ values in such a way as to make the $\mathcal{K}=0$ line the first line of the ${}^rQ$ branch. A choice between the two systems of notation is entirely a matter of convenience; our way of assigning $\mathcal{K}$ values leads to simpler formulas.

(2) Although the rather arbitrary index $\mathcal{K}$ and the rotational quantum number K are obviously closely related, we prefer to denote them by different symbols (many authors use a K throughout).

(3) If we neglect the Coriolis coupling between ω_s and $\omega_{s'}$ (put $\zeta_{ss'}{}^{(xz)}=0$ or assume that $|\omega_{s'}-\omega_s|$ predominates the square root term), Eq. (6) reduces to the following two:

$$\omega_A=\omega_s-(B_e{}^{(zz)}-B_e{}^{(xx)})$$
$$+2\mathcal{K}\{[1-\zeta_{ss}{}^{(zz)}]B_e{}^{(zz)}-B_e{}^{(xx)}\} \quad (7a)$$

$$\omega_B=\omega_{s'}-(B_e{}^{(zz)}-B_e{}^{(xx)})$$
$$+2\mathcal{K}\{[1-\zeta_{s's'}{}^{(zz)}]B_e{}^{(zz)}-B_e{}^{(xx)}\} \quad (7b)$$
$$(\mathcal{K}=0, \pm1, \pm2, \pm3, \cdots).$$

These formulas are of course well known. They appear in a slightly different form than elsewhere, which is partly because of our choice of notation as explained in remarks (1) and (2) above. In addition one usually gives $\mathcal{K}$ positive values only, in which case the term multiplying this index has to be written with a $\pm$ sign, $+$ referring to the $\Delta K=+1$, and $-$ to the $\Delta K=-1$ transitions. Our notation eliminates this $\pm$ sign and thus avoids confusion with the $\pm$ sign in Eq. (6), which is of entirely different origin.

(4) If $\zeta_{ss}{}^{(zz)}=\zeta_{s's'}{}^{(zz)}=0$, Eq. (6) reads

$$\omega({}_A{}^B)=\frac{\omega_s+\omega_{s'}}{2}-(B_e{}^{(zz)}-B_e{}^{(xx)})$$
$$\pm\sqrt{\left[\left(\frac{\omega_{s'}-\omega_s}{2}\right)^2+4\mathcal{K}^2(B_e{}^{(zz)}\zeta_{ss'}{}^{(zz)})^2\right]}$$
$$+2\mathcal{K}(B_e{}^{(zz)}-B_e{}^{(xx)})$$
$$(\mathcal{K}=0, \pm1, \pm2, \pm3, \cdots). \quad (8)$$

This formula should be valid if the interacting vibrations are nondegenerate. Indeed, Eq. (8) is identical with the formula, derived by Nielsen[5,7] to explain the structure of two resonating bands in the formaldehyde spectrum.[15] This was the formula used by Miller and Thompson[1] in describing the perpendicular bands in allene. We have here demonstrated that Eq. (6) should be used instead and a comparison of these equations clearly shows that an essential differences arises as a result of the appearance of a term linear in $\mathcal{K}$ in the square root term of Eq. (6). We shall see in sec. IV that this term is by no means negligible. This difference between Eqs. (6) and (8) is not immediately apparent from the less explicit form in which these formulas were given by Nielsen.[7]

IV. INTERPRETATION OF THE OBSERVED SPECTRUM

In Table II we have collected the observed frequencies for eighteen lines (nine at each side of the center) of both band A and band B.[1] Since we have neglected centrifugal stretching and differences between the constants B_V and B_e, we cannot expect our equations to be valid to a great degree of accuracy when values of $\mathcal{K}$ higher than these are involved. We stress again that although our $\mathcal{K}=0$ lines are the same as Miller and Thompson's $K=0$ lines, our $\mathcal{K}$ has been defined in a different way.

From Eq. (6) we obtain

$$[\omega(B)]\mathcal{K}+[\omega(A)]\mathcal{K}=(\omega_s+\omega_{s'})-2(B_e{}^{(zz)}-B_e{}^{(xx)})$$
$$+4\mathcal{K}\{[1-(\zeta_{ss}{}^{(zz)}+\zeta_{s's'}{}^{(zz)})/2]B_e{}^{(zz)}-B_e{}^{(xx)}\} \quad (9a)$$

$$\{([\omega(B)]\mathcal{K}-[\omega(A)]\mathcal{K})/2\}^2=\{(\omega_{s'}-\omega_s)/2\}^2$$
$$+\mathcal{K}B_e{}^{(zz)}(\zeta_{ss}{}^{(zz)}-\zeta_{s's'}{}^{(zz)})(\omega_{s'}-\omega_s)$$
$$+\mathcal{K}^2\{(\zeta_{ss}{}^{(zz)}-\zeta_{s's'}{}^{(zz)})^2(B_e{}^{(zz)})^2+4(\zeta_{ss'}{}^{(zz)}B_e{}^{(zz)})^2\}. \quad (9b)$$

By using Eqs. (9a) and (9b), and the method of least squares, we find that the frequencies of the thirty-six lines of Table II can be best represented by the

[15] E. S. Ebers and H. H. Nielsen, J. Chem. Phys. 5, 822 (1937).

following formula,

$$\omega(_A{}^B)=932.6\pm\sqrt{[9181.4+36.60\mathcal{K}+36.34\mathcal{K}^2]}+9.00\mathcal{K}. \quad (10)$$

Deviations from this equation average 0.4 cm^{-1} and are at most (in very few cases) 0.8 cm^{-1}. This is certainly as good as could be expected as a result of a first-order perturbation treatment of this kind.

In order to calculate the band centers and the various Coriolis coefficients, we have to make certain assumptions about the geometry of the allene molecule. Miller and Thompson suggested

$$\begin{cases} r_{C-C}=1.33\text{A} & \text{(a "pure" C=C distance)} \\ r_{C-H}=1.07\text{A} & \text{(a slightly shortened C–H bond)} \\ \angle\text{H–C–H}=120^\circ & \text{(pure } sp_2 \text{ hybridization of the end C atoms).} \end{cases}$$

At present there is no evidence to support an essentially different choice of these constants. They yield

$$I_e^{(zz)}=5.8\times10^{-40}\text{ g cm}^2, \quad \text{hence,} \quad B_e^{(zz)}=4.83\text{ cm}^{-1},$$

and

$$I_e^{(xx)}=96\times10^{-40}\text{ g cm}^2, \quad \text{hence,} \quad B_e^{(xx)}=0.29\text{ cm}^{-1}.$$

Using these B_e values, we can calculate the ω's and ζ's by comparing Eqs. (6) and (10). The final results are

$$\text{Band centers}\begin{cases}\omega_s = 850.0\text{ cm}^{-1}\\ \omega_{s'}=1{,}042.3\text{ cm}^{-1}\end{cases}$$

$$\text{Coriolis constants}\begin{cases}\zeta_{ss}^{(zz)} = 0.067\\ \zeta_{s's'}^{(zz)}=-0.050^5\\ \zeta_{ss'}^{(zz)} = 0.621.\end{cases}$$

In deriving Eq. (6), we tacitly assumed that

$$B_V^{(\alpha\alpha)}=B_0^{(\alpha\alpha)}=B_e^{(\alpha\alpha)}.$$

Without making this assumption the following extra terms would occur in the expression for the frequencies:

$$(B_{V_s}^{(xx)}-B_0^{(xx)})J(J+1)+\mathcal{K}^2(B_{V_s}^{(zz)}-B_{V_s}^{(xx)}-B_0^{(zz)}+B_0^{(xx)})$$

(compare Eqs. (5) and (5a)). The only consequence of the term in $\mathcal{K}^2$ would be that Eqs. (6) and (10) will become inaccurate at high values of this index. Dr. Harald H. Nielsen has drawn the author's attention to the fact that the term $(B_{V_s}^{(xx)}-B_0^{(xx)})J(J+1)$ may very well be responsible for the appearance of "satellites" of the main Q branches as observed by Miller and Thompson (Fig. 1). In particular, such a term might in principle account for the satellites in band A, provided we assume

$$B_{V_s}^{(xx)}>B_0^{(xx)} \text{ (in other words, } \alpha_{V_s} \text{ is negative).}$$

As far as we can see, this phenomenon alone cannot give a satisfactory explanation for the occurrence of satellites at *both* sides of the main peaks, such as we observe in band B. It seems desirable that additional information, obtained with a higher spectral resolution, become available before a more complete and more satisfactory explanation can be aimed at.

TABLE II. Calculated and observed frequencies.

$\mathcal{K}$	Band A (ω in cm^{-1}) Observed[a]	Band A (ω in cm^{-1}) Calculated[b]	Band B (ω in cm^{-1}) Observed[a]	Band B (ω in cm^{-1}) Calculated[b]
−8	755.5	754.7	967.2	966.5
−7	766.6	766.1	973.3	973.1
−6	777.1	777.3	980.0	979.9
−5	787.7	788.1	986.8	987.1
−4	798.1	798.5	994.2	994.7
−3	808.2	808.7	1002.4	1002.5
−2	818.3	817.9	1010.5	1011.3
−1	827.6	827.8	1019.4	1019.4
0	836.5	836.8	1028.5	1028.4
1	845.5	845.4	1038.0	1037.8
2	854.0	853.7	1047.1	1047.6
3	862.0	861.5	1058.3	1057.7
4	869.5	869.1	1068.5	1068.1
5	876.5	876.2	1079.1	1079.0
6	883.5	883.1	1090.2	1090.1
7	889.6	889.7	1101.6	1101.5
8	895.8	896.0	1113.3	1113.2
9	901.8	902.5	1125.1	1124.7

[a] Miller and Thompson, reference 1.
[b] This paper, Eqs. (6) and (10).

ACKNOWLEDGMENT

The author wishes to express his gratitude to Professor Harald H. Nielsen for suggesting this problem to him and for many valuable discussions during the course of this investigation.

Note added in proof:—After this paper went to press, the author was informed that R. C. Lord and P. Venkateswarlu, at M.I.T., recently carried out a new spectroscopic study of gaseous allene, and also investigated allene-d_4. In interpreting some of their data, they independently derived certain results, reported in Secs. II and III of the present paper. Although the author has not yet seen a copy of the manuscript, which will be submitted for publication by Lord and Venkateswarlu, private correspondence with the former has established that no discrepancy exists between our theoretical investigations. It appears, however, that some of the numerical results derived in Sec. IV of the present paper may have to undergo minor revisions in the light of the new experiments referred to above.

Visco-Elastic Effect in Solutions of Simple Particles

GEORGE K. FRAENKEL*
Baker Laboratory of Chemistry, Cornell University, Ithaca, New York
(Received October 29, 1951)

Calculations are performed on a simple model to show that dilute solutions of asymmetric particles possess a frequency dependent intrinsic viscosity and a rigidity. The model used is that of a solution containing elastic dumbbells, that is, particles consisting of two rigid bodies held together by elastic forces. Part of the rigidity would also arise from inelastic dumbbells and is caused by a force, usually neglected, as a result of Brownian motion. An additional rigidity is caused by the elastic nature of the dumbbells. At sufficiently low or high frequencies the results approximate a form similar to the ordinary dispersion formula for the dielectric constants of solutions and involve two relaxation times, one at low frequencies and one at high frequencies. The results for inelastic dumbbells are described by one relaxation time and follow the usual dispersion curve for all frequencies.

INTRODUCTION

RECENT measurements performed at the Bell Telephone Laboratories[1] on the viscosity of dilute solutions of high polymers have shown the existence of both a shear viscosity and a rigidity. The rigidity was found to be caused by the characteristics of the individual, noninteracting, polymer molecules, whereas previous measurements had shown a rigidity attributable only to the intertwining of separate molecules. In an attempt to ellucidate the fundamental nature of the visco-elastic behavior of solutions as illustrated by these experiments, the following investigation was undertaken of a very simple model: a solution containing elastic dumbbells, that is, particles consisting of two rigid bodies held together by elastic forces.

At about the same time that the present work was originally carried out, Kirkwood[2] formulated a general approach to the visco-elastic behavior of polymer solutions, but in this first paper he made no attempt to obtain detailed results. In a second paper, Kirkwood and Auer[3] investigated the behavior of a rigid rod-like macromolecule consisting of a large number of equally spaced identical friction centers lying in a straight line. The present work is in substantial agreement with the results of Kirkwood and Auer but also includes the effects of inherently elastic particles. In general, a dispersion in the viscosity accompanied by a rigidity is found to result from the rotation of a rigid, asymmetric, inelastic body, as well as from an inherently elastic body. The contribution of the rigid body motion arises from a hitherto neglected force as a result of the molecular impacts of the solvent.

In conventional analyses of the viscosity of solutions, the forces considered may be one or more of the following: the hydrodynamic forces, which may be caused by an over-all fluid flow or be a result merely of the resistance that the fluid offers to motion of the body; external forces, such as an electric field tending to orient a body containing a dipole; and internal forces, of which an example is the hindering torques in polymer chains. Inertial effects are usually neglected. The sum of these forces and torques sometimes averaged over all orientations is ordinarily set equal to zero, thus neglecting the forces caused by Brownian motion. It is these latter forces that have been included in both Kirkwood's work and in the present paper.

The first stage in the following calculation is the determination of the Brownian motion distribution function which describes the probability of a dumbbell being at a given position with a given orientation. This distribution function is used to calculate the contribution of the Brownian motion to the forces on the particles. From these forces the stresses added to the solution by the particles are determined, and from the stresses the incremental viscosity is calculated.

SPECIFICATION OF THE MODEL

The dumbbells are considered to be immersed in a homogeneous liquid. They consist of two identical centers of friction with friction constant f at the ends of an elastic rod of negligible cross section and of sufficient length to prevent hydrodynamic interaction between the friction centers. Thus, the hydrodynamic forces on a dumbbell are determined, if one neglects acceleration, by the forces on the two ends. These are given by

$$(\mathbf{v}_1-\dot{\mathbf{R}}_1)f, \tag{1}$$

where $\dot{\mathbf{R}}_1$ is the velocity of the end of the dumbbell designated by (1), and $\mathbf{v}_1$ is the velocity of the fluid at the location of this end. The concentration of the dumbbells will be considered to be small enough to avoid complications caused by interactions between adjacent dumbbells.

The elastic forces are specified by a potential energy V given by

$$V=\tfrac{1}{2}\kappa[|\mathbf{R}_1-\mathbf{R}_2|-a]^2, \tag{2}$$

where κ is the force constant, a the equilibrium separa-

* National Research Council Predoctoral Fellow; now at Columbia University, New York 27, New York.

[1] Baker, Mason, and Heiss, Phys. Rev. **75**, 1301 (1949). W. P. Mason, Trans. Am. Soc. Mech. Engrs. **69**, 359 (1947).

[2] J. G. Kirkwood, Rec. trav. chim. **68**, 649 (1949).

[3] J. G. Kirkwood and P. L. Auer, J. Chem. Phys. **19**, 281 (1951).

tion between the two ends, and $\mathbf{R}_1$ and $\mathbf{R}_2$ the vectors locating the ends.

The fluid is subject to an external transverse oscillatory motion in the X-direction of velocity $v(Z)\exp(i\omega t)$. This motion is propagated in the Z-direction and the circular frequency of oscillation is given by ω. In the neighborhood of the center of a dumbbell, located by the vector $\bar{\mathbf{R}}$ with components $\bar{X}$, $\bar{Y}$, and $\bar{Z}$, the velocity may be represented by the first two terms of a Taylor series,

$$v(Z)=v(\bar{Z})+\alpha(Z)[Z-\bar{Z}], \tag{3}$$

where $\alpha(Z)=(\partial v/\partial Z)_{\bar{Z}}$. This approximation is valid if the wavelength of the transverse motion is large compared to the length of the dumbbell.

It will be convenient to specify the position of a dumbbell by a vector to its center,

$$\bar{\mathbf{R}}=(\mathbf{R}_1+\mathbf{R}_2)/2, \tag{4}$$

with components $\bar{X}$, $\bar{Y}$, $\bar{Z}$, and by a vector representing the separation of one dumbbell end from the other,

$$\mathbf{r}=(\mathbf{R}_1-\mathbf{R}_2)/2, \tag{5}$$

with components x, y, z. The components of the separation of the ends will be expressed in polar coordinates r, θ, φ with the polar angle θ measured from the y-axis, and the azimuthal angle φ measured from the z-axis. Thus,

$$x=r\sin\theta\sin\varphi,\quad y=r\cos\theta,\quad z=r\sin\theta\cos\varphi. \tag{6}$$

The six Cartesian components of $\mathbf{R}_1$ and $\mathbf{R}_2$ will be represented by the general symbol Q^k. The components $\bar{X}$, $\bar{Y}$, $\bar{Z}$, r, θ, and φ will be designated by the general symbol q^k. The quantities $\mathbf{i}$, $\mathbf{j}$, and $\mathbf{k}$ will represent unit vectors along the x, y, and z directions. In transforming from the Q^k's to the q^k's in the ensuing calculations, use will be made of the following quantities:

The metric tensor g_{ij} is defined by

$$g_{ij}=\Sigma_k\frac{\partial Q^k}{\partial q^i}\frac{\partial Q^k}{\partial q^j}. \tag{7}$$

It has the values: $g_{\bar{X}\bar{X}}=g_{\bar{Y}\bar{Y}}=g_{\bar{Z}\bar{Z}}=g_{rr}=2$; $g_{\theta\theta}=2r^2$; and $g_{\varphi\varphi}=2r^2\sin^2\theta$. The other components vanish. The determinant of the metric tensor, $g=det|g_{ij}|$, is $64r^4\sin^2\theta$.

A component of the force F_k on a dumbbell end in the Q^k coordinates is related to a component G_j in the q^j coordinates by

$$G_j=\Sigma_k F_k\frac{\partial Q^k}{\partial q^j},\qquad F_k=\Sigma_j G_j\frac{\partial q^j}{\partial Q^k}. \tag{8}$$

THE BROWNIAN MOTION DISTRIBUTION FUNCTION

It will be assumed that the Brownian motion is adequately described by a distribution function which is the solution of the appropriate generalized diffusion equation, the Fokker-Planck equation.[4] In the q^j coordinates this equation is

$$\frac{\partial\Psi}{\partial t}=\frac{1}{g^{\frac{1}{2}}}\Sigma_j\frac{\partial}{\partial q^j}\left\{g^{\frac{1}{2}}\left[\Sigma_i D^{ij}\frac{\partial\Psi}{\partial q^i}-\dot{q}^j\Psi\right]\right\}, \tag{9}$$

where Ψ is the distribution function and D^{ij} is a component of the diffusion tensor. The $\dot{q}^j$ are the velocities caused by the action of the external forces and are determined by the condition that, neglecting accelerations, the work done on the particles must vanish. The relations obtained are

$$\dot{q}^j=\Sigma_i f^{ji}G_i=\frac{1}{f}\Sigma_i F_i\frac{\partial q^i}{\partial Q^j},\qquad G_i=\Sigma_j f_{ij}\dot{q}^j, \tag{10}$$

where the friction tensor f_{ij} is given by $f_{ij}=fg_{ij}$ and where f^{ij} is the reciprocal of f_{ij}. The forces F_k on the dumbbells are the sum of the components of the first term, $f\mathbf{v}$, of Eq. (1) and of the negative gradient of the potential energy V in Eq. (2). The velocity $\mathbf{v}$ in Eq. (1) is determined from Eq. (3).

The diffusion tensor D^{ij} is evaluated by the condition that, when equilibrium is established in a force field derivable from a potential, the distribution function is represented by the appropriate Boltzmann factor and each component of the diffusion current,

$$-\Sigma_i D^{ij}\frac{\partial\Psi}{\partial q^i}+\dot{q}^j\Psi, \tag{11}$$

vanishes. These considerations lead to the well-known result

$$D^{ij}=kTf^{ji}. \tag{12}$$

It is of interest to note that each component of the total convection velocity, caused by both external forces and Brownian motion, is given by

$$-\Sigma D^{ij}\frac{\partial\ln\Psi}{\partial q^i}+\dot{q}^j. \tag{13}$$

With Eqs. (10) and (12) it is seen that the Brownian motion may be thought of as exerting an additional force on the particles of magnitude

$$kT\frac{\partial\ln\Psi}{\partial q^j}. \tag{14}$$

[4] S. Chandrasekhar, Revs. Modern Phys. 15, 41 (1943).

If the indicated calculations are performed, the diffusion equation in r, θ, φ may be written as

$$\frac{2f}{kT}\frac{\partial\Psi}{\partial t}=\frac{1}{r^2}\frac{\partial}{\partial r}\left\{r^2\left[\frac{\partial\Psi}{\partial r}+\frac{2\kappa a}{kT}\left(\frac{2r}{a}-1\right)\Psi-\frac{\alpha f r}{kT}\sin^2\theta\sin 2\varphi\right]\right\}$$
$$+\frac{1}{r^2\sin^2\theta}\frac{\partial}{\partial\theta}\left\{\sin\theta\left[\frac{\partial\Psi}{\partial\theta}-\frac{\alpha f}{2kT}r^2\Psi\sin 2\theta\sin 2\varphi\right]\right\}$$
$$+\frac{1}{r^2\sin^2\theta}\frac{\partial}{\partial\varphi}\left[\frac{\partial\Psi}{\partial\varphi}-\frac{2\alpha f}{kT}r^2\Psi\sin^2\theta\cos^2\varphi\right]. \quad (15)$$

The terms in $\overline{\mathbf{R}}$, the coordinates of the center of a dumbbell, have been omitted because the distribution function may be considered to be independent of these coordinates. The center of a dumbbell follows the motion of the fluid, $\overline{\mathbf{R}}=\mathbf{i}v(\bar{Z})$.

We will be interested in solutions of this equation which are linear in the velocity gradient $\alpha=\alpha_0\exp(i\omega t)$, so that the distribution function may be written in the form

$$\Psi(r,\theta,\varphi,t)=\Psi_0(r,\theta,\varphi)[1+\alpha\Omega(r,\theta,\varphi)]. \quad (16)$$

Ψ_0 is the steady state solution for $\alpha=0$ and is therefore given by the Boltzmann distribution with the potential energy V of Eq. (2):

$$\Psi_0=A\exp(-V/kT)=A\exp(-s^2),$$

where

$$s=1/\epsilon[(2r/a)-1],$$
$$\epsilon=(2kT/\kappa a^2)^{\frac{1}{2}} \quad (17)$$

and A is a normalization constant.

An exact solution of the equation resulting from the substitution to first order in α of Eqs. (16) and (17) in Eq. (15) has not been obtained. Before proceeding to the approximate solution, however, it is of interest to consider two special cases. The first case is that of inelastic dumbbells for which $2r=a$. The solution is readily found to be

$$\Psi(\theta,\varphi,t)=A\left[1+\frac{3\alpha\tau_0}{1+i\omega\tau_0}\sin^2\theta\sin\varphi\cos\varphi\right], \quad (18)$$

where $\tau_0=fa^2/12kT$. The second special case is that for elastic dumbbells held at a fixed orientation θ_0, φ_0. The appropriate distribution function is

$$\Psi(s,t)=A\exp[-s^2]\left\{1+\frac{\alpha f}{2\kappa}\left[\frac{2s}{\epsilon(1+i\omega\tau_1)}+\frac{s^2-\frac{1}{2}}{1+i\omega\tau_2}\right]\sin^2\theta_0\sin\varphi_0\cos\varphi_0\right\}, \quad (19)$$

where $\tau_1=3\epsilon^2\tau_0=f/2\kappa$ and $\tau_2=\tau_1/2$. For the case of negligible interaction between the rotational and vibrational motion, a superposition of these two special solutions should be an approximate description of the distribution of rotating elastic dumbbells. Such a solution would thus involve the relaxation time τ_0 related to the rotational motion, and the two relaxation times τ_1 and τ_2 related to the vibrational motion. The effect of the vibration on the rotation is reduced if the motion is restricted in such a way that the relative vibrational displacements $(2r-a)/a$ are small. The mathematical expression for this condition corresponds to ϵ being small, as can be seen from the following considerations: we note first that if $\epsilon\ll 1$, then $|s|\gg|\epsilon s|$. Because of the Boltzmann factor $\exp(-s^2)$, the distribution function is negligible if $|s|$ is much larger than 2, and thus the distribution function is only appreciable if $|\epsilon s|\ll 2$. Since ϵs is the relative displacement, the condition of small ϵ insures that the relative displacement is small under conditions where the distribution function is not negligible.

The mean square vibrational displacement in the absence of a velocity gradient is kT/κ and thus ϵ^2 is twice the ratio of the mean square displacement to the square of the equilibrium separation of the dumbbell ends. The variable s is $1/\sqrt{2}$ times the ratio of the relative displacement to the mean square relative displacement. Small ϵ means, of course, that the elastic forces in the dumbbell are large compared to the thermal forces.

Proceeding to the solution of Eq. (15) for small ϵ, we obtain to first order in α after substituting Eqs. (16) and (17) and putting

$$\Omega(r,\theta,\varphi)=R(s)\sin^2\theta\sin\varphi\cos\varphi, \quad (20)$$

$$R''(s)-2[s-\epsilon(1+\epsilon s)^{-1}]R'(s)$$
$$-6\epsilon^2[i\omega\tau_0+(1+\epsilon s)^{-2}]R(s)+12\tau_0\epsilon s(1+\epsilon s)=0. \quad (21)$$

Expanding in powers of ϵ, this equation becomes

$$R''(s)-2[s-\epsilon+\epsilon^2 s-\epsilon^3 s^2+\epsilon^4 s^3+\cdots]R'(s)$$
$$-6\epsilon^2[1+i\omega\tau_0-2\epsilon s+3\epsilon^2 s^2+\cdots]R(s)$$
$$+12\tau_0\epsilon s(1+\epsilon s)=0.$$

Three solutions are possible depending on the value of $\omega\tau_0$: (1) $0\leqq\omega\tau_0\ll\epsilon^{-1}$; (2) $0\ll\omega\tau_0\sim\epsilon^{-1}\ll\epsilon^{-2}$; and (3) $\epsilon^{-1}\ll\omega\tau_0\sim\epsilon^{-2}$. These solutions are

(1) $0\leqq\omega\tau_0\ll\epsilon^{-1}$

$$R_1(s)=\frac{3\tau_0}{\gamma_0}\left[1+\frac{\epsilon^2}{2}(\gamma_0^{-1}-1-5i\omega\tau_0)\right]$$
$$+6\tau_0\epsilon s[1-3\epsilon^2(\gamma_0-\gamma_0^{-1})]$$
$$+\tfrac{3}{2}\tau_0\epsilon^2 s^2[1-\tfrac{3}{2}\epsilon^2(i\omega\tau_0-3+3\gamma_0^{-1})], \quad (22)$$

(2) $\omega\tau_0\sim\epsilon^{-1}$

$$R_2(s)=\frac{9\tau_0\epsilon^2}{i\omega\tau_1}\Big[1-\tfrac{5}{6}i\omega\tau_1+\tfrac{3}{4}(i\omega\tau_1)^2-\frac{3\epsilon^2}{i\omega\tau_1}+\frac{9\epsilon^4}{(i\omega\tau_1)^2}+2\epsilon^2\Big]+6\tau_0\epsilon s\Big[1-i\omega\tau_1+(i\omega\tau_1)^2-(i\omega\tau_1)^3-3\epsilon^2+\frac{9\epsilon^4}{i\omega\tau_1}+\frac{13}{2}\epsilon^2 i\omega\tau_1\Big]+3\tau_0\epsilon^2 s^2\Big[1-i\omega\tau_2+(i\omega\tau_2)^2+\frac{9}{2}\epsilon^2\Big], \quad (23)$$

(3) $\omega\tau_0\sim\epsilon^{-2}$

$$R_3(s)=\frac{3\tau_0\epsilon^2}{i\omega\tau_1\gamma_1\gamma_2}\Big[3+2i\omega\tau_1-\frac{3\epsilon^2}{i\omega\tau_1\gamma_1\gamma_2}\times\Big(3+7i\omega\tau_1+\frac{13}{3}(i\omega\tau_1)^2+(i\omega\tau_1)^3\Big)\Big]+\frac{6\tau_0\epsilon s}{\gamma_1}\Big[1-\epsilon^2\frac{3+i\omega\tau_1}{\gamma_1\gamma_2}\Big]+\frac{3\tau_0\epsilon^2 s^2}{\gamma_2}\Big[1+\epsilon^2\frac{9+2i\omega\tau_1}{2\gamma_1\gamma_2}\Big], \quad (24)$$

where $\gamma_0=1+i\omega\tau_0$, $\gamma_1=1+i\omega\tau_1$, and $\gamma_2=1+i\omega\tau_2$. To higher order in ϵ, terms in s^3 and higher powers must be included in the solution. It will be noticed that, to order ϵ^2, $R_1(s)$ and $R_3(s)$ reduce to $R_2(s)$. If $-27\tau_0\epsilon^4 s^2(2\gamma_0\gamma_2)^{-1}$ and $18\tau_0\epsilon^3 s(\gamma_0\gamma_1)^{-1}$ are added to $R_3(s)$, the terms in s and s^2 hold for all three cases, but $R_1(s)$ and $R_3(s)$ involve a simple superposition of relaxation times only to order ϵ. The solutions to Eq. (15) may thus be put in the form

$$\Psi(r,\theta,\varphi,t)=A\exp(-s^2)[1+\alpha R(s)\sin^2\theta\sin\varphi\cos\varphi], \quad (25)$$

where $R(s)$ is given by one of Eqs. (22) to (24).

THE INCREMENTAL VISCOSITY

The increase in the viscosity of the solution over that of the pure solvent, the incremental viscosity, is readily determined for a solution of dumbbells by calculating the total shearing stress in the solution. If S_{xz} is the total shearing stress in the x-direction across a plane with normal in the z-direction, S_{xz}^0 that part of the stress caused by the pure solvent, and S_{xz}' that part caused by the dumbbells, then

$$S_{xz}=S_{xz}^0+S_{xz}'=\eta(\partial v/\partial Z), \quad (26)$$

where η is the viscosity of the solution and $(\partial v/\partial Z)$ is the rate of shearing strain in the x-direction caused by a fluid velocity v.

The contribution of the dumbbells to the stress S_ν' across an arbitrary plane with normal ν arises from the force transmitted by dumbbells which are cut between their two ends by this plane. Let $\mathbf{U}_1$ be the force exerted by the liquid above the plane on one end of a dumbbell. This force is transmitted through the dumbbell to its other end, which exerts a force of $-\mathbf{U}_2=\mathbf{U}_1$ on the liquid. The stress is the sum of these forces for all the dumbbells which cut unit area of the plane. Consider a cylinder of length, given by $2r$, equal to that of a dumbbell with its midpoint cutting unit area of the arbitrary plane and with its axis making an angle γ with the normal ν. The number of dumbbells with centers in this cylinder is $2nr\cos\gamma$ where n is the number of dumbbells per cubic centimeter. Those dumbbells with centers in the cylinder and length $2r$, which are oriented along its axis, cut the arbitrary plane. The number of such dumbbells is $2nr\cos\gamma\Psi r^2 dr\sin\theta d\theta d\varphi$, where Ψ is the normalized Brownian motion distribution function and γ must be expressed in terms of θ and φ for any given orientation of the arbitrary plane. Multiplying this quantity by the force $\mathbf{U}$ and integrating over all r, θ, and φ gives the total stress, which may be expressed as

$$\mathbf{S}_\nu'=\mathbf{i}S_{x\nu}'+\mathbf{j}S_{y\nu}'+\mathbf{k}S_{z\nu}'=2n\langle\mathbf{U}_1 r\cos\gamma\rangle_{Av}, \quad (27)$$

where the average of a function $f(r,\theta,\varphi,t)$ is given in terms of the Brownian motion distribution function Ψ by

$$\langle f(r,\theta,\varphi,t)\rangle_{Av}=\frac{\int_0^\infty dr\int_0^\pi d\theta\int_0^{2\pi} f(r,\theta,\varphi,t)\Psi(r,\theta,\varphi,t)r^2\sin\theta d\varphi}{\int_0^\infty dr\int_0^\pi d\theta\int_0^{2\pi}\Psi r^2\sin^2\theta d\varphi}.$$

The forces are proportional to α, so the linear effects are obtained by using Ψ_0 in place of Ψ in performing the averages in Eq. (27).

The force on a dumbbell end is given by Eq. (1), where the particle velocity $\dot{\mathbf{R}}_1$ is obtained from an equation of the form of Eq. (13). It is most convenient to calculate these forces in the q^k coordinates. The contributions from the fluid velocity cancel, leaving a term in the logarithmic derivative of the distribution function and, in the radial part only, a term resulting from the elastic force. This elastic term is cancelled by the derivative of the Boltzmann factor Ψ_0, and each component can be reduced, to first order in α, to an equation of the form

$$U_r=\alpha kT(\partial\Omega/\partial r), \quad (28)$$

where Ω is given by Eq. (20) with $R(s)$ by Eqs. (22) to (24). Similar expressions hold for the other components.

Examination of these forces for the case of rigid dumbbells is of interest. With Eq. (18) for $\Psi(\theta, \varphi)$,

$$\begin{aligned} U_\theta &= (fa^2/2)(\dot\theta_l - \dot\theta_p) \\ &= (\alpha f a^2/8)(1+i\omega\tau_0)^{-1} \sin 2\theta \sin 2\varphi, \\ U_\varphi &= (fa^2/2)(\dot\varphi_l - \dot\varphi_p) \\ &= (\alpha f a^2/4)(1+i\omega\tau_0)^{-1} \sin^2\theta \cos 2\varphi. \end{aligned} \tag{29}$$

At high frequencies U_θ and U_φ vanish, so that the motion follows the rotational component of the fluid flow with velocities $\dot\theta_l = \dot\theta_p = (\alpha/4)\sin 2\theta \sin 2\varphi$ and $\dot\varphi_l = \dot\varphi_p = \alpha \cos^2\varphi$. This conclusion is not unreasonable if it is recalled that inertial effects have been neglected. At low frequencies $\dot\theta = 0$ and $\dot\varphi = \alpha/2$, velocities that correspond to the average values which would have been obtained if Brownian motion had been neglected and the dumbbells had been assumed to be in random orientations. These are the values of the velocity which would have been used in the conventional treatment of intrinsic viscosity.[5]

The forces given by Eq. (28), together with the equations for the other components, are transformed to the Q^k coordinates using Eq. (10). After performing the integrations over the angles, the nonvanishing stress components become

$$S_{xz} = S_{zx} = \alpha(nkT/15)\langle r(\partial R/\partial r) + 3R\rangle_{Av}.$$

The integrals over r reduce, when s is substituted for r, to expressions of the form

$$\int_{-1/\epsilon}^{\infty} (1+\epsilon s)^n R(s)\Psi_0(s)\,ds.$$

By using an asymptotic series for the error integral,[6] it may be shown that the lower limit can be replaced by $-\infty$ to the order of ϵ that has been retained in the solutions. If $R(s)$ is written as

$$R(s) = A^{(0)} + A^{(1)}s + A^{(2)}s^2,$$

the stress becomes

$$\begin{aligned} S_{xz} = S_{zx} = \alpha(nkT/15)[&3A^{(0)} + A^{(1)}\epsilon^{-1} \\ &+ (4A^{(1)} + 2A^{(2)}\epsilon^{-1})(\epsilon - \tfrac{1}{2}\epsilon^3) + (5/2)A^{(2)}(1+\epsilon^2)]. \end{aligned}$$

If we write the intrinsic viscosity, which will be complex, as

$$\begin{aligned} \eta &= \eta_0 + \Delta\eta = \eta' - i\eta'' \\ &= \eta_0 + \Delta\eta' - i\Delta\eta'', \end{aligned}$$

where η_0 is the viscosity of the solvent and $\Delta\eta$ is the incremental viscosity as a result of the presence of the dumbbells, we have, with Eq. (26) with $\alpha = (\partial v/\partial Z)$,

$$\Delta\eta' - i\Delta\eta'' = \alpha^{-1}S_{xz}.$$

The rigidity is given by $\mu = \Delta\mu = \omega\Delta\eta''$. The results, which for simplicity are given to only first order in ϵ, become, for the three frequency ranges,

(1) $0 \leqq \omega\tau \ll \epsilon^{-1}$

$$\Delta\eta_1' = (nfa^2/60)\left[2 + \frac{3}{1+\omega^2\tau_0^2}\right],$$

$$\Delta\eta_1'' = (nfa^2/20)\cdot\frac{\omega\tau_0}{1+\omega^2\tau_0^2}.$$

(2) $\omega\tau_0 \sim \epsilon^{-1}$

$$\Delta\eta_2' = nfa^2/30,$$

$$\Delta\eta_2'' = \epsilon(nfa^2/60)\left[\frac{9\epsilon}{i\omega\tau_1} + \frac{2\omega\tau_1}{\epsilon}\right].$$

(3) $\omega\tau_0 \sim \epsilon^{-2}$

$$\Delta\eta_3' = (nfa^2/30)(1+\omega^2\tau_1^2)^{-1},$$

$$\Delta\eta_3'' = (nfa^2/30)(\omega\tau_1)(1+\omega^2\tau_1^2)^{-1}.$$

For the range of low or high frequencies there is the usual type of relaxation effect, depending on a single relaxation time, either τ_0 or τ_1. The second vibrational relaxation time τ_2 does not appear to first order in ϵ, and to higher orders in ϵ the results can no longer be represented by a simple superposition of relaxation phenomena.

At low frequencies the imaginary part of the incremental viscosity vanishes and the real part reduces to the results which would have been obtained by the conventional type of treatment that neglects Brownian motion and makes use of velocities averaged over random orientations.

The vibrational contribution, unlike the rotational relaxation effects, does not depend, in the case of small interaction between rotation and vibration, on Brownian motion. Thus, if it is assumed that the rotational motion follows the liquid motion, the results to first order in ϵ, for $\omega\tau_0 \sim \epsilon^{-2}$, could also be obtained from purely mechanical considerations. The radial motion would be determined by the equilibrium between the hydrodynamic and elastic forces:

$$\dot r + (a/2\tau_1)[(2r/a) - 1] = 2\alpha r \sin^2\theta \sin\varphi \cos\varphi$$

which gives, for small displacements,

$$(2r/a) - 1 = (\alpha\tau_1)(1+i\omega\tau_1)^{-1} \sin^2\theta \sin\varphi \cos\varphi.$$

The radial force on the dumbbell is then

$$U_r = (\alpha f a)(1+i\omega\tau_1)^{-1} \sin^2\theta \sin\varphi \cos\varphi.$$

Calculation of the stress using Eq. (27), assuming random orientations, gives results identical to those above for $\omega\tau_0 \sim \epsilon^{-2}$.

If the parameters, such as the viscosity of the solvent, the friction constant, and the dumbbell force constant, are independent of temperature, the temperature de-

[5] P. Debye, J. Chem. Phys. 14, 636 (1946).
[6] E. T. Whittaker and G. N. Watson, *Modern Analysis* (Cambridge University Press, London, England, 1927), p. 341.

pendence of the incremental viscosity is determined only by the temperature dependence of the relaxation time. Under these restrictions, the rotational relaxation time would vary inversely with the absolute temperature, whereas the vibrational relaxation time would be independent of the temperature.

It is to be expected that any unsymmetrical body which will tend to be oriented in a transverse velocity gradient should show dispersion of the viscosity of the rigid body type, and thus protein solutions should exhibit a dispersion of viscosity and a rigidity.

The rotational relaxation time for the dumbbells is inversely proportional to the rotational diffusion constant, $2kT/fa^2$, and it would be expected that other types of bodies would have relaxation times related to their particular rotational diffusion constants. There should thus be a direct correlation between the rotational friction constants found from measurements of flow birefringence and the rotational relaxation times.

ACKNOWLEGDMENT

The writer would like to thank Professor P. Debye for suggesting this problem and for valuable discussions during the course of the work.

THE JOURNAL OF CHEMICAL PHYSICS VOLUME 20, NUMBER 4 APRIL, 1952

The Measurement of Bond Moments and Derivatives in HCN and DCN from Infrared Intensities*†

G. E. HYDE‡ AND D. F. HORNIG
Metcalf Chemical Laboratories, Brown University, Providence, Rhode Island

(Received January 21, 1952)

The absolute infrared absorption intensities of the fundamental vibrations of HCN and DCN have been measured, using the pressure broadening technique. These measurements yield the bond moments $\mu_{C-H} = \pm 1.13$d, $\mu_{C\equiv N} = \pm 1.80$d and show that if C is positive in the C≡N dipole, H is positive in the C−H dipole. The change in moment with internuclear distance is found to be $\partial\mu/\partial r_{C-H} = \pm 1.05$d/A, $\partial\mu/\partial r_{C\equiv N} = \mp 0.66$d/A. Two of the three anomalous peaks in the band ν_1 of HCN are shown to arise from the dimer of HCN.

INTRODUCTION

THE change in dipole moment due to the displacement of the atoms of a molecule determines the absorption intensity of a fundamental vibration. If the intensities of enough normal vibrations can be measured, therefore, the "effective bond moment" of the various bonds and the change in this moment with internuclear distance can be calculated. Such calculations usually involve the approximation that the intensities depend only on the first-order terms in the dipole moment expansion and the quadratic (i.e., harmonic) terms in the potential energy function.[1]

Both of these approximations are good ones for fundamentals. Of course, it is necessary to know the complete harmonic potential function in order to calculate the atomic displacements correctly and in the case of some molecules (e.g., N_2O,[2] CNCl,[3] COS[4]), this has been the chief problem. Finally, the additional assumption has been made in some reported work that all moments are developed along bond directions (stretching motions) or perpendicular to them (bending motions). This assumption is equivalent to the assumption that there are no induced moments in a molecule and has led to serious difficulties and contradictions (e.g., in ethylene[2]).

This work was undertaken chiefly to compare the C−H bond in HCN with that in CH_4, for which apparently reliable measurements are available, both from infrared absorption[5] and infrared dispersion measurements.[6] In addition it was of some interest to compare the C≡N bond with those previously studied in cyanogen and cyanogen chloride, although in these cases the potential function was known only approximately.[3] In HCN and DCN one could expect to have a reasonably exact potential function and consequently reliable normal coordinates; in addition, the symmetry of a linear molecule restricts the dipole moment change to directions along the molecular axis (stretching vibrations) or perpendicular to it (bending vibrations) so that no assumptions are necessary on this score. A comparison of the results in HCN and DCN affords an over-all check on the reliability of the experimental techniques

* Based on a thesis presented by G. E. Hyde in partial fulfillment of the requirements for the degree of Doctor of Philosophy, Brown University, 1951.

† While not directly supported, this work received assistance from ONR.

‡ Present address: E. I. duPont de Nemours and Company, Parlin, New Jersey.

[1] B. L. Crawford, Jr., and H. L. Dinsmore, J. Chem. Phys. **18**, 983 (1950).

[2] Thorndike, Wells, and Wilson, Jr., J. Chem. Phys. **15**, 157 (1947).

[3] E. R. Nixon and P. C. Cross, J. Chem. Phys. **18**, 1316 (1950).

[4] D. Z. Robinson, J. Chem. Phys. **19**, 881 (1951).

[5] A. M. Thorndike, J. Chem. Phys. **15**, 868 (1947).

[6] R. Rollefson and R. Havens, Phys. Rev. **57**, 710 (1940).

and on the effect of higher order terms in the dipole moment and potential energy expansions. Furthermore, it eliminates certain ambiguities of sign which occur in the calculations.

A second reason for our interest in these molecules is the peculiar envelope of the weak C≡N stretching vibration ν_1 of HCN which, instead of the characteristic $P-R$ structure of a parallel band in a linear molecule, shows three sharp closely spaced peaks. The structure of this band has never been satisfactorily explained.

The only previously reported absorption intensities in HCN are the high resolution measurements by Foley[7] on individual vibration-rotation lines of the bending mode ν_2. After correcting for the effect of finite resolution and pressure broadening, he used his data to calculate the "effective dipole moment" of the vibrational transition. If these results are used to calculate the dipole moment of the C—H bond, a value of 1.04d is obtained.§ This is sufficiently different from the value 0.31d in CH_4 to warrange further study.

EXPERIMENTAL METHOD

The present investigation employed the pressure broadening technique of Wilson and Wells[8] to measure the integrated absorption intensity over a complete vibration-rotation band. This quantity is defined as

$$A=\int \alpha_\nu d\nu=\frac{1}{pl}\int \ln\frac{I_0}{I}d\nu, \tag{1}$$

where α_ν is the absorption coefficient at the frequency ν, p is the sample pressure, l is the path length of the cell, I_0 is the intensity of the radiation of frequency ν which is incident on the cell, and I is the intensity transmitted. It has been shown by Wilson and Wells that although the real spectrometer does not measure this quantity, the two experimental quantities

$$B=\frac{1}{pl}\int \ln\frac{T_0}{T}d\nu \tag{2}$$

and

$$C=\frac{1}{pl}\int\left(\frac{T_0-T}{T_0}\right)d\nu, \tag{3}$$

where T_0 and T are the measured intensities of incident and transmitted radiation, both approach A as $pl\to 0$ under certain conditions. These are that I_0 does not vary rapidly over a slit width and (a) that the absorption coefficient is nearly constant over a spectral slit width or (b) that the resolving power does not change much over a spectral slit width.

The rotational structure of a band normally causes α_ν to change radically within a slit-width but this is remedied by the introduction of a sufficient pressure of broadening gas. In this work the rotational structure was broadened with 63 lb/in.^{2} absolute of nitrogen. The adequacy of this broadening pressure was checked by studying the area (C) under the measured absorption bands of ν_2 and ν_3 in HCN at both 29 lb/in.^{2} and at 63 lb/in.^{2} Over a range of pl from 0.0154 to 0.130 cm atmos for ν_3 and 0.0083 to 0.074 cm atmos for ν_2 the results were sufficiently similar so that it was concluded that the higher pressure was adequate.

The measurements were carried out on a double beam infrared spectrophotometer, which plotted percentage transmission directly.[9] A CaF_2 prism was used to study the two stretching vibrations and a KBr prism for the bending vibration. The resolution varied from 6 to 13 cm^{-1} but the integrated intensity is very insensitive to the resolution. The approximate peak to peak noise level on the records was 1 percent and the stray light in the KBr region did not exceed 1 percent.

The quantity plC for ν_1 and ν_3 of HCN and DCN was measured directly with a planimeter on the recorder tracings. In each of these cases there was a change of about 10 percent in dispersion from one end of the band to the other. Since most of the area lay within a region of much smaller change, it was not considered necessary to replot the records and the dispersion was taken as that at the band center.

The bending vibration ν_2 of both HCN and DCN occurs in a spectral region where the frequency scale on the record is quite nonlinear. The records were therefore replotted with a linear frequency scale. To minimize the errors resulting from the strong Q-branch they were replotted on semilog paper and the quantity B, which converges faster to A than does C, was measured.

The cell used in this work had a path length of 26.0 cm. Both windows (KBr) were at one end of the brass cell and an internal mirror reflected the beam from the entrance to the exit window. It was found that the Neoprene gaskets originally used on the windows ab-

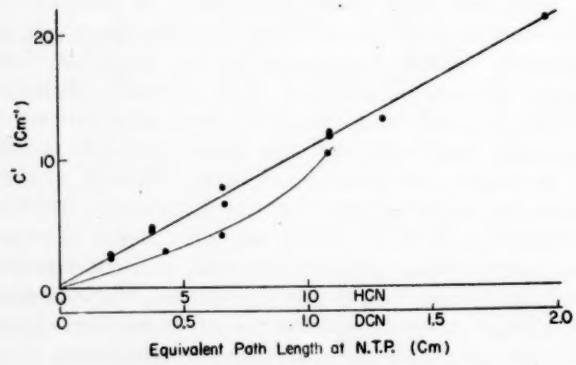

FIG. 1. Experimental intensity measurements for ν_1 of HCN and DCN. The lower curve is HCN.

[7] H. M. Foley, Phys. Rev. **69**, 628 (1946).

§ Thorndike and Wilson obtained 0.57d from the same calculation but apparently made an error.

[8] E. B. Wilson, Jr., and H. A. Wells, J. Chem. Phys. **14**, 578 (1946).

[9] Hornig, Hyde, and Adcock, J. Opt. Soc. Am. **40**, 497 (1950).

sorbed HCN so that Teflon gaskets were substituted. Under these circumstances there was a slight leakage problem so that runs were made at 10-minute intervals and extrapolated back to the filling time. In a typical extrapolation the measured areas were 12.48 cm² (11 minutes), 12.22 cm² (20 minutes), and 12.10 cm² (30 minutes). The extrapolated area at zero time was 12.6 cm².

When DCN was introduced into the cell, exchange took place, presumably the result of adsorbed water on the metal and windows. In this case the DCN band and the corresponding band of the HCN impurity were measured alternately and extrapolated separately to the areas at zero time. The DCN absorption was then corrected for the presence of the HCN.

The HCN was prepared by the reaction of H_2S with reagent grade $Hg(CN)_2$ and by the reaction of H_2O, P_2O_5, and KCN. The DCN was prepared from D_2O, P_2O_5, and KCN. The gas was mixed and diluted with N_2 to a pressure of one atmosphere in a glass bulb. Portions

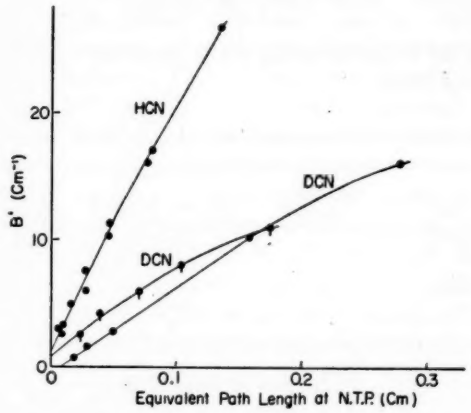

FIG. 2. Experimental intensity measurements for ν_2 of HCN and DCN.

of the diluted gas were then passed into the cell where nitrogen was added to a total pressure of 63 lb/in.² for pressure broadening. In the case of the lower gas pressures two successive dilutions were carried out.

Only a single band was studied at a time and, for each cell filling, the band was scanned two or three times. Thereafter the cell was evacuated, the gas mixture discarded, and an entirely new gas mixture used for the next measurement at another sample pressure. For all but ν_1 of HCN, the very weak band, two completely independent sets of runs were made, including separate preparations of the gas.

RESULTS

The results obtained are plotted in Figs. 1–3. The slopes of these curves are the quantities C (Figs. 1 and 3) and B (Fig. 2), and the slopes at zero equivalent path length are the desired quantities A. The curious upward curvature exhibited by the HCN curve in Fig. 1 will be discussed later. The failure of some of the

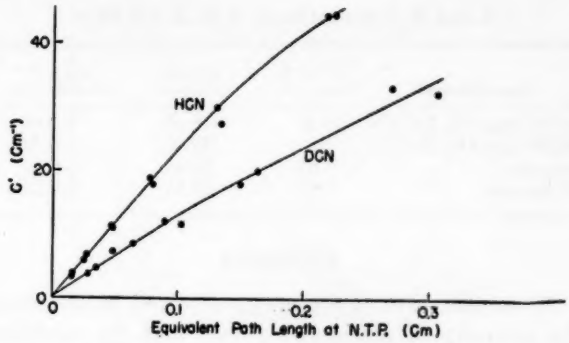

FIG. 3. Experimental intensity measurements for ν_3 of HCN and DCN.

curves to pass through zero is probably the result of base line errors and window absorption. In particular, the perfluoro grease used to seal the windows had an absorption band near ν_2 of DCN and on one of the two runs on this band such absorption could be observed on the records. So long as it was constant throughout the run it caused no error in the slopes. The limiting slopes of the two curves for ν_2 of DCN are nearly equal.

The derivative of the dipole moment with respect to the normal coordinate is given in terms of the quantity A by the expression[1]

$$A = N\pi/3c^2(\partial\mu/\partial Q)^2, \tag{4}$$

where A is in units of $cm^{-1}/(cm\ atmos)$, N is the number of molecules of gas in 1 ml at N.T.P. and c is the velocity of light in cm/sec. The measured values of A and $\partial\mu/\partial Q$ are given in Table I. For the bending vibration ν_2 the experimental A must be divided by two before applying Eq. (4) to take account of the double degeneracy.

These results may be compared with those of Foley who obtained for the dipole moment matrix element of the ν_2 transition (Foley's d) 1.47×10^{-19} cgs units. Since he apparently took no account of the degeneracy of ν_2, this value should be divided by $\sqrt{2}$, yielding

$$D/\sqrt{2} = |\mu_{01}| = \frac{\partial\mu}{\partial Q}(h/8\pi^2\nu)^{\frac{1}{2}} = 1.04\times10^{-19}\ \text{cgs units} \tag{5}$$

and

$$\pm\partial\mu/\partial Q = 52.5\ \text{esu}. \tag{6}$$

This result is 8.1 percent smaller than that given in Table I, but the results certainly agree to within the combined experimental errors. The agreement is particularly gratifying because the experimental methods used are so different.

TABLE I. Infrared intensities and $(\partial\mu/\partial Q)$'s in HCN and DCN.

	HCN			DCN		
Band	Frequency (cm^{-1})	A (cm^{-1}/cm atmos)	$\pm\partial\mu/\partial Q$ (esu)	Frequency (cm^{-1})	A (cm^{-1}/cm atmos)	$\pm\partial\mu/\partial Q$ (esu)
ν_1	2089	0.64	4.5	1921	12	20
ν_2	712	204	57	569	61	31
ν_3	3312	241	88	2629	136	66

TABLE II. Force constants of HCN and DCN.

Equation used	$k_1\times10^{-5}$ dyne/cm	$k_2\times10^{-5}$ dyne/cm	$k_{12}\times10^{-5}$ dyne/cm
HCN (8 and 9), DCN 8	5.62	18.66	−0.64
DCN (8 and 9), HCN 8	5.62	19.04	−0.24
Average	5.62	18.85	−0.44
Richardson	5.63	19.15	−0.22

ACCURACY

A consideration of the errors involved in measuring the intensity of absorption shows that the combined errors in the measurement of C (or B) probably do not exceed 10 percent. The uncertainty in the slope of the extrapolations is of the order of 3 to 5 percent in ν_1 and ν_3 of HCN and DCN, and 10 to 15 percent for ν_2 of both gases. The two independent determinations of the intensity of each band checked to from 4 to 10 percent. Therefore, the absolute accuracy of the intensities reported is probably in the range of ten to twenty percent; the moments and derivatives are probably accurate to better than ten percent.

POTENTIAL FUNCTION AND NORMAL COORDINATES

The most general form of the vibrational potential energy for the stretching vibrations of HCN and DCN in the harmonic approximation is

$$2V=k_1(\Delta r_1)^2+k_2(\Delta r_2)^2+2k_{12}\Delta r_1\Delta r_2. \quad (7)$$

Where V is the potential energy, Δr_1 and Δr_2 are the displacements from equilibrium of the C−H (or C−D) and C−N distances, k_1 and k_2 are the corresponding force constants and k_{12} is the interaction constant. From the standard treatment of the vibrational problem one then obtains

$$\lambda_1+\lambda_3=(\mu_H+\mu_C)k_1+(\mu_C+\mu_N)k_2-2\mu_C k_{12}, \quad (8)$$

$$\lambda_1\cdot\lambda_3=(\mu_H\mu_C+\mu_H\mu_N+\mu_C\mu_N)(k_1k_2-k_{12}^2), \quad (9)$$

where $\lambda_i=4\pi^2\nu_i^2c^2$, ν_i is the frequency in cm^{-1} and μ_i is the reciprocal of the mass of the ith atom. If it is assumed that the corresponding k's are identical in HCN and DCN, the frequencies of Table I may be used in Eqs. (8) and (9) to solve for the force constants. Because of the effect of anharmonicity two solutions can be obtained, depending on which set of three equations is used. The results are summarized in Table II together with those obtained by Richardson from the study of $DC^{12}N$ and $DC^{13}N$.[10] For lack of any better choice the averaged values were used in subsequent calculations. The normal coordinates for HCN are then

$$Q_1=0.528\times10^{-12}\Delta r_1+3.26\times10^{-12}\Delta r_2, \quad (10)$$

$$Q_3=1.141\times10^{-12}\Delta r_1-0.808\times10^{-12}\Delta r_2, \quad (11)$$

and those of DCN are

$$Q_1=1.290\times10^{-12}\Delta r_1+2.85\times10^{-12}\Delta r_2, \quad (12)$$

$$Q_3=1.213\times10^{-12}\Delta r_1-1.858\times10^{-12}\Delta r_2. \quad (13)$$

The bending motion is one-dimensional and the results obtained for the two molecules are

$$k_\theta=2.46\times10^{-12}\ (\text{HCN})\ \frac{\text{dyne cm}}{\text{radian}^2}$$
$$=2.48\times10^{-12}\ (\text{DCN}), \quad (14)$$

$$Q_2=1.17\times10^{-20}\Delta\theta\ (\text{HCN})$$
$$=1.47\times10^{-20}\Delta\theta\ (\text{DCN}), \quad (15)$$

where k_θ is the bending force constant and $\Delta\theta$ is the angle of bend.

TABLE III. Bond moments in HCN and DCN.

	$(d\mu/d\theta)/\mu$	$\pm\mu_{C-H}$	$\pm\mu_{C\equiv N}$
HCN	+	1.11d	1.82d
	−	−0.23	3.16
DCN	+	1.16	1.77
	−	0.24	2.69

TABLE IV. Bond moment derivatives in HCN and DCN.

Gas	$(\partial\mu/\partial Q_1)/(\partial\mu/\partial Q_3)$	$\pm\partial\mu/\partial r_1$ (d/A)	$\pm\partial\mu/\partial r_2$ (d/A)
HCN	+	1.025	−0.562
	−	0.977	−0.856
DCN	+	1.055	−0.664
	−	0.547	−1.786

BOND MOMENTS

If μ_{C-H} and $\mu_{C\equiv N}$ are the dipole moments of the respective bonds, the dipole moment of the molecule is

$$\mu_{HCN}=\mu_{C-H}+\mu_{C\equiv N}. \quad (16)$$

The moment developed perpendicular to the axis when the molecule is bent is

$$\frac{d\mu}{d\theta}=\mu_{C-H}\frac{\partial\alpha}{\partial\theta}-\mu_{C\equiv N}\frac{\partial\beta}{\partial\theta}, \quad (17)$$

where α and β are the angles between C−H and C≡N bonds in the bent molecule and the axis of the molecule at equilibrium. The positive sign of both bond moments is taken in the same direction. From Table I and Eq. (15), $d\mu/d\theta$ for HCN and DCN is ±0.669d and ±0.460d, respectively, and Smyth[11] has determined μ_{HCN} as ±2.93d. If Eqs. (16) and (17) are solved simultaneously and it is assumed that μ_{DCN} is equal to μ_{HCN}, the results given in Table III are obtained.

Comparison of the results for HCN and DCN shows that the positive value of the ratio is correct;

[10] W. S. Richardson, J. Chem. Phys. **19**, 1213 (1951).

[11] C. P. Smyth and K. B. McAlpine, J. Am. Chem. Soc. **56**, 1697 (1934).

that the mean bond moment of the C—H and C—D bonds is ±1.13d and of the C≡N bond is ±1.80d.

In solving Eqs. (17) and (18) simultaneously we have assumed that the effective moments in the bending vibration are equal to those in the equilibrium configuration. However, the validity of this assumption (which has been customary heretofore) is a serious question in the interpretation of infrared intensities and it is not at all obvious that it must be correct. For example, if the hybridization about the carbon atom does not change when the proton is displaced perpendicular to the axis of the molecule, the effective moment would be just that of the proton, er_{C-H} or 5.06d, and independent of the electronic charge distribution. If the hybridization does change, one can still not be certain that the moment of the deformed bond is the same as that at equilibrium since the amplitude of deformation in the first vibrational state is about 15°. Nevertheless, the fact that the moments obtained in HCN and DCN check so well, although the amplitudes differ considerably, supports the original assumption.

Alternatively, these moments can be calculated without assumption or recourse to dipole moment data from the solution of Eq. (17) for both molecules. This yields $\mu_{C-H}=1.14$d, $\mu_{C\equiv N}=1.75$d and predicts a dipole moment of 2.89d for the molecule, in excellent agreement with that found directly by Smyth.

Although we cannot establish the absolute sign of the dipole moments, these results do demonstrate that the sign of the H—C and C≡N dipoles is the same in HCN, i.e., if C is the positive end of the C≡N dipole, then H is the positive end of the H—C dipole. This is of some importance since there is considerable doubt about the sign of the C—H dipole whereas it seems quite certain that carbon is the positive end of the C≡N dipole. Most of the quantum-mechanical arguments which have been advanced with regard to the moment of covalent bonds reduce essentially to the statement that the atom with the smaller covalent radius, in this case nitrogen, is negative when only the bonding electrons are considered. Since the moment of the unshared pair in nitrogen enhances this effect, there appears to be little reason to doubt that nitrogen is indeed the negative end of the C≡N dipole. The same conclusion is reached from electronegativity arguments. Consequently, it is highly probable that the hydrogen is positive in the C—H dipole of HCN.

THE CHANGE IN BOND MOMENT WITH INTERNUCLEAR DISTANCE

The bond moment derivatives are given by the expression

$$\frac{\partial\mu}{\partial r_i}=\frac{\partial Q_1}{\partial r_i}\frac{\partial\mu}{\partial Q_1}+\frac{\partial Q_2}{\partial r_i}\frac{\partial\mu}{\partial Q_2}. \qquad (18)$$

From Table I and Eqs. (10)–(13), two values of $\partial\mu/\partial r_i$ may be calculated for each gas, depending on whether the $\partial\mu/\partial Q$'s have the same or opposite sign. The results obtained are given in Table IV. It is clear

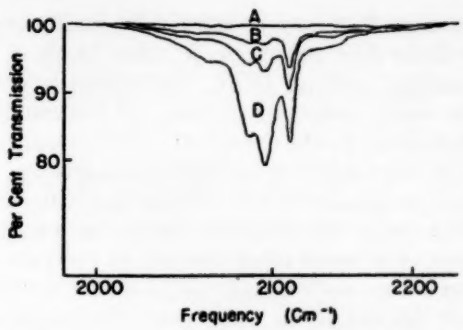

FIG. 4. Infrared spectrum of ν_1 in HCN with nitrogen added to a total pressure of 63 lb/in.² The path length is 26 cm and the HCN pressures used were (*A*) 0.00 atmos (*B*) 0.18 atmos, (*C*) 0.28 atmos, and (*D*) 0.50 atmos.

that the positive value of the radio is the correct one. If the intensities in HCN are calculated from the values of $\partial\mu/\partial r_i$ found for DCN, the calculated intensity of ν_3 agrees to 8 percent with that found experimentally whereas the calculated intensity of the very weak band ν_1 is four times less than was found. Because this band is so weak, however, the *difference* between calculated and observed values is within the experimental error. Nevertheless, it will be shown later that there is good reason to believe that some of the absorption ascribed to ν_1 is probably the result of HCN dimer, so that the DCN value should be the more reliable. Consequently, we conclude that $\partial\mu/\partial r_{C-H}=\pm1.05$d/A, that $\partial\mu/\partial r_{C\equiv N}=\mp0.66$d/A and that the signs of the two derivatives are opposite.

EVIDENCE FOR HCN DIMER

The spectra obtained in the vicinity of the fundamental frequency ν_1 at three different pressures of HCN are illustrated in Fig. 4. It is readily seen that whereas at low pressures the high frequency peak is most intense, the central peak becomes more intense at high HCN pressures. The relative heights of the three peaks are compared with the sample pressure and its square in Table V. It is apparent that although the intensity of the peak at 2110 cm^{-1} varies directly with the pressure as expected, the intensity of the other two peaks depends on the square of the pressure.

This p^2 dependence can only arise if these peaks are the C≡N stretching vibrations of HCN dimer in equilibrium with the monomer, for which indirect evidence has been available previously from vapor density measurements[12] and from dipole moment

TABLE V. Relative intensity of the peaks in HCN as a function of pressure.[1]

p	p^2	2087 cm^{-1}	2096 cm^{-1}	2110 cm^{-1}
0.36	0.13	0.17	0.14	0.37
0.56	0.31	0.35	0.33	0.56
1.0	1.0	1.0	1.0	1.0

[12] W. F. Giauque and R. A. Ruehrwein, J. Am. Chem. Soc. **61**, 2626 (1939).

measurements.[11] It may be asked why similar evidence for the dimer does not appear in other bands or in the corresponding band of DCN. The reason is probably that the nearly vanishing intensity of this band is the result (as shown by the calculation of its intensity from the DCN intensities) of accidental cancellation of the moments produced in the C−H and C≡N bonds. Any slight change in the vibration amplitudes would make this band very much more intense. In the case of the other bands no such enhancement of the intensity is expected. Moreover, in these cases the bands of the dimer would have to be observed against a background of strong monomer absorption rather than the very weak absorption of ν_1 of HCN.

THE ANOMALOUS SHAPE OF ν_1 IN HCN

It has been pointed out previously[13] that the explanation given by Choi and Barker[14] for the presence of three peaks in this region cannot be correct. In the preceding paragraph it was shown that the intensity of the two low frequency peaks depends on p^2 and must be the result of HCN dimer. The remainder of the bands in Fig. 4 (which agree with the high resolution curves of Choi and Barker) consist of a strong peak at 2110 cm^{-1} and wings extending from the neighborhood of 2025 cm^{-1} to 2150 cm^{-1}. This structure is almost certainly because of the Q-branch of the second overtone $3\nu_2$ of the bending vibration superimposed on the normal $P-R$ structure of the parallel band ν_1 with a band center at 2089 cm^{-1} as found by Kastler[15] in the Raman spectrum of HCN gas.

This view is supported by the fact that the width of the wings is almost identical with that found in the other parallel band ν_3. To check the reason for the appearance of $3\nu_2$ in such great intensity, the spectrum of 0.35 atmos of DCN, where $3\nu_2$ does not coincide in frequency with ν_1, was studied, and it shows no absorption as great as 2 percent in the region where $3\nu_2$ is expected. Consequently, except for interaction with ν_1, $3\nu_2$ would not be expected to be nearly as intense in HCN as it appears. It must, therefore, derive most of its intensity from ν_1 as a consequence of Coriolis interaction between levels differing by one in their rotational quantum number.

DISCUSSION

The effective dipole moment of the C−H bond found in HCN and DCN, 1.13d, is very much greater than that found in methane, 0.31d. Although these moments include moments induced in the rest of the molecule as well as the "true" moments, the difference is probably chiefly the result of the use of an sp orbital from the triply bonded carbon in HCN instead of an sp^3 orbital as in methane. Evidence for this difference in hybridization is also found in the decreased internuclear distance, 1.06A *vs* 1.09A, and the high stretching force constant, 5.62×10^5 dynes/cm *vs* 4.50×10^5 dynes/cm. It would be interesting to have similar measurements on the iso-electronic molecule acetylene, whose C−H bonds should be very similar to that in HCN.‖

This difference in dipole moment is consistent with the theoretical expectations[15,16] which lead to an increasingly positive polarity of H as the hybridization changes from sp^3 to sp. A question that arises is the polarity in methane where Coulson[17] predicts a negative hydrogen. In this connection, the fact that the C−H moment in ethylene, with the intermediate hybridization sp^2 is intermediate between ethane and HCN rather suggests that the hydrogen is also positive in methane, since if the moment passed through zero as the hybridization varied it might be expected to be small in ethylene.

The value found for the change of C−H bond moment with distance, 1.05d/A, is also greater than that found in methane, 0.56d/A. The rate of change of C≡N moment, 0.66d/A, is very nearly that found by Nixon in cyanogen, 0.72d/A, but considerably smaller than the range, 1.03 to 1.12d/A, found for cyanogen chloride. Both the cyanogen and cyanogen chloride values are somewhat uncertain because the value of the interaction constant in the potential energy expression is unknown, but it seems fairly certain that $\partial\mu/\partial r_{C\equiv N}$ is greater in CNCl. This can be related to the much greater polarizability of the C−Cl bond, leading to considerable induced moments. An alternative statement is that the increase may be the result of the contribution of the resonance form $Cl^+=C=N^-$ as the C≡N bond is stretched whereas no corresponding resonance forms are important in $(CN)_2$ or HCN.

Since the stretching of the C≡N bond increases the contribution of the resonance structure $H-C^+=N^-$ it seems likely that $\partial\mu/\partial r_{C\equiv N}$ is positive. If this is correct, our measurements lead to the conclusion that $\partial\mu/\partial r_{C-H}$ is negative, the moment decreasing as the bond is stretched, just as in the case of HCl.[18] This conclusion is also consistent with the resonance picture since hydrogen should become more negative as the hybridization is changed from sp to sp^2. It may be noted, finally, that if the chief resonance structure is $H-C^+=N^-$ for which both the C−H and C−N distances are greater than at equilibrium, the negative cross term in the potential function becomes reasonable.

ACKNOWLEDGMENT

One of us (G. E. H.) is indebted to the E. I. du Pont de Nemours and Company for its assistance in the form of a graduate fellowship.

[13] R. E. Hoffman and D. F. Hornig, J. Chem. Phys. **17**, 1163 (1949).
[14] K. N. Choi and E. F. Barker, Phys. Rev. **42**, 777 (1932).
[15] A. Kastler, Compt. rend. **194**, 858 (1932).

‖ *Note added in proof:*—From infrared dispersion Kelly, Rollefson, and Schurin, J. Chem. Phys. **19**, 1595 (1951) have found $\mu_{C-H}=\pm1.05d$ and $\partial\mu/\partial r_{C-H}=\pm.52d/A$ in acetylene.
[15] D. Z. Robinson, J. Chem. Phys. **17**, 1022 (1949).
[16] C. R. Mueller and H. Eyring, J. Chem. Phys. **19**, 193 (1951).
[17] C. A. Coulson, Trans. Faraday Soc. **38**, 433 (1942).
[18] R. P. Bell and I. E. Corp, Trans. Faraday Soc. **34**, 1209 (1938).

The Azomethane Induced Oxidation of Propane*

MILTON D. SCHEER AND H. AUSTIN TAYLOR
Research Division, University Heights and Department of Chemistry, New York University, New York 53, New York
(Received July 3, 1951)

The effect of methyl radicals from the photolysis of azomethane on propane-oxygen mixtures in Pyrex vessels has been shown to include a slow oxidation in the temperature range 35° to 200°C and cool flames at 250°C. Azomethane decomposed thermally induces cool flames in propane-oxygen mixtures at 255° and 270°C, temperatures below those at which cool flames occur in the system propane-oxygen alone. A rapid photo-oxidation has been observed in a quartz vessel in the temperature range 230 to 250°C.

INTRODUCTION

HYDROCARBON oxidations are generally accepted as involving a degenerate branched chain mechanism.[1] The complexity of possible chain participants is such that in no single example may it be said that the detailed mechanism is completely known. This paper describes a study of the effect of introducing methyl radicals into a propane-oxygen mixture. The methyl radicals were derived both by pyrolysis and by photolysis of azomethane. In particular, the region of onset of cool flames[2] in propane oxidation was studied.

It has been well established that both the pyrolysis and photolysis of azomethane involve initially the production of methyl radicals. Rice and Evering[3] removed lead and antimony mirrors by the pyrolysis while Blacet and Taurog[4] similarly used the photolysis of azomethane. Jahn and Taylor[5] showed that nitric oxide almost completely suppresses hydrocarbon production in azomethane pyrolysis, a result similar to that found in the photolysis.[6] Finally the decomposition of numerous organic materials has been induced by the thermal decomposition of azomethane[7] explicable on the basis of the introduction of methyl radicals. Since azomethane decomposes rapidly at the temperatures of the occurrence of cool flames in propane-oxygen systems, namely 300–400°C, and absorbs light effectively for photolysis around 3400A in which region propane-oxygen mixtures are transparent, it is possible to control the initiating azomethane decomposition with a minimum disturbance of the propane system. Observed changes in the propane-oxygen system may thus be traced to the methyl radical introduction.

EXPERIMENTAL

Azomethane was prepared according to the method described by Jahn[8] and stored as the cuprous chloride complex which was heated to liberate the gas as required. Cp propane and oxygen were taken from tanks without further purification.

The reaction vessel was a Pyrex cylinder 925 ml in volume, 60 mm in diameter with a wall thickness of 2.4 mm. This thickness transmits only at wavelengths greater than 3000A. A high pressure Hanovia AH-3 mercury arc backed by a parabolic aluminum reflector was used as light source when required. A hot air oven using forced draft and regulated by a bimetallic thermoregulator served in both the thermal and photochemical runs. A 10-cm quartz window separated the arc from the oven. The reaction vessel was connected to a manifold leading to a vertical manometer, a sloping manometer, a McLeod gauge, and a Toepler pump. Evacuation of the system was achieved by a two-stage mercury diffusion pump backed by a Hypervac oil pump. The sloping manometer at an incline of 11.0° covered the range 0–200 mm. It was graduated in 0.25-mm units and could be read to 0.05 mm. The Toepler pump delivered the product gases to a modified Burrell gas analyzer after drawing them from the reaction vessel through a trap in liquid nitrogen. The noncondensable products consisted of oxygen, nitrogen, traces of carbon monoxide, hydrogen, and a hydrocarbon, which combustion showed was propane. Oxygen was absorbed in alkaline pyrogallol. The carbon monoxide and hydrogen were oxidized over copper oxide. The propane was oxidized catalytically with a known amount of added oxygen and nitrogen was obtained by difference from the total volume. The condensable fraction on vaporization always left several drops of liquid remaining in the trap. Anhydrous copper sulfate on addition to this liquid turned blue at once, indicating the presence of water and on standing turned a greenish-brown indicating a reduction to the cuprous state probably by aldehyde. The condensable fraction after vaporization was analyzed for residual azomethane by absorption in acid stannous chloride, for carbon dioxide by absorption in potassium hydroxide solution, for unsaturates by bromine water, and the residue was almost wholly

* Abstract from a dissertation presented in partial fulfillment of the requirements for the degree of Doctor of Philosophy at New York University, June 1951. The work described in this paper was done with the support of the Office of Naval Research, Dept. of Navy and Office of Air Research, Dept. of Air Force under Contract N6-ori-11, Task Order 2, as part of Project Squid.

[1] N. Semenoff, Z. physik. Chem. **11B**, 464 (1930).
[2] D. M. Newitt and L. S. Thornes, J. Chem. Soc. 1656 (1937).
[3] F. O. Rice and B. L. Evering, J. Am. Chem. Soc. **55**, 3898 (1933).
[4] F. E. Blacet and A. Taurog, J. Am. Chem. Soc. **61**, 3024 (1939).
[5] F. P. Jahn and H. A. Taylor, J. Chem. Phys. **7**, 474 (1939).
[6] Davis, Jahn, and Burton, J. Am. Chem. Soc. Soc. **60**, 10 (1938).
[7] D. V. Sickman and O. K. Rice, J. Chem. Phys. **4**, 239, 608 (1936); A. O. Allen and D. V. Sickman, J. Am. Chem. Soc. **56**, 2031 (1934); Rice, Walters, and Knoff, J. Chem. Phys. **8**, 259 (1940).
[8] F. P. Jahn, J. Am. Chem. Soc. **59**, 1761 (1937).

TABLE I. Azomethane photo-induced oxidation of propane.*

Temp °C	Time (hr)	Initial Azo	Initial C_3H_8	Initial O_2	$\Delta P/\Delta t$ (mm/hr)	Reacted Azo	Reacted C_3H_8	Reacted O_2	Formed N_2	Formed Condens	Formed CO	Formed H_2
35	1	0.42	2.6	3.5	0.40	0.12	0.07	0.11	0.11	0.29	0.01	0.00
	2	0.45	2.6	3.4	0.40	0.15	0.12	0.13	0.15	0.35	0.01	0.01
	3	0.47	2.6	3.5	0.37	0.15	0.10	0.14	0.14	0.36	0.01	0.01
	4	0.32	2.6	3.5	0.31	0.16	0.11	0.18	0.14	0.40	0.01	0.01
	5	0.40	1.4	2.1	0.24	0.21	0.17	0.25	0.19	0.53	0.02	0.01
	5	0.67	2.7	4.8	0.35	0.30	0.29	0.34	0.30	0.69	0.01	0.01
	5	0.46	8.2	6.9	0.46	0.22	0.18	0.25	0.23	0.49	0.01	0.01
	5	0.43	2.6	3.5	0.38	0.22	0.16	0.26	0.18	0.45	0.01	0.01
85	5	0.05	0.3	1.6	0.00	0.05	0.03	0.04	0.05	0.03	0.01	0.01
	5	0.43	1.5	2.4	0.39	0.21	0.17	0.24	0.17	0.47	0.02	0.01
	5	0.35	1.5	3.4	0.65	0.13	0.14	0.19	0.14	0.44	0.02	0.02
	5	0.59	8.3	7.0	0.72	0.30	0.23	0.35	0.37	0.55	0.02	0.01
135	5	0.41	1.4	2.2	0.74	0.19	0.18	0.24	0.17	0.54	0.03	0.02
	5	0.44	8.5	6.9	0.70	0.17	0.17	0.25	0.19	0.60	0.03	0.02
185	5	0.43	1.5	2.3	0.60	0.22	0.18	0.24	0.20	0.46	0.03	0.01

* All quantities are in millimoles.

propane. Analysis thus yielded directly the amounts of azomethane, propane, and oxygen which had reacted. The pressure, volume, and temperature on completion of a run being known, the total number of moles of gas in the reaction vessel could be calculated. From the volume and analysis of the noncondensable products, the number of moles of each of these present is calculable. Similarly, from the volume of the condensable fraction after vaporization and its analysis the number of moles of azomethane, carbon dioxide and so on, are known. The difference between the total number of moles at the conclusion of a run and the moles specifically recovered gives the number of moles of liquid condensate even though no quantitative analysis of the liquid was made.

RESULTS

The azomethane photo-induced oxidation of propane which occurs in the range 35° to 185°C is a slow process. The reaction exhibits a small pressure increase of about 0.5 mm per hour. The products formed are condensables, containing water and aldehydes and traces of carbon monoxide and hydrogen. Table I lists the data obtained in these runs. For an average run in which 0.2-millimole azomethane is photolyzed in five hours, the rate of the slow oxidation is approximately 10^{-11} moles cc^{-1} sec^{-1}.

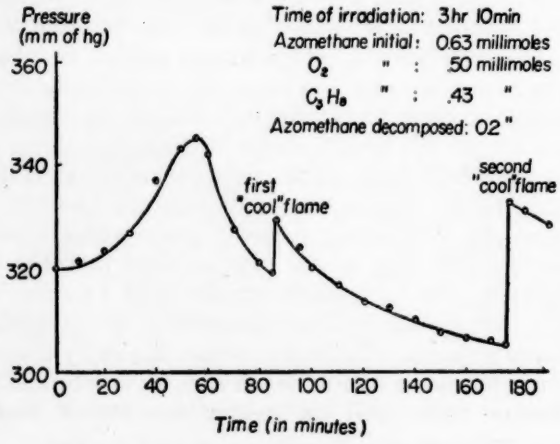

FIG. 1. Pressure time curve for experiment 81-C.

Above 200°C the photo-induced oxidation proceeds more rapidly with increasing temperature. In addition to the products formed in the slow oxidation, carbon dioxide and unsaturated hydrocarbons were detected. At 250°C "cool flames" were observed. Figure 1 shows a pressure-time curve and Table II contains the analytical data from runs at 200°, 230°, and 250°C.

Since azomethane decomposes thermally at temperatures above 250°C by a free radical mechanism similar to the photolytic process, the possibility of inducing cool flames thermally was explored. An equimolar mixture of propane and oxygen at a total pressure of 325 mm was introduced into the reaction vessel at 300°C. A cool flame with a rapid pressure change of 60 mm was observed after an induction period of about 20 minutes. This is in good agreement with the observations of Newitt and Thornes.[2]

A similar equimolar propane-oxygen mixture containing about six percent azomethane was introduced into the reaction vessel at 270°C which according to Newitt and Thornes is below the normal limit for cool flames. A very intense cool flame, a mild explosion, was observed after a 60-min induction period, with a pressure change of 240 mm. A similar run at 255°C showed a slight cool flame with a pressure change of 10 mm after an induction period of 140 min. An appreciable pressure increase occurred during this induction period. A summary of the results is given in Table III.

TABLE II. Azomethane photo-induced oxidation above 200°C

Temp °C	200	230	250
Time hr	3	3	3.17
Azo millimoles	0.57	0.60	0.63
O_2 millimoles	4.1	4.2	5.0
C_3H_8 millimoles	4.3	4.3	4.3
Av $\Delta P/\Delta t$, mm/hr	0.83	1.17	cool flames
Azo reacted	0.17	0.20	0.22
O_2 reacted	0.24	0.43	4.8
C_3H_8 reacted	0.27	0.36	1.9
N_2 formed	0.14	0.14	0.25
Condensable formed	0.50	0.76	4.7
H_2 formed	0.01	0.01	0.07
CO formed	0.03	0.05	1.6
CO_2 formed	0.03	0.10	0.57
Unsat formed	0.06	0.09	0.14

In an attempt to increase the production of alkyl radicals and at the same time render intermediates less stable photolytically, a quartz reaction vessel, spherical in shape, with a volume of 338 cc and a surface to volume ratio of 1.1 cm^{-1} was used. The surface to volume ratio of the Pyrex cell was 0.7 cm^{-1}. Runs were made at 230°, 240°, and 250°. It is possible that some photosensitization might occur under these circumstances but the resonance emission of the lamp used is very small. The rate of oxidation in all three cases was more rapid than in the corresponding runs in the glass vessel although even at 250°C no cool flame was observed. The pressure-time plots are shown in Fig. 2 and the analytical data in Table IV.

DISCUSSION

Examination of the data in Table I for the reaction at temperatures below 190°C, shows that the rate of propane oxidation is independent of temperature, of total pressure and of the partial pressures of propane and oxygen. The rate varies linearly with the rate at which azomethane decomposes. When due allowance is made for the poor precision of the small amounts of propane and of oxygen reacting, each deduced as the difference of two relatively large quantities, it is seen that the rate of oxygen consumption is roughly fifty percent greater than that of propane. Furthermore, the ratio of azomethane to propane reacting is, on the average, slightly greater than unity.

The photolysis of azomethane yields two methyl radicals per molecule decomposed. From the work of Vaughan and co-workers,[9] methyl radicals in the presence of oxygen under conditions similar to those used here, react rapidly to form methyl peroxyl radicals,

TABLE III. Thermally-induced reaction above 250°C.

Temp °C	300	270	255
Azo millimoles	0.00	0.59	0.44
O_2 millimoles	4.56	4.96	4.31
C_3H_8 millimoles	4.39	5.03	4.25
Induction min	20	60	140
ΔP(induction) mm	0	0	17
ΔP(cool flame) mm	60	240	10
Azo reacted	–	0.23	0.20
O_2 reacted	4.31	4.40	3.84
C_3H_8 reacted	2.18	2.55	1.52
N_2 formed	–	0.29	0.27
Condensable formed	4.68	4.07	4.33
H_2 formed	0.11	2.70	0.03
CO formed	2.24	3.76	0.48
CH_4 formed	0.03	2.59	0.60
C_2H_6 formed	0.17	0.08	0.06
CO_2 formed	0.70	0.39	0.66
Unsat formed	0.54	0.93	0.24

which, in turn, are rapidly transformed into methoxyl radicals

$$CH_3N{:}NCH_3+h\nu\rightarrow 2CH_3+N_2, \quad (1)$$

$$CH_3+O_2\rightarrow CH_3O_2, \quad (2)$$

$$2CH_3O_2\rightarrow 2CH_3O+O_2. \quad (3)$$

Methoxyl radicals are shown to act readily as hydrogen acceptors to form methyl alcohol. It seems probable then, that methoxyl radicals are responsible for the attack on propane,

$$CH_3O+C_3H_8\rightarrow CH_3OH+C_3H_7, \quad (4)$$

the resulting propyl radicals, like methyl, reacting rapidly with oxygen,

$$C_3H_7+O_2\rightarrow C_3H_7O_2. \quad (5)$$

Walsh[10] has shown that attack of hydrogens on secondary atoms is about three times more probable than attack on the terminal hydrogens; the propyl radical is therefore CH_3CHCH_3 and the propyl peroxyl, $CH_3CH(OO)CH_3$.

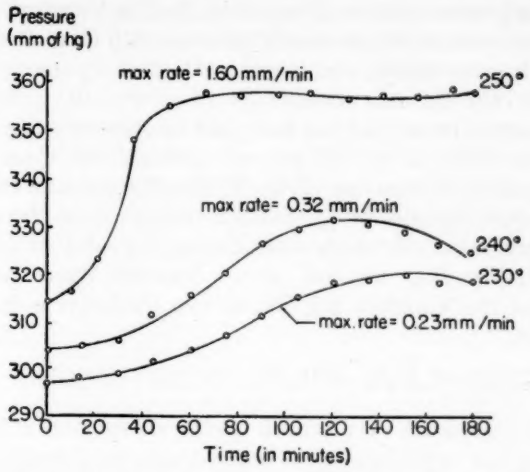

FIG. 2. Pressure time curves for experiment 82 A, B, C.

The low yield of propane oxidation and the approximately unit ratio of azomethane to propane reacting suggest that the reaction under the conditions studied is probably not a chain reaction, or at most has a very short chain length. A possible reaction of the propyl peroxyl radical at higher temperatures, frequently postulated in the direct oxidation of propane, is its abstraction of hydrogen from a propane molecule to produce the hydroperoxide. Such a reaction, by producing a propyl radical, being chain forming, cannot be occurring extensively in this low temperature range. An alternative reaction of the propyl peroxyl is dissociation into acetaldehyde and methoxyl. This too, being chain forming, must not occur appreciably at lower temperatures. The ultimate fate of methoxyl radicals in the work of Vaughan is accounted

$$2CH_3O\rightarrow CH_3OH+HCHO,$$

although further reaction of methoxyl and formaldehyde to yield methyl alcohol and carbon monoxide is assumed in order to account for the products found.

TABLE IV. Photo-induced oxidation in a quartz vessel.

Temp °C	230	240	250
Time hr	3	3	3
Azo millimoles	0.35	0.30	0.31
O_2 millimoles	1.90	1.98	1.96
C_3H_8 millimoles	1.91	1.92	2.00
Max $\Delta P/\Delta t$ mm/min	0.23	0.32	1.60
Azo reacted	0.20	0.18	0.22
O_2 reacted	1.73	1.79	1.86
C_3H_8 reacted	0.74	0.77	0.94
N_2 formed	0.26	0.21	0.22
Condensable formed	2.27	2.28	2.66
H_2 formed	0.02	0.01	0.03
CO formed	0.21	0.37	0.50
CO_2 formed	0.21	0.26	0.17
Unsat formed	0.04	0.04	0.05

[9] Raley, Porter, Rust, and Vaughan, J. Am. Chem. Soc. **73**, 15 (1951).

[10] A. S. Walsh, Trans. Faraday Soc. **42**, 269 (1946).

The present system differs from that of Vaughan and co-workers in the presence of propane with its secondary hydrogens which are readily attacked by methoxyl with the ultimate production of propyl. It is to be expected from what has been said above concerning the dissociation of propyl peroxyl radicals and from the sequence of reactions (1) to (5) that the concentrations of methoxyl and propyl peroxyl radicals would become comparable with each other during the reaction and a radical-ending reaction occur between them rather than the Vaughan reaction of two methoxyl radicals, thus,

$$CH_3O+C_3H_7O_2\rightarrow CH_3OH+HCHO+CH_3CHO. \quad (6)$$

This sequence of reactions yields an over-all rate of propane oxidation dependent only on the intensity of the light absorbed by the azomethane as is observed. The Vaughan reaction would make the propane oxidation dependent on the propane concentration which is not found.

Reactions (1) to (6) thus account for the observations derivable from the data in Table I, namely, the reaction rate is independent of the partial and total pressures, is independent of temperature and depends only on the azomethane. A molecule of propane is oxidized indirectly to propyl peroxyl through a reaction with methoxyl and thence to acetaldehyde by reaction with a second methoxyl, the two methoxyls resulting from one molecule of azomethane. The ratio of one found for azomethane to propane is thus explained. The oxygen consumed should be twice the amount of propane reacting whereas it is only about fifty-percent greater. The condensables expected from the above mechanism should equal four times the propane reacting, whereas the average of all runs is only three. This may be in part experimental error though it is probable that the postulated mechanism is oversimplified and that the reaction is more complex than pictured. Thus the presence of water among the condensables might suggest a hydroperoxide decomposition. Vaughan specifically states that the formation of methyl hydroperoxide cannot definitely be ruled out as a possible reaction though the amount of water found did not warrant its consideration as a major product. Similarly, in the present system, the water found could originate from oxidation of formyl radicals resulting from secondary reactions of methoxyl and formaldehyde. Until more detail is available on the nature of the products and their quantities, it serves no purpose to speculate on further refinements of the mechanism in the lower temperature range.

Above 200°C Table II shows that the course of reaction is quite different from that below 190°C. The ratio of propane to azomethane reacting is greater than unity and increases steadily with increase in temperature. Cool flames are observed at 250°C and considerable amounts of oxides of carbon and unsaturated hydrocarbons are formed. The reaction parallels that found in the thermal propane oxidation, proceeding comparably, however, at a lower temperature presumably sensitized by methoxyl radicals. The thermal reaction has been attributed to a chain reaction with some chain branching resulting from reaction between peroxides and aldehydes.[11] There is, however, no general agreement on the mechanism and it may not be amiss to speculate on a possibility not so far considered. It is well known that the nature of the surface, especially a KCl-coating, has a marked effect on peroxides and also on acetaldehyde oxidation. It appears possible that aldehydes may poison the walls preventing a heterogeneous decomposition of peroxides and favoring a gas phase reaction leading to chain branching and a nonstationary state. Such reactions being exothermal, the system will self-heat to such temperatures that a molecular decomposition of peroxides into aldehyde and water becomes effective and applies a brake causing the process to come to a halt. Peroxide build-up occurs again and a repetition of events results in successive cool flames until the amounts of fuel are used up. In the run described in Fig. 1 about 95 percent of the initial oxygen had reacted after the second cool flame.

It is felt that this mechanism could receive support in the present work by accounting for the pressure changes shown in Fig. 1. It serves also to correlate other phenomena previously observed in many systems. Chamberlain and Walsh[12] have shown that formaldehyde inhibits the decomposition of *t*-butyl hydroperoxide at 200°C. Thus if the peroxide decomposes both homogeneously and heterogeneously as these authors suggest, the addition of aldehyde should inhibit the heterogeneous decomposition and consequently the over-all rate would be decreased as is observed. Despite a claim by Cullis and Hinshelwood[13] that added acetaldehyde is without effect in the combustion of pure hexane, there are numerous references in the literature to the accelerating effect of added acetaldehyde in hydrocarbon oxidations, a recent one is by Antonovski[14] on propane oxidation which shows that the effect decreases with increasing temperature. This conceivably could result from a decreased wall poisoning as the temperature is increased. Further experimentation is required, with particular attention to the elucidation of surface effects at present not adequately accounted for, before a definite opinion can be expressed on the suggested machanism or the precise steps involved. The same sequence is presumably present in the thermally-induced cool flames at temperatures above 250°C with reaction (1) occurring thermally. The appearance of cool flames in the sensitized system, at temperatures

[11] See B. Lewis and G. von Elbe, *Combustion, Flames and Explosions of Gases* (Academic Press, New York, 1951), p. 172.

[12] G. H. N. Chamberlain and A. D. Walsh, *Third Symposium on Combustion, Flame and Explosion Phenomena* (The Williams and Wilkins Company, Baltimore (1949)), p. 381.

[13] C. F. Cullis and C. N. Hinshelwood, Disc. Faraday Soc. 2, 117 (1947).

[14] V. L. Antonovski and V. Ya. Shtern, Doklady Akad. Nauk S.S.S.R. **78**, 303 (1951).

lower than those found in the unsensitized propane oxidation reflects the greater difficulty of chain initiation in the latter system.

The reaction in the quartz vessel where the rate even at 230°C far exceeds that in the Pyrex vessel is undoubtedly to be attributed to the increased illumination. The rate at 240°C is increased by 40 percent over that at 230°C while at 250°C a better than fivefold increase over that at 240°C is found. This effect must be caused by the possibility of chain-branching setting in at 250°C as was observed in the runs in Pyrex where cool flames were found. That no cool flame was found in quartz may be the result of the larger surface to volume ratio tending to break chains as rapidly as formed leading to a stable velocity. There can be no doubt, however, judging from the large increase in rate at 250°C, that some process is occurring that was relatively unimportant at 230°C. It would appear that this process is the chain branching process usually associated with peroxide breakdown.

THE JOURNAL OF CHEMICAL PHYSICS VOLUME 20, NUMBER 4 APRIL, 1952

The Lennard-Jones 12:6 Potential and the Viscosity of Gases

E. WHALLEY* AND W. G. SCHNEIDER
National Research Council, Ottawa, Canada

(Received December 10, 1951)

The viscosity of several simple gases is discussed with reference to the Lennard-Jones 12:6 potential. The predicted and experimental viscosities agree well at moderate temperatures, but the agreement is not so good at higher temperatures, and for some gases, no possible choice of the force parameters will predict the correct temperature variation of the viscosity at high temperatures.

1. INTRODUCTION

THE Lennard-Jones 12:6 (abbreviated to 12:6) potential function for the interaction between molecules

$$U(r)=4\epsilon\{(r_0/r)^{12}-(r_0/r)^6\}, \tag{1}$$

where $U(r)$ is the potential energy of two molecules separated by the distance r, ϵ is the depth of the potential energy minimum, and r_0 is the low velocity collision diameter, i.e., the value of r for which $U=0$ has had some success in correlating the compressibility, and the critical and transport properties of gases over moderate temperature ranges.[1,2] In this paper we report an investigation of the validity of this model for gases with particular reference to viscosity over a wide temperature range.

The transport properties which might have been chosen for this investigation are viscosity, thermal conductivity, concentration diffusion, and thermal diffusion. Data on thermal conductivity, concentration diffusion, and thermal diffusion are rather scanty. They are seldom accurate to better than several percent and are not usually accurate enough for good assignments of the potential parameters. In addition, the thermal conductivity of all but monatomic molecules depends upon the rate of interchange between internal and translational energy. It can therefore be used in assigning the parameters only to the inert gases. These transport properties, however, can be calculated using the parameters obtained from other data and may provide a useful check. Data on viscosity, on the other hand, are good and exist over wide temperature ranges. We therefore confine ourselves to using the viscosity to evaluate the potential parameters.

2. EVALUATION OF PARAMETERS

The coefficient of viscosity η of a single gas is given by[1]

$$\eta=2.6693\times10^{-5}(MT)^{\frac{1}{2}}r_0^{-2}A(\tau), \tag{2}$$

where M is the molecular weight, T is the temperature, r_0 is the low velocity collision diameter in angstroms, and $A(\tau)$ is a function of $\tau(=kT/\epsilon)$ given by

$$A(\tau)=V/W(2)(2), \tag{3}$$

where V and $W(2)(2)$ are functions of τ tabulated by Hirschfelder, Bird, and Spotz[1] (abbreviated to HBS). Several methods can be used to fit the viscosity data to give values of ϵ/k and r_0.

1. Trial and Error.—This method was used by HBS. Approximate values of ϵ/k are obtained from the boiling point or critical temperature and adjusted until the ratios of the $A(\tau)$'s obtained from experimental data agree.

2. From Sutherland Constant S and Temperature Exponent of the Viscosity s.—HBS give values of S/T and s as functions of τ. One need only, therefore, obtain S/T or s at any temperature and read from the theoretical plot the corresponding value of τ; ϵ/k is then easily

* National Research Laboratories Postdoctorate Fellow.

[1] Hirschfelder, Bird, and Spotz, J. Chem. Phys. **16**, 968 (1948); Chem. Revs. **44**, 205 (1949); Trans. Am. Soc. Mech. Engrs. **71**, 921 (1949).

[2] K. E. Grew, Proc. Phys. Soc. (London) **57**, 655 (1949); E. R. S. Winter, Trans. Faraday Soc. **46**, 81 (1950).

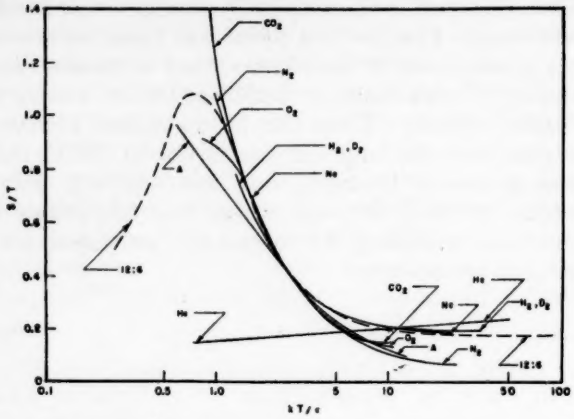

FIG. 1. Experimental values of S/T *vs* log$T$ for several gases superimposed on the theoretical S/T *vs* logkT/ϵ for the 12:6 potential.

calculated. A more informative procedure is to plot the theoretical S/T or s against logτ and the experimental S/T or s against log$T$ on the same scale. The experimental and theoretical curves should then be superposable by shifting along the log$T$−logτ axis, and the amount of the shift gives logϵ/k. This is probably the most convenient way of showing the degree of fit which can be obtained with a 12:6 potential.

3. Adaptation of the Buckingham Method[3] *for the Second Virial Coefficient.*—We define the two quantities

$$X=2.6693\times10^{-5}M^{\frac{1}{2}}r_0^{-2}, \tag{4}$$

$$Y=\epsilon/k=T/\tau. \tag{5}$$

Taking logs of Eq. (2) and rearranging we obtain

$$\log X=\log\eta T^{-\frac{1}{2}}-\log A(\tau), \tag{6}$$

and taking logs of (5) we obtain

$$\log Y=\log T-\log\tau. \tag{7}$$

For each value of the viscosity log$X$ *vs* log$Y$ is plotted for various values of τ around the value expected. The intersection of two lines gives the values of X and Y (i.e., r_0 and ϵ/k) which is the solution of the simultaneous Eq. (2) for two values of the viscosity. This method can also be used by obvious adaptations for thermal conductivity and for diffusion data.

It is found on plotting the log$X$−log$Y$ curves that they cross one another at a rather small angle. A small change in the viscosity therefore may result in a comparatively large change in the point of intersection. To obtain reliable values of ϵ/k and r_0 it is essential that the viscosities be known to better than about 0.5 percent, and should preferably be known to 0.1 percent. Similar remarks apply to the use of S/T and s in evaluating ϵ/k, since small errors in the viscosity result in comparatively large errors in S/T and s. The same remarks also apply to diffusion and to thermal conductivity and a few trial plots showed that existing data are quite inadequate. The reason for this is discussed below.

[3] R. A. Buckingham, Proc. Roy. Soc. (London) **A168**, 264 (1938).

3. RESULTS

Large scale plots were made of all the available viscosity data in the literature for the following gases: hydrogen,[4] deuterium,[5] helium,[6] carbon dioxide,[7] nitrogen,[8] oxygen,[9] neon,[10] and argon[11] and the "best" curves drawn through the points. The viscosities given by various authors are fairly concordant, and the curves are

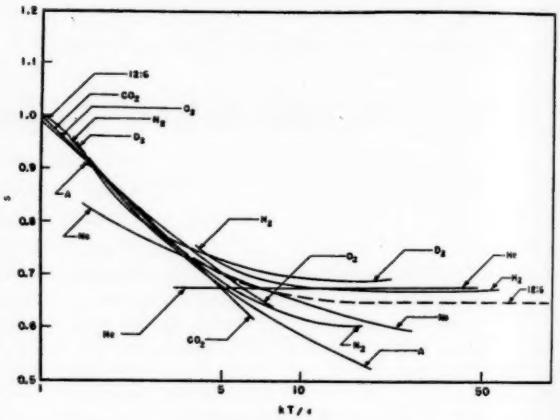

FIG. 2. Experimental values of s *vs* log$T$ for several gases superimposed on the theoretical s *vs* logkT/ϵ for the 12:6 potential.

[4] M. Trautz *et al.*, Ann. Physik **5**, 561 (1930); **7**, 409, 431 (1930); **9**, 981 (1931); **22**, 189 (1935); B. P. Sutherland and O. Maass, Can. J. Research **6**, 428 (1932); A. van Itterbeek *et al.*, Physica **5**, 938 (1938); **7**, 265 (1940); W. H. Keesom and G. E. MacWood, Physica **5**, 749 (1938); W. H. Keesom and P. H. Keesom, Physica **7**, 29 (1940); H. L. Johnston and K. E. McCloskey, J. Phys. Chem. **44**, 1038 (1940); R. Wobser and F. Müller, Kolloid-Beihefte **52**, 165 (1940).

[5] A. B. Van Cleave and O. Maass, Can. J. Research **12**, 57 (1935); A. van Itterbeek *et al.*, Physica **5**, 938 (1938); **7**, 265 (1940).

[6] M. Trautz *et al.*, Ann. Physik. **5**, 561 (1930); **7**, 427 (1930); **22**, 189 (1935); A. van Itterbeek and W. H. Keesom, Physica **5**, 257 (1938); A. van Itterbeek and O. van Paemel, Physica **7**, 265 (1940); R. Wobser and F. Müller, Kolloid-Beihefte **52**, 162 (1940); H. L. Johnston and E. R. Grilly, J. Phys. Chem. **46**, 948 (1942).

[7] M. Trautz *et al.*, Ann. Physik. **7**, 427 (1930); **9**, 981 (1931); B. P. Sutherland and O. Maass, Can. J. Research **6**, 428 (1932); P. Bremond, Compt. rend. **196**, 1472 (1933); H. L. Johnston and K. E. McCloskey, J. Phys. Chem. **44**, 1038 (1940); R. Wobser and F. Müller, Kolloid-Beihefte **52**, 165 (1940); V. Vasilesco, Ann. phys. **20**, 137, 292 (1945).

[8] C. J. Smith, Proc. Phys. Soc. (London) **34**, 155 (1922); M. Trautz *et al.*, Ann. physik **2**, 733 (1929); **7**, 409, 427 (1930); H. L. Johnston and K. E. McCloskey, J. Phys. Chem. **44**, 1038 (1940); R. Wobser and F. Müller, Kolloid-Beihefte **52**, 165 (1940); V. Vasilesco, Ann. Phys. **20**, 137, 292 (1945).

[9] M. Trautz *et al.*, Ann. Physik. **7**, 409, 427 (1930); H. L. Johnston and K. E. McCloskey, J. Phys. Chem. **44**, 1038 (1940); R. Wobser and F. Müller, Kolloid-Beihefte **52**, 165 (1940).

[10] R. S. Edwards, Proc. Roy. Soc. (London) **A119**, 578 (1928); M. Trautz *et al.*, Ann. Physik. **5**, 561 (1930); **7**, 427 (1930); A. van Itterbeek and O. van Paemel, Physica **7**, 265 (1940); R. Wobser and F. Müller, Kolloid-Beihefte **52**, 165 (1940); H. L. Johnston and E. R. Grilly, J. Phys. Chem. **46**, 948 (1942).

[11] M. Trautz *et al.*, Ann. Physik. **3**, 409 (1929); **5**, 561 (1930); **7**, 427 (1930); A. van Itterbeek and O. van Paemel, Physica **5**, 1009 (1938); R. Wobser and F. Müller, Kolloid-Beihefte **52**, 165 (1940); H. L. Johnston and E. R. Grilly, J. Phys. Chem. **46**, 948 (1942); V. Vasilesco, Ann. phys. **20**, 137, 292 (1945).

easily drawn. From these plots S/T and s were evaluated and plotted against $\log T$. The temperature ranges covered are quoted in Table II. The "best" superposition of the experimental and theoretical S/T and s curves is shown in Figs. 1 and 2, respectively. It is evident that neither S/T nor s are universal functions of the reduced temperature, as predicted by the 12:6 potential. From the shift required for best superpositions, the "best" values of ϵ/k for all the gases have been calculated and compared with the values assigned by HBS in Table I. For most of the gases considered, the fit is very good over the range $\tau=1.2-3$, and gives reasonable values of ϵ/k and r_0, i.e., values close to those obtained from critical and virial data.

It will be evident that if we use the experimental values of S/T or s at various temperatures to calculate the apparent ϵ/k at each temperature, by reading off the corresponding value of τ from the theoretical S/T or s plots, the values obtained will have a temperature dependence, and when the experimental s or S/T values fall below the minimum predicted by the 12:6 model, i.e., 0.6438 for s and 0.1680 for S/T[1], no values of ϵ/k and r_0 will give an exact fit. The same temperature dependence is also found when we use method (3) for fitting ϵ/k and r_0 to the viscosity. All the gases considered except hydrogen, deuterium, and helium show a decrease in the apparent ϵ/k at high temperatures, and if the viscosity has been measured to a high enough temperature, decreases to zero. At higher temperatures no exact fit to a 12:6 potential is possible, and the experimental S/T for many gases falls to less than half the minimum theoretical value. In Table II we show the temperature range for the viscosity data and the approximate maximum temperatures for fit with a 12:6 potential. It would seem that the potential though excellent at moderate temperatures, is not so satisfactory for extrapolation of viscosities to high temperatures, and such extrapolations should be made with care.† However, the viscosity calculated is not very dependent on the value of ϵ/k chosen. It seems that at the moderately high temperatures (to ~1500°K) an accuracy of 5 percent or better can be expected for simple gases, using the constants obtained at lower temperatures. The viscosity of neon appears to be particularly well described by a 12:6 potential, as seen from the almost exact fit with the theoretical S/T curve. It is somewhat surprising that argon does not fit the S/T curve very well. Hydrogen and helium can be fitted over the whole range if one allows ϵ/k and r_0 to vary with temperature. With helium, for example, the variation in ϵ/k necessary is from 6° at low temperatures to about 185° at 1000°K. There is a similar variation also for hydrogen. Nevertheless, the viscosity is moderately well predicted with a single choice of ϵ/k and r_0, in spite of the fact that for accurate predictions ϵ/k and r_0 have to be varied.

The apparent variation in the values of the parameters does not of course mean that the force field is temperature dependent, but is simply a reflection on the inadequacy of the 12:6 potential.

TABLE I. Comparison of ϵ/k from viscosity data.

Gas	From S/T curve	From s curve	From HBS
H_2	27.6	22.3	33.3
He	no value possible		6.03
CO_2	216	216	190
N_2	94	79	91.46
O_2	117	104	113.2
Ne	34	40	35.7
A	120	129	124.0

† Since this work was completed Keyes (Trans. Am. Soc. Mech. Engrs. 73, 589 (1951)) has reported that he has arrived at this conclusion and gives the apparent variation in ϵ/k for carbon dioxide up to 773°K.

TABLE II.

Gas	Temp. range °K for η data	Approx. max. temp. for fit with 12:6
H_2	15–1100	—
He	15–1100	—
CO_2	200–1700	1230
N_2	80–1700	500
O_2	80–1100	730
Ne	80–1100	—
A	55–1900	830

Helium

It has been shown that a 12:6 potential is quite inadequate to explain in detail the temperature variation of the viscosity of helium, and Yntema and Schneider[12] have shown that the second virial coefficient over the range 0–1200°C is not fitted by this potential.

Hydrogen-Deuterium

Neither the s nor the S/T curves for hydrogen and deuterium were identical, though the S/T curves were superposable by shifting along the $\log T$ axis. The reason for this is not immediately evident, as it seems unlikely that hydrogen and deuterium have different force fields.

Carbon Dioxide

The second virial coefficient of carbon dioxide over the temperature range 0–600°C cannot be represented by a single 12:6 potential.[13] This, and the failure of the viscosity to obey a 12:6 potential is undoubtedly due, in part at least, to the fact that the carbon dioxide molecule possesses a permanent quadrupole which introduces attractive terms in r^{-3} and r^{-4}, etc., into the potential function. Also the carbon dioxide molecule is not spherical, and though this has little effect on the second virial coefficient,[13] it probably has greater in-

[12] J. L. Yntema and W. G. Schneider, J. Chem. Phys. 18, 646 (1950).

[13] K. E. MacCormack and W. G. Schneider, J. Chem. Phys. 19, 849 (1951).

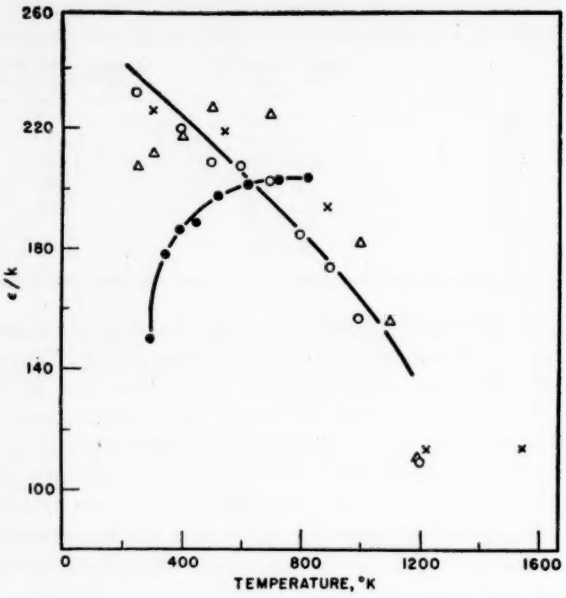

FIG. 3. Temperature variation of the apparent ϵ/k for carbon dioxide. From viscosity data—○ from S/T, Δ from s, × from method 3. From second virial coefficient data ●.

fluence on the viscosity. We illustrate this failure for carbon dioxide by plotting in Fig. 3, the apparent values of ϵ/k from viscosity and second virial data against the mean temperature of the two measurements used to obtain ϵ/k. The trend in ϵ/k with temperature from the two properties are in opposite directions.

The viscosities of fluorine and bromine have been considered since both seemed anomalous, and also uranium hexafluoride, for which data have recently been reported.

Fluorine

As pointed out by HBS, the 12:6 potential cannot be fitted to the data of Kanda[14] who measured the viscosity at nine temperatures between 87 and 273°K. However, if the highest and lowest values are omitted, the remaining seven between 120 and 250°K are well fitted within the experimental error by

$$\epsilon/k=117\pm 8°,$$
$$r_0=3.620.$$

The values obtained at 87 and 273°K are ~12 percent higher and lower respectively than predicted with these parameters. This assignment agrees well with the ϵ/k's obtained from the critical temperature and the boiling point. According to Cady and Hildebrand[15] the critical temperature is 144°K. Using the relation[1]

$$T_c=1.28\epsilon/k,$$

we obtain

$$\epsilon/k=112°.$$

According to Clausen[16] and Kanda,[17] the boiling point is 85.2°K. Using the relation[1]

$$T_b=0.769\epsilon/k,$$

we find

$$\epsilon/k=111°.$$

Bromine

The viscosity data of Rankine[18] were used by HBS to assign an ϵ/k and an r_0 to bromine. This gave an r_0 smaller than that for chlorine. An attempt has been made to include the more recent data up to 800°K of Braune *et al.*[19] The two measurements do not agree too well over the common range, but the "best" fit is described almost equally well by any value of ϵ/k between about 520 and 700°, with corresponding values of r_0 between 4.268 and 3.956A. r_0 for chlorine from viscosity data is 4.115A. The values of ϵ/k for bromine indicated by the critical temperature and the boiling point are 431° and 461°, respectively. The data on the diffusion of bromine into various gases[20] do not appear to fit any reasonable values of ϵ/k and r_0 for the gases.

Uranium Hexafluoride

The viscosity has been measured recently over the temperature range 14–48°C by K. Kigoshi.[21] These data are well fitted by $S/T=1.87$ and by $s=1.16$, neither of which will fit a 12:6 potential.

4. DISCUSSION

The reason for the comparative insensitivity of the viscosity to the value of ϵ/k is, that the main part of the temperature variation of the viscosity is described by the $T^{\frac{1}{2}}$ term and the function $A(\tau)$ is a comparatively slowly varying correction term which increases by a factor of only 5.8 over the range of τ of 0.3–400. With $\epsilon/k=100°$ $T^{\frac{1}{2}}$ increases by a factor of 36.5 over the same range of τ. A change in τ due to change in either T or ϵ/k therefore has a comparatively small effect on the value of $A(\tau)$ for any particular temperature, and even the small change is partly compensated by the necessary change in r_0 due to change in ϵ/k, to obtain a fit to the viscosity at a standard temperature. Similar remarks also apply to diffusion and thermal conductivity.

In view of the fact that the 12:6 potential is a highly simplified approximation to the true potential, its failure to describe molecular properties over a wide range of temperature is perhaps not too surprising. A better approximation might be obtained by using an exponential repulsive term in place of the inverse 12th-power repulsion, and also by taking into account higher

[14] E. Kanda, Bull. J. Chem. Soc. (Japan) **12**, 463 (1937).
[15] G. H. Cady and J. H. Hildebrand, J. Am. Chem. Soc. **52**, 3839 (1950).
[16] W. H. Clausen, J. Am. Chem. Soc. **56**, 614 (1934).
[17] E. Kanda, Bull. J. Chem. Soc. (Japan) **12**, 416 (1937).
[18] A. O. Rankine, Proc. Roy. Soc. (London) **A89**, 575 (1913).
[19] H. Braune, R. Basch and W. Wentzel, Z. Phys. Chem. **A137**, 176, 447 (1928).
[20] J. E. MacKenzie and H. W. Melville, Proc. Roy. Soc. (Edinburg) **52**, 337 (1932).
[21] K. Kigoshi, Bull. Chem. Soc. Japan **23**, 67 (1950).

terms in r^{-8}, r^{-10}, etc., in the dispersion energy. Such a potential involves at least three, or possibly four unknown constants, and to evaluate these constants from viscosity data alone would be a very laborious task. Moreover, in such a task it would probably not be advisable to make use of one or more of the constants which may have been derived from say, the second virial coefficient. With present procedures of deriving the force constants it appears that, when a fairly wide temperature range is considered, the set of constants derived from the second virial coefficient may be quite different from the corresponding set derived from viscosity data. Such a difference can be expected in particular for unsymmetrical molecules, as for example, carbon dioxide (see Fig. 3). It is not possible at present to determine whether this behavior is due entirely to an incorrect choice of the form of the molecular force field, or whether it can be traced in part to other causes. It is possible that there is a variation in the proportion of inelastic collisions with temperature, and this would have different effects on different properties.

A more general force law than the 12:6 is

$$U(r)=\epsilon f(r/r_0), \tag{8}$$

where ϵ and r_0 are characteristic parameters for the particular interacting pair. The viscosity of the gas obeying this potential is given by an equation exactly similar to Eq. (2), where $A(\tau)$ depends on the particular form of f.[22] If f is a universal function, as is assumed in developing the theory of corresponding states,[23] then both s and S/T should be universal functions of the reduced temperature τ. From Figs. 1 and 2 it would appear that some potential of type (8) other than the 12:6 may give rather better agreement with experiment, since it seems that the value of S/T and s at high temperatures for oxygen, nitrogen, argon, and carbon dioxide are considerably lower than predicted by the 12:6. It is not possible to say at present whether a higher or lower power for the repulsive potential would be needed for this. However, no potential of type (8) would give exact agreement since the experimental S/T and s curves are not coincidental.

[22] Hirschfelder, Curtiss, Bird, and Spotz, *Properties of Gases*, preliminary circulated edition, University of Wisconsin, CF1507, November, 1950, Chapter X, p. 5.

[23] K. S. Pitzer, J. Chem. Phys. **7**, 583 (1939).

5. CONCLUSIONS

The 12:6 model fits viscosity data very well over the range of τ of 1.2–3. Outside this range it is frequently impossible to choose any values of the parameters which will fit the viscosity data exactly.

Extrapolation of viscosity data to high temperatures using the 12:6 model should be done with care. Up to 1500°K, an accuracy of 5 percent or better can be expected using the parameters obtained at lower temperatures, but at higher temperatures the accuracy decreases rapidly.

ACKNOWLEDGMENT

We wish to thank Mr. M. Badior for assistance with the computations.

APPENDIX: THE TRAUTZ RELATION AND THE 12:6 POTENTIAL

Trautz[24] found empirically that for many gases at the critical temperature the viscosity η_c of the dilute gas is approximately related to the temperature by the equation

$$\left.\frac{d\eta}{dT}\right|_c=\frac{\eta_c}{Tc} \quad \text{or} \quad \left.\frac{d\ln\eta}{d\ln T}\right|_c=1.$$

By differentiating Eq. (2) and using the integrals for the 12:6 potential and the relation

$$kT_c/\epsilon\equiv\tau_c=1.28$$

it is easily shown that

$$\left.\frac{d\ln\eta}{d\ln T}\right|_c=0.946.$$

[24] M. Trautz, Ann. Phys. **11**, 130 (1931).

On the Decomposition of Metallic Azides

J. G. N. THOMAS AND F. C. TOMPKINS
Department of Inorganic and Physical Chemistry, Imperial College of Science and Technology, S.W.7, London, England

(Received October 15, 1951)

The mechanisms suggested previously for the formation and growth of nuclei in the decomposition of barium azide have been examined in detail. It is concluded that these cannot adequately account for the experimental results available on the thermal decomposition, and photo and ionic conductivity of this salt.

WE have recently measured[1] the specific ionic conductance of a series of solid inorganic azides and oxalates, as a part of a general program of research on the mechanism of decomposition of these two groups of compounds. The detailed results will be presented in a separate communication, but we shall here consider the results obtained with barium azide since both experimental and theoretical work on this decomposition is more extensive than for the other compounds. The specific ionic conductance of solid barium azide can be accurately represented by

$$\log\sigma = -5.991 - 11{,}620/4.576T$$

so that at 373°K, σ is 6.3×10^{-12} ohm^{-1} cm^{-1}. Here the activation energy E_m of 11,620 cal/mole refers to the mobility of the conducting species, since the measurements were obtained in the structure-sensitive region. Values of E_m are reproducible to within 2 percent and of σ to 30 percent.

I. GROWTH OF NUCLEI

When barium azide is heated to about 100°C there is an initial slow decomposition and localized specks of barium, which increase in size with time, become visible. In explanation of nuclear growth, Mott[2] assumes that:

1. Barium azide is an ionic conductor at room temperature by reason of the presence of mobile interstitial Ba^{2+} ions in thermal equilibrium with the salt; the azide ions are immobile.

2. At the metal (nucleus)-salt interface, electrons are transferred from adjacent azide ions thereby leaving azide radicals (positive holes) in the full band; these latter are mobile and diffuse to the surface of the crystal where decomposition, giving nitrogen, ensues.

3. Growth of the nucleus then proceeds by alternate trapping of interstitial Ba^{2+} ions and electrons transferred from adjacent azide ions.

4. The activation energy of growth E_g, obtained by Wischin[3] from the temperature coefficient of the increase of radius of the approximately hemispherical specks of Ba with time, is 23.5 kcal or *ca* 1 ev. The energy has been identified by Mott as that required to transfer an electron from an adjacent azide ion to the metal nucleus.

By using this postulated mechanism and our experimental values of σ and E_g, the maximum rate of addition of Ba atoms to the nucleus at 100°C can be calculated.

We consider a hemispherical nucleus of radius r cm and denote by ne the average negative charge on the nucleus during growth, where e is the electronic charge and n is a small number. The average potential at the surface of the hemisphere is thus ne/Kr, where K is the static dielectric constant of the solid azide, and the total current flowing per second resulting from the trapping of interstitial barium ions is

$$2\pi\sigma ne/K. \tag{1.1}$$

The number of Ba atoms incorporated in the nucleus per second is therefore

$$\pi\sigma n/K. \tag{1.2}$$

Now the velocity of radial growth at 100°C has been directly measured[3] for nuclei having radii greater than 3×10^{-4} cm and is 8×10^{-8} cm/sec.

Taking a value of 2A for the radius of the Ba atom, it follows that $2\pi r^2\times10^{16}$ atoms of barium/second are added to a nucleus of radius r. Hence,

$$\begin{aligned}\sigma &= 2\times10^{17}r^2/n \text{ esu}\\ &= 2\times10^{5}r^2/n \text{ ohm}^{-1}\text{ cm}^{-1},\end{aligned} \tag{1.3}$$

where K has been given the reasonable (maximum) value of 10. An acceptable value of n is now required and it is sufficient for our purpose to evaluate its maximum value.

We therefore place the lowest vacant level of the uncharged metal nucleus at its minimum value, i.e., that corresponding to the highest level in the full band of the azide ion. The energy levels of the metal are raised by the trapping of electrons, consequently the maximum value of n is the number of electrons required to raise the metal levels by 23.5 kcal or 1 ev, the activation energy for electron transfer.

For a nucleus of radius r, the potential at the surface is

$$ne/K^1r, \tag{1.4}$$

and when $ne^2/K^1r > 1$ ev, further electrons cannot be trapped. K^1 is assumed to be unity because the process here involves an electron transfer from an azide ion

[1] P. W. M. Jacobs and F. C. Tompkins, unpublished.
[2] N. F. Mott, Proc. Roy. Soc. (London) A172, 325 (1939).
[3] A. Wischin, Proc. Roy. Soc. (London) A172, 314 (1939).

adjacent to the metal. Hence

$$n_{max}=r/1.5\times10^{-7}; \quad (1.5)$$

combining (1.3) and (1.5),

$$\sigma=3\times10^{-2}r \text{ ohm}^{-1} \text{ cm}^{-1}. \quad (1.6)$$

The smallest nucleus measured by Wischin had a radius of 3×10^{-4} cm, hence

$$\sigma=9\times10^{-6} \text{ ohm}^{-1} \text{ cm}, \quad (1.7)$$

which is 10^6 times larger than the experimental value (6.3×10^{-12} ohm^{-1} cm^{-1}). We further note that the value given in (1.7) is a minimum one, because (1) in evaluating n_{max}, the maximum repulsive potential between the negatively charged nucleus and an electron was taken to be 1 v, whereas it is almost certainly nearer 1/10 v; (2) Wischin's measurements of r extend to $r=10^{-3}$ cm, while dr/dt remains constant. The effect of (1) and (2) gives $\sigma=10^{-3}$ ohm^{-1} cm^{-1} in (1.7), i.e., 10^8 times larger than our measured specific conductance. From Wischin's experimental results growth is definitely three-disional; nevertheless, growth may proceed to give nuclei in the form of lenticular disks. The effect would decrease the discrepancy of 10^8 by a factor of 10 or 100 and therefore does not affect our conclusions. It is therefore highly improbable that growth can proceed by a process of internal electrolysis.

There is a further, but less critical, comment to make here. We have, following Mott and Littleton,[4] calculated that the ratio of the number of interstitial Ba^{2+} ions to barium ion vacancies is about 10^{-6}. It might be anticipated that since the dielectric constant[5] of barium azide (*ca* 10) approaches that of the silver halides (12–13) (where there is some evidence of the presence of interstitial cations), the formation of interstitial Ba^{2+} ions might be favored energetically, but the effect of this ion possessing a double charge more than compensates for the high dielectric constant; thus barium azide is similar to the alkali metal halides and we note that with NaCl, Mott and Littleton's calculations give a similar order for the ratio of number of interstitial cations to cation vacancies. It must be stressed, however, that Mott's general mechanism for the decomposition of azides can be modified, so as to be equally applicable for vacant cation site as for interstitial ions.

Finally, it is most unlikely that barium azide is a cationic conductor. We have unfortunately, as yet failed to measure the transport numbers of the Ba^{2+} and N_3^- ions on account of the low ionic conductance of barium azide at temperatures sufficiently low for the decomposition to be negligible over the long periods required. There are, however, two sound reasons for the statement that this salt is an anionic conductor:

(1) The very similar halides[6] $BaCl_2$, $BaBr_2$, BaF_2, and the halides PbF_2, $PbCl_2$, PBr_2 are all anionic conductors ($t_{cation}=0$).

(2) The activation energy for mobility[7] of Ba^{2+} in barium azide is expected to be similar to that of Pb^{2+} in its halides, i.e., *ca* 20 kcal whereas we obtain from the temperature coefficient of σ a value of only 11 kcal—this low activation energy we believe, therefore, refers to the mobility of the azide ion.

If we accept mobility of vacant anion sites as the most likely mode of transport of ions, Mott's growth mechanism could be retained with minor modifications, i.e., growth would involve alternate trappings of electrons and of vacant anion sites which are attracted to the negatively charged nucleus. Nevertheless, the main criticism that the measured ionic conductance is 10^{6-8} too small for the observed growth still stands.

The only reasonable alternative process of growth is a decomposition, to give nitrogen, taking place at the metal-salt interface. This is certainly true for the decomposition of silver oxalate[8] since x-ray photographs prove that the metallic silver is a pseudomorph of the original crystals and is universally true in the decomposition of hydrates and carbonates. The apparent objection to this process, pointed out by Mott, the difficulty of escape of the gaseous product from the interface, is therefore a general one and is not confined to the barium azide decomposition. Both from visual observation and from the fact that all these decompositions are catalyzed at the interface, there is little doubt that the actual interface remains intact. We suggest therefore that the nucleus grows by transformation of lattice Ba^{2+} ions to Ba atoms such that these atoms on formation occupy the lattice sites of the salt. Since the $Ba^{2+}-Ba^{2+}$ distance in the azide is greater than the Ba—Ba distance in the Ba metal, the nucleus originally has an expanded structure. On further growth, with the interface remaining intact, "recrystallization" to the normal metal lattice takes place in the interior of the nucleus, the body of which becomes permeated with cracks through which diffusion of N_2 can occur. This is, in fact, the mechanism of escape of water molecules during the dehydration of chrome alum[9] and the photographs of the nuclei given by Garner leave no doubt that this process takes place, and a similar phenomenon occurs in the decomposition of silver oxalate.[8] Furthermore, the barium azide used by Garner *et al.*, by Wischin, and by us was the dehydrated monohydrate. This dehydration proceeds rapidly at room temperature and H_2O molecules escape from the interior of the crystals with ease. Now the minimum dimension of the water molecule is 3.2A, whereas that of

[4] N. F. Mott and M. J. Littleton, Trans. Faraday Soc. **34**, 485, 500 (1938).

[5] N. F. Mott and R. W. Gurney, *Electronic Processes in Ionic Crystals* (Oxford University Press, London, 1940), p. 12.

[6] W. Jost, *Diffusion und Chemische Reaktion in festen Stoffen* (Steinkopf, Leipsiz, 1937), p. 80.

[7] G. von Hevesey and W. Seith, Z. Physik **56**, 790; **57**, 869 (1929).

[8] R. Griffiths, J. Chem. Phys. **11**, 499 (1943); **14**, 408 (1946).

[9] J. A. Cooper and W. E. Garner, Trans. Faraday Soc. **32**, 1739 (1936).

the N_2 molecule is 3.0A—diffusion of N_2 out of the crystal can therefore take place without difficulty even at room temperature.

We conclude from the foregoing that:

(1) The number of interstitial Ba^{2+} ions present in equilibrium with the crystal is a very small fraction of the number of vacant cation sites.

(2) The Ba^{2+} ion is immobile and the azide ion mobile.

(3) The measured rate of growth is 10^6–10^8 times faster than that calculated from the measured ionic conductance of the salt.

(4) Reaction (growth) proceeds at the salt-metal interface, and the N_2 produced escapes by diffusion through the salt (or metal nucleus).

II. NUCLEAR FORMATION

Two mechanisms have been suggested by Mott; one involves the trapping of two conduction electrons,[2] and the other the bimolecular aggregation of interstitial Ba atoms.[10] Garner and Maggs,[11] and Wischin[3] give preference to the latter, but there is no suggestion[7] that the former is not an acceptable hypothesis. None of these authors have, however, considered these mechanisms in detail. We believe that neither hypothesis as originally proposed accounts adequately for the experimental results.

1. Bimolecular Aggregation of Interstitial Ba Atoms

(a) It is assumed that when $Ba(N_3)_2$ is heated N_2 is driven off from the surface at a constant rate, and that interstitial Ba atoms diffuse into the body of the crystals. Whenever two of these meet at some favored spot, a stable nucleus is formed. Now the energy necessary to create a Ba^{2+} interstitial ion is not less than 3 ev, so that the activation energy for the nucleus formation is therefore at least 6 ev or, taking regard of the activation energy of mobility of Ba^{2+} ions (which may approach 1 ev), probably 7 ev, whereas the experimental activation energy is only 3.2 ev. It is true, of course, that the energies for formation and mobility of interstitial atoms on the surface are smaller, but reduction to about one-half of the bulk value is unlikely. Furthermore, this high value of the energy for the production of interstitial Ba atoms means that the rate of production is very small, and it is not possible to account for the rate of nucleus formation directly observed by Wischin.

(b) We may, however, assume that there are originally present a number of interstitial Ba^{2+} ions in excess of that in thermal equilibrium with the crystal, and then calculate the energy necessary to transform these to interstitial atoms by the trapping of conduction electrons. The spectrum of solid $Ba(N_3)_2$ has an adsorption band commencing on the high wavelength side[1,11] at 2600A, corresponding to an electron transition to an exciton level. Assuming the electron transition from full to conduction band occurs at the shorter wavelength band at about 2500A, the optical excitation required for this process is about 114 kcal. Because of the Franck-Condon principle, this value exceeds the corresponding thermal energy in the ratio of the dielectric constant in static to high frequency fields, which is between about 1/3 and 2/5. The thermal excitation energy is therefore 35–48 kcal. The interstitial Ba^{2+} ion acts as a deep electron trap and a second electron will be trapped before the Ba^+ ion thermally dissociates to regenerate the Ba^{2+} ion. The rate of formation of interstitial Ba atoms thus depends linearly on the time, and the activation energy for their formation is 35–48 kcal. These atoms have mobility, and aggregate to form stable (two-atom) nuclei. The activation energy for this process will thus be 70–96 kcal, plus the activation energy of mobility. The latter is unknown but cannot be less than 11 kcal (the energy for mobility of the *mobile* azide ion), and by analogy with the energy for *cationic* mobility in predominantly *anionic* conductors, e.g., Pb^{2+} in $PbCl_2$ or PbI_2, it is probably 20–25 kcal. The total activation energy is thus 91–121 kcal compared with the experimental value of 74 kcal; we conclude that the formation of *internal* nuclei by this mechanism is energetically unlikely, but the possibility of production of *surface* nuclei cannot be definitely dismissed. Nevertheless, we believe that this is improbable, since the number of interstitial Ba^{2+} ions which have to be present in excess of the equilibrium number is large and thus highly improbable.

2. Bimolecular Trapping of Conduction Electrons

From the calculation in 1(b), this process is energetically possible at the surface. To obtain the dependence on t^3, the number of electrons in the conduction band is assumed to increase linearly with time at constant temperature. These electrons can be trapped at certain positions in the lattice, and by electrostatic forces attracts (in the original theory) an interstitial Ba^{2+} to give a Ba^+ center. (In general, however, this ion can be replaced by a mobile positively charged species). This center may now (1) dissociate on receipt of thermal energy giving Ba^{2+} and a free electron, or (2) trap a second electron before (1) occurs and so form a stable nucleus. There seems some confusion[2] about the nature of the original traps, which might be shallow (sensitivity specks) or deep (vacant anion sites); both possibilities are therefore considered below. We shall use the following notation:

N_o = number of (surface) azide ions from which electrons may be excited into the conduction band,

N_T = total number of nucleus-forming traps at which decomposition finally takes place,

[10] Reference 5, p. 266.

[11] W. E. Garner and J. Maggs, Proc. Roy. Soc. (London) **A172**, 299 (1939).

N_t', N_t'' = number of nucleus-forming traps containing one (two) electrons at time t,
n_t = number of electrons in the conduction band at time t,
E = thermal energy to raise an electron from the azide full band to the conduction band,
k', k'' = rate constants of trapping of electrons at empty (one-electron filled) traps,
k = rate constant for the dissociation of one or two-electron-filled traps thereby freeing one electron,
ν = lattice frequency,
M_T, M_t', M_t'', k_M', k_M'', k_M, etc., are corresponding symbols to N_T, N_t', N_t'', k', k'', k, etc., in the case where the traps are of the non-nucleus-forming type.

When only nucleus-forming traps are present, the rate of increase of the number of electrons in the conduction band is

$$dn_t/dt = \text{const}\ \nu N_o \exp(-E/kT) - k'(N_T - N_t' - N_t'')n_t + k'N_t' - k''N_t'n_t'. \quad (2.1)$$

We require that (1) $dn_t/dt = R = \text{const}$ (Mott's assumption) and (2) $N_t'' = \text{const}\ t^3$ (Wischin's experimental result) be compatible. After writing $Rt = n_t$,

$$C_1 = \text{const}\ \nu N_o \exp(-E/kt),$$

in (1) and solving for N_t',

$$N_t' = \frac{R - C_1 + k'N_TRt - k'N_t''Rt}{k'Rt + k - k''Rt}. \quad (2.2)$$

As a good approximation, $k' = k''$, and $k'N_t''Rt$ is small, particularly at small t; therefore,

$$N_t' = (R - C_1 + k'N_TRt)/k. \quad (2.3)$$

At $t = 0$, $N_t' = 0$, hence

$$R - C_1 \simeq 0, \quad (2.4)$$

i.e.,

$$N_t' = k'N_TRt/k, \quad (2.5)$$

and the rate of nucleus formation is

$$k'k''N_TR^2t^2/k, \quad (2.6)$$

or

$$N_t'' = \text{const}\ t^3. \quad (2.7)$$

Thus, with the restrictive condition that R is approximately equal to C, Wischin's experimental result follows from Mott's assumptions.

Case 1—Shallow Traps

In this case, there can be a high rate of trapping at empty traps because these centers can undergo rapid dissociation and thus condition (2.4) holds; the trapping of two electrons at the same trap will be a rare occurrence as demanded by theory. Since, however, vacant anion sites have a trap depth of about 2 ev, i.e., the life of a trapped electron is as long as 10^{12} sec at 100°C, these traps cannot be those at which nucleus formation is initiated, otherwise N quickly becomes proportional to t^2 and not to t^3. The alternative that the center, F center + interstitial Ba^{2+}, can be easily dissociated implies that it is not an effective electron trap, which is also clearly unacceptable. We further note that if the vacant anion site is not the center of ultimate decomposition, then Mott's theory, that the effect of pre-irradiation in shortening the induction period is the creation of additional vacant anion sites, must be modified.

Moreover, to maintain condition (2.4), the number of free electrons produced must approximate to the rate of production. The over-all activation energy is 74 kcal, of which at least 11 kcal is required for the mobility of the Ba^{2+} ion. Hence, 31.5 kcal are required at most to raise the electron to the conduction band; therefore at 400°K the rate of production will be $N_o\ 10^{-4}$ sec^{-1}. Assuming the electron production to be confined to the surface, then for 1 cm^2 $Ba(N_3)_2$ surface containing 10^{15} N_3^- ions, 10^9 free electrons are produced per sec corresponding to a photocurrent of about 10^{-9} amp/sec, since non-nucleus forming traps are assumed absent here, i.e., at least 10^5 greater than has been experimentally detected.[1]

Case 2—Deep Traps

Here the rate of dissociation of one- and two-electron traps is negligible. If the number of traps is very large so that only a small fraction are filled with electrons, then the number of one-electron filled traps increases as t^2 and of two-electron filled traps as t^3 as required. However, this is clearly impossible, for with a large number of deep traps, the condition (2.4), $R \simeq C$, cannot hold over the long periods (400 min) observed by Wischin. If, on the other hand, to maintain $R \simeq C$ the number is small, then the number of empty traps decreases rapidly with t, and N'', although initially varying as t^3, will quickly vary as t^2.

Case 3—Presence of Non-Nucleus Forming Traps

In this case,

$$R = C_1 - k'(N_T - N_t' - N_t'')Rt + kN_t' - k''N_tRt - \sum_{\text{all traps}} k_M'(M_T - M_t')Rt + \sum_{\text{all traps}} k_MM_t' = 0.$$

For $R \simeq C$, it is clear that

$$-\sum_{\text{all traps}} k_M'(M_T - M_t')Rt + \sum_{\text{all traps}} k_MM_t' = 0,$$

i.e., equilibrium is quickly established and the presence of non-nucleus forming traps has no effect on our

previous argument. Any alternative to this disobeys the restrictive condition (2.4).

Case 4—Loss of Conduction Electrons by Rapid Recombination with Positive Holes or Falling into Exciton Levels

This represents in this case the general fate of the conduction electron, consequently as a first approximation, the number of positive holes (and number of exciton levels, since these are always associated here with the presence of positive holes) equals the number of free electrons. Consequently,

$$N_i' = (R - C_1 + k' N_T R t + k_+ (Rt)^2)/k.$$

For rapid recombination, k_+, the rate constant for the recombination process, is large and again the conditions, (a) R=const and (b) $N_i'' \propto i^3$, are incompatible.

CONCLUSIONS

We have considered all reasonable variations of nucleus formation involving (1) Ba^{2+} interstitial ions and (2) the bimolecular trapping of conduction electrons in some detail, because it is essential that mechanisms based on these concepts should be fully explored before other superficially less probable approaches based on the production and trapping of excitons which we develop in later papers are postulated. We conclude that neither the growth of nuclei nor their formation can be adequately explained by mechanisms which have as yet been postulated.

THE JOURNAL OF CHEMICAL PHYSICS VOLUME 20, NUMBER 4 APRIL, 1952

Determination of a Single Quadrupole for a Charge Distribution

EDWIN S. CAMPBELL*
Department of Chemistry and Chemical Engineering, University of California, Berkeley, California
(Received November 6, 1951)

A method is given for the reduction to a single quadrupole of the second-order term in the Taylor series expansion of the potential defined by a charge distribution.

I. INTRODUCTION

MANY problems involving the interaction of forces arising from distinct points can be simplified by using a Taylor series expansion of the potential around a conveniently chosen reference point. For example, although direct integration of the expression for the second virial coefficient of a gas is impossible if part of the potential energy is assumed to arise from point charges within each molecule, analytic approximations to the integral have been obtained using the Taylor expansion.[1]

Let S be a system of point charges or an integrable charge distribution contained within a sphere $C(O, R)$; let $\varphi(P)$ be the potential at P: (x, y, z) defined by the system S. If P belongs to the exterior domain of $C(O, R)$, the Taylor series expansion about O converges, and

$$\varphi(P) = p^{(0)}/r - (p_x^{(1)}\partial/\partial x + p_y^{(1)}\partial/\partial y + p_z^{(1)}\partial/\partial z)(1/r) + \tfrac{1}{2}!(p_{xx}^{(2)}\partial/\partial x^2 + \cdots + p_{yz}^{(2)}\partial/\partial y\partial z)(1/r) + \cdots \quad (1)$$

r: $(x^2+y^2+z^2)^{\frac{1}{2}}$
$p^{(0)}$: the total charge contained in $C(O, R)$
$p_x^{(1)}$, etc.: elements of the dipole vector
$p_{xx}^{(2)}$, etc.: elements of the quadrupole tensor.[2,3]

The Taylor series notation for $\varphi(P)$ can be simplified and the computation required in certain problems reduced through the introduction of the concept of spherical harmonics, i.e., of multipoles.[4] An nth-order multipole with moment $p^{(n)}$ and characteristic directions $\mathbf{s}_1, \cdots, \mathbf{s}_n$ (each $\mathbf{s}_i$ a unit vector) may be defined as a point singularity whose potential at the endpoint of $\mathbf{r} \neq (0, 0, 0)$ is

$$\varphi_n(\mathbf{r}) = (-1)^n p^{(n)}[(\mathbf{s}_n \cdot \nabla) \cdots (\mathbf{s}_1 \cdot \nabla)(1/r)]/n!. \quad (2)$$

If $\mathbf{s}_1 = \cdots = \mathbf{s}_n$, then $p^{(n)}$ is said to be a zonal or an axial multipole.

Stated in terms of this definition, the problem of simplifying the notation becomes: When can the $(n+1)(n+2)/2$ multipoles of the nth-order term of the Taylor series be reduced to a single multipole? Although for each spherical harmonic of degree n the existence of a unique set of n rays along which $\mathbf{s}_1, \cdots, \mathbf{s}_n$ must lie has been established, the method of the existence theorem requires the solution of an equation of the 2-nth order.[5] A general solution of the reduction prob-

* Present address: Department of Chemistry, University of Southern California, Los Angeles 6, California.

[1] J. S. Rowlinson, Trans. Faraday Soc. 47, 120 (1951).

[2] O. D. Kellogg, *Foundations of Potential Theory* (Julius Springer, Berlin, 1929), p. 135 ff.

[3] The notation used for the Taylor expansion is that of J. A. Stratton, *Electromagnetic Theory* (McGraw-Hill Book Company, Inc., New York, 1951), p. 178.

[4] For discussion of the use of the multipole concept see, e.g., H. Margenau, Revs. Modern Phys. 11, 5 (1939).

[5] The usual observations (A. G. Webster, *Partial Differential Equations of Mathematical Physics* [(Hafner Publishing Company, New York, 1947), p. 298] do not establish the existence of the representation. See E. W. Hobson, *The Theory of Spherical and Ellipsoidal Harmonics* (Cambridge University Press, 1931), p. 121. For the existence theorem and a clarifying discussion of the problem, see Hobson, *The Theory of Spherical and Ellipsoidal Harmonics* (Cambridge University Press, 1931), pp. 124–132, 135–137.

lem appears to be available in a simple form only for the trivial case $n=1$; a simple solution for $n=2$ follows.

II. REDUCTION OF THE SECOND-ORDER TERM TO A SINGLE QUADRUPOLE

Assuming that (x, y, z) constitutes the principal axis system for the charge distribution S,[6]

$$p_{xy}^{(2)}=p_{xz}^{(2)}=p_{yz}^{(2)}=0. \tag{3}$$

The three remaining axial quadrupoles $p_{xx}^{(2)}$, $p_{yy}^{(2)}$, and $p_{zz}^{(2)}$ may be represented by a single quadrupole of moment $p^{(2)}$ and characteristic directions

$$\mathbf{s}_1=(s_1^1, s_1^2, s_1^3), \quad \mathbf{s}_2=(s_2^1, s_2^2, s_2^3), \tag{4}$$

if and only if the coefficients of the quadratic forms obtained after differentiating and multiplying by r^5 are identical. Therefore,

$$2p_{xx}^{(2)}-p_{yy}^{(2)}-p_{zz}^{(2)}=p^{(2)}(2s_1^1s_2^1-s_1^2s_2^2-s_1^3s_2^3) \tag{5}$$

$$2p_{yy}^{(2)}-p_{xx}^{(2)}-p_{zz}^{(2)}=p^{(2)}(2s_1^2s_2^2-s_1^1s_2^1-s_1^3s_2^3) \tag{6}$$

$$2p_{zz}^{(2)}-p_{xx}^{(2)}-p_{yy}^{(2)}=p^{(2)}(2s_1^3s_2^3-s_1^1s_2^1-s_1^2s_2^2) \tag{7}$$

$$0=p^{(2)}(s_1^1s_2^2+s_1^2s_2^1) \tag{8}$$

$$0=p^{(2)}(s_1^1s_2^3+s_1^3s_2^1) \tag{9}$$

$$0=p^{(2)}(s_1^2s_2^3+s_1^3s_2^2). \tag{10}$$

Also,

$$1=(s_1^1)^2+(s_1^2)^2+(s_1^3)^2 \tag{11}$$

$$1=(s_2^1)^2+(s_2^2)^2+(s_2^3)^2. \tag{12}$$

If $p^{(2)}\neq 0$, then by (8, 9, 10) for some i, j: $s_i^j=0$. Since $\mathbf{s}_i$ is not a zero vector,

$$s_1^j=0 \quad s_2^j=0 \quad j=1, 2, 3. \tag{13}$$

[6] For a careful proof of the theorem that every real quadratic form is orthogonally equivalent to exactly one diagonal form, see G. Birkhoff and S. MacLane, *A Survey of Modern Algebra* (MacMillan Company, New York, 1948), Chapter IX, Sec. IX and Chapter X, Sec. IX. For a method of determining the principal axes, see e.g., J. L. Synge and B. A. Griffiith, *Principles of Mechanics* (McGraw-Hill Book Company, Inc., New York, 1949), p. 318.

The following solution for $(p^{(2)}, \mathbf{s}_1, \mathbf{s}_2)$ may be deduced by using the observation that Eqs. (5)–(13) are symmetric in all variables.

1. Find the principal axes of the charge distribution by solving for the eigenvalues of the charge distribution matrix.[6]

2. (a) $p^{(2)}=0$ if and only if $p_{xx}^{(2)}=p_{yy}^{(2)}=p_{zz}^{(2)}$.

(b) If and only if exactly two of the three principal moments are equal, can the second-order term be represented by a single nonvanishing axial quadrupole. Suppose $p_{yy}^{(2)}=p_{zz}^{(2)}$, then

(1) $\mathbf{s}_1$ and $\mathbf{s}_2$ are both parallel or both antiparallel to the x axis and $p^{(2)}=(p_{xx}^{(2)}-p_{yy}^{(2)})$.

(2) $\mathbf{s}_1$ is parallel and $\mathbf{s}_2$ antiparallel to the x axis and $p^{(2)}=-(p_{xx}^{(2)}-p_{yy}^{(2)})$.

(c) If and only if no two of the three principal moments are equal, can the second-order term be represented by a single nonvanishing quadrupole with two linearly independent characteristic directions. In this case, arrange the three principal moments in order of increasing magnitude. It may be shown that the direction numbers of $\mathbf{s}_1$, $\mathbf{s}_2$ relative to the axis with the intermediate moment must be zero. For example, suppose

$$p_{zz}^{(2)}<p_{yy}^{(2)}<p_{xx}^{(2)}. \text{ Set } s_1^2=s_2^2=0.$$

Then

$$(s_1^1=-(+)s_2^1) \text{ and } (s_1^3=+(-)s_2^3)$$

$$p^{(2)}=-(+)(p_{xx}^{(2)}-p_{zz}^{(2)})$$

$$s_1^1=\pm[(p_{xx}^{(2)}-p_{yy}^{(2)})/(p_{xx}^{(2)}-p_{zz}^{(2)})]^{\frac{1}{2}}$$

$$s_1^3=\pm[(p_{zz}^{(2)}-p_{yy}^{(2)})/(p_{zz}^{(2)}-p_{xx}^{(2)})]^{\frac{1}{2}}.$$

Although, for a given reference point $(p^{(2)}, \mathbf{s}_1, \mathbf{s}_2)$ are unique (save for compensating changes of sign), it must be noted that all three quantities depend on the reference point selected.

In terms of the alternative notation for spherical harmonics, the axial quadrupole has the potential $p^{(2)}P_2^0(\cos\theta)/r^3$ provided $\mathbf{s}_1=\mathbf{s}_2=z$; the quadrupole with $\mathbf{s}_1$ perpendicular to $\mathbf{s}_2$ has the potential $p^{(2)}P_2^1(\cos\theta)\cos\varphi/2r^3$ provided $\mathbf{s}_1=z$, $\mathbf{s}_2=x$. $p^{(2)}$ is the quadrupole moment and $P_n^m(\cos\theta)$ is the associated Legendre polynomial.

The Spectra of HCl, NH_3, H_2O, and H_2S from 100 to 700 Microns*

T. KING MCCUBBIN, JR.
The Johns Hopkins University, Baltimore, Maryland

(Received November 23, 1951)

This paper reports the pure rotation spectra of HCl, NH_3, H_2O, and H_2S in the region of the far infrared from 100 to 700 microns. Observations were made using an instrument which had a resolving power of from .1 to 2 cm^{-1} in that region of the spectrum.

INTRODUCTION

THIS paper is a report of some studies of molecular spectra which have been made using a far infrared grating spectrometer which the author and William M. Sinton have constructed.[1] The spectrometer, shown in Fig. 1, used one-foot square milling machine produced diffraction gratings, a quartz mercury arc source, and a Golay cell detector. Gratings spacings were $66\frac{2}{3}$ lines per inch for the region from 100 to 300 microns and 25 lines per inch for from 300 to 700 microns. Atmospheric water vapor absorption, especially at wavelengths shorter than 200 microns, was still evident even after the entire optical path of the instrument had been flushed with prepurified nitrogen which had passed through a liquid nitrogen trap. The resolving power of this spectrometer is from 1 to 2 cm^{-1} in the region from 100 to 700 microns. Except for the work at the University of Michigan with Randall's spectrometer,[2] which was capable of resolving spectral lines as close together as 1 cm^{-1} out to 140 microns, the best previous resolution in the infrared beyond 100 microns has been of the order of from 5 to 10 cm^{-1}.

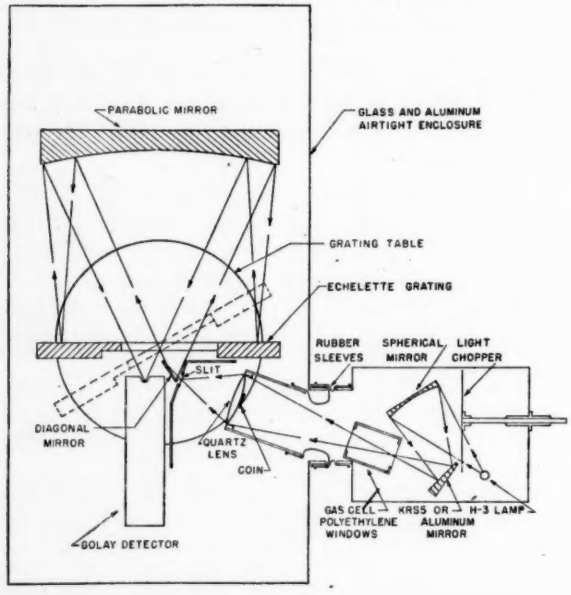

FIG. 1. The one-foot far infrared grating spectrometer.

HYDROGEN CHLORIDE

Figure 2(a) shows the four longest wavelength pure rotation lines of HCl. These lines were measured using an absorption cell having a 5-cm path length. The polyethylene windows on this cell were too thin to permit evacuation. Therefore, the following procedure for filling the cell was necessary: First, the cell was flushed with prepurified dry nitrogen in order to remove atmospheric water vapor. Next, enough of the absorbing gas was allowed to enter the nitrogen-filled cell to cause the desired intensity of absorption. Total pressure in the cell was always atmospheric pressure. Observed frequencies of the HCl lines are given in Table I. The average value for B_0 computed from observed frequencies of these four lines is 10.40 cm^{-1}. This value is in close agreement with Czerny's[3] value of 10.395 cm^{-1}. Czerny observed pure rotation lines having final J values of 4 through 11 in the spectral region from 45 to

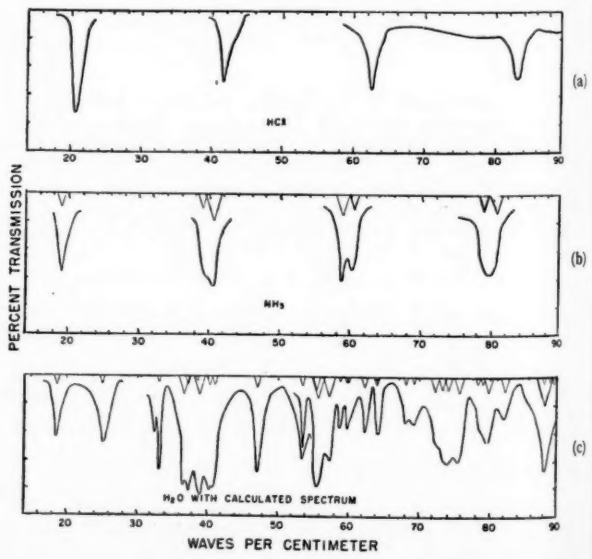

FIG. 2. Far infrared transmission spectra of hydrogen chloride, ammonia, and water vapor. Triangles representing computed frequencies and intensities of absorption lines are drawn with equal apex angles and have areas proportional to intensities.

* This paper is part of the author's doctorial dissertation at The Johns Hopkins University. The equipment used was constructed with the support of the ONR, Contract N5-ori-166, Task Order V.

[1] T. K. McCubbin, Jr., and W. M. Sinton, J. Opt. Soc. Am. 42, 113 (1952).

[2] Randall, Dennison, Ginsburg, and Weber, Phys. Rev. 52, 160 (1937).

[3] M. Czerny, Z. Physik 34, 227 (1925).

TABLE I. HCl rotation lines.

J''	J'	ν in cm^{-1} Calculated[a]	Observed	B[b] in cm^{-1}
0	1	20.79	20.8	10.40
1	2	41.57	41.6	10.40
2	3	62.33	62.5	10.42
3	4	83.06	83.1	10.40

[a] $\nu_{calc} = 20.79J' - .0016J'^2$. Czerny (reference 3) evaluated these molecular constants from his observations of rotation lines having $J' = 4$ through 11.
[b] $B = \frac{\nu_{obs} + 0.0016J'^2}{2J'} = \frac{\nu_{obs}}{2J'} + 0.008J'^2$.

130 microns. Measurements[4] of the vibration-rotation bands give a value of $B_0 = 10.44$ cm^{-1}. The value $B_0 = 10.45$ cm^{-1} is obtained from Strong's[5] measurements of the HCl pure rotation emission spectrum from 13 to 30 microns (final J's 17 through 33).

AMMONIA

The absorption spectrum of NH_3 showing the four longest wavelength rotation lines is presented in Fig. 2(b) and Table II. This spectrum was obtained using the 5-cm cell containing a mixture at atmospheric pressure of nitrogen and ammonia. All of the ammonia lines except the lowest frequency line should show a splitting having a separation equal to twice the inversion frequency of the molecule in the zero vibrational state. The spectrometer did not have enough resolution to resolve the splitting of the $J=3 \rightarrow J=4$ line at 79.45 cm^{-1}. The lower of the $J=0$ energy levels does not occur.[6] Therefore, only the lower frequency component of the doublet for $J=0 \rightarrow J=1$ should be observed. Table II is a tabulation of calculated and observed frequencies of the ammonia lines. Wright and Randall[7] have observed the splitting of the pure rotation lines of ammonia having final J's of 5, 6, and 7.

WATER VAPOR

Atmospheric water vapor in the optical path of the spectrometer caused enough absorption to permit study of the far infrared water vapor spectrum. Figure 3 is a trace with the noise removed of the spectrum drawn by the recording potentiometer showing water vapor

TABLE II. NH_3 rotation lines.

J''	J'	ν in cm^{-1} Calculated[a]	Observed	$\delta\nu$ in cm^{-1} Observed	B[b] in cm^{-1}
0	1	19.89[c]	19.1	...	9.90
1	2	39.77	39.8	1.4	9.95
2	3	59.62	59.5	1.4	9.93
3	4	79.45	79.4	not resolved	9.92

[a] $\nu_{calc} = 19.890J' - 0.00178J'^2$ (reference 9, p. 175).
[b] $B = (\nu_{obs}/2J') + 0.0009J'^2$.
[c] Values of calculated frequencies refer to the frequency midway between the two inversion components. The observed frequency for the $0 \rightarrow 1$ line should be $\delta\nu/2$ lower than the calculated frequency because this line is not doubled.

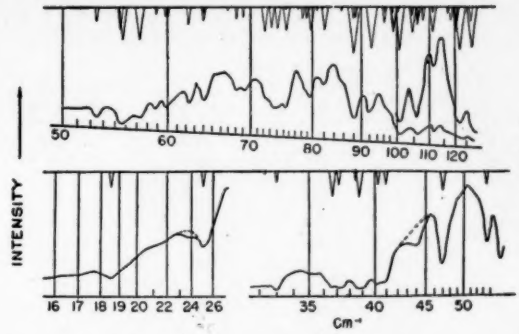

FIG. 3. Water vapor spectra traced directly from recorder charts. Triangles represent computed lines. The false lines at 44 and 23.5 cm^{-1} are the second-order spectra of the lines at 88 and 47 cm^{-1}. Areas of the triangles are portional to computed intensities.

TABLE III. Water vapor spectrum.

Line number	Transition J_{τ}''	J_{τ}'	Calculated frequency cm^{-1}	Observed frequency cm^{-1}	Calculated relative intensity
1	1_{-1}	1_1	18.58	18.7	44.2
2	2_{-2}	2_0	25.09	25.2	35.6
3	4_2	5_{-2}	32.28	32.4	1.1
4	1_0	2_{-2}	32.96	33.0	20.4
5	3_{-3}	3_{-1}	36.61	36.5	115
6	0_0	1_0	37.14	37.2	37.1
7	2_1	3_{-1}	38.47	b	16.8
8	3_{-1}	3_1	38.79		116
9	4_{-2}	4_0	40.25	40.2	33.4
10	2_0	2_2	41.00	40.9	30.4
11	5_{-3}	5_{-1}	47.05	47.0	69.2
12	4_{-4}	4_{-2}	53.44	53.5	33.0
13	2_{-1}	2_1	55.41	b	89.6
14	1_{-1}	2_{-1}	55.71		222
15	2_{-1}	3_{-3}	57.27	57.3	195
16	6_{-2}	6_0	58.82	58.8	11.1
17	6_{-4}	6_{-2}	59.79	b	14.6
18	7_{-3}	7_{-1}	60.02		17.6
19	5_{-1}	5_1	62.29	62.3	58.4
20	4_1	5_{-1}	64.01	64.2	10.6
21	3_{-2}	3_0	64.02	b	38.5
22	8_{-4}	8_{-2}	67.11		2.25
23	4_0	4_2	68.13	68.1	26.9
24	3_0	4_{-2}	69.19	69.3	18.7
25	2_{-2}	3_{-2}	72.21	72.3	110
26	3_1	3_3	73.24	b	83.4
27	5_{-5}	5_{-3}	74.09		89
28	4_{-3}	4_{-1}	75.55[a]	75.5	116
29	9_{-3}	9_{-1}	77.52		2.56
30	7_{-5}	7_{-3}	78.21	b	29.0
31	3_0	3_2	78.97		29.1
32	3_{-2}	4_{-4}	79.77[a]	79.5	111
33	9_{-5}	9_{-3}	80.98		3.88
34	8_{-2}	8_0	81.68		2.44
35	4_{-1}	4_1	82.11[a]	81.9	101
36	6_1	7_{-1}	85.60[a]	c	3.97
37	5_{-2}	5_0	87.88		27.6
38	3_{-3}	4_{-3}	88.06	88.1	405
39	7_{-1}	7_1	88.87[a]	c	16.8
40	5_{-4}	5_{-2}	89.53[a]	c	27.9

[a] (Reference 2).
[b] Observed as a single line.
[c] Not seen clearly enough to permit accurate assignment of frequency.

[4] S. M. Naudé and H. Verleger, Proc. Phys. Soc. (London) A63, 470 (1950).
[5] J. Strong, Phys. Rev. 45, 887 (1934).
[6] D. M. Dennison and J. D. Hardy, Phys. Rev. 39, 938 (1932).
[7] N. Wright and D. M. Randall, Phys. Rev. 44, 391 (1933).

TABLE IV. Hydrogen sulfide spectrum.

Calculated spectrum lines $T=300°K$				
ν cm^{-1}	$J_{\tau''}$	$J_{\tau'}$	Intensity	Frequency of observed bands
10.24	3_1	3_3	21.0	
12.24	3_{-1}	3_1	30.6	
12.29	4_0	4_2	10.6	
13.05	2_{-2}	2_0	7.7	
13.09	2_2	3_{-2}	0.053	
13.76	5_1	5_3	30.7	
14.52	4_2	4_4	8.57	
15.11	0_0	1_0	10.6	
16.89	6_2	6_4	9.22	
16.91	2_{-1}	2_1	25.9	17
18.30	7_1	7_3	23.8	
18.72	6_0	6_2	12.4	18.9
19.08	3_0	3_2	13.7	
19.61	8_2	8_4	4.94	
19.80	5_3	5_5	32.76	
20.26	5_{-1}	5_1	69.58	20.4
21.67	7_3	7_5	22.95	21.5
21.94	4_1	4_3	44.59	
22.13	4_{-2}	4_0	45.6	
22.90	1_0	2_{-2}	28.6	
23.58	3_{-3}	3_{-1}	68.1	
24.57	1_{-1}	2_{-1}	117.45	24.7
24.90	3_{-2}	3_0	23.0	
25.36	5_2	5_4	14.1	
25.39	6_4	6_6	7.73	
25.57	4_{-1}	4_1	79.1	
26.82	5_0	5_2	24.6	
27.07	8_0	8_2	8.95	
27.67	8_4	8_6	5.60	
27.74	4_2	5_{-2}	0.29	
27.74	7_1	8_{-3}	0.083	
28.81	6_1	6_3	58.05	28.80
29.06	6_3	6_5	30.81	
29.58	7_{-1}	7_1	61.46	
30.93	3_3	4_{-1}	3.15	
31.15	7_2	7_4	12.9	
31.74	6_{-2}	6_0	27.1	
33.13	2_{-1}	3_{-3}	263.4	
33.21	5_{-3}	5_{-1}	108.3	33.21
33.45	2_{-2}	3_{-2}	105.7	
33.96	4_{-4}	4_{-2}	30.3	
34.18	5_{-2}	5_0	36.7	
34.23	4_{-3}	4_{-1}	91.3	37.2
34.24	8_3	8_5	19.3	
34.26	6_{-1}	6_1	92.9	
34.90	8_6	8_8	3.58	
34.98	7_0	7_2	19.79	
35.84	1_1	2_1	240.9	35.9
36.03	8_1	8_3	36.5	
36.33	8_5	8_7	11.5	
39.80	2_1	3_{-1}	161.5	39.8
40.30	6_2	7_{-2}	0.308	
41.47	8_{-2}	8_0	18.0	
42.72	3_{-2}	4_{-4}	197.6	42.7
42.75	7_{-3}	7_{-1}	92.1	
42.76	3_{-3}	4_{-3}	596.3	
43.21	8_{-1}	8_1	56.79	
43.26	1_0	2_2	57.0	
43.44	7_{-2}	7_0	31.9	
43.53	6_{-4}	6_{-2}	44.3	43.5
43.69	6_{-3}	6_{-1}	133.2	
43.89	5_{-5}	5_{-3}	124.6	
43.93	5_{-4}	5_{-2}	41.6	
45.30	2_0	3_0	141.1	45.1
47.40	4_4	5_0	3.24	
47.90	5_3	6_{-1}	3.99	
50.80	8_2	9_{-2}	0.10	
51.78	3_0	4_{-2}	163.3	51.4
52.19	4_{-3}	5_{-5}	889.4	52.0
52.19	4_{-4}	5_{-4}	298.3	
52.92	8_{-4}	8_{-2}	28.2	
53.08	8_{-3}	8_{-1}	85.0	
53.41	3_{-1}	4_{-1}	550	53.2
53.44	7_{-5}	7_{-3}	128.5	

Calculated spectrum lines $T=300°K$				
ν cm^{-1}	$J_{\tau''}$	$J_{\tau'}$	Intensity	Frequency of observed bands
53.46	7_{-4}	7_{-2}	42.8	
53.70	6_{-6}	6_{-4}	43.9	
53.71	6_{-5}	6_{-3}	131.6	
54.83	3_2	4_0	51.14	55.5
57.07	2_2	3_2	226.7	57.2
61.62	5_{-4}	6_{-6}	439.8	59.9
61.62	5_{-5}	6_{-5}	1141	
61.85	4_{-1}	5_{-3}	766.5	
62.16	4_{-2}	5_{-2}	297	
62.28	2_1	3_3	630	61.7 to 62.7
62.36	5_5	6_1	13.3	
62.52	7_3	8_{-1}	2.0	
62.93	9_{-4}	9_{-2}	22.7	
62.93	9_{-5}	9_{-3}	68.0	
63.26	8_{-5}	8_{-3}	108.1	
63.26	8_{-6}	8_{-4}	36.05	
63.46	7_{-6}	7_{-4}	42.17	
63.46	7_{-7}	7_{-5}	126.5	
66.74	3_1	4_1	644.7	66.6
66.85	6_4	7_0	3.09	
67.81	4_3	5_1	99.6	
68.95	2_{-1}	3_1	135.5	69.0
69.39	4_1	5_{-1}	520.2	
71.07	6_{-5}	7_{-7}	1288	
71.07	6_{-6}	7_{-6}	470	
71.39	5_{-2}	6_{-4}	319.9	
71.44	5_{-3}	6_{-3}	960	71.4
72.98	9_{-6}	9_{-4}	29.61	
72.98	9_{-7}	9_{-5}	88.83	
73.24	8_{-7}	8_{-5}	108.8	73.0
73.24	8_{-8}	8_{-6}	36.28	
74.21	4_3	5_0	229.3	
76.44	6_6	7_2	3.9	74.4
77.43	2_{-2}	3_2	39.5	
78.44	3_3	4_3	1231	78.2
79.02	5_4	6_2	17.5	
80.47	7_{-6}	8_{-8}	442.3	
80.47	7_{-7}	8_{-7}	1308	
80.74	5_3	6_{-2}	246.9	80.7
80.82	6_{-3}	7_{-5}	1040.7	
80.83	6_{-4}	7_{-4}	339.7	
81.64	3_2	4_4	411	
81.92	5_{-1}	6_{-1}	801	82.0
82.73	10_{-7}	10_{-5}	64.6	
82.73	10_{-8}	10_{-6}	21.5	
82.99	9_{-8}	9_{-6}	29.1	
82.99	9_{-9}	9_{-7}	87.2	
84.06	7_5	8_1	11.8	
85.66	5_2	6_0	123.1	
86.20	3_0	4_2	138.9	
88.74	4_2	5_2	300	
89.07	6_5	7_3	24.6	
89.86	8_{-8}	9_{-8}	398.0	89.5
89.86	8_{-7}	9_{-9}	1209	
90.25	7_{-4}	8_{-6}	338	
90.25	7_{-5}	8_{-5}	991.5	
90.57	6_{-1}	7_{-3}	799.2	
90.76	6_{-2}	7_{-2}	269.8	
92.71	10_{-9}	10_{-7}	65.6	
92.71	10_{-10}	10_{-8}	21.9	
95.92	3_{-1}	4_3	93.6	95.6
95.92	5_1	6_1	706.2	
98.81	3_{-2}	4_0	40	
99.28	9_{-8}	10_{-10}	346.6	
99.28	9_{-9}	10_{-9}	1021	
99.58	4_4	5_4	553	99.5
99.61	8_{-5}	9_{-7}	879	
99.61	8_{-6}	9_{-8}	304	
99.83	6_3	7_1	194	
100.05	7_{-2}	8_{-4}	260.1	
102.39	11_{-10}	11_{-8}	14.9	
102.39	11_{-11}	11_{-9}	44.8	
102.46	6_0	7_0	209	

absorption. For the region from 50 to 120 cm^{-1} the absorption is caused by a path of about 4 inches of air at 20°C and 60 percent relative humidity. The spectrum from 33 to 55 cm^{-1} was obtained with a path through the air of about a foot. The lowest frequency spectrum was obtained with about 6 feet of laboratory air path. Figure 2(c), the H_2O spectrum plotted as percent transmission, was computed from the envelope obtained by drawing a curve through the intensity maxima of the spectrum taken after the entire optical path had been flushed with prepurified nitrogen which had passed through a liquid nitrogen trap. Even this degree of drying failed to remove the strong water lines.

The triangles drawn above the observed spectra in Figs. 2(c) and 3 represent the calculated frequencies and intensities of the pure rotation lines of water vapor. They were calculated by W. S. Benedict[8] using energy levels based on a restudy of the complete rotation-vibration spectrum. These levels differ only slightly from those of Dennison.[9] Transition probabilities were interpolated for $\kappa=-0.438$ in the tables of Cross, Hainer, and King.[10]

Table III, a tabulation of the observed and computed water vapor spectrum, reports the observation of 35 lines in the region of 89 to 15 cm^{-1}. Previously, the pure rotation spectrum of water vapor had been mapped with high resolution only to frequencies as low as 75 cm^{-1} in the infrared.[2]

HYDROGEN SULFIDE

Observed and computed spectra of H_2S are presented in Table IV and Fig. 4. The 5-cm cell containing a mixture of the absorbing gas and dry nitrogen at atmosphere pressure was used again. The computed spectrum is represented by lines with lengths proportional to the intensities of the absorbing lines. This method of representation was chosen instead of the triangles because it was better suited to the regions of the spectrum where many lines are crowded together. The energy levels used in the calculation are those of Cross.[11] These energy levels are complete through $J=8$ and include some of the lower levels for J as high as 12. Most of the lines which cannot be computed from these levels are either very weak or are of higher frequency than 100 cm^{-1}. Intensities are calculated from the tables of Cross, Hainer, and King[6] for a temperature of 300°K and with the asymmetry parameter of $\kappa=0.5$.

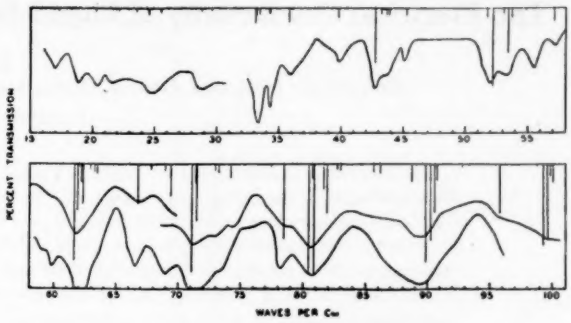

FIG. 4. The far infra spectrum of H_2S with computed spectrum.

ACKNOWLEDGMENTS

The construction of the equipment used for this work was carried out under the supervision of John Strong. The author wishes to acknowledge the help of William M. Sinton and W. S. Benedict.

[8] Written communication; cf. W. S. Benedict and E. K. Plyler, J. Research Nat. Bur. Standards 46, 246 (1951).
[9] D. M. Dennison, Revs. Modern Phys. 12, 189 (1940).
[10] Cross, Hainer, and King, J. Chem. Phys. 12, 200 (1944).
[11] P. C. Cross, Phys. Rev. 47, 12 (1935).

The Electrical Conductivity of Liquid Selenium and Selenium-Tellurium Mixtures*

B. LIZELL
Laboratory for Insulation Research, Massachusetts Institute of Technology, Cambridge, Massachusetts
(Received October 29, 1951)

The electrical conductivity of liquid selenium and selenium-tellurium mixtures was studied in detail. Measurements in the temperature range 230° to 500°C from dc to 1 mc/sec indicated the conductivities to be frequency-independent at low field strength (<5 v/cm). For larger fields (5 to 250 v/cm) the conductivity increases and higher dc than ac values result. Adding increasing amounts of tellurium to selenium produced a continuous rise in conductivity from 1.26×10^{-4} ohm^{-1} cm^{-1} (pure Se) to 2.08×10^{-1} ohm^{-1} cm^{-1} (50.3 percent Se, 49.7 percent Te) at 480°C and a decrease in activation energy from 1.14 ev to 0.84 ev. Comparatively good reproducibility was obtained in the measurements. An attempt to study ionic migration in liquid selenium by tracer methods has thus far not given satisfactory results. The conductivity values obtained for pure selenium are in good agreement with those presented by Henkels but disagree with those of Borelius. The electrical characteristics of liquid selenium and selenium-tellurium mixtures indicate that hole conduction as pictured for selenium in the solid state cannot be considered as an adequate explanation of the conduction process in these liquids. A complex mixture of conduction by electrons, holes, and ions is believed to exist.

INTRODUCTION

A LONG-RANGE research program on the transition from electric insulators to metals in the VI_b group of the periodic system is under way in this laboratory. As a link in this work an investigation of the electrical conductivity of liquid selenium and selenium-tellurium mixtures has been undertaken. A recent x-ray investigation of solid selenium-tellurium alloys in this laboratory by Grison[1] gave valuable evidence as to the substitution of Te for Se and connects this phase of our research to proposed electrical measurements on single crystals of the solid Se-Te copolymers.

While no previous research on the electrical conductivity of liquid Se-Te mixtures has apparently been reported, for the liquefied elements themselves the following work preceded ours. Pélabon[2] undertook a single series of conductivity measurements on Se between 390° and 690°C. Borelius and co-workers[3] reported on the conductivity of liquid and solid selenium from room temperature to 500°C. For liquid selenium the specific resistance followed the law $\log\rho=A+B/T$ in the range measured. The factor B which is related to the activation energy of the conduction process was found to vary from 2550 to 6700 and the measured conductivities were dependent on the time of heating, the particular specimen, and the depth of immersion of the platinum electrodes in the melt. Much more reproducible data were recently obtained by Henkels;[4] his average value of B is 5850 (max deviation, 3.4 percent) and A is -3.81 (with 10 percent deviation). A slight change in the temperature coefficient at about 300°C was attributed to the presence of selenium dioxide. Kraus and Johnson[5] reported measurements on liquid and solid tellurium and tellurium-sulfur mixtures. A continuously increasing resistivity from 6.410×10^{-4} ohm cm at 440°C (undercooled) for pure tellurium to 2.317×10^{5} ohm cm at the same temperature for tellurium containing 85 percent sulfur was found. Several investigations on the conductivity and photoconductivity of solid selenium-tellurium mixtures have been reported.[6]

CONDUCTIVITY CELLS

Experimental Procedure

Our conductivity cells were made of quartz because it is more resistant to selenium attack than any other glass. Very pure graphite served as the electrodes as this material proved to be the only one inert to selenium attack in our test of the most inactive elements: gold, platinum, and graphite. The pure selenium and mixtures with a low tellurium content were measured in a coaxial cell (Fig. 1) designed to give an even field distribution and to enable measurements up to 1 mc. The capillary cell of Fig. 2 was used for mixtures rich in tellurium. Both cells were mounted in the furnace shown. The selenium or Se-Te mixture was introduced into the cell in a two-step distillation in Vycor apparatus under a pressure of 2×10^{-5} mm Hg. An evacuation time of about 10 hr insured complete outgassing before sealing the cells.

The cells were calibrated with $M/50$ and $M/100$ KCl solutions at 10 kc. From the results a series lead resistance of 0.2 ohm and a geometrical cell constant (length/cross section) of 0.0415 cm^{-1} (electrode capacitance 2.13 $\mu\mu$f) were calculated for the coaxial conductivity cell. A cell constant of 369 cm^{-1} was obtained for the capillary cell. The inductive effect in the leads of the coaxial cell was found to be 1.4×10^{-6} h from measurements on conductivity water at 100 kc, 1 mc, and 3.45 mc.

* Sponsored by the ONR, the Army Signal Corps, and the Air Force under ONR Contract N5ori-07801.

[1] E. Grison, J. Chem. Phys. **19**, 1109 (1951).
[2] H. Pélabon, Compt. rend. **173**, 295 (1921).
[3] Borelius, Phihlstrand, Andersson, and Gullberg, Arkiv Mat. Astron. Fysik **30A**, No. 14 (1944).
[4] H. W. Henkels, J. Appl. Phys. **21**, 725 (1950).
[5] C. A. Kraus and E. W. Johnson, J. Phys. Chem. **32**, 1281 (1928).
[6] For a survey see *Gmelins Handbuch der anorganischen Chemie* (Verlag Chemie, G.m.b.H., Weinheim/Bergstrasse, Theil 10, Selen A2, 1950), p. 356.

Measurement Technique

The dc measurements were carried out on a Wheatstone bridge (galvanometer sensitivity, 1.4×10^{-6} amp). The ac measurements up to 10 kc were made by the resistance substitution method using a General Radio capacitance bridge, while at radio frequencies a susceptance variation circuit was used. The temperature in the furnace was determined with a chromel-alumel thermocouple calibrated together with the potentiometer at the condensing points of steam and sulfur with an estimated accuracy of ±1°C.

The errors in the resistance measurements at dc and 1 to 10 kc amounted to one percent except for the measurements on the field-strength dependence of the conductivity, where they were 2 percent. The error at radio frequencies and high temperatures was 5 to 10 percent since the large conductivity resulted in a flattened resonance band with sample in. At intermediate temperatures the error was reduced below 5 percent. The accuracy of the cell calibrations for measurements from dc to 10 kc equaled 3 percent, and above 300°C the error was estimated to be 5 percent for measurements at radio frequencies.

Purity of the Selenium and Tellurium

Spectrographic analysis of the selenium[7] for 70 elements showed only traces of copper, potassium, magnesium, and sodium. The copper and the magnesium may have come from the electrodes. The total amount of impurities was <30 parts per million. A spectrographic analysis of the tellurium[7] for 20 elements by the manufacturer gave evidence of very faint traces of iron, copper, and silicon, and some trace of arsenic.

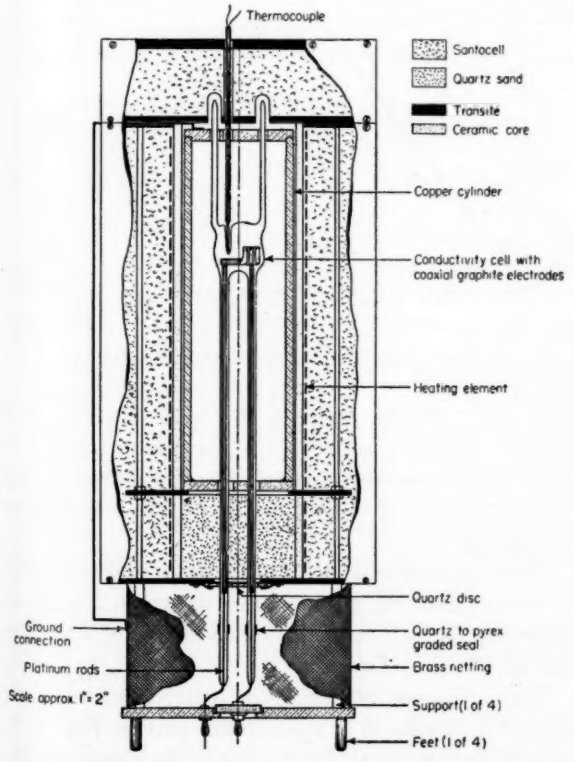

FIG. 1. Furnace and cell for conductivity measurements on liquid Se and Se-Te mixtures.

[7] Our selenium and tellurium was obtained from the American Smelting and Refining Company, New York, New York.

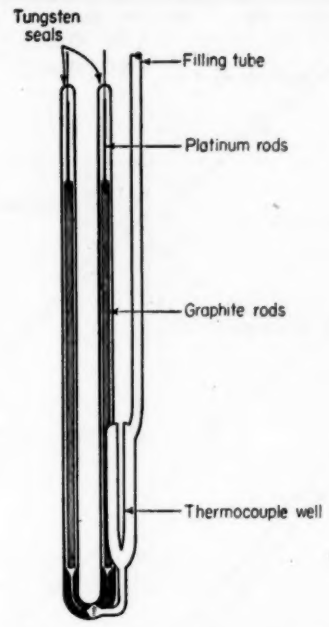

FIG. 2. Conductivity cell for measurements on Se-Te mixtures with high Te content.

EXPERIMENTAL RESULTS

Temperature Dependence of the Conductivity

Pure Selenium

Two complete conductivity curves from 230° to 500°C and back (designated as Runs 1 and 2) were obtained for pure selenium. Most measurements were taken at low field strength (below 5 v/cm). The conductivities measured at dc, 300 c, 1 kc, and 10 kc agree within 2 percent. The higher experimental error for measurements on the susceptance variation circuit caused a larger spread of the data at 100 kc and 1 mc. The data at temperatures above 300°C show the conductivity to be independent of frequency (dc to 1 mc). A nonlinear relationship between $\log\sigma$ (σ is the volume conductivity) and $1/T$ found in the return run of Run 1 proved to be due to the presence of SeO_2 (see insert, Fig. 3). This effect of the oxide was found previously by Henkels.[4] A crack had formed in the seal of the cell at elevated temperatures and a small amount of air had leaked in. Evaporation in vacuum removed the SeO_2 and the linear relationship between $\log\sigma$ and $1/T$ became restored.

Selenium-Tellurium Mixtures

Runs 3 to 6 refer to samples containing 0.1, 1.0, 5.0, and 19.8 percent of tellurium. A few checks proved the

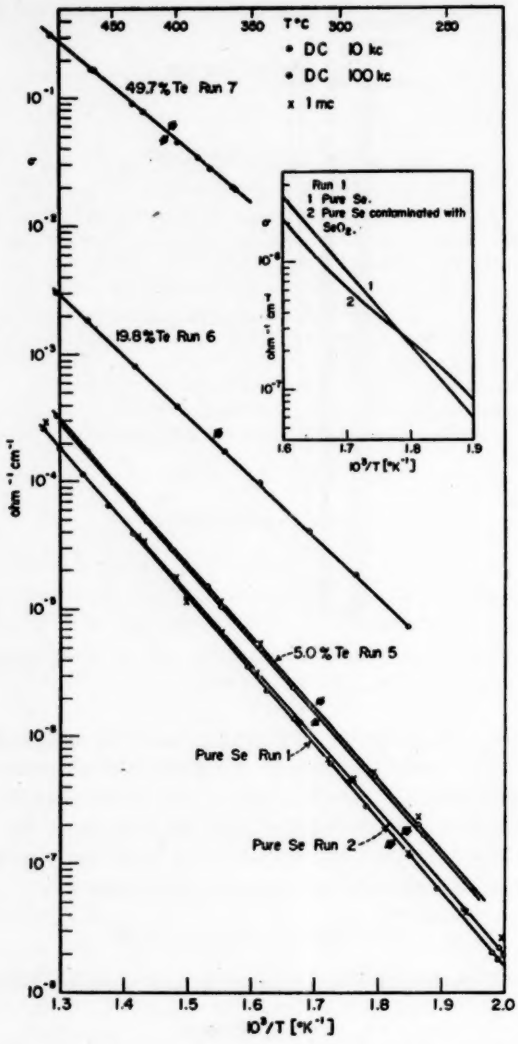

FIG. 3. Electrical conductivity of liquid Se and Se-Te mixtures. Insert, effect of SeO_2 on conductivity of pure Se.

conductivity still to be independent of frequency up to 1 mc. Most data were taken from dc to 100 kc. Good agreement was found in the measurements taken with rising and falling temperature in Run 3. A small decrease in slope was observed above 330°C but the direction of the change was opposite to that found for melts containing oxide. Trapped air in the bottom of the leads unfortunately contaminated the melt for Run 4 at high temperatures and caused the familiar nonlinear relationship between $\log\sigma$ and $1/T$ in the curve taken with falling temperature. A close agreement was obtained for rising and falling branches in the conductivity *vs* temperature curves in Run 5. For Run 6 only the rising branch of the curve is given as experimental difficulties made the results obtained with falling temperature unreliable.

Run 7, with 49.7 percent of tellurium in the melt, was carried out with the capillary cell because the mixture was too conducting for the coaxial sample holder to be used. To avoid the formation of gas bubbles in the capillary, the cell was sealed off at about 400°C under 50 cm of helium pressure. Measurements were taken from dc to 100 kc between the melting point of the mixture (~345°) and 500°C. The design of the cell prevented measurements at 1 mc. No change in slope was observed after reversal of the direction of temperature change.

TABLE I. Electrical conductivity of liquid selenium and selenium-tellurium mixtures at 480°C.

Composition of melt	Conductivity (ohm^{-1} cm^{-1})
Pure selenium, Run 1	1.25×10^{-4}
Pure selenium, Run 2	1.26×10^{-4}
99.9% Se, 0.1% Te, Run 3	1.30×10^{-4} } not shown
99.0% Se, 1.0% Te, Run 4	1.45×10^{-4} } in Fig. 3
95.0% Se, 5.0% Te, Run 5	2.13×10^{-4}
80.2% Se, 19.8% Te, Run 6	2.15×10^{-3}
50.3% Se, 49.7% Te, Run 7	2.08×10^{-1}

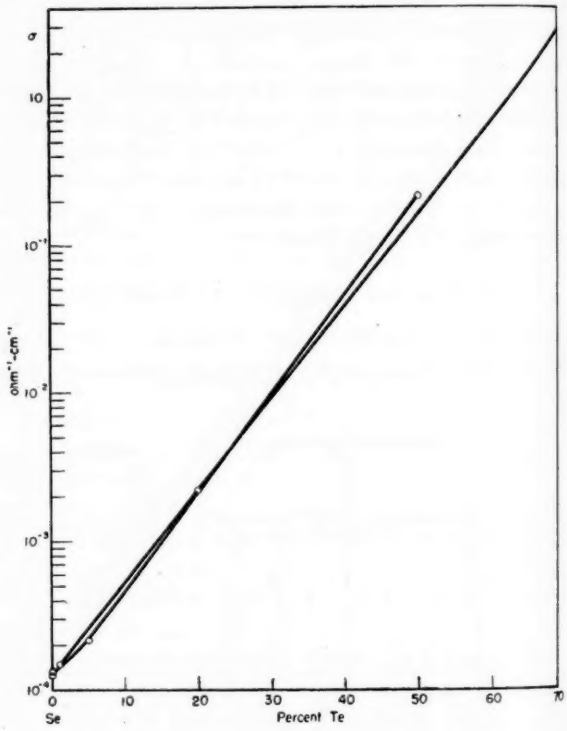

FIG. 4. Conductivity of Se-Te mixtures at 480°C.

The data obtained for pure selenium and the various selenium-tellurium mixtures are shown in Fig. 3; the values for the various melts are compared at a temperature of 480°C in Table I.

The continuous increase in conductivity with tellurium content is shown in a logarithmic plot in Fig. 4. The straight line connecting the value of the conductivity of pure selenium observed by the author, with the value of pure tellurium reported by Kraus and Johnson,[5] fits the data relatively well.

Activation Energies

The temperature dependence of the conductivity may be expressed by an activation energy equation

$$\sigma = \sigma_0 e^{-(U/kT)},$$

which can be rewritten as

$$\log\sigma = A' - (B/T),$$

where $A' = \log\sigma_0$ and $B = (U/k)(\log e)$. The values obtained for A', σ_0, B, and U are given in Table II.

Field-Strength Dependence of the Conductivity of Liquid Selenium

The conductivity characteristics reported above refer to an applied field strength of less than 5 v/cm. At higher fields the conductivity was found to depend on the duration and magnitude of the applied voltage. This effect was investigated in detail during Run 2 on pure selenium (Figs. 5 and 6). The conductivity rises at constant voltage to a final value, and returns slowly again to the original after removal of the voltage. The effect of reversal of the polarity during a continuous run was recorded for a field strength of 250 v/cm at 256° and for several field strengths at 402°C.

TABLE II. Constants in the activation energy equation for liquid selenium and selenium-tellurium mixtures in the temperature range 230°–500°C.

Run no.	A'	σ_0 ohm^{-1} cm^{-1}	B	U ev
Run 1 up (pure selenium)	3.81	6.5×10^3	5810	1.15
Run 1 after removal of SeO_2	4.31	2.1×10^4	6140	1.22
Run 2 up (pure selenium)	3.67	4.7×10^3	5700	1.13
Run 2 down	4.12	1.3×10^4	6040	1.20
Run 3 up and down (0.1% Te)				
low temperature	4.50	3.1×10^4	6210	1.23
high temperature	3.78	6.1×10^3	5780	1.15
Run 4 up (1% Te)	4.08	1.2×10^4	5960	1.18
Run 5 up (5% Te)	3.83	6.8×10^3	5650	1.12
Run 5 down (5% Te)	3.86	7.2×10^3	5680	1.13
Run 6 up (19.8% Te)	3.60	4.0×10^3	4730	0.94
Run 7 up and down (49.7% Te)	4.92	8.3×10^4	4220	0.84

Summarizing, we found that:

1. The conductivity rises with an increase in field strength.
2. This increase is appreciably larger for dc than for ac.
3. The effect is larger with the center electrode as anode than as cathode.
4. Reversal of the polarity during a continuous run results in an abrupt decrease of the conductivity followed by a slow increase.
5. When the applied voltage is removed the original value of the conductivity is slowly restored.
6. The effect of the field strength on the conductivity is decreased by over 50 percent when the measurements are made at 402° instead of 256°C.

The dependence of the conductivity on the electrode polarity was even apparent at low field strengths (1 to 5 v/cm). Higher values resulted with the center electrode as anode than as cathode, the difference increasing at lower voltage, but the effect is of the order of one percent and can therefore be neglected in the discussion of activation energies.

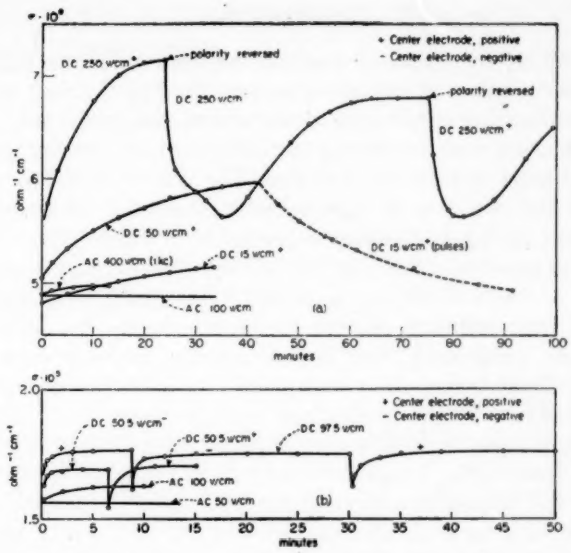

FIG. 5. Field-strength dependence of the conductivity of pure liquid Se (a) at 256°C, (b) at 402°C.

Similar measurements on the mixture containing 19.8 percent tellurium at 289° and 402°C showed only a small field-strength and practically no polarity dependence of the conductivity. For a field strength below 100 v/cm all changes were within 2 percent, i.e., within the experimental error. An increase in the conductivity of about 3 percent at 100 v/cm was partially due to the clearly noticeable heating of the sample by the current.

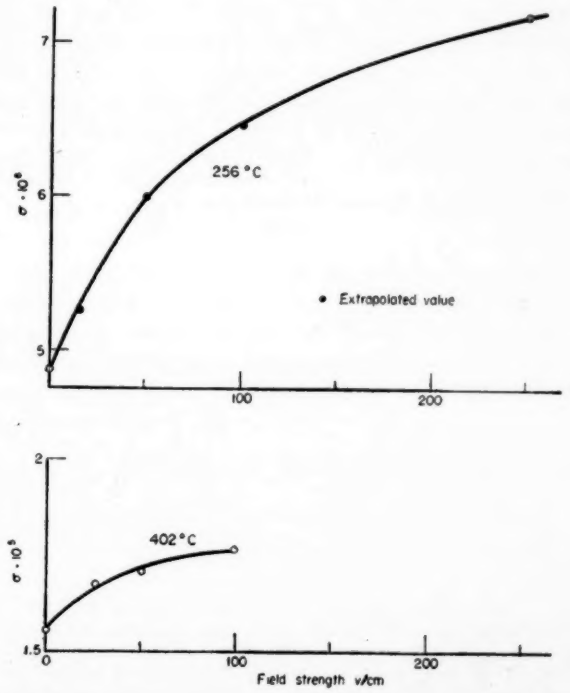

FIG. 6. Field-strength dependence of the conductivity of pure liquid Se (dc, center electrode positive, equilibrium values).

DISCUSSION

Since, by chemical reaction between selenium and quartz, traces of impurities seemed to enter the melt on long heating at elevated temperatures, the initial measurements with increasing temperature were considered the most reliable for each run. The values so obtained for the two runs on pure selenium showed good agreement giving an average value for B of 5760 (1.14 ev) with an error of less than 1.0 percent. The average value of A' was 3.74 with an error of 1.9 percent. If all curves on pure selenium (except for those affected by SeO_2) were considered, the corresponding numbers were: $B=5920$ (error, 3.7 percent) and $A'=3.98$ (error, 8.3 percent). These results are in agreement with the measurements presented by Henkels[4] with a B (average) of 5850 (error, 3.4 percent) and an A' (average) of 3.81 (error, 10 percent), but disagree with those by Borelius.[3] Henkels made his measurements in an open beaker and obtained SeO_2 contamination in the melts as indicated by some of his curves. In the present investigation a nonlinear relationship between $\log\sigma$ and $1/T$ was observed only when air leaked into the cell. The presence of oxide gives a higher slope above *ca* 330°C, and the value of 5850 reported as average for B by Henkels (compared to 5760 found by the author) can thus be explained. However, the difference is small (1.6 percent) and the results support each other.

CONDUCTION MECHANISM IN LIQUID SELENIUM AND SELENIUM-TELLURIUM MIXTURES

The semiconductor theory as applied to a periodic lattice in the solid state cannot be assumed to hold for the random structure of a liquid. To account for the exponentially increasing conductivity with temperature of liquid selenium, an ionic conduction by positive and negative ions was suggested.[8] The lowered viscosity and shortened chain length at elevated temperatures would favorably influence an ionic conductivity. Attempts made by the author to achieve direct evidence of ionic migration by a tracer technique have thus far given no results which justify a statement in one direction or another. Conductivity measurements cannot give information on the conduction mechanism involved, since both electronic and ionic conduction are expected to follow an exponential law

$$\sigma=\sigma_0 e^{-(U/kT)}$$

in their temperature dependence.

The measurements on selenium-tellurium mixtures indicate that a simple electronic conduction process does not occur. Selenium and tellurium form true copolymers by replacement of a selenium atom in a chain by a tellurium atom.[1] Additions of small amounts of tellurium to a selenium melt would therefore be expected to decrease hole conductivity along the chains due to the interrupted periodicity of the molecule. The continuous increase in conductivity from 1.26×10^{-4} ohm^{-1} cm^{-1} for pure selenium at 480°C to 2.08×10^{-1} ohm^{-1} cm^{-1} for a mixture containing 49.7 percent tellurium at the same temperature, with a subsequent change in activation energy from 1.14 ev to 0.84 ev, does not give evidence of such a phenomenon. The comparatively long time required for the final values to be established in the measurements on the field-strength dependence of conductivity suggests that a migration process takes place. For a proper interpretation of the results additional information is required. The observed electrical characteristics suggest a complicated mixture of conduction through holes, electrons, and ions.

ACKNOWLEDGMENTS

The author is indebted to Professor A. R. von Hippel for suggesting the subject of this investigation and for his helpful advice throughout the work, and to J. Kalnajs and W. B. Westphal for their kind assistance in several problems of chemical preparation and measuring techniques.

[8] A. von Hippel, personal communication.

Flow Birefringence in Polydisperse Systems of Rod-Like Molecules Having a Montroll-Simha Distribution

MARTIN GOLDSTEIN*
The Polytechnic Institute of Brooklyn, Brooklyn, New York
(Received December 7, 1951)

Values of the quantities measured in flow birefringence experiments (extinction angle χ and optical factor F) are calculated for polydisperse systems of rigid rod-like molecules, where the polydispersity is assumed to arise from random degradation of a system of molecules all having the same initial length. The recent calculations of Scheraga, Edsall, and Gadd, and the distribution function of Montroll and Simha are used. A number of simplifying assumptions are made, and their effect on the results is discussed.

INTRODUCTION

THE usefulness of flow birefringence as a tool for the study of the size and shape of large molecules has been greatly enhanced by the work of Scheraga, Edsall and Gadd,[1] who have solved the equation of Peterlin and Stuart[2] by numerical methods for large values of the velocity gradient. As SEG points out, it is possible with the aid of these computations to deal with polydisperse systems in a more quantitative way than has previously been possible.

The equations that determine the quantities measured in a flow birefringence experiment when the system is polydisperse have been given by Sadron.[3] These were tested experimentally on systems of two chemically different components by Sadron, and applied by Edsall and Foster[4] to the case of a molecule associating to form a dimer.

In the study of flow birefringence in certain systems in which there was some reason to believe that the molecules were essentially rigid, as is required by the theory of Peterlin and Stuart,[2] deviations from the theoretical curve of SEG for extinction angle against gradient were observed; these deviations were consistent with the assumption that these systems are polydisperse in the sense of having a distribution of sizes among molecules that are essentially similar otherwise.[5]

In a preliminary attempt to deal with this situation theoretically, a form of size distribution was assumed that was easily treated mathematically. This was a "rectangular" distribution; i.e., one in which the number of molecules having a given length was constant over a specified range of lengths and zero outside this range.

On comparison of the calculated values with experimental data, it was found that the theoretical curve for this type of distribution accounted for only a part of the observed deviations from the curve of SEG. On examination of the results of the calculation, a possible reason for this failure could be deduced; in flow birefringence observations at low and moderate velocity gradients, the largest molecules contribute most heavily to the phenomenon; in a distribution where these are present in molar amounts comparable to the smaller molecules they dominate the situation, and while the calculated curves for such systems will deviate from the monodisperse curve, they will not deviate by much. In other words, flow birefringence is sensitive not merely to the existence of polydispersity, but sensitive to the form of the distribution at the high molecular weight end.[5]

Obviously a more realistic form of molecular distribution is needed for this type of calculation. Perhaps the most generally useful would be a Gaussian one. Scheraga has treated this case in a preliminary way.[6]

However, in some systems of large molecules having a biological origin, there is reason to postulate that in the living tissue there exist parent molecules having a fixed length; polydispersity arises from some degradation of the parent molecule that takes place on extraction from the tissue.[7] For this type of system the distribution function worked out by Montroll and Simha[8] is the appropriate one.

THEORY

Montroll and Simha treat the distribution of t-mers resulting when N molecules, all composed of $p+1$ monomers, are subjected to a degradation process involving the random breaking of a fraction s† of the total of Np bonds in the system. They find for the number of t-mers N_t

$$N_t = Ns(1-s)^{t-1}[2+(p-t)s] \quad t \leqq p \tag{1}$$

and for the number of undegraded molecules N_{p+1}

$$N_{p+1} = N(1-s)^p. \tag{2}$$

* U. S. Public Health Service Postdoctoral Fellow of the National Institutes of Health. Present address: Department of Chemistry, Harvard University, Cambridge, Massachusetts.

[1] Scheraga, Edsall, and Gadd, J. Chem. Phys. **19**, 1101 (1951). This paper will be referred to as SEG.

[2] A. Peterlin and H. A. Stuart, Z. Physik. **112**, 1, 129 (1939).

[3] C. Sadron, J. phys. et radium **9**, 381, 384 (1938).

[4] J. T. Edsall and J. F. Foster, J. Am. Chem. Soc. **70**, 1860 (1948).

[5] M. Goldstein, 119th Meeting Am. Chem. Soc., Boston, (April, 1951).

[6] H. A. Scheraga, J. Chem. Phys. **19**, 983 (1951).

[7] See for example Scatchard, Oncley, Williams and Brown, J. Am. Chem. Soc. **66**, 1980 (1944).

[8] E. W. Montroll and R. Simha, J. Chem. Phys. **8**, 721 (1940).

† The symbol s is used in place of the α of Montroll and Simha to avoid confusion with the α used later in this paper to represent the ratio of the gradient to rotary diffusion constant.

To determine the flow birefringence parameters of such a system, the weight fractions of t-mer and $p+1$-mer are needed; these are proportional to tN_t and $(p+1)N_{p+1}$.

It was found convenient to simplify the expressions for the weight fractions by the neglect of unity compared to p and t, and with the introduction of the approximations

$$\begin{aligned}(1-s)^{t-1} &\cong e^{-st} \\ (1-s)^{p} &\cong e^{-sp}.\end{aligned} \tag{3}$$

These approximations fail under two conditions. One is when s is appreciable compared to unity; this represents physically a system in a very advanced degree of degradation. The other is when st and sp are large compared to unity (equal to 10 or greater); under these conditions the number of highly polymerized molecules at somewhat advanced degrees of degradation is in error, but this is under conditions when this number is so small that these large molecules are no longer contributing appreciably to the observed birefringence. It is interesting to note that with the approximations (3), the correct value for the number average molecular weight of the distribution is obtained regardless of the value of s.

With the aid of the above approximations, tN_t is expressible as a function of two parameters only: sp, which has the meaning of the average number of bonds broken per parent molecule; and st.

We obtain

$$tN_t = N[(2-sp)st - s^2t^2]e^{-st}. \tag{4}$$

For convenience we introduce two new variables $\gamma = sp$ and $x = t/p$. x varies from 0 to 1 over the distribution. We find

$$tN_t = N[(2+\gamma)\gamma x - \gamma^2 x^2]e^{-\gamma x}. \tag{5}$$

As we wish to replace a sum over the distribution by an integral, we must integrate with respect to the variable that takes on successive integral values, namely t. Since $dt = p\,dx$ we obtain for the weight fraction of material in the range dx:

$$tN_t\,dt/pN = [(2+\gamma)\gamma x - \gamma^2 x^2]e^{-\gamma x}dx. \tag{6}$$

Neglecting unity compared to p, the weight fraction of undegraded parent molecule is given by

$$pN_p/pN = e^{-\gamma}. \tag{7}$$

Thus we see that although the ratio of the weight of t-mer to weight of parent molecule is dependent explicitly on p, the number of bonds in the molecule, the ratio of weight within a range of t values covered by dx is not. This is to be expected intuitively.

We find

$$\int_0^1 [(2+\gamma)\gamma x - \gamma^2 x^2]e^{-\gamma x}dx = 1 - e^{-\gamma}, \tag{8}$$

so the distribution is normalized.

In flow birefringence measurements two quantities, χ, the extinction angle, and Δ, the amount of birefringence, are obtained. In monodisperse systems of rigid ellipsoidal molecules these are functions of two parameters; α, the dimensionless ratio of velocity gradient G to the rotary diffusion constant θ of the molecule, and the axial ratio. At large axial ratios (greater than 20) χ is almost independent of axial ratio and Δ is only slightly sensitive. Hence for elongated molecules, the limiting values for axial ratio equal to infinity from SEG are used.

χ is given as a function of α in tabular form by SEG. Δ is given by the relation[1]:

$$\Delta = (2\pi c/n_s)(g_1 - g_2)f(\alpha), \tag{9}$$

where $f(\alpha)$ is a function of α given in tabular form in SEG, c is the volume fraction of macromolecule, $g_1 - g_2$ an optical parameter of the molecule,[2] and n_s the refractive index of the solution at rest.

The following assumptions are made in this treatment:

I. The rotary diffusion constant θ varies inversely as the cube of the molecular length. This follows from the exact relation for θ when axial ratio is greater than five[9]:

$$\theta = \frac{kT}{8\pi\eta a^3}\frac{3}{2}\left(-1 + 2\ln 2\frac{a}{b}\right). \tag{10}$$

η is the solvent viscosity, a and b are the semi-major and semi-minor axes of the ellipsoid of revolution, and kT has its usual meaning.

At large axial ratio θ varies rapidly with a and only slowly with axial ratio. The conditions under which the approximation will break down are discussed below.

II. The optical factor $g_1 - g_2$ is independent of length. This means physically that the maximum amount of birefringence that could be obtained is dependent on the volume fraction of polymer only. That this should be so for rigid elongated molecules was pointed out by Kuhn[10] and observed experimentally in systems of rod-like molecules by De Rosset.[11]

Sadron's[3] theoretical treatment of polydispersity gives the following relations among the observed χ and Δ in a birefringent system and the extinction angles φ_i and birefringences δ_i of the individual components:

$$\begin{aligned}\tan 2\chi &= (\textstyle\sum_i \delta_i \sin 2\varphi_i)/(\sum_i \delta_i \cos 2\varphi_i) \\ \Delta^2 &= (\textstyle\sum_i \delta_i \sin 2\varphi_i)^2 + (\sum_i \delta_i \cos 2\varphi_i)^2.\end{aligned} \tag{11}$$

It may readily be shown that an optical factor F for a polydisperse system obeying the second assumption may be so defined that

$$F^2 = (\textstyle\sum_i \delta_i' \sin 2\varphi_i)^2 + (\sum_i \delta_i' \cos 2\varphi_i)^2 \tag{12}$$

[9] See for example E. J. Cohn and J. T. Edsall, *Proteins, Amino Acids and Peptides* (Reinhold Publishing Corporation, New York, 1943), Chapter 21.

[10] W. Kuhn, Z. Physik Chem. **A161**, 1 (1932).

[11] A. J. De Rosset, J. Chem. Phys. **9**, 766 (1941).

and

$$\Delta=(2\pi c/n_s)(g_1-g_2)F,$$

where δ_i' is the product of the optical factor f_i of the ith component by its weight fraction. Then

$$\tan 2\chi=(\sum_i\delta_i' \sin 2\varphi_i)/(\sum_i\delta_i' \cos 2\varphi_i).$$

These sums are to be expressed as integrals over the distribution function. To do this the variable x must be expressed in terms of α. Remembering that x may be looked upon as the ratio of the length of the t-mer l_t to the undegraded molecule l_0 and that θ is assumed to vary inversely as the cube of the length, we have

$$\begin{aligned} x&=l_t/l_0=(\alpha_t/\alpha_0)^{\frac{1}{3}} \\ dx&=\tfrac{1}{3}(\alpha_t/\alpha_0)^{-\frac{1}{3}}d(\alpha_t/\alpha_0), \end{aligned} \tag{13}$$

where the subscript zero denotes the values of l and α for the undegraded molecule.

Hence we have

$$\sum_i\delta_i' \sin 2\varphi_i=f(\alpha_0)\sin 2\varphi(\alpha_0)e^{-\gamma}$$
$$+\frac{1}{3}\int_0^{\alpha_0}[(2+\gamma)\gamma(\alpha/\alpha_0)^{-\frac{1}{3}}-\gamma^2]$$
$$\times\exp[-\gamma(\alpha/\alpha_0)^{\frac{1}{3}}]f(\alpha)\sin 2\varphi(\alpha)(d\alpha/\alpha_0) \tag{14a}$$

$$\sum_i\delta_i' \cos 2\varphi_i=f(\alpha_0)\cos 2\varphi(\alpha_0)e^{-\gamma}$$
$$+\frac{1}{3}\int_0^{\alpha_0}[(2+\gamma)\gamma(\alpha/\alpha_0)^{-\frac{1}{3}}-\gamma^2]$$
$$\times\exp[-\gamma(\alpha/\alpha_0)^{\frac{1}{3}}]f(\alpha)\cos 2\varphi(\alpha)(d\alpha/\alpha_0). \tag{14b}$$

The first term in each expression arises from the undegraded molecules, the integral from the degradation products.

The conditions under which assumption I, that θ varies inversely as the cube of the length, breaks down may now be examined in a semiquantitative fashion. It is readily seen from Eq. (11) that the breakdown occurs not necessarily when the diffusion constant θ of a particular molecule is in *error* by some specified amount, but rather when the contribution to χ and Δ made by this molecule is sufficiently in *error* to affect seriously the integrals of Eqs. (14). This contribution depends on the value of the optical factor f and on the weight fraction of molecules this size.

Let us consider a system in which the axial ratio of the undegraded molecules is 100, at such a gradient that the α-value for the undegraded molecules is 200. The smaller molecules have α-values varying from 200 down; these α-values are in *error* as a result of assumption I by amounts that are greater the smaller the molecule. The contribution of molecules having, say, $\frac{1}{5}$ the length of the largest molecule is underestimated as a result of assumption I: the value of α ascribed to these molecules is 1/125 of 200 or 1.60; the correct value of α when the factor $(-1+2\ln a/b)$ used is 2.40. The factors $f\sin 2\varphi$ for the assumed is 0.10, and for the true α is 0.14. Since the φ's are near 45 degrees for these molecules, $f\cos 2\varphi$ is smaller in proportion to the values of these quantities at higher α's than $f\sin 2\varphi$, and the main *error* in $\tan 2\chi$ comes from the integral involving $f\sin 2\varphi$.

The discrepancy in $f\sin 2\varphi$ for molecules $\frac{1}{4}$ the length of the undegraded molecules is less; the ascribed value being 0.18 while the true value would be 0.21.

The α-values ascribed to smaller molecules are, of course, more seriously in error than in the two examples above, but this tends to be compensated for by the rapid decrease in f for these molecules. It is reasonable then to regard assumption I, and hence the theory of this paper, as no longer valid when molecules having $\frac{1}{4}$ or less the length of the undegraded molecules make a significant contribution to the integrals of (14). This situation comes about under conditions of large gradient and advanced degrees of degradation, as will be seen below.

In addition the theory should not be applied to systems in which the axial ratio of the undegraded molecules is less than 100.

CALCULATIONS

Simpson's rule was used for evaluation of the integrals.[12] Integrals were evaluated for γ values of 0.2, 0.5, 0.75, 1.0, 1.5, 2.0, 2.5, and 3.0, and for α_0 values of 1, 2, 4, 8, 16, 40, 80, and 160. Values calculated for $\alpha_0=80$ and 160 are to be considered dubious, because of the uncertainty in the calculations of SEG for α greater than 60. This is less important at the larger γ-values, due to the decreasing contribution made by molecules having these α_0 values. The values for α_0 above were chosen to allow as much use as possible of the values given in the tables of SEG. It was necessary to determine some values of $f\sin 2\varphi$ and $f\cos 2\varphi$ for values of α not given in the tables; for α less than 1.25 the limiting law $\tan 2\chi=6/\alpha$, and the assumption that f is proportional to α were used,[2] and for higher α, graphical interpolation of the values of SEG was performed.

The values of the integrand at 8 equal intervals were first computed. For low α_0 and low γ values these increased monotonically. As either α_0 or γ increased, a maximum appeared, and shifted toward lower α_t/α_0 values. If the first nonzero ordinate (that for $\alpha_t/\alpha_0=\frac{1}{8}$) was the largest of the 8, the integrand was evaluated further by dividing the first quarter of the range of integration into either 8 or 10 parts depending on which division better served the purpose of using the SEG values as much as possible. Integrals for which the first value of the integrand was the greatest under this further subdivision are ones for which assumption I is about to break down; the values of χ and F for these

[12] H. Margenau and G. M. Murphy, *The Mathematics of Physics and Chemistry* (D. Van Nostrand, Company, Inc., New York, 1943).

TABLE I. Birefringence parameters χ and F as functions of α_0 for various values of the degradation parameter γ.

Degradation parameter γ	α_0	Calculated extinction angle χ	$\theta_{rel}=\alpha_0/\alpha_{apparent}$	Log θ_{rel}	Optical factor F	Weight fraction of undegraded molecules $e^{-\gamma}$
0.2	1	40.43	1.02	0.009	0.0582	0.819
	2	36.27	1.02	0.009	0.1117	
	4	29.72	1.03	0.014	0.1959	
	8	22.38	1.06	0.026	0.2964	
	16	16.35	1.10	0.042	0.3947	
	40	10.90	1.16	0.065	0.5148	
	80	7.78	1.17	0.068	0.6042	
	160	(4.83)	1.23	0.090	(0.6631)	
0.5	1	40.65	1.05	0.022	0.0489	0.607
	2	36.67	1.08	0.034	0.0940	
	4	30.43	1.11	0.046	0.1660	
	8	23.35	1.16	0.065	0.2544	
	16	17.45	1.24	0.094	0.3450	
	40	12.02	1.43	0.156	0.4616	
	80	8.80	1.45	0.162	0.5496	
	160	(5.87)	1.54	0.188	(0.6147)	
0.75	1	40.82	1.11	0.046	0.0423	0.472
	2	36.98	1.13	0.054	0.0814	
	4	30.88	1.16	0.065	0.1447	
	8	24.13	1.26	0.100	0.2245	
	16	18.17	1.36	0.134	0.3076	
	40	12.88	1.67	0.223	0.4221	
	80	9.63	1.74	0.241	0.5090	
	160	(6.68)	1.83	0.263	(0.5776)	
1	1	40.98	1.15	0.062	0.0367	0.368
	2	37.30	1.18	0.072	0.0709	
	4	31.48	1.23	0.090	0.1263	
	8	24.92	1.35	0.130	0.1986	
	16	19.23	1.57	0.196	0.2774	
	40	13.73	1.89	0.277	0.3865	
	80	10.43	2.10	0.323	0.4722	
	160	(7.47)	2.18	0.339	(0.5435)	
1.5	1	41.33	1.27	0.104	0.0280	0.223
	2	37.87	1.29	0.111	0.0541	
	4	32.60	1.38	0.140	0.0976	
	8	26.42	1.54	0.188	0.1565	
	16	20.93	1.84	0.266	0.2249	
	40	15.30	2.41	0.382	0.2666	
	80	12.00	2.86	0.458	0.4073	
	160	(8.95)	3.00	0.478	(0.4819)	
2.0	1	41.63	1.43	0.156	0.0215	0.135
	2	38.55	1.43	0.156	0.0417	
	4	33.60	1.52	0.182	0.0760	
	8	27.85	1.76	0.246	0.1244	
	16	22.60	2.17	0.337	0.1835	
	40	16.97	2.96	0.472	0.2759	
	80	13.47	3.67	0.566	0.3532	
	160	(10.33)	4.06	0.610	(0.4287)	
2.5	1	41.93	1.54	0.188	0.0167	0.082
	2	39.13	1.56	0.194	0.0326	
	4	34.63	1.68	0.226	0.0599	
	8	29.20	1.98	0.298	0.0998	
	16	24.25	2.55	0.407	0.1504	
	40	18.47	3.54	0.550	0.2349	
	80	(14.87)	4.57	0.660	(0.3078)	
	160	(11.60)	5.33	0.728	(0.3821)	
3.0	1	42.22	1.72	0.236	0.0132	0.050
	2	39.67	1.71	0.234	0.0256	
	4	35.53	1.88	0.275	0.0474	
	8	30.50	2.18	0.339	0.0807	
	16	25.53	2.86	0.457	0.1253	
	40	19.67	4.09	0.612	0.2011	
	80	(16.20)	5.40	0.734	(0.2693)	
	160	(12.78)	6.66	0.824	(0.3415)	

are considered to be unreliable, and are placed in parentheses in the tables.

It may be of interest to mention that whenever the maximum value of the integrand occurred at α_l/α_0 values less than $\frac{1}{4}$, the integrals obtained by subdivision of the first quarter of the range agreed within a percent or less with those obtained using only 8 values of the integrand. For the first γ-value for a given α_0 at which the integrand at $\alpha_l/\alpha_0=\frac{1}{8}$ was the maximum, the $f \sin 2\varphi$ integral evaluated using $\frac{1}{8}$-intervals was 2–3 percent lower than the integral obtained by subdivision. This may be a measure of the error in the numerical method in those integrals for which the first ordinate is maximal even after subdivision; the direction of the

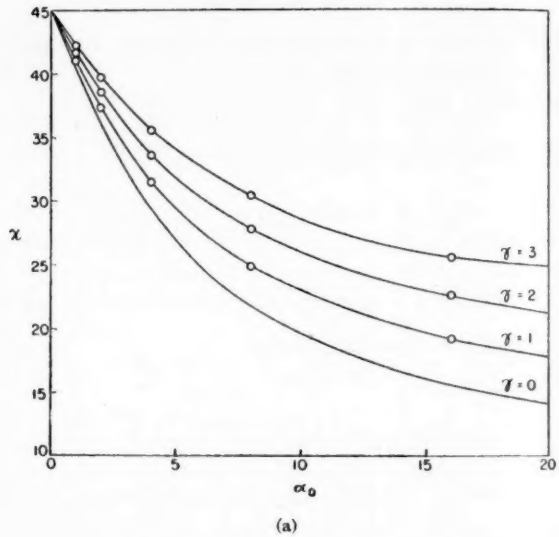

(a)

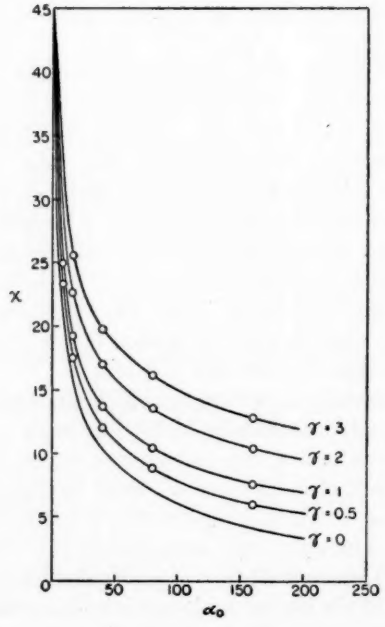

(b)

FIG. 1. Extinction angle χ as a function of α_0 for various values of the degradation parameter γ.

error is the same as that due to assumption I, also causing an underestimation of the contribution of smaller molecules. It will be noticed that in the plot of the apparent θ (defined below) against gradient (Fig. 2) there is a flattening of the curves at these dubious values, which is the effect to be expected from these two cooperating sources of error.

RESULTS

The results of the calculations are given in Table I. A plot of the calculated χ against α_0 for several values of γ is shown in Figs. 1(a) and 1(b). Since the general course of the curve is less significant than its deviation from the monodisperse curve, other methods of plotting are more useful, both to demonstrate the extent of the effect of polydispersity and to aid in determining θ_0 and γ-values from experimental data.

In polydisperse systems of this and similar types, the apparent value of the diffusion constant θ, as determined

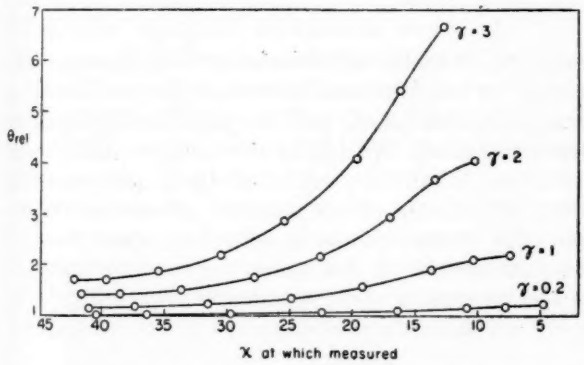

FIG. 2. θ_{rel}, the ratio of the apparent rotary diffusion constant θ to the rotary diffusion constant θ_0 of the undegraded molecule, plotted as a function of the extinction angle χ at which the measurement was made, for various values of the degradation parameter γ.

from the tables of SEG, is a function of the gradient at which the measurement is made; θ rises with the increase in gradient, as the smaller molecules begin to make their contribution to the birefringence. For a given calculated value of χ in Table I, the ratio θ_{rel} of the apparent θ (determined from SEG) to the θ_0 of the undegraded molecule may be readily determined (it is equal to the ratio of α_0 to the apparent α); this ratio is plotted against the χ-value at which it was determined in Fig. 2.

It may be seen from Figs. 1 and 2 that below $\gamma=0.5$ the differences between the curves for the undegraded and degraded systems are small, being of the order of what is presently the experimental precision of flow birefringence measurements. At advanced degrees of degradation the differences become quite readily observable, θ/θ_0 for $\gamma=3$ changing by a factor of 4 as we go from χ's near 45° to lower values.

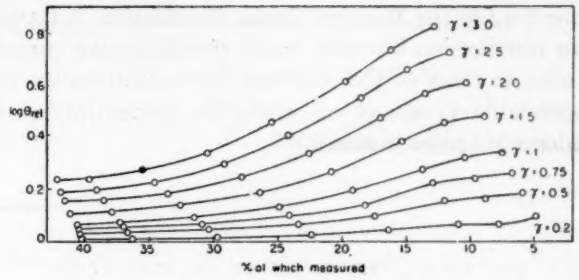

FIG. 3. The logarithm of θ_{rel} plotted as a function of χ for various values of γ.

An interesting conclusion is that the θ's do not extrapolate to the diffusion constant of the longest molecules at zero gradient, even for relatively low values of γ, when the weight fraction of undegraded molecules (Column 7 of Table I) is appreciable. This probably has its origin in the fact that there is always a finite concentration of molecules having lengths close to that of the undegraded molecule; these somewhat shorter molecules are still large enough to make a contribution comparable to that of the undegraded molecules.

In Fig. 3 the logarithm of θ/θ_0 is plotted against χ. If a plot of the logarithm of the apparent θ against χ from experimental data is made to the same scale on transparent paper and placed over the $\log\theta/\theta_0$ plot, the γ-value best fitting the experimental data may readily be ascertained by vertically shifting the plots relative to each other to give the best coincidence of the curve. The log of the ratio θ/θ_0 for any χ-value may be subtracted from the log of the experimental apparent θ to give the logarithm of θ_0.

It should be mentioned that other types of molecular weight distributions will give curves showing the same general features as those given here. Fitting a γ-value to experimental data using the theory of this paper requires an observation of what is essentially the magnitude of the deviation of the shape of the experimental curve from the theoretical curve of SEG. To choose between different distribution functions would require an observation of the shape of the shape deviation—the relation is similar to that between first and second derivatives. It is doubtful whether the present state of the theory of flow birefringence on the one hand, and the experimental accuracy on the other, will permit this to be done except in a gross way. As an example of what can be done in this direction, it may be recalled that the calculated curves for a polydisperse system having a rectangular distribution did not deviate sufficiently from the monodisperse curve to account for experimental results on some nucleic acid preparations;[5] in addition, for as polydisperse a system as is possible for a rectangular distribution (equal numbers of molecules of all lengths up to a maximum length), the maximum variation in θ/θ_0 over the whole range of χ for which the calculations were performed was 1.7 as compared with

4 for $\gamma=3$ in the Montroll-Simha distribution. A Gaussian distribution however would probably give curves similar to those of the Montroll-Simha distribution at appreciable values of γ, when the concentration of undegraded molecules is small.

ACKNOWLEDGMENTS

I would like to thank Dr. H. A. Scheraga and Dr. R. Ullman for comments on this paper, Dr. K. G. Stern for his encouragement and interest, and Mr. E. Farber for performing the tedious computations.

THE JOURNAL OF CHEMICAL PHYSICS VOLUME 20, NUMBER 4 APRIL, 1952

Spin-Orbit Interaction in Aromatic Molecules*

DONALD S. MCCLURE
Department of Chemistry and Chemical Engineering, University of California, Berkeley, California
(Received August 14, 1951)

The matrix elements of spin-orbit interaction are obtained for polyatomic molecules using M.O. wave functions, taking account of configurational interaction. These results are then applied to the calculation of singlet-triplet transition probabilities in aromatic compounds. It is shown without evaluation of integrals that intercombination transitions in these compounds should be much weaker than in most other classes of organic compounds. This is in agreement with experimental results on the phosphorescence lifetimes of these compounds.

I. INTRODUCTION

INTERCOMBINATION transition probabilities in most molecules can be estimated as to order of magnitude by taking the intercombination probability for the heaviest atom of the molecule. This is true because the spin-orbit interaction which brings about such transitions is chiefly determined by the heaviest atom. Such estimates have been made and compared with experiment, and apparently there is agreement in all cases except where an aromatic ring system is involved.[1] The metastable triplet state lifetimes of polynuclear aromatic hydrocarbons and of many of their substitution products and heterocyclic analogs appeared from these estimates to be from 10 to 1000 times too great. More recent experimental work has only served to increase the discrepancy. When the measured lifetimes are corrected for simultaneous radiationless processes, the lifetimes are increased many fold.[2] For example, the measured triplet state lifetime for benzene is 7 sec while the corrected value is 30 sec. For triphenylene we have 15.9 sec measured and 30 sec corrected, and for naphthalene 2.6 sec measured and 22 sec corrected. Electronic transitions as weak as this are unusual, even when they are intercombinations.

A possible explanation is that there is accidental cancellation among the terms of the dipole matrix element of the transition. This seems to explain some weak, but formally allowed transitions among the singlet states of aromatic hydrocarbons. The discrepancies seemed far too common, however, since practically no exceptions were found, and this prompted the present theoretical study. We will be able to show that the experimental results are explained by a more unusual effect, namely, the nearly complete cancellation of the spin-orbit interaction among π-electron states. Some of the consequences of this result, for example its effect on the assignment of the metastable triplet state symmetry of benzene, will be discussed in another paper.

II. THE SPIN-ORBIT INTERACTION OPERATOR

In order to calculate singlet-triplet transition probabilities, we must first calculate the mixing of singlet with triplet and of triplet with singlet. The most important effect causing singlet-triplet mixing is, ordinarily, the electron spin-orbit interaction in the electric field of the nuclei.

The part of the Hamiltonian which represents the spin-orbit interaction for a system of n electrons and m nuclei is[3]

$$H_s=\frac{e^2}{2m^2c^2}\sum_i^n\sum_k^m\frac{Z_k(\mathbf{r}_{ik}\times\mathbf{p}_i)\cdot\mathbf{s}_i}{r_{ik}^3}, \tag{1}$$

where Z_k is the atomic number of nucleus k, $\mathbf{r}_{ik}$ is the vector distance of electron i from nucleus k, r_{ik} is the magnitude of the latter, $\mathbf{p}_i$ is the linear momentum of electron i and $\mathbf{s}_i$ is its spin angular momentum. The expression $r_{ik}\times p_i$ is the orbital angular momentum, $\mathbf{l}_{ik}$ of electron i with respect to nucleus k. Now $\mathbf{l}_{ik}$ and $\mathbf{s}_i$ are vector operators, so that (1) can be written for each

* *Note added in proof:*—In work to be published, M. Mizushima and S. Koide (private communication) have demonstrated which of the possible mechanisms of singlet-triplet mixing is of most importance in benzene. The same mechanism can safely be assumed to be the most important one in other aromatic hydrocarbons.

[1] D. S. McClure, J. Chem. Phys. **17**, 905 (1949).

[2] Gilmore, Gibson, and McClure (to be published).

[3] H. A. Kramers, *Die Grundlagen der Quantentheorie* (Akademische Verlagsgesellschaft MBH., 1938), p. 239.

electron as

$$\frac{e^2}{2m^2c^2}\left[\left(\sum_k^m \frac{Z_k \mathbf{l}_{xk}}{r_k^3}\right)\mathbf{s}_x+\left(\sum_k^m \frac{Z_k \mathbf{l}_{yk}}{r_k^3}\right)\mathbf{s}_y+\left(\sum_k^m \frac{Z_k \mathbf{l}_{zk}}{r_k^3}\right)\mathbf{s}_z\right], \quad (2)$$

since $\mathbf{s}_i$ is independent of space coordinates. The subscript i has been omitted from (2) for clarity. For the problems to be dealt with here, this component form of the operator will prove very useful. The problem of computing spin-orbit interaction in a molecule therefore involves finding the components of the orbital angular momentum of each electron with respect to each nucleus of the molecule.

The value of Z_k to use in (2) should depend upon where the electron is in the molecule, as the shielding by the other electrons depends upon the distance from a given nucleus. This effect may be taken into account crudely in a manner analogous to that used in calculating atomic multiplet separations, where an "inner" and "outer" Z value are used. In a more elegant treatment, (2) would be modified by adding the terms of opposite sign corresponding to the interaction of the spin of one electron with the relative orbital motions of the others. By adding this so-called $l_1 \cdot s_2$ interaction, we lose a desirable property of (2), namely its one electron character, and introduce terms depending directly on the correlations between the electrons. Instead of adding these complications we will use a single average Z value for each nucleus. Fortunately, the arguments that will be used in this paper do not depend on the exact values of the integrals and will be practically independent of any errors introduced by this procedure.

Selection rules for determining which of the elements of (1) are different from zero have been published.[4,5] The presentation of the author is more convenient for application to the component form of the operator (2), although Weissman's is certainly the more elegant. We will limit ourselves to the case of small spin-orbit coupling, so the molecular analog of Russell-Saunders coupling prevails. The wave functions of the zeroth-order set will then be eigenfunctions of the energy and of S^2 and S_z. The axis of spin quantization will be chosen to suit the problem and will be called the z axis.

III. APPLICATION OF MOLECULAR ORBITALS

We will assume at first that configurational interaction may be neglected and set up the proper linear combinations of d determinantal eigenfunctions for the states of interest

$$\psi_j=\frac{1}{d^{\frac{1}{2}}}\sum_i^d A_{ij}D_i; \quad D_i=\frac{1}{n!^{\frac{1}{2}}}|a_1\alpha_1 a_2\beta_2 b_3\alpha_3 b_4\beta_4\cdots|, \quad (3)$$

where the a_1, etc., represent the orthogonal normalized molecular orbitals and α_i and β_i are spin wave functions corresponding to $s_z=1$ and -1, respectively. We will not consider the case of degenerate configurations for two reasons. Very few molecules have them, and since vibrational perturbations are greater than spin-orbit perturbations, the degeneracies will be removed by the former, even if for some state they are not already removed by the electronic interaction. For a nondegenerate configuration with only one electron excited, the ψ_j for singlet states can be represented by four D_i, two of the triplets by two D_i and the other triplet by four D_i. They are represented in short form by writing down only the diagonals of the D_i and only the orbitals corresponding to half-filled shells (for configuration $\cdots w^1 v^1$):

$$\begin{aligned}
&\tfrac{1}{2}(n!)^{-\frac{1}{2}}(\text{filled orbitals})\times(w_1v_2+w_2v_1)(\alpha_1\beta_2-\alpha_2\beta_1)\ \text{singlet}\\
&\tfrac{1}{2}(n!)^{-\frac{1}{2}}(\text{filled orbitals})\times(w_1v_2-w_2v_1)(\alpha_1\beta_2+\alpha_2\beta_1)\ \text{triplet}\\
&2^{-\frac{1}{2}}(n!)^{-\frac{1}{2}}(\text{filled orbitals})\times(w_1v_2-w_2v_1)(\alpha_1\alpha_2)\ \text{triplet}\\
&2^{-\frac{1}{2}}(n!)^{-\frac{1}{2}}(\text{filled orbitals})\times(w_2-w_2v_1)(\beta_1\beta_2)\ \text{triplet}.
\end{aligned} \quad (4)$$

Since we are interested only in the total transition probability from the three triplet levels of (4) to a singlet state, any linear combination of the triplet functions in (4) will suit our purposes just as well. This is the justification for choosing the axis of quantization in the direction most convenient for calculation.

The interaction operator (1) is of the form $\sum F_i$ with F_i depending only on the coordinates of the ith electron. The matrix elements of (1) between singlet and triplet states are therefore limited to those involving states which differ at most in the orbital assignment of one electron.[6] This makes it unnecessary to use the entire determinant in the wave function as no new terms arise aside from the ones given by using the diagonal. The normalizing factors of $n!^{\frac{1}{2}}$ are canceled out in the usual way when the determinants are multiplied together and the terms collected. This part of the calculation is the same as the evaluation of electric dipole matrix elements, except that one of the wave functions and the effective part of the spin-orbit operator are antisymmetric under electron interchange.[5] Since the spin operators are independent of the space coordinates, the integration over the spins can be performed immediately. As a result of the foregoing, a matrix element of (1) between a singlet and a triplet state can be reduced to one of the following integrals,

[4] S. I. Weissman, J. Chem. Phys. 18, 232 (1950).

[5] D. S. McClure, J. Chem. Phys. 17, 665 (1949). There is a typographical error in the formula for A_i which should read:

$$A_i=\sum_k^m 1/r_{ik}\cdot\partial V(r_{ik})/\partial r_{ik},$$

and in the 9th line from the bottom, one should read $B_{1u}\rightarrow B_{2u}$. The form of the operator H' used in this note is not the same as is used here and is not strictly correct even though the resulting selection rules are correct.

[6] E. U. Condon and G. H. Shortley, *The Theory of Atomic Spectra* (Cambridge University Press, London, 1935), p. 169.

depending on which triplet component (in the form (4)) is being used, and on which component of the spin-orbit operator (in the form (2)) is being used:

	$\alpha_1\alpha_2$	$\beta_1\beta_2$	$\alpha_1\beta_2+\alpha_2\beta_1$
X	$2^{-\frac{1}{2}}(vH_xu)$	$2^{-\frac{1}{2}}(vH_xu)$	0
Y	$2^{-\frac{1}{2}}i(vH_yu)$	$2^{-\frac{1}{2}}i(vH_yu)$	0
Z	0	0	(vH_zu)

(5)

Here, v and u are the excited orbitals. That is, the configurations belonging to the singlet and triplet states are $\cdots w^1v^1$ and $\cdots w^1u^1$. The configurations may differ only insofar as u, v, and w are different orbitals. H_x, etc., represents one of the components of (2) without the spin operator and multiplied by $h/2$. That is,

$$H_x=\frac{e^2h}{4m^2c^2}\sum_k^m\frac{Z_k\mathbf{l}_{xk}}{r_k^3}.$$

The integration is over the coordinates of only one electron, so the corresponding subscript is omitted.

As Craig[7] has shown, configuration interaction among *ASMO* states leads to large changes in the final energies. If a complete set of configurational wave functions of a given symmetry type is used, the wave function for a final electronic state will be the best that is consistent with the initial use of $2p_z$ atomic functions. Such a wave function can be written

$$\Psi_c=\sum_i a_i^c\psi_i^c, \tag{6}$$

where a_i^c is the coefficient of the n-electron determinantal eigenfunction ψ_i^c of (orbital) symmetry species c, for configuration i. ψ_i^c is analogous to the wave function (3). The coefficients a_i^c are determined by the variation method with (6) as a linear variation function, and using the Hamiltonian without spin. The spin-orbit interaction can be calculated as a perturbation between the final states so obtained. This calculation will be more complicated than when using (3) as a wave function because of the larger number of terms, and because the triplet states with several electrons excited which contribute to the wave function (6) cannot be represented as simply as (4). There are some simplifying factors, however. A term in the complete matrix element can only appear when it comes from two configurations differing in only one orbital. Further, the main contribution to the complete wave functions may arise from only a few configurations. Finally, there will be no new types of integrals. All will be of the type found in (5). We can therefore represent the z-component, for example, of the matrix element between two complete states by

$$S_{cc'}=\sum_i\sum_j a_i^c b_j^{c'}(v_iH_zu_j)\delta_{j,i-1} \tag{7}$$

where c and c' refer to the symmetry species of the two wave functions, and $\delta_{j,i-1}$ indicates that the occupation numbers corresponding to configuration j must differ from those of i by only one; δ is one when this is so, otherwise zero. In many important cases, $S_{cc'}$ should not differ greatly from $S_{vu}=(vH_zu)$ in (5). All of the qualitative results of this paper hold equally well with either one, so that S_{vu} will be used in the remainder.

[7] D. Craig, Proc. Roy. Soc. (London) **A200**, 474 (1950).

IV. TRIPLET-SINGLET TRANSITION PROBABILITY

After obtaining the matrix elements of the spin-orbit interaction between a triplet state of interest and the important perturbing singlet states, the perturbed eigenfunction of the triplet state can be set up and used to calculate the transition amplitudes to singlet states. The wave function for one component of the perturbed triplet state is

$$\psi_T'=\psi_T^0+\sum_{N\neq T}\frac{S_{TN}}{E_T-E_N}\psi_N^0, \tag{8}$$

with ψ_T^0 the unperturbed triplet eigenfunction, ψ_N^0 an unperturbed singlet eigenfunction, E_T and E_N the triplet and singlet state energies, respectively (we will use experimental values of these energies), and S_{TN} some matrix element of (5). The transition amplitude to the ground state will be of interest and is

$$\int\psi_G^*M\psi_T'd\tau=\sum_{N\neq T}\frac{M_{NG}S_{TN}}{E_T-E_N}, \tag{9}$$

where M is the electric moment operator and M_{NG} are some of its matrix elements. The transition probability for emission from the three triplet components to the ground state is

$$A_{TG}=\frac{1}{\tau_T}=\frac{64\pi^4\nu_{TG}^3}{3hc^3}\sum_{T=1}^{3}\left[\sum_N\frac{M_{NG}S_{TN}}{E_T-E_N}\right]^2, \tag{10}$$

where τ_T is the lifetime of the triplet state.

V. SPIN-ORBIT INTERACTION IN THE AROMATIC HYDROCARBONS

The matrix elements of the spin-orbit interaction in an aromatic hydrocarbon can be calculated using the general results of Sec. III. If we consider at first only π-electron states, the molecular orbitals which enter into the integrals of (5) can be represented by their normalized, orthogonal LCAO forms

$$v=\sum_j^n c_j^v\phi_j \qquad u=\sum_i^n c_i^u\phi_i, \tag{11}$$

where ϕ_j represents a $2p_z$ atomic orbital‡ on carbon atom j and the z axis is taken perpendicular to the plane of the carbon atoms. By choosing the z axis this way,

‡ The final result will be qualitatively the same if we use a more general atomic function. We could, for example use an expansion involving some $3d_z$ function, or in fact any atomic function having $m_l=0$.

only one of the triplet components, *viz.*, $\alpha_1\beta_2+\alpha_2\beta_1$, contributes to the transition probability. The molecular orbitals are assumed to belong to the irreducible representations of the symmetry group of the molecule and to be the right ones to mix under the influence of the operator H_s. They all have one symmetry property in common, regardless of the symmetry group of the molecule, namely, all are antisymmetric toward reflection in the plane of the carbon atoms. This has the important consequence that the only component of H_s which can cause singlet-triplet perturbations among π-electron states of aromatic compounds is the z-component, since only this one is symmetric toward reflection. The only nonzero element in (5) is therefore $S_{vu}=(vH_zu)$.

In order to yield physically significant results, the matrix of the spin-orbit operator must be Hermitean. The operator (1) is not Hermitean for an arbitrary distribution of nuclei, so that we must take the average of (1) with its Hermitean conjugate. The nondiagonal matrix elements which we must consider will therefore be of the form

$$S_{vu}=\tfrac{1}{2}[(vH_zu)-(uH_zv)], \tag{12}$$

since v and u are real and H_z is pure imaginary. Substituting the expressions for v and u into (12) gives

$$S_{vu}=\sum_{i>j}\sum(c_i^{v}c_j^{u}-c_i^{u}c_j^{v})[(\phi_iH_z\phi_j)-(\phi_jH_z\phi_i)], \tag{13}$$

where the terms with $i=j$ have canceled out. Thus there are no contributions to spin-orbit interaction when the electron is localized on a single atom.

Further simplification results when we examine the effect of the individual terms of H_z on ϕ_i and ϕ_j. The latter will be assumed to be Slater type $2p_z$ functions. The operator H_z is understood to be written in terms of a coordinate system appropriate for the molecule. Individual terms, as expressed in this coordinate system will be of the form

$$\frac{ie^2h^2}{4m^2c^2}\cdot\frac{Z}{r_k^3}\left[(x-x_k^0)\frac{\partial}{\partial y}-(y-y_k^0)\frac{\partial}{\partial x}\right],$$

where x_k^0 and y_k^0 are the coordinates of nucleus k in the molecular coordinate system. It is readily seen that if $k=j$ in the first integral of (13) or if $k=i$ in the second integral, the result of carrying out the operation with the kth term of H_z will be zero. This is because ϕ_i and ϕ_j belong to the eigenvalue zero of l_{zi} and l_{zj}, respectively. The two remaining terms corresponding to $k=i$ and $k=j$ of the operator can be combined and written in terms of a coordinate system with x axis on the line joining the atoms i and j. The result, apart from a constant multiplier is

$$\sum_{i>j}\sum(c_i^{v}c_j^{u}-c_i^{u}c_j^{v})t_{ij}\int\frac{\phi_i\phi_j}{r_ir_j}y\left(\frac{1}{r_i^2}-\frac{1}{r_j^2}\right)d\tau, \tag{14}$$

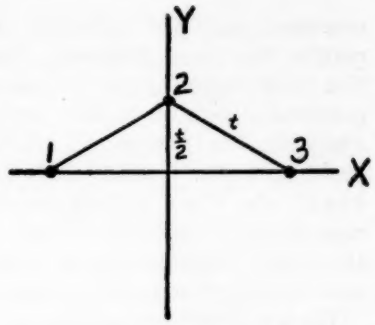

FIG. 1. Arrangement of atomic centers used in calculating I.

where t_{ij} is the distance between atoms i and j. The integrand changes sign when y changes sign as the y coordinates of r_i and r_j are the same in the coordinate system chosen. Therefore the integral is zero, and no terms of (13) having $k=i$ or $k=j$ contribute to S_{vu}. Thus all two-center integrals vanish and the only integrals left to consider are three-center types for which $i\neq j\neq k$. If any of these exist, they will certainly be small. At this point, therefore, one sees that S_{vu} will be small and as a result, singlet-triplet mixing among π-electron states should be much less than normal.

The largest of the three-center integrals are of the types $(\phi_jH_{z,j+1}\phi_{j+2})$ and $(\phi_jH_{z,j+2}\phi_{j+1})$. The first of these is probably of greater importance than the second because the overlap falls off less rapidly with distance than does the function r^{-3}. If we consider only integrals of the first type and transform each integrand to a coordinate system of the type shown in Fig. 1 (for ease of integration), we can write

$$S_{vu}=\frac{iR\sqrt{3}t}{256\pi}I_{123}\sum_{j}^{n}(c_j^{v}c_{j+2}^{u}-c_j^{u}c_{j+2}^{v}), \tag{15}$$

where $R=Z^4e^2h^2/2m^2c^2a_0^3$ and Z is a value of the effective nuclear charge whose determination we will not have to consider in detail here; a_0 is the Bohr radius; t is the bond length; I_{123} is an integral involving a triple of atoms arranged as in the figure. Its value is independent of where the atoms are in the molecule if we assume, as has been done, that all bond lengths and angles are equal. This is practically true for all aromatic hydrocarbons made up of hexagonal ring networks. The exact form of I_{123} is

$$I_{123}=\int\frac{\phi_1\phi_3}{r_2^3}\left[\left(y-\frac{t}{2}\right)\left(\frac{1}{r_1}+\frac{1}{r_3}\right)-\frac{x}{\sqrt{3}}\left(\frac{1}{r_1}-\frac{1}{r_3}\right)\right]dxdydz.$$

In order to be properly appreciated, (15) should be compared with the theoretical and experimental results on intercombination probabilities in atomic spectra. In the quantum-mechanical treatment, both the diagonal and off-diagonal elements of the spin-orbit interaction matrix are of the same order of magnitude and are proportional to a parameter ζ. This parameter can be determined experimentally from the easily

measured multiplet splittings, and with it and the matrix, the more difficultly measured intercombination probabilities can be calculated. Actually, some experimental data on atomic triplet state lifetimes are available. The lifetimes calculated as above were compared with the experimental ones by King and Van Vleck[8] who found fair agreement. An additional parameter which took into account the difference between the radial eigenfunctions in singlet and triplet states was added and found to produce excellent agreement.

We will therefore compare S_{vu} with the ζ value for the lowest-lying configuration of the carbon atom, $2p^2$. Theoretically, $\zeta_{2p}=R/24$.[6] Experimentally, it is about 28 cm^{-1} (although configuration interaction makes this somewhat uncertain; see reference 1, p. 908). The ratio of the absolute value of S_{vu} to ζ_{2p} is

$$\frac{|S_{vu}|}{\zeta_{2p}}=\frac{3\sqrt{3}t}{32\pi}I_{123}\sum_{i}^{n}(c_j{}^{v}c_{j+2}{}^{u}-c_j{}^{u}c_{j+2}{}^{v}). \qquad (16)$$

Since the sum over the molecular orbital coefficients cannot be greater than two and $t\simeq 8$ and I_{123} must have a very small value, $|S_{vu}|\ll 28$ cm^{-1}. Of course, the value used for Z (or R) for the atom will differ somewhat from that used in the molecule, but this does not alter the qualitative result.

Let us assume that $|S_{vu}|\simeq 1$ cm^{-1} and make a rough estimate of the strength of the singlet-triplet transition in benzene. Assuming that there is only one important perturbing singlet state, and applying the well-known relation between f, the oscillator strength, μ the electric moment operator and A_{12} the Einstein spontaneous transition probability, Eq. (10) can be expressed as

$$f_{T\to G}=f_{S\to G}\left(\frac{S_{vu}}{\Delta E_{ST}}\right)^2.$$

Let us take the singlet state near 50,000 cm^{-1} as the perturbing state. The oscillator strength of the band corresponding to the transition from the ground state to this excited state is $f_{S\to G}=0.10$.[9] The triplet is at 30,000 cm^{-1} so $\Delta E_{ST}=20{,}000$ cm^{-1}. Therefore $f_{T\to G}=0.25\times 10^{-9}$. This is about equal to the uncorrected experimental value[1] of 0.24×10^{-9}, to which more than one state must contribute. Therefore, 1 cm^{-1} is probably an upper limit to the value of S_{vu}. We wish only to indicate the order of magnitude of S_{vu} by this calculation. It will vary from one aromatic compound to another, but will be small in all of them because only three-center integrals can contribute to its value.

We can be much more certain of this result than, for example, of a molecular orbital calculation of energy levels. We have already noted that configuration interaction does not introduce any profound changes in the matrix elements (5). Its only effect on our final result will be to alter slightly the value of the summation over molecular orbital coefficients in (15). We would therefore have obtained the same qualitative result using a complete set of configurations, i.e., using the best possible wave functions consistent with the initial use of atomic $2p_z$ functions or other atomic functions having $m_l=0$ (with respect to the direction perpendicular to the ring plane). This means that our qualitative result will hold with a very general wave function and would undoubtedly hold true with the correct wave functions.

Since S_{vu} is small it follows that all singlet-triplet perturbations among π-electron states will be small, and since the non-π-electron states should have a relatively small effect because of their high energy, the low-lying triplet states of aromatic hydrocarbons should have little singlet character. This completes the qualitative explanation of the unusually long triplet state lifetimes of the polynuclear aromatic hydrocarbons.

As a consequence of the abnormally small π-electron spin-orbit interaction, perturbations which one ordinarily neglects in comparison with (1), are now relatively important causes of singlet-triplet mixing, and may well be responsible for the intercombination transitions that are actually observed. Some of these are: (1) spin-spin interaction; (2) spin-orbit interaction involving non-π-electron states of the molecule; (3) vibrational perturbations which destroy the symmetry plane of the molecule; (4) heavy atom substituents. In a paper to follow, these questions will be dealt with in more detail.

[8] G. W. King and J. H. Van Vleck, Phys. Rev. **56**, 464 (1937).
[9] Platt and Klevens, Chem. Revs. **41**, 301 (1947).

The Microwave Spectrum of Ketene*

H. R. JOHNSON AND M. W. P. STRANDBERG
Research Laboratory of Electronics, Massachusetts Institute of Technology, Cambridge, Massachusetts

(Received November 29, 1951)

The microwave absorption spectra of the ketene molecules $H_2{}^1C_2{}^{12}O^{16}$, $H^1D^2C_2{}^{12}O^{16}$, and $D_2{}^2C_2{}^{12}O^{16}$ have been investigated. Reciprocal moments of inertia have been determined for each from the measurements. The centrifugal distortion theory of Hillger and Strandberg has been found valid for both Q and R branches. The structure has been calculated and dipole moment measured; results check and extend the accuracy of values previously determined by other methods. Intensities of satellites of the lightest molecule corresponding to the lowest three vibrational fundamentals have also been measured and changes in the average reciprocal moments determined. The vibrational frequencies have been calculated and found different from values reported in the literature by infrared workers. References and suggestions for further work are given.

INTRODUCTION

A. General Properties

KETENE is an organic compound, $CH_2C=0$, which at room temperature is a colorless, heavy, extremely poisonous[1] gas. It melts at $-151°C$ and boils at approximately $-50°C$. Ketene is chemically reactive and a dimer exists at room temperature. There is a large body of literature on the molecule, bearing mainly on its chemical properties. Because its spectrum is difficult enough to be interesting but perhaps simple enough to be precisely analyzed, considerable spectroscopic work has been published. Ketene has C_{2v} symmetry and an electric dipole moment and is nearly a prolate symmetric rotor.

B. Early Microwave History

Early in 1948, J. Goldstein of Harvard located four microwave rotational absorption lines of ketene in the 20,000-Mc/sec region, where the $J=0\rightarrow J=1$ transition would be expected on the basis of the known structure. At his request, the precise frequencies of those lines were measured in this laboratory, and the Stark coefficients were determined. The higher frequency transitions $J=1\rightarrow 2$ and $J=2\rightarrow 3$ were also measured since our laboratory was equipped to work in those regions (40,000 and 60,000 Mc/sec, respectively).

Early in 1950, Bak and co-workers at Copenhagen measured the $J=0\rightarrow 1$ of $H_2{}^1C_2{}^{12}O^{16}$, $D^2H^1C_2{}^{12}O^{16}$, and $D_2{}^2C_2{}^{12}O^{16}$ (hereafter, briefly referred to as H_2C_2O, DHC_2O, and D_2C_2O, respectively) as well as some vibrational satellites.[2] The reported absorption frequencies (wavemeter accuracy) check fairly well with our measurements, although some discrepancies amount to 20 Mc/sec. A preliminary report of our work herein described has been given.[3]

C. Reason for Interest

The values of the three moments of inertia of H_2C_2O would enable calculation of thermodynamic gas functions of possible engineering interest; also using those of D_2C_2O the structure of ketene could be calculated; the combination of Q and R branch transitions that occur would give an interesting check on the theory of centrifugal distortion in asymmetric tops developed in this laboratory[4,5]; the relative intensities of the vibrational satellites which occur would help in the correct assignment of the fundamental vibrational frequencies; and the measurement of the Stark effect would enable accurate evaluation of the dipole moment independent of impurities. Consequently, intensive work has recently been begun in this laboratory.

I. EXPERIMENTAL WORK

A. Preparation of Ketene and Heavy Ketene

Ketene was made by pyrolysis of acetone using a lamp described by Williams and Hurd.[6] Their method

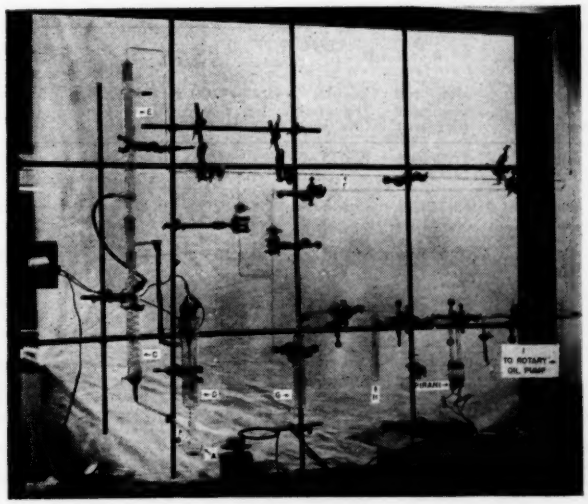

FIG. 1. System for ketene synthesis.

* This work has been supported in part by the Signal Corps, the Air Materiel Command, and ONR.

[1] Wooster, Lushbaugh, and Redeman, J. Am. Chem. Soc. **68**, 2743 (1946).

[2] Bak, Knudsen, Madsen, and Rastrup-Anderson, Phys. Rev. **79**, 190L (1950).

[3] Johnson, Ingersoll, and Strandberg, Phys. Rev. **82**, 327(A) (1951).

[4] R. B. Lawrance and M. W. P. Strandberg, Phys. Rev. **83**, 363 (1951).

[5] R. E. Hillger and M. W. P. Strandberg, Phys. Rev. **83**, 575 (1951).

[6] J. W. Williams, and C. D. Hurd, J. Org. Chem. **5**, 122 (1940).

TABLE I.

$H_2{}^1C_2{}^{12}O^{16}$

Assignment	Measured frequency (Mc/sec)	Calculated frequency (Mc/sec)	Intensity (cm^{-1}) (100 percent abundance)	Distortion correction (Mc/sec)	Vibrational state	Error (Mc/sec)
$0_{00}\rightarrow1_{01}$	20,209.20	20,209.15	1.8×10^{-6}	0.01	G	−0.05
$0_{00}\rightarrow1_{01}$	20,266.86	···	5.2×10^{-7}	···	$\nu_9=1$	···
$0_{00}\rightarrow1_{01}$	20,219.92	···	3.6×10^{-7}	···	$\nu_8=1$	···
$0_{00}\rightarrow1_{01}$	20,231.59	···	2.1×10^{-7}	···	$\nu_7=1$	···
$1_{01}\rightarrow2_{02}$	40,417.90	40,417.84	1.4×10^{-5}	0.08	G	−0.06
$1_{01}\rightarrow2_{02}$	40,532.78	···	4.0×10^{-6}	···	$\nu_9=1$	···
$1_{01}\rightarrow2_{02}$	40,440.17	···	2.8×10^{-6}	···	$\nu_8=1$	···
$1_{01}\rightarrow2_{02}$	40,462.26	···	1.6×10^{-6}	···	$\nu_7=1$	···
$1_{10}\rightarrow2_{11}$	40,793.62	40,038.92	3.2×10^{-5}	1.99	G	+0.12
$1_{10}\rightarrow2_{11}$	40,926.95	···	1.0×10^{-6}	···	$\nu_9=1$	···
$1_{10}\rightarrow2_{11}$	40,809.98	···	4.2×10^{-7}	···	$\nu_7=1$	···
$1_{11}\rightarrow2_{12}$	40,038.80	40,793.74	3.1×10^{-5}	1.99	G	+0.12
$1_{11}\rightarrow2_{12}$	40,135.35	···	9.9×10^{-7}	···	$\nu_9=1$	···
$1_{11}\rightarrow2_{12}$	40,087.77	···	6.8×10^{-7}	···	$\nu_8=1$	···
$1_{11}\rightarrow2_{12}$	40,110.92	···	4.0×10^{-7}	···	$\nu_7=1$	···
$2_{02}\rightarrow3_{03}$	60,625.68	60,625.64	4.8×10^{-6}	0.27	G	−0.04
$2_{12}\rightarrow3_{13}$	60,057.92	60,057.98	1.2×10^{-4}	3.13	G	+0.06
$2_{11}\rightarrow3_{12}$	61,190.24	61,190.22	1.3×10^{-4}	3.13	G	−0.02
$2_{21}\rightarrow3_{22}$	60,615.88	60,615.76	2.5×10^{-4}	11.71	G	−0.12
$2_{20}\rightarrow3_{21}$	60,617.30	60,617.32	2.5×10^{-4}	11.71	G	+0.02
$6_{1,6}\rightarrow6_{1,5}$	7,925.18	7,925.17	2.3×10^{-7}	0.51	G	+0.01
$9_{1,9}\rightarrow9_{1,8}$	16,980.97	16,981.07	6.8×10^{-7}	2.34	G	−0.10
$10_{1,10}\rightarrow10_{1,9}$	20,753.90	20,753.85	9.0×10^{-7}	3.50	G	+0.05
$11_{1,11}\rightarrow11_{1,10}$	24,903.53	24,903.53	1.1×10^{-6}	5.04	G	0.00
$12_{1,12}\rightarrow12_{1,11}$	29,430.02	29,430.00	1.4×10^{-6}	7.04	G	+0.02
$13_{1,13}\rightarrow13_{1,12}$	34,333.14	34,333.08	1.7×10^{-6}	9.59	G	+0.06
$14_{1,14}\rightarrow14_{1,13}$	39,612.55	39,612.62	2.0×10^{-6}	12.76	G	−0.07
$27_{2,26}\rightarrow27_{2,25}$	9,188.20	···	2.8×10^{-6}	10.62	G	···
$28_{2,27}\rightarrow28_{2,26}$	10,588.88	···	3.2×10^{-6}	13.15	G	···

$H^1D^2C_2{}^{12}O^{16}$

Assignment	Measured frequency (Mc/sec)	Calculated frequency (Mc/sec)	Intensity (cm^{-1}) (50 percent abundance)	Distortion correction (Mc/sec)	Vibrational state	Error (Mc/sec)
$0_{00}\rightarrow1_{01}$	18,821.68	18,821.68	1.2×10^{-6}	···	G	···
$0_{00}\rightarrow1_{01}$	18,877.65	···	1.2×10^{-7}	···	$\nu_9=1$	···
$0_{00}\rightarrow1_{01}$	18,832.76	···	7.9×10^{-8}	···	$\nu_8=1$	···
$0_{00}\rightarrow1_{01}$	18,846.86	···	4.7×10^{-8}	···	$\nu_7=1$	···
$6_{1,6}\rightarrow6_{1,5}$	9,919.95	9,919.95	9.2×10^{-8}	0.80	G	0.00
$9_{1,9}\rightarrow9_{1,8}$	21,254.31	21,254.30	2.8×10^{-7}	3.66	G	−0.01
$10_{1,10}\rightarrow10_{1,9}$	25,975.83	25,975.85	3.6×10^{-7}	5.47	G	+0.02
$21_{2,20}\rightarrow21_{2,19}$	7,901.08	7,901.08	3.9×10^{-8}	8.87	G	0.00
$22_{2,21}\rightarrow22_{2,20}$	9,462.69	9,462.70	5.1×10^{-8}	11.64	G	+0.01
$27_{2,26}\rightarrow27_{2,25}$	20,855.93	20,855.93	1.4×10^{-7}	38.35	G	0.00

$D_2{}^2C_2{}^{12}O^{16}$

Assignment	Measured frequency (Mc/sec)	Calculated frequency (Mc/sec)	Intensity (cm^{-1}) (100 percent abundance)	Distortion correction (Mc/sec)	Vibrational state	Error (Mc/sec)
$0_{00}\rightarrow1_{01}$	17,673.44	17,673.46	2.2×10^{-6}	0.00	G	+0.02
$0_{00}\rightarrow1_{01}$	17,726.71	···	1.1×10^{-7}	···	$\nu_9=1$	···
$1_{01}\rightarrow2_{02}$	35,345.13	35,345.06	1.8×10^{-6}	0.00	G	−0.07
$1_{01}\rightarrow2_{02}$	35,431.86	···	8.6×10^{-8}?	···	$\nu_9=1$?	···
$1_{10}\rightarrow2_{11}$	35,913.66	35,913.64	8.3×10^{-6}	1.35	G	−0.02
$1_{10}\rightarrow2_{11}$	36,048.40	···	6.5×10^{-7}?	···	$\nu_7=1$?	···
$1_{11}\rightarrow2_{12}$	34,777.36	34,777.37	7.8×10^{-6}	1.35	G	+0.01
$1_{11}\rightarrow2_{12}$	34,842.81	···	6.1×10^{-7}?	···	$\nu_7=1$?	···
$1_{11}\rightarrow2_{12}$	34,835.26	···	1.0×10^{-6}?	···	$\nu_8=1$?	···
$5_{1,5}\rightarrow5_{1,4}$	8,521.53	8,521.51	9.0×10^{-8}	0.43	G	−0.02
$8_{1,8}\rightarrow8_{1,7}$	20,448.71	20,448.77	3.2×10^{-7}	2.45	G	+0.06
$9_{1,9}\rightarrow9_{1,8}$	25,558.93	25,558.94	4.3×10^{-7}	3.83	G	+0.01
$10_{1,10}\rightarrow10_{1,9}$	31,235.60	31,235.54	5.7×10^{-7}	5.72	G	−0.06
$18_{2,17}\rightarrow18_{2,16}$	8,687.06	8,687.05	1.4×10^{-7}	9.33	G	−0.01
$22_{2,21}\rightarrow22_{2,20}$	18,737.62	18,737.66	4.3×10^{-7}	24.36	G	+0.04
$23_{2,22}\rightarrow23_{2,21}$	22,181.36	22,181.37	5.3×10^{-7}	30.24	G	+0.01
$24_{2,23}\rightarrow24_{2,23}$	26,050.17	26,050.05	6.4×10^{-7}	37.24	G	−0.12
$25_{2,24}\rightarrow25_{2,23}$	30,368.36	30,368.24	7.9×10^{-7}	45.50	G	−0.12
$26_{2,25}\rightarrow26_{2,24}$	35,159.06	35,159.13	1.1×10^{-6}	55.19	G	+0.07

was modified in that a vacuum system was used to minimize loss of the deuterium compounds. With reference to Fig. 1, acetone was cracked at about atmospheric pressure in subsystem *ADCB*, and products bled off through capillary *F* to liquid nitrogen cooled traps *GH* and rotary vacuum pump *I*. Acetone in bulb *A* was surrounded by a water bath at 55°C. Vapors rising from *A* cannot pass the drop condensed in constriction *B*, so they rise into *D* and make contact with the dull-red hot nichrome filament there. Most of the acetone is returned by the water-cooled condensers *C* and *E* to *A*; ketene, some acetone, and other products pass through capillary *F* (1 meter long, 0.4 mm bore) into large cold traps *G* and *H*; the pressure on this side of the capillary is low enough so that the two traps are essentially 100 percent effective in condensing ketene and less volatile compounds (the second trap condenses very little). The pump removes at least some of a more volatile product, probably CH_4. Purification of the ketene is carried out by fractional distillation in the following way. The substance is first triple-distilled at the temperature of dry ice in acetone. This removes impurities, mainly acetone, less volatile than ketene; they are returned to *A* for recycling. The ketene is then placed in a microwave spectroscope and slowly warmed. The absorption of the effluent vapor at the frequency of the $J=0\rightarrow1$ line is monitored as the vapor is being pumped off. When the spectroscope indicates ketene, and the absorption shows little increase with time, the pump is shut off. This results in discarding more volatile impurities, roughly 5 to 20 percent of the mixture. The ketene has been stored in vacuum for months at liquid nitrogen temperatures with no deterioration; some decomposition is noticeable in a week of storage at dry-ice acetone temperatures.

Heavy ketene was made in the same way as the light, but 1.5 cc of 96 percent pure heavy acetone, supplied to us by R. C. Lord of M.I.T. was used. DHC_2O was made from a mixture of 50 percent each of heavy and light acetones (attempts to make it by exchange of light ketene and heavy water were unsuccessful).

B. Systems Used

The spectroscope used for most of this work[7] employed square-wave Stark modulation at 6 kc/sec, and a 6 kc/sec amplifier, phase detector, and remodulator. The system band width was roughly 10 cps. Reflex klystrons were used as sources on this system. Its ultimate sensitivity, used with a two-meter *X*-band cell of the usual type, appeared to be between 1 and 5×10^{-8} cm^{-1}. A one-meter *K*-band Stark cell was used when the system was operated at frequencies above 30,000 Mc/sec. Measurements in the vicinity of 60,000 Mc/sec and initial measurements at 40,000 Mc/sec were made with a direct absorption (no Stark) doubling system with superheterodyne detection, using an *X*-band cell ten meters long.

[7] Weiss, Strandberg, Lawrance, and Loomis, Phys. Rev. 78, 202 (1950).

C. Observed Spectrum

Table I shows the observed frequencies of the three molecules studied, namely H_2C_2O, DHC_2O, and D_2C_2O. Lines were identified by Stark effect, intensity, and frequency. The identification given is thought to be the only one possible. Figure 2 shows log intensity plotted against log frequency for the lines of D_2C_2O. Neither instability nor dimerization of the sample was serious enough to render the microwave measurements difficult; nevertheless, effects which could be assigned to these actions were observed. In a brass wave guide at room temperature, after ten microns of ketene pressure had been maintained for some time, there was a decrease in peak line intensity of a factor of two in a few hours with an associated drop in Pirani gauge reading. When the wave guide was surrounded by dry ice, the intensity and pressure seemed even more stable. Furthermore, and fortunately for intensity measurement, if at room temperature the pressure were initially high enough (>100 microns) to broaden the line considerably, the peak intensity would not change as the pressure dropped. This indicates that the remaining gas was at least 80 percent pure after an hour. These observations, however, are essentially only approximate.

D. Relative Intensity Measurement

To obtain the vibration frequencies, we measured relative intensities of the $J=0\rightarrow1$ transitions in ground and excited vibrational states. With reference to Figs. 3 and 4, the method used was to inject into the 6-kc/sec amplifier of the Stark spectrograph a signal 180° out of phase with the 6-kc/sec signal from the detector crystal, and adjust the amplitude of this added voltage to exactly balance out the peak gas absorption signal. The only factor limiting the precision of this procedure appears to be the presence of noise. The amplitude uncertainty is roughly equal to the noise voltage present, so the percentage error in the ratio of ground-state to satellite line is smaller, the greater the signal-to-noise ratio of the line.

The results of about ten independent determinations of the intensity ratio at 27°C yield the result that the intensities of the four lines in the $J=0\rightarrow1$ region of H_2C_2O are in the ratio 1: (0.295±7 percent): (0.205±10 percent): (0.121±15 percent). These errors are limits within which the true intensity ratio is expected to fall.

II. INTERPRETATION OF ABSORPTION FREQUENCIES

A. General

The rotational spectrum of a molecule is, to a good first approximation, that of a rigid rotor. Because of the high resolution of microwave techniques, relatively small perturbing effects of rotation-vibration interaction must also be considered.[8] The terms "zero-point vibration correction" and "centrifugal distortion correction" are given to those parts of the effect of vibration on rotation which depend on vibrational and rotational quantum numbers, respectively (there is also a small constant vibration-rotation interaction term). In addition, rotation-electronic interaction occurs. These terms are generally very small because of the large mass ratio between electrons and nuclei.

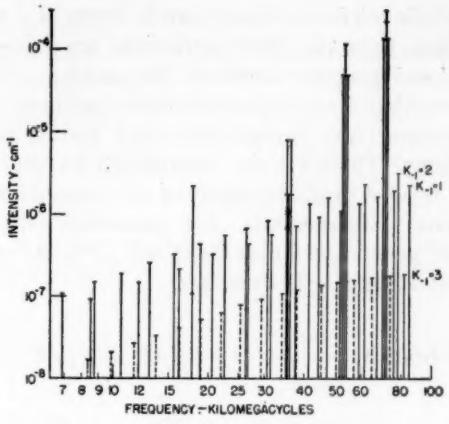

FIG. 2. Spectrum of $D_2{}^2C_2{}^{13}O^{16}$.

B. Rigid Rotor

The rigid rotor frequencies were calculated by the methods of King, Hainer, and Cross.[9] Their power series in δ was used for the R branch, and for Q branch lines with $K_{-1}=1$; their continued fraction expansion was used for Q branch lines with $K_{-1}=2$.

C. Centrifugal Distortion

The centrifugal distortion correction to the rigid rotor is the only one necessary for reasonable prediction

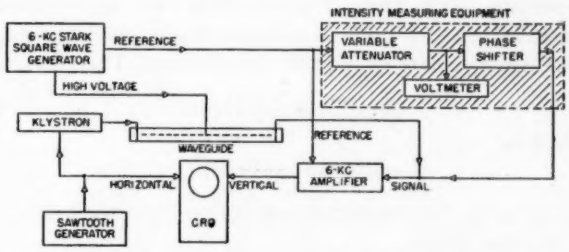

FIG. 3. Block diagram of connection of intensity measuring equipment to Stark system.

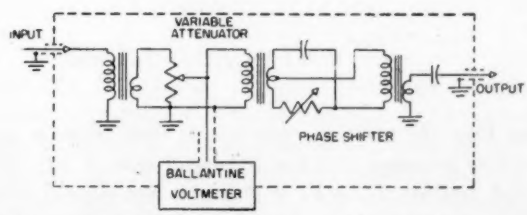

FIG. 4. Detailed diagram of intensity measuring equipment.

[8] H. H. Nielsen, Phys. Rev. **60**, 794 (1941); **61**, 540 (1942).

[9] King, Hainer, and Cross, J. Chem. Phys. **11**, 27 (1943).

of the whole microwave spectrum in terms of a selected set of lines, since the other corrections are independent of rotational quantum numbers. The problem of making this correction for asymmetric rotors has been treated by Lawrance and Strandberg,[4] and by Hillger and Strandberg.[5] There are six "centrifugal distortion constants" related to the structure of the molecule and the vibrational fundamentals. For molecules with $\delta \ll 1$, there are general formulas for $Q(\Delta K_{-1}=0,\ \Delta J=0)$ and $R(\Delta K_{-1}=0,\ \Delta J=+1)$ branches,

$$Q \text{ branch: } \frac{\nu_{\text{dist}}}{\nu_{\text{rigid}}} = J(J+1)f_1(K_{-1}) + f_2(K_{-1}); \quad (1)$$

$$R \text{ branch: } \frac{\nu_{\text{dist}}}{\nu_{\text{rigid}}} = (J+1)^2 \frac{4D_J}{b+c} + K_{-1}^2 \frac{D_{JK}}{b+c}. \quad (2)$$

Here, ν_{rigid} is the absorption frequency of the rigid rotor; ν_{dist} is the frequency correction to be added to ν_{rigid} to get ν_{meas}; ν_{meas} is the actual measured absorption frequency; D_J and D_{JK} are two centrifugal distortion constants. $f_1(K_{-1})$ and $f_2(K_{-1})$, used here temporarily for purposes of discussion, contain the other four centrifugal distortion constants.

A considerable amount of numerical calculation is involved in determining the six centrifugal distortion constants from the vibrational fundamentals. In view of some uncertainty in the assignment of these fundamentals for ketene, we will instead fit the microwave data to Eqs. (1) and (2).

The fit was attempted in the following way for Q branch lines with $K_{-1}=1$: for $\delta \ll 1$

$$\nu_{\text{rigid}} = k(b-c), \quad (3)$$

where k is a constant involving δ only in second and higher powers, and b and c are the usual reciprocal moments of inertia. Suppose that an approximate value of $(b-c)$ is used to calculate ν_{rigid}; we will designate approximate quantities with primes. Then let

$$(b-c) = (b-c)'(1+\alpha), \quad (4)$$

whence,

$$\nu_{\text{rigid}} = \nu'_{\text{rigid}}(1+\alpha), \quad (5)$$

where α is the fractional correction by which $(b-c)'$ is in error. Then,

$$\nu_{\text{rigid}} = k(b-c)'(1+\alpha), \quad (6)$$

whence,

$$\frac{\nu_{\text{meas}} - \nu'_{\text{rigid}}}{\nu'_{\text{rigid}}} = J(J+1)f_1(1) + f_2(1) + \alpha. \quad (7)$$

From Eqs. (1) and (3), this means that when a value $(b-c)'$ is assumed and the left-hand side of Eq. (7) is plotted against $J(J+1)$, a straight line should result. This is experimentally found true. The slope of the line is $f_1(1)$ and the intercept is $[f_2(1)+\alpha]$, or a combination of J-independent centrifugal distortion and the necessary fractional correction to the assumed $(b-c)'$. Similarly treating the $K_{-1} \geqslant 2$ lines of the Q branch, we may assume a value δ' as a first approximation to the true value δ of the asymmetry,

$$\nu_{\text{rigid}} = j(K_{-1})\delta^{K_{-1}^2}, \quad (8)$$

where $j(K_{-1})$ is a constant involving J and $(b-c)$ but involving δ only as a first-order correction. Writing

$$\delta = \delta'(1+\beta), \quad (9)$$

where β is the necessary fractional correction to the estimated value δ', we get

$$\frac{\nu_{\text{meas}} - \nu'_{\text{rigid}}}{\nu'_{\text{rigid}}} = J(J+1)f_1(K_{-1}) + f_2(K_{-1}) + (K_{-1}-1)\beta. \quad (10)$$

Again, this means that when a value of δ' is assumed and the left-hand side of Eq. (10) plotted against $J(J+1)$, a straight line should result. This is experimentally verified for $K_{-1}=2$ with D_2C_2O and HDC_2O. The intercept of the $K_{-1}=3$ line as well as the $K_{-1}=2$ and $K_{-1}=1$ plots would be required, however, to obtain f_2 and β. Unfortunately, only for D_2C_2O would such lines be strong enough to be detected, and none of the latter were searched for.

The effect of this situation is to introduce uncertainty into the values of $(b-c)$ and δ extrapolated to zero centrifugal distortion of about 1:5000 and 1:1000, respectively; fortunately, the amount of this uncertainty is smaller than the uncertainty in the equilibrium moments of inertia caused by zero-point vibration, and hence has no effect on the accuracy of the structure determination. The limits of error given above are suggested by a definite deviation from linearity in the case of D_2C_2O of the plot of Eq. (10) for $K_{-1}=2$ when a change of 1:1000 in δ is made; $f_2(2)$ was estimated in this way. The fitting process described was carried out by least squares.

Values of effective $(b-c)$ and δ in the ground vibrational state as well as measured centrifugal distortion constants are given in Table II. The number of significant figures given is much greater than the quoted error because of their empirical value for prediction of lines with $K_{-1} \leqslant 2$.

R branch lines pose less of a problem. First we consider lines in the ground vibrational state. For H_2C_2O, values of $(b-c)$ and δ found from the Q branch lines were assumed correct, and D_J, D_{JK} and $(b+c)$ solved for from the many observed R branch lines by the method of least squares. For D_2C_2O, no lines of the group $J=2\rightarrow3$ were searched for. $D_J=0$ was assumed since otherwise it calculated to be a small negative value with an uncertainty greater than its absolute value. For DHC_2O, only the $J=0\rightarrow1$ transition was measured, so calculation of D_J and D_{JK} is impossible. This frequency is listed as $(b+c)$.

TABLE II. Constants of isotopes of ketene.

Quantity	H_2C_2O	HDC_2O	D_2C_2O
$b+c$, Mc/sec	20,209.16±0.05	18,821.68±0.15	17,673.46±0.05
$b-c$, Mc/sec	377.414±0.080	472.421±0.100	568.136±0.100
δ	0.0013776±0.0000020	0.00254186±0.00000400	0.0042700±0.0002000
μ, $v_i=0$, debye	1.414±0.010	1.423±0.015	1.442±0.013
D_J, Mc/sec	0.0025±0.0020	···	0.000±0.005
D_{JK}, Mc/sec	0.4766±0.0060	···	0.353±0.030
f_1 (1)	$(1.53\pm0.10)\times10^{-6}$	$(1.91\pm0.10)\times10^{-6}$	$(1.66\pm0.10)\times10^{-6}$
f_1 (2)	$(1.53\pm0.17)\times10^{-6}$	$(2.428\pm0.033)\times10^{-6}$	$(1.375\pm0.025)\times10^{-6}$
f_2 (2)	···	···	$(604\pm200)\times10^{-6}$
v_9 cm^{-1}	487±15	···	···
v_8 cm^{-1}	565±20	···	···
v_7 cm^{-1}	674±30	···	···
μ, $v_9=1$, debye	1.430±0.012	···	···
μ, $v_8=1$, debye	1.387±0.010	···	···
μ, $v_7=1$, debye	1.386±0.010	···	···
$\alpha_b+\alpha_c$, Mc/sec $v_9=1$	57.66±0.05	55.97±0.05	53.27±0.05
$v_8=1$	10.72±0.05	11.08±0.05	···
$v_7=1$	22.39±0.05	25.18±0.05	···
$\alpha_b-\alpha_c$, Mc/sec $v_9=1$	18.39±0.05	···	···
$v_8=1$	−27.0±0.05	···	···
$v_7=1$	−27.88±0.05	···	34.66±0.05?
D_J, Mc/sec $v_9=1$	+0.020±0.004	···	···
$v_8=1$	−0.026±0.004	···	···
$v_7=1$	0.019±0.004	···	···
D_{JK}, Mc/sec $v_9=1$	0.505±0.030	···	···
$v_8=1$	···	···	···
$v_7=1$	0.550±0.030	···	···

D. Zero-Point Vibration

There are two well-known methods for finding the equilibrium moments of inertia from the microwave "effective" values, the first from vibrational data and the second from microwave data. In the calculations of the first method, anharmonic force constants which are generally unknown contribute effects of the same order as harmonic force constants so the calculation is seldom feasible. Rough calculations of the harmonic correction can be used to calculate the order of magnitude of the error, however. This idea is later applied to calculation of the error to be assigned to the structure determination. The second method consists of finding rotational transitions of the molecule in each of the fundamental excited vibrational states. The reciprocal moment a for ketene in a vibrational state characterized by vibrational quantum numbers $n_1, n_2, \cdots n_9$ is then

$$a(n_1, n_2, \cdots n_9)=a(0, 0, \cdots 0)+\sum_{i=1}^{9}\alpha_a{}^i(n_i+\tfrac{1}{2}), \quad (11)$$

and similarly for b and c. Here the α are interaction constants and $a(0, 0, \cdots 0)$ is the equilibrium reciprocal moment of inertia, which can then be calculated.

A considerable number of R branch lines of the molecule in excited vibrational states was found. For the $J=0\rightarrow1$ transition of H_2C_2O, all but one of the interaction lines from vibrations ν_7, ν_8, and ν_9 were measured, enabling calculation of $\alpha_b{}^9$, $\alpha_c{}^9$, $\alpha_b{}^8$, $\alpha_c{}^8$, $\alpha_b{}^7$, and $\alpha_c{}^7$ as well as D_{JK} for each state. Since we have no knowledge of the other α-values, however, we cannot correct for zero-point vibration. The known values are nevertheless interesting since they give the order of magnitude of this correction. The measured values of α and D_{JK} are listed in Table II.

E. Electronic Interaction

There is a small effect on the rotation spectrum caused by the coupling of the electronic motion to the rotation. Recent work by Eshbach and Strandberg[10] has shown how this coupling gives rise to a molecular magnetic moment which can be measured. We shall now show that the magnetic moment can be used to obtain the effect of the electronic interaction on the rotational frequencies. The Hamiltonian of the rigid rotor plus the electrons is (negligible error in calculating the electronic interaction is made here by omitting the vibrational part)

$$H=H_r+H_e+H', \quad (12)$$

where

$$H_r=\tfrac{1}{2}\sum_{i=a,b,c}\frac{P_i^2}{I_i}, \quad (13)$$

$$H_e=\frac{1}{2m}\sum_j\sum_{i=a,b,c}p_{ij}{}^2+V(a, b, c), \quad (14)$$

$$H'=-\sum_{i=a,b,c}\frac{L_iP_i}{I_i}. \quad (15)$$

Here N_a, N_b, N_c are the components of the nuclear angular momentum $\mathbf{N}$ resolved along the nuclear a, b, and c principal axes of inertia; I_a, I_b, I_c are the principal moments of inertia of the nuclear system; m is the mass of the electron; p_{aj}, p_{bj}, p_{cj} are the components of linear momentum of the jth electron in a space-fixed system, resolved along the axes a, b, and c; and $V(a, b, c)$ is the potential energy of the electrons. The terms in

TABLE III. Moments of inertia of HDC_2O, *AMU-A*[2].

	Calculated	Measured	Error (%)
I_A	2.5946	2.5914	0.12
I_B	52.320	52.377	0.03
I_C	54.972	55.089	0.21

$L_a^2/2I$, etc., have been neglected. Shift in the center of mass has also been neglected. Also

$$\mathbf{P}=\mathbf{N}+\mathbf{L} \tag{16}$$

where P_a, P_b, P_c are the components of the total angular momentum $\mathbf{P}$ of the electrons plus nuclei in a space-fixed system resolved along a, b, c; L_a, L_b, L_c are the components of the angular momentum $\mathbf{L}$ of the electrons in a space-fixed system resolved along a, b, c. Choose now the matrix representation in which $\mathbf{P}^2$, H_e, and H_r are simultaneously diagonal. This can be done since these operators mutually commute.[10] The eigenvalues of H_r are the first approximation to the energy levels of the rotational spectrum. The subscript n labels the eigenvalues E_n and eigenfunctions ψ_n^0 of H_e with $n=0$ corresponding to the lowest state. H' is a small coupling between H_e and H_r which will influence the energy of each rotational level. After diagonalizing H in n by second-order perturbation theory, the $n=0$ elements of H are found to be

$$H=\tfrac{1}{2}\sum_i \frac{P_i^2}{I_i}-\sum_i\sum_j \frac{P_iP_j}{I_iI_j}A_{ij}, \tag{17}$$

where

$$A_{ij}\overset{\Delta}{\equiv}\sum_n{}' \frac{\langle o|L_i|n\rangle\langle n|L_j|o\rangle}{E_n-E_0}. \tag{18}$$

In these and later equations, indices i, j and k run over a, b, and c.

We define

$$G_{ij}{}^e\overset{\Delta}{\equiv}-\frac{e}{2mv}\frac{A_{ij}+A_{ji}}{I_j} \tag{19}$$

and a symmetric tensor $G_{ij}{}^n$ cyclical in a, b, c of which typical elements are

$$\left.\begin{aligned} G_{aa}{}^n&=\frac{e}{2vI_a}\sum_k Z_k(b_k^2+c_k^2)\\ \text{and}\qquad G_{ab}{}^n&=-\frac{e}{2vI_b}\sum_k Z_ka_kb_k. \end{aligned}\right\} \tag{20}$$

Eshbach and Strandberg[10] showed for $^1\Sigma$ states that if m_i is the component of the vector rotational magnetic moment $\mathbf{m}$ along a principal inertial axis i

$$m_i=\sum_j G_{ij}P_j, \tag{21}$$

[10] J. R. Eshbach and M. W. P. Strandberg, Phys. Rev. **85**, 24 (1952).

where

$$G_{ij}=G_{ij}{}^e+G_{ij}{}^n. \tag{22}$$

Here e is the electronic charge; v is the velocity of light; a_k, b_k, and c_k are the coordinates of the kth nucleus in the principal inertial axis system; and Z_k is the atomic number of the kth nucleus.

If $A_{ij}=A_{ji}$, Eq. (17) can be written,

$$H=\tfrac{1}{2}\sum_i \frac{P_i^2}{I_i}-\sum_i\sum_j \frac{P_iP_j}{I_iI_j}\left(\frac{A_{ij}+A_{ji}}{2}\right). \tag{23}$$

A sufficient condition for this assumption is that G_{ij} be diagonal. With Eqs. (19) and (22), Eq. (23) becomes

$$H=\tfrac{1}{2}\sum_i \frac{P_i^2}{I_i}-\frac{mv}{e}\sum_i\sum_j G_{ij}{}^n\frac{P_iP_j}{I_i}+\frac{mv}{e}\sum_i\sum_j G_{ij}\frac{P_iP_j}{I_i}. \tag{24}$$

The second term of the right-hand side of Eq. (24) can be written, using Eq. (20), as

$$\frac{mv}{e}\sum_i\sum_j G_{ij}{}^n\frac{P_iP_j}{I_1}=\tfrac{1}{2}\sum_i\sum_j I_{ij}{}^e\frac{P_iP_j}{I_iI_j}, \tag{25}$$

where typical elements of the tensor $I_{ij}{}^e$, symmetric and cyclic in a, b, c, are

$$\left.\begin{aligned} I_{aa}{}^e&=\tfrac{1}{2}\sum_k mZ_k(b_k^2+c_k^2)\\ I_{ab}{}^e&=-\tfrac{1}{2}\sum_k mZ_ka_kb_k \end{aligned}\right\}.$$

That is, $I_{ij}{}^e$ is the moment of inertia tensor of the electrons considered concentrated at their respective nuclei, in the nuclear principal axis system. Using Eqs. (24) and (25), we have

$$H=\tfrac{1}{2}\sum_i\sum_j\left[\frac{\delta_{ij}}{I_i}-\frac{I_{ij}{}^e}{I_iI_j}\right]P_iP_j+\frac{mv}{e}\sum_i\sum_j G_{ij}\frac{P_iP_j}{I_i}, \tag{26}$$

where δ_{ij} is the usual Kronecker delta. The quantity in the brackets in Eq. (26) is obviously the reciprocal of a moment of inertia tensor; we will now find the corresponding moment of inertia tensor. The bracketed quantity is nearly diagonal, so its reciprocal will be of the form

$$\left[\frac{\delta_{ij}}{I_i}-\frac{I_{ij}{}^e}{I_iI_j}\right]^{-1}=I_i\delta_{ij}+\beta_{ij}, \tag{27}$$

where $\beta_{ij}\ll I_k$ for all i, j, k. Thus,

$$\sum_k\left[\frac{\delta_{ik}}{I_i}-\frac{I_{ik}{}^e}{I_iI_k}\right][I_k\delta_{kj}+\beta_{kj}]=\delta_{ij}, \tag{28}$$

whence

$$\beta_{ij}=I_{ij}{}^e, \tag{29}$$

$$H=\tfrac{1}{2}\sum_i\sum_j[I_i\delta_{ij}+I_{ij}^{e}]^{-1}P_iP_j+\frac{mv}{e}\sum_i\sum_j G_{ij}\frac{P_iP_j}{I_i}. \quad (30)$$

This last equation states that in the limit when the molecular magnetic moment is zero, the case of "perfect slip" which is approached by the large number of inner shell electrons in molecules made up of heavy nuclei, the effect of electronic interaction is to change the rotational energy from that calculated using nuclear masses to that using atomic masses, the method generally used. Exact correction for electronic interaction can be made from experimental magnetic moment measurements using Eq. (30). This entire derivation is of course based on the assumption $A_{ij}=A_{ji}$ made in connection with Eq. (23); although it covers a very important class of molecules, molecules of very low symmetry are excluded. Generalization appears feasible but more involved.†

The tensor G_{ij} has at worst the same symmetry as the nuclear system. For H_2C_2O and D_2C_2O, symmetry C_{2v}, it is diagonal. An estimate of G_{ij} for H_2C_2O is $G_{aa}=+0.48e/2\ Mv$, $|G_{bb}\simeq G_{cc}|<0.05e/2\ Mv$ where M is the proton mass. Use of these figures results in decreasing the H—H distance by 2.45×10^{-4}A below the value that results from using atomic masses, and introducing a correction of less than $\pm4\times10^{-5}$A in the C=C=O distance.

F. Structure

The equilibrium structure is to be calculated from the equilibrium moments of inertia. We do not know the equilibrium moments, so the structure has been calculated from the moments of inertia extrapolated to zero centrifugal distortion. The errors assigned are taken roughly equal to an estimate of the correction resulting from the harmonic force constants, calculated on the assumption of a simple harmonic oscillator.

Unfortunately, the structure of ketene is such that the carbon nucleus is, for all feasible isotopic configurations, so close to the center of gravity of the molecule that its position (±0.10A) has no effect upon the rotational spectrum. Consequently, only three structural parameters can be deduced from this work. First, the H to axis distance can be calculated from I_A of H_2C_2O and D_2C_2O. This gives values 0.9399A and 0.9406A, respectively (uncertainties in extrapolation to zero centrifugal distortion amount to ±0.0010A here). Solving the expressions for I_B of H_2C_2O and D_2C_2O simultaneously gives the length of the C=C=O chain and the projection of the C—H bond length along the symmetry axis as 2.4751A and 0.5210A, respectively. The first of these is to be compared to the electron diffraction result[11] of 2.52±0.04A. The inertia defect

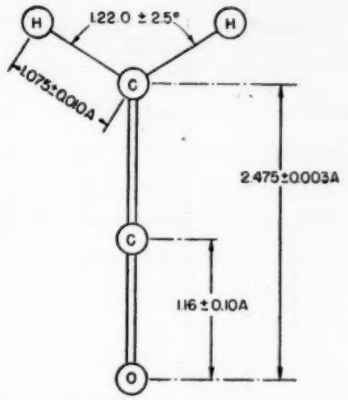

FIG. 5. Equilibrium structure of ketene from microwave data.

Δ in the expression $I_C=I_A+I_B+\Delta$ here amounts to 5 percent and 3 percent of I_A for H_2C_2O and D_2C_2O, respectively, so that I_C calculated from this structure is in error by something of the order of 0.2 percent. The measured moments of HDC_2O were used as a check, with the result shown in Table III.

These errors are well outside the experimental error; calculations show that the length of the C=C=O chain varies only 6×10^{-5}A per Mc/sec frequency change of the $J=0\rightarrow1$ line, and that the component of the C—H distance along the symmetry axis varies 5×10^{-4}A per Mc/sec. In this work, Planck's constant times Avogadro's number is taken as 39.9066×10^{-4} cgs; the present fractional error in this value[12] of $1:2.3\times10^{-4}$, is not the limiting error in the final result, but is of the same order as the electronic correction.

The structure is shown in Fig. 5.

III. STARK EFFECT AND ABSORPTION INTENSITIES

A. Stark Effect

The electric dipole moments determined from the Stark effect of the $J=0\rightarrow1$ transition of each molecule in the ground state, and of H_2C_2O in excited vibrational states, are listed in Table II. The difference in dipole moment between different isotopic forms is nearly within the experimental error. Some of the vibrational states have dipole moments differing from that of the ground state by more than the experimental error. Errors are estimated limits. Agreement with the more impurity-sensitive method of Hannay and Smyth,[13] which yielded 1.45 Debye units, seems good.

In general, the Stark effect is quadratic. Because the molecule is nearly symmetric, however, R branch transitions with $K_{-1}=1$ have a quadratic Stark at low fields which changes to linear at high fields. R branch lines with $K_{-1}\gtrsim2$ have essentially a linear Stark.

B. Intensities in the Ground Vibrational State

The line breadth parameter was measured on the $J=0\rightarrow1$ line of H_2C_2O as 19.8±2.0 Mc/mm.‡ Line in-

† The assumption that A is diagonal, as made above, is not drastic since it may be shown that the off-diagonal elements of A contribute to the energy only in the second and higher orders anyway.

[11] J. Y. Beach and D. P. Stevenson, J. Chem. Phys. **6**, 75 (1938).

[12] J. W. M. DuMond and E. R. Cohen, Revs. Modern Phys. **20**, 82 (1948).

[13] N. B. Hannay and C. P. Smyth, J. Am. Chem. Soc. **68**, 1357 (1946); A. D. Walsh, J. Am. Chem. Soc. **68**, 2408L (1946).

‡ Half-width at half-intensity.

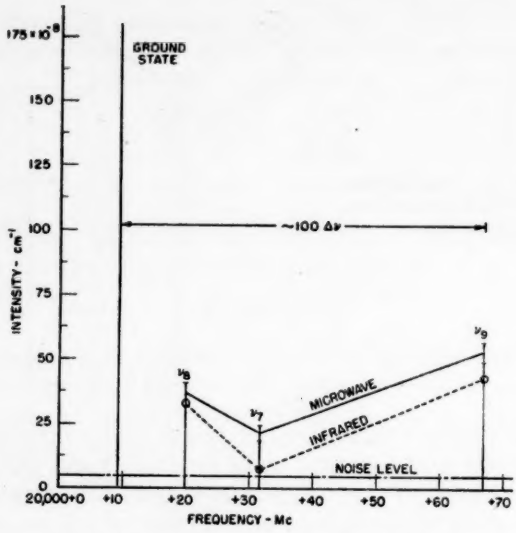

FIG. 6. $J=0\rightarrow J=1$ pattern of $H_2{}^{13}C_2{}^{12}O^{16}$.

tensities were then calculated from the Van Vleck-Weisskopf formula, with results consistent with rough estimates of intensity relative to nearby ammonia lines. In particular, the intensity alternation associated with the identical hydrogen nuclei in H_2C_2O and D_2C_2O was observed. The specific effect of this nuclear identity on transitions between levels in the ground vibrational state for H_2C_2O is the increase of transition intensities between levels of odd K_{-1} by a factor of three. Intensities are increased by the same factor for even K_{-1} values in transitions between levels in accessible vibrational states. For D_2C_2O, ground vibrational state intensities for even K_{-1} are increased by a factor of two; again, transition intensities in accessible excited vibrational states have the opposite dependence on the parity of K_{-1}. These facts further substantiate the C_{2v} symmetry of the molecule.

Lines with $K_{-1}=3$ are weak. H_2C_2O lines in K band with $K_{-1}=3$ have intensities of 10^{-9} cm^{-1}. D_2C_2O lines in K band with $K_{-1}=3$ are about 1.1×10^{-7} cm^{-1} in a pure sample, and so could be detected, but $K_{-1}=4$ lines are 7×10^{-9} cm^{-1}. No $K_{-1}=3$ lines were searched for, however.

Cooling the wave guide to dry ice temperatures is calculated to give an increase in line strength of a factor of about 4 for low-lying transitions. The vapor pressure of ketene at dry ice temperature was measured as roughly 200 mm of mercury.

Intensities recorded in Table I for H_2C_2O and D_2C_2O are calculated on the basis of a pure sample, but for DHC_2O, on the basis of a 50 percent pure sample, which is the maximum easily obtainable.

C. Intensities in Excited Vibrational States

For H_2C_2O, the intensity ratio of the ground-state line to the vibration satellites corresponding to vibration fundamentals ν_9, ν_8, and ν_7 is $1:3\exp(-\nu_9/kT):3\exp(-\nu_8/kT):3\exp(-\nu_7/kT)$. This involves the highly reasonable assumption that the lowest three modes of vibration are antisymmetric or "B" type. Thus, the intensity measurements already described imply the vibrational fundamentals listed in Table IV. The errors assigned are calculated from the estimated error of the intensity measurement (at room temperature, the frequency error in cm^{-1} is twice the percent error in the intensity).

Figure 6 shows the actual pattern of the $J=0\rightarrow1$ transition of H_2C_2O. The solid line connects our measured values, and limits of error assigned to these values are also shown. Intensity points calculated from the vibrational fundamental assignments of Halverson and Williams[14] have also been plotted and connected by a dashed line. Barring an accidental and very unlikely coincidence of the satellites from vibrations ν_6 and ν_7, there is a definite disagreement for ν_7. Although calculation of vibrational fundamentals from rotational relative intensity measurement gives far less accuracy than the usual infrared techniques, the former method has the great advantage of freedom from the confusion of combination bands near the same frequency. The infrared spectrum of ketene has a large number of these which might result in difficulty of assignment of some of the fundamentals.

IV. CONCLUSION

A more accurate structure evaluation for ketene depends mainly upon correct calculation or measurement of the zero-point vibration interaction. It appears that this would be difficult at present.

Further measurement of the spectrum of D_2C_2O would be extremely interesting as a more complete check on centrifugal distortion theory applied to a molecule with both Q and R branch transitions; besides investigating how well the rotational spectrum can be fitted to the theory, actual calculation of the coefficients from the vibrational fundamentals would be feasible for ketene because of its symmetry. R branch sets measurable are $J=0\rightarrow1^*$, $1\rightarrow2^*$, $2\rightarrow3$, $3\rightarrow4$, and $4\rightarrow5$; Q branch series measurable have $K_{-}=1^*$, 2^*, and 3. Those starred have actually been measured.

Possibly, further work on the vibrational spectrum is also indicated.

TABLE IV. Comparison of microwave and infrared measurements of vibration frequencies, cm^{-1}.

	ν_9	ν_8	ν_7	ν_6
Microwave	487±15	565±20	674±30	···
Halverson and Williams	529	588	909	1011
Drayton and Thompson	540	600	910	995

[14] H. Halverson and V. Z. Williams, J. Chem. Phys. **15**, 552 (1948).

ACKNOWLEDGMENT

The authors are grateful to R. C. Lord of M.I.T., who supplied the deuterated acetone; to J. G. Ingersoll, who participated in most of the experimental work; to B. V. Gokhale for many profitable discussions; and to J. Goldstein of Harvard for his cooperation in the initial phases of this work. Miss Mida Karakashian and Mrs. Neria Ryder assisted in the numerical computations.

BIBLIOGRAPHY

(1) Infrared: H. Gershinowitz and E. B. Wilson, Jr., J. Chem. Phys. **5**, 500L (1937).
(2) Infrared: W. R. Harp and R. S. Rasmussen, J. Chem. Phys. **15**, 778 (1948).
(3) Infrared: L. G. Drayton and H. W. Thompson, J. Chem. Soc., 1416 (1948).
(4) Raman, Liquid: H. Kopper, Z. Phys. Chem. **B34**, 396 (1937).
(5) Ultraviolet: Forster, Skrabal, and Wagner, Z. Elektrochem. **43**, 290 (1937).
(6) Magnetic moment estimation: G. C. Wick, Phys. Rev. **73**, 51 (1948).

THE JOURNAL OF CHEMICAL PHYSICS VOLUME 20, NUMBER 4 APRIL, 1952

The Heat Capacities of Uranium, Uranium Trioxide, and Uranium Dioxide from 15°K to 300°K

W. M. JONES,* JOSEPH GORDON,† AND E. A. LONG‡
Department of Chemistry, University of California, Berkeley, California

(Received August 13, 1951)

Heat capacity measurements have been made over the temperature range 15–300°K for uranium metal, uranium trioxide, and uranium dioxide. A maximum was observed at 28.7°K in the heat capacity curve of UO_2 which is probably the result of the changing population of the magnetic quadrivalent uranium ions among their available energy states. The entropies of these substances at 298.16°K are 12.03, 23.57, and 18.63 cal deg^{-1} mole^{-1}, respectively. The free energies of formation of UO_3 and UO_2 are -273.1 ± 3 and -246.6 ± 0.6 kcal mole^{-1}, respectively.

THE measurements reported in this paper were performed at the University of California during the late summer and fall of 1942 for the purpose of securing data needed by the Manhattan Project. The work was conducted as part of a contract between the University of California and Columbia University. High temperature data for the present compounds, obtained with samples representative of our own in composition (except possibly for UO_3, as discussed in the following material), have already been reported.[1]

Two calorimeters were employed. The first was used for the measurements on uranium metal and has been described by Giauque and Meads.[2] The second calorimeter used with UO_3 and UO_2 was provided with 12 radial vanes to facilitate heat conduction and has been described by Giauque and Archibald.[3] For general features of the measurements reference may be made to Giauque and collaborators.[4] In each case a small amount of helium, for which correction was made, was added to the calorimeter to facilitate heat conduction. The gold resistance thermometers were calibrated against a standard copper-constantan thermocouple, of laboratory designation W-26, the working junction of which was imbedded with Rose metal in a well at the bottom of the calorimeter. The calibrations were carried out concurrently with the heat capacity measurements at intervals of approximately five degrees. The defined thermochemical calorie equal to 4.1833 international joules is used throughout, and 0°C is taken to be 273.16°K. The atomic weight of uranium was taken as 238.07. A smooth curve through the data should be accurate to 0.2 percent above 35°K. The error may be 1 percent at 20°K and 2–3 percent at 15°K.

MATERIALS

The uranium sample had been cast in the shape of a cylinder and was provided by Dr. J. W. Marden. The material was thoroughly cleaned with benzene before placing in the calorimeter. The analysis by Moore and Kelley[1] on a sample which was cast with the present material from the same block of metal indicated 99.71 percent uranium.

The uranium trioxide was prepared by Mr. H. F. Priest by heating a quantity of uranyl nitrate for eight hours in a muffle furnace at 300°C until complete decomposition had occurred. The muffle was kept closed in order to maintain an oxidizing atmosphere of NO_2 over the sample. After removal from the furnace the sample was ground in an agate mortar and sifted

* Present address: Los Alamos Scientific Laboratory of the University of California, Los Alamos, New Mexico.
† Present address: Chemical Industries Week, 330 West 42nd Street, New York 18, New York.
‡ Present address: Institute for the Study of Metals, The University of Chicago, Chicago, 37, Illinois.

[1] G. E. Moore and K. K. Kelley, J. Am. Chem. Soc. **69**, 2105 (1947).
[2] W. F. Giauque and P. F. Meads, J. Am. Chem. Soc. **63**, 1897 (1941).
[3] W. F. Giauque and R. C. Archibald, J. Am. Chem. Soc. **59**, 561 (1937).
[4] (a) W. F. Giauque and R. Wiebe, J. Am. Chem. Soc. **50**, 101 (1928); (b) W. F. Giauque and H. L. Johnston, **51**, 2300 (1929).

TABLE I. Heat capacity of uranium metal.

cal deg^{-1} g-atom^{-1}		atomic weight 238.07		0°C = 273.16°K	
T, °K	C_p	T, °K	C_p	T, °K	C_p
Series I		87.07	5.072	192.61	6.154
15.38	0.432	92.78	5.194	198.51	6.203
16.61	0.496	98.95	5.325	Series III	
18.55	0.665	104.83	5.435	205.17	6.232
21.01	0.914	111.02	5.532	211.12	6.274
23.92	1.211	117.43	5.591	217.81	6.295
27.56	1.639	123.51	5.639	224.94	6.335
31.20	2.080	128.26	5.697	231.93	6.348
35.33	2.530	134.61	5.754	238.78	6.381
40.11	2.954	140.93	5.823	245.64	6.417
45.28	3.369	147.09	5.874	252.95	6.441
50.50	3.731	153.38	5.924	259.42	6.476
55.54	4.011	159.80	5.964	266.38	6.486
60.64	4.231	166.69	6.008	273.08	6.524
65.79	4.446	173.65	6.053	280.22	6.544
Series II		180.08	6.091	287.56	6.548
71.58	4.657	186.41	6.131	294.94	6.556
76.01	4.807			297.77	6.574
81.54	4.955				

through a 120-mesh brass screen. Separate portions were tested for reducing action with dilute $KMnO_4$ solution and for nitrate. Both tests gave negative results. A quantitative analysis by Mr. S. J. Kiehl, Jr., using the silver reductor-ceric sulfate method, showed that the uranium content was 99.9±0.1 percent of the theoretical value. It had been found during the analysis that the finely ground oxide took up small amounts of water from the atmosphere. For this reason the UO_3, which had been received by us in an airtight screw-cap container, was heated in an oven at 100°C for three hours immediately before sealing it into the calorimeter. The heat capacity at 270.95°K in Table III shows that the free water content was about 0.04 mole percent. Moore and Kelley[1] have reported that their sample, as received from us, contained 1.17 percent water not removable at 120°C. We have no detailed record of the history of their sample, but it seems possible that it had more opportunity than our own to pick up moisture. If our sample actually contained any significant amount of water, it was bound in such a manner as to give an almost normal heat capacity at 0°C. Fortunately, the fractional effect on the UO_3 heat capacity would be less than the fractional water content. No correction has been made. An analysis by Moore and Kelley on their final material gave 83.02 percent uranium, as compared with the theoretical value of 83.22 percent.

The uranium dioxide came from a one-pound lot originating with the Mallinckrodt Chemical Works of St. Louis. Their analysis, provided by Dr. J. A. Kyger, indicated 99.3 percent UO_2, 0.7 percent UO_3, and traces of other metal oxides. No correction has been made for the UO_3 content. An analysis by Moore and Kelley indicated 88.26 percent U against a theoretical 88.15 percent. The material was a powder of well-crystallized particles.

HEAT CAPACITY AND ENTROPY OF URANIUM METAL

The conditions for heat transfer from the calorimeter wall to the uranium cylinder were not very favorable, but the accuracy of the data was not significantly impaired by the somewhat abnormal temperature rise of the resistance thermometer-heater over the calorimeter wall during energy input. The weight of the uranium sample was 2135.21 grams in vacuum or 8.9688 gram atoms. The results of the measurements are presented in Table I. Table II gives values of C_p at rounded temperatures as read from a smooth curve through the data. The values of C_v given in Table II were computed from C_p and the empirical equation

$$C_p - C_v = ATC_p^2.$$

The constant A was evaluated at room temperature from the thermodynamic equation

$$C_p - C_v = \alpha^2 VT/\beta.$$

The isothermal compressibility α was taken to be $(8.4\pm0.5)\times10^{-13}$ cm^2 dyne^{-1}, derived from measurements on Young's and shear moduli on uranium bars by Birch and by Kilpatrick, Laquer, and McGee at Los Alamos.[5] The density of α-uranium was taken to be 18.95±0.05 g/cm^{-3},[6,7] giving a molal volume of 12.56 cm^3. The thermal coefficient of cubical expansion β was taken to be $(50\pm2)\times10^{-6}$ deg^{-1}.[8] A is then found to be 2.07×10^{-5} g-atom cal^{-1}. C_v attains the value $\frac{3}{2}R$ at 40.5°K and the value $3R$ at about 181°K.

The entropy was obtained by graphical evaluation of $\int C_p d \ln T$ and a Debye function extrapolation with

TABLE II. Heat capacity of uranium metal. Values at rounded temperatures from a smooth curve through the data.

cal deg^{-1} g-atom^{-1}		Atomic weight 238.07		0°C = 273.16°K	
T, °K	C_p	C_v	T, °K	C_p	C_v
15	0.416	0.416	160	5.970	5.852
20	0.809	0.809	170	6.031	5.903
25	1.334	1.333	180	6.092	5.953
30	1.938	1.936	190	6.152	6.003
40	2.946	2.938	200	6.211	6.051
50	3.700	3.686	210	6.268	6.097
60	4.208	4.186	220	6.313	6.132
70	4.601	4.571	230	6.355	6.163
80	4.910	4.870	240	6.395	6.192
90	5.134	5.085	250	6.437	6.222
100	5.345	5.286	260	6.475	6.250
110	5.503	5.435	270	6.511	6.274
120	5.623	5.545	280	6.539	6.291
130	5.722	5.634	290	6.556	6.298
140	5.814	5.716	300	6.571	6.302
150	5.897	5.789			

[5] We are indebted to Dr. H. L. Laquer for providing us with these data. See Laquer, McGee, and Kilpatrick, Trans. Am. Soc. Metals, 42, 771 (1950).

[6] C. W. Jacob and B. E. Warren, J. Am. Chem. Soc. 59, 2588 (1937).

[7] F. H. Driggs and W. C. Lilliendahl, J. Ind. Eng. Chem. 22, 516 (1930).

[8] We thank Dr. H. R. Nelson of the Battelle Memorial Institute for supplying this information.

TABLE III. The entropy of uranium.

0-15°K, Debye extrapolation	0.121
15-298.16°K, graphical integration	11.913
S at 298.16°K	12.03±0.03 cal deg^{-1} mole^{-1}

a characteristic temperature of 162°K. The calculation is summarized in Table III.

HEAT CAPACITY, ENTROPY, AND FREE ENERGY OF FORMATION OF URANIUM TRIOXIDE

The weight of the uranium trioxide sample was 277.429 grams in vacuum or 0.96979-gram atoms. The original data and smoothed values of C_p at rounded temperatures appear in Tables IV and V.

The entropy calculation is summarized in Table VI. The extrapolation was made with a single Debye function having a characteristic temperature of 140°K.

The heat of formation of UO_3 is taken to be 291,600 cal.[9] Taking the present entropies of U and UO_3 and the computed entropy of oxygen gas,[10] we obtain

$$U+\tfrac{3}{2}O_2=UO_3$$
$$\Delta H^\circ_{298.16}=-291{,}600\pm3000 \text{ cal}$$
$$\Delta S^\circ_{298.16}=-61.98\pm0.07 \text{ cal deg}^{-1}$$
$$\Delta F^\circ_{298.16}=-273{,}100\pm3000 \text{ cal.}$$

HEAT CAPACITY, ENTROPY, AND FREE ENERGY OF FORMATION OF URANIUM DIOXIDE

The heat capacity data are given in Tables VII and VIII and in Figs. 1 and 2. The first series of measurements revealed a region of high energy absorption in the neighborhood of 30°K. The measurements of Series II and III, made over temperature intervals of 0.1–0.5 degree, established satisfactorily the shape of the heat capacity curve, which rises smoothly to a maximum value of about 9 cal deg^{-1} mole^{-1} at 28.7°K and then falls rapidly on the high temperature side. The measurements indicate that the slope of the heat capacity curve changes continuously. There was no evidence of poor thermal equilibrium, and the agreement of the three series of measurements shows that there were no hysteresis effects. The total entropy, including that arising from the heat capacity maximum, is summarized in Table IX. The Debye extrapolation is somewhat uncertain because of the low temperature maximum. The characteristic temperature of 160°K is based on the measurements below 20°K; the uncertainty in the extrapolation is estimated to be 0.03 cal deg^{-1} mole^{-1}. The value for the total entropy assumes that there is no entropy below the lowest temperature of our measurements other than that given by the Debye extrapolation.

TABLE IV. Heat capacity of uranium trioxide.

cal deg^{-1} mole^{-1}	Molecular weight 238.07		0°=273.16°K
T, °K	C_p	T, °K	C_p
13.81	0.483	139.58	12.98
15.24	0.611	146.20	13.44
17.52	0.805	152.74	13.87
19.96	1.024	156.60	14.13
22.32	1.289	163.20	14.54
24.93	1.562	169.60	14.89
28.32	1.899	176.29	15.30
33.21	2.407	183.59	15.67
39.07	3.118	190.50	16.03
44.74	3.792	199.78	16.18
50.49	4.407	207.14	16.78
56.60	5.130	214.34	17.15
62.99	5.846	221.12	17.43
67.61	6.356	227.89	17.69
73.62	7.005	234.89	18.00
78.79	7.559	241.88	18.30
82.53	7.951	248.79	18.66
86.85	8.391	256.10	18.87
92.11	8.933	263.51	19.11
97.95	9.499	270.95	19.53
104.51	10.12	278.52	19.69
119.33	11.42	285.90	19.71
126.35	12.05	294.57	20.16
132.89	12.49		

TABLE V. Heat capacity of uranium trioxide. Values at rounded temperatures from a smooth curve through the data.

cal deg^{-1} mole^{-1}	Molecular weight 286.07		0°=273.16°K
T, °K	C_p	T, °K	C_p
15	0.590	160	14.34
20	1.050	170	14.91
25	1.567	180	15.48
30	2.074	190	16.00
40	3.234	200	16.49
50	4.356	210	16.95
60	5.514	220	17.39
70	6.612	230	17.81
80	7.694	240	18.24
90	8.675	250	18.65
100	9.675	260	19.03
110	10.62	270	19.39
120	11.51	280	19.72
130	12.31	290	20.02
140	13.03	300	20.30
150	13.70		

The heat of formation of UO_2 is 259.2±0.6 kcal.[11] Using the present entropies of U and UO_2 and the entropy of oxygen gas[10] we obtain

$$U+O_2=UO_2$$
$$\Delta H^\circ_{298.16}=-259{,}200\pm600 \text{ cal}$$
$$\Delta S^\circ_{298.16}=-42.41\pm0.11 \text{ cal deg}^{-1}$$
$$\Delta F^\circ_{298.16}=-246{,}600\pm600 \text{ cal.}$$

DISCUSSION OF THE HEAT CAPACITY ANOMALY IN UO_2

The state of the U^{+4} ion is $^3F_2$ for a $6d^2$ electronic configuration, assuming Hund's rule for L-S coupling. The state is $^3H_4$ for a $5f^16d^1$ or $5f^2$ configuration. The corresponding L-S coupling magnetic moments are

[9] Bichowsky and Rossini, *Thermochemistry of Chemical Substances* (Reinhold Publishing Corporation, New York, 1936).

[10] H. W. Wooley, J. Research Natl. Bur. Standards **40**, 163 (1948).

[11] Measurements at the Los Alamos Scientific Laboratory by Holley, Huber, and Meierkord. We wish to express our appreciation for permission to utilize this value in advance of publication.

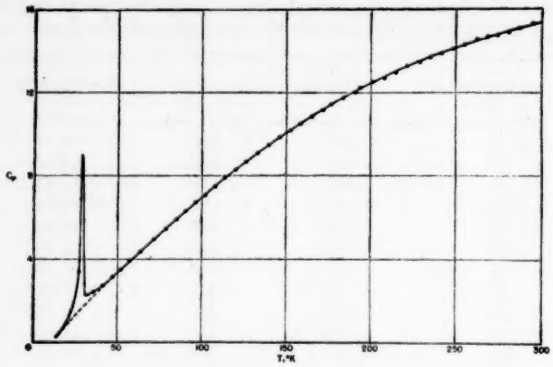

FIG. 1. Heat capacity in calories per degree per mole of uranium dioxide.

1.63 and 3.58-Bohr magnetons, while the spin-only moment for a triplet state is 2.83. Dawson and Lister[12] have found that UO_2 follows the Curie-Weiss law, $\chi(T+\theta)=C$, with $\theta=233°K$ and a derived magnetic moment of 3.20 (diamagnetic correction included), indicating a $5f^2$ or $5f^16d^1$ configuration with appreciable quenching of the orbital contribution. Haraldsen and Bakken[13] found a θ of 180°K and a moment of 2.92 (correction for diamagnetism would raise the moment by about 0.1 unit), suggesting slightly more orbital quenching. No magnetic measurements below about 90°K have been reported.

If the orbital contribution to the magnetic moment were completely quenched, then the magnetic ions would be equally distributed among three magnetic states at sufficiently high temperatures. With decreasing temperature an increasing fraction of the ions would move into the state of lowest energy, until at the absolute zero a completely ordered arrangement of zero entropy would be attained. We believe that the maximum in the heat capacity curve of UO_2 is associated with some such loss of magnetic entropy at low temperatures. For complete orbital quenching the magnetic entropy present at high temperatures amounts to R ln3 or 2.18 cal deg^{-1} mole^{-1}. For free ions with a $^3H_4$ ground state the magnetic entropy would approach R ln9 or 4.37 cal deg^{-1} mole^{-1} at high temperatures. In Figs. 1 and 2 we have indicated by a dashed line an estimate of the lattice heat capacity resulting from the crystalline vibrations. The entropy contributed by that portion of the observed heat capacity which lies above the dashed line corresponds to 0.87 cal deg^{-1} mole^{-1}. A large fraction of the magnetic entropy present at high temperatures must therefore be acquired in regions of temperature other than that in which the anomalous heat capacities occur. The situation considered most likely is that magnetic entropy continues to be acquired at higher temperatures in so gradual a manner that the magnetic and lattice contributions to the heat capacity are not readily separable. Such a separation has sometimes been assisted by comparison with a similar substance which is expected to have closely the same lattice contribution without magnetic complications. Unfortunately such data are not available in this case. Another possibility, considered less likely, is that there remains at the lowest temperatures of our measurements a substantial magnetic entropy which would be lost at lower temperatures. Further experiments at lower temperatures, perhaps including measurements of the magnetic susceptibility, will be necessary in order to prove positively that an ordered state has been reached.

TABLE VI. The entropy of uranium trioxide.

0–15°K, Debye extrapolation	0.196
15–298.16°K, graphical integration	23.378
S at 298.16°K	23.57±0.06 cal deg^{-1} mole^{-1}

TABLE VII. Heat capacity of uranium dioxide.

cal deg^{-1} mole^{-1} Molecular weight 270.07 0°C=273.16°K

T, °K	C_p	T, °K	C_p	T, °K	C_p	T, °K	C_p
Series I							
14.15	0.308	31.36	2.260	28.90	8.80	190.99	12.25
16.23	0.497	31.95	2.269	29.07	8.63	Series V	
18.77	0.807	32.73	2.287	Series IV		193.61	12.25
21.49	1.276	35.71	2.424	63.63	4.369	200.87	12.54
41.15	2.710	Series III		71.62	4.960	207.90	12.73
47.21	3.158	22.37	1.450	78.88	5.467	214.61	12.98
52.00	3.513	23.33	1.679	85.10	5.916	221.41	13.31
57.24	3.922	24.13	1.941	90.54	6.331	228.96	13.48
Series II		apparatus cooled		96.24	6.740	235.02	13.72
13.68	0.261	slightly		102.06	7.086	241.75	13.92
15.27	0.418	24.07	1.906	108.11	7.492	248.50	14.12
17.29	0.609	24.79	2.164	113.40	7.896	255.24	14.32
19.61	0.928	25.41	2.420	120.09	8.282	262.47	14.56
22.70	1.537	25.97	2.690	126.20	8.680	268.57	14.68
28.38	7.99	26.46	3.012	133.18	9.113	274.33	14.76
28.59	8.79	26.92	3.403	139.74	9.503	281.10	14.88
28.84	8.89	27.31	3.918	146.23	9.868	287.57	15.08
29.08	8.55	27.65	4.723	152.48	10.20	294.82	15.31
29.33	8.24	27.93	5.73	158.65	10.53	300.21	15.53
29.61	7.31	28.17	6.95	165.25	10.87		
29.90	5.86	28.37	7.92	171.90	11.18		
30.29	2.828	28.55	8.71	176.61	11.47		
30.89	2.282	28.72	8.98	183.85	11.76		

The narrowness of the heat capacity curve in the anomalous region, the sharpness of the maximum, and the rapid drop on its high temperature side are characteristic of cooperative behavior. The behavior of UO_2, as well as that of many other concentrated paramagnetic compounds at low temperatures, is probably caused by the phenomenon of antiferromagnetism, an approximate theory of which has been given by Van Vleck.[14] This theory predicts a gradual rise of the magnetic heat capacity to a maximum, followed by a discontinuous fall to zero. At this temperature the complete magnetic entropy would have been acquired. Our results do not agree with this picture. It must be mentioned, however, that the Van Vleck theory applies as it stands only to spin-only cases in which the magnetic species are in simple cubic or body-centered cubic array. The orbital contribution to the magnetic moment is not completely quenched in UO_2 over the temperature range in which

[12] J. K. Dawson and M. W. Lister, J. Chem. Soc. 2181 (1950). Other pertinent references are given in this paper.
[13] H. Haraldsen and R. Bakken, Naturwiss. 28, 127 (1940).
[14] J. H. Van Vleck, J. Chem. Phys. 9, 85 (1941).

magnetic measurements have been made. In addition UO_2 has a structure of the fluorite type[15] in which the uranium ions have a face-centered cubic arrangement. The prediction of zero magnetic heat capacity above a critical temperature is the same as that of the Weiss-Heisenberg theory of ferromagnetism, of which the Van Vleck theory is the analog for the case in which antiparallel alignment of spins is favored. It has been mentioned by Seitz[16] that this discrepancy with experiment might be removed by consideration of short-range order in the theory. This would occur in much the same way that Bethe's treatment of the analogous phenomenon of order and disorder removes, at least qualitatively, a similar discrepancy of the Bragg-Williams theory with experiment. Improved approximations with specific application to the face centered cubic lattice have recently been given by Kikuchi.[17]

TABLE VIII. Heat capacity of uranium dioxide. Values at rounded temperatures from a smooth curve through the data.

cal deg^{-1} mole^{-1}	Molecular weight 270.07		0°C=273.16°K
T, °K	C_p	T, °K	C_p
15	0.382	80	5.563
16	0.475	90	6.298
17	0.582	100	6.958
18	0.704	110	7.619
19	0.842	120	8.276
20	1.001	130	8.923
21	1.178	140	9.518
22	1.380	150	10.07
23	1.610	160	10.60
24	1.888	170	11.11
25	2.243	180	11.60
26	2.725	190	12.05
27	3.50[a]	200	12.47
28	6.10[a]	210	12.87
29	8.70[a]	220	13.23
30	5.15[a]	230	13.57
31	2.275	240	13.89
32	2.267	250	14.16
35	2.382	260	14.43
40	2.637	270	14.69
50	3.367	280	14.92
60	4.103	290	15.14
70	4.841	300	15.36

[a] These values are of reduced accuracy because the heat capacity is changing rapidly in this temperature region.

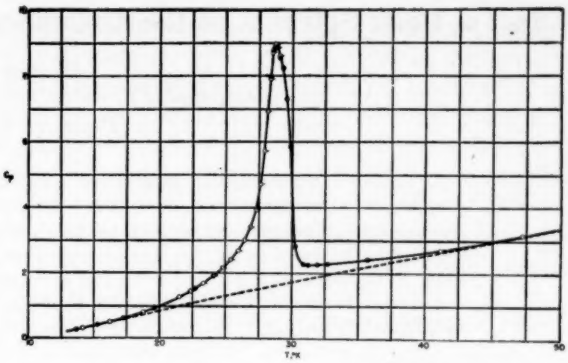

FIG. 2. Heat capacity of uranium dioxide in calories per degree per mole in the anomalous region.

It is expected that other compounds of quadrivalent uranium would exhibit similar behavior. The heat capacity of UF_4,[18] measured down to temperatures approximately as low as ours, appears normal, but it seems likely that experiments at lower temperatures would reveal a heat capacity anomaly.

TABLE IX. Entropy of uranium dioxide.

0–15°K, Debye extrapolation	0.12
15–298.16°K, graphical integration	18.507
Total S at 298.16°K	18.63±0.1 cal deg^{-1} mole^{-1}

ACKNOWLEDGMENT

We thank Professor W. F. Giauque for the use of the facilities of his laboratory.

[15] R. W. G. Wyckoff, *Structure of Crystals* (Chemical Catalog Company, New York, 1931), p. 239.
[16] F. Seitz, *Modern Theory of Solids* (McGraw-Hill Book Company, Inc., New York, 1940), p. 611.
[17] R. Kikuchi, Phys. Rev. **81**, 988 (1951).
[18] Brickwedde, Hoge, and Scott, J. Chem. Phys. **16**, 429 (1948).

Effect of Polar Solvents on the Absorption Frequency of $n \rightarrow \pi$ Electronic Transitions*

HARDEN MCCONNELL†
Department of Physics, University of Chicago, Chicago 37, Illinois
(Received November 23, 1951)

A variety of spectroscopic data shows that the absorption frequencies of $n \rightarrow \pi$ electronic transitions progressively increase in the series of solvents, paraffin, alcohol, and water. This general effect of polar solvents on the frequency of $n \rightarrow \pi$ transitions is related to the characteristic change in the molecular charge distribution accompanying this type of transition. In certain cases solvation effects can be of considerable value in distinguishing between $n \rightarrow \pi$ and $\pi \rightarrow \pi$ electronic transitions.

Evidence is presented which indicates that the absorption bands of the ions, NO_3^- (32,000 cm^{-1}), $CO_3^=$ (46,000 cm^{-1}) and $CS_3^=$ (20,000 cm^{-1}) are $n \rightarrow \pi$ transitions.

I. INTRODUCTION

THE dependence of the electronic spectra of solute molecules on the properties of solvent media can be used to establish empirical classifications of electronic spectra. Such empirical classifications have been made by Coggeshall and Pozefsky[1] for catacondensed aromatic $\pi \rightarrow \pi$ spectra in paraffin hydrocarbon and benzene solvents, and by Burawoy[2] for various spectra in polar solvents. Our empirical classification, which is similar to that used by Burawoy, is: All absorption bands whose maxima are progressively displaced to lower frequencies in the series of solvents, a paraffin hydrocarbon, alcohol, and water, are called *red-shift* bands and all absorption bands whose maxima are progressively displaced to higher frequencies in the same series of solvents are called *blue-shift* bands. Current interest in the *blue-shift, red-shift* classification of electronic spectra stems from the possibility that, in certain cases, it may be possible to relate this classification to classifications of spectra based on electronic configurations.

Planar conjugated organic molecules containing double- or triple-bonded hetero atoms ($=O$, $=S$, $\equiv N$) frequently show singlet-singlet $n \rightarrow \pi$ transitions.[3] These transitions arise from the excitation of an n (nonbonding) electron of the hetero atom to a π molecular orbital extending over the entire conjugated molecule. In Sections II and III of the present paper, it is shown that (a) all known $n \rightarrow \pi$'s give *blue-shift* bands, and (b) solvation effects can be useful for distinguishing between $n \rightarrow \pi$ and $\pi \rightarrow \pi$ transitions. These two possibilities were apparently first suggested by M. Kasha,[4] but relatively little substantiating evidence has been published. Section IV deals with the identification of $n \rightarrow \pi$ transitions for the ions, NO_3^-, $CO_3^=$, and $CS_3^=$. All the electronic transitions discussed in the present paper are believed to be singlet-singlet (see Section III).

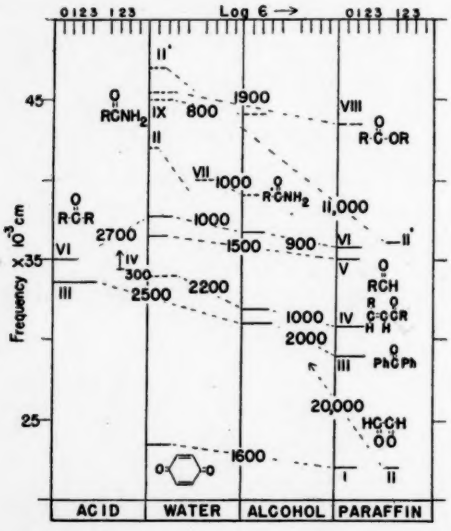

FIG. 1. The *blue-shift* bands of molecules containing the C=O group. The symbols *R, R', Ph, Ph'* denote alkyl, substituted alkyl, phenyl and substituted phenyl groups, respectively.

II. CLASSIFICATION OF SPECTRA INTO BLUE-SHIFT AND RED-SHIFT BANDS

This section presents a compilation of data on the *blue-shift* and *red-shift* bands of a typical group of planar conjugated organic molecules containing hetero atoms. Most of the data has been taken from the literature and, whenever possible, the data of several investigators on a particular compound have been compared. No inconsistencies in experimental results have been found which would invalidate our conclusions. The data on *s*-trinitrobenzene and benzonitrile (Section III) and nitrosobenzene[5] are reported here for the first time. Our experimental procedure was similar to that described elsewhere[6] except that 1.0 and 10.0 cm light paths were employed, and that the nitrosobenzene was

* The experimental portion of this work was assisted by the ONR under task order IX of contract N6ori-20 with the University of Chicago.
† National Research Council Postdoctoral Fellow, 1950–1952.
[1] N. D. Coggeshall and A. Pozefsky, J. Chem. Phys. **19**, 980 (1951).
[2] A. Burawoy, J. Chem. Soc., 1177 (1939).
[3] For recent discussions of $n \rightarrow \pi$ transitions, see J. R. Platt, J. Chem. Phys. **19**, 101 (1951); J. R. Platt, *Radiation Biology*; (McGraw-Hill Book Company, Inc., New York, 1952), Chapter 4 (to be published).
[4] M. Kasha, Disc. Faraday Soc. No. 9, 14 (1950).
[5] See references to figures at end of this paper.
[6] Ham, Platt, and McConnell, J. Chem. Phys. **19**, 1301 (1951).

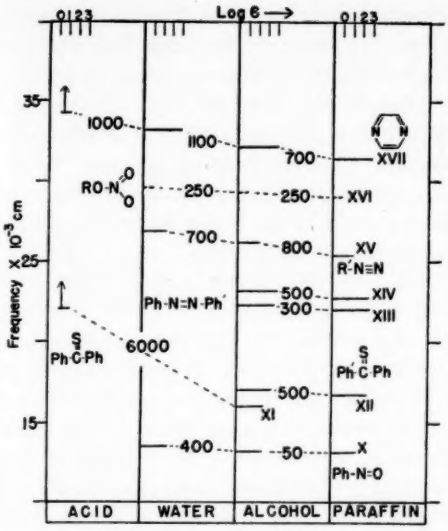

FIG. 2. The *blue-shift* bands of molecules containing nitrogen, oxygen or sulfur hetero atoms. The symbols *R, R', Ph, Ph'* denote alkyl, substituted alkyl, phenyl, and substituted phenyl groups, respectively.

prepared and purified according to the method described by Coleman *et al.*[7]

Figures 1–2 give the *blue-shift* bands, and Fig. 3 the *red-shift* bands, of the above mentioned group of organic molecules containing hetero atoms. Literature references for compounds are listed at the end of this paper according to the Roman numerals in the figures.[5] A horizontal full heavy line in Figs. 1–3 gives the frequency (vertical scale) and logϵ[8] (horizontal scale) for an absorption maximum; a dashed horizontal heavy line gives the frequency and logϵ for a point on the long wavelength side of an absorption band whenever the absorption maximum is obscured by a neighboring band or is otherwise unknown. Most of the absorption frequencies in Figs. 1–3 are accurate to *ca*$\pm$150 cm^{-1}.

A vertical arrow indicates that an absorption band has "disappeared"; that is, the band has moved so far to higher frequencies as to be completely obscured by other absorption bands. The frequency of the absorption maximum is equal to or greater than the frequency indicated by the tail of the arrow.

The paraffin hydrocarbon solvent in the three figures is hexane, heptane, or isooctane. The frequencies of an absorption maximum of a polar solute molecule in these solvents generally differ by less than 200 cm^{-1}; this frequency variation is usually negligible relative to the larger frequency shifts produced by alcohol and water. The alcohol is ethanol. Slightly different solvents are used for a few compounds.[5] Arabic figures give the differences in frequency (cm^{-1}) of absorption maxima in the pairs of solvents indicated by the dashed connecting lines. Uncertainties in determining absorption frequencies from curves in the literature produce an estimated *average* error of 25 percent in the frequency shifts; in all cases the frequency shifts are accurate as to order of magnitude and sign. For the polar solute molecules of Figs. 1–3, the changes in absorption frequency in passing from the paraffin to alcohol, and from alcohol to water, are usually between 200 and 2000 cm^{-1}. Absorption frequencies of unsaturated hydrocarbons with no hetero atoms ($\pi \rightarrow \pi$ transitions only) are considerably less affected by polar solvents.[9]

Also included in the figures are data for acid solvents. The acid is concentrated or dilute aqueous sulfuric acid. Acid solvents have been used by Kasha[4] and Burawoy[2] for classifications of electronic spectra. The acid solvent frequently, but not always, gives a blue shift relative to water solvent for the *blue-shift* bands of Figs. 1–2. One reason for not including acid solvents in our classification of spectra is discussed in Section III.

III. CORRELATION OF BLUE-SHIFT BANDS WITH $n \rightarrow \pi$ TRANSITIONS

An $n \rightarrow \pi$ electronic transition in a planar conjugated molecule represents the excitation of an n (nonbonding) electron from a *MO* or *AO* (molecular or atomic orbital) symmetric to the molecular plane to a π *MO* (molecular orbital antisymmetric to the molecular plane). For the present discussion, only conjugated atoms need be coplanar. The *blue-shift* bands in Figs. 1–2 have intensities ($\epsilon \approx 10$–1000) which have been used previously to identify singlet-singlet $n \rightarrow \pi$ transitions: forbidden $^1A - {}^1U$, $\epsilon \approx 10$–100; allowed $^1A - {}^1W$, $\epsilon \approx 100$–1000. The investigations of McMurry and Mulliken,[10a]

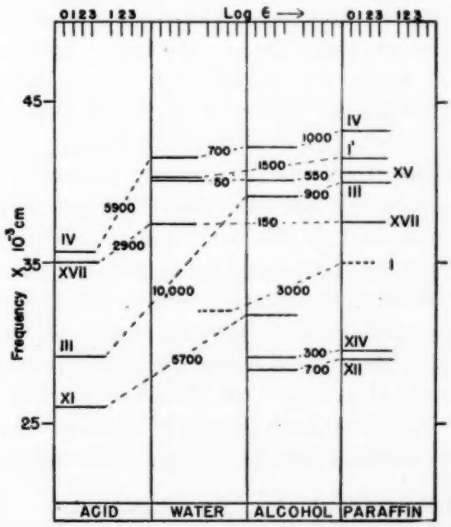

FIG. 3. The *red-shift* bands of molecules containing nitrogen, oxygen or sulfur hetero atoms. The numbering of compounds in this figure is the same as in Figs. 1–2.

[7] Coleman, McCloskey, and Stuart, Org. Syntheses **25**, 80 (1945).

[8] In standard notation, $\epsilon = (1/lc) \log_{10} I_0/I$.

[9] K. L. Lauer and R. Oda, Ber. **69**, 851 (1936).

[10a] H. L. McMurry and R. S. Mulliken, Proc. Natl. Acad. Sci. U. S. **26**, 312 (1940).

McMurry,[10b] Platt,[3] Kasha,[4] and Halverson and Hirt,[11] are the basis for our assertion that all of the *blue-shift* bands in Figs. 1–2 arise from $n\rightarrow\pi$ (singlet-singlet) transitions.[12] An examination of the $n\rightarrow\pi$ spectra of about thirty compounds reported in the literature has led the present author to the conclusion that *all* $n\rightarrow\pi$ transitions give *blue-shift* bands. As yet, no exception to this rule has been found.

Our qualitative theoretical explanation for the fact that $n\rightarrow\pi$ transitions give *blue-shift* bands is the following. In the ground state of the polar solute molecule, the solvent molecules orient themselves around the solute molecule so as to bind most strongly with the ground-state charge distribution of the solute molecule. If the excited state charge distribution of the solute molecule is markedly different from the ground-state charge distribution, then by the Frank-Condon principle it is plausible to suppose that the polar solvent molecules will not have the proper positions and orientations to bind most strongly with the excited state charge distribution. (In fact the net solute-solvent intermolecular force may even be repulsive in the excited state.) This condition can give rise to a *blue-shift* band since the solvation energy of the solute molecule in the excited state may be less than the solvation energy in the ground state (relative to an inert or nonpolar solvent). Allowed $n\rightarrow\pi$ transitions are weak, and symmetry forbidden $n\rightarrow\pi$ transitions very weak, because the ground and excited state charge distributions are markedly different.[3] For an $n\rightarrow\pi$ transition, the excited state charge distribution has a node through the molecular plane whereas (for the compounds of Figs. 1–2) the ground-state charge distribution has no nodes.

The above discussion and the fact that all $n\rightarrow\pi$ transitions give *blue-shift* bands have led us to propose the rule: *Electronic transitions in molecules which have low intensities because the ground and excited state charge distributions do not overlap strongly are likely to give blue-shift bands.* This rule is clearly based on the approximations that (a) the nuclear geometry of the solute molecule is not essentially changed in passing from one solvent to the next, and (b) solute-solvent interactions may be treated by first-order perturbation theory. These approximations are probably not valid for frequency shifts of the order of 10,000 cm^{-1} or more. Frequency shifts of this magnitude are observed for the $n\rightarrow\pi$ bands of glyoxal (see II and II′ in Fig. 1) and chloral[13] in passing from hexane to water solvent; both of these molecules are so strongly hydrated in water that approximations (a) and (b) do not hold.[14] Approximation (b) amounts to neglecting the frequency shifts commonly attributed to the high frequency refractive index of the solvent[15] and also solute-solvent interactions which give rise to visible or near ultraviolet intermolecular charge transfer spectra.[16] The possibility that approximations (a) and (b) may frequently break down in acid media is the reason for not including acid solvents in our empirical classification of spectra.

Most of the *red-shift* bands in Fig. 3 have intensities of allowed $\pi\rightarrow\pi$ transitions, $\epsilon\approx 10{,}000$. The intensities of $n\rightarrow\pi$'s and allowed $\pi\rightarrow\pi$'s are usually so different that there is little difficulty in distinguishing between the two. However, the intensities of allowed $n\rightarrow\pi$'s and forbidden or weakly allowed $\pi\rightarrow\pi$'s are sometimes in the same range, $\epsilon\approx 200$–1000. It is therefore of interest to inquire as to whether solvation effects may be used to distinguish between the two types of transitions. Some weak $\pi\rightarrow\pi$'s do give *blue-shift* bands. For example, the well known $\pi\rightarrow\pi$ bands of benzene at 2600A ($\epsilon\approx 200$) are *blue-shift* bands.[9] Therefore our classification is of value only in that (a) a weak ($\epsilon\approx 10$–1000) *blue-shift* band may be taken as tentative evidence for an $n\rightarrow\pi$ transition, and (b) it is exceedingly improbable that a weak *red-shift* band is an $n\rightarrow\pi$. Possibilities (a) and (b) are illustrated for the particular cases of *p*-quinone and *s*-trinitrobenzene.

The absorption spectrum of *s*-trinitrobenzene shows no absorption maximum or inflection with an extinction coefficient between 10 and 100 in heptane, alcohol, or water solvent at room temperature. However, the long wavelength portion of an absorption shoulder (4000A, $\epsilon\approx 20$) undergoes a small blue shift, ~ 100 cm^{-1}, in passing from heptane to water solvent whereas at wavelengths less than 3860A the entire spectrum undergoes a strong red shift. These data suggest that there may be an $n\rightarrow\pi$ transition in this molecule in the 4000A region; if this is the case then the absorption maximum for this $n\rightarrow\pi$ is completely obscured by $\pi\rightarrow\pi$'s which have high intensities at shorter wavelengths. Such tentative assignments of $n\rightarrow\pi$'s are of value in that they do suggest cases where low temperature measurements may be particularly informative.[17]

According to the intensity criteria for $n\rightarrow\pi$'s and $\pi\rightarrow\pi$'s, the weak transition in *p*-quinone at 35,000 cm^{-1} ($\epsilon\approx 320$) might be a forbidden $\pi\rightarrow\pi$ or an $n\rightarrow\pi$. If the conclusions of this paper are correct, this transition is *not* $n\rightarrow\pi$ since the absorption band is a *red-shift* band.

[10b] H. L. McMurry, J. Chem. Phys. **9**, 242 (1941).

[11] F. Halverson and R. C. Hirt, J. Chem. Phys. **19**, 711 (1951).

[12] Some of the transitions called singlet-singlet $n\rightarrow\pi$ in the present paper are regarded as singlet-triplet ($\pi\rightarrow\pi$) by A. Burawoy, Disc. Faraday Soc., No. 9, pp. 70–73 (discussion with M. Kasha). Although the evidence favoring the singlet-singlet $n\rightarrow\pi$ assignments is very strong (see references 3, 4, 10a, 10b, 11) the possibility that some of these transitions may be singlet-triplet has not been completely eliminated.

[13] S. A. Schou, J. chim. phys. **26**, 69 (1929).

[14] J. B. Conant and A. H. Blatt, *The Chemistry of Organic Compounds* (MacMillan Company, New York, 1947), pp. 146 and 247.

[15] N. S. Bayliss, J. Chem. Phys. **18**, 292 (1950).

[16] R. S. Mulliken, J. Chem. Phys. **19**, 514 (1951).

[17] Another case is phenyl cyanide. For this molecule we have found a *blue-shift* band ($\log\epsilon\approx 0$, 33,000 cm^{-1}—inflection) which may be $n\rightarrow\pi$. J. R. Platt, J. Chem. Phys. **19**, 101 (1951) has already suggested this assignment. Experiments are planned which will determine whether or not this band comes from the vibrational structure of a neighboring *red-shift* $\pi\rightarrow\pi$ band ($\epsilon\approx 500$, 37,000 cm^{-1}) or the presence of impurities.

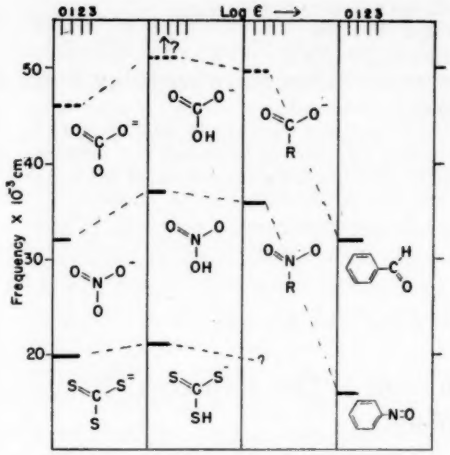

FIG. 4. The low intensity absorption bands of NO_3^-, $CO_3^=$, CS_3^-, and related molecules and ions.

(See compound I in Fig. 3.) The other weak band of *p*-quinone at 23,000 cm^{-1} is $n \rightarrow \pi$ and is a *blue-shift* band. (See compound I in Fig. 1.)

IV. $n \rightarrow \pi$ TRANSITIONS IN IONS

According to simple electronic theory, each of the ions NO_3^-, $CO_3^=$, and $CS_3^=$ has two outer electron shells, one of which contains six π-electrons and the other six n electrons. Each of these ions exhibits a weak absorption band (shoulder for $CO_3^=$) with $\epsilon \approx 10$–100, and a much more intense band ($\epsilon \approx 10^4$) at shorter wavelengths. The similarity between the electronic structures and spectra of these ions indicates that these spectra may be interpreted in terms of the n and π electrons. This section attempts to answer only one question: Do the weak bands arise from $n \rightarrow \pi$ or $\pi \rightarrow \pi$ transitions?

Figure 4 gives the absorption frequencies and intensities of the weak bands of NO_3^-, $CO_3^=$, and $CS_3^=$, together with the weak $n \rightarrow \pi$ bands of a number of related molecules and ions.[5] Figure 4 provides rather strong evidence that the weak bands of these trigonal ions arise from $n \rightarrow \pi$ transitions. This evidence is: (a) All the bands in Fig. 4 have intensities of $n \rightarrow \pi$ transitions. The intensity criteria given in Section III would indicate these transitions to be forbidden or weakly allowed $n \rightarrow \pi$'s. (b) All the molecules and ions in Fig. 4 show absorption bands whose intensities differ by a factor of ten or less. The only symmetry property, or approximate symmetry property, common to all the molecules and ions in Fig. 4 is σ_h (reflection in the molecular plane). Only those transitions which are weak because of this symmetry property ($n \rightarrow \pi$ transitions, not $\pi \rightarrow \pi$ transitions) should remain weak and have roughly constant intensities for the variety of molecular symmetries and charge distributions evident for the molecules in Fig. 4. (The weak bands of benzaldehyde and nitrosobenzene have already been classified as $n \rightarrow \pi$.)[3] Final confirmation of this $n \rightarrow \pi$ assignment for these weak bands in NO_3^- and $CO_3^=$ may lie in the analysis of the polarization and vibrational structure of these bands in ionic crystals.

ACKNOWLEDGMENTS

Special acknowledgment is due M. Kasha whose work on the effect of acids on $n \rightarrow \pi$ *N*-heterocyclic spectra stimulated this investigation. Discussions with Professor J. R. Platt and Professor R. S. Mulliken and Mr. Joe Ham, as well as the technical assistance of Mr. J. Landauer and Mr. D. Lawrey (supported by the ONR), have been most helpful. The author has been supported by the National Research Council.

REFERENCES FOR FIGURES

Abbreviations

ICT —V. Henri, International Critical Tables (McGraw-Hill Book Company, Inc., New York, 1929), Vol. V, p. 359.
API —American Petroleum Institute Catalog of Ultraviolet Spectrograms (API Research Project 44, Natl. Bur. Standards, 1945–1950).
UP —McConnell, Landauer, and Lawrey, unpublished.
FN —See footnote to text.

Figure 1

I —*p*-quinone, ICT 86.
II, II′—Glyoxal, ICT 76. Two $n \rightarrow \pi$ bands shown in Fig. 1.
III —Benzophenone,* G. Scheibe, Ber. deut. chem. Ges. **59**, 2619 (1926).
IV —Mesityl oxide, FN 2; API 96; ICT 68, 74.
V —Acetaldehyde, FN 13.
VI —Acetone, ICT 74, 85; API 96; UP (spectrum in sulfuric acid); G. Scheibe, Ber. deut. chem. Ges. **59**, 2617 (1926).
VII —Chloroacetamide, W. Herold, Z. physik. Chem. **B18**, 265 (1932). Methanol instead of ethanol solvent.
VIII —Ethyl acetate, see reference for VII.
IX —Acetamide, see reference for VII. Methanol instead of ethanol solvent.

Figure 2

X —Nitrosobenzene, UP. Instead of water the solvent is a 1:1 mixture (by vol.) of ethanol and water.
XI —Thiobenzophenone,* FN 2. Ether instead of alcohol solvent.
XII —*pp*′-diethoxythiobenzophenone,* FN 2.
XIII —*o*-methoxybenzeneazobenzene, A. Burawoy, J. Chem. Soc., 1865 (1937).
XIV —*p*-methoxybenzeneazobenzene, FN 2.
XV —Diazoacetic ester, E. Wolf, Z. physik. Chem. **B17**, 46 (1932).
XVI —Ethyl nitrate, H. v. Halban and J. Eisenbrand, Z. physik. Chem. **132**, 433 (1928); G. Scheibe, Z. Electrochem. **34**, 497 (1928).
XVII —Pyrazine, FN 11.

* Molecule not planar so the notation $n \rightarrow \pi$ has only approximate significance.

Figure 3

The numbering of compounds is the same in Fig. 3 as in Figs. 1–2. References for Figs. 1–2 contain the data used for Fig. 3.

Figure 4

Carbonate ion, H. Ley and B. Arends, Z. physik. Chem. **B17**, 192 (1932).

Bicarbonate ion, see reference for carbonate ion.
Acetate ion, H. Ley and B. Arends, Z. physik. Chem. **B4**, 234 (1929) and ref. to carbonate ion.
Benzaldehyde, ICT 88. Benzaldehyde is used here so that a direct comparison can be made with the isoelectronic nitrosobenzene molecule. The $n \rightarrow \pi$ band of acetone at 36,000 cm^{-1} could be used instead of benzaldehyde without essentially modifying the relative spacing of the absorption frequencies in Fig. 4.
Nitrate ion, L. I. Katzin, J. Chem. Phys. **18**, 789 (1951).
Nitric acid, see reference to nitrate ion.
Nitromethane, API 104.
Nitrosobenzene, UP, FN 3.
Thiocarbonate ion, Halban, Mackert, and Ott, Z. Electrochem. **29**, 445 (1923).
Bithiocarbonate ion, see reference to thiocarbonate ion. Absorption frequency estimated as being half-way between frequencies of corresponding bands for thiocarbonate ion and thiocarbonic acid.

THE JOURNAL OF CHEMICAL PHYSICS VOLUME 20, NUMBER 4 APRIL, 1952

A Single Crystal Neutron Diffraction Determination of the Hydrogen Position in Potassium Bifluoride*

S. W. PETERSON AND HENRI A. LEVY
Chemistry Division, Oak Ridge National Laboratory, Oak Ridge, Tennessee
(Received December 10, 1951)

Neutron diffraction measurements on KHF_2 single crystals show that the hydrogen atom occupies the central position, within 0.1A, in the linear F−H−F ion. The data also indicate asymmetry in thermal motion, which suggests that the bifluoride ion undergoes rotatory oscillation with appreciable amplitude. The study demonstrates the usefulness of single crystal neutron diffraction data for crystal structure determination.

INTRODUCTION

THE question of the nature of the hydrogen bond in bifluoride ion has attracted much experimental and theoretical treatment. X-ray crystallography has shown that the two fluorine atoms in potassium bifluoride are separated by the short interatomic distance of 2.26A. The location of the proton which is presumed responsible for the binding, has been the aim of several investigations. If the forces in the bifluoride ion are chiefly electrostatic, the proton would be expected to be centrally situated between the fluorine atoms. If exchange forces are important, a potential function with a double minimum might be expected and the proton probably would be situated at random in the two positions close to one or the other fluorine atom. Ketelaar[1] and Glockler and Evans,[2] utilizing infrared data, came to the conclusion that the double minimum model was the correct one; their respective calculations led to distances of 0.70A and 0.52A between the potential minima. Some doubt was cast upon these conclusions by the dielectric constant measurements of Polder[3] and the calculations of Davies.[4] More recently, in a complete thermodynamic study, Westrum and Pitzer[5] showed that there is no residual entropy at absolute zero in the KHF_2 crystal and no specific heat anomaly above 15°K, strongly supporting the single potential minimum. In addition, they suggested a new assignment of the infrared frequencies consistent with their conclusion. This reinterpretation has been corroborated by Ketelaar and Vedder,[6] and by Newman and Badger,[7] who have recently reported polarized infrared studies of KHF_2, a method which allows increased certainty in assignment of frequencies. The present neutron diffraction investigation was begun before the appearance of the three latter papers. Even though the works of Westrum and Pitzer seem decisive, it is desirable to have confirmation of their conclusions by the essentially more direct method of a diffraction study. The result, which incidentally provides more detailed knowledge of the thermal motion of the bifluoride ion than was previously available, is presented below.

PROCEDURE

X-ray studies[8,9] indicate that KHF_2 is tetragonal with $a_0=5.67$, $c_0=6.81$, of space group $D_{4h}{}^{18}-I\,4/mcm$, with four molecules to the unit, potassium occupying the fourfold positions[10] (a) and fluorine the eightfold positions (h); the one parameter for fluorine was evaluated as 0.1408 by Helmholz and Rogers,[9] giving an F−F distance of 2.26A. If the hydrogen is centrally

* This work was performed for the AEC at the Oak Ridge National Laboratory.
[1] J. A. A. Ketelaar, Rec. trav. chim. **60**, 523 (1941); J. Chem. Phys. **9**, 775 (1941).
[2] G. Glockler and G. E. Evans, J. Chem. Phys. **10**, 607 (1942).
[3] D. Polder, Nature **160**, 870 (1947).
[4] M. Davies, J. Chem. Phys. **15**, 739 (1947).
[5] E. F. Westrum, Jr. and K. S. Pitzer, J. Am. Chem. Soc. **71**, 1940 (1949).
[6] J. A. A. Ketelaar and W. Vedder, J. Chem. Phys. **19**, 654 (1951).
[7] R. Newman and R. M. Badger, J. Chem. Phys. **19**, 1207 (1951).
[8] R. M. Bozorth, J. Am. Chem. Soc., **45**, 2128 (1923).
[9] L. Helmholz and M. T. Rogers, J. Am. Chem. Soc. **61**, 2590 (1939).
[10] *International Tables for the Determination of Crystal Structures* (J. W. Edwards, Ann Arbor, Michigan, 1944), revised edition, Vol. 1, p. 226.

situated in the bifluoride ion, it occupies the fourfold positions (*d*): $0\frac{1}{2}0$, $\frac{1}{2}00$, B. C. If asymmetrically situated, it can fit into the x-ray unit only if the orientation of the ion is random; with a colinear asymmetric ion, for example, $\frac{1}{2}H$ would occupy each of the eightfold positions (*h*): x, $\frac{1}{2}+x$, 0, etc. For a zero value of the parameter x, these positions reduce to the central positions (*d*). If the ion is asymmetric and the structure ordered, either an enlarged tetragonal unit or a departure from tetragonal symmetry is required.

The initial attack by neutron diffraction employed the usual powder method, with deuterated material to avoid heavy diffuse scattering due to hydrogen. The pattern was consistent in all respects with the x-ray unit, showing that the hydrogen positions do not call for an enlarged unit. An evaluation of the parameter x from the powder intensities was next undertaken. Although a zero value gave the closest approach, fully satisfactory agreement between calculated and observed intensities was not achieved. The difficulty was eventually traced to preferential orientation in the packed powder samples, with *c* axes tending to lie parallel to the vertical cylindrical axis of the sample container; this was clearly demonstrated when, in a test measurement, a pattern was obtained with the sample tilted at 90° to the normal orientation, and the intensity anomalies were reversed.

An attack by means of single crystal measurements was next undertaken. Recent work[11] has demonstrated that single crystal methods are applicable in neutron crystallography. The success achieved clearly confirms this conclusion and demonstrates that single crystal methods have many advantages over powder methods in the neutron field as well as in the x-ray field. For this reason, the work will be reported in some detail.

For single crystal measurements a deuterated specimen is not required, because of the greatly enhanced ratio of intensity in a Bragg reflection to that in diffuse scattering. This arises from the fact that the entire single crystal specimen contributes simultaneously to a Bragg reflection. Hence, the ordinary hydrogen compound was used in the single crystal portion of this study.

Potassium bifluoride was prepared by direct reaction in platinum of aqueous KF and HF in equivalent quantity. Analysis by alkali titration of several preparations, dried to constant weight, showed less than 0.3 percent impurity. Several samples were deuterated and analyzed for deuterium in a manner to be described elsewhere[12] for use in collecting powder data. Single crystals of KHF_2 were grown by slow evaporation of aqueous solutions of the pure salt, yielding rectangular platelets up to nearly 2 mm in thickness (perpendicular to (*c*) and several millimeters on an edge (bisecting (*a*) and (*b*)). A specimen approximately 1.4×2.6×3.6 mm was selected for study.

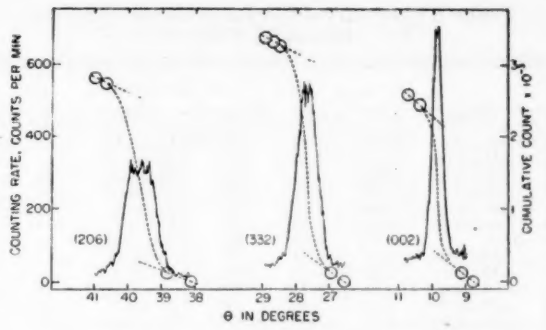

FIG. 1. Typical neutron diffraction reflections from a single crystal of KHF_2. The solid curves (left-hand ordinate scale) are traced from strip-chart records of the counting rate. The circled points (right-hand ordinate scale) show the observed cumulative count.

The manner of collection of diffraction data from powder samples will be described elsewhere.[12] For single crystal data, the spectrometer was used with minimum collimation, the wavelength spread being of the order of ±1.5 percent at half-maximum intensity, and the sensitive angle subtended by the detector about 2°. The crystal specimen was mounted on a fine glass fiber set on a goniometer head and its orientation adjusted until alternately the [110], [010], [120], [230], and [001] zone axes were parallel to the spectometer axis. Measurements were made with the crystal and detector rotating synchronously through the Bragg angle in the usual way, with a crystal angular speed of usually 8° per hour. The diffracted intensity was recorded automatically, as with powder samples. Simultaneously, the cumulative count across the reflection was recorded with a scaler. The integrated intensity was taken as the accumulated count during the scanning, reduced by the background count as measured with the crystal out of reflecting orientation. Typical data for reflections at different scattering angles are shown in Fig. 1. Integrated intensities were easily reproducible to a few percent. The wavelength was 1.16A.

TREATMENT OF DATA

Observed integrated intensities were corrected for absorption with a correction factor calculated as though the specimen were cylindrical with a cross section equal to its average cross section for the orientation under consideration. The linear absorption coefficient was measured on a sample of KHF_2 powder. In the case of reflections taken with the [001] zone vertical, which brought the maximum dimensions of the specimen into the equatorial plane, an extinction correction was necessary also. Only the strong (310) and (400) planes were appreciably affected. The latter was measured also in the [010] zone and served to evaluate the extinction

[11] S. W. Peterson and H. A. Levy, J. Chem. Phys. **19**, 1416 (1951); G. E. Bacon, Proc. Roy. Soc. (London) **209A**, 397 (1951).
[12] H. A. Levy and S. W. Peterson (to be submitted for publication).

TABLE I. Observed and calculated neutron structure. Factors for KHF_2.

hkl	$\|F\|_{obs}$	F_{calc} $x=0$	F_{calc} $x=.02$	hkl	$\|F\|_{obs}$	F_{calc} $x=0$	F_{calc} $x=.02$
110	1.16±0.05	1.16	1.13	332	2.70±0.11	−2.64	−2.77
002	1.37±0.06	1.30	1.30	215	2.10±0.10	2.12	2.15
200	0.93±0.06	−0.96	−0.92	422	1.45±0.08	−1.49	−1.35
112	1.59±0.07	−1.50	−1.52	006	0.53±0.05	0.54	0.54
211	3.08±0.10	3.06	3.10	116	1.21±0.08	−1.19	−1.20
202	3.40±0.10	−3.43	−3.39	334	0.38±0.11	−0.22	−0.32
220	<0.19	0.10	0.18	206	2.39±0.10	−2.34	−2.31
222	2.39±0.09	−2.35	−2.27	424	0.59±0.12	0.71	0.83
004	3.49±0.11	3.44	3.44	440	2.56±0.10	2.62	2.81
213	2.64±0.09	2.70	2.74	325	1.10±0.07	−1.14	−1.20
114	1.10±0.07	1.05	1.03	226	1.67±0.09	−1.67	−1.62
321	1.60±0.08	−1.65	−1.76	442	0.35±0.20	0.52	0.69
204	0.62±0.08	−0.59	−0.55	600	1.80±0.06	1.75	1.94
400	3.28±0.11	−3.15	−3.01	662	<0.27	0.22	−0.04
330	0.53±0.08	−0.44	−0.58	046	3.32±0.12	−3.41	−3.33
402	5.04±0.15	−5.23	−5.10	008	1.99±0.09	1.97	1.97
224	0.15±0.08	0.23	0.30	064	1.48±0.09	1.49	1.64
323	1.48±0.08	−1.46	−1.55	550	1.21±0.09	1.19	1.01
420	0.79±0.07	0.73	0.88				

coefficient in the Darwin expression.[13] Because of uncertainties involved in this correction and greater importance of absorption, data taken with the [001] zone vertical were not used for parameter determination.

The tetragonal symmetry of KHF_2 was confirmed by establishing the equality of neutron intensities of several pairs of reflections of type ($hk0$), ($kh0$) with the [001] zone vertical. The possibility of ordered asymmetric structures was thus eliminated with reasonable certainty.

Structure factors $|F|$ were obtained from the corrected integrated intensities E by application of the following expression adapted from the standard x-ray expression[14]

$$E=\frac{I_0\lambda^3N^2V}{\omega}\frac{|F|^2}{\sin 2\theta},$$

I_0 being the incident intensity, λ the wavelength, ω the angular velocity of rotation of the crystal, N the number of unit cells per unit volume, V the volume of the specimen, and θ the Bragg angle. The value of I_0 was established from similar measurements on a crystal of NaCl which had previously been carefully studied and shown not to be subject to appreciable extinction.[11]

Structure factors for models incorporating symmetric ions and linear asymmetric ions in disorder were calculated in the usual way. The nuclear scattering amplitudes were those reported by Shull and Wollan,[15] namely, $f_K=0.35$, $f_F=0.55$, and $f_H=-0.40$. The fluorine parameter value was that established by x-ray studies, 0.1408. The calculation was carried out for several values of the parameter x governing the degree of asymmetry. It was clear that use of a single Debye-Waller temperature factor would not bring satisfactory agreement with experimental values for any value of x. Separate temperature factors for K, H, and F were then introduced, and systematic variation led to much improved agreement. Careful examination of the comparison at this stage disclosed that planes with large l index were yielding calculated structure factors consistently too large in absolute value, suggesting the need for an asymmetric temperature factor. No improvement resulted from the application of an asymmetric factor to K or H; however, the application to F brought about final satisfactory agreement. The form of the factor was

$$\exp[-B_F(\sin\theta/\lambda)^2-B_F'(l/2c)^2],$$

in which B_F represents the effect of ordinary spherically symmetrical temperature motion, and B_F' the effect of an asymmetric component in the c direction. This temperature factor is similar to that applied to the CN group in NH_4CN by Lely and Bijvoet.[16] Final values of the temperature factor coefficients were $B_K=1.25$, $B_H=3.0$, $B_F=1.85$, and $B_F'=1.0$.

Table I lists experimental structure factors for 37 reflections examined in the equators of the [110], [230], [120], and [010] zones of the single crystal specimen, together with estimated uncertainties in these values. Also listed are calculated structure factors for the symmetrically placed hydrogen ($x=0$) and for the asymmetric random case corresponding to $x=0.02$. The same values of the temperature factors, listed above, were used in both calculations. Similar data taken in the equator of the [001] zone are collected in Table II. The symmetric model gives excellent agreement, while the asymmetric one gives agreement definitely less than satisfactory. The effect of change of temperature factors, particularly B_H, on the asym-

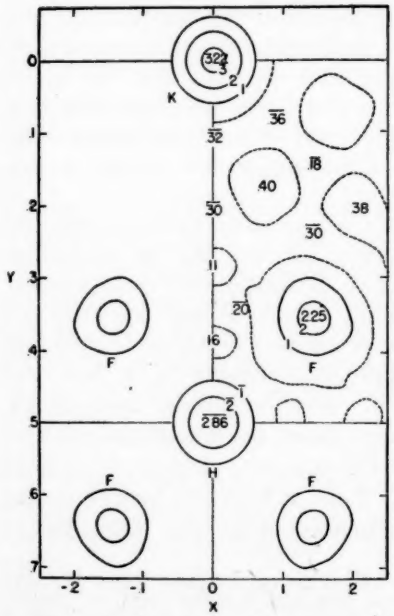

FIG. 2. A projection on the $a-b$ plane of the neutron scattering density in KHF_2. The figures indicate the values of the function at the contours and the extremes in units of 10^{-12} cm/A^2. The dashed lines represent zero contours.

[13] See, for example, R. W. James, *The Optical Principles of the Diffraction of X-Rays* (G. Bell and Sons, Ltd., London, 1948), p. 292.

[14] Reference 10, Vol. 2, p. 560.

[15] C. G. Shull and E. O. Wollan, Phys. Rev. **81**, 527 (1951). Hughes, Burgy, and Ringo, Phys. Rev. **77**, 291 (1950), have reported the somewhat smaller value $f_H=-0.38$. This value does not affect our conclusions in the current study.

[16] J. A. Lely and J. M. Bijvoet, Rec. trav. chem. **63**, 39 (1944).

metric model was carefully studied: the majority of the disagreements in column 4 of Table I can be made to approach agreement if a smaller value of B_H is used, for example, (222) and (400); however, the disagreement of (321), (213), and (325) is left essentially unchanged and the good agreement of a large number of other reflections, for example (226), (006), and (008), is rapidly destroyed by this change. We conclude that the asymmetric random model with $x=0.02$ cannot give agreement with the data for any values of the temperature factor coefficients. Careful study of intermediate parameter values, with similar consideration of temperature factor changes, places the upper limit of x at about 0.01. This modest precision, in view of the excellence of the agreement, is somewhat disappointing. It results primarily from the rather large temperature and zero point motion of the hydrogen atom, which reduces its contribution to the high angle reflections. Broadening of these high angle reflections due to wavelength spread in the primary neutron beam, with attendant reduction of peak to background ratio and loss of precision in intensity measurement, also contributes.

The ($hk0$) data were used to construct a projection of the neutron scattering density on the $a-b$ plane, shown in Fig. 2. The hydrogen atom, because of its negative amplitude, appears as a well rather than a peak on the map. Effects of termination of the Fourier series are apparent, particularly around the potassium atom, which has the smallest temperature factor; these could probably be reduced by application of a convergence factor to the data. The map is presented as an illustration of the possibility of applying series methods in neutron diffraction crystal analysis.

The powder data from KDF_2, after allowance for effects of preferred orientation, are fully consistent with the final model.

DISCUSSION

This investigation has shown that the hydrogen position is within 0.1A of the center of the F−H−F link. This may be taken as confirmation of Westrum and Pitzer's result that the bifluoride ion is symmetric.

The root-mean-square displacements of the atoms corresponding to the temperature factors found are for K, 0.22A; for H, 0.34A; and for F, 0.29A. It seems appropriate to interpret the asymmetry of the fluorine displacement in terms of components, perpendicular to and along the axis of the bifluoride ion. If it is assumed that displacements perpendicular to the ion axis have cylindrical symmetry, the data yield 0.10A and 0.27A, respectively, for the mean displacements parallel and in the perpendicular plane. The perpendicular displacement suggests a rotatory oscillation of the bifluoride ion with a mean half-amplitude of some 14°. The relatively high displacement for hydrogen is not unusual; it probably represents mostly zero-point motion. The absence of appreciable asymmetry for hydrogen is consistent with recent assignments of spectroscopic frequencies which make the bending and asymmetric stretching frequencies not greatly different.[6,7]

The excellence of the agreement confirms previous reports[11] that single crystal neutron data are useful in favorable cases for structure determination. The absence of extinction in nearly all the measurements is consistent with Bacon and Lowde's[17] criterion; a rough application of their theory to the strong (211) reflection, assuming the low value of 5 minutes for the mosaic spread parameter, yields a limiting thickness of 2.1 mm, not greatly different from the smaller dimensions of our specimen. In the case of reflections measured in the equator of [001], where extinction appeared appreciable, the cross section of the specimen was 2.6×3.6 mm, which might well exceed the limiting value.

TABLE II. Neutron diffraction data for equatorial reflections in the [001] zone of KHF_2.

$hk0$	Intensity, counts/128 Obs.	Corrected[a]	F_{obs}	F_{calc} ($x=0$)
310	70.2	110	4.62±0.20	4.64
400	34.0	45.5	3.28±0.15	−3.15
510	17.6	22.4	2.52±0.12	2.50
530	4.0	4.4	1.16±0.10	1.03
620	0.3	0.3	0.3 ±0.20	0.04
710	<0.5	<0.5	<0.4	0.01
640	3.7	4.1	1.14±0.10	−0.72
730	23.8	26.5	2.87±0.30	2.90

[a] Corrected for absorption and, in the case of (310) and (400), for extinction. The latter, together with the appropriate value from Table I, was used to establish the magnitude of the extinction correction.

[17] G. E. Bacon and R. D. Lowde, Acta Cryst. 1, 303 (1948).

The Host Crystal Luminescence of Zinc Sulfide Phosphors

RICHARD H. BUBE
Radio Corporation of America, RCA Laboratories Division, Princeton, New Jersey
(Received November 12, 1951)

Effects produced on the host crystal luminescence of zinc sulfide phosphors by increasing the preparation temperature without any additives in the preparation, are compared with effects produced by adding halide in the preparation at a fixed temperature.

Both methods of altering the luminescence properties of the phosphors produce qualitatively the same results on (1) intensification of the host crystal emission for excitation by 3650A ultraviolet and by 6 kv cathode rays, and for phosphors of both cubic and hexagonal crystal structure, (2) glow curves after excitation by 3650A ultraviolet, (3) diffuse reflectivity for light in the wavelength range from 3400 to 4200A, and (4) the variation of the emission intensity during excitation as a function of operating temperature.

Data on the variations, with preparation procedure, of the emission intensity during excitation and of the glow intensity during thermostimulation show that a possible correlation exists between shallow traps and isolated omission defects, and between deep traps and pairs of omission defects; and that a correlation is suggested between luminescence centers and particular perturbed (SZn_4) groups in the crystal.

At least a part of the intensification caused by adding halide in the preparation must be attributed to a classical "flux" action.

INTRODUCTION

LUMINESCENCE centers and trapping centers in zinc sulfide phosphor, prepared without added impurity, are caused by defects in the crystal structure. Considerable study has been concentrated on determining the nature of these defects and the various methods by which they may be formed.

An increase in the emission intensity during excitation and an increase in the glow intensity during thermostimulation may be caused (1) by increasing the temperature at which the phosphor is heated in preparation[1] without any additives, at least in the range 950° to 1350°C, (2) by the addition of a halide in the preparation without altering the preparation temperature,[2,3] and (3) by the addition of a trivalent cation in the preparation without altering the preparation temperature.[4] It is possible to consider all of these methods as increasing the number of defects responsible for luminescence centers and trapping centers.

Several hypotheses concerning the identity of the defects have been advanced.

(1) Schleede's proposal that the blue emission of "pure" ZnS is caused by the simultaneous presence of the cubic and hexagonal crystal forms was one of the earliest.[5] Later results[1] showing that the emission intensity increases with preparation temperature for temperatures from 1100° to 1350°C, these being above the transition temperature from cubic to hexagonal, have eliminated the acceptability of this proposal.

(2) The analogy between ZnS and ZnO later led Schleede and many others[6–10] to propose that the blue-emitting centers in ZnS phosphor were associated with neutral interstitial zinc atoms. It was known that the best ZnO phosphors were made by preparation in H_2, and it was assumed that some of the zinc was reduced to the free atoms. An additional argument for zinc as the activating defect was the finding of a negative Hall coefficient for ZnO by Fritsch.[11] Garlick, Wells, and Wilkins[12] proposed that both luminescence centers and traps in ZnS phosphor are probably due to a stoichiometric excess of zinc.

Thomsen,[13] however, has reported that all efficient ZnO phosphors give a test for sulfide, that an efficient ZnO phosphor can be prepared by neating ZnS in air, and that nonluminescent ZnO can be made luminescent by heating with sulfide. Thomsen suggested, therefore, that the luminescence center in ZnO is associated with sulfide ion. He attributed the success of the method of making efficient ZnO phosphor by heating in H_2 to a reduction of a small amount of sulfate in the original ZnO material, to sulfide in the final phosphor.

Riehl and Ortman[14] reported failure in an attempt to prove that free zinc atoms were the luminescence centers by diffusing zinc atoms into ZnS.

The gradual shift of the emission band to longer wavelengths in the system (Zn:Cd)S as the proportion of CdS is increased, has led Leverenz[15] to propose that neither interstitial zinc in ZnS nor interstitial cadmium in CdS are intimately associated with the luminescence center, but that the luminescence center in this family is associated with the sulfide.

[1] R. H. Bube, Phys. Rev. **80**, 655 (1950).
[2] W. P. Jorissen and W. E. Ringer, Chem. Zentralblatt. **1**, 644 (1906).
[3] MacDougall, Stewart, and Wright, Chem. Soc. (London) J., Trans. **111**, 663 (1917).
[4] F. A. Kroeger and J. Dikhoff, Physica **16**, 297 (1950).
[5] A. Schleede, Angew. Chem. **48**, 277 (1935).
[6] B. Gudden, Ergeb. Exakt. Naturw. **13**, 223 (1934).
[7] C. Wagner, Z. physik. Chem. **22**, 181 (1933).
[8] W. Schottky and C. Wagner, Z. physik. Chem. **11**, 163 (1931).
[9] F. Seitz, Trans. Faraday Soc. **35**, 74 (1939); J. Chem. Phys. **6**, 454 (1938).
[10] N. Riehl and G. Ortmann, Z. physik. Chem. **188**, 109 (1941).
[11] O. Fritsch, Ann. Physik **22**, 374 (1935).
[12] Garlick, Wells, and Wilkins, J. Chem. Phys. **17**, 399 (1949).
[13] S. M. Thomsen, J. Chem. Phys. **18**, 770 (1950).
[14] N. Riehl and G. Ortmann, Doklady Akad. Sci. USSR **66**, 613 (1949).
[15] H. W. Leverenz, *Introduction to Luminescence of Solids* (John Wiley and Sons, Inc., New York, 1950), p. 197.

(3) Both the assumption that the blue-emitting center is associated with the simultaneous presence of cubic and hexagonal crystal forms, and the assumption that the center is associated with interstitial zinc, fail to give an explanation of the long-known increase in emission intensity caused by the addition of a halide in the preparation. It was originally believed that the action of the halide was principally that of a flux, that it "provided (1) a fluid phase for solvation and transport of ingredients, and (2) increased surface reactivity (lowered activation energy) and atomic mobility to facilitate crystal growth,"[16] and that the halide could be completely washed out after the phosphor was made. In recent years, this point of view has been somewhat altered. Smith[17] suggested that the halide acted not only to increase crystal size, but that it was also incorporated into the crystal in such a way as to cause crystal defects. Strange[18] and Rothschild[19] also attributed an intimate role to incorporated chloride ions. Kroeger and Hellingman[20] have reported that the emission intensity is roughly proportional to the proportion of chloride incorporated. It has been shown[21–23] that whether luminescence centers associated with copper in ZnS:Cu phosphors are green-emitting or blue-emitting depends on the relative proportion of incorporated copper and chloride for all but very low copper proportions. Kroeger and his associates have developed an hypothesis from originally considering the luminescence centers in ZnS phosphor to be neighboring Zn^+ and Cl^-, to a broader view based on the principle of charge and volume compensation[4] in which Zn^+ is considered as an essential element of the luminescence center, the formation of Zn^+ being allowed by the incorporation of singly charged anions, such as the halides, or by triply charged cations, such as aluminum.

The present investigation has for its principal purpose a comparison of two methods of increasing the blue emission intensity of ZnS phosphor: (1) by increasing the preparation temperature without any additives in the preparation, and (2) by adding halide in the preparation at a fixed temperature.

In the interpretation of the results, further use is made of a hypothesis introduced in a previous publication:[1] luminescence phenomena caused by impurities in interstitial positions will be different when observed in cubic and hexagonal ZnS phosphors, whereas luminescence phenomena caused by impurities in substitutional positions will be identical or practically identical whether observed in cubic or hexagonal ZnS phosphors.[24] This hypothesis is supported in the only case where definite evidence is known concerning the location of an impurity in ZnS phosphors. It is known that Mn is located in substitutional sites[25,26] in ZnS:Mn phosphors, and it is found that there is no difference in the emission spectra between cubic and hexagonal phosphors.[27]

The application of this hypothesis in the past work with ZnS:Cu phosphors[1] led to the deduction that traps were associated with omission defects. This deduction is supported by further evidence in the present paper.

The answers to two questions are sought: (1) Are the two methods of increasing the blue emission intensity—by increasing the preparation temperature without any additives in the preparation, and by adding halide in the preparation at a fixed temperature—basically equivalent? (2) Is there a relation between the emission intensity during excitation and the glow intensity during thermostimulation, as both of these are varied by the preparation procedure?

EXPERIMENTAL

Preparation of Materials

All of the phosphors used in the present investigation were prepared from the same lot of purified ZnS (RCA 33Z19). Spectrographic analysis[28] of this material showed traces of calcium and manganese, and ≤ 0.00001 percent copper, which did not affect the luminescence properties of the finished phosphors. Table I presents a summary of the materials prepared, together with quantitative data on emission intensity and glow intensity for 3650A ultraviolet and cathode-ray excitation, as is discussed later. X-ray analysis of the phosphors showed that phosphors prepared below 1050°C were cubic, that prepared at 1050°C was 98 percent cubic and 2 percent hexagonal, that prepared at 1100°C was 95 percent cubic and 5 percent hexagonal, and those prepared above 1100°C were hexagonal.[29]

For preparations without added halide, 30 grams of ZnS were placed directly into a 30 ml Vycor crucible. In the cases where halide was added in the preparation, a triple-distilled-water solution of the halide was added to a slurry of 30 grams of ZnS. After thorough mixing and drying, the material was placed into a 30 ml Vycor crucible. The crucible had a ground rim and was covered with a tight-fitting ground silica lid. The crucible was placed into a hot furnace at the desired temperature, was allowed to remain in the furnace for 10 min, and was then immediately removed. Only the core of each batch was used.

[16] Reference 15, p. 78.
[17] A. L. Smith, J. Electrochem. Soc. **96**, 75 (1949).
[18] J. W. Strange, Proc. Phys. Soc. (London) **55**, 364 (1943).
[19] S. Rothschild, Trans. Faraday Soc. **42**, 635 (1946).
[20] F. A. Kroeger and J. E. Hellingman, J. Electrochem. Soc. **93**, 156 (1948); **95**, 68 (1949).
[21] Kroeger, Hellingman, and Smit, Physica **15**, 990 (1949).
[22] A. A. Cherepnov and T. S. Drobrolyubski, Doklady Akad. Sci. USSR **66**, 621 (1949).
[23] R. H. Bube, J. Chem. Phys. **19**, 985 (1951).
[24] This is because interstitial positions are different in cubic and hexagonal phosphors, but substitutional positions are identical out to third nearest neighbors.
[25] F. A. Kroeger, Z. Krist. **100**, 543 (1939).
[26] Jenkins, McKeag, and Rooksby, Nature **143**, 978 (1939).
[27] Reference 15, p. 217.
[28] Spectrographic analysis by S. Larach.
[29] X-ray analysis by I. J. Hegyi.

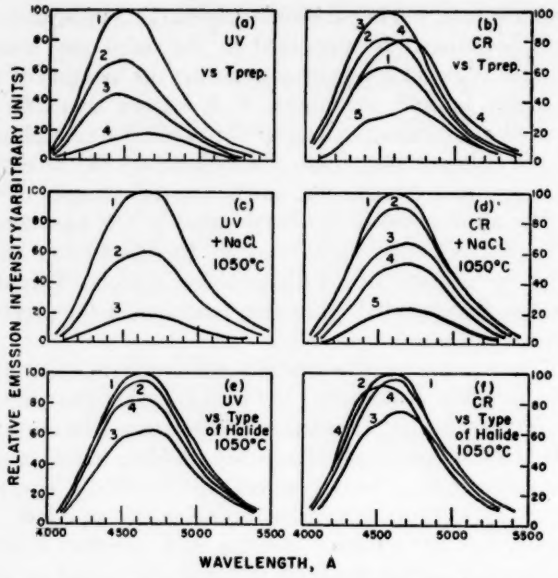
(a) UV vs Tprep.
(b) CR vs Tprep.
(c) UV +NaCl 1050°C
(d) CR +NaCl 1050°C
(e) UV vs Type of Halide 1050°C
(f) CR vs Type of Halide 1050°C
RELATIVE EMISSION INTENSITY (ARBITRARY UNITS)
WAVELENGTH, A

FIG. 1. Spectral emission curves for 3650A ultraviolet and 6 kv, 1 $\mu a/cm^2$ cathode-ray excitation. (a) and (b) Phosphors prepared without any additives in the preparation—(1) 1350°C, (2) 1250°C, (3) 1150°C, (4) 1100°C, (5) 1050°C. (c) and (d) Phosphors prepared at 1050°C with (1) 1.0 percent NaCl, (2) 0.1 percent NaCl, (3) 0.03 percent NaCl, (4) 0.01 percent NaCl, (5) 0.003 percent NaCl. (e) and (f) Phosphors prepared with different halides at 1050°C—(1) 1.0 percent NaCl, (2) 1.0 percent NaBr, (3) 1.0 percent NaI, (4) 1.0 percent KCl.

Measurements

Luminescence emission spectra and peak emission intensities were measured with a recording spectroradiometer.[30] Excitation was by 3650A ultraviolet (hereafter designated UV) from a 100-watt C-H4 mercury projector spot lamp with appropriate filters, or by 6 kv, 1 $\mu a/cm^2$ cathode rays (hereafter designated CR).

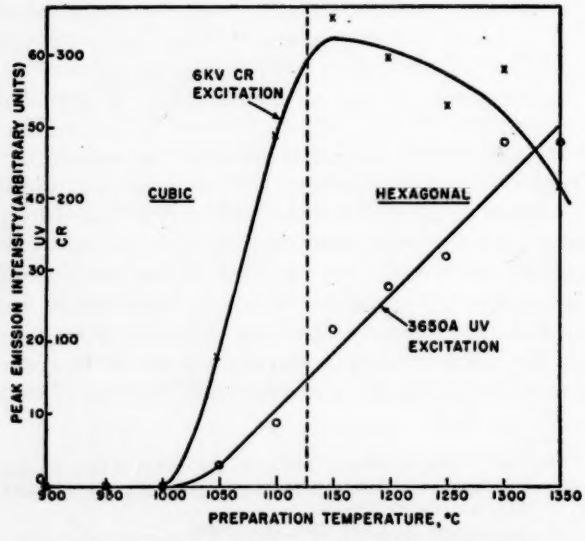

FIG. 2. The variation of peak intensity with preparation temperature for the phosphors prepared without additives.

[30] V. K. Zworykin, J. Opt. Soc. Am. **29**, 84 (1939).

Measurements involving temperature variation were made with the specially insulated apparatus which was used in previous studies.[1] The emission was detected by a 1*P*21 multiplier phototube attached to a sensitive microammeter (10^{-8} amp full scale). A Wratten 47 filter was placed between the phosphor and the phototube. Glow curves were obtained with a heating rate of 0.12°/sec.

Measurements of diffuse reflectivity were made with the assistance of R. E. Shrader, using a photographic method and a grating spectrograph of his own design and construction. Near normal reflection from an effectively infinitely thick sample was observed for the sample under excitation through a large solid angle. Data is taken from densimetric measurements of the photographic record.

RESULTS

Emission Spectra

All of the phosphors prepared in this study show only the normal blue luminescence emission of the ZnS phosphor. The peak of this emission is located at about 4500A for the hexagonal phosphors, and at about 4700A for the cubic phosphors.

Figure 1 shows some typical emission spectra during UV and CR excitation. The curves show that the effect of increasing preparation temperature without any additives, and the effect of adding halide in the preparation at a fixed temperature, is to increase the intensity of the emission without changing its spectral distribution. These are cases, therefore, of true luminescence intensification, i.e., the number or efficiency of host crystal luminescence centers is increased. Similar effects are obtained regardless of the halide used.

The curves of Figs. 1(a) and 1(b) also indicate that the shift of the peak of the emission band between cubic and hexagonal phosphors could be explained as a variation in the prominence of two emission bands, both of which are present in both cubic and hexagonal phosphors. This suggestion was previously made by Shrader as the result of measurements on the variation with operating temperature of the emission spectrum of a hexagonal ZnS phosphor;[31] it was found that the peak of the emission had shifted to about 4700A at a temperature of 152°C. If the same two bands are present in both cubic and hexagonal phosphors, it is possible for the luminescence center to be associated with a substitutional defect. It need not, therefore, necessarily be concluded, in accordance with the hypothesis correlating different luminescence phenomena in cubic and hexagonal phosphors with interstitial imperfections, that the difference in peak wavelength between cubic and hexagonal phosphor emission means that the center is associated with an interstitial defect.

[31] R. E. Shrader (private communication); data given in H. W. Leverenz, reference 15, p. 188.

Peak Intensities

Figures 2 and 3 show the details of the variation of the peak intensity of the blue emission with increasing preparation temperature without any additives, or with proportion of halide added in the preparation at a fixed temperature, for both UV and CR excitation.

Figure 2 shows that the intensification during UV excitation increases almost linearly with preparation temperature, with no indication of an irregular variation at the transition from the cubic to the hexagonal crystal form. The CR-excited emission intensity, however, reaches a maximum at approximately the temperature of the crystal structure transition.

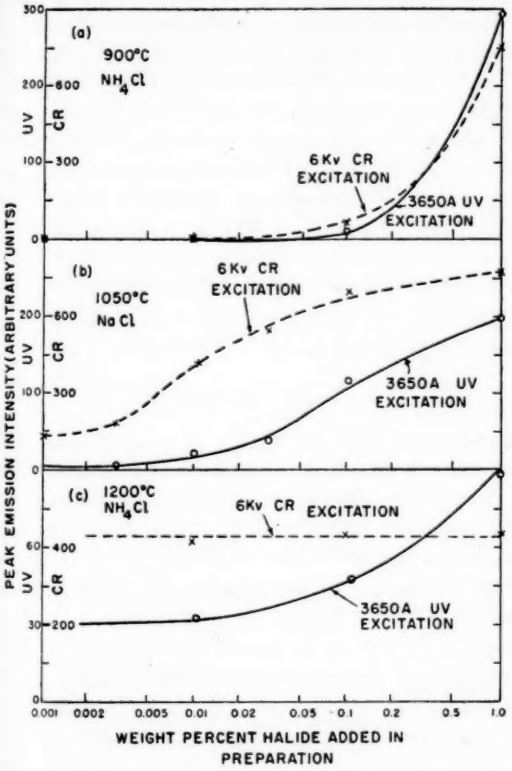

FIG. 3. The variation of peak intensity with proportion of halide added in the preparation at a fixed temperature. (a) Variation with proportion of NH_4Cl added in preparation at 900°C. (b) Variation with proportion of NaCl added in preparation at 1050°C. (c) Variation with proportion of NH_4Cl added in preparation at 1200°C.

Figure 3 shows that intensification is obtained for the UV-excited emission by the addition of chloride in the preparation for both cubic and hexagonal phosphors, but that the CR-excited emission is intensified only for cubic phosphors.

Table I presents a summary of the quantitative data. The units of peak intensity for UV excitation and for CR excitation are relative to the peak intensity of hex.-ZnS:Ag (0.015), 1250°C (RCA 33Z20A) as standard equal to 1000 for both types of excitation. The units of area under glow peaks are arbitrary, but are the same within the table.

TABLE I. A summary of quantitative data.

Prep. temp., °C	Additive in prep.	UV-excited peak intensity	CR-excited peak intensity	Area (above −140°C) under glow peak at −110°C, UV exc.	Area under glow peak at −20°C, UV exc.
900	None	<1	<1	1	0
	0.01% NH_4Cl	<1	<1	7	0
	0.1% NH_4Cl	8	63	50	0.5
	1.0% NH_4Cl	300	760	330	20
1050	None	3	91	80	9
	0.0003% NaCl	3	91	115	7
	0.001% NaCl	3	140	170	12
	0.003% NaCl	4.5	181	195	8
	0.01% NaCl	19	422	630	65
	0.03% NaCl	39	542	845	65
	0.1% NaCl	117	705	1650	230
	1.0% NaCl	200	783	1550	245
1050	1.0% NaBr	191	815	1780	100
	1.0% NaI	124	606	1060	75
	1.0% KCl	165	740	1390	345
1200	None	28	300	1300	730
	0.01% NH_4Cl	32	418	1490	890
	0.1% NH_4Cl	47	438	2635	2045
	1.0% NH_4Cl	87	438	1950	3020
900	None	<1	<1	1	0
950	None	<1	<1	2.3	0.13
1000	None	<1	<1	7	0.3
1050	None	3	91	80	9
1100	None	9	246	355	105
1150	None	22	327	595	310
1200	None	28	300	1300	730
1250	None	32	264	1250	615
1300	None	48	291	1460	1280
1350	None	48	209	2930	3180

Incorporated Chloride

The technique of chemical determination of incorporated chloride in zinc sulfide phosphors has been established.[20,21,23] The proportion of chloride incorporated in ZnS phosphors containing impurity activators, Ag, Cu, and Mn, is dependent upon the particular activator, and is dependent, up to a certain limit, upon

TABLE II. A summary of incorporated chloride.

Preparation temperature, °C	Additives in preparation	Mole ppm of chloride
Unheated raw material	...	140
900	None	80
	0.01% NH_4Cl	110
	0.1% NH_4Cl	140
	1.0% NH_4Cl	150
1050	None	<50
	0.01% NaCl	<50
	0.1% NaCl	140
	1.0% NaCl	205
1200	None	<50
	0.01% NH_4Cl	<50
	0.1% NH_4Cl	110
1350	None	<50

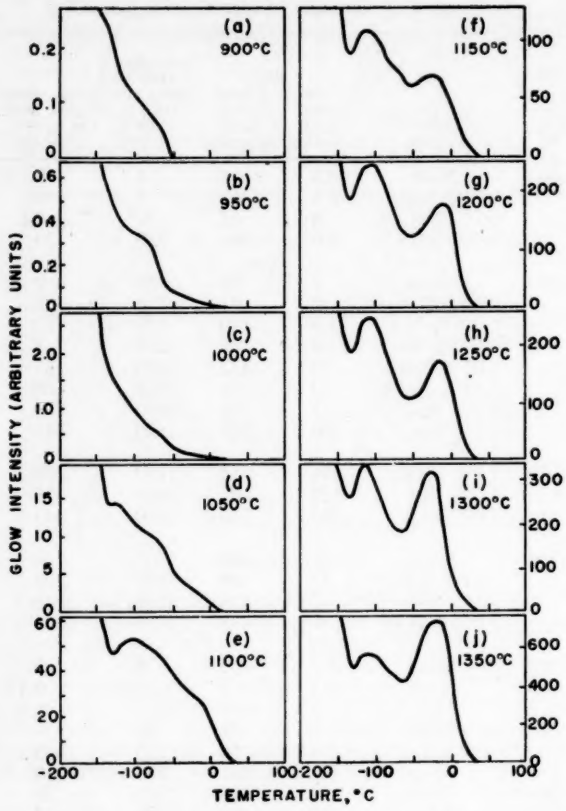

FIG. 4. Glow curves for the series of phosphors prepared at increasing temperatures without any additives in the preparation. UV excitation.

the proportion of chloride added in the preparation. Whereas the incorporation of Cu greatly increases the proportion of chloride incorporated,[21,23] the incorporation of Ag or Mn has no effect on the proportion of chloride incorporated.

The analysis for incorporated chloride in the phosphors involved in the present study is difficult because of the small proportions of chloride present. Table II presents a summary of such analyses for representative members of the series studied. The minimum proportion of incorporated chloride which could be meaningfully detected is about 50 mole ppm.[32]

The ZnS material which was used to prepare all the phosphors was found to contain an appreciable proportion of chloride, probably in the form of zinc chloride, but only a minor fraction, if any, of this chloride was incorporated in the final phosphors for preparation temperatures greater than 1000°C. The data obtained show that the proportion of incorporated chloride does increase with the proportion added in the preparation, but that (1) the amount incorporated is not proportional to the amount added, but reaches a maximum value of about 150 to 200 mole ppm, and (2) the amount incorporated is not proportional to the peak intensity of the phosphor. These facts are especially noticeable for the phosphor prepared at 900°C, where a 10 percent increase in incorporated chloride is found for an increase from 0.1 percent to 1.0 added NH_4Cl, and for which the peak intensity increases by a factor of about 40 for UV excitation and about 12 for CR excitation.

Glow Curves

Glow curves after excitation at −150°C by 3650A ultraviolet are shown in Figs. 4–8. The heating for the glow curve measurement was started at the same time as the cessation of excitation, in order to detect the presence of traps with glow peak very close to the temperature at which the phosphor was excited. The heating rate was linear throughout.

Figure 4 presents the glow curves for the phosphor series prepared at increasing temperatures without any additives in the preparation. The curves may be conveniently separated into a low temperature glow peak

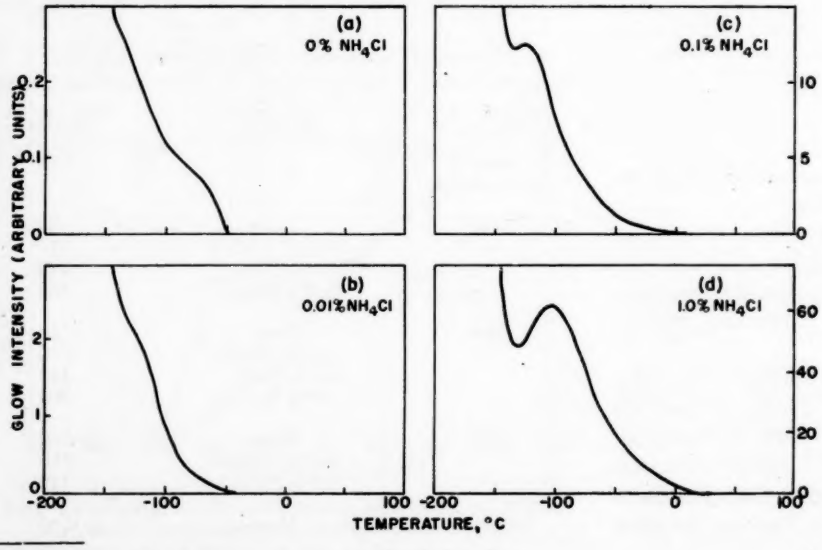

FIG. 5. Glow curves for the series of phosphors prepared at 900°C with increasing proportions of NH_4Cl added in the preparation. UV excitation.

[32] 1 mole ppm = 1 microgram atom per mole of phosphor.

at −110°C, caused by shallow traps, and a high temperature glow peak at about −20°C, caused by deep traps. Closer inspection of the glow curves shows that the low temperature glow peak has a component with glow peak at about −75°C. It may be noted from Figure 4 that there is no indication of a sudden change in the glow curves at the crystal transition from cubic to hexagonal. The deep traps are found in both cubic and hexagonal phosphors, although the glow peak corresponding to the deep traps is resolved only in the hexagonal phosphors.

Because of the difficulty of separation, the glow peaks at −110° and at −75°C are considered together as a unit in the measurements of glow curve areas given in Table I.

Figure 8 shows that the glow curves obtained for the addition of different halides in the preparation are closely similar. It is established that the phenomenon of intensification depends comparatively little on the choice of halide.

Emission Intensity *vs* Operating Temperature

Figure 9 shows the dependence of emission intensity for UV excitation, on the operating temperature for several representative phosphors of the present study. All of the curves for phosphors without added halide show two peaks, one at about −20°C and the other at about 30°C, but only one peak is found when halide is added in the preparation.

Absorption Spectra

Measurements of diffuse reflectivity at room temperature were used to obtain a measure of the absorption of the phosphors of the present study over the wavelength range from 3400 to 4200A. The curves of absorption in Figure 10 are determined by simply subtracting the percent reflection from 100 percent, and therefore absolute values of absorption are not quantitatively determinable. The curves of Fig. 10 show that absorption over the whole range is (1) decreased in cubic phosphors by increasing the preparation temperature without any additives in the preparation, or by adding halide in the preparation at a fixed temperature, and (2) not affected in hexagonal phosphors either by increasing the preparation temperature or by adding halide in the preparation.

That the measured changes in reflectivity are not caused by a simple change in particle size with prepara-

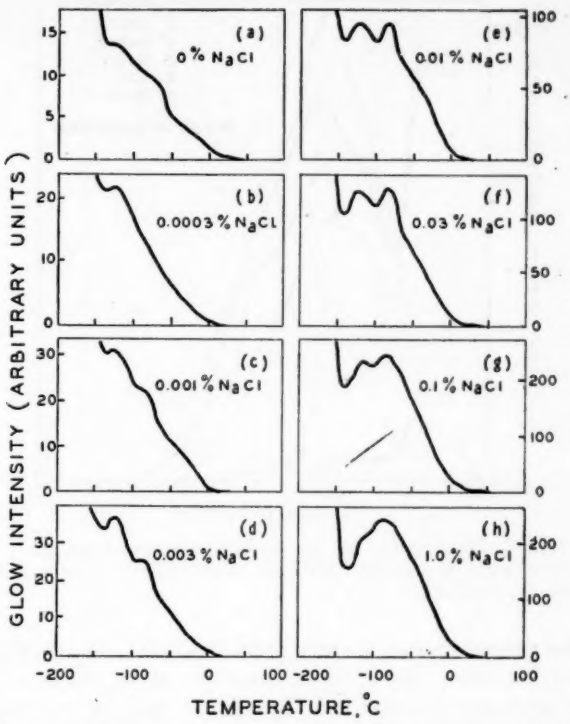

FIG. 6. Glow curves for the series of phosphors prepared at 1050°C with increasing proportions of NaCl added in the preparation. UV excitation.

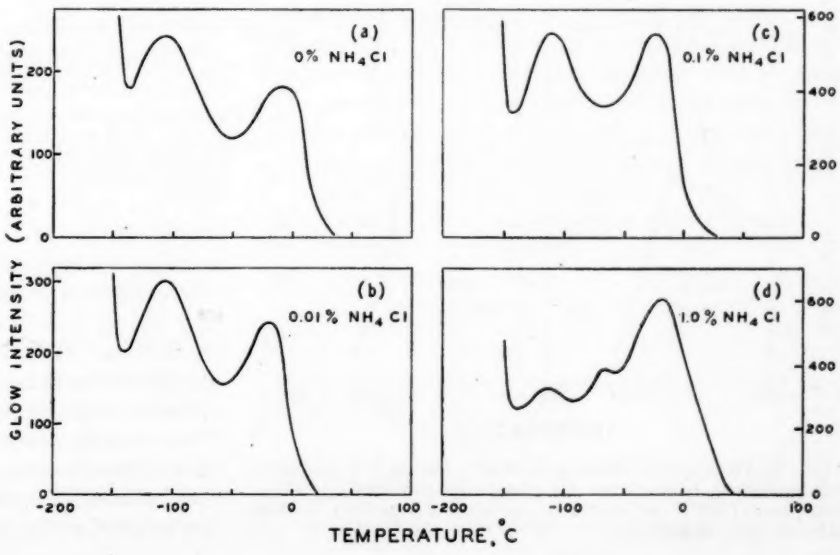

FIG. 7. Glow curves for the series of phosphors prepared at 1200°C with increasing proportions of NH_4Cl added in the preparation. UV excitation.

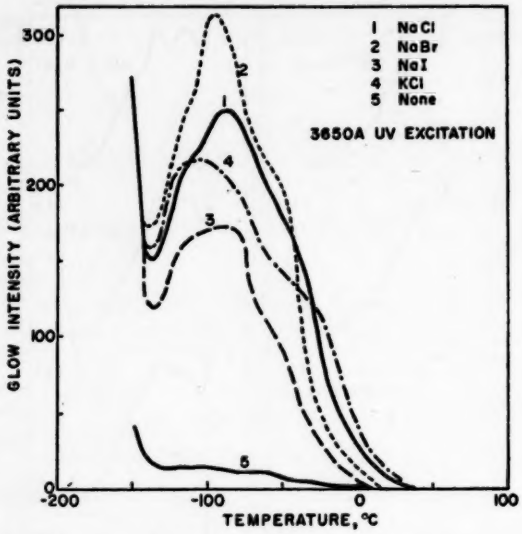

FIG. 8. Glow curves for the series of phosphors prepared at 1050°C with 1.0 percent of different halides added in the preparation. UV excitation.

tion procedure may be seen from Table III. The average particle sizes given for a number of representative phosphors were obtained by microscopic examination with a magnification of 675×. For the phosphor series prepared at increasing temperatures, a decrease in reflectivity would be expected as the result of increasing particle size; actually an increase in reflectivity is found.

A portion of the intensification effect observed in cubic phosphors may possibly be associated with a reduction in absorption for the wavelength region of the luminescence emission. The effect, if present, is concluded to be a minor one, however, for the following reasons: (1) the *greatest* average absorption found in any of the phosphors in the region of the emission is less than 40 percent; (2) small factors of decrease in absorption in the range of low absorption where such factors

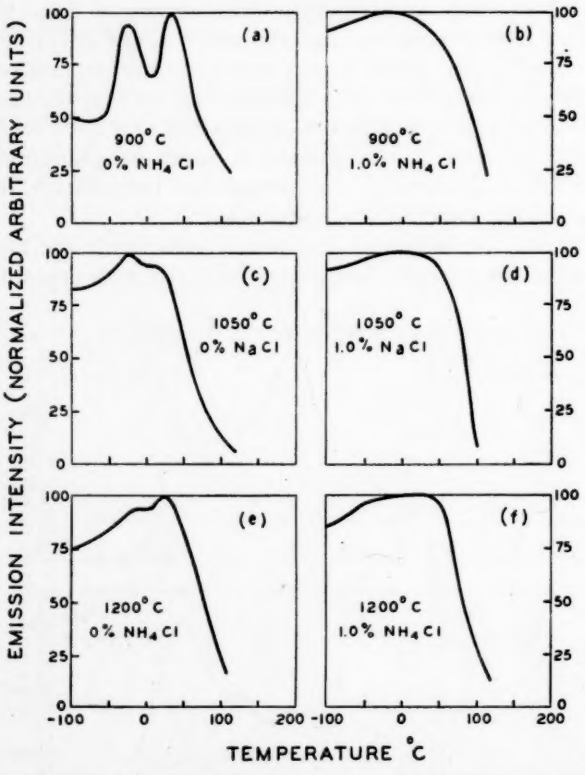

FIG. 9. Variation of emission intensity during UV excitation with operating temperature for phosphors prepared at 900°C, 1050°, and 1200°C without any and with 1.0 percent chloride added in the preparation.

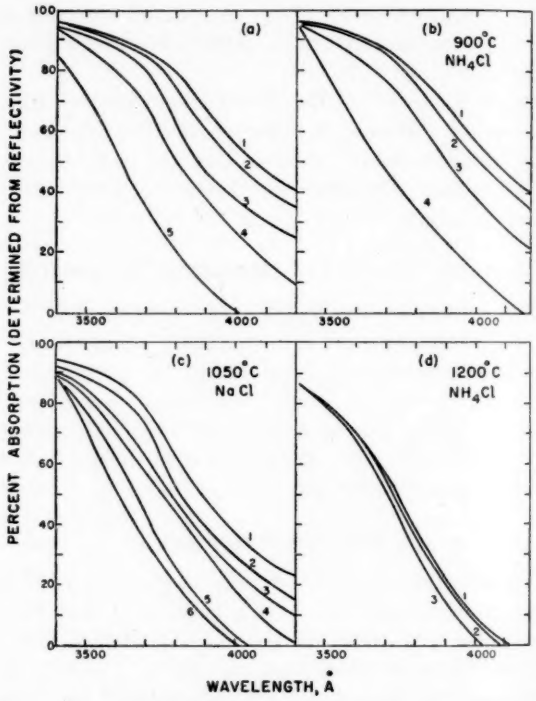

FIG. 10. Curves of absorption, as determined from measurements of diffuse reflectivity. (a) Phosphors prepared at increasing preparation temperatures without any additives in the preparation—(1) 900°C, (2) 950° and 1000°C, (3) 1050°C, (4) 1100°C, (5) 1150°C, 1200°, 1250°, 1300°, 1350°C. (b) Phosphors prepared at 900°C with increasing proportions of NH_4Cl—(1) None, (2) 0.01 percent, (3) 0.1 percent, (4) 1.0 percent. (c) Phosphors prepared at 1050°C with increasing proportions of NaCl—(1) None, 0.0003 percent, 0.001 percent, (2) 0.003 percent, (3) 0.01 percent, (4) 0.03 percent, (5) 0.1 percent, (6) 1.0 percent; also for 1.0 percent NaBr, NaI, and KCl. (d) Phosphors prepared at 1200°C with increasing proportions of NH_4Cl—(1) 0.01 percent, (2) 0.1 percent, (3) 1.0 percent.

are valid, are accompanied by much larger factors of increase of emission intensity; (3) intensification for UV excitation occurs in hexagonal phosphors without any change of absorption, and (4) using preparations in H_2S and HCl, Kroeger and Hellingman[20] have reported intensification to be accompanied by an actual increase in absorption in the region 3500 to 4000A.

For these reasons, and from the fact that intensification increases as the absorption of 3650A UV decreases, it is believed that variations in absorption are a secondary effect for the phosphors of the present study, and

are only indirectly connected with variations in luminescence.

DISCUSSION OF RESULTS

Comparison of Methods of Intensification

Luminescence effects caused by increasing the preparation temperature without any additives in the preparation, and luminescence effects caused by adding halide in the preparation at a fixed temperature, are found to be qualitatively the same. Both methods produce (1) true intensification, i.e., an increase in the intensity of the blue emission band of ZnS phosphor without a change in the spectral distribution; (2) intensification for both UV and CR excitation in cubic phosphors, but intensification only for UV excitation in hexagonal phosphors; (3) an increase in the total glow intensity after UV excitation, and the same relative variation of individual glow peaks with intensification; (4) a decrease in absorption for light in the wavelength range from 3400 to 4200A; (5) a smoothing of the curve of UV-excited emission intensity during excitation as a function of operating temperature. It appears, then, that the mechanism of intensification involved in the two processes is essentially the same.

TABLE III. Particle sizes for representative phosphors.

Phosphor	Average particle size (microns)
ZnS, 900°C	1
ZnS, 1050°C	5
ZnS, 1150°C	7
ZnS, 1250°C	19
ZnS, 1350°C	34
ZnS, [NH_4Cl(1)], 900°C	7
ZnS, [NaCl(1)], 1050°C	6
ZnS, [NH_4Cl(1)], 1250°C	5

The principal quantitative differences between the two methods of producing intensification can be obtained from Table I. The addition of halide in the preparation at a fixed temperature is much more efficient in increasing the peak intensity than is increasing the preparation temperature without any additives in the preparation, but the glow intensity during thermostimulation is increased somewhat more by increasing the preparation temperature than by adding halide in the preparation. The glow intensity is primarily limited by the temperature of preparation, but may be increased to some extent by the addition of halide in the preparation.

If the luminescence centers and the trapping centers in ZnS phosphor are the result of crystal defects, it is natural to look for a dependence of emission and glow intensity on preparation temperature in the usual exponential relation, involving an activation energy for defect formation. Figure 11 is a plot of the log of the number of traps (as determined from glow curves areas) and the log of the blue emission intensity as a function of the reciprocal of the preparation temperature for UV excitation for the phosphors prepared without halide. Table IV presents a summary of the activation energy values obtained from the curves of Fig. 11. Different activation energies are found for the cubic and hexagonal phosphors. This difference may be caused to some extent by the change of absorption with increasing preparation temperature for the cubic phosphors, but it is interesting to note that the ratio of activation energies for the shallow traps in the cubic and hexagonal phosphors is the same as the ratio for the deep traps in the two crystal forms. It is also found that the ratio of activation energy for defect formation to the average

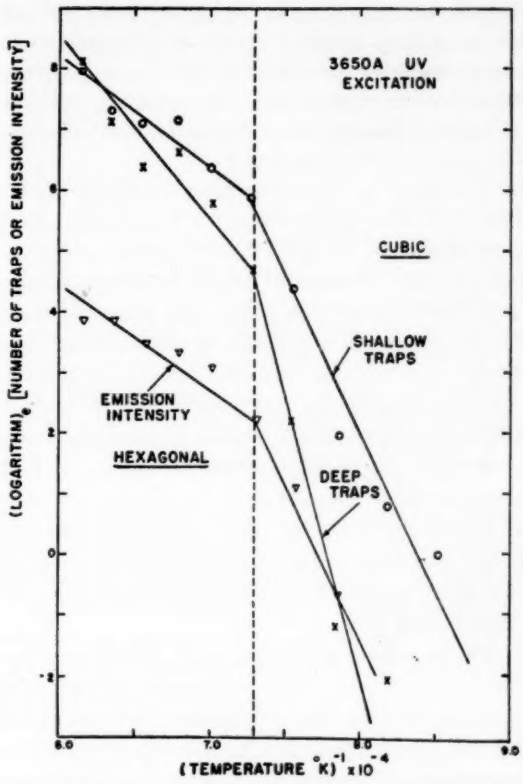

FIG. 11. The variation of low and high temperature glow peak areas and of blue emission intensity during UV excitation, as a function of preparation temperature for the series of phosphors prepared at increasing temperatures without any additives in the preparation.

TABLE IV. Activation energies for defect formation.

	E^*_{hex}	$^*E_{cub}$	Approximate trap depth, ϵ	E^*_{cub}/E^*_{hex}	E^*_{hex}/ϵ
Blue emission	1.5 ev	4.5 ev	—	3.0	—
Traps with glow peak at −110°C	1.6	4.5	0.37 ev	2.8	4.3
Traps with glow peak at −20°C	2.6	7.4	0.60 ev	2.8	4.3

trap depth corresponding to the defect, is a constant for shallow and deep traps. Finally, it is found that the activation energies for defect formation corresponding to luminescence centers are the same in both cubic and hexagonal phosphors as the activation energies for shallow trap defect formation.[33]

The variation of blue emission intensity with the number of shallow traps and with the number of deep traps is shown in Fig. 12 for the series prepared at increasing temperatures and for the series prepared with NaCl at 1050°C. For the phosphors prepared without halide, the emission intensity is proportional to the number of shallow traps and proportional to the square root of the number of deep traps. For the phosphors prepared with NaCl, the emission intensity is found to be proportional to the square of the number of shallow traps and directly proportional to the number of deep traps. The variation of emission intensity with number of shallow and deep traps is approximately the same for the two short series with added NH_4Cl as for the series with added NaCl.

It may be concluded, then, that intensification (at least for UV excitation) by increasing the preparation temperature without any additives in the preparation involves a process wherein luminescence centers and shallow traps are formed simultaneously, and that intensification by adding halide in the preparation at a fixed temperature involves a process wherein luminescence centers and deep traps are formed simultaneously.

Trapping Centers

The continuous variation of glow curve form shown in Fig. 4 for the transition from cubic to hexagonal crystal form supports the previously suggested hypothesis[1] identifying trapping centers in ZnS phosphors with omission defects. At least it may be concluded that trapping centers are located at substitutional sites, and the relations of Fig. 11 indicate that the formation of traps is associated with the formation of omission defects by thermally induced disorder in the preparation.

Although it is found that the dependence between blue emission intensity and number of shallow or deep traps is different depending on whether intensification is achieved by adding halide in the preparation or increasing the preparation temperature without any additives, the same relation is always found between the number of shallow and deep traps. The number of deep traps is proportional to the square of the number of shallow traps.

The variation of the number of pairs of defects with the number of isolated defects in ZnS, assuming a random distribution of defects, has been calculated.[34] It is found that the number of pairs of omission defects in ZnS is proportional to the square of the number of isolated defects. Figure 13 presents a plot of the number of pairs of omission defects per lattice site in ZnS as a function of the number of isolated omission defects per lattice site. The same relation results regardless of whether two like omission defects make up the pair,

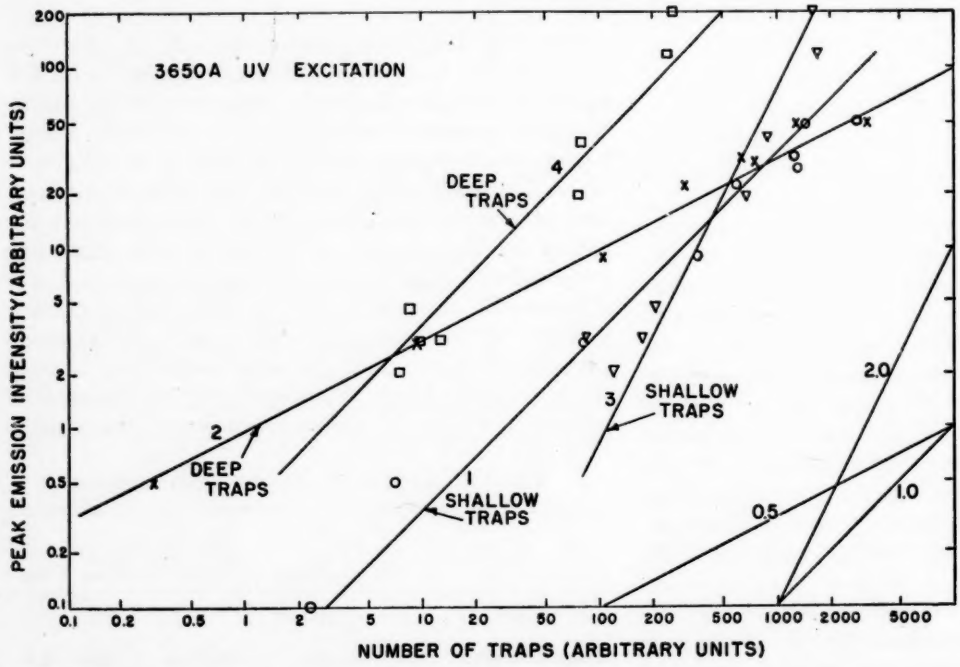

FIG. 12. The variation of peak emission intensity for UV excitation as a function of low and high temperature glow peak areas, for the series of phosphors prepared at increasing temperatures without any additives in the preparation (curves 1 and 2), and for the series of phosphors prepared at 1050°C with increasing proportion of NaCl added in the preparation, (curves 3 and 4).

[33] The particle size of the phosphors, as given in Table III, is found to vary exponentially with the reciprocal of the preparation temperature. If an activation energy, related to the activation energy for diffusion, is calculated from this relation, a value of 1.3 ev is obtained. This value is reasonable for the diffusion activation energy, and is also very close to the activation energy for shallow trap and luminescence center formation.

[34] Reference 15, p. 478.

or whether two unlike omission defects constitute the pair.

A relation is suggested, therefore, between isolated omission defects and shallow traps, and between pairs of omission defects and deep traps in these ZnS phosphors. A difference is found, however, between the ratio of theoretically expected number of pairs of emission defects to number of isolated omission defects, and the ratio of deep to shallow traps found for some of the phosphors, especially those prepared at high temperatures. Additional assumptions about the processes of trap filling and emptying as a function of trap depth, or about the formation of defects, would be required to allow the conclusion that isolated omission defects and pairs of omission defects are associated with the shallow and deep traps found in the phosphors of the present study.

A detailed study of the variation of the glow curves of ZnS:Cu phosphors as a function of incorporated copper proportion has previously[1] also led to the hypothesis that the deepest traps of ZnS phosphor (with glow peak at about −20°C) are associated with pairs of neighboring omission defects.

Luminescence Centers

A consideration of the evidence concerning the blue luminescence emission of zinc sulfide phosphors leads to the conclusion that the luminescence centers are probably associated with particular (SZn_4) groups in the crystal which are perturbed by nearby crystal defects. (1) The present study and the previous results of Shrader[31] indicate that the same two emission bands are present in both cubic and hexagonal phosphors, and that therefore the luminescence centers are located at substitutional sites. (2) The observation of Leverenz[15] on the system (Zn:Cd)S indicates that the luminescence centers are not associated with the zinc or the cadmium as the central element, but with the common ion, the sulfide. (3) Measurements of the spectra distribution of the luminescence emission in the Zn(S:Se) system[35] indicate that two bands are clearly discernible for proportions of ZnSe in ZnS of less than 20 percent, such as would be expected if perturbed (SZn_4) groups were the centers in ZnS and perturbed ($SeZn_4$) groups were the centers in ZnSe.

The spectral distribution of the luminescence emission in the (Zn:Cd)(S:Se) system is also partially determined by the lattice spacing of the particular composition.[36] In every possible substitution, the replacement of either cation or anion by an ion of larger ionic radius results in a luminescence emission with peak at a longer wavelength. This effect can be interpreted as a decrease in the width of the forbidden energy band with increasing lattice spacing.

[35] Reference 15, p. 200.

[36] The author is indebted to Dr. A. L. Smith for calling to his attention this general variation of peak emission wavelength with lattice spacing.

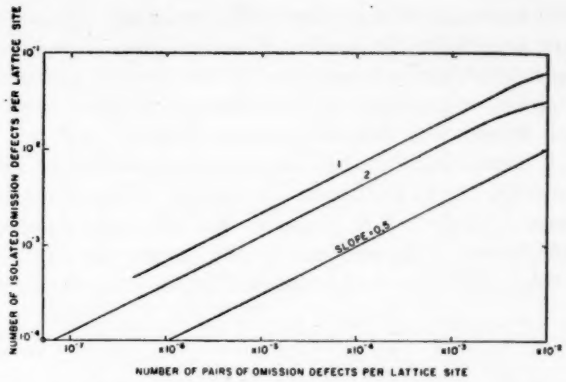

FIG. 13. The theoretical variation of the number of pairs of omission defects per lattice site with the number of isolated omission defects per lattice site. (1) Unlike omission defects make up the pair. (2) Like omission defects make up the pair.

Although there appears to be a relation between the variation with intensification procedure of blue emission intensity during excitation and the number of traps, it does not appear that the perturbing defects responsible for luminescence centers can be directly identified as the omission defects which are responsible for traps. (1) Phosphors with 1.0 percent chloride added in the preparation at 900° and 1050°C have a much more intense emission during excitation than the phosphor prepared at 1350°C without chloride, but the latter phosphor has many more luminescence-active traps. (2) The emission intensity during UV excitation is proportional to the number of shallow traps where intensification is caused by increasing the preparation temperature without any additives in the preparation, but is proportional to the number of deep traps where intensification is caused by adding halide in the preparation at a fixed temperature.

It is found that the emission intensity does increase with the proportion of chloride incorporated in the final phosphor (except for CR excitation of hexagonal phosphors), but the complete lack of proportionality between emission intensity and proportion of chloride incorporated suggests that the use of chloride causes some such "flux" action as that which was originally believed to be the whole effect. A one-to-one correlation between luminescence centers and incorporated chloride ions is not indicated by the results of the present study.

SUMMARY

The same mechanism is involved in intensification of the host crystal luminescence emission of ZnS phosphors by increasing the preparation temperature without any additives in the preparation, and by adding halide in the preparation at a fixed temperature. Both methods of intensification introduce defects which are responsible for the luminescence characteristics of the phosphors.

Further evidence is found to support the hypothesis that trapping centers in ZnS phosphors are associated

with omission defects. The variation of the number of deep traps with the number of shallow traps, for changing intensification procedure, is found to be the same as would be expected for the variation of pairs of omission defects with isolated omission defects.

A correlation between luminescence centers in ZnS phosphor and particular perturbed (SZn_4) groups seems indicated. It is probable that the same omission defects which act as trapping centers are not the perturbing defects in the formation of luminescence centers.

It is found that a portion of the intensification which results from the addition of NH_4Cl or NaCl in the preparation is due to a type of classical "flux" action, in addition to whatever intensifying effect actual incorporation of chloride ions has.

ACKNOWLEDGMENTS

The author is indebted to Dr. R. E. Shrader for helpful suggestions and for his assistance in obtaining the data on diffuse reflectivity.

THE JOURNAL OF CHEMICAL PHYSICS VOLUME 20, NUMBER 4 APRIL, 1952

Disproportionation in Deuterated Ammonia

D. F. STEDMAN
Applied Chemistry Section, National Research Laboratories, Ottawa
(Received May 8, 1951)

Infrared absorption spectra indicate that in NH_3 containing equal molar proportions of D and H, the proportions of the various molecular species appear to depart very seriously from what would be expected if all configurations are intrinsically equally probable.

INTRODUCTION

THE determination of the molecular species present in partially deuterated ammonia is complicated by the fact that the molecules are highly labile, and consequently only the end members are directly available for test purposes. Infrared absorption spectra, however, were found to be peculiarly well adapted to examine this system, since the range from 700 to 1000 cm^{-1} includes but one fundamental vibration mode for both NH_3 and ND_3 with very strong absorption and the background consists only of the relatively much weaker rotational components of this same vibration.

Preliminary experiments showed that the difficulties of analyzing partially deuterated NH_3 could be avoided by synthesizing each mixture from pure ND_3 and NH_3 since at room temperature in glass these gases exchange and reach equilibrium very rapidly. When for instance 1 volume of ND_3 was added to 9 volumes of NH_3, the exchange process was virtually complete before the spectrum could be recorded (about 5 min). This exchange may take place as a wall effect, but this was not investigated as the exchange mechanism should not affect the ultimate result.

In the above case the spectrum showed no trace of the ND_3 band, but a doublet very similar to the NH_3 doublet appeared in a position displaced to slightly longer wavelengths. If more ND_3 was added, another similar doublet appeared, still further displaced, and with further addition the ND_3 band eventually appeared also. There seems no reason to doubt that these absorption bands are caused by NH_3; NH_2D; NHD_2, and ND_3, respectively. The spacing between the doublets becomes progressively less in the order listed, and with ND_3 a single broader peak only appears since this doublet is not resolved under the conditions used.

Method Adopted

Investigation of the concentration of each of these molecular species is complicated by the fact that NH_2D and NHD_2 cannot be prepared and examined as such. The positions of their major absorptions can be determined readily as noted above, but their extinction coefficients cannot be determined directly.

If it can be assumed that the mixed molecules do not interfere at the NH_3 and ND_3 peaks, the concentration of NH_3 and ND_3 in any mixture can be obtained directly from the heights of these peaks. Unfortunately, the rotational terms caused by the mixed molecules add an appreciable unknown complexity to the entire background and even these analyses for NH_3 and ND_3 are therefore none too satisfactory.

A further complication is also caused by the fact that with four molecular species the concentrations of the end members are extremely sensitive to the percent deuteration. For instance at 30 or 70 percent deuteration the peaks for ND_3 or NH_3, respectively, are hardly perceptible, and even at 40 or 60 percent deuteration the background disturbance is very severe. Fifty percent deuteration, however, provides the maximum simultaneous peak heights for both end members, and if each peak is measured from both longer and shorter wavelengths, the results are reasonably concordant, and it would not appear that the average obtained can be far from the truth.

Measurement Details

Figure 1 gives the spectrum of NH_3 containing equal atomic proportions of H and D, taken at 6 and 4-cm pressure in a cell 1.5 cm thick with NaCl windows using a Perkin-Elmer recording spectrograph. The lower curves are for the empty cell and include the drum calibration ticks for drum numbers 570 to 1100, covering the range from 733 to 982 cm^{-1}. The slit widths used for these curves were 0.46 mm below drum No. 800 and 0.29 mm above No. 800, and the drum numbers are used to characterize the curves rather than the reference wavelength, since the latter has but little application in the present discussion.

Several methods might be used to characterize the peak heights; e.g., total height above the baseline for the empty cell, height above the tangent to the base of the peak, and several other methods. It was felt most satisfactory, however, to select wavelengths from the calibration spectra of NH_3 and ND_3, giving the characteristic peak heights from both longer and shorter wavelengths and to use the same wavelengths in examining Fig. 1. This choice was made on the basis that this method involves errors in background densities in a directly additive fashion, and does not concern itself with further complexities as a result of the form of the curves at the tangent to the base of the peaks. Any method by which the peak heights may be properly determined will of course give closely the same results with such pronounced peaks, but the method chosen seems more satisfactory statistically than the use of tangents which are themselves complex and variable functions of the background.

Calibration

The absorption spectra of NH_3 and ND_3 are well known and the calibration spectra are therefore not reproduced. As recorded under the same conditions they are essentially very similar to the regions of Fig. 1 at drum numbers 580 and 630 and from 1000 to 1100, both regions being exaggerated vertically.

The densities of the NH_3 peaks were found to obey Beer's law quite exactly up to at least 0.5 D.U., and the wavelengths used and their extinction coefficients were:

Drum No.	1010	1029	1038	1070	1081	1095
Cm⁻¹	918.2	929.8	935.7	957	964.8	976.8
K/cm press.		0.05558	0.05125		0.05667	0.06292

For ND_3 the following wavelengths were used:

Drum No.	580	607.5	635
Cm⁻¹	735.9	744.5	753.3

but presumably because of the unresolved nature of the doublet (Δ cm^{-1} = approximately 2.9, only), Beer's law was not obeyed at very low densities, and Fig. 2 gives the relation of the density difference for this peak as measured from both longer and shorter wavelengths.

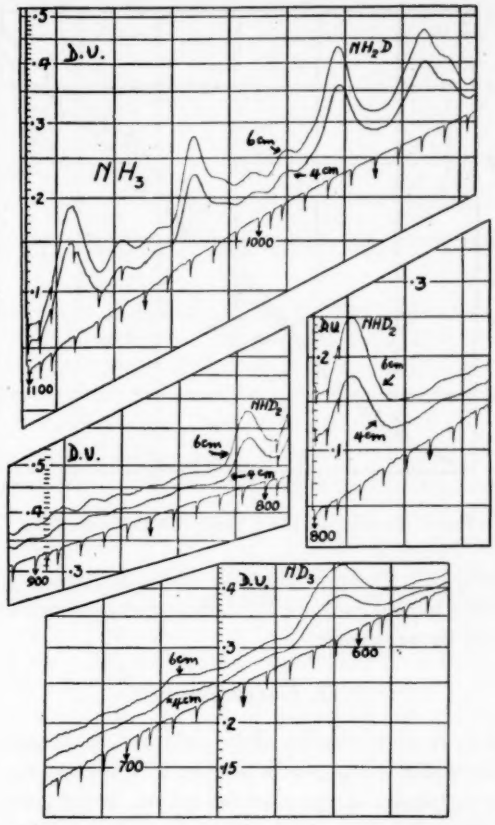

FIG. 1. Infrared absorption spectrum of 50 percent deuterated NH_3 in D.U. *vs* drum number.

RESULTS

In view of the fact that the method involves the measurement of peak heights from an unknown, although rather faint, background, it is felt desirable to present the measurements in more detail than is generally necessary for such an elementary examination, so that their self-consistency may be examined by the usual statistical methods.

NH_3 Determination

The results obtained, in determining the amount of NH_3 present in the pure anhydrous gas containing an equal atomic ratio of H and D after equilibration at room temperature for several hours in glass receivers, is presented in Table I.

These results give 8 versions of the analysis of this gas for NH_3 species, and the final average, 27.14 percent involves the total of errors from recording and reading the spectrum at 24 points, combined with the possibility of 8 systematic errors from background residuals. Examined in the usual statistical manner, the value of $[v]^2$ for these 8 analyses is 22.80, so that v for each value is ± 1.21 percent. The probable error of the arithmetic mean is therefore ± 0.43 percent. The averages for 4 cm and 6 cm differ from the mean by less than double the probable error, and these differences are therefore

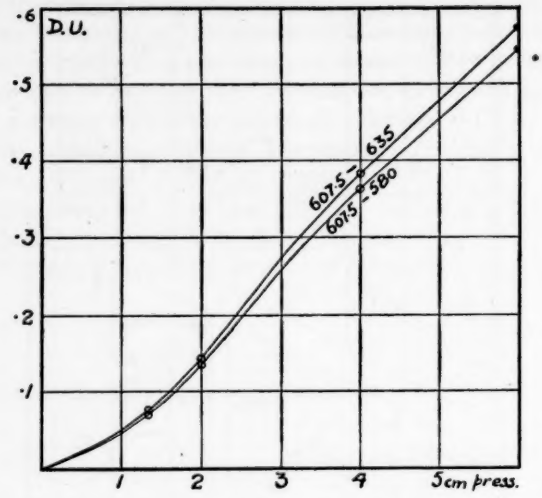

FIG. 2. Density of 744.5 band of ND_3 *vs* pressure.

insignificant. Pressure could have no influence on this exchange in any case, as the number of molecules is not affected by exchange.

ND_3 Determination

Table II gives similar data obtained in determining the amount of ND_3 species present in this same mixture.

These results happen to be rather more consistent than those for NH_3, and although only 4 analyses are provided by the one band, their deviation is comparatively small. For these results $[v]^2=2.18$; v therefore $=\pm 0.58$ percent, and the P.E.A.M. $=\pm 0.29$ percent.

SYSTEMATIC ERROR

Since the details of the background spectra are not known for NH_2D or NHD_2, the variations in background density appear not only as random variations in each analysis, but leave a possibility of systematically affecting the average result. Only certain wavelengths are used in the analysis, and irrespective of the number of analyses made or the percent deuteration, the relation of the background with the main peaks is uniform and repetition therefore will not reduce this effect.

To investigate the possibility of this type of error a set of 9 other readings were taken from the spectra at regions as far removed from the peaks as possible, and in order to avoid deliberate selection, wavelengths were selected at the drum number ticks, taking alternate ticks as far as suitable. These background densities were then taken serially as three groups of three, and the "peak heights" taken for each pair in the same manner as was done in the analyses. The average density differences should of course be zero in this case if no systematic error occurred. The values found are listed in Table III.

In the mean analysis for NH_3 using 8 values, the mean peak height was 0.0782 D.U. in which a probable systematic error of ± 0.00106 might therefore be present. This is equivalent to 1.36 percent of the NH_3 content or ± 0.37 percent NH_3.

For the ND_3 analysis using 4 values, the mean peak height was 0.0718 D.U. in which Table III shows that a probable systematic error of ± 0.0015 D.U. might occur. Because of deviations from Beer's law, variations in ND_3 content at this density are only 0.66 of the percentage of the density variation, and the probable residual systematic error would therefore be ± 0.35 percent ND_3.

TABLE I. Determination of NH_3 in 50 percent deuterated NH_3 Gas phase at room temperature.

Drum No.	D.U. above baseline 4 cm	Δ	6 cm	Δ	cm NH_3 4 cm	6 cm	% NH_3 4 cm	6 cm
1010	0.032		0.056					
1029	0.096	0.064	0.147	0.091	1.15	1.64	28.9	27.4
1038	0.028	0.068	0.049	0.098	1.18	1.73	29.5	28.8
1070	0.030		0.047					
1081	0.089	0.059	0.131	0.084	1.04	1.48	26.0	24.7
1095	0.022	0.067	0.036	0.095	1.06	1.51	26.6	25.2
							27.75	26.52
							Av. 27.14%	

TABLE II. Determination of ND_3 in 50 percent deuterated NH_3 Gas phase at room temperature.

Drum No.	D.U. above baseline 4 cm	Δ	6 cm	Δ	cm ND_3 4 cm	6 cm	% ND_3 4 cm	6 cm
580	0.019		0.037					
607.5	0.070	0.051	0.131	0.094	1.09	1.70	24.2	25.2
635	0.019	0.051	0.040	0.091	1.17	1.75	26.0	26.0
							25.1	25.6
							Av. 25.35%	

ANALYSIS OBTAINED

It has already been shown by examination of Tables I and II that the average analyses for NH_3 and ND_3 have a total P.E.A.M. of 0.43 percent and 0.29 percent, respectively; while examination of the background shows that from this source alone a P.E.A.M. of 0.37 percent and 0.35 percent might be included in these uncertainties. The total determinable error of the results is therefore not of a greater order than the systematic background error alone, and recording and reading the curves therefore is of adequate accuracy for the number of readings taken and does not affect the average result to a determinable extent.

The average analyses reported for NH_3 and ND_3 therefore should not be in error by more than double this systematic error or ± 0.7 percent.

By simple calculation the amount of NH_2D and NHD_2 species may then be obtained, without further regard to their spectra, giving the analysis in Table IV for the gas within the above accuracy.

The last column gives the amount of each species which would be obtained by purely random distribution of the H and D atoms.

It is clear therefore that these results would indicate serious deviations from random distribution for this system of a magnitude far greater than can be explained as residual error, and owing to the rather unexpected nature of this result it was felt desirable to present the data in some detail.

DISCUSSION

It is perhaps premature to discuss the cause for these deviations, but the gases were prepared from pure materials and were purified with the greatest care by repeated distillation. It was checked that the cell itself did not liberate H (or D) in adequate amount to produce detectable results in the spectra, and such contamination would not produce this type of deviation in any case, but would deplete ND_3 or NH_3 as the case might

TABLE III. Examination for systematic error in determining NH_3 and ND_3.

Drum No.	D.U.	v	v^2 ($\times 10^6$)
650	0.039		
670	0.041	+0.002	4
690	0.039	+0.002	4
710	0.046		
730	0.048	+0.002	4
850	0.061	−0.013	169
870	0.057		
1000	0.052	−0.005	25
1050	0.050	+0.002	4
			$[v^2]$ 210

$\therefore\ v = 3.01 \times 10^{-3}$. P.E.A.M. $= 1.50 \times 10^{-3}$ D.U. for 4 observations, or P.E.A.M. $= 1.06 \times 10^{-3}$ D.U. for 8 observations.

be while the present results show both to be about equally too high.

It might be noted that these spectra were recorded in an air conditioned constant temperature laboratory, and consequently there is little possibility of detectable instrumental error during the few seconds required to record each peak. Further, the analyses obtained from each peak are completely independent of each other. It will also be seen by examination of the method of calculation that the absolute position of the base-line for the empty cell is not of the slightest importance in this determination, since the difference between the curves does not appear in the calculation but only their slopes.

TABLE IV.

	Expt. Mol. %	Random Mol. %
NH_3	27.14	12.5
NH_2D	21.07	37.5
NHD_2	26.44	37.5
ND_3	25.35	12.5

From these results it would appear that the symmetrical end members, NH_3 and ND_3, are indicated as being markedly preferred configurations over the much less symmetrical mixed molecules. There is one possibility, however, which cannot be overlooked, i.e., that the spectra of these highly unsymmetrical molecules may in fact be more complex than a simple isotope shift of the absorption maxima. It would, however, be necessary to assume that the additional features in their spectra retain considerable similarity to the original NH_3 and ND_3 spectra, otherwise the analyses would be much more confused.

Unfortunately, other stable molecules of the same configurations do not appear to be available for comparison with the spectra of these mixed molecules. These gases are not themselves available for direct examination, and in view also of the other complications already noted it is difficult to clarify the results any further by the present method, and unfortunately other absorbing wavelengths in the infrared give such complex spectra with these gases that it does not appear that analyses at other wavelengths would be very useful. Since, however, this examination is extremely simple and no other source of gross error can at present be located, it is indicated that either NH_2D and NHD_2 are unfavorable configurations, or else their infrared spectra include faint bands at the same wavelengths as the NH_3 and ND_3 absorption maxima used in the analysis. Unfortunately, it is not at present clear how the infrared absorption spectra of these inaccessible molecular species can be determined unambiguously.

ACKNOWLEDGMENTS

Grateful acknowledgment is made of assistance in preparing the gases for this work by Mr. J. B. Palmer and Mr. B. Ogden, also for recording the spectra by Mr. W. L. Ross.

A Molecular Orbital Theory of Reactivity in Aromatic Hydrocarbons

KENICHI FUKUI, TEIJIRO YONEZAWA, AND HARUO SHINGU
Faculty of Engineering, Kyoto University, Kyoto, Japan

(Received October 29, 1951)

In the search for a quantitative correlation between reactivity and electronic configuration of aromatic hydrocarbons, the electron density, at each carbon atom, of the highest occupied π-orbital in the ground state of the molecule is calculated by means of the LCAO method. Comparing the result of such a calculation on fifteen condensed aromatic hydrocarbons with their chemical reactivities, we find that the position at which the electron density is largest is most readily attacked by electrophilic or oxidizing reagents.

It is, therefore, concluded that distinct from other π-electrons the pair of π-electrons occupying the highest orbital, which is referred to as *frontier* electrons, plays a decisive role in chemical activation of these hydrocarbon molecules. The theoretical significance of this discrimination of the *frontier* electrons in relation to the chemical activation is discussed.

INTRODUCTION

CONSIDERABLE progress has been made of late in the quantum-mechanical treatments for explaining the chemical reactivity of organic compounds. Especially, the problem of predicting the reactivity of an organic molecule in a particular position has been solved to some extent by means of the LCAO molecular orbital method in the case of the well-known "orienting effect" of substituents in aromatic nuclei. On treating such a problem, two methods have been applied by several authors: the one may be called the "transition state method"[1,2] and the other the "π-electron density method.[3,4]

In the former method the configuration of transition complex is assumed *a priori* on the basis of some other theoretical or empirical arguments, and this method is usually confined to tedious calculations, as it is necessary to compute the energies of all the possible configurations.*

In the latter method, on the other hand, the π-electron density was computed as a resultant of the contributions of all π-electrons in the molecule, and no distinction between individual π-electrons has ever been considered. The defect of the method arising from this indiscrimination appears most evidently in the treatment of nonsubstituted aromatic hydrocarbons, in which the π-electron density has always the same value at each position in the molecule according to the Coulson-Rushbrooke theorem,[2] so that this method is of no use for predicting the reactivity of different positions in such molecules.†

In the present paper it is shown that on the ground of the latter method, if we distinguish the pair of π-electrons in the highest occupied orbital in the ground state from the others and assume that this pair of π-electrons plays a decisive role in the reaction in question, we can obtain an illuminating explanation of the difference of reactivity at each position in a molecule.

In the first place we will report on the treatment of nonsubstituted aromatic hydrocarbons. The orienting effect of substituents in aromatic nuclei will be treated in the next publication.

CALCULATION OF ELECTRON DENSITY

In the present paper our treatment is restricted to condensed aromatic hydrocarbons which are "alternant."[5] Namely, they consist of several fused six-membered rings and have the Kékulé-type structure in their ground state.

The energy spectrum can be obtained by the LCAO method, using one-electron approximation function

$$\Psi=\sum_{i=1}^{2N} c_i\varphi_i, \tag{1}$$

where φ_i is the $2p\pi$-atomic orbital of the ith carbon atom.‡

The secular equations for a series of aromatic hydrocarbons are reduced according to the modes shown in Appendix, where the symmetry operations σ_h, σ_v, and i are not considered.

The density of each electron occupying the nth electronic level at the ith carbon atom is represented by $|c_i|^2$, where c_i is the coefficient in Eq. (1) corresponding to the nth eigenvalue.

[1] G. W. Wheland, J. Am. Chem. Soc. **64**, 900 (1942).
[2] H. C. Longuet-Higgins, J. Chem. Phys. **18**, 283 (1950).
[3] G. W. Wheland and L. Pauling, J. Am. Chem. Soc. **57**, 2086 (1935).
[4] H. C. Longuet-Higgins and C. A. Coulson, Trans. Faraday Soc. **43**, 87 (1947).

* This method has never been applied to unsubstituted hydrocarbons except to naphthalene (see reference 1). Whether such a calculation is successfully applicable to the condensed aromatic hydrocarbons which are treated in the present paper, is not known.

† In relation to this problem two other quantum-mechanical methods have been proposed in which the distribution of π-electron density is discussed without using LCAO method. The one is called by O. Schmidt (Z. physik. Chem. **39**, 59 (1938); **42**, 83 (1939); **44**, 185, 194 (1939)) the "Kastenmodel" method in which certain ambiguities are involved as to the model used, resulting in an insufficient accuracy of the method. The other is the "molecular diagram" method after A. and B. Pullman (Rev. sci. **84**, 145 (1946); **86**, 219 (1948); Chem. Abst. **43**, 6905 (1949)) which is almost inapplicable to complex molecules, owing to the laboriousness in calculating the contributions of all possible bond structures, including excited ones, to the normal state of the molecule.

[5] C. A. Coulson and H. C. Longuet-Higgins, Proc. Roy. Soc. (London) **A192**, 16 (1947).

‡ All σ-electrons which form a closed shell in the ground state are left out of account.

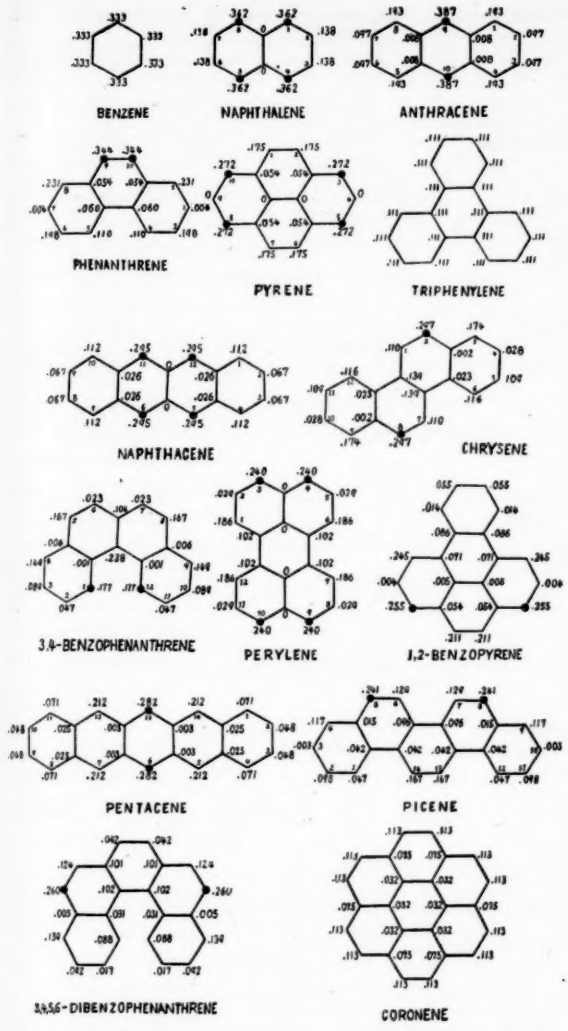

FIG. 1. The distribution of density of the frontier electrons. ●: Position of the largest frontier electron density.

In discussing the reactivity of the π-electron system in these molecules, we make here an assumption that the two electrons occupying the highest π-orbital in the ground state, distinct from the other π-electrons, are essential to the reactivity of the system. We shall refer hereafter to this sort of π-electrons as *frontier electrons*.

The discrimination of the pair of *frontier* π-electrons in relation to the reactivity is considered reasonable so far as, in photochemical processes in which a conjugated double bond system takes part, the triplet state has often been demonstrated as an intermediate step essential to the reaction.[6]

It is our opinion, furthermore, that for ordinary, nonphotochemical, organic reactions—not only for oxidation and other reactions of radical nature, but also, with certain reservations, for reactions of ionic character such as the electrophilic substitutions in aromatic nuclei—a transition of the *frontier* electrons into the triplet state under the influence of the attacking reagent may be essential to the process of chemical activation. Thus, this will be described as a rate process in which the *frontier* electrons solely play an orienting or guiding role, so that the density distribution of the *frontier* electrons will determine the configuration of the transition complex for the reaction.

In view of these considerations we have numerically calculated the density distribution of the *frontier* electrons at each carbon atom in the molecule. The result for 15 hydrocarbons is shown in Fig. 1. The points marked in each diagram of molecules indicate the position of the largest density of the *frontier* electrons.

In this calculation the exchange integrals, except those between two adjacent carbon atoms, and all the overlap integrals, are neglected and the Coulomb integral, as well as the exchange integral, is assumed to be constant.

It is a simplifying circumstance for the present treatment that the distribution of the π-electron density in the triplet state is always the same as that for the ground state, so far as the hydrocarbon systems in the present consideration are concerned. We can, therefore, proceed with our discussion without settling the question as to which of these two states is essential to the reaction. This problem is discussed in some detail in the last section.

COMPARISON WITH EXPERIMENT

In Table I the structures of the reaction products of oxidation, halogenation, nitration, and sulfonation of ten condensed aromatic hydrocarbons are tabulated along with, in the second column, the positions of the highest density of the *frontier* electrons in each hydrocarbon indicated in Fig. 1. No experimental results could be found in the literature for 1,2-benzopyrene and 3,4,5,6-dibenzophenanthrene.

As can be seen from the Table I, there is a perfect agreement between calculation and the result of experiment in the cases of naphthalene, anthracene, phenanthrene, chrysene, naphthacene, perylene, pentacene, and picene.

In the case of 3,4-benzophenanthrene our calculation seems to disagree with the experiment. But this is explicable from the consideration that the position of the largest electron density, 1, is sterically hindered, so that the position 5 where the density is second to the position 1 may be attacked, in conformity with the experiment.

The apparent exceptions in the examples of sulfonation, that of anthracene in particular, may be attributed to the instability of primary sulfonation products, as is widely recognized by preparative organic chemists.

As to picenequinone, the 13,14-structure has been reported by Burg,[7] but later on Cook[8] proved experi-

[6] G. N. Lewis and M. Kasha, J. Am. Chem. Soc. **67**, 994 (1945).

[7] O. Burg, Ber. deut. chem. Ges. **13**, 1836 (1880).

[8] J. W. Cook, J. Chem. Soc. **1941**, 685.

TABLE I. Comparison of the predicted positions of the highest reactivity with experimental results. "1-Cl" means, e.g., "1-Chloronaphthalene," "3,9-di-SO_3H" means, e.g., "Perylene-3,9-disulfonic acid," etc.

Compounds	Position of the highest density of the frontier electrons	Structure of the reaction products: Oxidation	Halogenation	Nitration	Sulfonation
Naphthalene	1,4,5,8	1,4-quinone[a] (5,8-quinone)	1-F[l] 1-Cl[m] 1-Br[n] 1,4-di-Cl[o] 1,5-di-Cl[o]	1-NO_2[cc] 1,5-di-NO_2[dd] 1,8-di-NO_2[dd]	1-SO_3H[ii] (2-SO_3H at higher temp.)
Anthracene	9,10	9,10-quinone[b]	9-Cl[p] 9,10-di-Cl[q] 9-Br[p] 9,10-di-Br[r]	9-NO_2[ee] 9,10-di-NO_2[ee]	(9-SO_3H unstable?) 1,5-, 1,8-di-SO_3H[ii]
Phenanthrene	9,10	9,10-quinone[c]	9,10-di-Cl[s] 9-Br[t]	9-NO_2[ff]	9-SO_3H[kk] (2 or 3-SO_3H at higher temp.)
Pyrene	3,5,8,10	3,8-quinone[d] 3,10-quinone[e]	3,5,8,10-tetra-Cl[u] 3,5,8-tri-Br[v]	...	3,5,8,10-tetra-SO_3H[ll]
Naphthacene	5,6,11,12	5,12-quinone[f] (6,11-quinone)	5,12-di-Cl[w] 5,12-di-Br[w]	...	...
3,4-Benzophenanthrene	1,12	5,6-quinone[g]	...	...	...
Chrysene	2,8	1,2-quinone[h]	2-Cl[x] 2-Br[x]	2,8-di-NO_2[gg]	2-SO_3H[mm]
Perylene	3,4,9,10	3,9-quinone[i] 3,10-quinone(?)[i]	3,9-di-Cl[y] 3,4,9,10-tetra-Cl[z] 3,9-di-Br[aa] 3,10-di-Br[aa]	3,10-di-NO_2[hh] 3,4,9,10-tetra-NO_2[hh]	3,9-di-SO_3H[nn] 3,10-di-SO_3H[nn]
Pentacene	6,13	6,13-quinone[j]	...	...	...
Picene	5,8	5,6-quinone[k]	13,14-di-Br(?)[bb]	...	...

[a] C. E. Groves, Ann. Chem. **167**, 357 (1873).
[b] J. Fritzsche, J. prakt. Chem. (1) **106**, 287 (1869).
[c] R. Fittig and E. Ostermayer, Ann. Chem. **166**, 365 (1873).
[d] R. Scholl and C. Seer, Ann. Chem. **394**, 125 (1912).
[e] Rütgerswerke, A.-G. Germ. Pat. 613, 914 (May 31, 1935).
[f] S. Gabriel and E. Leupold, Ber. deut. chem. Ges. **31**, 1277 (1898).
[g] J. W. Cook, J. Chem. Soc., 3524 (1931).
[h] C. Liebermann, Ann. Chem. **158**, 309 (1871).
[i] A. Zinke and E. Unterkreuter, Monatshefte Chemie **40**, 408 (1919).
[j] E. Phillipi, Monatshefte Chemie **53/54**, 639 (1929).
[k] J. W. Cook, J. Chem. Soc., 685 (1941).
[l] Schiemann, Gueffroy, and Wikelmüller, Ann. Chem. **487**, 270 (1931).
[m] A. Töhl and O. Eberhard, Ber. deut. chem. Ges. **26**, 2945 (1893).
[n] C. Glaser, Ann. Chem. **135**, 41 (1865).
[o] J. S. Salkind and S. B. Faerman, J. Russ. Phys.-Chem. Ges. (U.R.S.S.) **62**, 1021 (1930).
[p] W. H. Perkin, Chem. News **34**, 145 (1876).
[q] Ed. Lippmann and I. Pollak, Ber. deut. chem. Ges. **34**, 2768 (1901).
[r] C. Graebe and C. Liebermann, Ber. deut. chem. Ges. **1**, 186 (1868).
[s] J. Schmidt and R. Schall, Ber. deut. chem. Ges. **39**, 3893 (1907).
[t] L. F. Fieser and C. C. Price, J. Am. Chem. Soc. **58**, 1838 (1936).
[u] I. G. Farbenind, A.-G. Fr., 261, 627 (March 23, 1934).
[v] E. Clar, Ber. deut. chem. Ges. **69**, 1671 (1936).
[w] I. J. Postovskii and R. G. Beyles, Compt. rend. Acad. Sci. U.R.S.S. **39**, 102 (1943).
[x] I. G. Farbenind, A.-G. Fr., 793, 893 (February 3, 1936).
[y] Zinke, Funke, and Pongratz, Ber. deut. chem. Ges. **58**, 330 (1925).
[z] A. Zinke and K. Funke, Ber. deut. chem. Ges. **60**, 580 (1927).
[aa] Zinke, Linner, and Wolfbauer, Ber. deut. chem. Ges. **58**, 328 (1925).
[bb] O. Burg, Ber. deut. chem. Ges. **13**, 1837 (1880).
[cc] R. Piria, Ann. Chem. **78**, 32 (1851).
[dd] Ch. Gassman, Ber. deut. chem. Ges. **29**, 1243, 1521 (1896).
[ee] J. Meisenheimer and E. Connerade, Ann. Chem. **330**, 164 (1903).
[ff] J. Schmidt and M. Strobel, Ber. deut. chem. Ges. **36**, 2511 (1903).
[gg] I. G. Farbenind, A.-G. Fr., 794, 534 (February 19, 1936).
[hh] Zinke, Hirsch, and Brozek, Monatshefte Chemie **51**, 205 (1929).
[ii] O. N. Witt, Ber. deut. chem. Ges. **48**, 743 (1915).
[jj] J. Houben, *Das Anthracen und die Anthrachinone* (1929), p. 109.
[kk] A. Werner, Ann. Chem. **321**, 270 (1902).
[ll] I. G. Farbenind, A.-G. Germ. Pat., 620, 635 (October 26, 1935).
[mm] I. G. Farbenind, A.-G. Fr., 789, 461 (October 29, 1935).
[nn] C. Marschalk, Chem. Zentr. **I**, 1833 (1927).

mentally that the quinone obtained from picene by oxidation must have the 5,6-structure which coincides with our results.

In view of these excellent agreements of our theory with experiment we believe that some essential relations must exist between the reactivity and the density of the *frontier* electrons.

As for the significance of the absolute value of the *frontier* electron density, two examples may be of value to be mentioned here: triphenylene is more stable than naphthacene in relation to oxidation;[9] and anthracene is more readily oxidized than phenanthrene.[10] Comparing the largest values of the density in those hydrocarbons having the same number of carbon atoms and π-electrons, we can observe a parallelism between the reactivity and the absolute value of the *frontier* electron density.

[9] Ward, Kirner, and Howard, J. Am. Chem. Soc. **67**, 246 (1945).
[10] R. Anschütz and G. Schultz, Ann. Chem. **196**, 38 (1879).

THEORETICAL DISCUSSION

In our treatments so far disclosed the physical ground of discriminating the highest occupied π-orbital in the ground state from the other π-orbitals is left untouched. We shall try here to add some theoretical considerations.

Anyhow, it can be concluded from the successful results obtained above that certain differences must exist between the *frontier* electrons and the other π-

electrons in respect to their behaviors in the course of electronic interaction during the chemical activation. This fact may be understood in two different ways: the one way of understanding consists in the possibility that the frontier electrons, on account of their valence-electron-like nature, can pass into the next higher orbital, forming a triplet state, presumably under the influence of the field arising from the approaching reagent. From the symmetry consideration of the wave function of the whole system, it seems to be quite reasonable that, in order to retain the singlet spin symmetry of the whole system, the spin state of two electrons in the C−Hσ bond to be substituted by the electrophilic reagent is simultaneously changed into a triplet in the course of the reaction which is considered to take place adiabatically.

To understand that the triplet formation of the *frontier* electrons can be effective for bond formation between the molecule and the electrophilic reagent, we can make use of the following analogy. Considering that, as shown by Bartlett,[11] a strong bond of a $^3\sum_u^+$ state is formed between two $p\sigma$ orbitals, we may assume that between the hydrocarbon molecule and the electrophilic reagent in a transition complex a $\{(sp^3)\sigma, (sp^3)\sigma\}$-like bond is formed in the same way by a participation of the *frontier* electrons with parallel spins.

The reagent is thus attracted to the position of the largest *frontier* electron density, while the hydrogen ion, formerly in the C−Hσ-bond, may be repelled from the molecule because of the triplet property of the C−Hσ-part of the electronic system in the transition complex.

On the other hand, the contributions of all the π-electrons in the molecule must, in general, be taken into account on the occasion of chemical reaction. From this point of view, we come to the second way of understanding. When it is assumed that in the electronic interaction with an electrophilic attacking reagent the highest occupied π-orbital would always act as *attractive* and the other π-orbitals as *repulsive*, it can be expected that the formation of a transition complex at the position of the largest *frontier* electron density might be preferred in consequence of the resultant effect of all π-electrons, in either attractive or repulsive orbitals, upon the potential energy of the whole system in the process of formation of the transition complex. In another expression, this way of understanding consists in attributing the distinction of the highest occupied orbital from the others to the difference in the nature of each orbital in reference to the interaction with the attacking reagent. Of course, the repulsive effect represents a resultant contribution of all π-electrons other than *frontiers*. Some of them may give attractive effects but in this case the contribution must be smaller than those of *frontier* electrons. The possibility of a fact that a certain orbital in an atom attracts and that another orbital in the same atom repels a certain orbital of another atom has been shown by Araki and Watari[12] in the case of C_2-molecule.

The two ways of theoretical approach as discussed above may be considered as corresponding to the two different interpretations in the description of the process of electronic interaction. A correlation between them needs to be confirmed by further investigations.

The concept of the frontier electron, as well as the principle involved in the above discussion, is hoped to find applications more widely to problems on the reactivity of π-electron systems.

ACKNOWLEDGMENTS

The authors are grateful to Professor S. Kodama and Professor G. Araki for valuable suggestions and encouragements. Especially are the authors indebted to Professor Araki for enlightening them on the arguments developed in the part of discussion.

APPENDIX. SYMMETRY GROUP AND MODES OF REDUCTION OF SECULAR EQUATIONS.[a]

Compounds	Symmetry group	Modes of reduction of secular equations
Benzene	D_6	$\Gamma(\Psi)=\Gamma A_1+\Gamma B_1+\Gamma E_1+\Gamma E_2$
Coronene	D_6	$\Gamma(\Psi)=3\cdot\Gamma A_1+\Gamma A_2+\Gamma B_1+3\cdot\Gamma B_2+4\cdot\Gamma E_1+4\cdot\Gamma E_2$
Triphenylene	D_3	$\Gamma(\Psi)=3\cdot\Gamma A_1+3\cdot\Gamma A_2+6\cdot\Gamma E$
Anthracene	D_2	$\Gamma(\Psi)=4\cdot\Gamma A_1+3\cdot\Gamma B_1+3\cdot\Gamma B_2+4\cdot\Gamma B_3$
Naphthacene	D_2	$\Gamma(\Psi)=5\cdot\Gamma A_1+4\cdot\Gamma B_1+4\cdot\Gamma B_2+5\cdot\Gamma B_3$
Naphthalene	D_2	$\Gamma(\Psi)=3\cdot\Gamma A_1+2\cdot\Gamma B_1+2\cdot\Gamma B_2+3\cdot\Gamma B_3$
Pentacene	D_2	$\Gamma(\Psi)=6\cdot\Gamma A_1+5\cdot\Gamma B_1+5\cdot\Gamma B_2+6\cdot\Gamma B_3$
Perylene	D_2	$\Gamma(\Psi)=6\cdot\Gamma A_1+4\cdot\Gamma B_1+6\cdot\Gamma B_2+4\cdot\Gamma B_3$
Pyrene	D_2	$\Gamma(\Psi)=5\cdot\Gamma A_1+3\cdot\Gamma B_1+3\cdot\Gamma B_2+5\cdot\Gamma B_3$
3,4-Benzophenanthrene	C_2	$\Gamma(\Psi)=10\cdot\Gamma A+8\cdot\Gamma B$
1,2-Benzopyrene	C_2	$\Gamma(\Psi)=10\cdot\Gamma A+10\cdot\Gamma B$
3,4,5,6-Dibenzophenanthrene	C_2	$\Gamma(\Psi)=11\cdot\Gamma A+11\cdot\Gamma B$
Phenanthrene	C_2	$\Gamma(\Psi)=7\cdot\Gamma A+7\cdot\Gamma B$
Picene	C_2	$\Gamma(\Psi)=11\cdot\Gamma A+11\cdot\Gamma B$
Chrysene	C_2	$\Gamma(\Psi)=9\cdot\Gamma A+9\cdot\Gamma B$

[a] $\Gamma(\Psi)$: reducible representation. ΓA, ΓB, $\cdots$: irreducible representations of character A, B, $\cdots$.

[11] J. H. Bartlett, Phys. Rev. **37**, 505 (1931).

[12] G. Araki and W. Watari, Prog. Theoret. Phys. **6**, 945 (1951).

The Mean Amplitudes of Thermal Vibrations in Polyatomic Molecules. I. $CF_2=CF_2$ and $CH_2=CF_2$

YONEZO MORINO, KÔZO KUCHITSU, AND TAKEHIKO SHIMANOUCHI
Chemical Laboratory, Faculty of Science, Tokyo University, Tokyo, Japan
(Received December 19, 1951)

A normal coordinate treatment based on the potential function of Urey-Bradley type has been applied to $CF_2=CF_2$ and $CF_2=CH_2$ molecules by taking into account the repulsions between nonbonded atoms in addition to the valence force field. The mean-square amplitudes of thermal vibration of the atomic distances in these molecules have been calculated by the use of the normal coordinates and compared with those obtained by I. Karle and J. Karle from the electron diffraction investigation.

RECENTLY the technique of electron diffraction by gases has been so much improved that we can measure not only the outer halos up to $s=30$ by the ordinary visual method but also minor features of each halo by the sector method. So it becomes necessary for the interpretation of the diffraction patterns to take into account the thermal motion of atoms in the molecule. Actually some of the workers have already used temperature factor for the computation of the intensity curves. For instance, Schomaker[1,2] and Bauer[3] assumed adequate values for temperature factors, but they have not given the details of their derivation. On the other hand, I. Karle and J. Karle[4] measured by their elegant sector apparatus the mean-square amplitudes of thermal vibrations in $CF_2=CF_2$ and $CH_2=CF_2$ molecules. They stated that it would be worthwhile to perform detailed computations of the mean amplitudes from spectroscopic data to compare them with the electron diffraction data, but they have not carried out the actual calculations.

Fortunately, the Raman and infrared spectra of these molecules have been reported by Smith, Claassen, and Nielsen,[5,6] and by Edgell and Byrd.[7] Hence, we will calculate the normal modes of vibrations of these molecules, compute the mean amplitudes of atomic distances using the normal coordinates thus obtained, and compare them with those measured by I. Karle and J. Karle.

1. THE METHOD OF ESTIMATION OF MEAN AMPLITUDES

As is well known in the theory of small vibrations, any displacement R_i of atomic distance from the equilibrium value can be expressed by a linear combination of the normal coordinates x_k,

$$R_i=\sum_k L_{ik}x_k, \tag{1}$$

so that the mean of the square of the displacement may be calculated as

$$\langle R_i^2\rangle=\sum_{k,j} L_{ik}L_{ij}\langle x_k\cdot x_j\rangle. \tag{2}$$

There are two sorts of terms in Eq. (2): the one, those for which $k=j$; and the other, those for which $k\neq j$. It is easily shown that the latter vanishes because the normal vibrations are mutually independent. Accordingly, we have

$$\langle R_i^2\rangle=\sum_k L_{ik}^2\langle x_k^2\rangle. \tag{3}$$

That is, the mean of the square of an atomic distance is given by the sum of the mean-square amplitudes of the normal vibrations multiplied by the square of the coefficients L_{ik}.

As is well known, the mean-square amplitude of a normal vibration is given by[8]

$$\langle x_k^2\rangle=\frac{h}{8\pi^2\nu_k}\coth\frac{h\nu_k}{2kT}, \tag{4}$$

where ν_k is the frequency of the normal vibration. Therefore, in order to compute the mean-square amplitude, the first task is to calculate the coefficient L_{ik}. If R_i is a symmetry coordinate which is composed of a linear combination of the displacements of bond distances or of bond angles according to the symmetry requirement, the transformation matrix L_{ik} can be obtained by solving the linear simultaneous equations (5), derived from the F and G matrices by Wilson's method,[9]

$$\sum_i[(GF)_{ji}-\delta_{ji}\lambda_k]L_{ik}=0, \quad (j, k=1, 2, \cdots n). \tag{5}$$

These equations provide only the ratios of the coefficients but not their absolute values. The latter can be obtained by normalizing x_k to satisfy the following equations, since x_k are the normal coordinates:

$$2V=X'\Lambda X=R'FR, \tag{6}$$

[1] Spitzer, Howell, and Schomaker, J. Am. Chem. Soc. **64**, 2693 (1942).
[2] K. Hedberg and V. Schomaker, J. Am. Chem. Soc. **73**, 1482 (1951).
[3] J. M. Hasting and S. H. Bauer, J. Chem. Phys. **18**, 13 (1950).
[4] I. Karle and J. Karle, J. Chem. Phys. **18**, 963 (1950).
[5] Nielsen, Claassen, and Smith, J. Chem. Phys. **18**, 812 (1950).
[6] Smith, Nielsen, and Claassen, J. Chem. Phys. **18**, 326 (1950).
[7] W. F. Edgell and W. E. Byrd, J. Chem. Phys. **17**, 740 (1949); **18**, 892 (1950).
[8] R. W. James, Physik Z. **33**, 737 (1932).
[9] E. B. Wilson, Jr., J. Chem. Phys. **9**, 76 (1941); **15**, 736 (1947).

which may be written in a more simple expression,

$$L'FL=\Lambda. \tag{7}$$

The mean-square amplitude of the displacement of distance between any atoms can be calculated by expanding them in terms of the symmetry coordinates and then transforming each term to the normal coordinates. The details of the actual calculations will be shown in Sec. 3.

In this place a few words should be added with regard to the mean-square amplitudes to be used in the discussion of electron diffraction. J. Karle and I. Karle[10] quoted that the quantity which is significant in electron diffraction is not the average of the square of the amplitudes, but "the average of the square of the amplitudes projected on the line joining the pairs of atoms in their equilibrium position." When the distance between a pair of atoms $r=(x^2+y^2+z^2)^{\frac{1}{2}}$ is expanded about the equilibrium value r_e,

$$r=r_e+\left(\frac{x_e}{r_e}\Delta x+\frac{y_e}{r_e}\Delta y+\frac{z_e}{r_e}\Delta z\right)+\cdots. \tag{8}$$

J. Karle and I. Karle called the absolute value of the displacement vector (Δx, Δy, and Δz) the "amplitude" and $\Delta r=r-r_e$ which is the quantity in parentheses in Eq. (8), the "projected amplitude." It seems, however, more reasonable to define the amplitude of thermal vibration with $\Delta r=r-r_e$, not with the relative displacement (Δx, Δy, and Δz). According to this definition it is the mean-square amplitude itself that is actually needed for the discussion of electron diffraction. Of course this quantity coincides in the first approximation with Karle's mean-square projected amplitude. In the following, the term "mean-square amplitude" is used in this sense. Furthermore, for simplicity "root mean-square amplitude" will be abbreviated to "mean amplitude."

2. NORMAL COORDINATE TREATMENT OF MOLECULAR VIBRATIONS IN $CF_2=CF_2$ AND $CH_2=CF_2$ MOLECULES

As for the calculations of the normal vibrations of ethylene type molecules ethylene itself was treated by Manneback and Verleysen,[11] Bernard and Manneback,[12] Bonner,[13] and Arnett and Crawford,[14] tetrachloroethylene by Verleysen[15] and Torkington,[16] and vinylidene fluoride by Edgell and Byrd.[7] Manneback *et al.*, Bonner, and Torkington used extended valence force field, including the cross terms of internal coordinates. Edgell and Byrd paid special attention to the interaction between F atoms and CF_2 groups, but the type of force field assumed by them leads to a C−F force constant which seems to be unreasonably small.

It was shown by one of the present authors[17] that the Urey-Bradley field is a reasonable assumption for the treatment of molecular vibration in methane derivatives and the like, so that it is also interesting to investigate the case of ethylene type molecules by the same force field, taking into account the repulsions between nonbonded atoms in addition to the valence force field.

I. $CF_2=CF_2$

Equilibrium distances and angles of this molecule were determined by I. Karle and J. Karle[3] by electron diffraction investigation: C−F: 1.313A, C=C: 1.313A, and ∠FCF: 114°. This molecule has the symmetry of V_h, so that the normal vibrations divide themselves in the following manner:

$$\Gamma=3A_g+2B_{1g}+2B_{2u}+2B_{3u}+A_u+B_{1u}+B_{2g}, \tag{9}$$

of which the last three are the out-of-plane vibrations and can be put aside from our present consideration, since in a planar molecule the out-of-plane vibrations do not give any influences in the first approximation upon the mean amplitudes. As stated above for the potential energy of this molecule the repulsive energies between alternate atoms such as those of the F···F atoms in CF_2 groups and those of the C···F atoms in the $C=CF_2$ groups are taken into account. But those terms between the F···F atoms in the adjacent CF_2 groups are neglected, since the distance (2.737A) between the latter is larger than that between the F···F atoms in CF_2 group (2.204A), so that the forces between them diminish until they become negligible. Thus the potential function for this molecule may be expressed as follows:[18]

$$\begin{aligned}V=&\tfrac{1}{2}K_{CC}(\Delta r_0)^2+\tfrac{1}{2}K_{CF}\{(\Delta r_1)^2+(\Delta r_2)^2\\&+(\Delta r_1')^2+(\Delta r_2')^2\}.\\&+\tfrac{1}{2}H_{FCF}\{(r\Delta\alpha)^2+(r\Delta\alpha')^2\}+\tfrac{1}{2}H_{CCF}\{(r\Delta\beta_1)^2\\&+(r\Delta\beta_2)^2+(r\Delta\beta_1')^2+(r\Delta\beta_2')^2\}+\tfrac{1}{2}F_{FF}\{(\Delta q_1)^2\\&+(\Delta q_1')^2\}+\tfrac{1}{2}F_{CF}\{(\Delta q_2)^2+(\Delta q_2')^2+(\Delta q_2'')^2\\&+(\Delta q_2''')^2\}+F_{FF}'\{q_1\Delta q_1+q_1\Delta q_1'\}\\&+F_{CF}'\{q_2\Delta q_2+q_2\Delta q_2'+q_2\Delta q_2''+q_2\Delta q_2'''\},\end{aligned} \tag{10}$$

where r_0 denotes the length of the C=C bond, r those of the C−F bonds, α the bond angles ∠FCF, β the bond angles ∠C=CF, q_1 the distances between F atoms in each CF_2 group, and q_2 those between the C and F atoms not bonded directly, as shown in Fig. 1.

[10] J. Karle and I. Karle, J. Chem. Phys. **18**, 957 (1950).
[11] C. Manneback and A. Verleysen, Ann. soc. sci. Bruxelles **56**, 349 (1936).
[12] E. Bernard and C. Manneback, Ann. soc. sci. Bruxelles **59**, 113 (1939).
[13] L. G. Bonner, J. Am. Chem. Soc. **58**, 34 (1936).
[14] R. L. Arnett and N. L. Crawford, Jr., J. Chem. Phys. **18**, 118 (1950).
[15] A. Verleysen, Ann. soc. sci. Bruxelles **59**, 267 (1939).
[16] P. Torkington, Proc. Phys. Soc. (London) **63A**, 804 (1950).
[17] T. Shimanouchi, J. Chem. Phys. **17**, 245, 734, 848 (1949).
[18] Strictly speaking, the potential energies given in Eqs. (10) and (17) should include linear terms in Δr_0, Δr, Δ_α, etc. However, all the coefficients of these terms are expressed by F', so that they are unnecessary for the calculation (see reference 17).

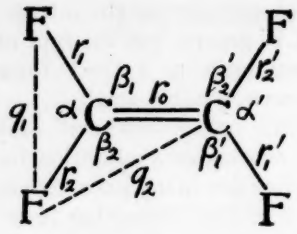

FIG. 1. The internal coordinates of $CF_2=CF_2$ molecules.

The symmetry coordinates used to set up the secular equation are as follows:

$$R_1=\Delta r_0,$$

$$R_2=\tfrac{1}{2}\{(\Delta r_1+\Delta r_2)+(\Delta r_1'+\Delta r_2')\},$$

$$R_3=\frac{1}{\sqrt{3}}(r\Delta\alpha+r\Delta\alpha')-\frac{1}{2\sqrt{3}}\{(r\Delta\beta_1+r\Delta\beta_2)+(r\Delta\beta_1'+r\Delta\beta_2')\},$$

$$R_4=\tfrac{1}{2}\{(\Delta r_1-\Delta r_2)+(\Delta r_1'-\Delta r_2')\},$$

$$R_5=\tfrac{1}{2}\{(r\Delta\beta_1-r\Delta\beta_2)+(r\Delta\beta_1'-r\Delta\beta_2')\},$$

$$R_6=\tfrac{1}{2}\{(\Delta r_1-\Delta r_2)-(\Delta r_1'-\Delta r_2')\},$$

$$R_7=\tfrac{1}{2}\{(r\Delta\beta_1-r\Delta\beta_2)-(r\Delta\beta_1'-r\Delta\beta_2')\},$$

$$R_8=\tfrac{1}{2}\{(\Delta r_1+\Delta r_2)-(\Delta r_1'+\Delta r_2')\},$$

$$R_9=\frac{1}{\sqrt{3}}(r\Delta\alpha+r\Delta\alpha')-\frac{1}{2\sqrt{3}}\{(r\Delta\beta_1+r\Delta\beta_2)-(r\Delta\beta_1'+r\Delta\beta_2')\}. \tag{11}$$

And the G and F matrices in these coordinates can be written as[19]

$$G$$

$$A_g\begin{matrix}R_1\\R_2\\R_3\end{matrix}\begin{pmatrix}2\mu_0, & & \\ -2c\mu_0, & 2c^2\mu_0+\mu, & \\ 2\sqrt{3}s\mu_0, & -2\sqrt{3}sc\mu_0, & 6s^2\mu_0+3\mu\end{pmatrix},$$

$$B_{1g}\begin{matrix}R_4\\R_5\end{matrix}\begin{pmatrix}2s^2\mu_0+\mu, & \\ -2sp\mu_0, & 2p^2\mu_0+\mu\end{pmatrix},$$

$$B_{2u}\begin{matrix}R_6\\R_7\end{matrix}\begin{pmatrix}2s^2\mu_0+\mu, & \\ -2sc\mu_0, & 2c^2\mu_0+\mu\end{pmatrix},$$

$$B_{3u}\begin{matrix}R_8\\R_9\end{matrix}\begin{pmatrix}2c^2\mu_0+\mu, & \\ -2\sqrt{3}sc\mu_0, & 6s^2\mu_0+3\mu\end{pmatrix},$$

$$F$$

$$\begin{pmatrix}A_0, & & \\ 2C_0, & A+C, & \\ -\frac{2}{\sqrt{3}}K_0, & \frac{2}{\sqrt{3}}K_1-\frac{1}{\sqrt{3}}K_2, & \frac{2}{3}B_0+\frac{1}{3}B\end{pmatrix},$$

$$\begin{pmatrix}A-C, & \\ K_2, & B\end{pmatrix}$$

$$\begin{pmatrix}A-C, & \\ K_2, & B\end{pmatrix},$$

$$\begin{pmatrix}A+C, & \\ \frac{2}{\sqrt{3}}K_1-\frac{1}{\sqrt{3}}K_2, & \frac{2}{3}B_0+\frac{1}{3}B\end{pmatrix}, \tag{12}$$

where the following abbreviations are adopted:

$$\mu=\frac{1}{m_F},\qquad \mu_0=\frac{1}{m_C},$$

$$s=\sin\frac{\alpha}{2},\qquad c=\cos\frac{\alpha}{2},$$

$$p=2\frac{r}{r_0}+c,\qquad q^2=r_0^2+r^2+2rr_0c,$$

$$s_1=(r+r_0c)/q,\qquad s_0=(r_0+rc)/q,$$

$$t_1=r_0s/q,\qquad t_0=rs/q, \tag{13}$$

and

$$A_0=K_{CC}+4(s_0^2F_{CF}+t_0^2F_{CF}'),$$

$$A=K_{CF}+s_1^2F_{CF}+t_1^2F_{CF}'+s^2F_{FF}+c^2F_{FF}',$$

$$B_0=H_{FCF}+c^2F_{FF}-s^2F_{FF}',$$

$$B=\frac{r_0}{r}(H_{CCF}+t_1t_0F_{CF}-s_1s_0F_{CF}'),$$

$$C_0=s_1s_0F_{CF}-t_1t_0F_{CF}',$$

$$C=s^2F_{FF}-c^2F_{FF}',$$

$$K_0=t_1s_0F_{CF}+t_0s_1F_{CF}',$$

$$K_1=cs(F_{FF}+F_{FF}'),$$

$$K_2=\frac{r_0}{r}(t_0s_1F_{CF}+t_1s_0F_{CF}'). \tag{14}$$

[19] Only elements on and below the main diagonals are listed since the matrices are symmetrical.

TABLE I. The force constants for $CF_2=CF_2$ and $CH_2=CF_2$ molecules in 10^5 dynes/cm.

$K_{CF}=5.5$	$K_{CH}=4.8$
$H_{FCF}=0.25$	$H_{HCH}=0.3$
$H_{CCF}=0.25$	$H_{CCH}=0.25$
$F_{FF}=1.15$	$F_{HH}=0.1$
$F_{CF}=0.8$	$F_{CH}=0.4$
$K_{CC}=9.2(CF_2=CF_2)$	$K_{CC}=8.4(CH_2=CF_2)$

TABLE II. The comparison of the calculated frequencies with the observed ones for $CF_2=CF_2$ molecules.

Symmetry group	ν_{calc}	ν_{obs}	$\Delta\%$	Designation
A_g	1871	1872	−0.0	C=C stretching
	805	778	+3.5	C−F stretching
	390	394	−1.0	CF_2 deformation
B_{1g}	1434	∼1340	+7.0	C−F stretching
	516	∼544	−5.1	CF_2 rocking
B_{2u}	1300	1335	−2.8	C−F stretching
	238	∼245	−2.9	CF_2 rocking
B_{3u}	1168	1186	−1.5	C−F stretching
	579	558	+3.8	CF_2 deformation

The G matrices described above essentially coincide with those given by Arnett and Crawford.[14]

A set of force constants is chosen to give a reasonable fit with all of the observed frequencies. Such a set of constants is given in the first column of Table I. The constants F' are assumed to be one-tenth of the corresponding constants F. The frequencies calculated with these constants are compared in Table II with those observed by Nielsen *et al.* The agreement is satisfactory except in the case of the frequency 1340 cm^{-1} of B_{1g} group. In fact, it is worthwhile mentioning that the coupling terms in the secular equation of the A_g group makes the C−F stretching frequency far smaller (805 cm^{-1}) than the corresponding frequencies 1434, 1300, and 1186 cm^{-1} of the groups, B_{1g}, B_{2u}, and B_{3u} in conformity with the observed result.

For the calculation of mean amplitudes it is necessary to know L_{ik} in Eq. (1). Now that the reasonable set of force constants has been obtained, we can calculate L_{ik} by the method stated in Sec. 1, using Eqs. (5) and (7),

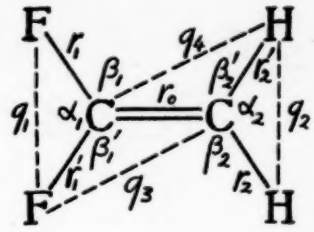

FIG. 2. The internal coordinates of $CH_2=CF_2$ molecule.

$$A_g:\ \begin{array}{c} \\ R_1 \\ R_2 \\ R_3 \end{array}\begin{array}{c} \begin{array}{ccc} x_1 & x_2 & x_3 \end{array} \\ \begin{pmatrix} 0.404 & 0.052 & -0.018 \\ -0.251 & 0.197 & -0.022 \\ 0.597 & 0.132 & 0.367 \end{pmatrix} \end{array}, \qquad B_{1g}:\ \begin{array}{c} \\ R_4 \\ R_5 \end{array}\begin{array}{c} \begin{array}{cc} x_4 & x_5 \end{array} \\ \begin{pmatrix} -0.405 & 0.075 \\ 0.961 & 0.456 \end{pmatrix} \end{array},$$

(15)

$$B_{2u}:\ \begin{array}{c} \\ R_6 \\ R_7 \end{array}\begin{array}{c} \begin{array}{cc} x_6 & x_7 \end{array} \\ \begin{pmatrix} -0.412 & -0.004 \\ 0.182 & 0.262 \end{pmatrix} \end{array}, \qquad B_{3u}:\ \begin{array}{c} \\ R_8 \\ R_9 \end{array}\begin{array}{c} \begin{array}{cc} x_8 & x_9 \end{array} \\ \begin{pmatrix} -0.317 & 0.041 \\ 0.484 & 0.524 \end{pmatrix} \end{array}.$$

The magnitudes of the values of L_{ik} gives us a means of classifying the vibrations. It is customary to name the frequencies as "bond stretching," "deformation," or "rocking," etc., as shown in Table II. At a first glance the values given above seems not to be consistent with these classifications. However, it can be easily seen that, by taking into consideration the contribution of each internal coordinate to the potential energy of the whole molecule, the usual classification such as those given in Table II can be safely applied to this molecule. The detailed discussions will be given in the later paper.

II. $CH_2=CF_2$

The same procedure as that of $CF_2=CF_2$ is applied to this molecule. The symmetry of this molecule is C_{2v}, so that the planar vibrations are divided as $\Gamma=5A_1+4B_1$. The potential function, the symmetry coordinates (see Fig. 2), and the G and F matrices for this molecule are as follows:

$$R_1=\Delta r_0,\quad R_2=\frac{1}{\sqrt{2}}(\Delta r_1+\Delta r_1'),\quad R_3=\frac{1}{\sqrt{2}}(\Delta r_2+\Delta r_2'),\quad R_4=\frac{(6)^{\frac{1}{2}}}{2}r_1\Delta\alpha_1,\quad R_5=\frac{(6)^{\frac{1}{2}}}{2}r_2\Delta\alpha_2;$$

$$R_6=\frac{1}{\sqrt{2}}(\Delta r_1-\Delta r_1'),\quad R_7=\frac{1}{\sqrt{2}}(\Delta r_2-\Delta r_2'),\quad R_8=\frac{1}{\sqrt{2}}r_{01}(\Delta\beta_1-\Delta\beta_1'),\quad R_9=\frac{1}{\sqrt{2}}r_{02}(\Delta\beta_2-\Delta\beta_2'),\quad (16)$$

$$\begin{aligned}2V=&K_{CC}(\Delta r_0)^2+K_{CF}\{(\Delta r_1)^2+(\Delta r_1')^2\}+K_{CH}\{(\Delta r_2)^2+(\Delta r_2')^2\}+H_{FCF}(r_1\Delta\alpha_1)^2+H_{HCH}(r_2\Delta\alpha_2)^2\\&+H_{CCF}\{(r_{01}\Delta\beta_1)^2+(r_{01}\Delta\beta_1')^2\}+H_{CCH}\{(r_{02}\Delta\beta_2)^2+(r_{02}\Delta\beta_2')^2\}+F_{FF}'q_1\Delta q_1+F_{FF}(\Delta q_1)^2\\&+F_{HH}'q_2\Delta q_2+F_{HH}(\Delta q_2)^2+F_{CF}'\{q_3\Delta q_3+q_3'\Delta q_3'\}+F_{CF}\{(\Delta q_3)^2+(\Delta q_3')^2\}+F_{CH}'\{q_4\Delta q_4+q_4'\Delta q_4'\}\\&+F_{CH}\{(\Delta q_4)^2+(\Delta q_4')^2\}\end{aligned}\quad (17)$$

$$G$$

$$A_1\begin{matrix}R_1\\R_2\\R_3\\R_4\\R_5\end{matrix}\begin{pmatrix} 2\mu_0, & & & & \\ -\sqrt{2}c_1\mu_0, & 2c_1^2\mu_0+\mu_1, & & & \\ -\sqrt{2}c_2\mu_0, & 0, & 2c_2^2\mu_0+\mu_2, & & \\ (6)^{\frac{1}{2}}s_1\mu_0, & -2\sqrt{3}s_1c_1\mu_0, & 0, & 6s_1^2\mu_0+3\mu_1, & \\ (6)^{\frac{1}{2}}s_2\mu_0, & 0, & -2\sqrt{3}s_2c_2\mu_0, & 0, & 6s_2^2\mu_0+3\mu_2 \end{pmatrix},$$

$$F$$

$$A_1\begin{matrix}R_1\\R_2\\R_3\\R_4\\R_5\end{matrix}\begin{pmatrix} A_0, & & & & \\ \sqrt{2}C_0, & A+C, & & & \\ \sqrt{2}C_0', & 0, & A'+C', & & \\ -\frac{2}{(6)^{\frac{1}{2}}}K_0, & \frac{1}{\sqrt{3}}(2K_1-K_2), & 0, & \frac{1}{3}\left(2B_0+\frac{1}{\rho_1}B\right), & \\ -\frac{2}{(6)^{\frac{1}{2}}}K_0', & 0, & \frac{1}{\sqrt{3}}(2K_1'-K_2'), & 0, & \frac{1}{3}\left(2B_0'+\frac{1}{\rho_2}B'\right) \end{pmatrix} \tag{18}$$

$$G$$

$$B_1\begin{matrix}R_6\\R_7\\R_8\\R_9\end{matrix}\begin{pmatrix} 2s_1^2\mu_0+\mu_1, & & & \\ 0, & 2s_2^2\mu_0+\mu_2, & & \\ -2s_1\sigma_1\mu_0, & -2s_2\rho_1\mu_0, & 2(\rho_1^2+\sigma_1^2)\mu_0+\frac{1}{\rho_1^2}\mu_1, & \\ -2s_1\rho_2\mu_0, & -2s_2\sigma_2\mu_0, & 2(\rho_2\sigma_1+\rho_1\sigma_2)\mu_0, & 2(\rho_2^2+\sigma_2^2)\mu_0+\frac{1}{\rho_2^2}\mu_2 \end{pmatrix},$$

$$F$$

$$B_1\begin{matrix}R_6\\R_7\\R_8\\R_9\end{matrix}\begin{pmatrix} A-C, & & & \\ 0, & A'-C', & & \\ K_2, & 0, & B, & \\ 0, & K_2', & 0, & B' \end{pmatrix}$$

$$\mu_0=\frac{1}{m_C},\quad \mu_1=\frac{1}{m_F},\quad \mu_2=\frac{1}{m_H}$$

$$r_{01}=(r_0r_1)^{\frac{1}{2}},\qquad r_{02}=(r_0r_2)^{\frac{1}{2}},$$

$$s_1=\sin\frac{\alpha_1}{2},\qquad c_1=\cos\frac{\alpha_1}{2},$$

$$s_2=\sin\frac{\alpha_2}{2},\qquad c_2=\cos\frac{\alpha_2}{2}, \tag{19}$$

$$s_{ij}=\frac{r_i-r_j\cos\alpha_{ij}}{q_{ij}},\qquad t_{ij}=\frac{r_j}{q_{ij}}\sin\alpha_{ij},$$

$$q_{ij}^2=r_i^2+r_j^2-2r_ir_j\cos\alpha_{ij},$$

$$\rho_1^2=r_1/r_0,\qquad \sigma_1=\rho_1+c_1/\rho_1,$$

$$\rho_2^2=r_2/r_0,\qquad \sigma_2=\rho_2+c_2/\rho_2,$$

and

$$\begin{aligned}
A_0&=K_{CC}+2(s_{01}^2F_{CF}+t_{01}^2F_{CF}'+s_{02}^2F_{CH}+t_{02}^2F_{CH}'),\\
A&=K_{CF}+s_{10}^2F_{CF}+t_{10}^2F_{CF}'+s_1^2F_{FF}+c_1^2F_{FF}',\\
A'&=K_{CH}+s_{20}^2F_{CH}+t_{20}^2F_{CH}'+s_2^2F_{HH}+c_2^2F_{HH}',\\
C_0&=s_{10}s_{01}F_{CF}-t_{10}t_{01}F_{CF}',\\
C_0'&=s_{20}s_{02}F_{CH}-t_{20}t_{02}F_{CH}',\\
C&=s_1^2F_{FF}-c_1^2F_{FF}',\\
C'&=s_2^2F_{HH}-c_2^2F_{HH}',\\
B_0&=H_{FCF}+c_1^2F_{FF}-s_1^2F_{FF}',\\
B_0'&=H_{HCH}+c_2^2F_{HH}-s_2^2F_{HH}',\\
B&=H_{CCF}+t_{10}t_{01}F_{CF}-s_{10}s_{01}F_{CF}',\\
B'&=H_{CCH}+t_{20}t_{02}F_{CH}-s_{20}s_{02}F_{CH}',\\
K_0&=s_{01}t_{10}F_{CF}+s_{10}t_{01}F_{CF}',\\
K_0'&=s_{02}t_{20}F_{CH}+s_{20}t_{02}F_{CH}',\\
K_1&=c_1s_1(F_{FF}+F_{FF}'),\\
K_1'&=c_2s_2(F_{HH}+F_{HH}'),\\
K_2&=(s_{10}t_{01}F_{CF}+s_{01}t_{10}F_{CF}')/\rho_1,\\
K_2'&=(s_{20}t_{02}F_{CH}+s_{02}t_{20}F_{CH}')/\rho_2,
\end{aligned} \tag{20}$$

where the G matrices perfectly coincide with those given by Edgell and Byrd.[7] The force constants used are listed in Table I. The constants, with which the F atoms are concerned, are assumed to be the same as those of $CF_2=CF_2$, and the constants, with which the H atoms are concerned, the same as those of $CH_2=CH_2$ molecule.[20] Because the force constant K_{CC} for the C=C stretching displacement has been found to have an appreciably different value for $CF_2=CF_2$ (9.2×10^5 dynes/cm) from that of $CH_2=CH_2$ (7.5×10^5 dynes/cm), an algebraic mean of them 8.4×10^5 dynes/cm is assumed for $CH_2=CF_2$. The calculated frequencies by the use of these constants are compared in Table III with the observed values. The assignment of the fundamental frequencies has been carried out both by Edgell and Byrd and by Nielsen, Claassen, and Smith. They have arrived at quite the same conclusion except the C–H deformation frequency of A_1 type. Our calculation gives 1422 cm^{-1} in good agreement with the Nielsen's value 1414 cm^{-1}. It is interesting, indeed, to note that the satisfactory agreement is obtained by assuming

(18)

TABLE III. The comparison of the calculated frequencies with the observed ones for $CH_2=CF_2$ molecules.

Symmetry group	ν_{calc}	ν_{obs} (Nielsen *et al.*)	Δ%	ν_{obs} (Edgell and Byrd)	Designation
	3034	3060	−0.8	···	C–H stretching
	1755	1728	+1.6	1734	C=C stretching
A_1	1422	1414	+0.6	1370	C–H deformation
	938	926	+1.3	924	C–F stretching
	526	550	−4.3	549	C–F deformation
	3085	3103	−0.6	···	C–H stretching
B_1	1371	1302	+5.3	1300	C–F stretching
	973	955	+1.9	954	C–H deformation
	458	438	+4.6	439	C–F deformation

the same force constants as those of the $CF_2=CF_2$ molecule. The transformation matrices L_{ik} are calculated as follows:

$$A_1:\quad \begin{array}{c} \\ R_1 \\ R_2 \\ R_3 \\ R_4 \\ R_5 \end{array} \begin{array}{c} \begin{array}{ccccc} x_1 & x_2 & x_3 & x_4 & x_5 \end{array} \\ \begin{pmatrix} 0.070 & 0.389 & -0.061 & -0.080 & -0.013 \\ -0.001 & -0.203 & 0.114 & -0.231 & 0.011 \\ -1.018 & 0.029 & 0.034 & -0.002 & -0.001 \\ 0.004 & 0.437 & 0.211 & 0.122 & 0.493 \\ 0.201 & 0.710 & 1.660 & 0.194 & 0.031 \end{pmatrix} \end{array} \tag{21}$$

(20)

$$B_1:\quad \begin{array}{c} \\ R_6 \\ R_7 \\ R_8 \\ R_9 \end{array} \begin{array}{c} \begin{array}{cccc} x_6 & x_7 & x_8 & x_9 \end{array} \\ \begin{pmatrix} 0.001 & -0.379 & 0.143 & -0.024 \\ -1.055 & -0.007 & -0.015 & -0.008 \\ 0.134 & 0.625 & 0.073 & -0.468 \\ 0.179 & 0.721 & 1.070 & 0.146 \end{pmatrix} \end{array}$$

3. THE MEAN-SQUARE AMPLITUDES OF THE ATOMIC DISTANCES IN $CF_2=CF_2$ AND $CH_2=CF_2$ MOLECULES

Let us consider first the case of $CF_2=CF_2$ molecule. As stated in Sec. 2, in order to calculate mean amplitudes of thermal vibration of atomic distances it is necessary to express the displacements of atomic distances in terms of the normal coordinates. In the first place the displacements of the bond distances, C=C and C–F, are easily written in terms of the symmetry coordinates by the use of the relations (11); thus

$$\Delta r_0 = R_1, \tag{22}$$

and

$$\Delta r_1 = \tfrac{1}{2}(R_2+R_4+R_6+R_8). \tag{23}$$

Secondly, as for the displacement Δq of the distance between the atoms which are bonded to the same carbon atom with the distances r_1, r_2 and with the bond angle α as shown in Fig. 3(a), the following relation is easily obtained,

$$\Delta q = \frac{1}{q}\{(r_1-r_2\cos\alpha)\Delta r_1+(r_2-r_1\cos\alpha)\Delta r_2 + r_1 r_2 \sin\alpha \Delta\alpha\}, \tag{24}$$

and for the displacement Δp of the distance between the atoms which are bonded to the adjacent carbon atoms with the distances r_1, r_2 and with the bond angles α and β as shown in Fig. 3(b), we get

$$\begin{aligned}\Delta q' = \frac{1}{q'}[&\{R-r_1\cos\alpha-r_2\cos\beta\}\Delta R \\ &+\{r_1-R\cos\alpha+r_2\cos(\alpha+\beta)\}\Delta r_1 \\ &+\{r_2-R\cos\beta+r_1\cos(\alpha+\beta)\}\Delta r_2 \\ &+\{Rr_1\sin\alpha-r_1r_2\sin(\alpha+\beta)\}\Delta\alpha \\ &+\{Rr_2\sin\beta-r_1r_2\sin(\alpha+\beta)\}\Delta\beta].\end{aligned} \tag{25}$$[21]

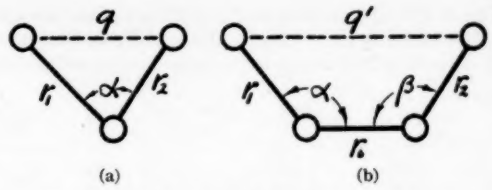

FIG. 3. Correlations between atomic distances.

Hence, inserting the numerical values of the molecular parameters, the displacement of the distance between the two F atoms in CF_2 group, that of the F atom and the C atom bonded to the same C atom, and those of the *cis* and the *trans* F···F distances can be written as follows:

$$\begin{aligned}\Delta q_{FF} &= 0.8387(R_2+R_8)+0.3144(R_3+R_9), \\ \Delta q_{CF} &= 0.8788R_1+0.4394(R_2+R_4+R_6+R_8) \\ &\quad -0.1378(R_3+R_9)+0.2386(R_5+R_7), \\ \Delta q_{cis}' &= R_1+0.5446(R_2+R_6)-0.4842R_3+0.8388R_7, \\ \Delta q_{trans}' &= 0.7798R_1+0.9498(R_2+R_4) \\ &\quad -0.1807R_3+0.3131R_5.\end{aligned} \tag{26}$$

[20] The result of the normal coordinate treatment of ethylene molecule will be published in the near future.

[21] In Eqs. (24) and (25) r_0, r_1, r_2, α, and β in the coefficients denote their equilibrium values.

TABLE IV. The mean-square amplitudes of the normal vibrations in $CF_2=CF_2$ and $CH_2=CF_2$ molecules.

Symmetry group	ν_i*	$\langle\Delta x_i^2\rangle$ (10^{-26}gA^2)	Symmetry group	ν_i*	$\langle\Delta x_i^2\rangle$ (10^{-26}gA^2)
	1872	1.495		3060	0.915
A_g	778	3.759		1728	1.620
	394	9.506	A_1	1414	1.983
				926	3.087
B_{1g}	1340	2.094		550	5.823
	544	5.911			
B_{2u}	1337	2.099		3103	0.902
	245	21.239	B_1	1302	2.157
				955	2.985
B_{3u}	1186	2.374		438	8.076
	558	5.711			

* The ν_i are the observed frequencies.

These displacements may be expressible in terms of the normal coordinates by the use of the coefficients (15). Squaring them and taking their mean, the required mean-square amplitudes of the displacements of these distances can be represented by the series of terms, the mean-square amplitudes of each normal coordinate times the coefficients L_{ik}, e.g.,

$$\langle\Delta r_0^2\rangle = L_{11}^2\langle x_1^2\rangle + L_{12}^2\langle x_2^2\rangle + L_{13}^2\langle x_3^2\rangle,$$
$$\langle\Delta r_1^2\rangle = \tfrac{1}{4}[L_{21}^2\langle x_1^2\rangle + L_{22}^2\langle x_2^2\rangle + L_{23}^2\langle x_3^2\rangle + L_{44}^2\langle x_4^2\rangle + L_{45}^2\langle x_5^2\rangle + L_{66}^2\langle x_6^2\rangle + L_{67}^2\langle x_7^2\rangle + L_{88}^2\langle x_8^2\rangle + L_{89}^2\langle x_9^2\rangle], \quad (27)$$

and so on. Now by the use of the mean-square amplitudes of the normal vibrations which are listed in Table IV together with the coefficients L_{ik} given in (15), the final result for the mean amplitudes of all the atomic distances in $CF_2=CF_2$ molecule are obtained. In Table V the contribution to the mean amplitude from each normal coordinate is tabulated. The same procedure has been applied to the case of $CH_2=CF_2$ as shown in Table VI. The calculated values are compared in Table VII with the values observed by I. Karle and J. Karle. As they have already pointed out, the mean amplitudes are in all cases a few percents of the atomic distances themselves, and they increase with longer atomic distances. Further, in the case of $CH_2=CF_2$ they are in very good agreement with the observed, whereas in the case of $CF_2=CF_2$ the observed values are larger than the calculated. I. Karle and J. Karle stated that it was one of their important results that the mean amplitudes are about 50 percent larger in $CF_2=CF_2$ than in $CH_2=CF_2$. Contrary to their result, the calculated amplitudes are found to be of almost equal values for both molecules. This is of course a natural conclusion, since the same force constants have been assumed in either case. Therefore, it seems to us very unlikely that such a great discrepancy could exist between the amplitudes of the two molecules.

Let us discuss the minute details of each mean amplitude. The amplitude of the C=C bond length, 0.039A, is almost entirely attributed to the vibration ν_1 just as expected. For this mean amplitude I. Karle and J. Karle assumed 0.03A which seems in fact to be slightly smaller. For the C−F bond length the calculated value perfectly coincides with that obtained by I. Karle and J. Karle (see Table V). They mainly consist of the terms due to the four C−F stretching vibrations ν_2, ν_4, ν_6, and ν_8. For the F···F distance in CF_2 group a slightly smaller value than the observed is obtained. It may be expected that the CF_2 deformation vibrations primarily contribute to this mean amplitude, but actually the C−F stretching vibration ν_2 contributes more than the deformation vibration ν_3. For the C···F distance the calculated value agrees well with the observed. This mean amplitude is mainly a result of the rocking vibrations ν_5 and ν_7, as expected, in addition to the stretching vibration ν_8.

TABLE V. The mean-square amplitudes of the atomic distances in $CF_2=CF_2$ molecules.

Symmetry group	Normal coordinate	The terms contributing to $\langle\Delta R^2\rangle$ from each normal coordinate (in 10^{-4} A^2)					
		C=C	C−F	F.....F \ C	F / C=C	*cis* F...F	*trans* F...F
A_g	x_1 ν(C=C)	14.72	1.42	0.05	2.39	0.04	0.09
	x_2 ν(C−F)	0.62	2.19	9.66	2.96	2.06	9.39
	x_3 δ(C−F)	0.18	0.07	5.42	3.29	24.66	5.83
B_{1g}	x_4 ν(C−F)	···	5.18	···	0.33	···	0.89
	x_5 γ(C−F)	···	0.49	···	7.13	···	16.22
B_{2u}	x_6 ν(C−F)	···	5.37	···	2.39	0.65	···
	x_7 γ(C−F)	···	0.00	···	4.75	60.79	···
B_{3u}	x_8 ν(C−F)	···	3.59	1.83	6.06	···	···
	x_9 δ(C−F)	···	0.15	13.69	1.00	···	···
	$\langle\Delta R^2\rangle$	15.52	18.46	30.65	30.30	88.20	32.42
	$(\langle\Delta R^2\rangle)^{\frac{1}{2}}$ A	0.0394	0.0430	0.0554	0.0550	0.0939	0.0569

TABLE VI. The mean-square amplitudes of the atomic distances in $CH_2=CF_2$ molecules.

		C=C	C−C	F.....F (C)	F (C=C)	C−H	H.....H (C)	H (C=C)	*cis* H....F	*trans* H....H
A_1	x_1 ν(C−H)	0.27	0.00	0.00	0.20	28.52	71.74	19.08	6.40	23.01
	x_2 ν(C=C)	14.78	2.01	0.09	1.79	0.04	11.12	4.35	0.75	0.10
	x_3 δ(C−H)	0.44	0.77	0.13	0.39	0.07	67.02	18.94	33.69	3.42
	x_4 ν(C−F)	1.19	4.95	8.19	10.61	0.00	1.20	2.50	15.85	13.03
	x_5 δ(C−F)	0.06	0.02	20.76	3.29	0.00	0.05	0.13	10.92	1.70
B_1	x_6 ν(C−H)	···	0.00	···	0.11	30.22	···	17.51	5.61	21.15
	x_7 ν(C−F)	···	9.31	···	0.15	0.00	···	7.70	6.45	0.25
	x_8 δ(C−H)	···	1.84	···	2.33	0.02	···	23.08	44.16	22.13
	x_9 δ(C−F)	···	0.14	···	13.71	0.02	···	1.00	59.53	3.87
	$\langle\Delta R^2\rangle$	16.74	19.04	29.17	32.58	58.89	151.13	94.29	183.36	88.66
	$(\langle\Delta R^2\rangle)^{\frac{1}{2}}$ A	0.0409	0.0436	0.0540	0.0570	0.0767	0.123	0.091	0.135	0.094

The most important result is that the *cis* F···F distance has the largest mean amplitude in spite of its shorter distance than the *trans* F···F distance. From the symmetry consideration it is evident that the vibrations of B_{1g} and B_{3u} groups do not contribute to this displacement. The contribution is constituted mainly of those by the rocking vibration ν_7 and the deformation vibration ν_3, both of which have low frequencies so that their contributions predominate in $\langle\Delta R^2\rangle$, as evident from Eq. (4). For the *trans* F···F distance the calculated value is definitely smaller than the observed. The displacement of this distance is caused by the rocking vibration ν_5 of B_{1g}, as well as the vibrations ν_2 and ν_3 of A_g group. The vibrations antisymmetric to the center of symmetry do not contribute to this amplitude.

As stated above, the *trans* distance, the longest in this molecule, has smaller amplitude than the *cis* distance. This is attributed to the facts that ν_2 and ν_5, which provide the greatest part of the amplitude of the *trans* distance, have larger frequencies than those of the vibration ν_3 and ν_7 which provide the greatest part of the amplitude of the *cis* distance and that the mean amplitude rapidly increases with decreasing frequencies. This fact is an important result of the present computation. It would be very interesting and, in fact, worthwhile to reinvestigate the mean amplitudes of the *trans* and the *cis* distances for the purpose of confirming the conclusions of this computation.

Almost the same discussions can be given for the case of $CH_2=CF_2$. It should be pointed out that the distances in which H atoms take part have exceptionally large mean amplitudes. Although their detailed discussions will be postponed till the second part of this article, it would be very interesting to note that the mean amplitude of the *cis* displacement is also larger than that of the *trans* one.

TABLE VII. The comparison of the calculated mean amplitudes with the observed values.

Atomic distance	$CF_2=CF_2$ R_g A	$CF_2=CF_2$ $(\langle\Delta R^2\rangle)^{\frac{1}{2}}$ calc A	$CF_2=CF_2$ $(\langle\Delta R^2\rangle)^{\frac{1}{2}}$ obs A	$CH_2=CF_2$ R_g A	$CH_2=CF_2$ $(\langle\Delta R^2\rangle)^{\frac{1}{2}}$ calc A	$CH_2=CF_2$ $(\langle\Delta R^2\rangle)^{\frac{1}{2}}$ obs A
C=C	1.313	0.0394	···	1.313	0.0409	···
C−F	1.313	0.0430	0.056	1.321	0.0436	0.042
F.....F (C)	2.204	0.0554	0.087	2.162	0.0540	0.060
F (C=C)	2.306	0.0550	0.095	2.335	0.0571	0.060
cis F.....F	2.737	0.0939	0.090	···	···	···
trans F.....F	3.515	0.0569	0.114	···	···	···
C−H	···	···	···	1.07	0.0767	···
H----H (C)	···	···	···	1.89	0.123	···
H (C=C)	···	···	···	2.06	0.09	···
cis H.....H	···	···	···	2.61	0.135	···
trans H.....H	···	···	···	3.29	0.094	···

ACKNOWLEDGMENTS

The authors wish to express their gratitude to Professor S. Mizushima for many helpful discussions during the course of this research. The expense of this work was defrayed from the Scientific Research Encouragement Grant of the Department of Education of Japan, to which the authors' thanks are also due.

On the Cubic Law of Oxidation*

J. T. WABER
University of California, Los Alamos Scientific Laboratory, Los Alamos, New Mexico
(Received January 2, 1952)

Experimental and theoretical studies are reviewed to indicate that a cubic law of oxidation occurs at low temperatures. Data for tantalum and titanium have been presented to indicate that this growth law may apply to more metals than suspected in the past.

THE purpose of this paper is to summarize the existing information on the cubic law of oxidation and to present new data obtained with tantalum and titanium which indicate that the law may have a greater range of applicability than has been generally expected. Mott[1] predicted this law in 1940 and showed that it might occur under conditions when the logarithmic law had failed. Experimentally it has been observed at temperatures between those at which the logarithmic and parabolic are obtained.

Mott proposed that a cubic law for oxidation might be obtained if large space charges formed in the oxide layers. Anderson[2] independently extended this idea and demonstrated that either a cubic or a quartic law would obtain over different thickness intervals as a result of the laws governing current limited by space charge in the oxide or scale. He plotted the data of others to indicate that parabolic, cubic, and quartic laws obtained over limited time intervals in the course of oxidation. Cabrera[3] reported that a cubic law could result from a specific distribution of lattice vacancies.

However, these authors cite no experimental evidence to substantiate the fact that this growth law would obtain over an extended time range. Rhodin[4] has confirmed the results of Campbell and Thomas[5] on copper. Both found that copper gave a cubic law at temperatures less than 100°C. Figure 6 of the paper by Campbell and Thomas indicates that a number of copper base alloys corrode according to this growth law. The slope on a log-log plot varies from 0.25 to 0.38 which is, of course, the reciprocal of the exponent n in the general growth law.

$$W^n = kt. \tag{1}$$

It should be noted that Vernon[6] found that his data on the oxidation of iron in the range 25° to 100°C could be represented by a law where

$$W^{2.5} = kt. \tag{2}$$

Apparently neither a cubic nor a log-log plot was made to determine the exact index, but the fact that the exponent is larger than two is significant.

The oxidation of copper at low temperatures proceeds according to a logarithmic law as Rhodin[4] and Mehl and Lustman[7] showed. Valensi[8] has reviewed the high temperature parabolic oxidation of copper. Analysis of such results indicates that the oxidation by

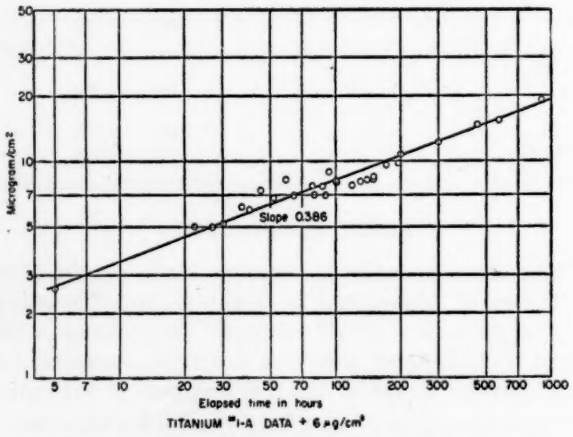

FIG. 1. Log-log plot demonstrating a cubic law for the oxidation of titanium.

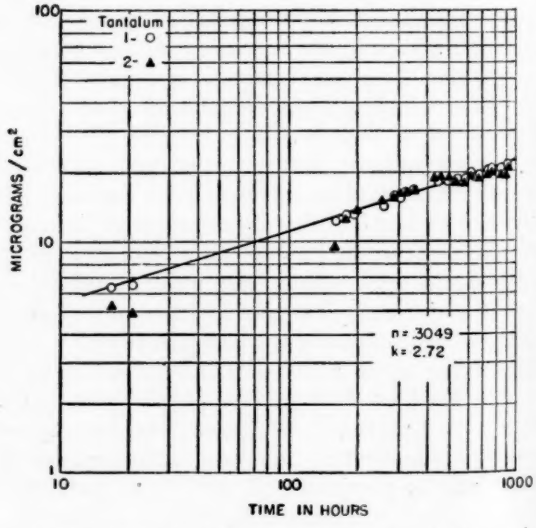

FIG. 2. Log-log plot demonstrating a cubic law for the oxidation of tantalum.

* Work done under the auspices of the AEC.
[1] N. F. Mott, Trans. Faraday Soc. **36**, 472 (1940).
[2] S. Anderson, Phys. Rev. **69**, 52 (1946).
[3] M. Cabrera, Phil. Mag. **40**, 175 (1949).
[4] T. N. Rhodin, J. Am. Chem. Soc. **72**, 5102 (1950).
[5] W. E. Campbell and U. B. Thomas, Trans. Electrochem. Soc. **91**, 623 (1947).
[6] W. H. J. Vernon, Trans. Faraday Soc. **31**, 1668 (1935).
[7] R. F. Mehl and B. Lustman, Trans. Am. Inst. Mining Met. Engrs. **143**, 246 (1941).
[8] G. Valensi, Pittsburgh International Conference on Surface Reactions, 156 (1948).

the cubic law occurs in the temperature range between the other two laws but overlaps the logarithmic ones.

Evans[9] states that iron corrodes logarithmically at temperatures below 195°C and parabolically at higher temperatures. Hence, Vernon's work indicates that the cubic law holds under some conditions where neither of the other two laws obtain. In this case the temperature range of the cubic law overlaps that of the logarithmic. A similar phenomenon occurs with titanium and tantalum.

The author[10] has shown in previous studies that both titanium and tantalum corrode at temperatures near 325°C by the logarithmic law and has shown that above 350°C a parabolic law obtains for tantalum. Gulbransen and Andrew[11] demonstrated that titanium oxidizes parabolically for temperatures above 350°C. Figures 1 and 2 show data for tantalum and titanium, respectively, which indicate cubic laws are obtained in the range that the logarithmic law is observed. In the former figure the run was conducted at 216°C; while in the latter the oxidation temperature was 350°C. How the metal decides which growth law to follow is not known nor are the factors which influence the choice in the overlap region of temperatures known.

[9] U. R. Evans, Trans. Electrochem. Soc. **91**, 547 (1947).
[10] J. T. Waber *et al.* [to be puslished in J. Electrochem. Soc. (1952)].
[11] E. A. Gulbransen and K. Andrew, J. Metals **1**, 741 (1949).

THE JOURNAL OF CHEMICAL PHYSICS VOLUME 20, NUMBER 4 APRIL, 1952

The Microwave Spectra and Molecular Structures of Methyl Bromoacetylene and Methyl Iodoacetylene*

JOHN SHERIDAN† AND WALTER GORDY
Department of Physics, Duke University, Durham, North Carolina
(Received December 11, 1951)

Pure rotation spectra of H_3CCCBr^{79}, H_3CCCBr^{81}, and H_3CCCI have been measured. For H_3CCCBr^{79}, $B_0=1561.11$ Mc/sec, $I_B=537.379\times10^{-40}$ g cm², and $D_{JK}=+11.4$ kc/sec; for H_3CCCBr^{81}, $B_0=1550.42$ Mc/sec, $I_B=541.082\times10^{-40}$ g cm², and $D_{JK}=+11.1$ kc/sec; for H_3CCCI, $B_0=1259.02$ Mc/sec, $I_B=666.316\times10^{-40}$ g cm², and $D_{JK}=+7.2$ kc/sec. The nuclear quadrupole coupling factors (eqQ) for the halogens are: for Br^{79}, +647 Mc/sec; for Br^{81}, +539 Mc/sec; for I^{127}, −2230 Mc/sec. On the basis of reasonable assumptions for $d_{C\equiv C}$, d_{CH}, and $\angle HCH$, it is shown that the C−C and C−Br bonds in H_3CCCBr are shortened to extents comparable with those found in methyl acetylene and cyanogen bromide, respectively, while the I_B of methyl iodoacetylene is consistent with a similar shortening of both C−C and C−I. This is supported by the force constants for the stretching of the C−Br and C−I bonds. Bond lengths and nuclear quadrupole couplings are discussed in relation to the structures of these molecules.

INTRODUCTION

METHYL bromoacetylene, H_3CCCBr, and methyl iodoacetylene, H_3CCCI, have been studied previously by Raman spectroscopy,[1] but no data have hitherto been available on the internuclear distances in these molecules. Since interest attaches to these distances, and to the nuclear quadrupole coupling factors of the halogens in these substances, we have measured the microwave pure rotation spectra of their principal isotopic combinations. From these the nuclear quadrupole coupling factors are obtained, and deductions can be made about the interatomic distances on the basis of justifiable assumptions about certain structural parameters.

* The research reported in this paper has been made possible through sponsorship extended by the Geophysical Research Directorate of Air Force Cambridge Research Laboratories under Contract No. W19-122-ac-35.
† Present address: Department of Chemistry, University of Birmingham, England.
[1] F. F. Cleveland and M. J. Murray, J. Chem. Phys. **11**, 450 (1943).

EXPERIMENTAL

Methyl bromo- and methyl iodoacetylene were made by the methods described by Cleveland and Murray.[1] Samples of about 50 g were finally distilled in vacuum and the center fractions collected. As slow decomposition occurred at room temperature, these were preserved at −70°C.

The spectra were observed with a video sweep spectometer[2] and measured with a frequency standard monitored against station WWV. Gas pressures of about 10^{-3} mm of Hg were used. For methyl bromoacetylene the temperature was −70°, but at this temperature the vapor pressure of methyl iodoacetylene was too small for spectra to be observed, and measurements were made at room temperature.

RESULTS

The regularity of the spectra confirmed that the molecules are symmetric tops. Transitions observed were $J=8\rightarrow9$, $9\rightarrow10$, and $11\rightarrow12$ for H_3CCCBr^{79};

[2] W. Gordy and M. Kessler, Phys. Rev. **72**, 644 (1947).

TABLE I. Molecular constants.

Molecule	Transition $J \rightarrow J'$	Unperturbed frequency Mc/sec ±0.1	B_0[a] Mc/sec	I_B[b] $\times 10^{-40}$ g cm^2	D_{JK} kc/sec	eqQ for halogen Mc/sec
H_3CCCBr^{79}	8→9	28,099.90	1561.11	537.378	+11.4	+647
H_3CCCBr^{81}	8→9	27,907.60	1550.42	541.082	+11.1	+539
H_3CCCI	12→13	37,770.57	1259.02	666.316	+7.2	−2230

[a] Calculated assuming $D_J = 0$.
[b] Calculated taking Planck's constant $= 6.62373 \times 10^{-27}$ erg sec and 1 amu. $= 1.65972 \times 10^{-40}$ g from J. W. M. Dumond and E. R. Cohen, Revs. Modern Phys. 21, 651 (1949). In view of possible error in Planck's constant, the last two figures quoted for I_B have relative significance only.

8→9 and 11→12 for H_3CCCBr^{81}; and $J = 12 \rightarrow 13$, 14→15, and 16→17 for H_3CCCI. Table I gives the unperturbed frequencies for accurately measured transitions, with values of B_0, moments of inertia I_B, distortion coefficients D_{JK}, and the halogen nuclear quadrupole couplings, eqQ. These values of D_{JK} and eqQ are those used in calculating the hyperfine structures of these transitions for CH_3CCBr^{81} and CH_3CCI^{127} which are compared with the observed frequencies in Tables II and III.

These measurements refer to molecules in the ground state. In all cases, further groups of lines were observed at frequencies slightly higher than those of the main transitions, and of somewhat weaker intensity. These are almost certainly due to molecules in excited bending vibrational states. The bending vibrations designated by Meister[3] as type E, ν_5 have frequencies of only 171 cm^{-1} and 163 cm^{-1} in methyl bromo- and methyl iodoacetylene, respectively, and their excited levels would, therefore, be considerably populated even at −70°. The λ bending vibration type E, ν_4 would also be easily excited, having a frequency of only 343 cm^{-1} in these molecules. The rotational spectra of these excited states correspond to a value of I_B roughly 0.7×10^{-40} g cm^2 less than that for the ground state, and they are well separated from the hyperfine structures of the ground-state spectra.

The intensities of the observed spectra show that methyl bromo- and methyl iodoacetylene have appreciable electric dipole moments, though these have not been previously studied. Bromoacetylene, HCCBr, though structurally simpler, has the disadvantage from the viewpoint of microwave spectroscopy of an extremely small dipole moment.[4] Since acetylene and bromoacetylene have very similar moments, we might expect methyl bromoacetylene to have roughly the same moment as methyl acetylene, $0.77D$.[5] We hope to determine the dipole moments of methyl bromo- and methyl iodoacetylene later by the Stark effect on their spectra.

[3] A. G. Meister, J. Chem. Phys. **16**, 950 (1948).
[4] L. O. Brockway and I. E. Coop, Trans. Faraday Soc. **34**, 1429 (1938).
[5] F. J. Krieger and H. H. Wenzke, J. Am. Chem. Soc. **60**, 2115 (1938).

DISCUSSION

The molecules treated here have five structural parameters. In the case of methyl bromoacetylene it is necessary to assume three of these until data for other isotopic combinations are obtained. Since the most interesting distances are those of the C−Br and C−C "single" bonds, and since it is known that the length of the C≡C triple bond and the configuration of the methyl group remain nearly constant despite considerable variations in the nature of the attached groups,[6-10] we have assumed $d_{C\equiv C}$, d_{CH}, and ∠HCH and so determined d_{C-C} and d_{CBr}. We have also determined the effects of variations in these assumed parameters on the values of d_{C-C} and d_{CBr}.

Table IV shows sets of parameters which are con-

TABLE II. Observed and calculated hyperfine structure for the $J = 8 \rightarrow 9$ transition of H_3CCCBr^{81}. Frequencies are calculated for $D_{JK} = 11.1$ kc/sec and $eqQ = 539$ Mc/sec.

$J \rightarrow J'$	Transition K	$F \rightarrow F'$	Calc. frequency Mc/sec	Obs. frequency Mc/sec
8→9	7	15/2→17/2	27,918.82	27,918.60
	5	17/2→19/2	27,918.68	
	6	15/2→17/2	27,916.26	27,916.40
	4	17/2→19/2	27,914.33	27,914.35
	5	15/2→17/2	27,914.10	
	4	15/2→17/2	27,912.33	27,912.39
	3	17/2→19/2	27,910.94	27,910.92
	3	15/2→17/2	27,910.90	
	2	15/2→17/2	27,909.98	27,910.00
		13/2→15/2	27,909.19	
	0	15/2→17/2	27,909.19	27,909.17
	1	15/2→17/2	27,909.38	
	2	17/2→19/2	27,908.52	27,908.37
	1	13/2→15/2	27,908.26	
	1	17/2→19/2	27,907.07	27,907.14
	0	19/2→21/2	27,906.59	27,906.60
		17/2→19/2		
	1	19/2→21/2	27,905.94	27,906.09
	2	13/2→15/2	27,905.48	27,905.53
	2	19/2→21/2	27,904.03	27,904.18
	3	13/2→15/2	27,900.85	27,900.86
	3	19/2→21/2	27,900.84	
	4	19/2→21/2	27,896.36	27,896.59
	4	13/2→15/2	27,894.36	27,894.38
	5	19/2→21/2	27,890.61	27,890.79

[6] R. Trambarulo and W. Gordy, J. Chem. Phys. **18**, 1613 (1950).
[7] Kessler, Ring, Trambarulo, and Gordy, Phys. Rev. **79**, 54 (1950).
[8] Westenberg, Goldstein, and Wilson, J. Chem. Phys. **17**, 1319 (1949).
[9] A. A. Westenberg and E. B. Wilson, J. Am. Chem. Soc. **72**, 199 (1950).
[10] Gordy, Simmons, and Smith, Phys. Rev. **74**, 243 (1948).

TABLE III. Observed and calculated hyperfine structure for the $J=12\rightarrow13$ transition of H_3CCCI. Frequencies are calculated for $D_{JK}=7.2$ kc/sec and $eqQ=-2230$ Mc/sec.

$J\rightarrow J'$	Transition K	$F\rightarrow F'$	Calc. frequency Mc/sec	Obs. frequency Mc/sec
12→13	6	29/2→31/2	32,753.14	32,752.83
	5	19/2→21/2	32,749.76	32,748.69
	5	29/2→31/2	32,748.11	32,747.90
	4	29/2→31/2	32,743.97	32,743.89
	4	19/2→21/2	32,743.23	
	3	29/2→31/2	32,740.76	32,740.77
	0	27/2→29/2	32,738.34	32,738.45
	2	29/2→31/2	32,738.48	
	1	27/2→29/2	32,737.79	32,737.72
	1	29/2→31/2	32,737.10	32,737.22
	0	29/2→31/2	32,736.64	32,736.69
	2	27/2→29/2	32,736.09	32,736.05
	0	25/2→27/2	32,735.44	32,735.35
	1	25/2→27/2	32,734.56	32,734.45
	2	19/2→21/2	32,734.51	32,734.26
	3	27/2→29/2	32,733.33	32,733.05
	1	19/2→21/2	32,732.32	32,732.18
	2	25/2→27/2	32,731.97	32,731.83
	0	19/2→21/2	32,731.60	32,731.52
	0	23/2→25/2	32,731.40	32,731.19
	1	23/2→25/2	32,730.74	32,730.52
	4	27/2→29/2	32,729.43	32,729.7
	0	21/2→23/2	32,729.26	
	1	21/2→23/2	32,729.18	32,729.00
	2	21/2→23/2	32,728.96	
	2	23/2→25/2	32,728.80	32,728.68
	3	21/2→23/2	32,728.58	
	4	23/2→25/2	32,728.07	32,728.14
	3	25/2→27/2	32,727.62	32,727.74
	3	19/2→21/2	32,727.49	32,727.32
	5	21/2→23/2	32,727.41	32,727.10
	6	21/2→23/2	32,726.58	32,726.06
	3	23/2→25/2	32,725.53	32,725.28
	7	21/2→23/2	32,725.62	
	5	27/2→29/2	32,724.42	32,724.73
	8	21/2→23/2	32,724.50	
	9	21/2→23/2	32,723.26	32,723.61
	4	25/2→27/2	32,721.53	32,721.36
	4	23/2→25/2	32,720.93	32,720.85
	6	27/2→29/2	32,718.28	32,717.22
	5	23/2→25/2	32,715.06	32,714.74
	5	25/2→27/2	32,713.72	32,713.35
	6	23/2→25/2	32,707.85	32,707.68

sistent with the I_B values, zero-point energy effects being neglected. The values for $d_{C\equiv C}$, d_{CH}, and $\angle HCH$ which are assumed are based on the values found in the related molecules methyl acetylene,[6] methyl cyanide,[7] or chloroacetylene.[8] In methyl acetylene d_{CH} is 1.097 ±0.01A and $\angle HCH$ is 108°14′±45′; in methyl cyanide, d_{CH} is 1.092A and $\angle HCH$ is 109°8′, to about the same degrees of accuracy. In methyl acetylene, $d_{C\equiv C}$ is 1.207A; and in chloroacetylene, $d_{C\equiv C}$ is 1.211A. The parameters in Table IV illustrate the effects of variations in each assumed parameter in turn on the values of d_{C-C} and d_{CBr}. The first two sets of parameters differ only in $\angle HCH$, and it is seen that a reduction of $\angle HCH$ by one degree lowers d_{C-C} by about 0.004A and has scarcely any effect on d_{CBr}. The next two sets differ only in d_{CH} and show that a decrease in d_{CH} of 0.01A raises d_{C-C} by 0.002A or less and lowers d_{CBr} by less than 0.001A. Finally, we see that lowering $d_{C\equiv C}$ from 1.211A to 1.207A increases d_{C-C} by 0.003A and increases d_{CBr} by only about 0.001A.

From these facts we can estimate that, if variations of ±0.01A in d_{CH}, ±1° in $\angle HCH$, and ±0.004 in $d_{C\equiv C}$ are allowed, the uncertainty in d_{C-C} will be about ±0.02A and that in d_{CBr} about 0.005A. If zero-point energy effects are neglected, the probable errors are likely to be less than these, but some allowance has been made for such effects. The chief source of uncertainty would seem to be the value assumed for $d_{C\equiv C}$.

A good choice of final parameters is:

$$\left.\begin{aligned} d_{C\equiv C}&=1.207\pm0.004\text{A}\\ d_{CH}&=1.092\pm0.01\text{A}\\ \angle HCH&=109°8'\pm1° \end{aligned}\right\}\text{assumed}\qquad \begin{aligned} d_{C-C}&=1.46\ \pm0.02\text{A}\\ d_{CBr}&=1.793\pm0.005\text{A} \end{aligned}$$

Since there is good probability that the assumed parameters lie within the quoted ranges, we may regard the calculated distances as reasonably reliable. The C−Br distance can be determined with considerably more precision than d_{C-C}.

The most striking property of the above parameters is that d_{C-C} is as short as it is in methyl acetylene[6] or methyl cyanide,[7] while d_{CBr} is also very short, being almost as short as it is in cyanogen bromide[11,12] and agreeing with the d_{CBr} found by electron diffraction in bromoacetylene,[4] which is 1.80±0.03A.

Table IV also shows that I_B for methyl iodoacetylene is consistent with a C−I distance of 1.99A on the basis of assumptions similar to those above for $d_{C\equiv C}$, d_{CH}, and $\angle HCH$, and taking d_{C-C} as 1.459A in this case also. Though d_{CI} must be subject to some uncertainty on account of the necessity of assuming d_{C-C} as well as the other parameters, it is worth noting that any longer value of d_{C-C} would probably require d_{C-I} to be even shorter, while if d_{CI} were much longer than 1.99A the d_{C-C} would have to be correspondingly shortened be-

TABLE IV. Structural parameters consistent with I_B values (neglecting zero-point energy effects).

Molecule	$d_{C\equiv C}$ (A)	d_{CH} (A) (assumed)	$\angle HCH$	d_{C-C} (A)	d_{CBr} or d_{CI} (A)
	1.211	1.092	109°8′	1.455_6	1.792_8
	1.211	1.092	108°14′	1.452_2	1.792_9
H_3CCCBr	1.211	1.082	109°8′	1.457_1	1.792_5
	1.211	1.102	109°8′	1.454_0	1.793_1
	1.207	1.092	109°8′	1.459_0	1.794_2
	1.211	1.092	109°8′	1.455_6	1.792_8
H_3CCCI	1.207	1.092	109°8′	1.459 (assumed)	1.99_1

Atomic masses used:
Carbon: 12.00386, and hydrogen: 1.00813 (R. T. Birge, Revs. Modern Phys. 13, 233 (1941)).
Bromine: 78.9417 and 80.9400 (F. W. Aston, Nature, 141, 1096 (1938)).
Iodine: 126.932 (F. W. Aston, Proc. Roy. Soc. (London) A115, 487 (1927)).

[11] Townes, Holden, and Merritt, Phys. Rev. 74, 1113 (1948).
[12] Smith, Ring, Smith, and Gordy, Phys. Rev. 74, 370 (1948).

TABLE V. Nuclear quadrupole couplings (eqQ in Mc/sec) for halogens in R−C≡C−X compared with those in H_3CX and XCN.

Nucleus (X)	H_3CX[a]	eqQ (Mc/sec) in R−C≡C−X		X−C≡N[c]
Cl^{35}	−75.1	−79.7	R=H[b]	−83.5
Cl^{37}	−59.93	−62.8		−65.0
Br^{79}	+577	+647	$R=CH_3$	+686
Br^{81}	+482	+539		+573
I^{127}	−1934	−2230		−2420

[a] From reference 10.
[b] From reference 8.
[c] From references 11 and 12.

low 1.459A. Shortening of either distance, however, below 1.99A or 1.459A, respectively, is not very likely, since these distances are already so short, and the indication is that both C−C and C−I are shortened in much the same way as the analogous bonds in methyl bromoacetylene. A length of 1.99A for C−I is close to that in cyanogen iodide[12] and much shorter than a normal C−I single bond.

Support for these conclusions is found in the measured stretching force-constants for C−Br and C−I in methyl bromo- and methyl iodoacetylene.[3] These are 4.3525×10^5 dynes/cm and 3.5707×10^5 dynes/cm, respectively, as compared with only 3.129×10^5 dynes/cm and 2.648×10^5 dynes/cm for the analogous bonds in methyl bromide and iodide. The shortened C−Br and C−I bonds in BrCN and ICN have stretching force constants of 4.2×10^5 dynes/cm and 3.0×10^5 dynes/cm.[13] The force constants in the methyl halogen acetylenes are therefore as high as those in the cyanogen halides, which supports a comparable shortness in these bonds in the methyl acetyle derivatives. It may be noted that the d_{CCl} in chloroacetylene[8] is found to be almost the same as that in ClCN, being much shorter than a single bond, while the C−Cl bonds in both have high and comparable stretching force constants.[13,14]

The explanation of such shortenings in C−C, C−Br, and C−I bonds in these substances is presumably to be found in the same causes suggested for the shortening of C−C in methyl acetylene[15] on the one hand, and for the shortening of carbon halogen bonds in halogen acetylenes and cyanogen halides on the other. It would thus chiefly involve postulation of hyperconjugated structures such as (I) for the C−C shortening, and structures such as (II) for the C−X shortening (X=Br or I):

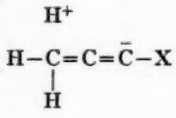

(I)

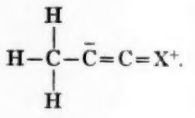

(II)

The halogen nuclear quadrupole couplings in the methyl halogen acetylenes are greater than those found in the methyl halides, but smaller than those found in the cyanogen halides. This is shown in Table V, which also shows that the same is true for the chlorine coupling in chloroacetylene. The explanation of the somewhat lower couplings compared with those in cyanogen halides, despite the similarity in bond lengths d_{CX} in the two series, may well depend on differences in contributions of the forms containing $C=X^+$ in the two series, and perhaps on differences in the ionic character of the C−X bonds in the two systems C≡C−X and N≡C−X.

[13] W. G. Penney and G. B. B. M. Sutherland, Proc. Roy. Soc. (London) **156**, 654 (1936).

[14] W. S. Richardson and J. H. Goldstein, J. Chem. Phys. **18**, 1314 (1950).

[15] Pauling, Springall, and Palmer, J. Am. Chem. Soc. **61**, 927 (1939).

THE JOURNAL OF CHEMICAL PHYSICS VOLUME 20, NUMBER 4 APRIL, 1952

Summer Symposium to be Held at University of Notre Dame

The St. Joseph Valley Section of the American Chemical Society and the Department of Chemistry of the University of Notre Dame will act as hosts for the 1952 joint summer symposium of the Division of Physical and Inorganic Chemistry of the American Chemical Society and the Division of Chemical Physics of the American Physical Society. The subject is "Electron Transfer and Isotopic Reactions." The three-day symposium will be held at the University of Notre Dame, June 11 to 13.

Because of limitation of facilities, registration will be limited to 200. It is essential for those who wish to obtain accommodations to register in advance. Abstracts of the symposium papers will be distributed to the members of the two divisions by their respective secretaries. Nonmembers of these divisions who register will be sent copies of the abstracts by the chairman in charge of arrangements for the symposium.

Preprints of the papers scheduled to be presented at the symposium will be distributed in May to all who register and pay for the preprints. Those who do not register for the symposium may obtain copies (until the supply is exhausted), from the chairman in charge of arrangements.

Physical and Inorganic Division of the American Chemical Society and the Division of Chemical Physics of the American Physical Society

Subject: Electron Transfer and Isotopic Reactions
Dates: June 11 to 13, 1952
Hosts: The St. Joseph Valley Section of the American Chemical Society and The Department of Chemistry of the University of Notre Dame
Chairmen: Dr. F. A. Long of Cornell University, Chairman-Elect of Division of Physical and Inorganic Chemistry
and
Dr. John R. Platt, University of Chicago, Secretary of Division of Chemical Physics.

—·—·—

Dr. J. V. Quagliano (in charge of arrangements), Department of Chemistry, University of Notre Dame

Program: *Wednesday* A.M., Introduction to Symposium
Chairman, Dr. John R. Platt, University of Chicago
Wednesday P.M., Reactions in Gases
Chairman, Dr. John L. Magee, University of Notre Dame
Wednesday Evening, General Mixer

—·—·—

Thursday A.M., Electron Transfer Reactions in Solution
Chairman, Dr. W. F. Libby, Inst. Nuclear Studies
Thursday P.M., Free Afternoon
Golf, swimming, visiting chemical concerns, inspecting University facilities, or just visiting with friends. Swimming, tennis, and golf facilities are available on the campus *for men only*. Within a radius of 30 miles there are state parks and Lake Michigan for picnicing, hiking, and swimming. No special "ladies' program" is being planned.
Thursday Evening, Buffet Supper or Dinner on campus
Thursday Evening (following Buffet Supper)
Electron Transfer Reactions in Solution
Chairman, Dr. R. W. Dodson, Brookhaven National Laboratory

—·—·—

Friday A.M. *and* P.M., Influence of Isotopes on Kinetics of Reactions
Chairman, Dr. Jacob Bigeleisen, Brookhaven National Laboratories

Room Reservations:

(a) *Hotel Accommodations*

Hotel accommodations are available in The Morris Inn on campus. The rooms in The Morris Inn, opened in April, 1952, are assigned only on the basis of 2 or 3 to a room.

Rates: Twin beds, private bath, $5.00 per person per night. 3 single beds, private bath, $4.00 per person per night.

Give name (or names) of roommates to share room, or indicate no choice and roommates will be assigned.

(b) *Dormitories*

Accommodations are available, *for men only*, in the University dormitories on the campus, at $2.50 per person per night. All rooms are equipped with running water.

Hotel reservations will be confirmed directly by the manager of The Morris Inn; dormitory reservations will be confirmed by the Housing Committee.

Transportation:

The TWA, American, and United Airline planes stop at the South Bend airport.

New York Central and Grand Trunk trains stop at the South Bend station. Michigan Central trains stop at Niles, Michigan (ten miles north of South Bend) and there is regular bus service from Niles to South Bend every half-hour. The nearest Baltimore and Ohio stop is at LaPaz, Indiana (16 miles south of South Bend), and the nearest Pennsylvania RR stop is at Plymouth, Indiana (24 miles south of South Bend). There is regular bus service between these points and South Bend.

There is service every hour between Chicago and South Bend on the South Shore and South Bend Electric line. These trains leave from the Randolph Street Illinois Central suburban station in Chicago on the hour; they also pick up passengers at the Van Buren and Roosevelt Road (Central) stations.

To register or to apply for preprints write to Dr. J. V. Quagliano, Department of Chemistry, University of Notre Dame, Notre Dame, Indiana before May 7, 1952. State name, address, and whether you are a member of either of the two Societies or of the Divisions, and enclose a check. Application for rooms should also be made.

Fees:

$2.50	for registration for members of the American Chemical Society or American Physical Society.*
$5.00	for registration for nonmembers.
$2.50	for buffet supper on Thursday evening.

Preprints:

$2.50	for all who register and attend and for all members of the sponsoring divisions who do not attend.
$3.50	for other members of the American Chemical Society or American Physical Society.
$5.00	for those who are not members of the American Chemical Society or the American Physical Society.

* Fees will be refunded if notification of nonattendance is given before June 1, 1952.

Letters to the Editor

THIS section will accept reports of new work, provided these are terse and contain few figures, and especially few half-tone cuts. The Editorial Board will not hold itself responsible for opinions expressed by the correspondents. Contributions to this section should not exceed 600 words in length and must reach the office of the Editor not later than the 15th of the second month preceding that of the issue in which the Letter is to appear. No proof will be sent to the authors. A publication charge of $10.00 per Letter is made which, when honored, will entitle the Institution to 100 free reprints.

Dipole Moments from Dielectric Data on Polar Liquids

JOHN D. HOFFMAN
General Electric Research Laboratory, The Knolls, Schenectady, New York
(Received January 21, 1952)

ONSAGER[1] has shown that a value for the dipole moment of a molecule in a pure polar liquid may be obtained from the equation

$$\mu_1^2=\frac{9MkT(\epsilon-n^2)(2\epsilon+n^2)}{4\pi Nd\epsilon(n^2+2)^2}. \quad (1)$$

ϵ is the static dielectric constant, n the index of refraction, and d the density; the other symbols have their usual meaning. μ_1 is often called the "Onsager moment," and it has sometimes been regarded as identical to the true gas moment μ_0(obs). This identity, however, is not generally to be expected and μ_1 is, in fact, frequently different from μ_0(obs). The object of this note is to point out that if μ_1^2 is plotted against $1/T$, the intercept with the ordinate axis will yield a value of μ_0, which is close to μ_0(obs).

The rationale of this extrapolation is evident from a comparison of Onsager's theory with that of Kirkwood.[2] Kirkwood's calculation of the dipole moment of molecules in pure polar liquids includes the effect of mutual orientation of dipoles as well as an internal field correction similar to that obtained by Onsager. Kirkwood's result is the same (for spherical molecules) as Eq. (1) except that the left-hand side is $\mu_0^2 g$, where $g=(1+z\langle\cos\gamma\rangle)$. γ is the angle between a central dipole and one of the z dipoles in the first coordination sphere. Comparison of the Onsager and Kirkwood equations shows that

$$\mu_0^2(1+z\langle\cos\gamma\rangle)=\mu_1^2, \quad (2)$$

where μ_0 is explicitly the gas moment. In general, $\langle\cos\gamma\rangle$ is given by

$$\langle\cos\gamma\rangle=\frac{\int\int\cos\gamma\exp[-(V_0/kT)\cdot f(\gamma,\omega)]\sin\gamma d\gamma d\omega}{\int\int\exp[-(V_0/kT)\cdot f(\gamma,\omega)]\sin\gamma d\gamma d\omega}, \quad (3)$$

where $f(\gamma,\omega)$ is a function which describes the variation of potential energy of the molecules in terms of the coordinates of the system represented by ω, as well as γ.

The relationship between μ_1, μ_0, and T may be found by expanding Eq. (3). The result, dropping terms $0(1/T^2)$ and higher, is

$$\langle\cos\gamma\rangle\doteq a(V_0/2kT), \quad (4)$$

where

$$a=\int\int\sin\gamma\cos\gamma f(\gamma,\omega)d\gamma d\omega.$$

Oster[3] has previously noticed that $\langle\cos\gamma\rangle$ may be approximated as a constant divided by T for a specific model. Combination of Eqs. (2) and (4) yields

$$\mu_0^2+\mu_0^2 azV_0/2kT\doteq\mu_1^2. \quad (5)$$

Thus, if a plot is made of μ_1^2 *vs* $1/T$, the intercept will be μ_0^2. If sufficient dielectric constant data are available to evaluate $\mu_1(T)$ from the Onsager equation, these data may be used to estimate μ_0. It would be preferable to have data for as high temperatures as possible.

TABLE I. Dipole moments in debyes.

Compound	Onsager moment[a] (μ_1) −1°	25°	55°C	Gas moment (μ_0) μ_0(calc)	μ_0(obs)[b]
C_2H_5Br	1.78	1.80	1.82	2.0[2]	2.02
n-bromides C-3 to C-16	1.76[c]	1.81[c]	1.85[c]	2.2[3]	2.15
C_6H_5Cl	1.44	1.45	1.46	1.5[5]	1.69
C_6H_5Br	1.32	1.37	1.42	1.8[4]	1.71
i-C_3H_7Br	2.04	2.06	2.08	2.2[5]	2.18

[a] See reference 4.
[b] See reference 5.
[c] Averages for 11 compounds.

The method of estimating gas moments from temperature dependent Onsager moments suggested by Eq. (5) has been tested for a few cases where values of $\mu_1(T)$ were available in the careful work of Heston, Hennelly, and Smyth.[4] Only cases where observed[5] values of the gas moments were available were considered and molecules where internal rotation of dipoles caused changes in μ_0 were avoided. The values of μ_0(calc) from Eq. (5) and the values of μ_0(obs) are shown in Table I. Even with the long extrapolation required, μ_0(calc) is always closer to μ_0(obs) than any of the values of μ_1 listed. μ_0(calc) is never in error by more than 9 percent and the standard deviation is 0.09 Debye. Dipole moments calculated from solution measurements[5] frequently lead to even greater errors when compared to μ_0.

[1] L. Onsager, J. Am. Chem. Soc. **58**, 1486 (1936).
[2] J. G. Kirkwood, J. Chem. Phys. **7**, 911 (1939); for the specific form used, see H. Fröhlich, *Theory of Dielectrics* (Oxford University Press, London, 1949), p. 52.
[3] G. Oster, J. Am. Chem. Soc. **68**, 2036 (1946).
[4] Heston, Hennelly, and Smyth, J. Am. Chem. Soc. **72**, 2071 (1950).
[5] L. Wesson, *Tables of Electric Dipole Moments* (The Technology Press, Massachusetts Institute of Technology, Cambridge, Massachusetts, 1948).

Errata: Paramagnetic Resonance Absorption of Microwaves

[J. Chem. Phys. **19**, 1181 (1951)]
FORREST W. LANCASTER AND WALTER GORDY
Department of Physics, Duke University, Durham, North Carolina

THE following corrections should be made for this paper:

The formula for cerous oxalate should be $Ce_2(C_2O_4)_3\cdot 9H_2O$, and the cerium ion should be Ce^{+++}.

The compound listed as chromic dirhodanato diethylene diammine rhodanate is chromic dithiocyanato diethylene diamine thiocyanate, and the formula is

$$[Cr(SCN)_2\{C_2H_4(NH_2)_2\}_2](SCN).$$

Cupric chromate should be cupric dichromate. The formula for lanthanum nitrate should be $La(NO_3)_3\cdot 6H_2O$.

Infrared Reflection Spectra of Phosphates and Arsenates

JOHN J. OBERLY
Crystal Branch, Metallurgy Division, Naval Research Laboratory, Washington, D. C.
AND
GEORGE WEINER
Chemistry Laboratories of Washington Square College, New York University, New York, New York
(Received January 18, 1952)

A STUDY has been made of the infrared reflection spectra of KH_2PO_4, $NH_4H_2PO_4$, KH_2AsO_4, and $NH_4H_2AsO_4$ crystals to (1) determine the local symmetry surrounding the phosphorus

and arsenic atoms, (2) locate the fourth fundamental frequency of the arsenate ion which could not be found in solution but which might well appear in the crystalline spectrum, and (3) inquire, if possible, into the nature of the vibrations of the hydrogen atoms common to these compounds.

Well-polished x-cuts were examined with a Perkin-Elmer infrared spectrometer 12-C using polarized radiation. Data were obtained at room temperature in the 1–25 micron region for all four crystals, and in addition, below the Curie point at liquid nitrogen temperature in the 2–15 micron region for the potassium compound. The ammonium crystals shatter at low temperature as a result of the ammonium transition.[1]

Our room temperature data for KH_2PO_4 confirm in substance the reflection spectrum recorded by C. La Lau[2] in the 4–14 micron region. Our spectrum shows somewhat improved resolution, possibly because we employed a Golay infrared detector. The new data are summarized in the table.

Above their respective Curie points x-ray crystallographers[3,4] assign these isomorphic crystals to the tetragonal space group V_d^{12}. The positions of the hydrogen atoms have not been revealed by x-ray analysis but those of all other atoms have been determined with reasonable accuracy; the phosphorus and arsenic atoms (to be designated X) lie[5,6] on site S_4 but the symmetry of the H_2XO_4 ions, if such exist in the crystals, might be of lower order. Judging from our data alone it would appear more likely that the ionic configuration, XO_4 or H_2XO_4, actually contains the symmetry element S_4 and is therefore probably of symmetry T_d. If such is the case, we might regard the H_2XO_4 ions, in approximation, as a five-particle system: $XO_2(OH)_2$. This tetrahedral symmetry might exist in spite of the fact that the frequency resulting from the totally symmetric vibration $\nu_1(A_1)$ is observed in all our spectra with both polarizations although this frequency is forbidden in the infrared by the selection rules for groups T_d and S_4. In the crystal, nevertheless, such a band might be activated because of its combination with a long-wave lattice frequency.[6,7] The $\nu_3(T_2)$ and $\nu_4(T_2)$ bands show splitting into normal and parallel bands in agreement with the mapping of the molecular group T_d onto site group S_4. Because of the incompleteness of present data, however, we cannot exclude the possibility of a lower ionic symmetry, e.g., C_{2v} or C_2, and a corresponding lower site symmetry.

Below the Curie point the space group is known[8,9] to be the orthorhombic group C_{2v}^{19}. The central atoms lie on site C_2 and the ionic configuration is likely to be C_{2v} or C_2. Our spectra show an increase in the number of bands at this temperature probably because of complete removal of the $\nu_3(T_2)$ degeneracy; contrary to expectation one of these bands occurs at almost the same wavelength with both polarizations. The bands are much narrower than at room temperature and more intense. Also, it appears that most bands are shifted to higher frequencies. This might be the result of the transition from hydrogen to hydroxyl bonding as discussed by Simon and Schulze.[10]

The bands in the range outside the region where typical XO_4 bands are known to occur are difficult to interpret. La Lau[2] identified the 1575 cm^{-1} band as a $P-O-H$ banding frequency.

Only three of the four frequencies typical of tetrahedral XO_4 molecules have been reported so far for the arsenate ion. Gupta and Guha[11] attribute this to accidental degeneracy of the ν_1 and ν_3 frequencies. From the spectra of our arsenate crystals it appears most likely that we have observed the missing frequency though our assignment is not unambiguous.

TABLE I. Observed infrared reflection bands (cm^{-1}).

KH_2PO_4				$NH_4H_2PO_4$		KH_2AsO_4				$NH_4H_2AsO_4$		
Above Curie point Polarization to z axis		Below Curie point Polarization to z axis		Above Curie point Polarization to z axis		Above Curie point Polarization to z axis		Below Curie point Polarization to z axis		Above Curie point Polarization to z axis		Probable assignments
normal	parallel	normal	parallel	normal	parallel	normal	parallel	normal	parallel	normal	parallel	
...	...	No data recorded		9090	9090	...	...	No data recorded		...	...	?
7690	6670			7690	7690	7690	6250			...	...	?
...	...	...	...	2085	2050	...	...	...	...	2085	2050	?
1578	1578	1544	1542	1550	1550	1578	1578	1578	1578	1578	1578	X−O−H bending vibration
1450	{1474}	1437	...	...	...	1465	1444	1506	1506	...	...	?
1435	{1420}	...	...	...	...	1400	1398	1416	1416	...	...	?
...	...	...	...	1415	1380	...	...	...	...	1403	1380	$\nu_4(T_2)$ of NH_4 ion
1297	1234	1305	1295b[a]	1255	1240	1240	1242	1277	1277	1190b[a]	1240	Combination band of $\nu_3(T_2)$ of XO_4 ion with some lattice band
...	...	...	...	...	...	1050	1000b[a]	...	...	1006b[a]	966b[a]	Possibly same assignment as above band
...	...	1160	1250?	...	...	...	...	1036	1037	...	...	$\nu_3(T_2)$ of XO_4 ion
...	...	1021	1030	...	...	...	...	865	...	...	...	
1090b[a]	1020b[a]	960	...	1095	1010	865b[a]	870	775	...	865b[a]	860b[a]	
889	893	904	907	895	880	745b[a]	735b[a]	750	765	745b[a]	735b[a]	$\nu_1(A_1)$ of XO_4 ion
847	847	...	...	...	...	...	...	...	...	...	...	Difference band of $\nu_1(A_1)$ of PO_4 ion and lattice band
547	...	No data recorded		546	...	...	...	No data recorded		...	...	Combination band of $\nu_4(T_2)$ of PO_4 ion and lattice band
455	476			455b[a]	465b[a]	435	...			435	...	$\nu_4(T_2)$ of XO_4 ion

[a] b = broad.

The measurements are now being extended to longer wavelengths and will be discussed in more detail in a future paper.

[1] Matthias, Merz, and Scherrer, Helv. Phys. Acta **20**, 273 (1947).
[2] C. La Lau, dissertation, University of Amsterdam, Amsterdam, The Netherlands (1947) (unpublished).
[3] S. B. Hendricks, Am. J. Sci. **14**, 269 (1927).
[4] J. West, Z. Krist. **74**, 306 (1930).
[5] R. S. Halford, J. Chem. Phys. **14**, 8 (1946).
[6] H. Winston and R. S. Halford, J. Chem. Phys. **17**, 607 (1944).
[7] D. F. Hornig, J. Chem. Phys. **16**, 1063 (1948).
[8] M. De Quervain, Helv. Phys. Acta **17**, 509 (1944).
[9] A. R. Ubbelohde and I. Woodward, Proc. Roy. Soc. (London) **188A**, 358 (1947).
[10] A. Simon and G. Schulze, Z. anorg. u. allgem. Chem. **242**, 329 (1939).
[11] J. Gupta and M. P. Guha, Indian J. Phys. **22**, 64 (1948).

The Free-Electron Model and the Diamagnetism of Aromatic Hydrocarbons

M. W. NATHANS
Great Lakes Carbon Corporation, Research Laboratory, Morton Grove, Illinois

(Received January 24, 1952)

PAULING'S semiclassical treatment[1] of the diamagnetic anisotropy of aromatic systems assumes mobile electrons to move freely over the hexagonal network of condensed benzene

rings which forms a set of closed circuits. Free-electron models which do not differ very much from Pauling's model have been proposed in recent years for the calculation of optical transition frequencies of aromatics.[2-4] Here the unsaturation electrons are assumed to move freely on the circumference of a circle of radius R. Pauling calculates the molar diamagnetic anisotropy of benzene from the expression

$$\Delta\chi = -n(Ne^2/4\,mc^2)\bar{\rho}^2, \tag{1}$$

where n is the number of mobile electrons, and $\bar{\rho}^2$ the mean square of the distance of the electron from the z axis, which is the axis of symmetry and the direction of the magnetic field. The anisotropy of higher condensed aromatics is calculated in terms of the $\Delta\chi$ if a six-electron hexagon.

The calculations can be simplified by applying the "spectroscopic" free-electron model and substituting the square of the radius of the circle for $\bar{\rho}^2$. Two assumptions have been made regarding the value of R.

(1) The area assumption

$$\pi R^2 = s(27/4)^{\frac{1}{2}}R_0^2, \tag{2}$$

where s = number of rings, R_0 = C−C distance. In this assumption the molecule is replaced by a circle with the same area.

(2) The perimeter assumption

$$2\pi R = nR_0. \tag{3}$$

Here the molecule is replaced by a circle with a perimeter approximately equal to the sum of all C−C bonds.

The results of the calculations are shown in Table I, columns 2 and 3, and are compared with Pauling's results and with the observed values. The agreement is not very good. The calculated values are too high. This is not too surprising, however, since insufficient account is taken of the possibility of the electrons taking shortcuts, which would reduce the effective area of the electron orbits. The perimeter assumption in particular tends to lead to a contradiction; the more shortcuts for a given number of rings the bigger R. In the application to optical transitions the perimeter assumption may be more satisfactory, since it leads to a zero frequency for the lowest transition of an infinite ship of catacondensed hydrocarbons in accordance with the results of Coulson and Rushbrooke's[5] molecular orbital calculations. The area assumption leads to a finite frequency for such systems.

TABLE I. Magnetic anisotropy of condensed aromatics.

1	2	3	4	5	6	7	8	9
Molecule	Area assumption	Perimeter assumption	Area assumption corrected	Perimeter assumption corrected	Pauling	Observed	s	n
C_6H_6	39	45	39	45	49	54	1	6
$C_{10}H_8$	143	215	72	108	104	146	2	10
$C_{14}H_{10}$	300	590	100	197	159	223[a] 164[b]	3	14
$C_{16}H_{10}$	457	891	114	223	222	222	4	16
$C_{18}H_{12}$	514	1237	129	309	214	218	4	18
$C_{24}H_{12}$[c]	1200	2972	171	425	572	...	7	24
$C_{54}H_{18}$[c]	7330	33,850	386	1780	2770	...	19	54
$C_{96}H_{24}$[c]	25,340	19,220	685	5141	8200	...	37	96
$C_{30}H_{18}$[d]	1498	5805	214	829	...	...	7	30
$C_{78}H_{42}$[d]	10,580	102,030	551	5370	...	...	19	78
$C_{150}H_{78}$[d]	39,630	725,620	1070	16,910	...	...	37	150

[a] Anthracene.
[b] Phenanthrene.
[c] Molecules with sixfold symmetry (D_{6h}).
[d] Linear strips of catacondensed benzene rings with the same number of rings as the preceding molecules with D_{6h} symmetry.

Actually, there is a certain arbitrariness in the value of R as has been pointed out by previous authors[2-4] and one might correct for the shortcuts by changing R. One may take s as a measure of the possibility that electrons take shortcuts and substitute R^2/s for $\bar{\rho}^2$ instead of R^2. The results are shown in columns 4 and 5. The agreement is much improved, in particular with the perimeter assumption. It is obvious, however, that the theory fails for large molecules. That is also evident from a comparison with the experimental value for graphite: $\Delta\chi = 270\times10^{-6}$. Pauling calculates that the graphitic layers are about 40A in diameter. Actually, the layers are much larger. The molecular orbital approach is much more promising as has been pointed out recently by McWeeny,[6] although his formulas, too, tend to give excessive values for large molecules, at least in the case of the polyphenyls.

[1] L. Pauling, J. Chem. Phys. **4**, 673 (1936).
[2] W. T. Simpson, J. Chem. Phys. **16**, 1124 (1948).
[3] J. R. Platt, J. Chem. Phys. **17**, 484 (1949).
[4] K. Rüdenberg and R. G. Parr, J. Chem. Phys. **19**, 1268 (1951).
[5] C. A. Coulson and G. S. Rushbrooke, Proc. Roy Soc. (Edinburgh) **A62**, 350 (1948).
[6] R. McWeeny, Proc. Roy. Soc. (London) **A209**, 261 (1951).

Raman Spectrum of *Para*-Dichlorobenzene

S. C. SIRKAR
Indian Association for the Cultivation of Science, Calcutta, India
(Received May 11, 1951)

IN a paper published recently in this journal Saksena[1] has pointed out that the data on the Raman spectra of *para*-dichlorobenzene reported by previous authors and those observed by him can be explained on the assumption that above 32°C the *para*-dichlorobenzene molecule in the crystal begins to rotate freely about an axis perpendicular to its plane. It has, however, to be pointed out that there are certain inaccuracies in this statement regarding the results reported by previous workers and that some of his arguments are not free from fallacies.

Saksena has stated that although Sirkar and Gupta[2] failed to observe changes in the Raman spectrum of *para*-dichlorobenzene with change of temperature of the crystal observed by previous workers, he has observed two different sets of lines in the low frequency region, one set being the result of the single crystal of the substance and the other set the result of a mass obtained by suddenly cooling the molten mass; and that Sirkar and Gupta observed only one set of such lines. This latter statement is not correct, because Sirkar and Gupta observed that when the crystal is once cooled in ice and again brought to a temperature of 32°C the lines at 40 and 82 cm^{-1} shift, respectively, to 46 and 92 cm^{-1}, while the position of the line at 50 cm^{-1} remains unchanged. These lines are identical with three of the four lines observed by Saksena in the case of his single crystal. The line at 27 cm^{-1} observed by him was not observed by Sirkar and Gupta, probably owing to the presence of a coma close to the Rayleigh line. The changes observed by the latter authors mentioned above have thus been overlooked by Saksena.

It has been suggested by Saksena that Sirkar and Gupta[3] failed to observe any change in the Laue photograph of single crystal of *para*-dichlorobenzene with change of temperature, probably because the crystal studied by them was of the disordered type, with each molecule rotating about an axis perpendicular to its plane in the crystal. In making this suggestion he has overlooked the fact that the same changes of conditions of the crystal which produce changes in its Raman spectrum fail to produce any change in its Laue pattern.

Saksena has tried to explain the discrepancies between the Raman spectra of mixed crystals of *para*-dichlorobenzene and *para*-dibromobenzene observed by Vuks[4] and those observed by Sirkar and Bishui[5] on the assumption that the mixed crystals studied by the latter authors were of the "disordered" type while the freedom of rotation of the molecules was absent in the mixed crystals studied by Vuks. In this assumption it has been overlooked by Saksena that the mixed crystal studied by Sirkar and Gupta was once cooled in ice, and therefore the Raman lines observed by them are not those of the "disordered" type. Further, it is difficult to understand how in calculating the frequencies of oscillations of the molecules pivoted in the lattice the statistical average of the moments of inertia of the different molecules can

be taken, because in the scattering of a single photon only the change in polarizability of either a single molecule or a small group of molecules is to be taken into consideration.

Finally, it has to be pointed out in this connection that according to the results obtained by Ray[6] in the case of some substituted benzene compounds, the frequencies of the new Raman lines in the low frequency region cannot be correlated with the moments of inertia of the molecules about their axes, and also the changes which these lines undergo with lowering of temperature of the crystals do not support the theory that these lines are the result of rotational oscillations of the molecules pivoted in the lattice.

[1] B. D. Saksena, J. Chem. Phys. **18**, 1653 (1950).
[2] S. C. Sirkar and J. Gupta, Indian J. Phys. **10**, 473 (1936).
[3] S. C. Sirkar and J. Gupta, Indian J. Phys. **11**, 283 (1937).
[4] M. Vuks, Acta Phys. Chem. U.S.S.R. **6**, 327 (1937).
[5] S. C. Sirkar and I. C. Bishui, Indian J. Phys. **11**, 417 (1937).
[6] A. K. Ray, Indian J. Phys. **25** (to be published).

Effect of Oxygen on the Ferrous-Ferric Exchange Reaction*

LOIS EIMER, A. I. MEDALIA, AND R. W. DODSON
Chemistry Department, Brookhaven National Laboratory, Upton, Long Island, New York
(Received December 17, 1951)

IT has recently been proposed by Weiss[1] that the rapid exchange observed in aqueous solutions between metal ions in different valence states may involve the oxidation and reduction of the metal ions by other substances present in the solution, such as O_2, H_2O, Br^-, etc. For example, Weiss suggests that in aqueous solutions of ferrous and ferric ions in the presence of oxygen, exchange will occur according to the following mechanism:

$$Fe^{++} + O_2 \rightarrow Fe^{+++} + O_2^- \quad (1a)$$
$$Fe^{+++} + O_2^- \rightarrow Fe^{++} + O_2 \quad (1b)$$

with the intermediate formation of the O_2^- ion. Weiss states[1] that the rate of this exchange should be given by the rate of step (1a), with rapid exchange expected in the presence of oxygen, and no exchange in its absence, i.e., the rate should depend on the amount of oxygen dissolved.

We have looked for such an effect by measuring the rate of this reaction at widely varying concentrations of dissolved oxygen, established by bubbling a stream of argon, nitrogen, air, or oxygen through the solutions. A specific set of conditions for the exchange was selected from the study by Silverman and Dodson[2a,b,c] to serve as a basis for the present investigation. The method of separation of the reacting species was that developed by these authors, namely, precipitation of ferric hydroxide after the reaction was quenched through formation of the ferrous tris-α-α'-dipyridyl complex at *p*H5.

A stock solution of ferrous perchlorate was prepared using the products of seven successive recrystallizations of G. F. Smith's ferrous perchlorate hexahydrate from 8*f* perchloric acid. It was analyzed for ferrous ion by titration with standard ceric sulfate and found to be 0.466*f*. The ferric ion concentration in this solution was found to be 1.6×10^{-3} *f* by spectrophotometric analysis using the thiocyanate complex.

A 1.33×10^{-3} *f* ferric perchlorate solution was prepared from a hydrochloric acid solution of high specific activity Fe^{55} (obtained from the Atomic Energy Commission). The method of preparation was the same as that used by Silverman[2c] but without the addition of inactive iron. In all experiments the ferric ion was the initially radioactive species.

The water used had been purified by successive distillation of ordinary distilled water from alkaline permanganate, acid dichromate, sodium hydroxide, and pure water in a continuous Pyrex quadruple still.

Perchloric acid (J. T. Baker Company 70 percent vacuum distilled) was diluted and standardized by titration with standard sodium hydroxide.It gave negative test for chloride.

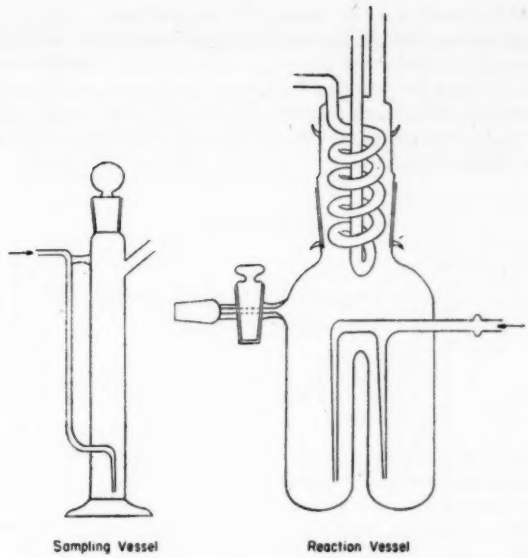

FIG. 1. Apparatus.

All[1] other chemicals were reagent grade.

Experiment 1. The ferric and ferrous fractions, each in 0.55 formal perchloric acid and of the reactant concentrations shown in Table I, were placed in the separate arms of the reaction vessel (Fig. 1) which was then heated in a water bath at 90°C for ten minutes while passing water at 0°C through the condenser and bubbling argon (Airco, 99.9 percent argon, 0.1 percent nitrogen) through the solutions. The argon was first passed through water in a gas bubbler at 0°C. The reaction vessel was then immersed in an ice bath in a Dewar flask; thirty minutes later the solutions were mixed. Aliquots were taken at intervals by tilting the vessel so that solution drained out the side arm into the sampling vessel, which contained the quenching solution, and through which argon was also passed. The amount of sample was determined by weighing. It was separately shown that the gas stream caused no significant changes in the weights of the reaction vessel or sampling vessel systems.

Separation and sample preparation were done as previously mentioned,[2c] and samples were counted with an end window GM tube filled with 71.5 cm of argon and 2.5 cm of ethyl acetate.

During each run approximately eight samples were taken. An "infinite time" sample (complete exchange) was taken after a lapse of about nine half-lives, at which time a total activity sample was also prepared by oxidizing an aliquot with hydrogen peroxide and precipitating the iron as ferric hydroxide in exactly the same manner as the other aliquots.

Experiment 2. This was carried out just as Experiment 1 but with nitrogen (Airco prepurified) passing through all solutions, in place of argon.

Experiment 3. This experiment was planned as a blank run and therefore was conducted as closely as possible to Experiment 1 but with tank compressed air bubbling through the solutions.

Experiment 4. In this experiment the vessel of Fig. 1 was used but tank oxygen (Matheson) was passed through the solutions at 0°C for 45 minutes before mixing, as well as during the reaction.

Experiment 5. The technique of this experiment was similar to that of Silverman.[2c] No attempt was made to remove the dissolved oxygen normally present in the aqueous solutions.

A typical exchange plot is shown in Fig. 2. Since the reaction has been shown[2c] to be first order in each of the two reactants, values of the specific rate constant were calculated from the reaction half-times (obtained from such curves) from the expression $k=0.693/t_{\frac{1}{2}}(a+b)$, where a and b are the concentrations of ferric and ferrous iron, respectively. The results are given in Table I.

It will be noted that the values of k obtained show no trend with oxygen concentration, and agree among themselves to within a conservative estimate of the experimental error. The close agreement between the value of k obtained in Experiment 5 and that reported by Silverman is particularly gratifying in view of the fact that all reagents used in the two sets of experiments came from different sources.

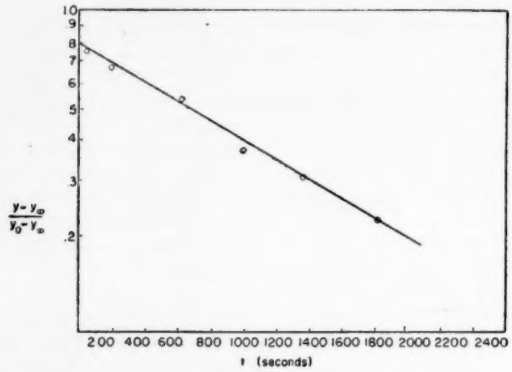

FIG. 2. Typical rate data. y, specific activity of ferric species at time t. y_0, initial specific activity of ferric species. y_∞, specific activity of ferric species after exchange equilibrium is established.

In order to estimate the reduction in concentration of dissolved oxygen brought about by the de-aeration procedure of Experiments 1 and 2, solutions of 0.1 M KCl were de-aerated in exactly the same manner, then transferred to a vessel (flushed with argon or nitrogen) for polarographic analysis with a rotating platinum micro-electrode, using a pool of mercury as the quiet electrode. The current was measured at −0.6-volt applied potential; aliquots of a solution of 0.1 M KCl, saturated with a gas mixture of 0.5 percent O_2—99.5 percent N_2 (Matheson) were then added, and the increments in current measured. By extrapolation it was estimated that the concentration of dissolved oxygen was not greater than 5×10^{-7} M with argon, and 4×10^{-7} M with nitrogen, thus showing a thousand-fold reduction from air-saturated solutions.

TABLE I. Effect of oxygen on exchange between ferrous and ferric iron in 0.55 f $HClO_4$ at 0°C.

Expt.	Apparatus	Gas	Fe^{++} ($f\times10^4$)	Fe^{+++} ($f\times10^4$)	$t_{\frac{1}{2}}$ (sec)	k (f^{-1} sec^{-1})
1	Fig. 1	Argon	3.79	1.07	1100	1.30
2	Fig. 1	N_2	3.58	1.15	1000	1.46
3	Fig. 1	Air	3.75	1.10	1030	1.39
4	Fig. 1	O_2	3.77	1.13	1040	1.36
5	Open vessel	···	3.92	1.08	1020	1.36
6[a]	Open vessel	···	3.92	1.08	1045	1.33

[a] Data of Silverman (see reference 2c).

The experimental results show that the rate of the ferrous-ferric exchange reaction is not significantly affected when the concentration of dissolved oxygen is varied by a factor of the order of 5000. Inasmuch as the mechanism suggested by Weiss, a reversible oxidation-reduction reaction with dissolved oxygen, would lead one to expect a rate directly proportional to the dissolved oxygen concentration, we conclude that this mechanism is not operative under the conditions of our experiments.

We are indebted to Dr. Everett Johnson for valuable suggestions, particularly in regard to the design of the reaction vessel.

* Research carried out under the auspices of the AEC.

[1] J. Weiss, J. Chem. Phys. **19**, 1066 (1951).

[2a] R. W. Dodson, J. Am. Chem. Soc. **72**, 3315 (1950). [b] J. Silverman and R. W. Dodson, BNL Quarterly Progress Reports (1950): BNL 64 (S-6) p. 31, BNL 82 (S-7) p. 54, BNL 93 (S-8) p. 65. [c] J. Silverman, thesis, Chemistry Department, Columbia University (1951).

Resonance Energy in Carbonium Ions

J. HALPERN
Department of Metallurgy, University of British Columbia, Vancouver, Canada
(Received October 29, 1951)

IN a recent issue of this journal[1] Franklin and Lumpkin have described and discussed the results of their measurements of the appearance potentials of various carbonium ions, including the allyl and phenyl dimethyl carbinyl ions in which the positive charge is conjugated with a double bond and with a benzene ring, respectively. The results of their measurements are of great interest, as only indirect evidence of the appearance potentials of these ions has previously been available. From these data it is possible to estimate the resonance energy arising from the conjugation of a positive charge or vacant orbital with adjacent π-bonds in a carbonium ion.

Franklin and Lumpkin conclude that the allyl and phenyl dimethyl carbinyl ions in which such conjugation is present have no resonance energy. This conclusion is based on their results, showing similar appearance potentials for the allyl and propyl carbonium ions from the corresponding chlorides and similar appearance potentials for the phenyl dimethyl carbinyl ion and the cyclohexyl dimethyl carbinyl ion from the corresponding methyl compounds. The assumption was also made that the saturated carbonium ions (i.e., the propyl and cyclohexyl dimethyl carbinyl ion) possess no resonance energy, although this was not demonstrated. In fact this assumption may be questioned, since several authors[2,3] have drawn attention to the resonance energy of these ions. In view of this, an attempt has been made to re-examine the results of Franklin and Lumpkin.

The appearance potential $A_{(R^+)}$ of a carbonium ion R^+ from the molecule $R-X$ is defined as the endothermicity of the reaction

$$R-X\rightarrow R^+ + X^\cdot + e - A_{(R^+)}. \tag{1}$$

Stevenson[4] has shown that $A_{(R^+)}$ may be related to the dissociation energy of the $R-X$ bond $D_{(R-X)}$ and the ionization potential of the $R^\cdot$ radical $I_{(R^\cdot)}$ as follows:

$$A_{(R^+)} = D_{(R-X)} + I_{(R^\cdot)}, \tag{2}$$

where $D_{(R-X)}$ is defined by

$$R-X\rightarrow R^\cdot + X^\cdot - D_{(R-X)} \tag{3}$$

and $I_{(R^\cdot)}$ is defined by

$$R^\cdot \rightarrow R^+ + e - I_{(R^\cdot)}. \tag{4}$$

The differences in dissociation energies of similar bonds in different molecules are due to differences in the resonance energies of the molecules and of the radicals formed on dissociation of the bond. Since there is no possibility for resonance in the molecules, CH_4 and R—H or in the CH_3 radical, the resonance energy $R_{(R^\cdot)}$, of the radical $R^\cdot$ may be expressed as

$$R_{(R^\cdot)} = D_{(CH_3-H)} - D_{(R-H)}. \tag{5}$$

Similarly differences in ionization potentials of different hydrocarbon radicals are due to differences in the resonance energies of the radicals and carbonium ions involved. Again, since there is no possibility of resonance in the $\overset{+}{C}H_3$ ion, the resonance energy of the carbonium ion R^+ may be related to the difference in ionization potentials of the $R^\cdot$ radical and the CH_3 radical, thus

$$R_{(R^+)} = I_{(CH_3)} - I_{(R^\cdot)} + R_{(R^\cdot)}. \tag{6}$$

Values of $I_{(R^\cdot)}$, $R_{(R^+)}$, and $R_{(R^\cdot)}$ calculated from the results of Franklin and Lumpkin[1] by means of Eqs. (2), (5), and (6) are listed in Table I. The values for CH_3 are given for comparison and serve as the basis of the resonance energy calculations. The resonance energies of the radicals are calculated from the differences in R—H bond dissociation energies.

The results in Table I present several striking features.

1. All the radicals $R^{\cdot}$ and carbonium ions R^{+} possess resonance energies relative to the $\dot{C}H_3$ radical and $\overset{+}{C}H_3$ ion, respectively.

2. The resonance energies of allyl and phenyl dimethyl carbinyl radicals, in which the free electrons are conjugated with adjacent π-bonds, are considerably larger (by about 15 kcal/mole) than in the corresponding saturated (i.e., propyl and cyclohexyl dimethyl carbinyl) radicals.

3. The resonance energies of all the carbonium ions are considerably larger than the resonance energies of the corresponding radicals.

4. The resonance energies of the allyl and phenyl dimethyl carbinyl carbonium ions are approximately the same as for the corresponding saturated (i.e., propyl and cyclohexyl dimethyl carbinyl) carbonium ions. Contrary to the conclusions of Franklin and Lumpkin that there is no resonance in these ions, the resonance energies are in fact very appreciable, amounting to about 58–59 kcal in the allyl and propyl ions and 81–84 kcal in the phenyl dimethyl- and cyclohexyl dimethyl-carbinyl ions.

In the unsaturated radicals and ions, the resonance energy is the result of the mobility of the π-electrons (π-conjugation energy)

TABLE I. All values in kcal/mole.

$R^{\cdot}$	$D_{(R-H)}$	$X^{\cdot}$	$D_{(R-X)}$ (from $R-X$)	$A_{(R^+)}$	$I_{(R^{\cdot})}$	$R_{(R^{\cdot})}$	$R_{(R^+)}$
$\dot{C}H_3$	101[a]	H	101[a]	333[b]	232	0	0
$CH_3-CH_2-\dot{C}H_2$	95[a]	Cl	77[a]	256[c]	179	6	59
$CH_2=CH-\dot{C}H_2$	77[a]	Cl	58[a]	256[c]	198	24	58
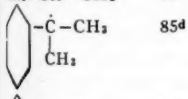	85[d]	CH_3	74[d]	241[c]	167	16	81
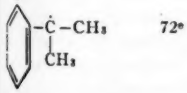	72[e]	CH_3	60[e]	237[c]	177	29	84

[a] M. Szwarc, Chem. Revs. **47**, 75 (1950).
[b] J. J. Mitchell and F. F. Coleman, J. Chem. Phys. **17**, 44 (1949).
[c] See reference 1.
[d] Estimated to be the same (see reference a) as for $R=(CH_3)_3\dot{C}$.
[e] Estimated from values (see reference a) for $R=$ 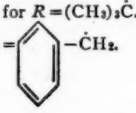 $-\dot{C}H_2$.

illustrated by the following resonance forms for the allyl radical and ion.

$$CH_2=CH-\dot{C}H_2\leftrightarrow\dot{C}H_2-CH=CH_2$$

$$CH_2=CH-\overset{+}{C}H_2\leftrightarrow\overset{+}{C}H_2-CH=CH_2.$$

In the saturated radicals and ions the resonance energy has been attributed[2] to hyperconjugation, illustrated by the following resonance forms for the propyl radical and ion:

$$CH_3-CH_2-\dot{C}H_2\leftrightarrow CH_3-\overset{H^{\cdot}}{CH}=CH_2$$

$$CH_3-CH_2-\overset{+}{C}H_2\leftrightarrow CH_3-\overset{H^{+}}{CH}=CH_2.$$

From the results in Table I it appears that the π-conjugation energy in unsaturated radicals is considerably greater than the hyperconjugation energy of the corresponding saturated radicals. In the case of hydrocarbon carbonium ions, both forms of resonance appear to be equally effective.

Evidence for the same conclusion was recently obtained and discussed by Evans and Halpern[5] on the basis of their measurements of the proton affinities of a variety of alkyl and aryl substituted olefins.

[1] J. L. Franklin and H. E. Lumpkin, J. Chem. Phys. **19**, 1073 (1951).
[2] A. G. Evans, *The Reactions of Organic Halides in Solution* (Manchester University Press, Manchester, England, 1946).
[3] Baughan, Evans, and Polanyi, Trans. Faraday Soc. **37**, 377 (1941).
[4] D. P. Stevenson, J. Chem. Phys. **10**, 291 (1942).
[5] A. G. Evans and J. Halpern (to be published).

Resonance Energy of Gaseous Ions—Reply to Halpern

J. L. FRANKLIN AND H. E. LUMPKIN
Technical and Research Divisions, Humble Oil and Refining Company, Baytown, Texas
(Received January 16, 1952)

HALPERN[1] has pointed out again the high degree of stabilization of alkyl carbonium ions caused by methyl groups attached to the charged atom and has attributed this to resonance. From this he concludes, contrary to our views,[2] that the allyl ion is stabilized by resonance and that the resonance energy of this ion is the same as that of the *n*-propyl ion.

That the higher alkyl radicals and positive ions are more stable than methyl will be apparent from a comparison of the C—H bond strength of the paraffin with that of methane and the appearance potential of the alkyl ion with that of methyl. For example, the strength of the C—H bond[3] is 102 kcal/mole in methane and 97 kcal/mole in ethane, the difference, 5 kcal/mole, representing the increased stability of the ethyl radical. Similarly, the appearance potentials of the methyl and ethyl ions from the corresponding paraffins are 332[4] and 295[5] kcal/mole, respectively. The ethyl ion is thus 36 kcal/mole more stable than the methyl. This increased stability of the higher alkyl radicals and positive ions has been attributed by Halpern,[1] Baughan, Evans, and Polanyi,[5] and A. G. Evans[6] to resonance on the basis that the radical or ion would be a hybrid of the following structures, again using ethyl as an example:

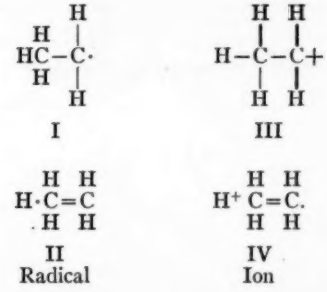

If there were no stabilization, the C—H bond strength and the appearance potential of the ion would be the same as those found with methane. From this we can calculate the heat of formation of the principal structure (I and III). The energies of structures II and IV are readily calculated as the sums of the ΔH_f of ethylene and, respectively, $H\cdot$ and H^+. The values for structures II and IV calculated in this way are probably low since both the C—C bond length and the hybridization of one of the carbons in the ethylene are probably not adjusted to minimum energy, i.e., are not the same as in an ethylene molecule at equilibrium.

Table I summarizes the results of such calculations for several alkyls. It will be apparent that the higher ions are stabilized for a far greater extent than the corresponding radicals. Resonance theory can account for this only if the difference in energies of structures IV and III is much smaller than that of structures II and I. Actually, from Table I we find the reverse to be true. In order to explain the stabilization of alkyl ions by resonance, Baughan, Evans, and Polanyi,[5] and A. G. Evans[6] have assumed that the energy of structure IV would be much less than that

shown because the proton, being very small, would have no significant repulsive energy. If this explanation is correct, we will find the stabilization energy to be greatly reduced if one or more atoms of high ionization potential are substituted for the hydrogen on the CH_3 group of the ethyl ion. Stevenson and Hipple[7] found the appearance potential of the

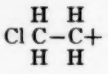

ion from *n*-propyl chloride to be 292 kcal/mole. From this we calculate the stabilization energy to be 40 kcal/mole, which is within the experimental error, a check on the stabilization energy of the ethyl ion. The energy of structure

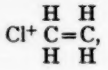

TABLE I. Energies of "resonance" structures of alkyl radicals and ions, kcal/mole.

R	D_{C-H}[a]	$\Delta H_f(R\cdot)$ Stab. energy ($R\cdot$)	Principal structure	Other structures	A_{R^+}	"ΔH"$_f(R^+)$ Stab. energy (R^+)	Principal structure	Other structures
CH_3	102	0	32	···	332[b]	0	262	···
CH_3CH_2	97	5	30	64	296[c]	36	260	379
$(CH_3)_2CH$	91	11	25	57	266[d]	66	255	372
$(CH_3)_3C$	86	16	19	49	247[e]	84	249	364
	···	···	···	···	292[f]	40	255	341[g] 372[h]

[a] See reference 3.
[b] See reference 4.
[c] D. F. Stevenson and J. A. Hipple, J. Am. Chem. Soc. **64**, 1588 (1942).
[d] Calculated from the appearance potential of 252 kcal/mole (see reference 5) for the *i*-propyl ion from *i*-butane.
[e] Calculated from the appearance potential of 237 kcal/mole for the *t*-butyl ion from *t*-butyl chloride (see reference 8).
[f] Calculated from the appearance potential of 277 kcal/mole for the ion from *n*-propyl chloride (see reference 8).
[g]
[h]

while somewhat below that of

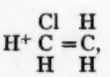

is still much higher than that of the principal structure. Of course, Cl^+ has a much greater radius than H^+, yet the stabilization energy of

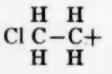

is substantially the same as that of the ethyl ion. Although more data on this point would be desirable, we are forced to doubt that the energy of structure IV is low and hence that more than a minor amount of the stabilization of alkyl ions is attributable to resonance.

We have recently measured the appearance potential of

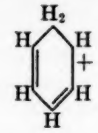

from

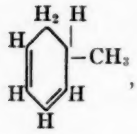

the value found being 10.6 volts (244 kcal/mole). From this we calculate a stabilization energy of 74 kcal/mole against $^+CH_3$. Now a simple valence bond treatment of the allyl ion gives a "resonance" energy of $\frac{1}{2}\alpha$. From Halpern's calculation of the empirical resonance energy we find $\alpha = 116$ kcal/mole. A valence bond treatment of

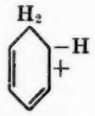

gives a value of 0.83α or 96 kcal/mole for the π-electron resonance alone. In addition, one would expect about the same hyperconjugation as is found in the ethyl ion, i.e., about 36 kcal/mole. If the ion were stabilized by resonance, the stabilization energy would be some 58 kcal/mole greater and the appearance potential 2.5 volts lower than is actually measured.

Thus, we have serious cause to doubt that either alkyl ions or ions with the charge conjugated with one or two double bonds are stabilized by resonance. Further, the fact that the *n*-propyl, allyl, and benzyl ions are stabilized by the same amount is a coincidence that is indeed striking and suggests that we seek an explanation other than that of resonance. Unfortunately, we can advance only a tentative partial explanation. Rough calculations indicate that the polarizability of a methyl group in the field of the ionic charge could result in stabilizing the ion by some 11–18 kcal/mole. This is only about $\frac{1}{3}$ to $\frac{1}{2}$ the total stabilization; however, this calculation usually gives results considerably below the measured values. Further, since polarizability is largely associated with the size of the group, one would expect the allyl and *n*-propyl groups to be stabilized by about the same amount.

[1] H. Halpern, J. Chem. Phys. **20**, 745 (1952), see preceding letter.
[2] J. L. Franklin and H. E. Lumpkin, J. Chem. Phys. **19**, 1073 (1951).
[3] Roberts and Skinner, Trans. Faraday Soc. **45**, 339 (1949).
[4] L. G. Smith, Phys. Rev. **51**, 263 (1937).
[5] Baughan, Evans, and Polanyi, Trans. Faraday Soc. **37**, 377 (1941).
[6] A. G. Evans, *The Reactions of Organic Halides in Solution* (Manchester University Press, Manchester, 1946).
[7] P. F. Stevenson and J. A. Hipple, J. Am. Chem. Soc. **64**, 2766 (1942).

α- and β-Bands in Potassium Bromide Crystals

CHARLES DELBECQ, PETER PRINGSHEIM, AND PHILIP YUSTER
Chemistry Division, Argonne National Laboratory, Chicago 80, Illinois
(Received January 29, 1952)

IN a paper[1] published about a year ago we described new types of absorption bands characteristic of alkali halides. In potassium iodide these bands, which we designated as α- and β-bands, were ascribed owing to the presence of negative ion vacancies and *F* centers, respectively. The last paragraphs of that paper mentioned the apparent existence of similar bands in potassium bromide in the region below 210 mμ, and in a report[2] we stated that the α-band in potassium bromide was observed at liquid nitrogen temperature at 203 mμ.

Further work with an instrument capable of measurement down to 185 mμ has shown that these two absorption bands which

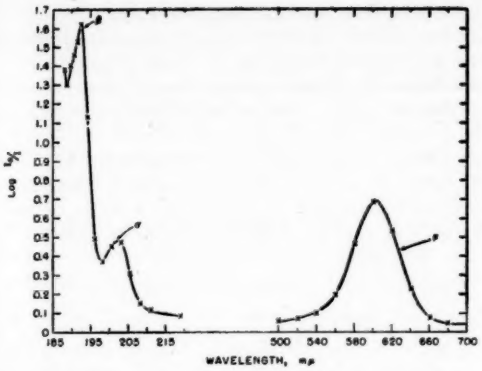

FIG. 1. KBr crystal x-rayed 10 minutes at liquid nitrogen temperature.

occur below 210 mμ in potassium bromide are analogous to the α- and β-bands first observed in potassium iodide. In additively colored potassium bromide bleached at −150°C with *F* light the α-band appeared and the β-band was lowered. A potassium bromide crystal colored by exposure to x-rays at liquid nitrogen temperature showed in its absorption spectrum the *F* band at 600 mμ, the α-band at 203 mμ, and the β-band at 193 mμ (Fig. 1), while a crystal colored at room temperature showed only the *F* and β-bands.

At an ionic crystals symposium at the University of Illinois, October 29–30, 1951, R. W. Pohl described an experiment in which a crystal of potassium bromide containing *U* centers was bleached at liquid nitrogen temperature by light absorbed in the *U* band. This bleaching gave rise to a new band on the short wavelength side of the *U* band which was given the name *U'*.[3] We repeated this experiment because we believed this *U'* band to be identical with our α-band. The *U'* band which we obtained in our experiment again seemed to coincide with the α-band.

Recently W. Martienssen has published a short note[4] which in the main contains the data on which Pohl's talk was based. In addition to the *U'* band another band with peak at about 192 mμ was observed by him when a crystal containing *U* centers was exposed to *U* light at room temperature. However, this band at 192 mμ as well as the *U'* band was also obtained in photochemically colored crystals free of *U* centers. Near the end of the note Martienssen mentions that his new bands may be connected with our "greek letter bands."

We would like to emphasize that all observations described in Martienssen's note can be explained by interpreting the new bands as α- and β-bands. The potassium bromide band at 192 mμ is a β-band and always appears when *F* centers are formed in the crystal, whether by photochemical coloration or by irradiation of *U* centers with *U* light at a temperature above −100°C. The *U'* band is identical with, or closely related to, the α-band which can be obtained in crystals photochemically colored at low temperature. If after absorption of light in a *U* center, which is supposed to be a hydride ion replacing a bromide ion, the electron is completely separated from the ion, and subsequently the neutral hydrogen atom also migrates away, the conditions are exactly those characteristic of a normal α-center. It may be, however, that at temperatures below −100°C the neutral hydrogen atom remains at the lattice point formerly occupied by the hydride ion and that the perturbation due to the presence of the hydrogen atom is similar to, but not identical with, that due to the presence of a negative ion vacancy. We hope to carry out further experiments to determine whether the *U'* center and the α-center are exactly the same. Another problem to be solved in this connection is the question of what becomes of the electron when it is separated from the hydride ion.

[1] Delbecq, Pringsheim, and Yuster, J. Chem. Phys. **19**, 574 (1951).
[2] ANL-4526, Section 1.7, Quarterly Progress Report, Chemistry Division, Sec. C-II (January 23, 1951).
[3] H. Thomas, Ann. Physik **38**, 601 (1940).
[4] W. Martienssen, Naturwiss. **38**, 482 (1951).

Theory of the Ozone Molecule*

B. T. DARLING AND J. A. WEISS
Department of Physics and Astronomy, The Ohio State University, Columbus, Ohio

(Received February 1, 1952)

THERE are two special features which distinguish the theoretical treatment of the ozone molecule from that of the usual nonlinear triatomic molecule. These are the existence of three equivalent equilibrium configurations (in the case of an isosceles model) and the further requirement, for O_3^{16}, that the wave functions be symmetrical under all permutations of the atoms. Furthermore, the usual treatment of molecules possessing isomeric forms cannot be applied because the molecule possesses more symmetry than can be described by the geometrical point groups and the rotation group; with the operations of these groups it is not possible to perform cyclic permutations of the nuclei. In order to investigate the situation we have used a coordinate system in terms of which these features may be conveniently described.

First, the set of three interatomic distances (r_1, r_2, r_3) specifying a configuration of the molecule is represented by a point in a three-dimensional rectangular coordinate system. We then adopt, in place of (r_1, r_2, r_3), the coordinates (u, z, χ) defined as shown in Fig. 1. Point 1 in the diagram represents an isosceles triangle

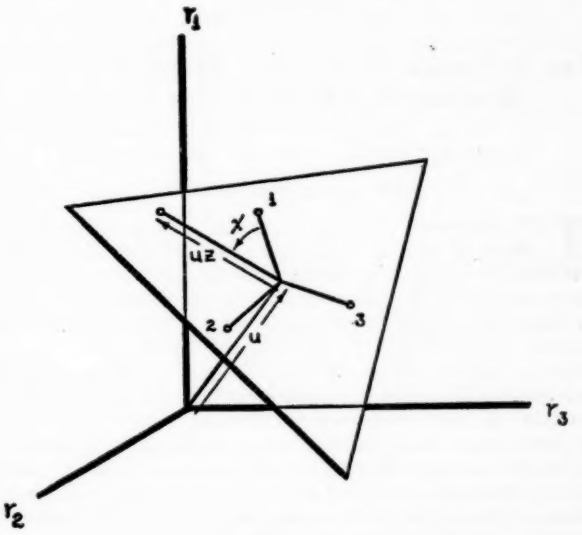

FIG. 1.

of obtuse apex angle, and points 2 and 3, the two triangles obtained from it by cyclic permutations. The variables u, z, χ correspond roughly to the normal coordinates of a nonlinear triatomic molecule, with $u \sim \nu_1$, $z \sim \nu_2$, $\chi \sim \nu_3$. The existence of three equilibrium configurations is accounted for by requiring that the potential be periodic of period $\frac{2}{3}\pi$ in χ. It must also be an even function of χ.

With the choice of principal axes as body-fixed axes and the requirement that the configuration vary continuously with χ relative to these axes, we find that the operations which superpose the molecule upon itself are: variation of χ from χ_0 to $\chi_0+\frac{2}{3}\pi$ with rotation of the body-fixed axes through π about the axis perpendicular to the plane of the nuclei, and variation of χ from χ_0 to $-\chi_0$ with rotation of the body-fixed axes through π about a specified principal axis in the plane of the nuclei.

Choosing the angular momentum diagonal in the component perpendicular to the plane and applying Bose statistics, we obtain the following symmetry properties of the vibrational states: they occur in pairs, one described by a periodic wave function $F_{n_3}(\chi+\frac{2}{3}\pi)=F_{n_3}(\chi)$, the other by an "antiperiodic" function

$Gn_3(\chi+\frac{2}{3}\pi)=-Gn_3(\chi)$, associated with even K and odd K, respectively, where K is the component of angular momentum perpendicular to the plane of the nuclei. We find that an estimate of the barrier height between the equilibrium configurations $\chi=0$ and $\chi=\frac{2}{3}\pi$, etc., based on the known features of the infrared spectrum, leaves these pairs degenerate to a very good approximation for the lowest vibrational states.

The 1040 cm^{-1} band of the solar ozone spectrum, as observed by Howard and Shaw,[1] apparently consists of three series of lines, such as would be expected for a very nearly symmetric rotator. For the obtuse isosceles equilibrium configuration of ozone we should expect alternate lines to be absent from two of the series. The fact that there are no missing lines suggests (in addition to the acute-angled model) the following possibilities: that the nearly-equal moments of inertia are sufficiently different, as in the obtuse-angled model of Hughes,[2] to produce additional lines giving the appearance of series as observed, or that the equilibrium configuration is not isosceles but nearly-isosceles, giving a potential in the form of a threefold double minimum. Analysis of the 1040 cm^{-1} band in the light of these hypotheses is in progress.

* Supported in part by a contract between the Geophysical Division of the Air Force Cambridge Research Center and the Ohio State University Research Foundation.

[1] J. N. Howard and J. H. Shaw, private communication.
[2] Richard H. Hughes, Phys. Rev. 85, 717(A) (1952).

The Application of the Hammett Equation to the Dissociation of Aromatic Free Radicals

NEWTON SCHWARTZ AND WAYNE K. WILMARTH
Department of Chemistry, University of Southern California, Los Angeles, California
(Received December 26, 1951)

THE Hammett rho-sigma equation[1] which correlates the effects of *meta*- and *para*-substituents in aromatic systems, has proved valid for free radical reactions in a single instance, although it is frequently mentioned in the discussions of such systems. It is generally recognized that it fails to predict the relative dissociation of the hexaphenyl ethanes, where all substituents increase the dissociation constant. Similarly, evidence has recently been presented indicating that the energies of dissociation of the benzyl bromides, forming benzyl radicals and bromine atoms, are lowered by substituents with either positive or negative sigma-values.[2] The only published instance where free radical dissociation has been successfully considered from the Hammett viewpoint is the unimolecular rate of dissociation of benzoyl peroxides to benzoyl radicals.[3] However, these systems are relatively insensitive to substituent effects (the rho-value for benzoyl peroxides is equal to -0.3).

If generalizations can be drawn from so few examples, the results would indicate that the formation of carbon radicals cannot be treated in this manner but that other radical systems might prove more amenable. Since the only successful application of the equation involves the calculation of rate constants, a correlation of dissociation constants, in even a single instance, would greatly strengthen the probability that the equation was of some general validity. Goldschmidt and his school of workers,[4,5] prepared and determined the equilibrium constants of the substituted 1,1,4,4, tetraphenyl-2,3 dibenzoyl tetrazanes (Fig. 1), where R_1 and R_2 were $-OCH_3$, $-CH_3$, $-H$, $-Br$, $-NO_2$. Despite the

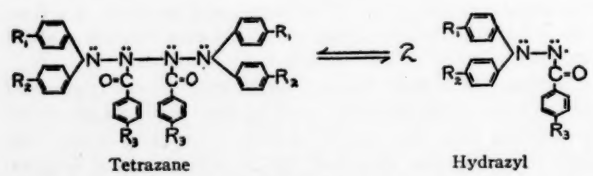

FIG. 1. Dissociation of the tetrazanes.

TABLE I. Equilibrium data for the tetrazanes.

R_1	R_2	T°C	Solvent	log$K$	logk/k_0	$\sigma_1+\sigma_2$
OCH_3	H	−18	acetone	−1.85	+1.49	−0.268
	[a]	−18	ϕCH_3	−1.97	+1.37	−0.268
CH_3	CH_3	−18	ϕCH_3	−2.17	+1.17	−0.340
CH_3	H	−18	ϕCH_3	−2.76	+0.58	−0.170
H	H	−18	ϕCH_3	−3.34	0	0
		−18	$CHCl_3$	−2.03		
		−18	acetone	−3.23		
Br	H	−18	ϕCH_3	−3.92	−0.58	+0.232
Br	Br	−18	ϕCH_3	−4.24	−0.90	+0.464
NO_2	H	−18	$CHCl_3$	−3.48	−0.14	+0.778
	[a]	−18	ϕCH_3	−4.79	−1.45	+0.778
NO_2	NO_2	0	$CHCl_3$	−5.62	−2.28	+1.56
	[b]	−18	ϕCH_3	−6.03	−4.73	+0.56

[a] Approximated by $\log K\,\phi CH_3=\log Kx+(\log K^0\,\phi CH_3-\log Kx^0)$ where K and K^0 are the dissociation constants for the substituted and unsubstituted compounds, respectively, and X is the solvent in which the compound was actually determined.
[b] Approximated by assuming heat of dissociation as 20 kcal/mole and use of van't Hoff equation, followed by use of above equation.

shortcomings that some of the radicals were studied in different solvents, and in one case at a different temperature, their data was subject to a rho-sigma treatment in this laboratory with approximate corrections for solvent and temperature effects (see Table I and Fig. 2). The results of the plot indicate that this is indeed a free radical equilibrium system in which the relative

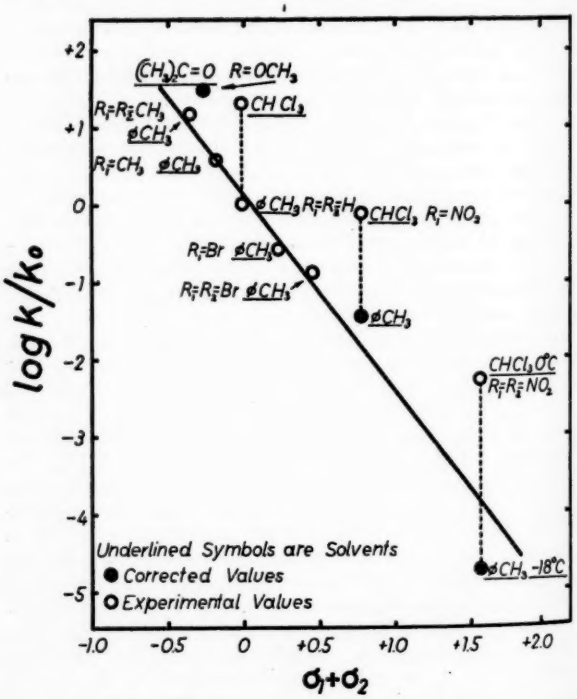

FIG. 2. Hammett rho-sigma for the tetrazanes at −18°C.

values of the dissociation constants can be predicted using the conventional sigma-values. The five compounds determined in the same solvent define a straight line with a rho-value equal to -2.6, indicating that the dissociation of the tetrazanes is strongly influenced by the various substituents. The compounds determined in chloroform and acetone scatter about this line when approximate corrections are made; if these corrections are ignored, the results still approximate linearity (i.e., satisfy the criterion

that substituents with positive and negative sigma-values act in opposing directions).

To establish firmly the above conclusions, work is underway to reinvestigate the tetrazane system. Compounds with *meta-* and *para*-substituents, mixed substituents, and substituents on the benzoyl ring will be determined in the same solvent. For the latter case, the previous workers determined only the effects of the $-NO_2$ and $-OCH_3$ groups; these points have not been included on the graph since they involve a different aromatic ring and the probable error was somewhat greater in these studies. An attempt will also be made to extend the range of sigma-values in order to test the recent proposal that a curvature should exist in such a plot.[3]

[1] L. P. Hammett, *Physical Organic Chemistry* (McGraw-Hill Book Company, Inc., New York, 1940), p. 184.
[2] Szwarc, Leigh, and Sehon, J. Chem. Phys. **19**, 657 (1951).
[3] Swain, Stockmayer, and Clarke, J. Am. Chem. Soc. **72**, 5426 (1950).
[4] Goldschmidt, Wolff, Wolffhardt, Drimmer, and Nathan, Ann. Physik 437, 194 (1924).
[5] St. Goldschmidt and J. Bader, Ann. Physik **473**, 137 (1929).

Paramagnetic Resonance Absorption of Microwaves

R. T. Weidner and C. A. Whitmer
Department of Physics, Rutgers University, New Brunswick, New Jersey
(Received December 26, 1951)

In a paper of the above title by Lancaster and Gordy[1] conclusions are drawn concerning the presence or absence of exchange interaction in paramagnetic salts on the basis of shape analyses of the resonance curves from powdered samples. We wish to point out that the experimental conditions for these measurements, in which the effects of anomalous magnetic dispersion were present, may affect the observed "absorption" curves considerably.

The presence of exchange interaction is deduced from the ratio of the root mean fourth moment to the root mean second moment of an absorption line; this ratio increases over the value 1.32, characteristic of the Gaussian shape, when exchange is present. The absorption curves for a resonance showing exchange interaction is then relatively narrow at the peak and strong in the wings. Clearly, the fourth to second moment ratio is very sensitive to small absorption in the wings of a line under the most favorable experimental conditions.

As Lancaster and Gordy point out, the observed signal registering the resonance will contain contributions from absorption alone only if the dispersion effects are removed by tuning the sample cavity or oscillator frequency at each magnetic field. In the balanced bridge method used by Lancaster and Gordy this procedure was not followed, and therefore both absorption and dispersion, i.e., both the imaginary and real parts of the microwave susceptibility of the sample, χ'' and χ', contribute to the observed signal. For sufficiently weak absorptions the unbalance power in a bridge is proportional to $\chi'^2+\chi''^2$; if a *single* resonance line having a Lorentz shape is observed, $\chi'^2+\chi''^2$ is closely proportional to χ'', which measures true absorption.[2] A properly unbalanced bridge will register pure χ' or pure χ'' when voltage unbalance rather than power unbalance is measured.[3]

The dispersion effects distort the line shape most severely when unresolved lines occur in the resonance. Lancaster and Gordy remark that a multiplicity of lines in the spectrum will tend to blunt the shape, and therefore give the opposite effect of exchange narrowing. If, however, there are χ' contributions to the observed signal, the interference or cancellation of χ' in the regions between adjacent lines may tend to narrow the observed shape near the peak and broaden it in the wings, where χ' contributions from the several lines will constructively interfere. This effect is all the more important in influencing the over-all absorption shape when it is recalled that the maximum value of $|\chi'|$ for a single resonance may be one-half the maximum value of χ''.

We have found the distortion effect of χ' to be quite large for some salts. Figure 1 shows the "absorption" for a single crystal of

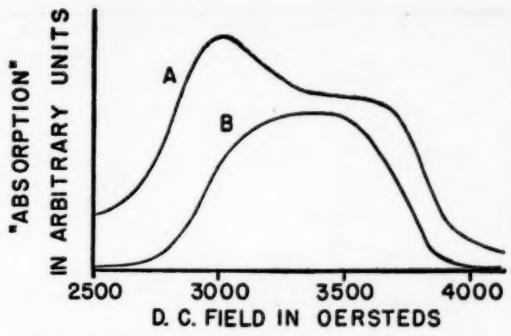

FIG. 1. Resonance curves for a single crystal of ferric ammonium sulfate. The dc magnetic field is perpendicular to the (110) face; the frequency is 9375 mc/sec. In curve *A* the ordinate is $\chi'^2+\chi''^2$; in curve *B* the ordinate is χ''.

ferric ammonium sulfate. In curve *A*, $\chi'^2+\chi''^2$ is plotted as ordinate; in curve *B*, χ'' is plotted. The interference in χ' clearly produces the asymmetry in the over-all shape in curve *A*. Curve *B* was obtained by retuning the oscillator frequency at each value of the magnetic field to remove the effects of χ'. The procedure for making these measurements is more fully described in a forthcoming article.[4]

Lancaster and Gordy report an asymmetrical shape for ferric ammonium sulfate. In view of these observations it appears to us that the evaluation of moment ratios without consideration of dispersion effects is highly questionable.

[1] F. W. Lancaster and W. Gordy, J. Chem. Phys. **19**, 1181 (1951).
[2] Whitmer, Weidner, Weiss, and Hsiang, Phys. Rev. **74**, 1478 (1948).
[3] G. E. Pake, Am. J. Phys. **18**, 473 (1950).
[4] R. T. Weidner and C. A. Whitmer, Rev. Sci. Instr. **23**, 75 (1952).

Emission Spectrum of HCl in the Near Infrared*

Roger Newman
Gates and Crellin Laboratories of Chemistry,† California Institute of Technology, Pasadena 4, California
(Received February 5, 1952)

THE infrared emission spectrum of a Cl_2, NH_3 flame was studied in the hope of observing the vibration-rotation spectrum of NH or NH_2 free radicals in the fundamental region. In this respect no success was obtained. In this flame, however, a portion of the HCl emission spectrum was observed which showed features of interest. For convenience subsequent work and that reported here was done with a Cl_2, H_2 flame. As the spectrum of this flame in the near infrared has, to our knowledge, not been previously reported, a brief description of the results seems worthwhile.

The flame consisted of a jet of chlorine burning in an atmosphere of hydrogen. The combustion was carried out in a tube open toward the tip of the flame. The flame was viewed axially by a vacuum grating spectrometer[1] equipped with a cooled PbS cell.

Because of the high degree of vibrational and rotational excitation in the flame-produced HCl molecules, portions of their spectrum are made accessible which are not observed in the usual absorption measurements.[2-4] Figure 1, showing part of the fundamental and first overtone bands, illustrates some of the effects accompanying such excitation.

The *R* branch band heads have been definitely observed for the (1−0), (2−0), and (3−1) transitions. These have been recorded at $3181._0$, 5833, and 5620 cm^{-1}, respectively. The empirical equations[5] for the rotational structure observed in absorption predict the values 3174, 5836, and 5629 cm^{-1} for these heads. In calculating the last quantity it was assumed that the convergence of the (2−0) and (3−1) bands was the same, which seems to be the case to a good approximation. The (2−1) band head is not too readily seen; we believe it to be the partially overlapped

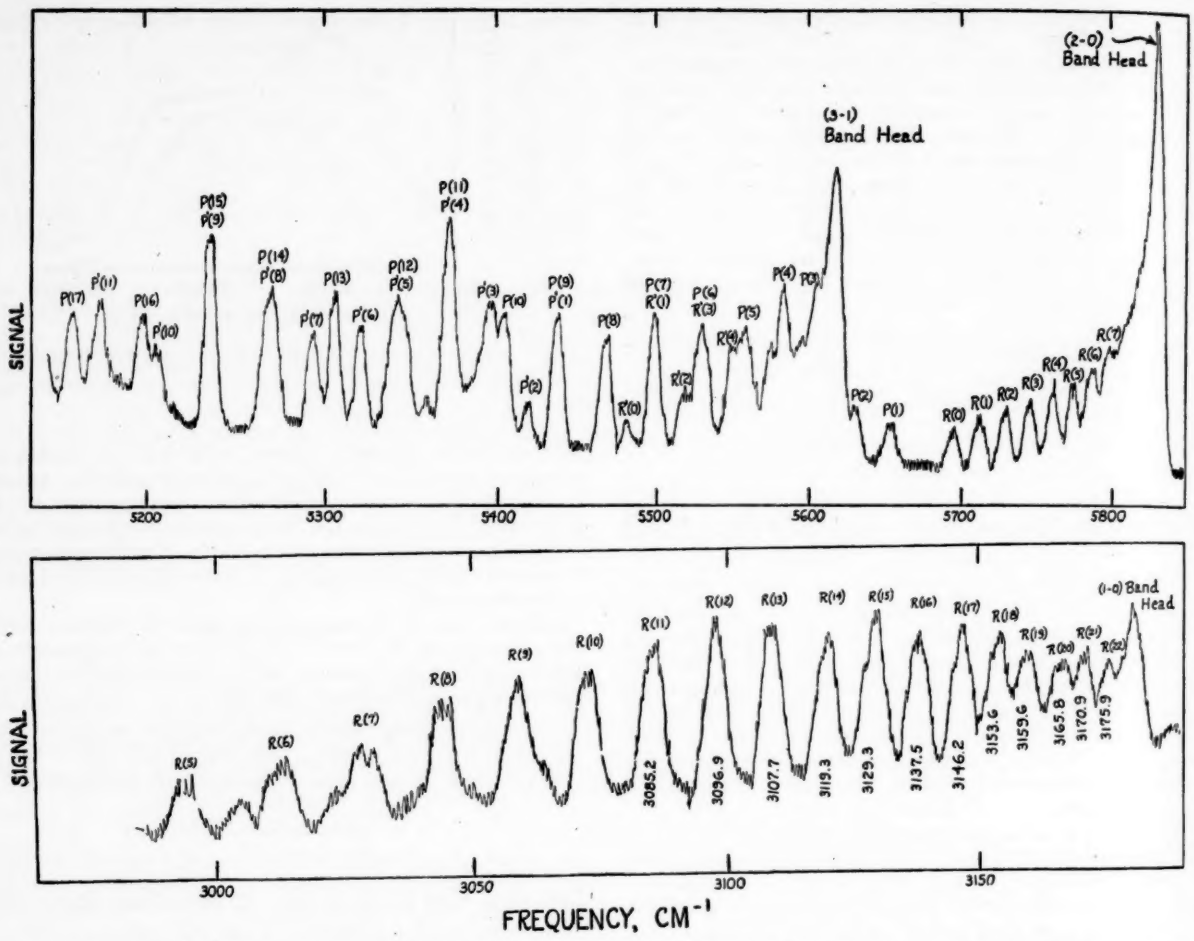

FIG. 1. A portion of the fundamental (lower figure) and first overtone bands (upper figure) of HCl in emission. The traces shown are uncorrected for changes in detector sensitivity. In the upper figure primes refer to the (3–1) transition, unprimed quantities to the (2–0) transition. The numbers in parentheses refer to the J level in the lower state.

maximum at 3063 cm^{-1} (predicted value 3070 cm^{-1}). The weak (4−2) head is probably obscured by overlapping lines.

In the figure we have indicated the frequencies of some of the higher J lines of the (1−0) band. These frequencies are good only to about ± 0.5 cm^{-1}. These new data are, unfortunately, insufficiently accurate to justify a refinement of the formula representing the rotational fine structure. With more regard paid to the design of the flame, higher accuracy could no doubt be obtained and such a refinement could be made.

The pattern of the overtone band is complicated by the superposition of the (2−0) and (3−1) transitions. The individual lines have been assigned as indicated in the figure.

A completely unambiguous estimate of rotational temperature from the data of the (1−0) band has not been made. The peak intensities of the well-resolved lines could not all be fitted to a single temperature parameter. Thus, for example, while the band maximum ($J'=12$ or 13) indicates a $T_{rot} \leqq 4500°K$, the intensity distribution of the lines for $J' \geqslant 13$ seem better fitted by a $T_{rot} \leqq 2500°K$. The discrepancy is perhaps due to reabsorption by the HCl present in the cooler portions of the flame and in the exhaust gas. If this is the case, then the 2500°K figure is probably the more reliable.

Our estimate of vibrational temperature is also not free from uncertainty. For purposes of calculation it is assumed that (1) the peak intensities of the (2−0) and (3−1) band heads characterize their respective band intensities; (2) the reabsorption at the band heads is small; (3) the ratio of dipole matrix elements M_{31}/M_{20} is equal to $\sqrt{3}$.[6] On this basis $T_{vib} \leqq 2500°K$. The agreement of the best estimates of T_{vib} and T_{rot} is probably accidental; however, these figures are not unreasonable in comparison with the maximum temperature attainable from the H_2, Cl_2 reaction, namely ~3000°K.

* This investigation was supported by the ONR under contract N6-ori 102, VI.
† Contribution number 1659.
[1] Badger, Zumwalt, and Geguére, Rev. Sci. Instr. **19**, 860 (1948).
[2] C. F. Meyer and A. A. Levin, Phys. Rev. **34**, 44 (1929).
[3] G. Herzberg and J. W. T. Spinks, Z. Physik **89**, 474 (1934).
[4] E. Lindholm, Naturwiss. **27**, 470 (1939).
[5] W. F. Colby, Phys. Rev. **34**, 53 (1929).
[6] B. L. Crawford and H. L. Dinsmore, J. Chem. Phys. **18**, 983 (1950).

Refined Free Electron Model of Porphine and Tetrahydroporphine

TAKESHI NAKAJIMA AND HIDEO KON
Glass Research Institute and Chemical Institute, Faculty of Science, Tohoku University, Sendai, Japan
(Received February 5, 1952)

THE electronic structures of porphine and tetrahydroporphine have been studied theoretically by several authors; Longuet-Higgins, Rector, and Platt[1] adopted the simple LCAO MO method and Simpson[2] and Kuhn,[3] the perimeter-free-electron model.

The present writers' calculation is based on a refined free-electron model, which takes into account explicitly the effect of the cross links and hetero-atoms.

The molecular skeleton of porphine is divided into twelve parts (six, in tetrahydroporphine) each of which has its π-electron wave function u_1, u_2, $\cdots$; respectively (Fig. 1). The total one-electron

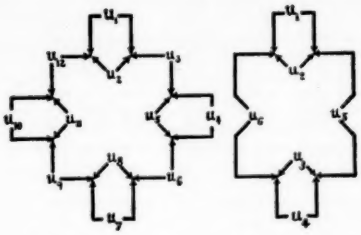

Porphine Tetrahydroporphine

FIG. 1. Structures of porphine and tetrahydroporphine.

wave functions Ψ's are constructed by connecting u's so as to make Ψ's the bases of the irreducible representations of the symmetry groups D_{4h} (porphine) and D_{2h} (tetrahydroporphine), so that u's must have one of the forms,

$$a\cos\tilde{\omega}x, \quad b\sin\tilde{\omega}x, \quad \text{or} \quad a\cos\tilde{\omega}x+b\sin\tilde{\omega}x.$$

For example, those belonging to the species A_{1u} of D_{4h} are written as

$$u_1=u_4=u_7=u_{10}=b_1\sin\tilde{\omega}x, \quad u_2=u_5=u_8=u_{11}=b_2\sin\tilde{\omega}x,$$
$$u_3=u_6=u_9=u_{12}=b_3\sin\tilde{\omega}x,$$

where x is measured by the one bond length l as a unit, and $\tilde{\omega}$ is related to the orbital energy E by the formula,

$$E=(h^2\tilde{\omega}^2)/(8\pi^2ml^2).$$

Moreover, Ψ's are required to be one-valued and continuous at the point of connection.[4]

These requirements are fulfilled by the following set of relations for the above species:

$$b_1\sin3\tilde{\omega}-b_2\sin2\tilde{\omega}=0,$$
$$b_1\sin3\tilde{\omega}+b_3\sin2\tilde{\omega}=0,$$
$$b_1\cos3\tilde{\omega}+b_2\cos2\tilde{\omega}-b_3\cos2\tilde{\omega}=0,$$

which leads to a determinantal equation,

$$\begin{vmatrix} \sin3\tilde{\omega} & -\sin2\tilde{\omega} & 0 \\ \sin3\tilde{\omega} & 0 & \sin2\tilde{\omega} \\ \cos3\tilde{\omega} & \cos2\tilde{\omega} & -\cos2\tilde{\omega} \end{vmatrix}=0.$$

The energy levels are computed by solving this equation for $\tilde{\omega}$. An entirely similar program is followed for the other species. The calculation is calibrated with the "color" of benzene.[2]

The singlet-triplet centers of gravity of several long wavelength transitions thus obtained are shown in Fig. 2 (a), and close agreement with the results of LCAO MO method is found there, except that, in porphine the two transitions $A_{1u}\rightarrow E_g$ and $B_{2u}\rightarrow E_g$ come out on the well-spaced positions and in tetrahydroporphine the transition $B_{1u}\rightarrow B_{3g}$ (24,000 cm^{-1}, $\perp$) is of shorter wavelength than the transition $B_{1u}\rightarrow B_{2g}$ (23,000 cm^{-1}, $\|$) in contrast with the LCAO results where the situations are reversed.

The effect of a nitrogen atom is taken into account by assuming a potential box of a certain length (one or two bond lengths) and depth V in place of the nitrogen atom.

The shift of a transition $\Psi_A\rightarrow\Psi_B$, thus caused, is given as

$$V\left|\int_{-\delta}^{+\delta}(\Psi_B^2-\Psi_A^2)dx\right|$$

by the first-order perturbation theory.

Several choices of the length and depth lead to the results shown in Fig. 2(b), (c).

In tetrahydroporphine the replacement of the two amino-nitrogens by the boxes (one bond length, $V=23{,}000$ cm^{-1}) presents the results considerably different from those of LCAO; the insertion of shallow supplementary boxes ($V'\doteqdot0.3$ ev) at the two aza-nitrogens or the extensions of lengths of boxes cause no significant changes. The computed 13,300 cm^{-1}, 16,400 cm^{-1}, and 24,100 cm^{-1} (Soret) transitions agree very well with the observation (Table I) and no transitions are computed near the observed 19,000 cm^{-1} (?) band. In agreement with the conclusion of reference 1, the predicted Soret and 13,000-cm^{-1} bands are polarized $\|$ along, and $\perp$ to, the long axis of the molecule, respectively, and remembering that this molecule is the typical case of the "long-field" spectra,[5] the predicted sequence may be expected to agree well with the observation.

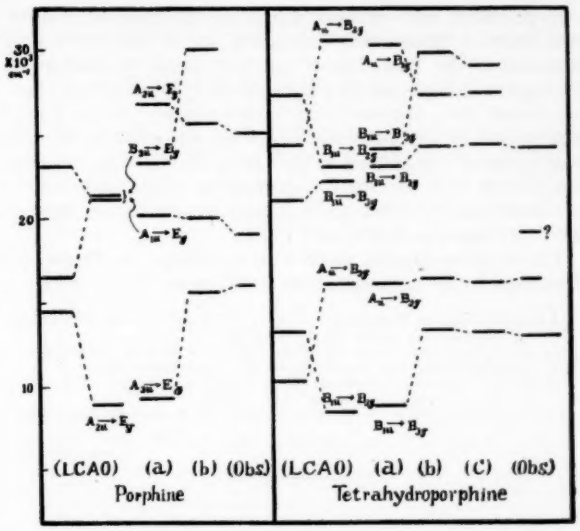

FIG. 2. Comparison of calculated with observed electronic energy states.

Porphine:
(a) $V=0$,
(b) $V=23{,}000$ cm^{-1}, two bond lengths.

Tetrahydroporphine:
(a) $V=0$, $V'=0$,
(b) $V=23{,}000$ cm^{-1}, $V'=0$, one bond length,
(c) $V=21{,}250$ cm^{-1}, $V'=2125$ cm^{-1}, one bond length.

TABLE I. Comparison of calculated centers of gravity with observed singlets.

Molecule	Trans. type	Pol.	Calc[a] (cm^{-1})	Obs (cm^{-1})	LCAO[b] (cm^{-1})
Porphine	$A_{2u}\rightarrow E_g$	$\perp$, $\|$	9300		9000
		Doub. deg	(15,600)	16,000	(14,500)
	$A_{1u}\rightarrow E_g$	$\perp$, $\|$	20,200		21,300
		Doub. deg	(20,200)	19,000	(16,500)
	$A_{2u}\rightarrow E_g$	$\perp$, $\|$	26,800		
		Doub. deg	(25,600)	25,000	
	$B_{2u}\rightarrow E_g$	$\perp$, $\|$	23,300		21,300
		Doub. deg	(30,100)	?	(23,000)
Tetrahydro-porphine	$B_{1u}\rightarrow B_{3g}$	$\perp$	8900 (13,300)	13,000	8700 (13,200)
	$A_u\rightarrow B_{3g}$	$\|$	16,200 (16,400)	16,300 19,000?	16,100 (10,300)
	$B_{1u}\rightarrow B_{2g}$	$\|$	23,000 (24,100)	24,000	23,000 (27,200)
	$B_{1u}\rightarrow B_{3g}$	$\perp$	24,100 (29,700)	?	22,200 (21,000)
	$A_u\rightarrow B_{2g}$	$\perp$	30,300 (27,200)	?	30,400 (24,300)

[a] Predicted energies in brackets are corrected for N atoms.
Potential boxes: Porphine; 2 bond lengths, $V=23{,}000$ cm^{-1}.
Tetrahydroporphine; 1 bond length, $V=23{,}000$ cm^{-1}, $V'=0$.

[b] See reference 1.

In porphine, four nitrogen atoms are assumed equivalent to each other. Although this molecule is one of the representative instances of the "round-field" spectra,[5] where the configuration interaction is supposed to play a more important role than in the former case, the predicted sequence is not so far from the observation, if the potential boxes are extended to two bond lengths and if it is allowed to infer from the experimental absorption curve[6] that the absorption maxima might plausibly exist at 16,000 cm^{-1}, 19,000 cm^{-1} (center of gravity of the bonds 500~600 $m\mu$) and 25,000 cm^{-1} (Soret).

The authors express their hearty thanks to Professor H. Tominaga for his encouragement in the course of this work.

[1] Longuet-Higgins, Rector, and Platt, J. Chem. Phys. **18**, 1174 (1950).
[2] W. T. Simpson, J. Chem. Phys. **17**, 1218 (1949).
[3] H. Kuhn, J. Chem. Phys. **17**, 1198 (1949). He says he has made a more elaborate calculation, but its details are not available to us.
[4] Y. Oshika, Busseiron-Kenkyu **29**, 16 (1950) (Japanese).
[5] J. R. Platt, J. Chem. Phys. **18**, 1168 (1950).
[6] J. G. Erdman and A. H. Corwin, J. Am. Chem. Soc. **68**, 1885 (1946).

The Second Virial Coefficient of a 6–9 Gas at High Temperatures

LEO F. EPSTEIN AND CELESTA J. HIBBERT
General Electric Company, Knolls Atomic Power Laboratory, Schenectady, New York*

(Received January 31, 1952)

THE second virial coefficient[1] of a gas which satisfies a Lennard-Jones 6–9 potential

$$U(r)=\epsilon[2(r_0/r)^9-3(r_0/r)^6] \tag{1}$$

can be obtained from the expression

$$B(T)=2\pi N\int_0^\infty r^2[1-\exp\{-U(r)/kT\}]dr. \tag{2}$$

Writing

$$B(T)=(2\pi Nr_0^3/3)G(\theta) \tag{3}$$

and

$$\theta=\epsilon/kT \tag{4}$$

it follows[2] that

$$G_9(\theta)=-(2^{1/3}/3)\sum_{n=0}^{\infty}a_n\theta^{(n+1)/3}, \tag{5}$$

where

$$a_n=\left(\frac{27}{4}\right)^{n/3}\left(\frac{1}{n!}\right)\Gamma\left(\frac{2n-1}{3}\right). \tag{6}$$

The convergence properties of this series are such that it is difficult to evaluate $G_9(\theta)$ for large values of θ, i.e., at low temperatures. It has been summed, however, for the range $0\leqslant\theta\leqslant 2$ using punched card computing machine techniques such as have previously been employed in determining the corresponding functions for a 6–12 potential.[3a, b] The results are given in Table I. In addition to the function $G_9(\theta)$ itself, the first three derivatives have been computed and tabulated

$$d^iG_9(\theta)/d\theta^i\equiv G_9{}^i(\theta)=-(2^{1/3}/3)\sum_{n=0}^{\infty}a_n{}^i\theta^{(n+1-3i)/3}, \tag{7}$$

where

$$a_n{}^0\equiv a_n \quad\text{and}\quad G_9{}^0(\theta)\equiv G_9(\theta) \tag{8}$$

as defined by Eq. (6) and

$$a_n{}^{i+1}=(1/3)(n+1-3i)a_n{}^i \quad\text{for}\quad i\geqslant 0. \tag{9}$$

All these computations were made by setting up the machines to carry the problem through with ten significant figures, and fifty terms in the series expansions were used. The final data have been rounded off to eight significant figures. These tables have been checked by differencing, out to the fourth differences in all cases, and in some regions to the sixth difference. Analysis of the results shows that the tables are accurate out to the last significant figure given, although it is difficult to conceive of any physical problem where such accuracy would be required. The zeros and turning points of the functions are listed in Table II.

TABLE I. Second virial coefficient and related functions for a 6–9 potential.

θ	G_9	G_9'	G_9''	G_9'''
0.01	+0.2683 6948	+4.2755 194	-403.1748 0	+107964.87
0.02	+0.3886 4795	+1.8307 604	-174.3587 4	+45738.813
0.03	+0.4825 5512	+0.5456 5819	-83.5073 88	+21671.8231
0.04	+0.5973 5888	-0.2968 6538	-49.4803 63	+12357.5453
0.05	+0.5922 3642	-0.7902 5846	-32.9325 41	+7890.4928
0.06	+0.6237 6288	-0.9790 9673	-23.6377 93	+5414.0 0
0.07	+0.6750 9644	-1.1048 325	-17.8911 07	+4159.1530 4
0.08	+0.7602 2585	-1.1433 167	-14.0886 56	+3157.2117 6
0.09	+0.8461 3554	-1.1708 215	-11.4421 85	+2822.8904 7
0.10	+0.8308 8562	-1.1745 784	-9.5867 348	+2164.1485 1
0.11	+0.9146 8801	-1.4683 633	-8.0864 683	+2124.3275 8
0.12	+0.1976 8999	-1.7376 179	-7.0009 865	+1.96.3388 79
0.13	+0.1789 7889	-1.8011 747	-6.1440 386	+1.76.0574 05
0.14	+0.1616 5194	-1.8610 785	-5.4616 215	+1.61.0955 68
0.15	+0.1487 7775	-1.9138 485	-4.9100 780	+1.49.7406 37
0.16	+0.1234 1172	-1.9596 109	-4.4582 215	+1.40.9878 64
0.17	+0.1035 9988	-2.0022 648	-4.0839 713	+1.34.1324 64
0.18	+0.0833 7788	-2.0414 938	-3.7708 891	+1.28.6867 16
0.19	+0.0687 9595	-2.0776 162	-3.5046 967	+1.24.3062 15
0.20	+0.0418 2903	-2.1117 593	-3.2820 487	+1.20.7427 10
0.21	+0.0205 5067	-2.1435 918	-3.0897 306	+1.17.8142 81
0.22	-0.0010 3690	-2.1736 427	-2.9241 011	+1.15.3655 85
0.23	-0.0229 1705	-2.2021 498	-2.7806 972	+1.13.3542 31
0.24	-0.0447 9545	-2.2292 188	-2.6539 540	+1.11.7458 81
0.25	-0.0674 9955	-2.2553 214	-2.5469 906	+1.10.1892 56
0.26	-0.0901 7847	-2.2803 034	-2.4514 642	+1.8.9479 401
0.27	-0.1131 0263	-2.3043 891	-2.3674 512	+1.7.8810 697
0.28	-0.1361 6368	-2.3276 854	-2.2933 608	+1.6.9582 702
0.29	-0.1596 8401	-2.3503 849	-2.2278 691	+1.6.1578 249
0.30	-0.1832 4786	-2.3723 478	-2.1698 661	+1.5.4581 201
0.31	-0.2070 9755	-2.3937 041	-2.1184 166	+1.4.8447 498
0.32	-0.2311 3973	-2.4146 553	-2.0727 275	+1.4.3043 670
0.33	-0.2553 8828	-2.4351 756	-2.0321 234	+1.3.8261 636
0.34	-0.2798 4196	-2.4553 128	-1.9960 250	+1.3.4016 163
0.35	-0.3044 9434	-2.4751 094	-1.9639 375	+1.3.0232 140
0.36	-0.3293 4314	-2.4946 034	-1.9354 281	+1.2.6848 155
0.37	-0.3543 8551	-2.5138 287	-1.9101 253	+1.2.3811 275
0.38	-0.3796 1832	-2.5328 156	-1.8877 046	+1.2.1077 338
0.39	-0.4050 4110	-2.5515 914	-1.8670 823	+1.1.8609 580
0.40	-0.4306 5013	-2.5701 810	-1.8504 092	+1.1.6372 714
0.41	-0.4564 4420	-2.5886 067	-1.8350 685	+1.1.4342 053
0.42	-0.4824 2179	-2.6068 889	-1.8216 654	+1.1.2492 637
0.43	-0.5085 8156	-2.6250 458	-1.8100 297	+1.1.0803 900
0.44	-0.5349 2234	-2.6430 948	-1.8000 101	+0.9257 914
0.45	-0.5614 4314	-2.6610 513	-1.7914 716	+0.7838 046
0.46	-0.5881 4310	-2.6789 288	-1.7842 960	+0.6533 446
0.47	-0.6150 2146	-2.6967 393	-1.7783 705	+0.5336 464
0.48	-0.6420 7772	-2.7145 001	-1.7736 033	+0.4237 888
0.49	-0.6693 1136	-2.7322 168	-1.7699 092	+0.3231 150
0.50	-0.6967 2128	-2.7499 018	-1.7672 045	+0.2310 45
0.51	-0.7243 0832	-2.7675 639	-1.7654 243	+0.1340 321
0.52	-0.7520 7052	-2.7852 129	-1.7645 037	+0.0510 435
0.53	-0.7800 1356	-2.8028 567	-1.7643 852	-0.0264 640
0.54	-0.8081 3703	-2.8205 031	-1.7650 172	-0.0990 747
0.55	-0.8364 3965	-2.8381 594	-1.7663 519	-0.1671 689
0.56	-0.8648 9360	-2.8558 323	-1.7683 468	-0.2311 684
0.57	-0.8935 4038	-2.8735 284	-1.7709 628	-0.2914 422
0.58	-0.9223 6426	-2.8912 535	-1.7741 643	-0.3483 133
0.59	-0.9513 5156	-2.9090 135	-1.7779 186	-0.4020 763
0.60	-0.9805 4466	-2.9268 136	-1.7821 944	-0.4529 962
0.61	-1.0099 020	-2.9446 591	-1.7869 700	-0.5013 120
0.62	-1.0394 380	-2.9625 546	-1.7922 147	-0.5472 402
0.63	-1.0691 533	-2.9805 048	-1.7979 075	-0.5908 730
0.64	-1.0990 463	-2.9985 142	-1.8040 275	-0.6323 005
0.65	-1.1291 238	-3.0165 868	-1.8105 553	-0.6725 727
0.66	-1.1593 803	-3.0347 266	-1.8174 733	-0.7107 411
0.67	-1.1898 185	-3.0529 375	-1.8247 649	-0.7475 401
0.68	-1.2204 393	-3.0712 234	-1.8324 153	-0.7826 927
0.69	-1.2512 432	-3.0895 869	-1.8404 103	-0.8163 112
0.70	-1.2822 313	-3.1080 324	-1.8487 374	-0.8488 283
0.71	-1.3134 042	-3.1265 627	-1.8573 845	-0.8803 456
0.72	-1.3447 638	-3.1451 811	-1.8663 408	-0.9107 495
0.73	-1.3763 114	-3.1638 904	-1.8755 964	-0.9401 193
0.74	-1.4080 489	-3.1826 940	-1.8851 444	-0.9687 096
0.75	-1.4399 821	-3.2015 941	-1.8949 677	-0.9964 116
0.76	-1.4720 738	-3.2205 941	-1.9050 671	-1.0233 661
0.77	-1.5043 625	-3.2396 965	-1.9154 405	-1.0495 707
0.78	-1.5368 474	-3.2589 038	-1.9260 565	-1.0751 186
0.79	-1.5695 530	-3.2782 185	-1.9369 330	-1.1000 992
0.80	-1.6024 328	-3.2976 433	-1.9480 564	-1.1244 988
0.81	-1.6355 062	-3.3171 805	-1.9594 212	-1.1483 275
0.82	-1.6687 762	-3.3368 325	-1.9710 224	-1.1717 772
0.83	-1.7022 432	-3.3566 017	-1.9828 553	-1.1947 335
0.84	-1.7359 086	-3.3764 903	-1.9949 157	-1.2172 806
0.85	-1.7697 738	-3.3965 007	-2.0071 926	-1.2394 502
0.86	-1.8038 390	-3.4166 351	-2.0197 035	-1.2612 721
0.87	-1.8381 068	-3.4368 955	-2.0324 240	-1.2827 757
0.88	-1.8725 774	-3.4572 841	-2.0453 580	-1.3039 811
0.89	-1.9072 520	-3.4778 028	-2.0585 027	-1.3249 183
0.90	-1.9421 329	-3.4984 536	-2.0718 556	-1.3456 085
0.91	-1.9772 221	-3.5192 412	-2.0854 141	-1.3660 716
0.92	-2.0125 198	-3.5401 640	-2.0991 763	-1.3863 288
0.93	-2.0480 260	-3.5612 254	-2.1131 401	-1.4063 986
0.94	-2.0837 424	-3.5824 274	-2.1273 037	-1.4262 989
0.95	-2.1196 710	-3.6037 721	-2.1416 655	-1.4460 441
0.96	-2.1558 091	-3.6252 614	-2.1562 241	-1.4656 486
0.97	-2.1921 607	-3.6468 973	-2.1709 782	-1.4851 375
0.98	-2.2287 305	-3.6686 816	-2.1859 262	-1.5045 134
0.99	-2.2655 549	-3.6906 164	-2.2010 665	-1.5237 931
1.00	-2.3025 711	-3.7127 036	-2.2164 021	-1.5429 891
1.05	-2.4810 887	-3.8254 982	-2.2959 341	-1.6381 049
1.10	-2.6851 088	-3.9483 759	-2.3802 031	-1.7386 519
1.15	-2.8853 191	-4.0635 914	-2.4692 064	-1.8276 238
1.20	-3.0907 841	-4.1893 764	-2.5629 459	-1.9230 145
1.25	-3.3043 578	-4.3199 709	-2.6616 191	-2.0218 746
1.30	-3.5237 054	-4.4556 008	-2.7653 239	-2.1257 501
1.35	-3.7489 478	-4.5962 874	-2.8741 637	-2.2357 544
1.40	-3.9834 559	-4.7430 986	-2.9878 444	-2.3524 446
1.45	-4.2258 758	-4.8954 521	-3.1068 584	-2.4758 081
1.50	-4.4731 089	-5.0539 136	-3.2328 085	-2.5574 180
1.55	-4.7298 987	-5.2187 695	-3.3630 273	-2.6763 460
1.60	-4.9950 814	-5.3903 174	-3.4989 143	-2.8000 343
1.65	-5.2690 411	-5.5688 663	-3.6431 154	-3.9288 037
1.70	-5.5520 681	-5.7548 384	-3.7928 846	-3.0629 746
1.75	-5.8448 426	-5.9482 692	-3.9495 083	-3.2028 749
1.80	-6.1470 606	-6.1498 083	-4.1132 736	-3.3488 388
1.85	-6.4587 598	-6.3597 197	-4.2844 990	-3.5011 808
1.90	-6.7811 584	-6.5781 870	-4.4635 084	-3.6602 445
1.95	-7.1177 843	-6.8068 069	-4.6506 436	-3.8264 347
2.00	-7.4639 886	-7.0435 537	-4.8468 738	-4.0000 563

It is of interest to compare the results for a 6–9 potential with those previously derived for a 6–12 potential.[3] From Fig. 1 it is evident that there is a striking similarity in the shape of the two curves. In fact, over a limited temperature range $G_{12}(\theta)$ can be approximated by $AG_9(\alpha\theta)$, where A and α are constants with quite reasonable accuracy. It is this fact which makes it nearly impossible to distinguish between a 6–9 and a 6–12 (or, perhaps, almost any other repulsive power) from second virial coefficient measurements. With a slightly different value of ϵ/k, corresponding to the multiplying factor α, and a simultaneous change in r_0

TABLE II. Points of special interest in $G_9(\theta)$.

θ	$G_9(\theta)$	$G_9'(\theta)$	$G_9''(\theta)$	$G_9'''(\theta)$
0	±0	$+\infty$	$-\infty$	$+\infty$
0.0347 2511$_9$	+0.2981 7550	0	−64.0435 08	+3362.6992
0.2195 2281	0	−2.1722 456	− 2.9314 682	+15.4916 85
0.5265 0764	−0.7702 3572	−2.7966 949	− 2.0444 51	0

to go with the factor A, either potential function can probably be made to give an equally satisfactory fit to any experimental data which can readily be obtained. Only if these parameters are known from other types of experiments (spectroscopic or x-ray scattering measurements, for example) or if the $B(T)$ data cover an extremely wide temperature range, does it seem feasible to distinguish between the two repulsive potentials from second virial coefficient measurements.

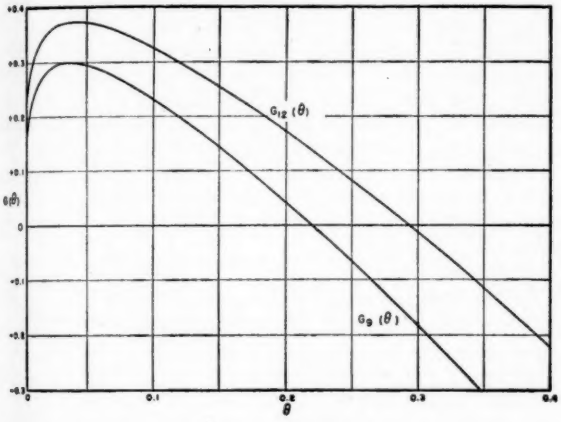

FIG. 1. Comparison of $G_9(\theta)$ and $G_{12}(\theta)$ at high temperatures.

The tables given here should be adequate for all of the permanent gases. They should also be suitable for a number of condensible gases since, according to the Lennard-Jones and Devonshire theory of liquids[4] as computed by Hirschfelder and his associates[5] (for a 6–12 rather than a 6–9 potential, it is true), $\theta_c = 1/1.30 = 0.76_9$ and the present tables go well above this. For higher values of θ (lower temperatures), special methods of evaluating $G_9(\theta)$ must be employed similar to those previously described[1] for $G_{12}(\theta)$. These have been devised and it is expected that they will be published shortly.

* The Knolls Atomic Power Laboratory is operated by the General Electric Company for the AEC. The work reported here was carried out under contract No. W-31-109 Eng-52.

[1] The notation used here is identical with that previously employed by L. F. Epstein and G. M. Roe, J. Chem. Phys. **19**, 1320 (1951).

[2] R. H. Fowler and E. A. Guggenheim, *Statistical Thermodynamics* (Cambridge University Press, London, 1939), p. 279.

[2a] Hirschfelder, Curtiss, Bird, and Spotz, *The Properties of Gases*, a book in eleven sections to be published soon. Individual chapters, prepared under Navy Bur. Ordnance contract, have been issued to a limited distribution list prior to April, 1951.

[2b] Hirschfelder, Bird, and Spotz, Trans. Am. Soc. Mech. Engrs. **71**, 921 (1949).

[4] J. E. Lennard-Jones and A. F. Devonshire, Proc. Roy. Soc. (London) **163A**, 53 (1937).

[5] Wentorf, Buehler, Hirschfelder, and Curtiss, J. Chem. Phys. **18**, 1484 (1950).

High Values for the Electrical Breakdown Strength of Liquids

W. D. EDWARDS
National Research Council of Canada, Ottawa, Ontario, Canada
(Received February 15, 1952)

RECENT experiments with an improved form of the apparatus described recently[1] have yielded breakdown strength values for pure organic liquids from 20 to 100 percent in excess of those reported in the literature. The "spread" in the results, in addition to the mean values, has increased and the former is as high as ±50 percent about the mean value for methylene chloride. The results given here are maximum values; spuriously low values, termed here subnormals, have been discarded.

TABLE I. Breakdown strengths found using rectangular voltage pulses.

Liquid	Max B.D.S.[a] found	Gap width used (microns)	Maximum previously reported values	Author
Carbon tet. CCl_4	4.79	36	{2.48 0.66	Edwards[b] Attwood, and Bixby[c]
Chloroform[d] $CHCl_3$	2.53	58	2.07	Edwards
Methylene chloride CH_2Cl_2	2.36	59	...	...
n-Hexane	2.46	73	1.37	Salvage[e]
Benzene	1.83	69	1.45	Bredner[f]
Ethyl alcohol	1.63	80	1.27	Edwards

[a] Breakdown strengths are expressed in megavolts/cm.
[b] See reference 1.
[c] S. S. Attwood and W. H. Bixby, J. Franklin Inst. **235**, 259 (1943).
[d] No attempt was made to remove the small percentage (0.5) of stabilizing alcohol present in the chloroform.
[e] B. Salvage, Inst. of Elec. Eng. (London) Monograph No. 2, 1951.
[f] R. Bredner, Arch. Elektrotech. **31**, 351 (1937).

Pure organic liquids of simple molecular structure, both polar and nonpolar, have been tested. The effect on the breakdown strength of replacing a specific atom of the molecule is being investigated by using members of series such as carbon tetrachloride, chloroform, and methylene chloride.

Single, rectangular voltage pulses of 10 μsec duration and positive, sawtooth voltage pulses with a time of rise to 16 kv of 45 μsec have been used. In conjunction with resistance voltage dividers a high speed oscilloscope was used to determine the amplitude and duration of the pulses used.

The miniature spark gap used was designed to operate within a completely enclosed glass system. The electrodes were highly polished phosphor bronze spheres which were carefully degreased before placing into the test liquid. With this spark gap and containing vessel it was possible to change the liquid sample and to present fresh, highly polished sphere surfaces to the gap after each breakdown. The spark gap was viewed and measured from outside the glass system with a travelling microscope. Stray particles visible after clearing the electrodes with cotton wool wipers were removed by the application of low voltage pulses. Except for drying, the "reagent grade" liquids were used as supplied by the manufacturers. The experiments were performed at atmospheric temperature and pressure.

A summary of the results found using rectangular pulses is presented in Table I. In Table II some of these are compared with values obtained using sawtooth pulses. As previously reported, the formative time lag or time to breakdown for such gap widths is much less than 10 μsec, and the breakdown strengths found using rectangular pulses should equal the dc breakdown strengths.

The major factor giving rise to subnormal breakdown strength values is the presence in the spark gap of minute particles which

TABLE II. A comparison of the breakdown strengths found using different types of voltage pulse.

Liquid	B.D.S. found using rectangular pulses	B.D.S. found using linearly rising voltage pulses
Benzene	1.83	2.08
Ethyl alcohol	1.63	1.68
Chloroform	2.53	2.47
Hexane	2.46	>2.39

may be as small as one micron in diameter. Such particles are products of breakdown or are introduced into the enclosed system at the time of assembly. If special precautions were not taken to eliminate stray particles, the subnormal breakdown strengths obtained would lay within ±10 percent of a mean value which for a given method of electrode polishing would be repeatable. These mean values, reported earlier,[1] are in agreement with the results published by other workers.

Experiments are continuing to determine whether the maximum values reported here are indeed the intrinsic electric strengths of the liquids concerned.

The author is indebted to the National Research Council of Canada for the award of a Fellowship which enabled him to carry out this work.

[1] W. D. Edwards, Can. J. Phys. **29**, 310 (1951).

Rapid Separations of Protactinium and Uranium Radioisotopes from Cyclotron Bombarded Thorium Nitrate

W. Wayne Meinke
Department of Chemistry, University of Michigan, Ann Arbor, Michigan
(Received February 12, 1952)

EXTENSION of work on collateral chains of the natural radioactive families[1–3] to short-lived members[4] has necessitated the development of new rapid chemical procedures for the separation of protactinium and uranium isotopes. Existing target procedures[5] were adaptable to separation times of 5 to 10 minutes, but new techniques were required for separation times of the order of one minute. Two techniques made these rapid separations possible. First the thorium was bombarded as the thorium nitrate salt in the jiffy-probe of the Berkeley 184-inch cyclotron with a pneumatic tube set-up which delivered the target to the processing area within 12–15 seconds after the end of bombardment.[3] Secondly, wet coarse filter paper was used as a separating medium for aqueous and organic layers in the extraction process.

To separate protactinium the thorium nitrate target material was emptied into a large funnel containing equal volumes of 4 *N* nitric acid and 0.25 *M* thenoyl trifluoroacetone (*TTA*)[6,7] in benzene. The funnel had been fitted with a ground glass stopcock and was lined with wet coarse filter paper. The mixture was stirred vigorously to effect the solution of the target material and to chelate simultaneously the protactinium in the organic layer. After 5 to 10 seconds of stirring (depending upon the protactinium yield desired) the stopcock was opened; the acid layer passed through the filter paper while the benzene layer remained in the funnel. 4 *N* nitric acid washes of the benzene layer were used to further remove alpha-emitting radioactive impurities.

Portions of the benzene fraction were then discharged onto platinum counting plates or dishes which were being heated with a heat lamp and hot plate. The samples were then immediately ignited to further speed evaporation. Flaming of the final plate in a Fisher burner flame left a weightless sample of protactinium ready for alpha-counting or alpha-pulse analysis.

Approximate times required for the above steps were solution, extraction, and separation 10–20 seconds; washing 5–10 seconds; and making of sample plate (~1 cc benzene) ~30 seconds.

The uranium procedure used the same techniques as above. The thorium nitrate target was emptied into the funnel containing 20 ml of 3 *M* magnesium nitrate (0.1 *N* in nitric acid) and 8 ml of diethyl ether. Solution and extraction were accomplished in one stirring. Wash solutions of magnesium nitrate removed other alpha-emitting impurities and the last traces of the thorium nitrate target material from the ether fraction. One final wash with ammonium nitrate solution insured that no nonvolatile material would remain in the ether fraction to give "thick" plates for counting. Two pre-extractions of the salting solutions with ether were required to further eliminate nonvolatile foreign material which would extract into the ether. Ignition of the ether sample gave a weightless plate of the uranium isotopes.

Approximate times required for the steps were: solution, extraction, and separation 10–20 seconds; washing 10–15 seconds; and making of sample plate (~1 cc ether) ~15 seconds.

In nuclear chemical work where the main interest is in characterizing particular isotopes, emphasis is on radiochemical purity of the isotope rather than on chemical yield. The above procedures give only a 10–20 percent chemical yield—$\frac{1}{10}$ of which can be rapidly placed on a plate for counting. These yields are quite satisfactory for the purpose, however, since contaminating isotopes have been reduced by a factor of 10^4 to 10^5. Experimental results have shown that about 1 part in 10^4 of actinium, 1 part in 10^5 of protactinium, and 1 part in 10^5 of thorium come through the uranium procedure. Even this maximum decontamination may prove inadequate, however, when alpha-bombardment conditions (energy, beam strength, and contamination by deuterons) are such that the contaminating isotopes are present initially in amounts 100 or more times greater than the uranium isotopes. Similarly the protectinium procedure removes all but about 0.1 percent of the thorium but still has proved too crude for certain branching ratio characterizations of protactinium isotopes.

The method of target solution and separation of organic and aqueous layers by wet filter paper has general applicability for rapid separations of other radioisotopes from their target materials.

The author wishes to thank Mr. C. Kalfian for his help in developing some of the techniques described here and also Professor Glenn T. Seaborg for his encouragement in this work.

[1] Ghiorso, Meinke, and Seaborg, Phys. Rev. **74**, 695 (1948).
[2] Meinke, Ghiorso, and Seaborg, Phys. Rev. **75**, 314 (1949).
[3] Meinke, Ghiorso, and Seaborg, Phys. Rev. **81**, 782 (1951).
[4] Meinke, Ghiorso, and Seaborg, Phys. Rev. (to be published).
[5] W. W. Meinke, AEC Declassified Documents AECD-2738 and AECD-2750 (August, 1949).
[6] J. C. Reid and M. Calvin, AEC Declassified Documents MDDC-1405 (August 13, 1947); also J. Am. Chem. Soc. **72**, 2948 (1950).
[7] TTA is obtainable from Dow Chemical Company, 310 Sansome Street, San Francisco, California.

Determination of the Heat of Dimerization of Tetrafluoroethylene by a Kinetic Method

Bernard Atkinson and Antony B. Trenwith
Department of Inorganic and Physical Chemistry, Imperial College of Science and Technology, London, S.W. 7, England
(Received February 18, 1952)

DURING a study of the pyrolysis of tetrafluoroethylene we observed that up to 600° the rates of the reaction,

$$2C_2F_4 = C_4F_8 \text{ (octafluorocyclobutane)}, \quad (1)$$

and the reverse reaction,

$$C_4F_8 = 2C_2F_4, \quad (2)$$

are much faster than the rates of any other homogeneous reactions occurring in the system at normal pressures. In a Pyrex vessel heterogeneous reactions including

$$C_2F_4 + SiO_2 = CO + SiF_4 \quad (3)$$

take place at a noticeable rate at 550°C. By using a steel vessel completely freed from iron oxide we have been able to show that an equilibrium

$$2C_2F_4 \rightleftharpoons C_4F_8 \quad (4)$$

is readily established at 550°C. The pressure change on heating perfluorocyclobutane at 520–590°C is in accord with that for a first-order reaction moving to equilibrium with a second-order reaction.

We have measured the rate of reaction (1) in a Pyrex vessel at temperatures from 300–550°C and the rate of reaction (2) in a Pyrex vessel at 520–550°C and in a steel vessel at 550–590°C. Values

of the rate constant for reaction (2) at 550°C calculated from the results obtained with the Pyrex vessel agreed with those obtained using the steel vessel. All measurements were made at 100–500 mm pressure.

Plots of log$k$ against I/T for both the forward and back reactions gave straight line graphs. Equilibrium constants were calculated from ratios of rate constants, and the heat of reaction for (1) was derived from a graph of log$K$ against I/T. For the forward reaction (1) the results gave the constants in the equation $k=PZe^{-E/RT}$ as $E=25.4$ kcal, $P=3.85\times10^{-4}$. For the reverse reaction, taking $k=Ae^{-E/RT}$, $E=74.1$ kcal, $A=8.9\times10^{15}$ sec^{-1}. The figures for the equilibrium constant gave $\Delta H=-49.8$ kcal, $\Delta S=-47.4$ cal per deg, both figures being for 550°C approximately.

The energy of activation for the forward reaction is distinctly lower than that for the polymerization of ethylene to butylene and higher olefines. For the latter reaction Pease[1] found $E=35$ kcal, $P=5\times10^{-4}$. Both our figure for the steric factor of reaction (1) and the figure of Pease for ethylene give support to the theory that association reactions between polyatomic molecules will in general have small steric factors.[2] The A factor found for the reverse reaction is similar to that for other reactions involving ring opening, thus for cyclopropane $A=1.48\times10^{15}$ cm^{-1} [3] and for trioxymethylene $A=1.43\times10^{16}$ cm^{-1}.[4] The A factor is much above the "normal" value of 10^{13}–10^{14} cm^{-1}.

From thermochemical data we estimate that for the reaction

$$2C_2H_4=C_4H_8 \text{ (cyclobutane)}, \qquad (5)$$

the value of ΔH is -25 kcal. As the cyclobutanes contain twelve bonds and the reacting olefine molecules ten bonds, the difference between this figure and that given above for reaction (1) cannot be said to indicate any great structural differences between the fluorocarbons and hydrocarbons involved.

A full account of experimental methods and results is being prepared.

We thank I.C.I. Ltd. for the gift of tetrafluoroethylene, the University of London for a grant towards the cost of apparatus, and the D.S.I.R. for a maintenance grant to one of us (A.B.T.).

[1] R. N. Pease, J. Am. Chem. Soc. **53**, 613 (1931).
[2] C. E. H. Bawn, Trans. Faraday Soc. **31**, 1536 (1935).
[3] T. S. Chambers and G. B. Kistiakowsky, J. Am. Chem. Soc. **56**, 399 (1934).
[4] R. LeG. Burnett and R. P. Bell, Trans. Faraday Soc. **34**, 420 (1938).

The Microwave Absorption Spectrum of Acetone Vapor*

THOMAS L. WEATHERLY AND DUDLEY WILLIAMS
Department of Physics and Astronomy, The Ohio State University, Columbus, Ohio
(Received February 6, 1952)

THE microwave spectrum of acetone vapor in the spectral region between 18,000 and 30,000 mc/sec has been examined. The observed spectrum includes the four strong lines whose frequencies are listed in Table I. The seventeen lines in the region 22,000 to 25,000 mc/sec reported by Bak *et al.*[1] were not observed in the present study and hence must be much weaker than the lines listed in the table.

TABLE I. Strong lines in the microwave spectrum of acetone.

26,661.5 mc/sec
28,340.0
28,622.3
30,070

An attempt to interpret the observed lines as transitions between the rotational energy levels of an asymmetric top has been unsuccessful. The asymmetry parameter $K=0.4$ for the acetone molecule if the interatomic distances and bond angles have values similar to those in related molecules.[2] The spectrum predicted for the region between 18,000 and 30,000 mc/sec on the basis of $K=0.4$ includes 23 lines for rotational transitions involving J values no higher than $J=6$. Moreover, the energy level populations and transition probabilities are such that one can expect relatively intense lines in this region for J values as high as 30. Thus, there seems little hope of positively identifying the strong lines observed. Although the lines were observed with a spectrograph employing ground-biased square wave Stark effect modulation, no clearly defined Stark patterns were observed; this probably indicates that the rotational transitions are between levels with high J values, since in this case the number of Stark components would be larger and the intensities of the individual components would be small. However, the behavior of the observed lines, when the wave guide was cooled with dry ice, indicates that the J values involved are less than $J=35$.

The intensities of the lines found in the present study are so much greater than those of the lines reported by Bak *et al.*[1] that they will probably prove to be the lines most suited for microwave spectrochemical analysis.

* This work was supported in part by a contract between the Geophysical Division of the Air Force Cambridge Research Center and the Ohio State University Research Foundation.
[1] Bak, Knudsen, and Madsen, Phys. Rev. **75**, 1622 (1949).
[2] G. Herzberg, *Infrared and Raman Spectra* (D. Van Nostrand Company, Inc., New York, 1945), p. 440.

X-Ray Diffraction Study of Crystalline Neopentane (Tetramethyl Methane)*

ARTHUR H. MONES AND BENJAMIN POST
Polytechnic Institute of Brooklyn, Brooklyn, New York
(Received February 18, 1952)

ON the basis of an optical study at −180°C, Wahl[1] reported that crystalline neopentane is birefringent at that temperature and probably tetragonal. He also noted that the crystals underwent a transition to an isotropic form well below the melting point (mp=−19.7°C). The existence of this transition has since been confirmed by Aston *et al.*[2] Some time after Wahl's observations were published, Mark and Noethling[3] reported (on the basis of Debye-Scherrer diagrams taken at the temperature of liquid air) that neopentane crystallized in the cubic system with $a_0=11.26$A and with 8 molecules per unit cell.

In this communication some results of an x-ray diffraction study of crystalline neopentane, above and below the transition temperature, are reported. The low temperature x-ray camera used in this investigation has been described elsewhere.[4]

Powder diagrams of the crystalline phase, stable above the transition temperature (−143°C), were not satisfactory. Only three or four very broad lines were observed. Single crystals of neopentane were then grown in thin-walled glass capillary tubes and oscillation diagrams were obtained at -50 ± 5°C. In this temperature region the crystals appeared isotropic. The x-ray diagrams were indexed on the basis of a face-centered cubic unit cell with $a_0=8.78\pm0.05$A and with four molecules per unit cell.

Intensities of reflections decreased very rapidly with increasing Bragg angles. Reflections were observed only from (111), (200), (220), (311), (222), (400), and (333). The large entropy of transition, 4.39 eu per mole, compared with an entropy of fusion of 3.03 eu per mole, indicates considerable disorder in the crystal above the transition temperature. The x-ray evidence, however, is too meagre to permit any definite conclusions to be drawn concerning the nature of the disorder. It may be noted, however, that structure factors computed on the assumption of random orientation of neopentane molecules above lattice points, with spherical symmetry on the average, showed good agreement with "observed" structure factors. Structure factors calculated, assuming the following models, showed poor agreement with observed structure factors: (a) an ordered structure; and (b) a disordered structure, with the four tetrahedrally disposed carbon atoms of each molecule occupying, statistically, the eight corners of a cube.

Single crystals of the high temperature form invariably broke

into fragments as the temperature was lowered through the transition point. Optical examination of the fragments with a polarizing microscope showed them to be weakly birefringent.

Debye-Scherrer diagrams were obtained at -150 ± 5°C. Several lines were observed in addition to those reported by Mark and Noethling.[3] The diagrams could be indexed tentatively, on the basis of a somewhat large tetragonal unit cell ($a_0=11.2\pm0.1$A; $c_0=11.5\pm0.1$A). However, in view of the small number of reflections observed and the breadth and spotty character of the lines, the unit cell choice and consequent indexing must be considered provisional.

* This research was supported in part by the ONR.

[1] W. Wahl, Proc. Roy. Soc. (London) **88**, 356 (1913).
[2] J. G. Aston and G. H. Messerly, J. Am. Chem. Soc. **58**, 2354 (1936).
[3] H. Mark and W. Noethling, Z. Krist. **65**, 435 (1927).
[4] Post, Schwartz, and Fankuchen, Rev. Sci. Instr. **22**, 218 (1951).

The Hydrogen Bond in an Amide Link

A. Elliott
Courtaulds Limited, Maidenhead, England
(Received January 28, 1952)

THE work of Newman and Badger[1] on the infrared spectrum of N-acetyl glycine raises an interesting point in connection with the linearity of the N—H···O atoms in a hydrogen bond. Pauling and Corey[2] have expressed the view that this structure should be linear in polypeptides and have used linearity as a criterion for accepting or rejecting a proposed fold in an α-protein or polypeptide. In N-acetyl glycine, if Newman and Badger's interpretation of their polarized infrared spectra is correct, not only in this bond nonlinear, but the N—H valency bond is apparently distorted from the usual assumed value (120°) *away* from the oxygen atom. As Newman and Badger point out, the N—H absorption band has nevertheless about the same frequency as in proteins.

A possible explanation of the configuration, should the distortion be confirmed, might be the tendency for the hydrogen bond to be directed towards the "lone pair" electrons of the double-bonded oxygen atom, which in some cases tend towards a tetrahedral arrangement with respect to the double bond.[3] When conditions allow, this requirement may be met by suitable orientation of the C=O group, retaining the linear N—H···O configuration. In N-acetyl glycine presumably the requirements of the strong O—H···O bonds prevent this.

In view of the above observations it appears doubtful whether enough is known about hydrogen bonds to justify rejection of a structure because of nonlinearity of this bond. It is perhaps worth noting that such information as does exist about O···H—N distances is chiefly obtained from structures in which one of the partners in the hydrogen bond is ionic in character.

Pauling and Corey have stated that the seven-membered ring proposed for synthetic α-polypeptides[4–6] must be rejected because the N—H···O angle differs from a straight angle by about 70°. Apart from the question of what divergence is allowable, this statement is incorrect; with bond distances and angles, as given by Pauling, Corey, and Branson,[7] and with a planar amide group the divergence is about 38° for a nitrogen-oxygen distance of 2.85A, and the angle between NH bond and N—O vector is about 25°. The magnitude of this angle in the 5.1 residue spiral is given by Pauling, Corey, and Branson as about 25°, and this they consider acceptable. The seven-membered ring fold has about the same degree of nonlinearity in the hydrogen bond and must be considered equally acceptable.

[1] R. Newman and R. M. Badger, J. Chem. Phys. **19**, 1147 (1951).
[2] L. Pauling and R. B. Corey, Proc. Natl. Acad. Sci. **37**, 241 (1951).
[3] Sir John Lennard-Jones and J. A. Pople, Proc. Roy. Soc. (London) **A205**, 155 (1951).
[4] E. J. Ambrose and W. E. Hanby, Nature **163**, 483 (1949).
[5] Bamford, Hanby, and Happey, Proc. Roy. Soc. (London) **A205**, 30 (1951).
[6] E. J. Ambrose and A. Elliott, Proc. Roy. Soc. (London) **A205**, 47 (1951).
[7] Pauling, Corey, and Branson, Proc. Natl. Acad. Sci. **37**, 205 (1951).

Errata: Irreducible Representations of Cubic Groups

[J. Chem. Phys. **19**, 1612 (1951)]

Frank Matossi
Naval Ordnance Laboratory, White Oak, Silver Spring, Maryland

1. The E-matrix for C_3 is valid for (123)(4) and equivalent axes with the same sense of rotation.
2. In the E-matrix for C_2, read 1 instead of -1.
3. On both pages, read (2 4) (1) (3) instead of (3 4) (1) (2).
4. On page 1613, read (3 4) (1) (2) instead of (1 2) (3) (4).

X-Ray Diffraction of Heat-Treated Carbon Blacks

H. T. Pinnick
Department of Physics, University of Buffalo, Buffalo, New York
(Received January 28, 1952)

ACCORDING to Franklin,[1] growth of microcrystallites in carbons occurs in the lowest part of the range 1000°C–3000°C at the expense of nonorganized carbon atoms surrounding each crystallite, while in the middle and upper part of this range it is due to the displacement of entire graphitic layers by thermal motion. This last assumption seems necessary to explain the gradual growth over such a wide temperature range; as the crystallites grow, an increasing amount of energy is required to move them and subsequent growth at a measurable rate will only occur at higher temperatures. Small crystallites have a turbostratic structure (perfect graphitic planes stacked parallel but randomly rotated). Franklin[2] found in studying polyvinyl chloride coke, that the percentage of oriented layers begins to be detectable in samples treated to 1800°C and increases rapidly for higher treatments, becoming 70 percent at 2500°C. It is difficult to see why the alignment does not occur as soon as growth starts to take place by movement of entire layers, and why it does take place in a relatively narrow temperature range.

As a part of extensive studies of heat-treated carbon blacks carried out in this laboratory, x-ray diffraction of various carbon blacks with particle sizes ranging from 50A–3000A, all graphitized to 3000°C, was investigated. The half-widths of the asymmetric 10 line were measured, and the crystallite diameters calculated using Warren's formula.[3] It was found that the average crystallite diameter is about one-third of the particle size. Electron micrographs made by dispersing these blacks directly in a substrate of Formvar cast on a small grating show that the particles retain their individuality after graphitization. Evidently the growth of crystallites is limited by the particle size, and one-third the particle size obtained by x-ray diffraction for the average crystallite diameter seems to be a reasonable figure for this limit.

For purposes of comparison a soft coke[4] was heat treated to various temperatures to give comparable crystallite sizes. As an indication of the degree of orientation of layers the appearance of the cross lattice 101 line as a broad maximum on the large angle side of the two-dimensional 10 line was observed. For the soft coke the 101 line first appears when the crystallite diameter has reached 150A, which agrees with the general trend of Franklin's results for polyvinyl chloride coke. The 101 line could first be clearly distinguished when its height was about one-tenth that of the 10 line.

It was suspected that the 101 line would appear in graphitized carbon blacks at smaller crystallite sizes, since it seemed that any restrictive forces in soft cokes should be overcome in the blacks by the more vigorous motion at the higher graphitization temperatures. Examination of the x-ray patterns shows, however, that the smallest diameter for which the 101 maximum appears is again about 150A. Furthermore, comparison of diffraction patterns for soft cokes and carbon blacks shows that the alignment for larger crystallite sizes proceeds similarly in the two series.

The agreement of dependence of alignment on crystallite diameter under such different temperature conditions is re-

markable. It may be that crystallites with diameters less than 150A have no preferred orientation. However, a more satisfactory explanation may lie in the existence of two opposing forces. Valence bonds between neighboring crystallites tend to stabilize the layers in rotated positions, while the attractive forces between the layers tend to align them. The latter increases as the square of the diameter, and evidently becomes the determining factor for crystallite diameters above 150A.

Further investigations of structure and diamagnetic susceptibility of carbons are in progress. The author is indebted to Professor S. Mrozowski, who suggested the problem, for his continued advice and encouragement and to Mr. E. A. Kmetko for making the electron micrographs.

[1] Rosalind E. Franklin, Proc. Roy. Soc. (London) **209**, 196 (1950).
[2] Rosalind E. Franklin, Acta Cryst. **4**, 253 (1951).
[3] B. E. Warren, Phys. Rev. **59**, 693 (1941).
[4] The meaning of the term "soft coke" is explained in a paper by S. Mrozowski, Phys. Rev. (to be published).

Direct Determination of the Sublimation Energy of Carbon

TH. DOEHAERD, PAUL GOLDFINGER, AND F. WAELBROECK*
Laboratory for Spectroscopical Analysis, Université Libre de Bruxelles, Brussels, Belgium
(Received January 28, 1952)

USING a powerful new apparatus, in which the relevant parameters could be easily varied over wide limits, rates of evaporation from a hot carbon surface and of effusion from a graphite furnace were investigated over the range of 2450–2840°K.

The sticking coefficient f was found to be much smaller than unity and the results lead to the spectroscopic value 141.26 kcal *for the heat of sublimation of carbon.*[1]

The rate of effusion per unit aperture area increases with decreasing aperture to total surface area ratio (σ). The results are compatible with a value of f between 1/500 and 1/5000. In each experiment, the rate of evaporation and the rate of effusion were observed simultaneously. They were estimated quantitatively by careful microphotometer analysis of the distribution of the carbon deposits on the glass microscope slides used as targets; in all cases a thick inner circular deposit was surrounded by a penumbra, the relative sizes agreeing beautifully with those predicted by the geometry of the system. For the ratio $\sigma = 1/24{,}000$, six measurements between 2620 and 2840°K were made, yielding 145.8 ±2.8 kcal.[2]

The apparatus was contained in a metal evaporation chamber manufactured for optics work by Leybolds (Cologne);[3] the large space available inside the high vacuum chamber, together with the great pumping speed (250 l/sec down to 10^{-4} and 10^{-5} mm Hg) enabled easy adjustment of the various components. Using remote control several runs could be made without touching the furnace with frequent temperature measurements during and between the runs.

The rate of evaporation results are in excellent agreement with those of previous workers.[4] The vapor pressure inside the Knudsen-cell at $\sigma = 1/400$ gives values in good agreement with those of Brewer and Mastick.[5] Hence it seems relatively easy to explain the discordant results of Brewer, Gilles, and Jenkins,[6] which, incidentally, seem to be the only direct evidence for a high value of the sublimation energy of carbon.

The present result, $L_c = 141$ kcal, is in good agreement with our first qualitative observations with a Knudsen-cell of adequate σ-value[7] and with the most recent conclusions of workers using the electron collision approach to this problem.[8] Earlier vapor pressure measurements,[9] especially those of Ribaud and Bégué[10] (see Fig. 1), as well as recent spectroscopic evidence[11] seem to favor also this value.

A detailed description of the apparatus and discussion of the results, together with those of previous investigators, is under preparation.

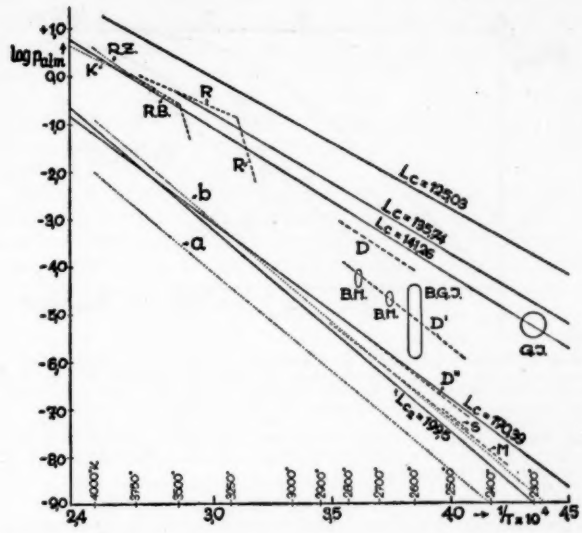

FIG. 1. Vapor pressure of carbon atoms calculated for $L_c = 125.03$; 135.74; 141.26; and 170.39 kcal (plain lines). (M) Marshall and Norton. (S) Simpson, Thorn, and Winslow. (D, D', D'') this work ($\sigma = 1/24.000$, 1/400, and 1, resp.). (G.J.) Goldfinger and Jeunehomme. (B.M.) Brewer and Mastick. (B.G.J.) Brewer, Gilles, and Jenkins. (K) Kohn and Guckel, as corrected by Warmuth (see reference 9). (R) Ryschkewitsch, as corrected by Warmuth (see reference 9). (R.Z.) Rochan Zaer, thèses, Paris, 1935. (R.B.) Ribaud and Bégué. The deviation from equilibrium shown by the ends to lines (R) and (R.B.) is easily explained and shall be discussed later. For vapor pressure curves of C_2 and lines (a) and (b), see following note.

We wish to express our thanks to Dr. G. J. Szasz for many valuable discussions.

We are greatly indebted to the E.C.A. Administration and to the Centre National Belge de Chimie Physique Moléculaire for grants which permitted us the purchase of vacuum apparatus.

* One of us (F.W.) wishes to express his thanks to the Institut pour l'Encouragement de la Recherche Scientifique dans l'Industrie et l'Agriculture for a "Bourse de Spécialisation," which enabled him to carry out this work.

[1] It is difficult to decide by vapor pressure measurements between this value and $L_c = 135.74$ kcal proposed by Hagstrum (reference 7).

[2] Using $k_g = 1.1 \times 10^5$ cm^2 g^{-1} for the absorption coefficient of carbon deposits and 0.2 for the sticking coefficient on the target according to Simpson *et al.* (reference 4).

[3] Our attention was called to this method of heating by Dr. M. Dunkel and Dr. G. W. Oetjen of C. Leybolds-Cologne; we are also indebted to them for valuable discussions on vacuum problems.

[4] A. L. Marshall and F. J. Norton, J. Am. Chem. Soc. **72**, 2166 (1950); Wertenstein and Jedrzejewky, Compt. rend. **177**, 316 (1923); Simpson, Thorn, and Winslow, AECD, 2680 (1949).

[5] L. Brewer and D. Mastick, UCRL, 572 (1949).

[6] Brewer, Gilles, and Jenkins, J. Chem. Phys. **16**, 797 (1948).

[7] P. Goldfinger and W. Jeunehomme, Colloque International sur les Réactions d'Inflammation, etc., Paris, April-May, 1948; Rev. de l'Institut Fr. du Pétrole **4**, 427 (1949); Third Symposium on Combustion, etc., Minneapolis, 1948.

[8] C. A. McDowell and J. W. Warren, Disc. Faraday Soc. **10**, 53 (1951); H. D. Hagstrum, Phys. Rev. **72**, 947 (1947), Revs. Modern Phys. **23**, 185 (1951).

[9] See the discussion of Goldfinger and Jeunehomme, Trans. Faraday Soc. **32**, 1591 (1936) and Hagstrum's (reference 8) remarks on them.

[10] G. Ribaud and J. Bégué, Compt. rend. **221**, 73 (1945); J. Bégué, thèses, Paris, 1945.

[11] H. G. Howell, Nature **163**, 773 (1949).

On the Mechanism of Evaporation of Graphite

F. WAELBROECK
Laboratory for Spectroscopical Analysis, Université Libre de Bruxelles, Brussels, Belgium
(Received January 28, 1952)

THE experiments communicated in the preceding note,[1] as well as earlier evidence on the rate of evaporation[2] and on the vapor pressure of graphite,[3] seem to show that the sticking coefficient of carbon is of a complex nature.

It is generally admitted[4] that the vapor pressure p inside a Knudsen-cell is related to the equilibrium vapor pressure p_{eq},

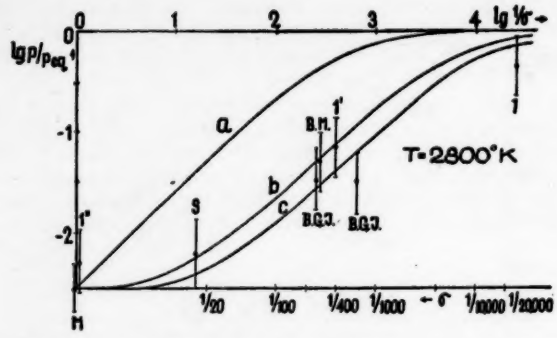

FIG. 1. Pressure p inside a Knudsen-cell *vs* aperture/total area ratio σ. Curve (*a*) (Eq. (1)); curves (*b*) and (*c*) (Eq. (2)), potential barrier of 50 and 52.5 kcal, respectively. Experimental points: (M) Marshall and Norton; (S) Simpson, Thorn, and Winslow; (BGJ) Brewer, Gilles, and Jenkins; (BM) Brewer and Mastick; (1, 1', 1'') results communicated in preceding note. Experiments (S), (BJG), and (BM) (at lower temperatures) were plotted as $\log p/p_{ev}$, since for large σ-values this ratio should be practically independent of temperature.

to the sticking coefficient f, and to the ratio of the aperture area to the total area σ by

$$p = p_{eq} f/(f+\sigma). \tag{1}$$

The plot of $\log p/p_{eq}$ *vs* $\log 1/\sigma$ (Fig. 1, curve (*a*)) gives a 45° straight line as long as $\sigma \gg f$. The intercept with the pressure axis gives practically the apparent pressure observed in rate of evaporation experiments.

The graph shows that the experimental points disagree with the theoretical curve (*a*). This could be accounted for if one considers that the speed of evaporation from a graphite surface is given mainly by the rate of evaporation of C_2, whereas C_1 is predominant in the equilibrium.

The value $L_c = 141.26$ kcal we advocate, combined with $Dc_2 = 83$ kcal proposed by Herzberg,[5] yields $Lc_2 = 199.5$ kcal ($Lc_2 = 2L_c - Dc_2$) and, using Gordon's entropy data,[6] the vapor pressure curve of C_2 (Fig. 1, preceding note).

Some time ago, Herzberg, Herzfeld, and Teller[7] have admitted that a potential barrier of about $L_c/3$ determines the rate of evaporation of C atoms, since two C−C bonds must be broken to evaporate the first C atom from the graphite plane and only one to evaporate the second. Hence the sticking coefficient of carbon atoms: $f_1 \approx 2 \cdot \exp[-(1/3)L_c/RT] \approx 2 \cdot \exp(-50.000/RT)$ and the apparent vapor pressure (p^*) of C atoms, as determined by rate of evaporation experiments, would be given by: $\log p^* = \log p_{eq} + \log f_1$ (curve *a*, Fig. 1, preceding note). The evaporation of C_2 molecules, treated according to Herzberg, Herzfeld, and Teller's model, does not, on the other hand, lead to any potential barrier.

The total apparent vapor pressure determined by rate of evaporation experiments, being calculated in mass units and not as a number of particles, should thus be: $p_{ev} = p_{1eq} f_1 + 2^{\frac{1}{2}} p_{2eq}$.

This function, plotted on Fig. 1 of the preceding communication (curve *b*), is seen to coincide very closely with the experimental "evaporation pressures," as determined by Marshall and Norton and Simpson *et al.*[2] Furthermore (even though there is a great danger in using determinations of the slope of the $\log p$ *vs* $1/T$ curve at such temperatures), its slope coincides very nicely with that of about 198 kcal obtained by Simpson *et al.* in their rate of evaporation experiments.

The apparent pressure determined by crucible experiments should now be

$$p = p_{1eq} \cdot f_1/(f_1+\sigma) + 2^{\frac{1}{2}} p_{2eq}. \tag{2}$$

The variation of $\log p/p_{eq}$ *vs* $\log 1/\sigma$ according to Eq. (2) is plotted on Fig. 1 (curves *b* and *c*) for two values of the potential barrier to C_1 evaporation (50 and 52.5 kcal, respectively). It is seen to be in excellent agreement with available experimental data.

The author wishes to thank Professor Goldfinger for continued interest and valuable help received during this research. He is indebted to the Institut pour l'Encouragement de la Recherche Scientifique dans l'Industrie et l'Agriculture and to the Centre National Belge de Chimie Physique Moléculaire for grants which allowed him to carry out this work.

[1] Doehaerd, Goldfinger, and Waelbroeck, preceding note.
[2] A. L. Marshall and F. J. Norton, J. Am. Chem. Soc. **72**, 2166 (1950); Simpson, Thorn, and Winslow, AECD, 2680 (1949).
[3] P. Goldfinger and W. Jeunehomme, Third Symposium on Combustion, Flame, and Explosion Phenomena, Minneapolis (1948); Brewer, Gilles, and Jenkins, J. Chem. Phys. **16**, 797 (1948); L. Brewer and D. F. Mastick, UCRL, 572 (1949).
[4] Although an experimental confirmation of Eq. (1) is not known to us.
[5] G. Herzberg, Phys. Rev. **70**, 762 (1946).
[6] A. R. Gordon, J. Chem. Phys. **5**, 530 (1937).
[7] Herzberg, Herzfeld, and Teller, J. Phys. Chem. **41**, 325 (1937).

Recent Determinations of the Vapor Pressure of Graphite

LEO BREWER
Department of Chemistry and Chemical Engineering, University of California, Berkeley, California
(Received February 14, 1952)

DOEHAERD, Goldfinger, and Waelbroeck[1] have greatly extended the range of measurements of the vapor pressure of graphite. If the details of their complete paper can confirm that the variation of vapor pressure with ρ, the ratio of orifice to evaporating area, is real, their work will be the definitive determination. However, certain internal inconsistencies are apparent in the information presented which cause one to be cautious in the acceptance of these new data and which indicate that well-established experimental errors may readily account for the observed variation.

The previous vapor pressure measurements[2–5] cover a range of values of ρ from 1 to 1/700. If f, the condensation coefficient, were small enough to allow reconciliation of these data with $L_C = 141$ kcal, a pronounced dependence of vapor pressure upon ρ would have been observed as indicated by curve (*a*) of Waelbroeck's letter.[6] Such a variation is not found, indicating that f cannot be very small. Also the direct determination[3,5] of the condensation coefficient of carbon vapor gives f greater than 0.1. The preceding authors[1,6] agree that one must accept a high f value for the range of ρ-values previously studied. They claim, however, that upon even further reduction of ρ, one finds a dependence indicating an extremely low f value. These observations are reconciled by assuming that the main species escaping when ρ is small is C_1 and that this species has a high f value. At very low ρ-values the concentration of C atoms, which have an extremely low f value, can build up, and the atomic beam consists largely of C atoms.

One can present arguments against C_2 playing such a role, but the significant point of the argument is that two species are present with vastly different condensation coefficients, and we need not debate here the possible nature of such species. Such an unusual situation is entirely possible. However, if this is the true situation in the case of graphite, it does not appear possible that the method used by the preceding authors[1,6] could indicate it. They[7] used the same method as that of Simpson, Thorn, and Winslow[3] and have indeed used the values of the absorption coefficient of carbon deposits and of the condensation coefficient of carbon vapor on such deposits determined by Simpson, Thorn, and Winslow. However, their hypothesis requires that Simpson's atomic beam, for which a high f value of 0.2 was obtained, consists largely of C_2. With a much smaller orifice and therefore presumably a beam largely of C atoms, with their very low f value, only a small fraction of the beam should condense. The carbon deposit would be due essentially only to the C_2 molecules in the beam and the C atoms should reflect off the carbon deposit. Thus the method used will not give appreciable detection of a species with an extremely low f value even when the atomic beam consists largely of that species. It would seem that some other explanation must be responsible for the abnormally high vapor pressure reported for the low ρ-value of 1/24,000. All the other

new data reported lie as close to or closer to $L_C=170$ than to $L_C=141$ kcal.

A possible clue to this explanation is given in the manner of presentation of the data given in the figures of the preceding letters. All of the determinations of Brewer, Gilles, and Jenkins[2] are presented out of context as if they were equivalent. Actually most of these pressures varying over a factor of ten were given by experiments designed to emphasize the error due to the "tar effect." Long heatings at very high temperatures are necessary to obtain graphite samples which do not give spuriously high vapor pressure values.[2,4,5] Their method of presentation of the data would indicate that the preceding authors might have overlooked this effect. Proper representation of the data gives much poorer agreement with curves *b* and *c* (reference 6). The figure of reference 1 presents two groups of data for $\rho=1/2400$ labeled *D* and *GJ*. The details of the *GJ* determinations are available.[8] The highest heating reported for the samples was 2100°K which would be much too low to have eliminated the "tar effect." Brewer and Mastick[6] have made a study of the various serious sources of errors involved in the determination of the vapor pressure of graphite. These cannot be reviewed here. However, the detailed paper of Doehaerd, Goldfinger, and Waelbroeck will be awaited with great interest to determine if these various errors have been adequately appraised. Because of the severe experimental difficulties inherent in these measurements, it is a difficult and time consuming task to carry out the experiments necessary to evaluate all the important variables. Doehaerd, Goldfinger, and Waelbroeck have greatly extended the available data and techniques and it is hoped that their work will soon lead to an unambiguous determination of this very important quantity.

[1] Doehaerd, Goldfinger, and Waelbroeck, J. Chem. Phys. **20**, 757 (1952).
[2] Brewer, Gilles, and Jenkins, J. Chem. Phys. **16**, 797 (1948).
[3] Simpson, Thorn, and Winslow, Argonne National Laboratory Declassified Report ANL-4264, May 6, 1949.
[4] A. L. Marshall and F. J. Norton, J. Am. Chem. Soc. **72**, 2166 (1950).
[5] L. Brewer and D. F. Mastick, paper submitted to *Journal of Chemical Physics;* based in part upon University of California Radiation Laboratory Declassified Report UCRL-572, November, 1949.
[6] F. Waelbroeck, J. Chem. Phys. **20**, 757 (1952).
[7] See reference 3 of Doehaerd, Goldfinger, and Waelbroeck letter.
[8] P. Goldfinger and W. Jeunehomme, Rev. de l'Institue Fr. du Petrole **4**, 427 (1949); Third Symposium on Combustion, Flame and Explosion Phenomena, pp. 618–621, Minneapolis (1948).

The Structure of the Molecules PH_3, AsH_3, and SbH_3*

H. H. NIELSEN
Department of Physics and Astronomy, The Ohio State University, Columbus, Ohio
(Received February 18, 1952)

THE two nearly coincident vibration frequencies ν_1 and ν_3 and the overlapping bands ν_2 and ν_4 (Herzberg's notation) of the molecules PH_3, AsH_3, and SbH_3 are coupled, respectively, by Coriolis interactions. It is possible to show in the case of ν_1 and ν_3 that the interaction is so slight that it may satisfactorily be taken into account in the effective moments of inertia of the molecule. Standard methods, where use is made of combination relations, may therefore be employed in the analysis of these bands. The Coriolis coupling between ν_2 and ν_4 in such molecules is not small, however, and since ν_2 and ν_4 are nearly alike, the interaction must be calculated by the use of degenerate perturbation methods.[1]

It may be shown, however, that for values of the quantum number K equal to J and K equal to $J-1$ (i.e., where the rotation of the molecule classically is almost entirely about the axis of symmetry) the perturbation is small enough so that the corresponding term values in the first excited state ν_4 may be obtained by an expansion of the secular determinant. One may show by this method that the frequency interval between two ${}^RR$ lines, ${}^RR(J,K)$ and ${}^RR(J+1,K+1)$ is equal to $\Delta\nu=2[(1-\zeta_4)C+2\xi_{2,4}{}^2B^2/\Delta]$ where $B=h/8\pi^2I_{xx}c$, $C=h/8\pi^2I_{zz}c$, I_{xx} and I_{zz} being the two moments of inertia, ζ_4 is the degenerate Coriolis coefficient coupling the angular momentum associated with ν_4 to the rotation of the molecule, $\xi_{2,4}$ is the Coriolis coefficient coupling the incipient angular momentum of ν_2 and ν_4 to the rotation of the molecule and where $\Delta=\omega_4-\omega_2$. Similarly one may show that the frequency interval between two ${}^RR$ lines ${}^RR(J,K-1)$ and ${}^RR(J+1,K)$ is equal to $\Delta\nu'=2[(1-\zeta_4)C+4\xi_{2,4}{}^2B^2/\Delta]$. One has, therefore, a direct means of determining the magnitude of the perturbation from the experimental data if the above lines can be identified.

The term values of ν_3 where $K=0$ (i.e., where the molecule is tumbling) may also readily be obtained from the secular determinant. Moreover, the frequency positions of the corresponding lines in the *P* branch are given by a rather simple equation. Here also the frequency interval between two lines in the *P* branch where $K=0$ gives a measure of the value $\xi_{2,4}{}^2B^2/\Delta$.

When applied to the PH_3 molecule,[2] this method leads to the values $2\xi_{2,4}B=4.77$ cm^{-1}, $B=4.4460$ cm^{-1}, $(1-\zeta_2)C=3.8360$ cm^{-1}, and $(1-\zeta_4)C=5.5425$ cm^{-1}. Recalling that $\zeta_2+\zeta_4=(B/2C-1)$,[3] the rotational constant C is determined and one may calculate the size and the shape of the molecule. For the H-P-H angle (α) we obtain the value 93° 50′, and for the PH distance (r_0) we find 1.424A. When the method is applied to the data on AsH_3, the following values are found $2\xi_{2,4}B=4.999$ cm^{-1}, $B=3.723$ cm^{-1}, $(1-\zeta_2)C=3.883$ cm^{-1} and $(1-\zeta_4)C=4.800$ cm^{-1}. These lead to the values $\alpha=91°\,35'$ and $r_0=1.523$A. The data on the SbH_3 molecule[4] treated in the same manner give these values: $2\xi_{2,4}B=3.28$ cm^{-1}, $B=2.935$ cm^{-1}, $(1-\zeta_2)C=2.975$ cm^{-1}, and $(1-\zeta_4)C=3.950$ cm^{-1}. These give for α and r_0 the values $\alpha=91°\,30'$ and $r_0=1.711$A.

The values of α and r_0 arrived at from infrared bands are, therefore, in substantial agreement with the value of these constants as determined from microwave spectra.[5] The values of α and r_0 given by Loomis and Strandberg for PH_3, AsH_3, and SbH_3 are, respectively, $\alpha=93°.5$, $r_0=1.419$A; $\alpha=92°.0$, $r_0=1.523$A; and $\alpha=91°.5$, $r_0=1.712$A.

The values of $2\xi_{2,4}B$ obtained from the bands ν_2 and ν_4 were, in each of the above cases, in good agreement.

* This work was assisted by the ONR under Contrct No. 6 onr-22526, NR 019-123 with the Ohio State University Research Foundation.
[1] H. H. Nielsen, Revs. Modern Phys. **23**, 133 (1951).
[2] V. M. McConaghie and H. H. Nielsen, Proc. Natl. Acad. **34**, 455 (1948).
[3] M. Johnston and D. M. Dennison, Phys. Rev. **48**, 868 (1935).
[4] W. Haynie, Doctoral dissertation, Ohio State University, Columbus, Ohio (1951).
[5] C. C. Loomis and M. W. P. Strandberg, Phys. Rev. **81**, 798 (1951).

Erratum: Ultrasonic Absorption in the Critical Temperature Region

[J. Chem. Phys. **18**, 1300 (1950)]
W. G. SCHNEIDER
National Research Council, Ottawa, Canada

VALUES of the sound velocity given in the above communication should be divided by two and the absorption coefficients per wavelength (as defined previously) divided by two. These corrections also apply to a later paper.[1]

The corrections are necessitated by a recent observation that on the recording of the resonance peaks of the double crystal acoustic interferometer every other peak was missing. This behavior can be accounted for by the presence of a superimposed emf having the same frequency as the resonant frequencies of the quartz crystals. At temperatures well below the critical temperature, where the sound attenuation is small, all the resonance peaks can be recorded with but a slight alternation of amplitude. As the critical temperature is approached, this alternation becomes very marked, alternate peaks appearing as small satellites. Very close to the critical temperature, where the sound absorption is very high, these "satellites" are completely obscured. This interpretation and the correct sound velocity was verified by employing a pulsing technique and measuring the transit time of a sound pulse between the two crystals at a known distance apart.

I am indebted to G. J. Thiessen, E. A. Shaw, and R. R. Aggarival for assistance in analyzing the resonance behavior of the double crystal ultrasonic interferometer, a more detailed account of which is to be given in a forthcoming publication.

[1] W. G. Schneider, Can. J. Chem. **29**, 243 (1951).

Erratum: Ultrasonic Propagation in Binary Liquid Systems Near Their Critical Solution Temperature

[J. Chem. Phys. **19**, 1566 (1951)]

A. G. CHYNOWETH AND W. G. SCHNEIDER
National Research Council, Ottawa, Canada

UNFORTUNATELY, through a mistake, the erratum immediately preceding this referring to another article was appended to the article with the title, "Ultrasonic Propagation in Binary Liquid Systems Near Their Critical Solution Temperature" as a note added in proof and immediately preceding the acknowledgment. The note has nothing to do with the article to which it was attached.

Excited Molecule Theory of Radiation Chemistry of Liquids*

MILTON BURTON, JOHN L. MAGEE AND ARYEH H. SAMUEL
Department of Chemistry, University of Notre Dame, Notre Dame, Indiana

(Received February 13, 1952)

AS a result of consideration of elementary physical processes produced by ionizing radiation in water we have concluded that the chemical effects start substantially from two classes of excited states, M^* and $M^\dagger$. The former is primarily produced, either in the primary ionization column or its "spurs," has comparatively small energy, and is relatively persistent; the excitation associated with M^* may diffuse as exciton or photon to a relatively remote position. The $M^\dagger$ is produced by ion neutralization and decomposes (if at all[1]) relatively rapidly near its production site. A brief summary of the bases of these conclusions follows.

1. A minor fraction (approximately one-third) of the ionization occurs in the primary ionization track, which initially contains two classes of excited entities, M^+ ions and M^* excited molecules. The number of the latter probably exceeds that of the former, but this point is not germane to the argument. The distance between successive ions in the primary track (and hence between spurs) d depends on the velocity of the incident particle; it is of the order of 5A for slow particles and of the order of 4000–5000A for fast particles.

2. The major fraction of the ionization occurs in spurs normal to the primary track at primary ion positions. The distance between successive M^+ ions in the spurs (in the cases of numerical importance) is of the order of 4A, as is the distance between successive M^* excited molecules. These distances are not significantly dependent on the nature of the incident radiation. The parameter d thus represents the principal significant physical differences between effects of fast and slow particles.[2]

3. For the most part, the entities M^* are in the lowest excited state.

4. Except under special circumstances, excluded from this discussion, the electrons produced simultaneously with the ions M^+ are recaptured within 10^{-13} second to give the reaction

$$M^+ + e \rightarrow M^\dagger.$$

In the case of water this definite conclusion represents a deviation from current ideas, which involve the assumption that electrons are captured by water molecules more or less remote from the site of their production to yield OH^- ions and isolated H atoms.

In liquid mixtures ion transfer may occur even before the neutralization process. In any event, the picture of ionization and excitation transfer previously developed is not greatly modified.[3–7]

5. Water may be taken as an illustrative case of special interest. Two classes of reaction resultant from decomposition of $H_2O^\dagger$ can be represented by the over-all scheme

$$H_2O^\dagger \begin{cases} \nearrow \tfrac{1}{2}(H_2+H_2O_2) & (F) \\ \searrow H+OH & (R) \end{cases}$$

The relative amounts of effects attributable to (F) and (R) are determined by local radical concentrations, which are, in turn, related to the parameter d. Except for the significance of this parameter, this aspect of the theory has been discussed frequently in a form not substantially different from our own.[8–10]

6. In water the weakly excited entities H_2O^* have relatively long life. The excitation may diffuse (as exciton or photon) considerably from the initial position and deactivation usually ensues. However, these activated molecules can participate in a true oxidation reaction when suitable traps are present in the water.

We may note that this view of the elementary processes in radiation chemistry accommodates such new findings as those of Dee and Richards[11] in the special case of water. It may demand some revisions of conventional concepts regarding elementary process in radiobiology and particularly of the role of H_2O^*.

A more complete discussion of these ideas will be presented in a forthcoming paper.

* A contribution from the Radiation Project of the University of Notre Dame, supported in part by the AEC under contract AT(11-1)-38.

[1] In substances like benzene, which are very resistant to radiation, neither M^* nor $M\dagger$ makes a significant contribution to the observed chemical effect. See reference 7.

[2] M. Burton and J. L. Magee, paper presented at International Congress of Pure and Applied Chemistry, September 1951, publication forthcoming. See a special effect discussed by T. J. Sworski and M. Burton, J. Am. Chem. Soc. **73**, 3790 (1951).

[3] S. C. Lind, *The Chemical Effects of Alpha Particles and Electrons* (Chemical Catalog Company, New York, 1928), p. 193.

[4] J. L. Magee and M. Burton, J. Am. Chem. Soc. **73**, 523 (1951).

[5] J. L. Magee, J. Phys. Chem. **56**, to be published (1952).

[6] J. P. Manion and M. Burton, J. Phys. Chem. **56**, to be published (1952).

[7] S. Gordon and M. Burton, Disc. Faraday Soc., to be published (1952).

[8] A. O. Allen, J. Phys. Colloid Chem. **52**, 478 (1948).

[9] E. J. Hart, J. Am. Chem. Soc. **73**, 68, 1891 (1951).

[10] C. J. Hochanadel, J. Phys. Chem. **56**, to be published (1952).

[11] P. I. Dee and E. W. T. Richards, Nature **168**, 736 (1951).

On the Origin of Low Frequency Raman Lines of *Para*-Dichlorobenzene and Reply to S. C. Sirkar*

B. D. SAKSENA
Department of Physics, University of Allahabad, Allahabad, India

(Received June 1, 1950)

THE changes referred to by Sirkar in the second paragraph of his letter have not been overlooked by me. I did not refer to them because there are considerable discrepancies between this work and the later work of Venkateswaran,[1] who kept the crystal for well over a week at ice-cold temperatures before the spectrum at 25°C was taken and reported frequencies at 48(6b) and 89(6b) at 25°C and 43(6), 55(5), and 88(5b) at 45°C. He did not find a change in the highest frequency as reported by Sirkar and Gupta[2] nor a constancy of frequency at 50 cm^{-1}. Moreover, at 45°C he finds the highest frequency at 89 cm^{-1}, while Sirkar and Gupta report it at 82.

The statement of Sirkar that the frequencies 46, 50, and 92 of the polycrystalline mass are identical with those of the four lines observed by me in a single crystal is not correct. I reported the frequencies 27, 54, and 92 for a single crystal and 45 and 82 for the disordered one. The main difference between the spectra of a

single and disordered crystal which I emphasized in my article was the disappearance of the frequency 27 for the latter. Sirkar and Gupta have never been able to obtain this frequency in their work, which would be the main argument for saying that the polycrystalline mass behaves as a single crystal. The agreement of the frequency 92 in the two spectra is not of much significance since this frequency is very broad and diffuse, and this is the reason why Venkateswaran measures it as 89 cm^{-1} and Sirkar and Gupta at 82 cm^{-1} at 45°C. The agreement of the frequency at 45 cm^{-1} in the two spectra would, however, suggest that the polycrystalline mass behaves as a disordered crystal.

In the third paragraph Sirkar states that changes in the condition of the crystal which produce changes in the Raman spectrum fail to produce any change in the Laue pattern. The changes to which Sirkar refers are very doubtful; the main test would be whether the two specimens—one of which shows the frequency 27 in its Raman spectrum and the other which does not—give identical Laue spots.

The contention of Sirkar that the mix crystal studied by Sirkar and Bishui[3] was once cooled in ice and therefore the Raman lines observed by them do not correspond to those of a disordered crystal does not appear to be very reasonable. It appears to me that since the crystal is very soft, internal strains will appear in the crystal due to sudden cooling and make it disordered.

Krueger, Reinkobar, and Holm[4] working with inorganic crystals and Vuks[5] with organic crystals have reported a variation of lattice frequency with concentration in the spectra of mix crystals. The idea of statistical average of moment of inertia for torsional lattice oscillations is able to explain this variation, but it is possible to account for this variation in a better way by adopting the idea of a unique lattice for the mix crystal suggested by Matossi.[6] Agarwal and myself[7] have considered this problem in a paper which is due to appear in this journal.

There is considerable experimental evidence which shows that the low frequency lines in crystals are lattice oscillations, for in a single crystal their intensity varies with orientation. The polarization work of Rousset and Linchet[8] on *p*-dichlorobenzene and of Nedungadi[9] on naphthalene shows that they are rotational oscillations, and to a first approximation their frequencies depend on the moments of inertia of the molecules.

[2] S. C. Sirkar, J. Chem. Phys. (to be published).
[1] C. S. Venkateswaran, Proc. Indian Acad. Sci. **A8**, 448 (1938).
[3] S. C. Sirkar and J. Gupta, Indian J. Phys. **10**, 473 (1936).
[3] S. C. Sirkar and I. C. Bishui, Indian J. Phys. **11**, 417 (1937).
[4] Krueger, Reinkobar, and Holm, Ann. Physik **85**, 110 (1928).
[5] M. Vuks, Acta Physicochim. U.R.S.S. **6**, 327 (1937).
[6] F. Matossi, J. Chem. Phys. **19**, 161 (1951).
[7] R. R. Aggarwal and B. D. Saksena, J. Chem. Phys. (to be published).
[8] A. Rousset and Linchet, J. phys. **3**, 146 (1942).
[9] T. M. K. Nedungadi, Proc. Indian Acad. Sci. **A13**, 161 (1941).

The Ionization Potential of the CF_3 Radical and Some Fluorocarbon Bond Energies Obtained by Electron Impact*

VERNON H. DIBELER, ROBERT M. REESE, AND FRED L. MOHLER
National Bureau of Standards, Washington, D. C.
(Received February 5, 1952)

THE purpose of this note is to report preliminary results obtained in a study of dissociation energies of fluorocarbons by electron impact. A Consolidated 21-103 mass spectrometer with several minor circuit changes was used to obtain the appearance potentials of the ions of methyl fluoroform, and hexafluoroethane given in Table I. Argon was used to calibrate the voltage scale and was added simultaneously with the fluorocarbon. Initial portions of the ionization efficiency curves were plotted on a semilog scale.[1] The resulting straight portions of each curve were very nearly parallel. Differences between the parallel portions of the curves of the fluorocarbon ions and of the A^+ ion were read on the abscissa and subtracted from the spectroscopic ionization potential of argon (15.76 ev).

TABLE I. Appearance potentials of several fluorocarbon ions.

Compound	Ion	Appearance potential (ev)
CH_3-CF_3	CH_3^+	15.2
	CF_3^+	14.0
CF_3-CF_3	CF_3^+	14.3

The minimum energy required to produce the CH_3^+ ion from CH_3-CF_3 without excess kinetic or excitation energy is given by the relation $A(CH_3^+)=D(CH_3-CF_3)+I(CH_3)$. The corresponding relation for the appearance potential of CF_3^+ is $A(CF_3^+)=D(CH_3-CF_3)+I(CF_3)$ where $D(CH_3-CF_3)$ represents the energy necessary to produce CF_3 and CH_3 radicals, and $I(CH_3)$ and $I(CF_3)$ are the ionization potentials of the radicals. From these relations, the observed appearance potentials of the CH_3^+ and CF_3^+ ions in CH_3-CF_3 and the known ionization potential of the CH_3 radical one can calculate $D(CH_3-CF_3)$ and $I(CF_3)$. The latter subtracted from the appearance potential of CF_3^+ in C_2F_6 gives the C—C bond energy in C_2F_6. Stevenson[2] has called attention to the evidence that such a procedure is not valid for a number of hydrocarbons. However, appearance potentials of CH_3^+ in methane[3] and in ethane[4] lead to values of the CH_3-H bond and the CH_3-CH_3 bond that are consistent with thermochemical data.

Subtracting the ionization potential of the CH_3 radical (10.07 ev)[2] from the observed appearance potential of CH_3^+ in methylfluoroform (15.2 ev) gives 5.1 ev (117 kcal) for the C—C bond energy. This value subtracted from the appearance potential of the CF_3^+ ion (14.0 ev) gives the ionization potential for the CF_3 radical as 8.9 ev. A similar calculation based on the appearance potential of CF_3^+ and I^+ in CF_3I and the spectroscopic ionization potential of iodine atoms (10.44 ev)[5] gave 8.3 ev for the ionization potential of CF_3. As measurements on CH_3I gave 9.5 ev for the ionization potential of CH_3 the values seem to be consistently low by 0.6 ev for reasons that are not obvious. By subtracting the value 8.9 ev from the observed values for the appearance potentials of CF_3^+ in C_2F_6 (14.3 ev) a value of 5.4 ev (124 kcal) is obtained for the C—C bond in C_2F_6.

The above values for the C—C bond energy are surprisingly high even in view of the demonstrated thermal stability of C_2F_6.[6] In general, bond energies derived from appearance potential measurements should be considered as upper limits because of the possible excess energy involved in the ionization process. We plan to extend the measurements to other compounds to see whether consistent values of the bond energies can be obtained.

* This work was supported in part by the Ordnance Department, Department of the Army.
[1] R. E. Honig, J. Chem. Phys. **16**, 106 (1948).
[2] D. P. Stevenson, Disc. Faraday Soc. on Hydrocarbons (1951).
[3] L. G. Smith, Phys. Rev. **51**, 263 (1937).
[4] J. A. Hipple, Phys. Rev. **53**, 530 (1938).
[5] K. Murakawa, Z. Physik. **109**, 173 (1938).
[6] L. White, Jr. and O. K. Rice, J. Am. Chem. Soc. **69**, 267 (1947).

Characteristic Infrared Absorptions Due to Aryl Deuterium

G. V. D. TIERS*,† AND J. H. TIERS
G. H. Jones Chemical Laboratory, University of Chicago, Chicago, Illinois
(Received January 29, 1952)

IT has long been recognized that the substituted benzenes exhibit intense absorptions in the 700–900 cm^{-1} region.[1–3] Thompson *et al.*[3–5] have examined these bands in detail, finding them characteristic of the position of the substituents and almost independent of their identity. These authors have assigned the bands as CH out-of-plane bending vibrations.

It is surprising that in no case have aryl deuterium compounds been considered in such correlations. In view of this, we have

TABLE I. Absorption frequencies and molar absorbancy indices. (a_m) for the 700–900 cm^{-1} region.

	Frequency in cm^{-1} (a_m in parentheses) Characteristic band	Neighboring bands
Benzene-d[a]	778 (vapor)	699
Toluene	729 (280)	694 (120)
Toluene-2d	775 (130)	721 (109)
Toluene-3d	806 (103)	692 (105)
Toluene-4d	838 (160)	710 (30)
Benzoic acid-2d	779 (180)	863 (46), 857 (61), 800 (43), 700 (120)
Benzoic acid-3d	820 (60)[b] 789 (57)	878 (72), 770 (116), 684 (138)
Benzoic acid-4d	873 (150)	796 (43), 783 (55), 697 (90)
Anisole-4d	843 (150)	783 (60)
Fluorobenzene-4d	851 (100)	818 (95), 778 (30), 713 (36)
Benzene-1,4d_2[a]	876 (vapor)	813

[a] See reference 7.
[b] A definite choice cannot be made between these and the 770 cm^{-1} peak. The 796–800 cm^{-1} peak present in the other two isomers and in benzoic acid itself does not appear, suggesting interaction.

examined the infrared spectra of a series of disubstituted benzenes in dilute solution, one of the substituents being deuterium in each case. Table I lists frequencies and molar absorbancy indices[6] for all bands in this region having an index greater than 20. Previously reported data are given for comparison.

For the disubstituted benzenes, the ranges listed by Thompson[3] fall in a definite sequence: *ortho*, 730–760 cm^{-1}, *meta*, 770–790 cm^{-1}, *para*, 800–830 cm^{-1}. When one of the substituents is deuterium, intense absorptions occur in the same order of increasing frequency, *ortho*, *meta*, and *para*; however, in each case the frequency is above the corresponding Thompson range, averaging 20 cm^{-1} higher. Benzoic acid-4d has the highest frequency, a difference of 43 cm^{-1}.

Of the deuterated benzenes reported by Ingold,[7] benzene-1,4d_2 exhibits a high frequency, 45 cm^{-1} above the Thompson range, as might be expected for two deuterium substituents; the benzene-d band at 778 cm^{-1} is 18 cm^{-1} above the range for monosubstituted benzenes.[3] It may be noted that the vibrational assignments for these bands in benzene-d and benzene-1,4d_2[7] resemble those given by Thompson[3] for the correspondingly substituted benzenes, except that the deuterium is considered to participate appreciably in the motion.

In the 500–650 cm^{-1} region, the deuterium substituted benzenes again show intense bands, probably due to out-of-plane bending vibrations involving deuterium,[7] while nondeuterated benzene derivatives generally have no strong absorptions in this region. Table II lists the frequencies and some molar absorbancy indices for aryl deuterium compounds, including some previously reported data for comparison. These bands appear adequate to show the presence of aryl deuterium, and perhaps also to identify the position substituted, at least within an isomeric series. In such cases, quantitative determination of the isomers will usually be feasible.[8]

The deuterotoluenes used have been described previously;[8] the fluorobenzene-4d was prepared in the same manner, and the infrared spectrum indicated 99 percent isotopic purity. In contrast, omission of the high vacuum treatment of the Grignard reagent[9] resulted in anisole-4d of 91 percent, and mesitylene-2d of only 60 percent, isotopic purity. Coinciding absorptions, strong in the parent compound and weak in the deutero derivative, were used for estimating isotopic purity; in each case good agreement was found between two such peaks. The spectra have been corrected for the estimated isotopic purity. The deuterobenzoic acids were prepared from the corresponding deuterotoluenes by alkaline permanganate oxidation. The D_2O was obtained through the Atomic Energy Commission. The infrared equipment was as previously used.[8] The solutions were 3.17 percent by volume for liquids, and 4.0 grams per 100 ml for the benzoic acids. Solvents employed were CS_2, tetrachloroethylene, and cyclohexane. The accuracy of the molar absorbancy indices is adequate for the purposes of this work, being highest for the low intensity peaks, although the most intense peaks are subject to as much as 30 percent error.

TABLE II. Absorption frequencies and intensities for aryl deuterium in the 500–650 cm^{-1} region.

	cm^{-1}	a_m
Benzoic acid-2d	628	232
Benzoic acid-3d	636	140
Benzoic acid-4d	612	285
Toluene-2d	631	190
Toluene-3d	645	162
Toluene-4d	607	324
Fluorobenzene-4d	602	298
Anisole-4d	598	310
Mesitylene-2d	632	190
Benzene-d[a]	612	vapor
Benzene-1,4d_2[a]	597	vapor
Benzene-1,3,5d_3[a]	527	vapor
Benzene-1,2,4,5d_4[a]	550	vapor

[a] See reference 7.

The authors wish to thank Professor R. S. Mulliken, who granted unlimited access to the infrared equipment, and Professor G. W. Wheland, who contributed helpful discussions.

* Charles A. Coffin Fellow, 1950–1951.
† Central Research Department, Minnesota Mining and Manufacturing Company, St. Paul, Minnesota.

[1] P. Lambert and J. Lecomte, Ann. phys. **18**, 329 (1932).
[2] N. Colthup, J. Opt. Soc. Am. **40**, 396 (1950).
[3] D. H. Whiffen and H. W. Thompson, J. Chem. Soc., 268 (1945).
[4] A. R. H. Cole and H. W. Thompson, Trans. Faraday Soc. **46** (2), 103 (1949).
[5] Bell, Thompson, and Vago, Proc. Roy. Soc. (London) **192A**, 498 (1948).
[6] F. A. Smith and E. C. Creitz, J. Research Natl. Bur. Standards **46**, 145 (1951).
[7] C. K. Ingold *et al.*, J. Chem. Soc. (London), 222–333 (1946).
[8] G. V. Tiers, J. Chem. Phys. **19**, 1072 (1951).
[9] L. H. P. Weldon and C. L. Wilson, J. Chem. Soc. (London), 235 (1946).

Electrical Polarizability as a Criterion for Molecular Wave Functions

J. A. ABBOTT AND H. C. BOLTON
Department of Physics, University of Durham, King's College, Newcastle upon Tyne, 1, England
(Received February 21, 1952)

THE object of this letter is to show that by making use of a simple expression for the polarizability suggested by Hassé,[1] considerable information may be obtained about the wave functions for molecules with particular reference to homonuclear diatomics. Results are reported here for H_2^+, H_2, and N_2. The electrical polarizabilities of H_2^+ and H_2 have recently been calculated by Bell and Long[2] by a method involving the complete Hamiltonian H_0+H_1 where H_0 is the unperturbed term and H_1 the perturbation term. This latter method is direct but very laborious since it involves a calculation of the total energy and is out of the question for more complicated molecules.

The present calculations start by assuming a perturbed wave function of the one-parameter form, *viz.*, $\psi=\psi_0(1+\lambda H_1)$, where ψ_0 is the unperturbed wave function and H_1 is the perturbation term in the Hamiltonian resulting from the field F; $H_1=eF\Sigma_i^n q_i$ where q_i is the coordinate of the ith electron measured from the center of the molecule. It may be shown that

$$\alpha_q=4\left[\int \psi_0^2\{\sum_i^n q_i\}^2 d\tau\right]^2 \Big/ a_0 n, \qquad (1)$$

when ψ_0 is the correct unperturbed wave function; a_0 is the first Bohr radius.

Experimental values for the longitudinal and transverse polarizabilities are known. A comparison can be made between these values and those calculated from Eq. (1) with wave functions containing two parameters, one of which is the scale factor c, and the other a measure of the hybridization. An LCAO MO composed of Rosen-type $s-p$ hybridized AO's was used in the

case of H_2^+ and H_2, and the following values obtained (σ is the usual Rosen parameter). For H_2^+, $c=1.31$, $\sigma=0.12$. These can be compared directly with the values of Dickinson[3] ($c=1.25$, $\sigma=0.16$) who made an accurate theoretical estimate of the binding energy. The discrepancies between the two sets of values is probably due to weighting different regions of the wave functions in the two methods. The true values of α_q for H_2^+ were taken to be those calculated by Bell and Long[2] using the James function (known to be very accurate). For H_2, $c=1.18$, $\sigma=0.09$; there is no energy calculation using such a wave function, but these figures lie in the range of values for c and σ given by other approximations[4] to ψ_0 using the minimum energy criterion. The agreement leads one to hope that valuable information about the wave functions for more complicated molecules, e.g., N_2, may be obtained using polarizability calculations.

For N_2 the following electronic structure was assumed:

$$(\sigma_g 1s)^2(\sigma_u 1s)^2(\sigma_g 2s)^2(\sigma_u 2s)^2(\sigma_g 2p)^2(\pi_y 2p)^2(\pi_x 2p)^2.$$

The total wave function was a completely antisymmetric determinant of the individual MO's. These MO's formed an *orthonormal* set which contained a variable parameter ω to represent a variation in the degree of hybridization ($\sigma 1s-\sigma 2s-\sigma 2p$). The orthonormal set was constructed by the Schmidt process from basic functions which were simple LCAO MO's, e.g., $[(2p_z)_a+(2p_z)_b]/[1+S(2p_z 2p_z)]$. The constituent AO's in these basic functions were Slater AO's with a variable scale factor c in all but the $1s$ functions.

By adjusting the values of c and ω to obtain agreement with experimental values for the longitudinal and the transverse polarizabilities, the following results were obtained: $c=0.87$, $|\omega|\approx 0.4$. The value $|\omega|=0.4$ represents the following degree of hybridization in the corresponding AO's of the $\sigma_g 2s$ orbital: $1s$, 3; $2s$, 78; $2p$, 19. It will be noticed that the orthogonalization process leads to some forced admixture of $1s$ functions as in Mulliken's[5] process. The ratio $2s/2p$ agrees with that predicted by Mulliken[5] and also by Greenhow and Smith[6] from quadrupole moment calculations. It is important to recognize that the polarizability calculations weight the outer regions of the wave functions; thus the value of $c(<1)$ shows that wave functions used with $c=1$ fall off too quickly at large distances. It is hoped to publish a full account of these calculations in the near future.

[1] H. R. Hassé, Proc. Cambridge Phil. Soc. **27**, 66 (1930).
[2] R. P. Bell and D. A. Long, Proc. Roy. Soc. (London) **A203**, 364 (1950).
[3] B. N. Dickinson, J. Chem. Phys. **1**, 317 (1933).
[4] J. O. Hirschfelder and J. W. Linnett, J. Chem. Phys. **18**, 130 (1950); E. F. Gurnee and J. L. Magee, J. Chem. Phys. **18**, 142 (1950).
[5] R. S. Mulliken, J. Chem. Phys. **19**, 900, 912 (1951).
[6] C. Greenhow and W. V. Smith, J. Chem. Phys. **19**, 1298 (1951).

Equation of State of Gases at High Temperature*

HARRY MILTON PEEK AND ZEVI W. SALSBURG†
University of California, Los Alamos Scientific Laboratory, Los Alamos, New Mexico
(Received February 18, 1952)

It has been shown by H. Jones[1] and also by Brinkley[2] that knowledge of the detonation velocity as a function of the initial density is not sufficient to determine the equation of state of the product gases at the temperature and pressure of the Chapman-Jouguet plane. The question arises: Given detonation velocity and initial density, what information does one gain if one measures the pressure or density of the product gases at the Chapman-Jouguet plane?

The Rankine-Hugoniot equations for conservation of mass, momentum, and energy across the detonation front may be written

$$P-P_0=\rho_0 uD;\quad \rho(D-u)=\rho_0 D;\quad E-E_0=\tfrac{1}{2}(P+P_0)\left(\frac{1}{\rho_0}-\frac{1}{\rho}\right), \quad (1)$$

where u is the particle velocity of the detonation products, D the detonation velocity, P the pressure, ρ the density, and E the specific internal energy. The subscript zero refers to the initial state of the explosive. From Eq. (1) it is obvious that P is determined for given D, ρ_0, and ρ; ρ is determined for given D, ρ_0, and P. We then know $E(P, \rho)$ of the detonation products if we measure, in addition to the usually measured D and ρ_0, either P or ρ.

Knowing $E(P, \rho)$ it is possible to determine the equation of state of the detonation products by the following scheme:

From thermodynamics it is easy to show that

$$T\left(\frac{\partial P}{\partial T}\right)_\rho - P = -\rho^2(\partial E/\partial \rho)_P - \rho^2(\partial E/\partial P)_\rho(\partial P/\partial \rho)_T. \quad (2)$$

Using

$$(\partial P/\partial \rho)_T = -(\partial T/\partial \rho)_P/(\partial T/\partial P)_\rho \quad (3)$$

in Eq. (2), we get

$$\rho^2(\partial E/\partial P)_\rho(\partial \ln T/\partial \rho)_P+[P-\rho^2(\partial E/\partial \rho)_P](\partial \ln T/\partial P)_\rho=1. \quad (4)$$

Equation (4) is a nonhomogeneous, first-order, linear partial differential equation which on integration will give the equation of state of the detonation products. Integration of Eq. (4) requires that $E(P, \rho)$ be measured over a wide range of P and ρ-values in order to compute its derivatives with respect to pressure and density. This requirement makes the above outlined procedure lucrative only for gaseous detonation. It is also necessary to know initial equation of state data in order to eliminate the arbitrary constants in the integration of Eq. (4).

One should now discuss the initial assumption of experimental measurement of P or ρ. The requirements of the measurement for determination of the equation of state are that one needs P or ρ at the Chapman-Jouguet plane. In order to determine P or ρ at the $C-J$ plane one must locate the $C-J$ plane. To this end one would like to have a pressure or density profile showing the behavior of pressure or density ahead of, within, and behind the steady zone. One could then say the $C-J$ plane is determined by a discontinuous change in slope of the pressure or density, occurring after the maximum value due to the shock.

It may be possible to determine a pressure profile using a piezoelectric gauge of the type well known in explosives work.[3] One of the most difficult problems is to obtain a gauge with very fast response time (i.e., for most detonations the reaction time is of the order 5×10^{-7} sec or less). Piezoelectric gauges of such fast response, capable of measuring the high pressures produced, are at the present time unknown.

It may be possible to determine a density profile by means of an x-ray densitometer as suggested by Kistiakowsky.[4] It cannot be said that equipment for such a measurement is commercially available, but it does not appear impossible to construct the necessary equipment.

It hardly seems necessary to point out that experimental determination of equation of state of detonation products of gaseous explosions will provide very useful thermodynamic data at high temperature (*ca* 5000°K) and pressures ($<10^4$ atmos). One might also mention that if one can determine P or ρ within the steady zone, one might be able to deduce information concerning the kinetics of the detonation process. This is seen to be plausible if one writes the necessary conservation equations in terms of the degree of reaction within the steady zone.

The authors wish to acknowledge helpful discussions with Dr. J. von Neumann, Dr. W. W. Wood, and especially, Professor G. B. Kistiakowsky, at whose suggestion this work has been done.

* Work done under the auspices of the AEC.
† Present Address: Department of Chemistry, Yale University, New Haven, Connecticut.
[1] H. Jones, *Third Symposium on Combustion and Flame and Explosion Phenomena* (The Williams and Wilkins Company, Baltimore, Maryland, 1949), pp. 590–595.
[2] S. R. Brinkley, Jr., Conference on Physics and Chemistry of Detonation sponsored by the ONR, Washington, D. C., January 11, 1951.
[3] See, for instance, R. H. Cole, *Underwater Explosions* (Princeton University Press, Princeton, New Jersey, 1948), Chapter 5.
[4] Professor G. B. Kistiakowsky, private communication.

Kinetics of Formation of Oxide Layer on Zinc

WALTER J. MOORE*
H. H. Wills Physical Laboratory, University of Bristol, Bristol, England
(Received February 5, 1952)

THE relation between the parabolic rate constant for metal oxidation k and the diffusion coefficient D_i for defects in the oxide is $k=2D_i(f_1-f_2)$, where f_1 and f_2 are the equilibrium defect fractions at the metal-oxide and oxide-oxygen interfaces. In the case of oxidation of copper to cuprous oxide, it was recently shown[1] that this equation reduces to $k=4D$, $D=\frac{1}{2}D_i(f_1+f_2)$ being the self-diffusion coefficient of copper in cuprous oxide measured with radioactive copper. In the case of copper oxidation, the defects are cation vacancies, and in both the oxidation-rate and the diffusion experiments they are formed by the same mechanism, solution of oxygen in cuprous oxide.

Recently Lindner[2] has measured D for radioactive zinc in zinc oxide from 800° to 1400°C, finding $D=1.4\exp(-74/RT)$ cm² sec^{-1} with the activation energy U in kcal mole^{-1}. The oxide was in the form of compressed sintered powder exposed to air. The k for zinc oxidation from 375° to 410° is[3] $3.8\times10^{-7}\exp(-29/RT)$ cm² sec^{-1}.

The diffusion of zinc in zinc oxide most probably proceeds via interstitial zinc ions, which arise from the dissociation ZnO $=Zn_i^{+2}+\frac{1}{2}O_2+2e$. For this reaction, $\Delta H=\Delta H_1+\Delta H_2$, where ΔH_1 is the heat of dissociation of ZnO to zinc vapor and oxygen, and ΔH_2 is the heat of solution of the zinc vapor to form interstitial ions in the oxide. At 1100°C, $\Delta H_1=110$ kcal,[4] $\Delta H_2=E_1+E_2+E_3$. E_1 is the heat of solution of an interstitial zinc atom in an octahedral hole in the zinc-oxide structure; it has been calculated to be about 5 kcal. E_2 is the heat of dissociation for $Zn_i=Zn_i^{+}+e$, which is 7 kcal from the activation energy of the low temperature electronic conductivity of ZnO.[5] E_3 is the heat of dissociation for $Zn_i^{+}=Zn_i^{+2}+e$, which is 45 kcal from the temperature coefficient of the high temperature conductivity, or from the threshold for photoconductivity in ZnO.[6]

The observed activation energy for the self-diffusion is $U=(\Delta H/3)+U_i$, where U_i is the activation energy for the mobility of an interstitial Zn_i^{+2} ion. Thus U_i is estimated to be 18 kcal. In the case of oxidation of zinc, the interstitial ions arise from solution of solid zinc in the oxide, and not from the dissociation reaction, which is negligible at the oxidation temperatures. In this case, the heat of formation of Zn_i^{+2} is $\Delta H'=\Delta H_3+\Delta H_2$, where ΔH_3 is the heat of sublimation of zinc, 30 kcal. The expected activation energy for diffusion of zinc in zinc oxide that is in equilibrium with solid zinc is therefore $(\Delta H'/3)+U_i=(87/3)+18=47$ kcal. This figure is considerably higher than the observed activation energy for the oxidation reaction.

It seems likely, therefore, that interstitial zinc ions diffusing during the oxidation of zinc do not arise from the thermal dissociation of interstitial zinc atoms, but by some process consisting of the transfer of electrons from interstitial zinc atoms to adsorbed oxygen. A possible process of this kind is $Zn_i+2O_2(\text{ads})=Zn_i^{+2}+2O_2^{-}(\text{ads})$. The heat of formation of Zn_i^{+2} in this case would be $\Delta H''=\Delta H'-2A$, where A is the electron affinity of O_2, about 23 kcal.[7] Thus $U=(\Delta H''/3)+U_i=32$ kcal. This is close to the experimental activation energy of 29 kcal.

The assumption that the diffusing interstitial ions are formed by electron transfer to adsorbed oxygen explains also the dependence of the parabolic rate constant on the oxygen pressure, and the assumption that the rate determining step involves adsorbed O_2 is consistent with the observation that the pressure dependence of k follows a Langmuir isotherm in P_{O_2}, and not $P_{O_2}^{\frac{1}{2}}$.[8] Although this interpretation explains the pressure and temperature dependence of the zinc oxidation, it should not be regarded as conclusive in view of (a) the reported independence of rate on oxygen partial pressure in O_2-N_2 mixtures[3] and (b) the possibility of grain-boundary diffusion of zinc and/or oxygen.

The author is glad to thank the John Simon Guggenheim Memorial Foundation and the U. S. Educational Commission in the U.K. for their support of this work.

* Permanent address: Catholic University, Washington, D. C.
[1] W. J. Moore and B. Selikson, J. Chem. Phys. **19**, 1539 (1951).
[2] R. Lindner, Z. Elektrochem. **54**, 430 (1950); Acta Chem. Scand. (to be published).
[3] W. J. Moore and J. K. Lee, Trans. Faraday Soc. **47**, 500 (1951).
[4] E. E. Mahn, J. Appl. Phys. **22**, 856 (1951); C. A. Hogarth, Z. physik Chem. **198**, 30 (1951).
[5] J. A. Kitchener and S. Ignatowicz, Trans. Faraday Soc. **47**, 1285 (1951).
[6] E. Mollwo, Ann. Phys. (6) **3**, 321 (1948); P. H. Miller, *Semi-Conducting Materials* (Butterworth Scientific Publications, London, 1951), p. 176.
[7] H. S. W. Massey, *Negative Ions* (Cambridge University Press, London, 1950), p. 28.
[8] C. Wagner and K. Grunewald, Z. physik. Chem. **B40**, 455 (1938).